A re-evaluation of the origins of Late Quaternary ramparted depressions in Wales

Neil Ross

School of Earth, Ocean and Planetary Sciences
Cardiff University

2006

UMI Number: U584973

UMI U584973

ProQuest LLC
789 East Eisenhower Parkway
P.O. Box 1346
Ann Arbor, MI 48106-1346

DECLARATION

This work has not previously been accepted in substance for any degree and is not concurrently submitted in candidature for any degree.

Signed .... *Neil Ross* ....,.................... (candidate)   Date *21st December 2006*

STATEMENT 1

This thesis is being submitted in partial fulfillment of the requirements for the degree of
.......PhD............/..(insert MCh, MD, MPhil, PhD etc, as appropriate)

Signed ...... *Neil Ross* .... (candidate)   Date *21st December 2006*

STATEMENT 2

This thesis is the result of my own independent work/investigation, except where otherwise stated.
Other sources are acknowledged by explicit references.

Signed ... *Neil Ross* .... (candidate)   Date *21st December 2006*

STATEMENT 3

I hereby give consent for my thesis, if accepted, to be available for photocopying and for inter-library loan, and for the title and summary to be made available to outside organisations.

Signed ... *Neil Ross* .... (candidate)   Date *21st December 2006*

STATEMENT 4 - BAR ON ACCESS APPROVED

I hereby give consent for my thesis, if accepted, to be available for photocopying and for inter-library loans **after expiry of a bar on access** approved by the Graduate Development Committee.

Signed ...... *N/A* .... (candidate)   Date

Summary

This thesis describes the results of sedimentological and near-surface geophysical investigations of the internal structure of late Pleistocene permafrost and glacial ice-related 'ramparted depressions' in Wales. These data were used to evaluate the possible origins of these landforms, which have previously been interpreted as the remains of open system pingos or lithalsas (mineral palsas). Six sites were investigated: i) Hirwaun valley; ii) Llanio Fawr; iii) Crychell Moor; iv) Cledlyn valley; v) Cletwr valley; and vi) Llanpumsaint. Each site investigation is presented as an individual case study. The precise origins of these landforms remain uncertain. The density of landforms at all sites however is inconsistent with their interpretation as relict open system pingos. Some sites (Hirwaun valley and Llanio Fawr) are unequivocally glacial in origin, whilst others (e.g. Llanpumsaint) are most probably a type of relict periglacial ground-ice mound, although formation via the grounding of icebergs in a proglacial lake cannot be ruled out. Conversely, the ramparted depressions of the Cledlyn and Cletwr valleys probably formed as a result of the meltout of stagnating glacier ice, although permafrost-related origins are also possible. The investigations of relict landforms are complemented by geophysical investigations (ground penetrating radar and electrical resistivity) of active open system pingos from Svalbard. Data from both the relict and active landforms suggests that groundwater seepage through geological discontinuities is important for ground-ice mound formation, and that there is a continuum of ground-ice mounds, from features cored with lenses of segregation ice (e.g. palsas and lithalsas) to others cored with massive, injection ice (pingos). Transitional forms between these two extremes will contain a mixture of ground-ice types.

Acknowledgements

List of Contents

List of Tables

List of Figures

Chapter 3: Research Methods

Chapter 8: Cletwr valley

Chapter 10: Svalbard

Chapter 11: Discussion

1   Introduction

1.1   Context of the research

Permafrost is ground that remains at or below 0°C for at least two consecutive years (Harris *et al.* 1988). Arctic regions currently underlain by permafrost are often characterised by the localised formation of ground ice (Mackay 1972) within both superficial sediments and bedrock, and the subsequent heaving and blistering of the ground surface in response to the progressive growth of an ice lens. Large ice-cored hills termed 'pingos', up to 50 m high and 600 m wide may result, though pingos and related ground-ice features (palsas, lithalsas, and seasonal frost mounds) range in size from large features such as these, down to much smaller mounds a few metres in diameter. During the Devensian, permafrost conditions became widely established across much of the southern regions of the British Isles, and a series of relict landforms thought to have been generated by the thaw and collapse of massive ground-ice bodies during permafrost degradation have been identified in Wales, Ireland, England and the Isle of Man (Watson 1977; Bryant and Carpenter 1987; Coxon and O' Callaghan 1987; Ballantyne and Harris 1994). These landforms, interpreted as the relict forms of periglacial ground-ice mounds, usually take the form of peat-filled basins enclosed by circular or complex debris-cored ridges, and are therefore referred to as 'ramparted depressions' or 'ramparted ground-ice depressions' (Sparks *et al.* 1972; Bryant and Carpenter 1987). They tend to occur in clusters, with tens to hundreds of individual landforms closely associated or superimposed across several square kilometres (Watson 1972; Bryant and Carpenter 1987; Coxon and O'Callaghan 1987; Gurney 2000). Because potentially they are one of the few known diagnostic indicators of permafrost (Mackay 1979, 1986, 1988), landforms of this type have been used to infer the existence and the distribution of late Pleistocene permafrost in currently temperate environments (Flemal 1976; De Gans 1988) or even to reconstruct palaeo-temperature regimes, based on the current distribution of active ground-ice mounds (Watson 1977; Washburn 1979, 1980; Isarin 1997; Pissart 2000, 2003). However, although enclosed circular depressions have been widely accepted by many as diagnostic of the former development of ground ice under permafrost conditions, there are a series of processes associated with the meltout of glacier ice that can also result in the development of a series of depressions

1

surrounded by enclosing ring-ridges (e.g. Hoppe 1952; Gravenor and Kupsch 1959; Stalker 1960; Parizek 1969; Flemal 1976; Eyles *et al.* 1999; Mollard 2000).

In the British Isles, groups of ramparted depressions are particularly widespread across parts of mid and west Wales (Pissart 1963; Watson 1972, 1977; Watson and Watson 1974; Ballantyne and Harris 1994). Originally interpreted as the remains of late Pleistocene open system pingos (Pissart 1963; Watson 1971, 1972; Watson and Watson 1972, 1974), these landforms have since been re-interpreted as the relict forms of mineral palsas (lithalsas), smaller ground-ice mounds formed by localised preferential ice segregation (Pissart and Gangloff 1984; Gurney 1994, 1995; Gurney and Worsley 1996; Worsley *et al.* 1995; Matthews *et al.* 1997; Pissart 2000, 2003). As well as supporting a range of important wetland habitats, the poorly drained central basins of many ramparted depressions in Wales are frequently infilled with organic-rich sediments that contain detailed Holocene palaeo-environmental records (Handa and Moore 1976; Walker and James 2001).

Despite potentially constituting important periglacial phenomena, highly diagnostic of ancient ground-ice conditions, little is known about the internal structure and precise cryogenic origins of many ramparted depressions in Wales. Accurate interpretation of these relict landforms requires data on the internal structure of both late Pleistocene ramparted depressions and active periglacial ground-ice mounds (Pissart 1988).

1.2 Thesis objectives

The primary objective of this thesis was to establish the internal structure of ramparted depressions in Wales, as a means of evaluating their cryogenic origins. This was achieved through the application of an integrated suite of sedimentological tools (sedimentological logging, clast fabric and grain-size analysis of boreholes, trial pits and trenches), and near-surface geophysical methods (electrical resistivity tomography, seismic refraction, induced polarisation and ground penetrating radar). Field investigations were undertaken at six sites in mid and west Wales (Hirwaun valley, Llanio Fawr, Crychell Moor, Cledlyn valley, Cletwr valley, and Llanpumsaint) (Figure 1.1). Preliminary results from these investigations, and a conservation assessment of these, as well as many other groups of ramparted
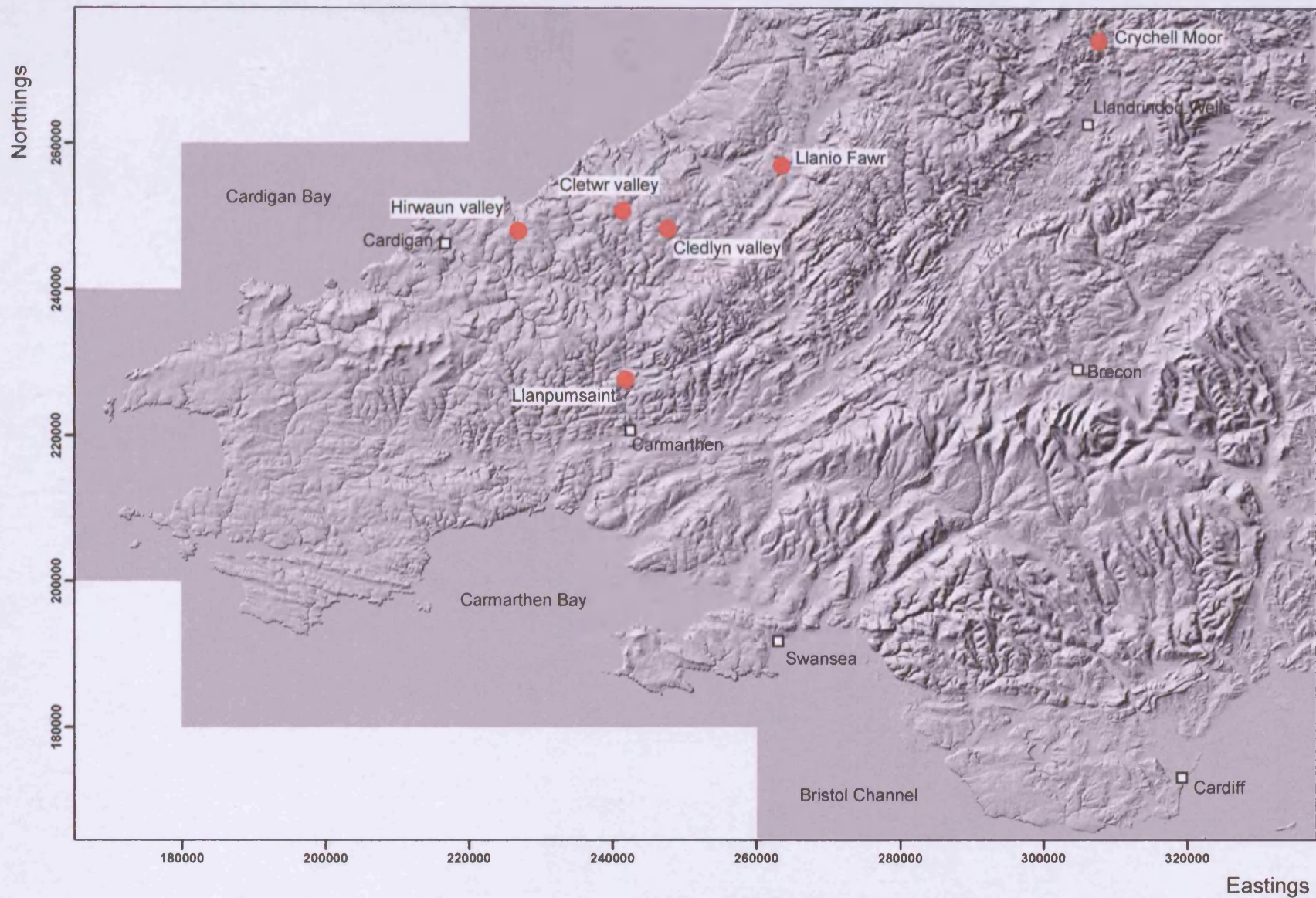
Figure 1.1: The locations of site investigations undertaken in west and mid Wales during this project. OS Panorama digital terrain model (© Crown Copyright/database right 2006. An Ordnance Survey/(Datacentre) supplied service).

depressions in Wales have already been presented in a series of interim reports (Ross *et al.* 2005a; Harris *et al.* 2005).

Because contemporary studies in permafrost regions aimed at assessing the processes of pingo decay and collapse are critical for the correct identification and classification of ramparted depressions (Pissart 1988), the interpretation of the Welsh landforms was complemented by data from geophysical investigations (ground penetrating radar, electrical resistivity) of the internal structure (ground ice geometry and physical characteristics) of active open system pingos in Svalbard, designed to establish the likely mode of formation. Of all the types of periglacial ground-ice mounds (closed system pingos, open system pingos, palsas, lithalsas, and seasonal frost mounds), knowledge of the internal description of open system pingos is perhaps the most limited, due to the lack of suitable exposures (Mackay 1985), and because of the difficulties associated with the transportation and deployment of drilling equipment. Geophysical methods provide an ideal solution to these problems as near-surface geophysical equipment is relatively portable and cheap to transport to remote locations, and significant volumes of data can be collected in short time periods.

1.3 Thesis format

Chapter 2 presents a review of research investigating the mechanisms that result in the formation of active periglacial ground-ice mounds, and the processes that lead to their collapse and the development of ramparted depressions. A review of ramparted depressions in northwest Europe (mainly Belgium and the British Isles) is presented. Chapter 2 also provides an outline of the bedrock and superficial geology, Quaternary environmental history and hydrogeology of mid and west Wales. Particular reference is made to the Afon Teifi catchment, within which four of the six sites investigated in Wales are located. Chapter 3 outlines the near-surface geophysical and sedimentological methods, and geographical information systems, used for the investigation and mapping of landforms in both Wales and in Svalbard, describing the equipment used and how data was acquired, processed and presented. Chapters 4-9 describe and interpret the geophysical and sedimentological data from a series of site investigations of ramparted depressions at six different localities in Wales (Chapter 4: Hirwaun valley; Chapter 5: Llanio Fawr; Chapter 6: Crychell Moor; Chapter 7: Cledlyn valley; Chapter 8: Cletwr valley; and Chapter 9: Llanpumsaint). Sections on

4

the mechanisms of landform formation are presented in two of the six 'Welsh' chapters (Chapter 4: Hirwaun valley, and Chapter 5: Llanio Fawr). The origins of the other six sites (Chapter 6: Crychell Moor; Chapter 7: Cledlyn valley; Chapter 8: Cletwr valley; and Chapter 9: Llanpumsaint) are specifically discussed in detail in the Discussion (Chapter 11). Geophysical investigations (ground penetrating radar and electrical resistivity) of the internal structure of active open system pingos in Svalbard are described and interpreted in Chapter 10. Chapter 11 discusses and evaluates the possible mechanisms of formation of the ramparted depressions in Wales, assessing the importance of regional and local hydrogeology, as well as outlining data and evidence that undermines or contradicts previous interpretations of these landforms. The role that glacial rather than periglacial processes may have played in the formation of these landforms is also evaluated. A summary of the possible genetic origins of ramparted depressions at Llanpumsaint, Crychell Moor and in the Cledlyn and Cletwr valleys is presented, followed by a short section outlining the implications of the current study for the interpretation of other ramparted depressions in the British Isles and for diagnostic criteria used to discriminate between, and interpret, ramparted depressions. Chapter 12 presents a summary of the main conclusions of this study and provides recommendations for areas of future work.

2 Literature Review

2.1 The nature and origins of pingos

Pingos are perennial, blister-like, intra-permafrost, ice-cored hills produced by the injection and subsequent freezing of water within superficial sediments or bedrock (Mackay 1979; Pissart 1988). They are circular to oval in plan, 30-600 m in diameter and generally less than 20 m in height (Pissart 1988), although some examples growing to elevations of 48 m (Mackay 1986) and 60 m (Ferrians 1988) have been reported. Formally classified as "a perennial *frost mound* consisting of a core of massive ice, produced primarily by injection of water, and covered with soil and vegetation" (Harris *et al.* 1988), the term 'pingo' originates from the Inuit language, and means 'conical hill' (Porsild 1938). Pingos develop in a variety of geological materials throughout the continuous and discontinuous permafrost zones, including till, slope deposits, alluvial silts, sands and gravels, and even in bedrock (e.g. Müller 1959; Cruickshank and Colhoun 1965; van Autenboer and Loy 1966; Åhman 1973; Liestøl 1977; Hamilton and Obi 1982; Pissart 1988; Seppälä 1988a; St-Onge 1990). A prerequisite for pingo initiation and growth is the availability of water under sufficient pressure to enable the development of injection or segregation ice (Mackay 1973, 1977, 1978a, 1983) and the upward displacement of overburden materials. Two mechanisms enable this, and on this basis, two types of pingo are recognised: i) closed (or hydrostatic) system; and ii) open (or hydraulic) system (Porsild 1938; Müller 1959; Mackay 1979) (Figure 2.1).

2.1.1 Closed system pingos

Closed system pingos are found, with few exceptions, in former lake basins or river channels on the low-lying coastal plains of the continuous permafrost zone of northwest Canada, Alaska and Siberia (Stager 1956; Mackay 1962; Péwé 1975; Ferrians 1988). The majority of closed system pingos in Canada are located in the flat low-lying tundra areas along the western Arctic coast around the Mackenzie Delta, the Tuktoyaktuk Peninsula and Richards Island, where there are 1350-1450 such landforms (Stager 1956; Müller 1959, 1962; Mackay 1962, 1963, 1966). In northern Alaska, more than 1000 closed system pingos have been described and mapped on the

6
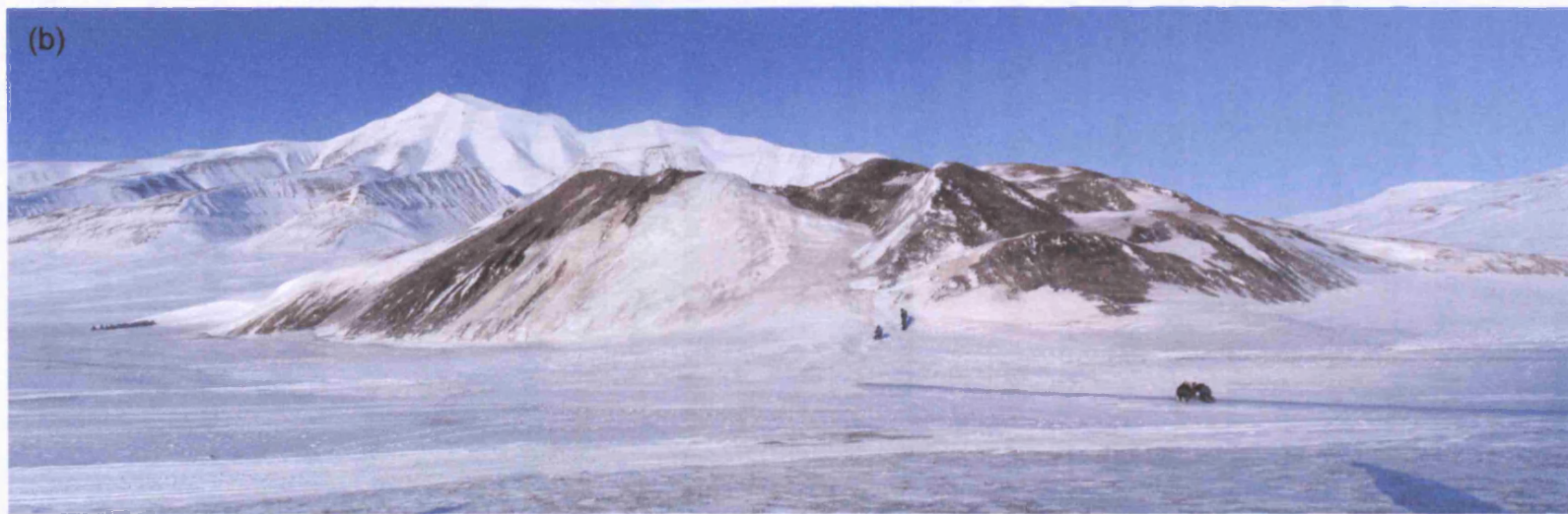
Figure 2.1: (a) Oblique aerial photograph of a closed system pingo, Mackenzie Delta, Canada (photo by C. Harris); (b) Open system pingo, Adventdalen, Svalbard.

Arctic Coastal Plain and on the Seward Pensinsula (Leffingwell 1919; Porsild 1938; Péwé 1975; Ferrians 1983, 1988).

The mechanism of closed system pingo growth is now well known (Mackay 1962, 1973, 1977, 1978a, 1979, 1983, 1998) (Figure 2.2). On the Tuktoyaktuk Peninsula and surrounding lowlands, surface water accumulates in summer to form pools and lakes. Where the water depth of a lake exceeds the maximum thickness of winter ice, the bottom waters of the lake will remain above 0°C throughout the winter and a talik (a zone of unfrozen, water-saturated sediment) will develop in the underlying permafrost. In simplified models of closed system pingo development, these taliks are enclosed, laterally and at depth, by impermeable, perennially frozen ground, although this may not always be the case (Mackay 1979). Thaw lakes, however, are highly susceptible to rapid catastrophic drainage from thermal erosion along ice wedge networks or coastline retreat. Subaerial exposure of the lake floor through lake drainage leads to refreezing of the underlying talik, with permafrost aggrading downwards and inwards from the sides (Figure 2.2). Because pore water is free to migrate to zones of lower pressure within coarse-grained, unfrozen sediments, as the talik gradually freezes, the 9% expansion associated with the phase change acts like a piston, expelling the remaining unfrozen pore water ahead of the freezing front and increasing the pore water pressure. This water is unable to percolate through the surrounding permafrost however and, as the talik freezes, becomes concentrated as a pressurised water lens in zones of lower pressures below areas of thinner permafrost (e.g. beneath a small residual pond). Freezing of this water lens from the surface downwards will then result in the growth of a massive ice-core, with water freezing to the base of the ice lens. As the ice is derived from 'internal' sources, the term 'closed system' is used to classify this type of pingo. Many old (10-20,000 years old), large lakes (>600 m in length), however, may not be enclosed at depth but will instead be characterised by through-going taliks (Mackay 1979). Theoretically, these enable groundwater to enter, or be lost from the system. Pingos can still grow despite the presence of through-going taliks however, providing that the rate of water expulsion is greater than the rate of water loss from the system (Mackay 1979). As a result of the possibility of groundwater migration via through-going taliks, Mackay (1979) argued that the term 'closed system' was inappropriate when used to classify the pingos of the Tuktoyaktuk Pensinsula area. Instead, these pingos should be classified
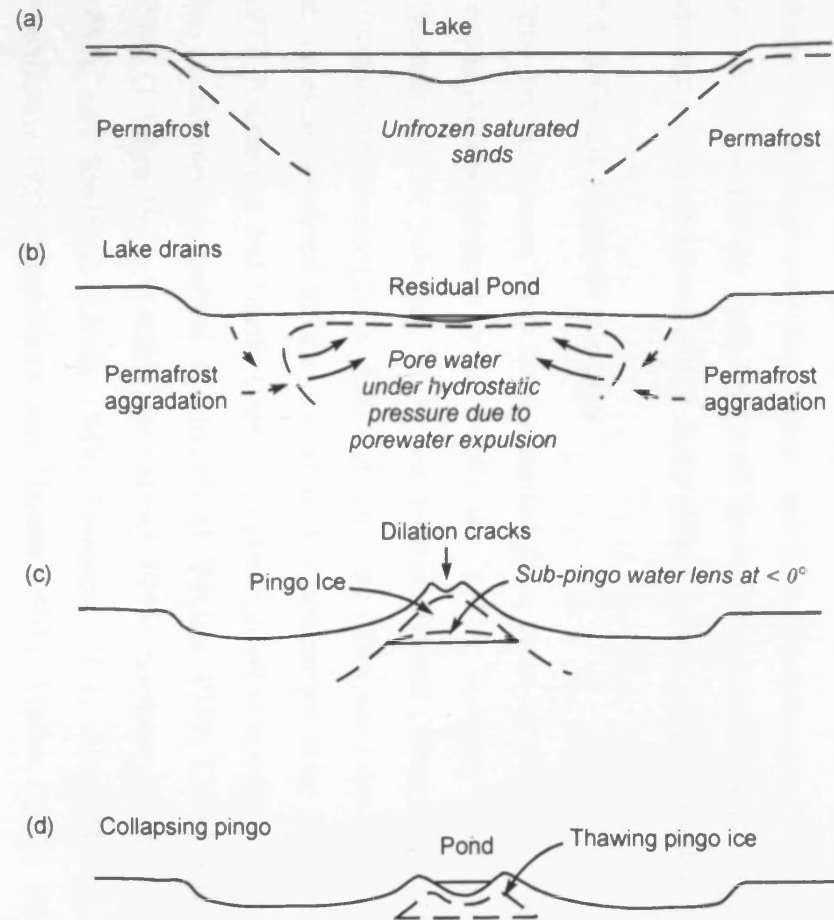
Figure 2.2: Formation of closed system pingos (after Mackay 1998). (a) Talik development beneath a thaw lake; (b) Lake drainage leads to permafrost aggradation, refreezing of the talik and pore water expulsion; (c) Growth of pingo ice-core as expelled water freezes; (d) Pingo collapse following development of dilation cracks and crater lake.

Figure 2.3: Drill-hole flow from the sub-pingo water lens of a closed system pingo ('Pingo 14'), 20 km east of Tuktoyaktuk, N.W.T., Canada (from Mackay 1998) (Photo: J.R. Mackay).

as 'hydrostatic' pingos (Mackay 1979, 1998). Although this recommendation, and the suggestion that open system pingos should be referred to as hydraulic pingos, have been adopted by some (e.g. Gurney 1998), many authors (e.g. Ballantyne and Harris 1994) still use the original terminology (open and closed system pingos), and it is this approach that will be adopted throughout this thesis.

If the addition of expelled pore water to the bottom of the pingo ice exceeds the downward rate of freezing, a sub-pingo water lens will develop in which the hydrostatic pressure is sufficient to cause uplift and deformation of the overlying ice core and its frozen overburden (Mackay 1973, 1979, 1983, 1998). Direct evidence for sub-pingo water lenses under artesian pressure has been obtained by drilling through closed system pingos on the Tuktoyaktuk Peninsula (Mackay 1973, 1977, 1978a, 1979, 1981, 1983, 1986) (Figure 2.3). Mackay argued that indirect, external evidence for the presence of pressurised water lenses takes the form of radial and concentric tension cracks, alternating periods of pingo uplift and subsidence, extensive peripheral failure and high-angle normal and reverse faulting, periodic spring discharge, and icing mound development (Mackay and Stager 1966; Mackay 1973, 1977; Rampton and Mackay 1971; French *et al.* 1982). At least some of these characteristics, however (e.g. pingo uplift, radial extension cracks), could equally have been caused by frost heave of the overburden generated by ice segregation, which has been observed within many closed system pingos (Mackay 1973, 1979).

2.1.2 Open system pingos

Open system pingos have been recorded from areas of discontinuous permafrost in central Alaska (Holmes *et al.* 1968), the Yukon Territory (Hughes 1969), Siberia (Shumskii 1959; Soloviev 1973), the Tibetan Plateau (Wang and French 1995), and Mongolia (Babinski 1982). Although they are often been described as characteristic of, or even restricted to, the discontinuous permafrost zone (e.g. Brown and Péwé 1973; Ballantyne and Harris 1994), this observation is at odds with their presence in the continuous permafrost of Greenland (Müller 1959; Cruickshank and Colhoun 1965; O' Brien 1971; Worsley and Gurney 1996), northern Alaska (Hamilton and Obi 1982), and Svalbard (Orvin 1944; Svensson 1971; Åhman 1973; Liestøl 1977; Yoshikawa 1993; Yoshikawa and Harada 1995). Müller (1959) believed that the distribution of pingos was concentrated in a belt where the permafrost was "...still

more or less continuous, but is nevertheless beginning to thin out perceptibly" (pg. 114). In truth however, open system pingos are most numerous in areas of thin permafrost (Holmes *et al.* 1968; Hughes 1969), and in the continuous permafrost zone where postglacial retreat of ice or a fall in relative sea level has allowed permafrost to aggrade in unfrozen sediments (e.g. in Svalbard and Greenland).

In the shallow discontinuous permafrost zone of central Alaska and the Yukon Territory, Canada, recharge of sub-permafrost groundwater aquifers occurs beneath upper slopes where permafrost is thin or absent (Holmes *et al.* 1968; Hughes 1969) (Figure 2.4). Downslope seepage of sub- or intra-permafrost groundwaters takes place through permeable, unfrozen, unconsolidated materials or bedrock discontinuities (Holmes *et al.* 1968). Beneath the lower valley-sides, where permafrost is thicker, the seepage of sub-permafrost groundwater is confined. This is highly conducive for the upward penetration and freezing of intruded groundwater under artesian pressure and, where the near-surface hydrogeology and permafrost regime are favourable, can lead to the formation of ice-cored, open system pingos (Holmes *et al.* 1968) (Figure 2.4). Groundwaters associated with open system pingo development can also originate from other sources however, including subglacial meltwaters from below polythermal glaciers (Liestøl 1977, 1996) (Figure 2.5) or relatively deep-seated sub-permafrost groundwaters (Müller 1959; O' Brien 1971; Allen *et al.* 1976; Worsley and Gurney 1996; Scholz and Baumann 1997). Many studies of open system pingos in the continuous permafrost zone have recognised the importance of groundwater migration from deep aquifers through faults and other structural discontinuities. The close association of pingos and structural features has been recorded in Alaska (Holmes *et al.* 1968; Hamilton and Obi 1982), Greenland (Müller 1959; O'Brien 1971; Worsley and Gurney 1996; Scholz and Baumann 1997), Svalbard (van Autenboer and Loy 1966; Liestøl 1977; Yoshikawa and Harada 1995; Pękala and Repelewska-Pękalowa 2004), Mongolia (Babinski 1982), and on the Tibetan Plateau (Wang and French 1995). Perennial groundwater flows that feed open system pingos from intra- or sub-permafrost sources remain unfrozen even under conditions of continuous permafrost due to high dissolved salt contents, artesian pressures and high flow rates, which all lower the freezing point. Geothermal heating of sub-permafrost waters may also play an important role in maintaining groundwater circulation through geologically controlled seepage zones in areas of continuous permafrost such

11
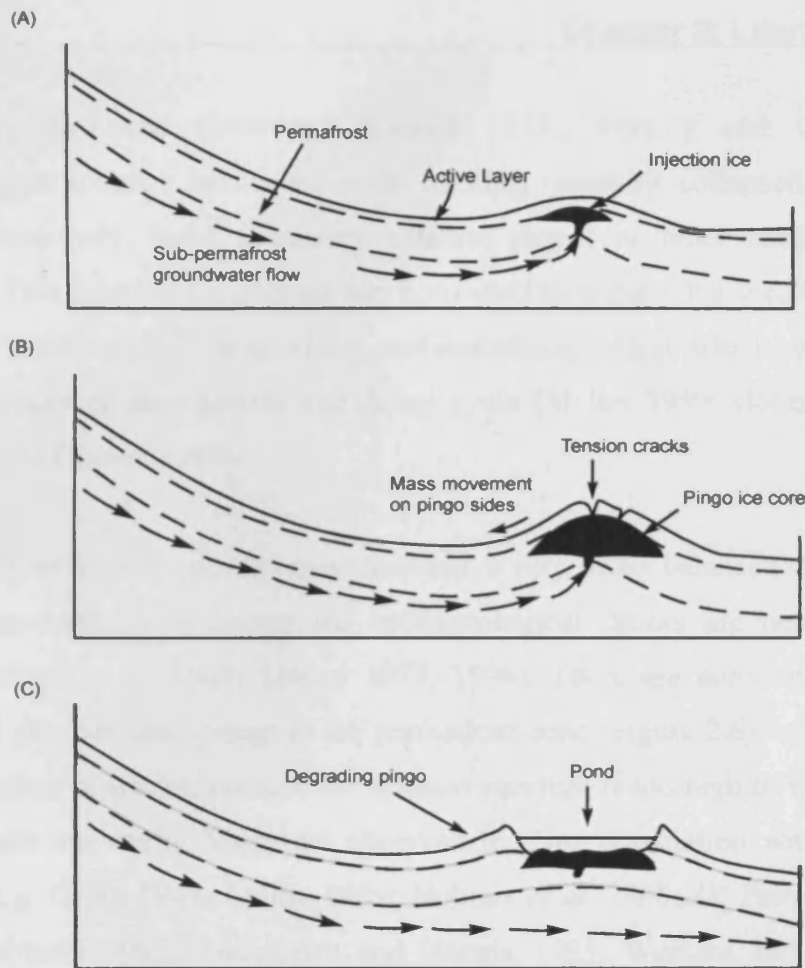
Figure 2.4: Cycle of formation and decay of open system pingos: (a) Downslope seepage of groundwater through a confined sub-permafrost aquifer, with upward injection in areas of thin permafrost, where freezing of groundwater leads to the formation of a pingo ice core; (b) Growth of pingo ice, leading to the development of tension cracks on the pingo surface (as a result of the tensional stresses caused by thinning and extension of the pingo overburden), and the mass movement of sediments on the steep pingo flanks; (c) Collapsing pingo, with a circular rampart (formed by the mass movement of sediments on the pingo flanks), enclosing a crater lake (after Holmes *et al.* 1968; and Ballantyne and Harris 1994).
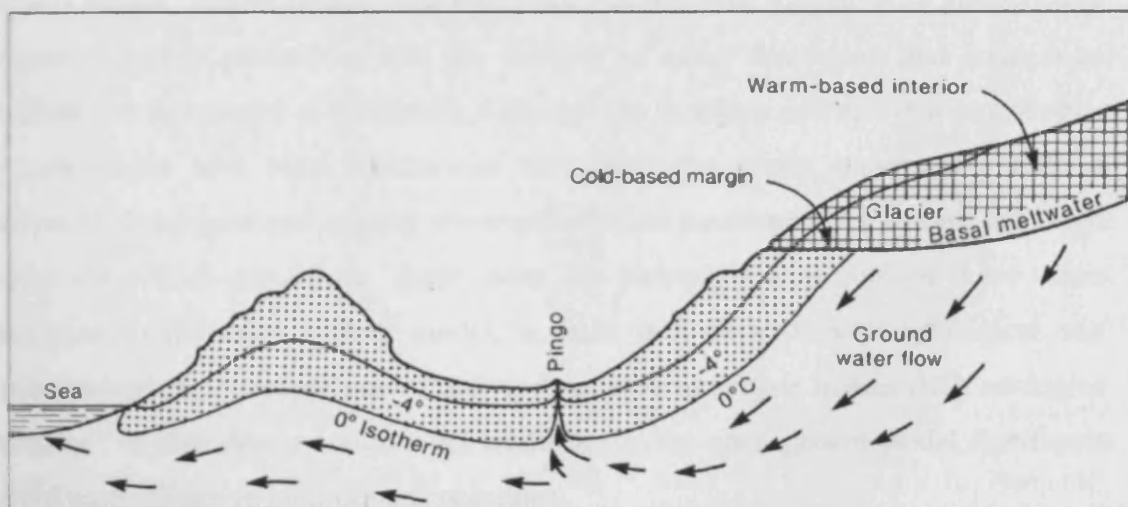
Figure 2.5: Formation of open system pingos in Svalbard, due to the upward injection of sub-permafrost groundwaters fed by meltwaters from polythermal glaciers (after Liestøl 1977; and Ballantyne and Harris 1994).

as in Svalbard and Greenland (Liestøl 1977; Worsley and Gurney 1996). Groundwater seepage associated with existing, partially collapsed, open system pingos commonly forms secondary satellite pingos or other smaller ground-ice mounds. This reactivation process has been used to explain the localised clusters of mutually interfering pingos in Alaska and eastern Greenland, which contain pingos at varying stages of their growth and decay cycle (Müller 1959; Holmes *et al.* 1968; Worsley and Gurney 1996).

For open system pingo development to occur, a very finely balanced selection of site-specific permafrost conditions and hydrogeological factors are necessary (Müller 1959; Holmes *et al.* 1968; Liestøl 1977, 1996). There are numerous examples of perennial groundwater springs in the permafrost zone (Figure 2.6), which form large surface icings in winter, because the artesian pressure is too high or the groundwater temperature too warm. Many are observed in close association with open system pingos (e.g. Orvin 1944; Müller 1959; Holmes *et al.* 1968; O' Brien 1971; Liestøl 1977; Babinski 1982; Yoshikawa and Harada 1995; Worsley and Gurney 1996; Scholz and Baumann 1997). Although these pingos consistently discharge mineralised groundwater at temperatures above zero, most authors advocate a meteoric, rather than juvenile (thermal) origin for the groundwaters.

In contrast to the intensive long-term investigations that have been undertaken on closed system pingos (e.g. Mackay 1998), there remains a lack of research on open system pingos. This is despite their importance as potential indicators of groundwater migration within permafrost and the number of relict landforms that have been attributed to this model of formation. Although the locations and distributions of open system pingos have been documented throughout the Arctic, surprisingly little is known of the origins and internal structures of these landforms. As a result, although many ramparted ground-ice depressions in permafrost-free regions have been attributed to the open system model, a basic lack of systematic geological and hydrogeological investigations of active open system pingos makes such analogies tentative. To confidently assign relict landforms to the open system model significant future work on active landforms is necessary.

13

Figure 2.6: (a) Seepage of saline groundwaters at Innerhytte pingo, Adventdalen, Svalbard on the 20th April 2004 (Photo: C. Harris); (b) Surface icing on the south-facing flanks of Innerhytte pingo on the 20th April 2004, formed by the freezing of saline groundwaters. The point of seepage in Figure 2.6a is located approximately at the feet of the person. Sheetflow of water was observed beneath the icing surface however, indicating that the true location of springflow was closer to the top of the icing visible in this photograph. The icing was covered with a deposit of salt, which had been expelled from solution during the freezing process.

2.1.3 Pingos of uncertain origins

Elongate pingo forms, not easily reconcilable with either the closed or open system models of pingo formation, have been reported from thick continuous permafrost in the Canadian Arctic (Pissart 1967; Pissart and French 1976; French and Dutkiewcz 1976; French et al. 1982; Zoltai 1983; Gurney and Worsley 1997). Pissart (1967) described two types of pingos from Prince Patrick Island, Canada. Despite being found in plateau-top locations, the formation of the first type of pingo appeared to be determined by geological structures in a manner similar to certain open system pingos. A second, elongate type of pingo found in low-lying near-shore areas was thought to have formed through permafrost aggradation in superficial estuarine sediments exposed by falling relative sea levels. Such a process is partly analogous to closed system pingo development. Similar elongate 'linear' pingos have been observed in inland areas of Banks Island, where their development was thought to be the result of permafrost aggradation on taliks exposed by the lateral migration of river channels (Pissart and French 1976; French and Dutkiewcz 1976). Other studies, however, have suggested that at least some of these pingos, located at distance from lake or river channels, may instead be a type of open system pingo, resulting from groundwater flow through structurally controlled groundwater pathways (Gurney and Worsley 1997).

2.1.4 The internal structure of pingos

The internal structure (ground-ice geometry and physical properties) of pingos and other ground-ice mounds can provide key data informing interpretation of the origins and growth of these landforms. However, such data are uncommon as the internal structure of these landforms is rarely revealed in natural exposure. Despite thirty field seasons in the Canadian Arctic, J.R. Mackay only observed thirty collapsing pingos, of which only ten had exposures large enough to study (Mackay 1985). Descriptions of open system pingo ice have been particularly limited (Müller 1959; Holmes et al. 1968; O' Brien 1971; Yoshikawa 1993), most observations of pingo ice having been made on closed system pingos (e.g. Müller 1959; Pihlainen et al. 1956; Tarnocai and Netterville 1976; Pissart and French 1976; Gell 1978; Mackay 1979, 1985, 1990, 1998; Mackay and Stager 1966; Rampton and Mackay 1971; Walker et al. 1985) or pingos of uncertain origin (Pissart 1967; Pissart and French 1976). These studies have

shown that the concept of the internal structure of pingos simply being composed of a clear plano-convex ice core is not always the most appropriate model (Mackay and Stager 1966). Many studies have emphasised the importance of segregation ice, as well as injection ice, for pingo development, even in medium-grained sands (Müller 1959, 1962; Mackay and Stager 1966; Mackay 1973, 1977, 1978a, 1979, 1983, 1985, 1998; Gell 1978; Rampton and Mackay 1971; Tarnocai and Netterville 1976; Pissart and French 1976).

2.1.5 Pingo decay and collapse

Because the topographic form of a pingo depends mainly on the presence of an underlying ice core, melting of this core leads to landform collapse. During pingo collapse, processes such as mass wasting, surface wash and deflation result in a net transfer of overburden material to the pingo flanks, leading to the development of a water-filled depression, surrounded by an annular ring-like ridge or rampart (Figure 2.7). The majority of work on the collapse of pingos has been conducted on closed system pingos (Mackay 1986, 1987, 1988). The basic processes associated with pingo decay are common to both types however (Mackay 1986), and information gained from the decay of closed system pingos can therefore be used to inform understanding of the collapse of open system pingos.

Pingo degradation is generally initiated by the development of radial dilation cracks and concentric cracking caused by tensional stresses arising from bending and extension of the frozen overburden during pingo growth (Figure 2.2, 2.4 and 2.8) (Müller 1959; Holmes *et al.* 1968; Babinski 1982; Mackay 1987, 1988). Sediment cover is also lost due to slumping and solifluction on the steep pingo sides, resulting in sediment accumulation around the base of the mound (Babinski 1982; Mackay 1987, 1988). Rupturing and collapse of overburden at the summit exposes the pingo ice-core, which thaws during the summer to form a summit crater (Mackay 1987, 1988). Meltwater collects within this crater to form a small pond, which further accelerates the rate of thaw (Müller 1959; Holmes *et al.* 1968; Babinski 1982). Thermal erosion of the surrounding frozen ridge causes lake expansion and the intermittent, sometimes seasonal breaching of the central pond, resulting in drainage outflow from the enclosed basin (Babinski 1982). Crater lakes (Figure 2.7a), many

Figure 2.7: (a) Partially collapsed closed system pingo ('Pingo 23'), Mackenzie Delta, Canada, with a central pond enclosed by an ice-cored rampart. External diameter of landform approximately 250 m (Mackay 1986, 1988, 1998) (Photo: J.R. Mackay); (b) Open system pingos in Reindalen, Svalbard, showing various stages of decay. From the background to the foreground, these features have heights of approximately 42 m, 28 m and 20 m (Photo: H.H. Christiansen).
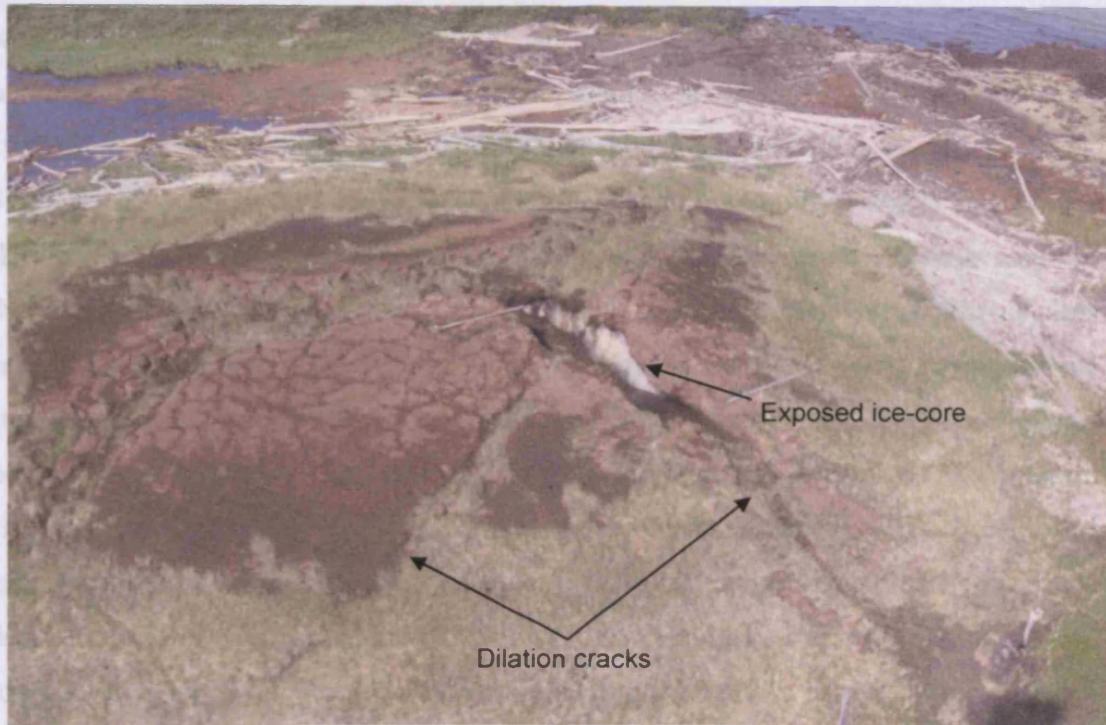
Figure 2.8: Closed system pingo in the Mackenzie Delta, Canada, showing development of radial dilation cracks caused by tensional stresses generated by upward growth. The exposed ice core is highly susceptible to summer thaw, which is likely to initiate pingo collapse (Photo: C. Harris).

with perennially flowing groundwater springs and outflow streams, have been reported from active pingos in Canada (Pihlainen *et al.* 1956; Hughes 1969; Mackay 1988), Greenland (Müller 1959; Cruickshank and Colhoun 1965; O' Brien 1971), Svalbard (Åhman 1973; Liestøl 1977; 1996), Mongolia (Babinski 1982) and Alaska (Holmes *et al.* 1968; Hamilton and Obi 1982). Short-lived streamflow events result in the development of small-scale outlet channels, associated with small alluvial fans around the periphery of the collapsing landform (Mackay 1988). By exposing the ice core to thaw or by affecting water pressures in sub-pingo water lenses, peripheral normal faulting, diking and associated spring flow can also play important roles in closed system pingo decay (Mackay and Stager 1966; Mackay 1987). Outflow of groundwater and lateral erosion by adjacent rivers can contribute significantly to the degradation of open system pingos (Müller 1959; Babinski 1982), whilst in mid- to low-latitudes solar radiation on pingo slopes with southerly aspects, causing rapid spring thaw, active layer instability and slumping, is also seen as important (Babinski 1982).

Once degradation is well advanced, inward movement of thawing sediment from the rim is likely, and this sediment may insulate the ice, slowing degradation of the core (Mackay 1986). Complete thaw often leaves a pond that is surrounded by a ridge of sediment that accumulated around the base of the former landform as a result of mass movement and the outward displacement of material (Figure 2.7) (Babinski 1982; Mackay 1988). Mature, collapsing or collapsed pingos with ramparts have been described from the current permafrost zone (Porsild 1938; Müller 1959; Holmes *et al.* 1968; Likens and Johnson 1966; O' Brien 1971; Mackay 1973, 1979, 1986, 1988; French 1975; Babinski 1982; Worsley and Gurney 1996; Gurney and Worsley 1997), but there have been few studies monitoring these landforms or investigating their internal structures. In relict Pleistocene ramparted depressions (Figure 2.9a), ramparts have been described with overturned, deformed, and tilted stratified sediments overlain by mass movement deposits showing crude, radially dipping stratification (Figures 2.9b, 2.9c). The presence of these structures often provides important evidence for an origin related to the decay of ground-ice mounds (e.g. Pissart 1963, 2000; Bastin *et al.* 1974; Watson 1975; Pissart and Juvigne 1980; De Gans 1988; van der Meulen 1988).

19
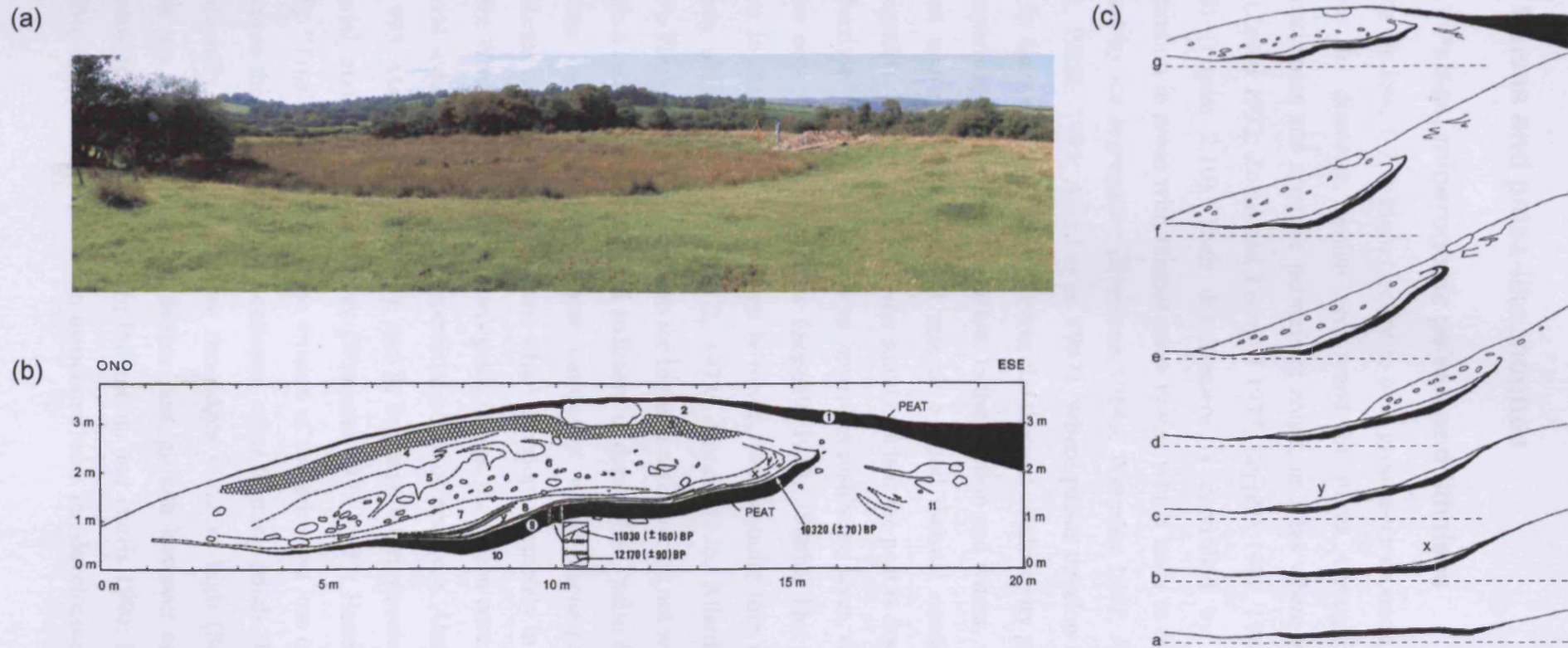
Figure 2.9: (a) A relict ramparted depression that may mark the former location of a periglacial ground-ice mound developed as a result of either groundwater migration (open system pingo) or ice segregation (lithalsa), near Llanpumsaint, Carmarthenshire, southwest Wales; (b) Section through the rampart of a landform thought to be the remains of a lithalsa, Konnerzvenn, Belgium. Two peat layers of Allerød (layer 9) and Holocene (layer 1) age are drawn in black. Note the deformation of layer 9 (from Pissart and Juvigne 1980; and Pissart 2003); (c) Reconstruction of the formation of the rampart in Figure 2.9b, demonstrating the uplift and deformation of existing sediments, and the mass movement of sediments down the flanks of the landform (from Pissart and Juvigne 1980; and Pissart 2003).

2.2 Palsas and palsa-like mounds

2.2.1 Paisas, minerogenic palsas and lithalsas

Palsas are low, 1-7 m high, circular to oval ground-ice mounds, up to several tens of metres in diameter, which are found in mires throughout the circumpolar discontinuous and sporadic permafrost zones, in areas where winter precipitation is low (Zoltai 1972; Zoltai and Tarnocai 1975; Seppälä 1982, 1988b; Sollid and Sørbel 1974) (Figure 2.10). Their development is controlled by deeper winter frost penetration in areas with thinner snow cover, which leads to differential frost heave caused by ice segregation (Svensson 1964a; Wramner 1967; Åhman 1976; Seppälä 1982, 1988b, 1995; Allard et al. 1987). Where palsas develop in thick sequences of peat in the sporadic permafrost zone, the thermal conductivity properties of peat play an important role in palsa formation. In the autumn and winter, when the surface peat is wet and/or frozen, the peat acts as a good thermal conductor, promoting ice segregation. In contrast, during the summer when the peat is dry, it has a low thermal conductivity and instead acts as an important insulating layer, vital for protecting the frozen core from summer thaw (Seppälä 1982, 1988b). The peat cover overlying palsas in the discontinuous zone however, can be quite thin (0-2.5 m) or may be entirely absent (Wramner 1972, 1973; Åhman 1976; Allard et al. 1987; Pissart 2002). The growth of segregation ice in these cases occurs not within peat, but instead within a zone of frozen mineral sediment at depth. The "palsa family" of ground-ice mounds therefore includes three categories which encompass a continuum of landforms (Figure 2.11): 1) palsas, which develop completely in peat (Seppälä 1972a, 1988b; Washburn 1983); 2) minerogenic palsas, the frozen core of which develops in mineral sediments but with a superficial cover of peat (e.g. Åhman 1976; Worsley et al. 1995; Matthews et al. 1997); and 3) lithalsas, which develop entirely in mineral material, and have no peat cover (Wramner 1972, 1973; Harris 1993; Pissart et al. 1998). "True" palsas decay when erosion of the sides and loss of peat cover from the top cause the core to melt and collapse, often forming ponds (Figure 2.10a) that are occasionally surrounded by low rim-ridges 0.5-2 m high (Seppälä 1988b). Such ponds are rapidly infilled by further peat growth however and their preservation potential is low (Seppälä 1988b; Ballantyne and Harris 1994; Pissart 2002). Due to the disturbance and deformation associated with the development of segregation ice

21

within mineral sediments however, the collapse of minerogenic palsas and lithalsas will more readily produce geomorphological and sedimentological features indicative of their former presence.

The distribution of minerogenic palsas and lithalsas is mainly restricted to northern Scandinavia (Lundqvist 1953; Ruuhijärvi 1960; Svensson 1964a; Wramner 1967; 1972, 1973; Åhman 1976; Svensson 1976; Lagerbäck and Rodhe 1985; Akerman and Malmström 1986; Matthews *et al.* 1997) and northern Canada (Figure 2.10b) (e.g. Harris 1993, 1998; Pissart *et al.* 1998). A significant number are found in northern Quebec, where they occur in fine-grained marine sediments exposed by Late Holocene isostatic uplift (Dionne 1978; Payette *et al.* 1976; Payette and Seguin 1979; Lagarec 1976, 1982; Seguin and Allard 1984; Pissart and Gangloff 1984; Allard *et al.* 1987, 1996; Worsley *et al.* 1995). This northern circum-Arctic distribution is a function of the requirement for a severe climate with very low summer temperatures to preserve the frozen core of the landform from year to year in the absence of a thick cover of insulating peat (Åhman 1976; Lagarec 1982; Allard *et al.* 1987; Pissart 2000, 2002, 2003).

Although the frozen core of minerogenic palsas and lithalsas is normally dominated by 1-10 mm thick ice lenses within a sedimentary matrix, thicker lenses and layers of massive injection ice up to 50 cm thick have also been recorded (Sollid and Sørbel 1974; Zoltai and Tarnocai 1975; Åhman 1976; Schunke 1983; Brown *et al.* 1983; Allard *et al.* 1987, 1996; Coultish and Lewkowicz 2003). Concentrations of ice lenses or units of massive ice are often found just below the permafrost table and at the base of permafrost (Åhman 1976; Lagerback and Rodhe 1986; Åkerman and Malmström 1986; Fortier *et al.* 1991; Sone and Takahashi 1993; An and Allard 1995; Allard *et al.* 1996; Delisle *et al.* 2003). The enrichment of ice at the base of the active layer suggests that the heave of these landforms is generated not only by the growth of segregation ice at depth, but also by aggradation ice that forms below the active layer as a result of downward migration of water during active layer thaw (Allard *et al.* 1996; Pissart 2002). Chaotic, faulted sequences of massive sub-horizontal to inclined ice lenses and veins, separated by highly distorted units of clay, have recently been observed in samples from boreholes drilled through lithalsas in Quebec (Allard and Rousseau 1999; Delisle *et al.* 2003). Although the majority of minerogenic palsas and

lithalsas are developed within fine-grained, frost-susceptible sediments, originally deposited in glaciolacustrine, marine and glacio-marine environments, ice lens growth within coarse-grained soils such as marine sands, gravel, till and stony glaciomarine diamictons has also been identified (Seguin and Allard 1984; Lagerbäck and Rodhe 1986; Allard *et al.* 1987; Worsley *et al.* 1995).

A variety of active permafrost mounds in Scandinavia (Wramner 1973; Lagerbäck and Rodhe 1985, 1986; Åkerman and Malmström 1986; Meier 1987) that were initially interpreted, tentatively, as open system pingos (Lagerbäck and Rodhe 1985) or as transitional forms between pingos and palsas (Lagerbäck and Rodhe 1986), have recently been re-interpreted as lithalsas (Pissart 2000). The internal structure of these landforms consists of massive ice cores, segregation ice and alternating layers of ice and sediment, (Lagerbäck and Rodhe 1985, 1986; Åkerman and Malmström 1986). Similar, but actively collapsing, ring-ridged features in northernmost Norway, interpreted by Svensson (1969, 1976, 1986) as transitional landforms between palsas and pingos, may be a form of collapsing lithalsas, being morphologically very similar to collapsing lithalsas in the Hudson Bay area of Quebec.

2.2.2 The decay and collapse of minerogenic palsas and lithalsas

Comparable to observations made on pingos, the development of radial and concentric cracks, small-scale landsliding, and solifluction have all been reported from minerogenic palsas and lithalsas (Allard *et al.* 1987; Worsley *et al.* 1995; Matthews *et al.* 1997; Allard and Rousseau 1999). Their collapse also results in the development of thermokarst pools and depressions surrounded by fragmented, arcuate and irregular ring-ridge ramparts of mineral sediments (Figure 2.12) that accumulate by mass movement of material off the former flanks, and through lateral compression of sediment due to the growth of segregation ice (Lagarec 1973; Dionne 1978; Seguin and Allard 1984; Pissart and Gangloff 1984; Matthews *et al.* 1997; Worsley *et al.* 1995; Gurney 2001; Pissart 2002). Because of the evidence suggesting lateral compression by ice segregation within minerogenic palsas and lithalsas, it has been argued that the ramparts of Pleistocene landforms should display very specific deformation structures. Theoretically, these can be used to distinguish between remnants of lithalsas and pingos (Pissart 2003), although arguably there is a shortage of suitable investigations on active pingos and lithalsas to validate this assertion. The

preservation potential of minerogenic palsas and lithalsas may be reduced because younger features commonly disturb older ramparts and depressions when they occur in extensive contiguous fields. External processes such as enhanced thaw associated with thermokarst ponds and fluvial erosion can also significantly modify the form of rim-ridges, resulting in a complex array of ridges and depressions (Matthews *et al.* 1997; Worsley *et al.* 1995).

Figure 2.10: (a) Palsa mire, northern Finland, with a number of low, abraded palsa mounds in the background and a pond, representing a collapsed palsa, in the foreground (Photo: M. Seppälä); (b) Minerogenic palsas or lithalsas, Maguse River Delta, west side of Hudson Bay, Nunavut, Canada. Mounds are 40-80 m in diameter and 1-2 m high. Developed in medium-grained sand, they are surrounded by seasonally flooded vegetation-free stony muds. Prominent radial cracks are visible on their surface from the tensional stresses associated with uplift and extension of the overburden (Photo: W.W. Shilts).

Peat   Silt   Segregation ice   Permafrost boundary
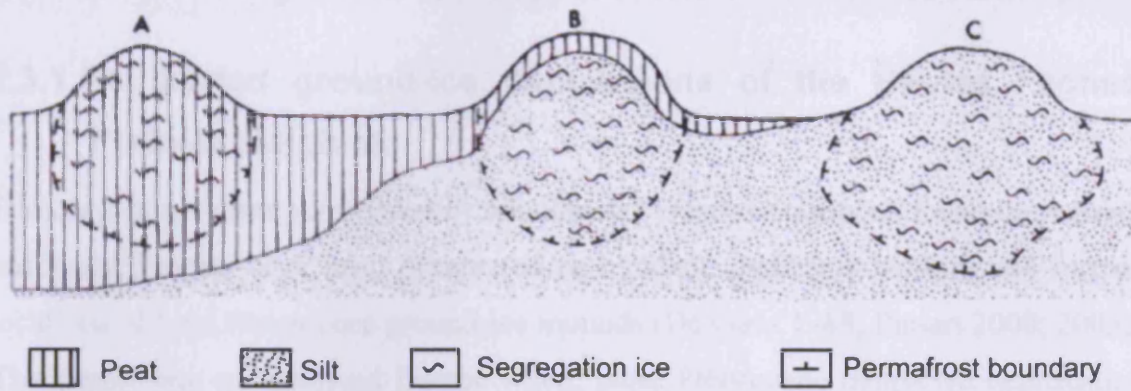
Figure 2.11: Classification of palsas and palsa-like mounds: (a) 'true' palsa, with segregation ice development entirely in peat; (b) minerogenic palsa with thin cover of peat, and segregation ice development almost entirely within mineral sediments; (c) lithalsa, segregation ice development entirely within mineral material (Åhman 1976).
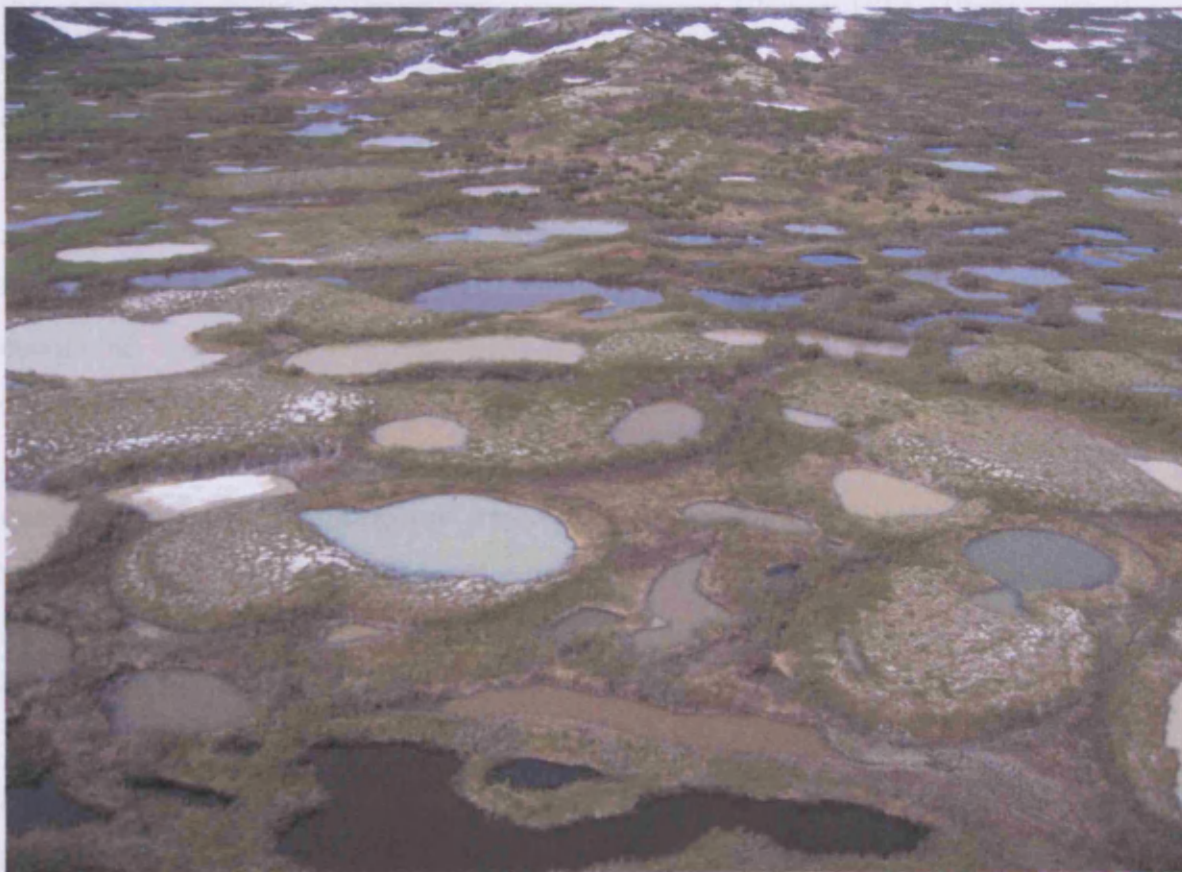
Figure 2.12: Decaying mineral palsas or lithalsas with central ponds and raised rims. These landforms are developed in marine silts, and are located 20 km inland from the eastern coast of Hudson Bay, near Umiujaq, northern Quebec, Canada (Photo: M. Allard).

2.3 Ramparted ground-ice depressions of northwest Europe

2.3.1 Ramparted ground-ice depressions of the Hautes Fagnes Plateau, Belgium

Enclosed depressions surrounded by annular ring ridges or ramparts found throughout northwest Europe have been interpreted as remnant landforms marking the former locations of Late Pleistocene ground-ice mounds (De Gans 1988; Pissart 2000; 2003). The classic site on mainland Europe where these Pleistocene ramparted depressions were first described in detail is the Hautes Fagnes Plateau, Belgium, where enclosed, peat-filled depressions, surrounded by distinct ramparts, are widespread. The ramparts are commonly less than 1 m high, but some reach a height of 5 m (Pissart 2000, 2003), and the thickness of the basin infill varies between 1 and 7.5 m, with diameters of up to several hundreds of metres. These features were first interpreted as the remains of Younger Dryas open system pingos (Pissart 1956, 1965), with the dating based on radiocarbon ages, tephra and pollen stratigraphy (Mullenders and Gullentops 1969; Bastin *et al.* 1974; Pissart and Juvigne 1980; Juvigne 1983; Pissart 1983, 2000, 2003). The impermeable nature of the local geology and the absence of an obvious aquifer to supply groundwater later led Pissart to reconsider this interpretation however (Pissart 1965, 1974, 1976; Pissart *et al.* 1972, 1975). Pissart concluded that segregation ice rather than injection ice was responsible for the development of these landforms, and they were subsequently reinterpreted as the remains of lithalsas rather than open system pingos. This was consistent with the density of the ramparted depressions on the Plateau, which is much greater than the recognised density of closed or open system pingos, and with structural evidence from rampart sections which suggested that lateral displacement (as well as slumping) of material had occurred during rampart formation (Figures 2.9b, 2.9c) (Bastin *et al.* 1974; Pissart and Juvigne 1980; Pissart 1974, 1983, 2000). Investigations of active and collapsing lithalsas in Quebec provided further evidence supporting this reinterpretation (Gangloff and Pissart 1983; Pissart and Gangloff 1984; Pissart 1983, 2000, 2003). Pissart later used similar lines of evidence to argue that ramparted depressions in Scandinavia (Rapp and Rudberg 1960; Svensson 1964b, 1976; Seppälä 1972b), and the British Isles (Pissart 1963; Watson 1971; Mitchell 1971, 1973; Sparks *et al.* 1972), previously interpreted as the remains of open system pingos, or as

27

transitional forms between pingos and palsas (Svensson 1976), should be reinterpreted as relict lithalsas (Pissart and Gangloff 1984; Pissart 2000, 2003). This reinterpretation has received strong support from UK-based researchers (Worsley *et al.* 1995; Gurney 1994, 1995; Gurney and Worsley 1996; Matthews *et al.* 1997).

2.3.2 Ramparted ground-ice depressions in the British Isles

Ramparted ground-ice depressions of Pleistocene age have been identified at numerous localities throughout the British Isles (Figure 2.13). Several wide-ranging reviews describing the research history and distribution of these landforms have already been presented (Bryant and Carpenter 1987; Coxon and O'Callaghan 1987; Ballantyne and Harris 1994; Gurney 2000; Harris 2002; Ross *et al.* 2005a). To avoid repeating the content of these reviews, the following section will focus only on key sites that have been interpreted as relict lithalsas and which have direct relevance to the current research project. Detailed information on sites investigated during this research project (e.g. Cledlyn and Cletwr valley) can be found in the relevant site investigation chapters (Chapters 4-9).

The first ramparted depressions in the British Isles interpreted as the remnants of ground-ice mounds are those near Llangurig in mid-Wales (Figure 2.13) (Pissart 1963). Here, peat-filled depressions, up to 5 m deep and 42-120 m wide, surrounded by distinct ramparts, are located at the bottom of a wide valley at 275-305 m OD (Pissart 1963; Gurney 1994). Based on their slope-foot locations and on pollen analysis of their basin-fill, these landforms were originally interpreted as open system pingos, which formed in shallow, discontinuous permafrost during the Younger Dryas (Pissart 1963; Trotman 1963a; Ballantyne and Harris 1994). Post-depositional deformation of sand and gravel in the rampart of one feature was attributed to the lateral thrust of expanding ground ice (Pissart 1963).

Groups of ramparted depressions morphologically similar to those near Llangurig were later documented throughout parts of southwest Wales, particularly between the Afon Teifi and the Cardigan Bay coast (Watson 1971, 1972; Watson and Watson 1972, 1974) (Figure 2.14). Based on comparisons with active pingos in central Alaska and Canada (Holmes *et al.* 1968; Hughes 1969), these ramparted depressions were originally interpreted as relict open system pingos (Watson 1971, 1972; Watson and

28
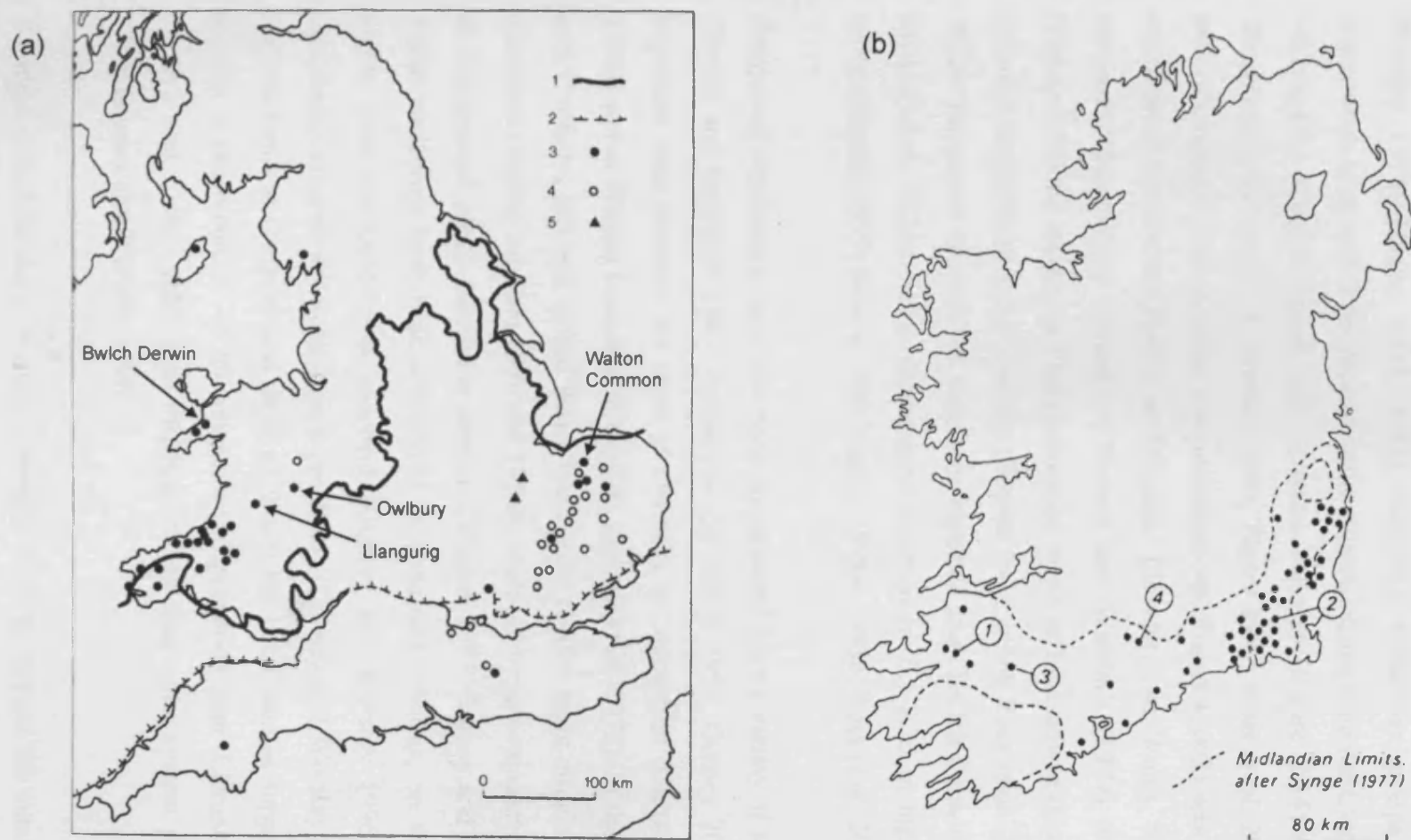
Figure 2.13: The distribution of groups of ramparted depressions, potentially representing the remains of permafrost ground-ice mounds, in Wales, England, the Isles of Man and Ireland: (a) Distribution of ramparted depressions in Wales, England and the Isles of Man (from Ballantyne and Harris 1994). (1) Maximum extent of Devensian glaciation; (2) Maximum extent of Pleistocene glaciation; (3) Ramparted depressions identified by surface relief; (4) Crop marks indicating possible locations of relict permafrost ground-ice mounds; (5) Sites of possible closed system pingos. Note that the distribution of ramparted depressions in Pembrokeshire, as displayed on this map, is highly inaccurate (see Ross *et al.* 2005a for details). There is also some uncertainty regarding the interpretation of the landforms marked as closed system pingos; (b) Distribution of ramparted depressions in Ireland (Coxon and O'Callaghan 1987).

Watson 1972, 1974). More recently however, the ramparted depressions of the Cledlyn and Cletwr valleys, along with those near Llangurig, have been reinterpreted as relict lithalsas (Pissart and Gangloff 1984; Gurney 1994, 1995; Gurney and Worsley 1996; Pissart 2000, 2003). Although numerous groups of ramparted depressions have also been mapped in the valleys surrounding the Cledlyn and Cletwr valleys (e.g. Ceri, Grannell and Hirwaun valleys) (Figure 2.14) (Watson 1972; Watson and Watson 1974; Bradley 1980; Taylor 1987; Ross et al. 2005a), due to a lack of evidence from detailed site investigations, Pissart (2003) was cautious about reinterpreting these landforms as lithalsas. Elsewhere in Wales, three groups of ramparted depressions marked on Watson and Watson's (1974) distribution map (Figure 2.14) are located at Ffald-y-brennin, north of Llansadwrn (Cors Farlais), and around Llanpumsaint and Pontarsais (Bowen 1974, 1999; Ross et al. 2005a). In north Wales, ramparted depressions have been reported from Bwlch Derwin and Clipau on Llŷn (Figure 2.13a), where depressions enclosed by 0.1-2.75 m high ramparts are found (Watson 1977; Moore 1980; Rogers 1998a, 1998b; Ross et al. 2005a).

Ramparted depressions have also been documented from a variety of sites in England (Bryant and Carpenter 1987; Ballantyne and Harris 1994; Gurney 2000). The most important sites however are those at Owlbury in Shropshire (Gurney and Worsley 1996), and at Walton Common in Norfolk (Sparks et al. 1972). In the Camlad valley near Owlbury, just east of the Wales-Shropshire border, eight circular hollows, with diameters ranging between 40 m and 105 m, enclosed by low ramparts, are developed in fine-grained, glacio-lacustrine deposits (Watson 1977; Gurney and Worsley 1996). These landforms have been interpreted as collapsed lithalsas, on the basis of the highly frost-susceptible host sediment (Gurney and Worsley 1996). The "strong morphological and sedimentological parallels" (Gurney and Worsley 1996) between the landforms at Owlbury and those in Wales has been used as supporting evidence for the reinterpretation of the ramparted depressions near Llangurig and in the Cledlyn and Cletwr valleys as lithalsas, rather than open system pingos (Gurney 1995; Gurney and Worsley 1996).

Ramparted depressions at Walton Common, Norfolk, beyond the maximum limits of the Devensian glaciation, are developed along springlines determined by the structure of the underlying permeable chalk (Worssam and Taylor 1969; Sparks et al. 1972).

Although they are restricted to footslope locations favourable for the seepage of subsurface groundwater under artesian pressure (and therefore open system pingo development under conditions of shallow discontinuous permafrost), Sparks *et al.* (1972) were not specific about their exact origins, describing them as the remains of "ground-ice features" or "ground-ice depressions", that could be related to the transitional forms between pingos and palsas observed in northern Norway (Svensson 1969). It has been suggested that the ramparted depressions at Walton Common could represent collapsed frost blisters (French 1979), open system pingos (Worsley 1977), or lithalsas (Pissart 2000, 2003).

In Ireland, a large number of depressions attributed to the former presence of ground-ice mounds are found south of the glacial limits of the last glaciation (Mitchell 1971, 1973; Coxon 1986; Coxon and O' Callaghan 1987) (Figure 2.13b). Originally interpreted as the remains of open system pingos, these too have been reinterpreted as lithalsa remnants (Pissart 2000, 2003).
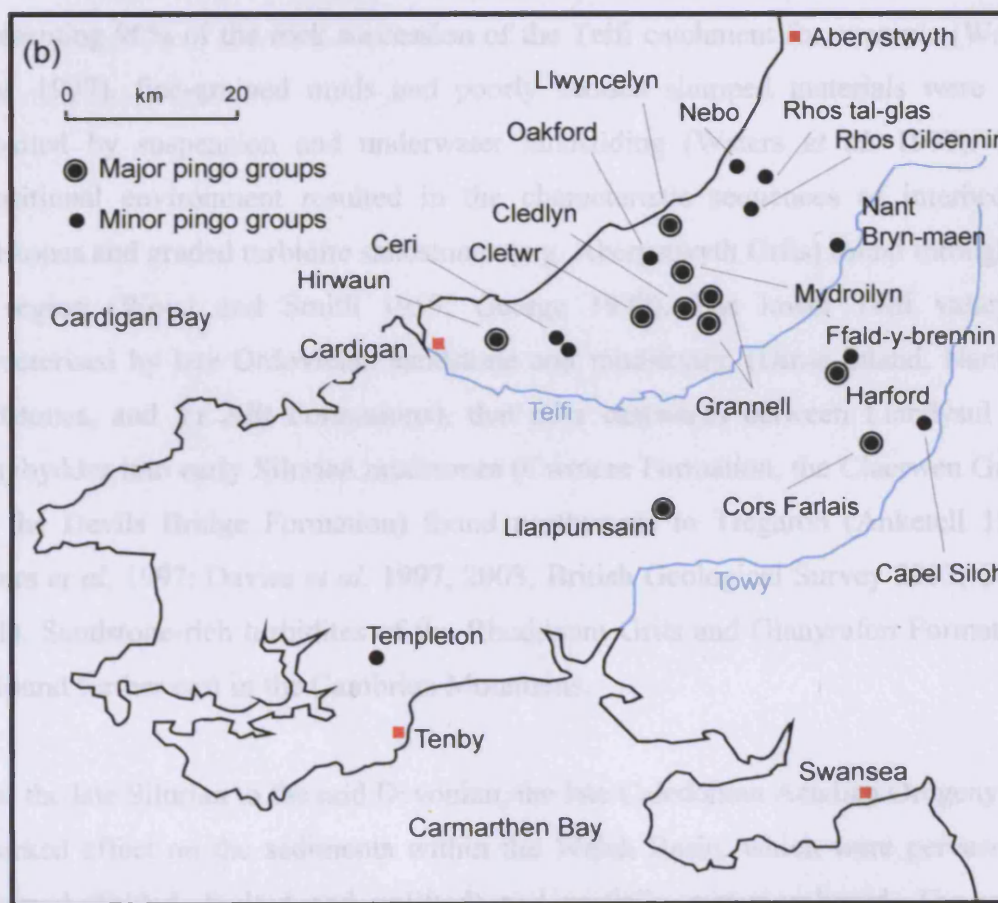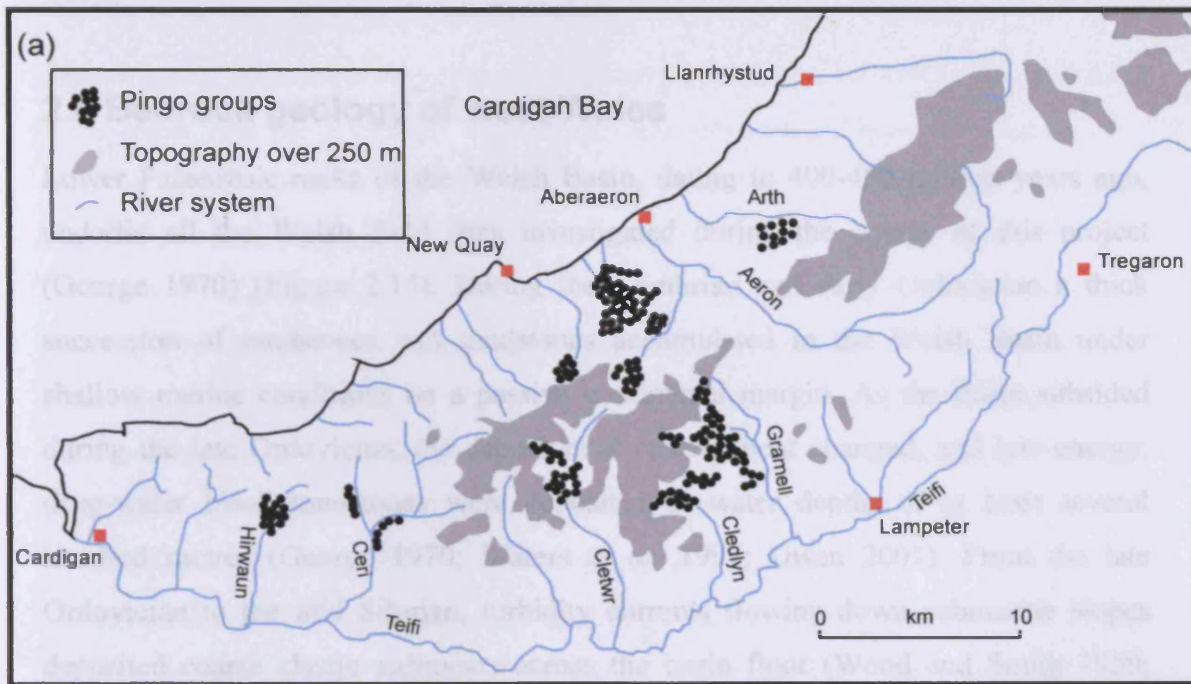
Figure 2.14: (a) The distribution of ramparted depressions ('pingos') in Ceredigion between the Afon Teifi and the Cardigan Bay coast (after Watson 1972); (b) The distribution of groups of ramparted depressions ('pingos') in southwest Wales (after Watson and Watson 1974). For details regarding each site (including grid references) please refer to Ross et al. (2005a).

2.4 Bedrock geology of west Wales

Lower Palaeozoic rocks of the Welsh Basin, dating to 400-450 million years ago, underlie all the Welsh field sites investigated during the course of this project (George 1970) (Figure 2.15). During the Cambrian and early Ordovician a thick succession of mudstones and sandstones accumulated in the Welsh Basin under shallow marine conditions on a passive continental margin. As the Basin subsided during the late Ordovician, the depositional environment changed, and low energy, deep-water black mudstones were deposited in water depths of at least several hundred metres (George 1970; Waters *et al.* 1997; Owen 2001). From the late Ordovician to the mid Silurian, turbidity currents flowing down submarine slopes deposited coarse clastic sediments across the basin floor (Wood and Smith 1959; Waters *et al.* 1997). Although these turbidites are the dominant rock facies, representing 90% of the rock succession of the Teifi catchment for example (Waters *et al.* 1997), fine-grained muds and poorly bedded slumped materials were also deposited by suspension and underwater landsliding (Waters *et al.* 1997). This depositional environment resulted in the characteristic sequences of interbedded mudstones and graded turbidite sandstones (e.g. Aberystwyth Grits) found throughout the region (Wood and Smith 1959; George 1970). The lower Teifi valley is characterised by late Ordovician sandstone and mudstones, (Dinas Island, Nantmel Mudstones, and Yr Allt Formations), that pass eastwards between Llandysul and Llanybydder into early Silurian mudstones (Cwmere Formation, the Claerwen Group and the Devils Bridge Formation) found northwards to Tregaron (Anketell 1987; Waters *et al.* 1997; Davies *et al.* 1997, 2003; British Geological Survey 2003; Owen 2001). Sandstone-rich turbidites of the Rhuddnant Grits and Glanyrafon Formations are found further east in the Cambrian Mountains.

From the late Silurian to the mid Devonian, the late Caledonian Acadian Orogeny had a marked effect on the sediments within the Welsh Basin, which were pervasively deformed (folded, faulted and uplifted) and partially metamorphosed. The major geological structures that developed are the regional folds of the Teifi Anticline, the Central Wales Syncline and the Towy Anticline (Jones 1912, 1938; George 1970; Waters *et al.* 1997; Davies *et al.* 1997) (Figure 2.15), but innumerable intermediate- and small-scale asymmetrical folds, with steeply dipping fold limbs, are

superimposed upon these major structures (Craig 1987; Anketell 1987). Regardless of scale, these folds are dominated by northeast to southwest and east-northeast to west-southwest trends (Figure 2.15) (George 1970; Craig 1987; Anketell 1987; Waters *et al.* 1997). The Ordovician and Silurian rocks are heavily faulted throughout the Welsh Basin (Anketell 1987; Craig 1987). The majority of these faults trend along two main orientations, northeast to southwest and north-northeast to south-southwest (Anketell 1987), but mapping along the coast has also revealed some minor faults between Aberporth and Newquay that are transverse to the regional northeast to southwest tectonic structure (Craig 1987). Although the Acadian Orogeny was mainly responsible for the majority of southwest-northeast trending faults and folds within the Lower Palaeozoic sequence (Craig 1987; Anketell 1987; Waters *et al.* 1997), tectonic movements associated with structures in the pre-Caledonian basement also caused faulting and folding that occurred contemporaneously with sedimentary accumulation (Cave and Hains 1986; Fitches and Woodcock 1987). Reactivation of major faults also occurred during post-Caledonian extension (Craig 1987).
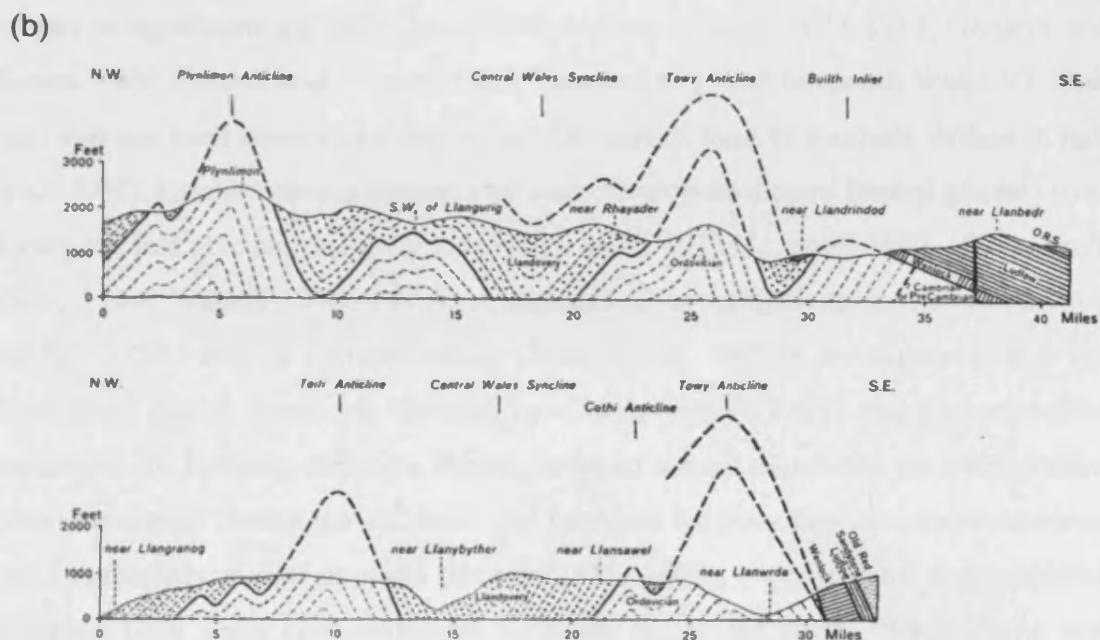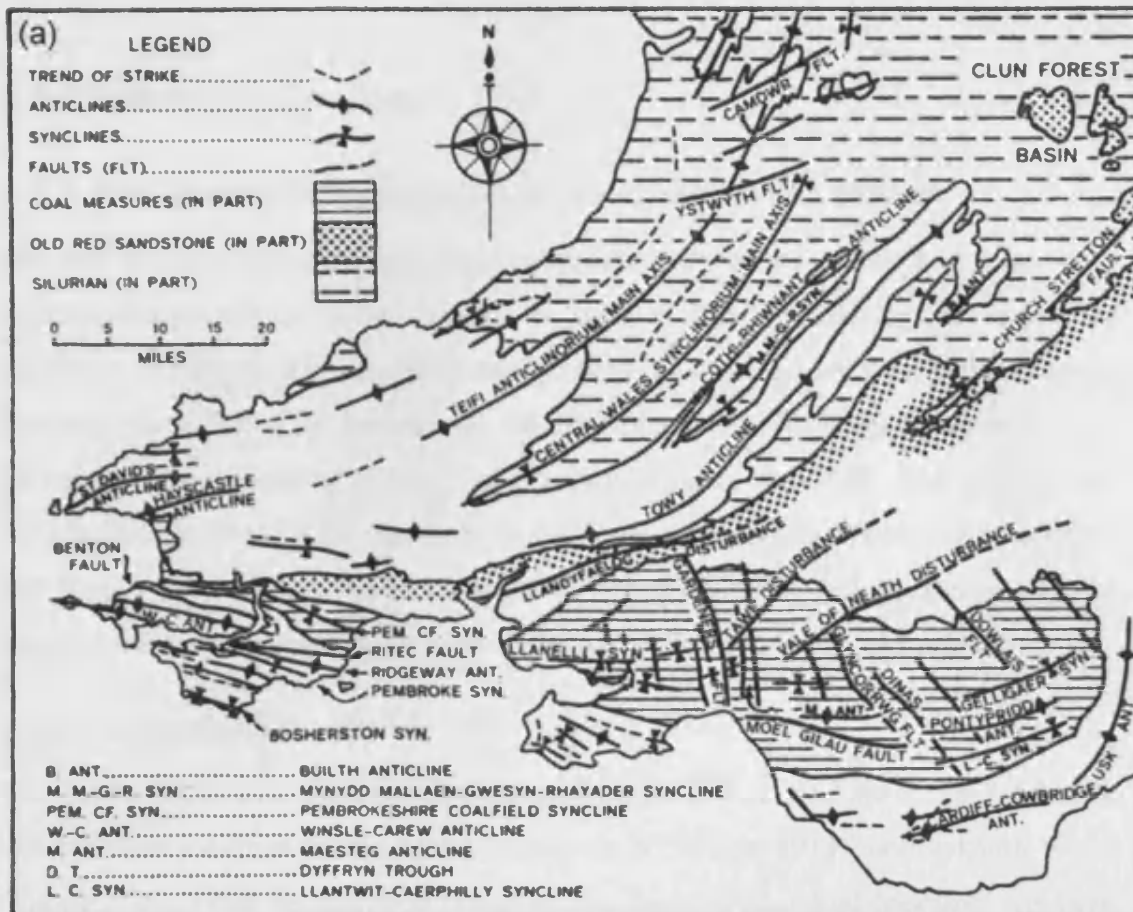
Figure 2.15: (a) Map of the major structures of south Wales (George 1970). The unshaded area between the Silurian rocks and the Old Red Sandstone in southwest Wales represents the area of Ordovician bedrock; (b) Schematic cross-sections across south Wales, demonstrating the development of the major Caledonian structures within the Ordovician and Silurian rocks (George 1970).

2.5 Quaternary Geology

2.5.1 The Devensian glaciation of south and west Wales

The aim of this section is to provide background information on the late Quaternary palaeoenvironments of south Wales. As well as briefly outlining the impact of glaciation during the last glacial period (Devensian) and the environmental changes that took place during the Lateglacial, detailed information on the glacial deposits and Devensian environments of the Teifi valley is also provided. The glacial and periglacial history of Wales has been extensively discussed elsewhere (e.g. Campbell and Bowen 1989; Ballantyne and Harris 1994; Bowen 2005), and readers looking for detailed information concerning these topics are referred to these publications.

2.5.1.1 Devensian ice limits

The South Wales End-Moraine of Charlesworth (1929) defined the maximum extent of Devensian ice (then known as the 'Newer drift' (Wright 1914)) across south Wales (Figure 2.16). From its inception however, the 'South Wales End-Moraine' has been subject to significant criticism (Jones 1929 *in Charlesworth 1929*, 1965; Gregory and Bowen 1966; Bowen and Gregory 1965; Bowen 1981) and the south Wales ice limit has been the most contentious part of the Devensian limit in southern Britain (Clark *et al.* 2004). Despite various attempts by some to propose a more limited glacial cover during the last glaciation (Figure 2.16) (e.g. Wirtz 1953; Mitchell 1960, 1972; Synge 1963, 1964; Watson 1970, 1972), stratigraphical investigations in Gower (Bowen 1973a, 1973b) and in Pembrokeshire (John 1970a, 1970b) demonstrated that the Devensian glacial limits, as defined by Charlesworth (1929) required extensive revision in the opposite direction. Inland, between coastal exposures, the interpolation of the maximum Devensian ice limits was based on the boundary between continuous and fragmentary glacial deposits (Bowen 1981, 2005), supported by stratigraphical evidence from open cast coalmines in south Wales (Donnelly 1988; Harris and Donnelly 1991). The southwards extension of the South Wales End-Moraine was particularly pronounced in Carmarthenshire, Cardiganshire and Pembrokeshire (Bowen 1970, 1973a, 1973b, 1974), where a continuous formation of glacial deposits exists south and west of Charlesworth's limit (Bowen 1981).
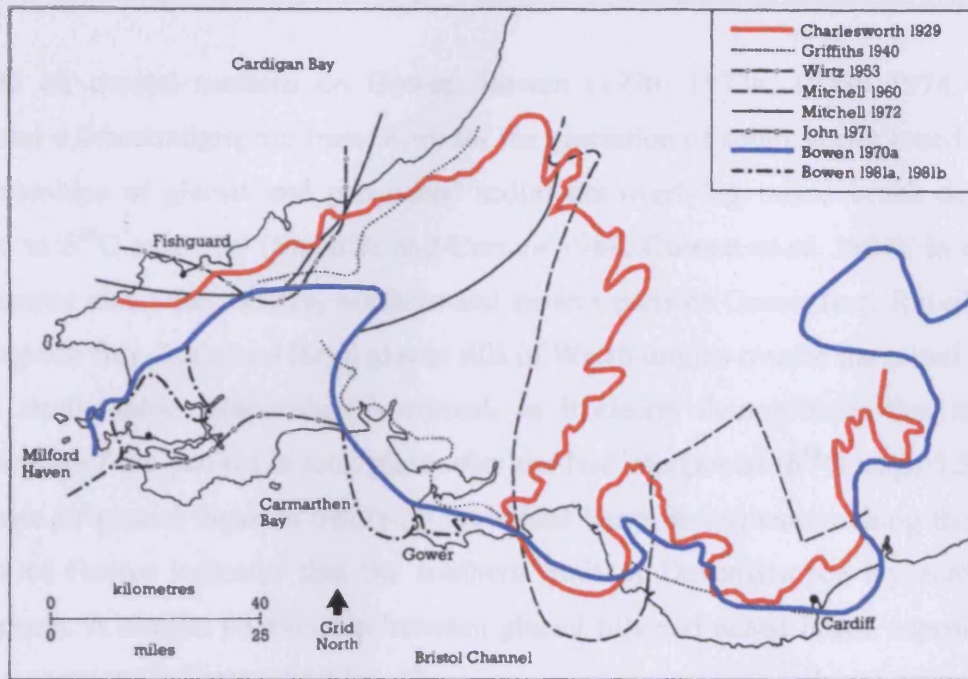
Figure 2.16: Suggested Late Devensian glacial limits in south Wales (from Campbell and Bowen 1989).
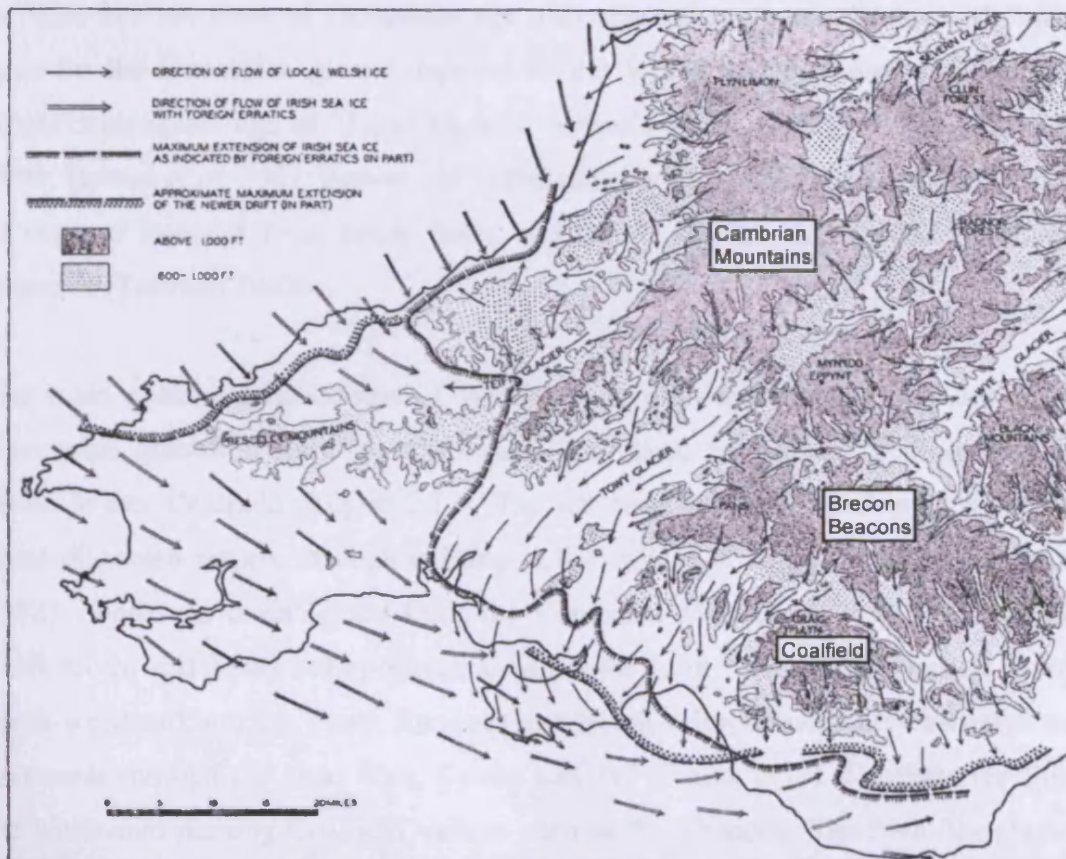
Figure 2.17: Ice flow directions of Welsh and Irish Sea ice masses in south Wales during the Pleistocene (from George 1970). No discrimination is made between the direction of ice flow during the Devensian glaciation (Newer Drift) and the more extensive pre-Devensian glaciation (Older Drift) when Irish Sea ice extended eastwards to the Vale of Glamorgan.

Based on coastal sections on Gower, Bowen (1970, 1973a, 1973b 1974, 1977) devised a lithostratigraphic framework for the glaciation of south Wales based on the relationships of glacial and periglacial sediments overlying raised beach deposits, dated to $\delta^{18}O$ stage 5.5 (Sutcliffe and Currant 1984; Currant *et al.* 1984). In coastal sequences along the western, northern and eastern parts of Gower (e.g. Rhosili Bay, Broughton Bay, Langland Bay), glacial tills of Welsh origins overlie the raised beach. This stratigraphic relationship is critical, as it clearly demonstrates that the last glaciation of the peninsula took place after the last interglacial ($\delta^{18}O$ stage 5.5). The absence of glacial deposits overlying the raised beach in sequences along the south coast of Gower indicates that the southern limit of Devensian ice lay across the peninsula. A similar relationship between glacial tills and raised beach deposits was also recognised in Pembrokeshire, where sequences incorporating glacial deposits and periglacial sediments are found overlying last interglacial raised beaches (John 1970a, 1970b; Bowen 1977). These sequences demonstrate that the southernmost margin of an Irish Sea ice sheet of Devensian age also reached southwest Wales. Minimum ages for the Devensian glacial deposits of the Welsh ice sheet are provided by a single cosmogenic age of 23.2±2 ka from Arthur's Stone, Cefn Bryn (Phillips *et al.* 1994; Bowen *et al.* 2002; Bowen 2005) and radiocarbon dating and/or pollen analysis of organic material from kettle holes at Llanilid (Walker *et al.* 2003) and near Swansea (Trotman 1963b).

The main accumulation centres of Welsh ice in mid- and south Wales during the Devensian glaciation were the Cambrian Mountains, the Brecon Beacons and the South Wales Coalfield (Figure 2.17). The ice caps that developed in these upland areas dispersed mainly through existing radial valleys (George 1970; Crimes *et al.* 1992). Westward draining ice from the Cambrian Mountains flowed through the Teifi, Cothi and Towy valley systems, whilst ice from the Brecon Beacons flowed south-westward into the Towy, Swansea and Neath valleys, and south-eastwards and eastwards through the Usk, Wye, Cynon and Taf (Figure 2.17). Coalfield ice filled the southward running Coalfield valleys such as the Rhondda. The Irish Sea glacier, which deposited tills and fluvioglacial sediments in southwest Wales, was sourced from ice accumulation centres in Scotland and Ireland. Based on these four areas of ice accumulation, the glacial deposits of the Devensian period in south Wales have now been divided into four formations (Bowen 1999, 2005):

1) Elenid Formation –glacial deposits of the middle and lower Teifi valley, across Carmarthenshire to Gower. These deposits overlie the raised beach at Broughton Bay (Campbell 1984; Davies 1988);

2) Brecknockshire Formation – glacial deposits characterised by distinctive old red sandstone content derived from the Brecon Beacons (David 1883; Bowen 1970);

3) Glamorgan Formation - glacial and fluvioglacial deposits containing erratics from the South Wales Coalfield (David 1883; Woodland and Evans 1964; Bowen 1970; Harris and Wright 1980; Donnelly 1988; Harris and Donnelly 1991);

4) St Asaph Formation – Irish Sea glacial and fluvioglacial deposits characterised by erratics from Scotland and North Wales, and by marine shells (Jehu 1904; Williams 1927; John 1970a; Lear 1986; Davies *et al.* 2003).

2.5.1.2 Periglacial and paraglacial conditions

Landforms and sediments in Wales indicative of periglacial conditions have been described by numerous studies (e.g. Pissart 1963; Watson 1968, 1970, 1972; Crampton and Taylor 1967; John 1973; Saunders 1973; Ballantyne and Harris 1994). Although the influence of processes associated with extensive permafrost has not been disputed, the belief that prolonged periglacial processes (e.g. solifluction or pingo formation) operated throughout the Devensian period under ice-free conditions (e.g. Watson 1968, 1970, 1972; Watson and Watson 1967) has been criticised. It is now widely accepted that whilst significant modification of the landscape did occur, this took place during and after deglaciation, as a result of both periglacial and paraglacial processes (Potts 1971; Bowen 1973a, 1973b, 1974, 1977; Cave and Hains 1986; Campbell and Bowen 1989; Davies *et al.* 1997; Harris 1998).

2.5.1.3 The Lateglacial period in south Wales

Palaeoenvironmental evidence for the Lateglacial in Wales (Coope and Brophy 1972; Campbell and Bowen 1989; Lowe and Lowe 2001; Walker *et al.* 2001; Walker *et al.* 2003) suggests that the environmental changes that took place during this period broadly follow the rapid and abrupt changes in climate established elsewhere in the British Isles following the Last Glacial Maximum (LGM) (Coope 1977; Watson

1977; Sissons 1979; Atkinson *et al.* 1987; Gray and Coxon 1991; Ballantyne and Harris 1994; Lowe *et al.* 1995, 1999). By the onset of the Lateglacial Interstadial at 14,500 cal yrs BP, mean July air temperatures in south Wales were around 20°C (Figure 2.18) with winter temperatures between 0°C to -4°C (Walker *et al.* 2003). South Wales would probably have been ice-free at this time (Bowen 2005), although buried ice may have persisted under favourable local conditions where it was insulated by fine-grained sediments. By 13,100 cal yr BP however, mean July air temperatures had declined to 11-12°C, with average winter temperatures of -6.6°C. The stepped cooling that occurred during the second half of the Lateglacial Interstadial (14,000-12,600 cal yr BP) (Coope 1977; Atkinson *et al.* 1987; Lowe *et al.* 1995; Walker *et al.* 2003), was followed by a period of very severe climate during the Younger Dryas (12,600-11,400 cal yr BP) with mean July air temperatures of 10-12°C and winter temperatures ranging between -3°C to -10°C (Walker *et al.* 2003). At this time cirque glaciers returned to the Brecon Beacons, Cadair Idris and Snowdonia (Campbell and Bowen 1989), and discontinuous permafrost became established even at very low elevations (Watson 1965, 1977; Potts 1971; John 1970a, 1973; Bowen 1970). At the beginning of the Holocene, at 11,400 cal yr BP, an abrupt 9°C rise in July temperatures to ca. 20°C, with winter temperatures of between 0°C and –1°C occurred (Walker *et al.* 2003), and would have resulted in the melting of any remaining ice masses and the thaw of permafrost.

2.5.2 The Quaternary geology of the Afon Teifi catchment

Four of the six site investigations in Wales described in this thesis (Cledlyn, Cletwr, and Hirwaun valleys, Llanio Fawr) are located within the tributary valleys of the Afon Teifi (Figure 2.19). As a result, this section describes the Quaternary geology of the Afon Teifi catchment (Figure 2.19) in some detail. However, because there is only limited information available on the Quaternary history and superficial geology of the areas surrounding the sites at Crychell Moor and Llanpumsaint, this information will be described in the introduction to their site investigations (Chapters 6 and 9).

Early descriptions of the glacial geology and geomorphology of the area around Cardigan Bay presented significant evidence that the Teifi valley and its surrounding areas were glaciated both by ice flowing down the Irish Sea and by Welsh sourced ice (Keeping 1882; Reade 1896; Jehu 1904; Williams 1927; Charlesworth 1929; Jones
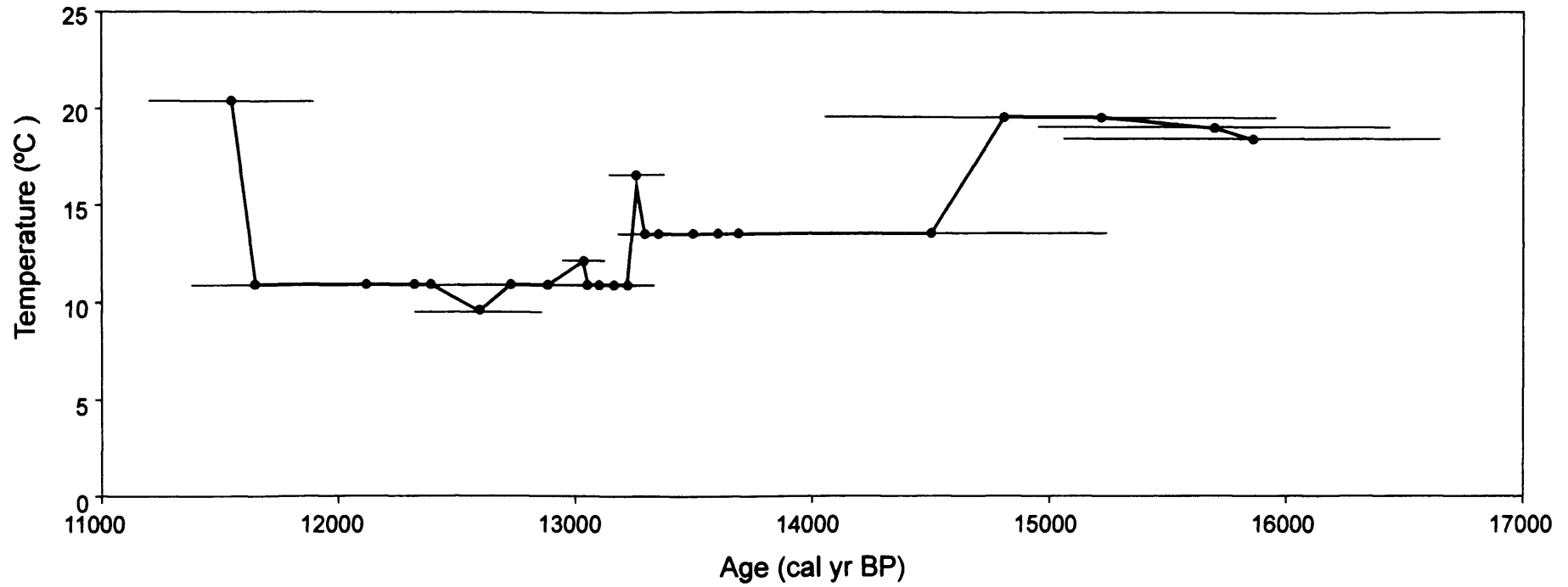
Figure 2.18: Lateglacial July temperature reconstruction (Tmax) from Llanilid, South Wales based on Mutual Climatic Range (MCR) coleopteran data (from Walker *et al.* 2003). The error bars show uncertainties in the age model associated with radiocarbon dating.
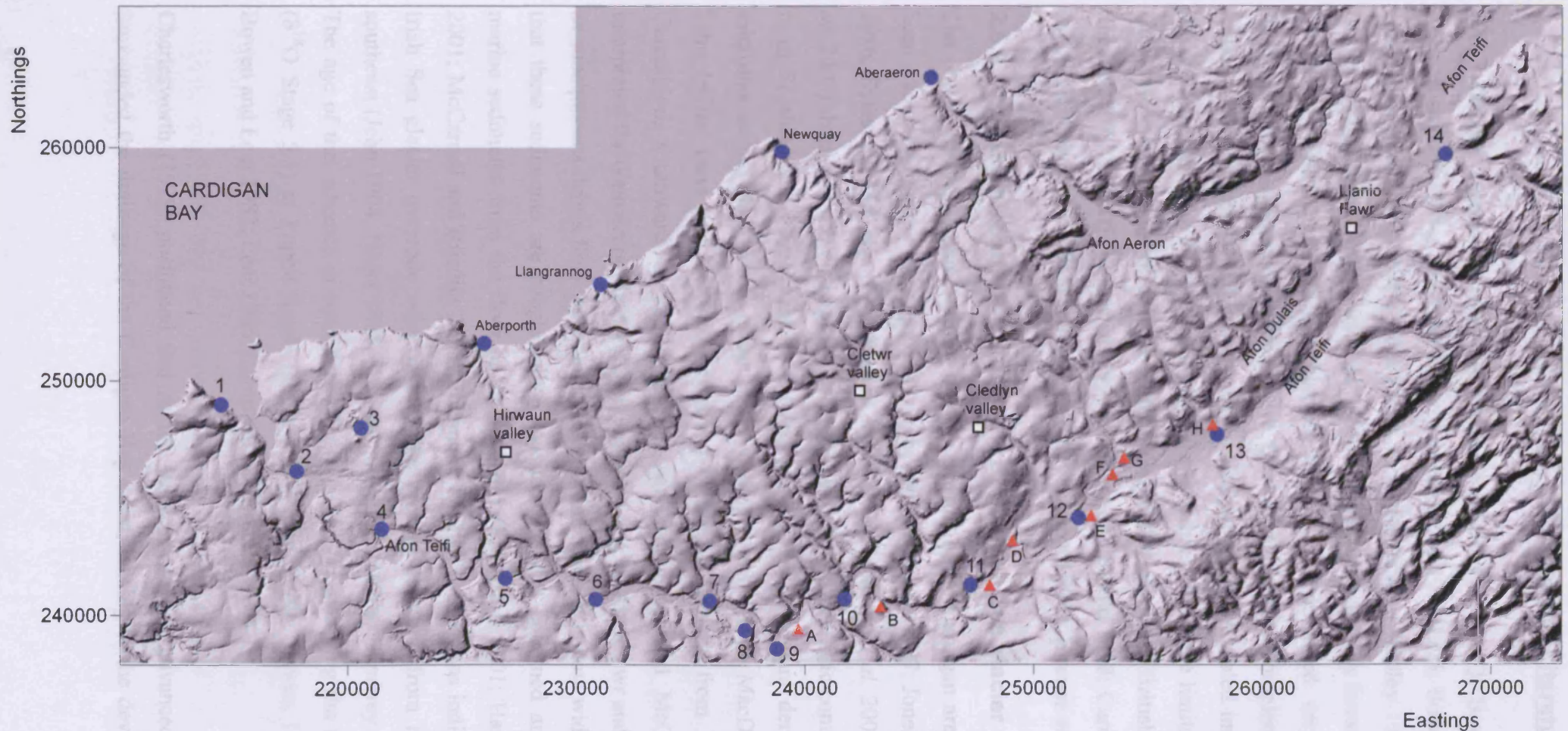
Figure 2.19: Locations within the Afon Teifi catchment and surrounding areas referred to in Section 2.5. Blue dots = key sites (1, Poppit Sands; 2, Cardigan; 3, Banc-y-warren; 4, Llechryd; 5, Cenarth; 6, Newcastle Emlyn; 7, Henllan; 8, Llangeler; 9, Pentrecwrt; 10, Llandysul; 11, Maesycrugiau; 12, Llanybydder; 13, Lampeter; 14, Tregaron). Red triangles = Lake Teifi 'deltas' (A, Pentrecwrt; B, Craig Gwytheryn; C, Llanllwni; D, Rhuddlan; E, Llanybydder; F, Pencarreg; G, Llanwnen; H, Lampeter). The site of Abermawr is located on the north Pembrokeshire coast approximately 30 km west of Cardigan. Of the six sites that have been investigated during this project, the four that are located within the Afon Teifi catchment are indicated (white squares). NEXTMAP digital terrain model (DTM) © Intermap Technologies Inc.

1965). Despite systematic mapping of the Teifi valley by D. Q. Bowen and his research students (Price 1976; M.S. Parry *unpublished* 1972-1975; Bowen and Lear 1982; Lear and Bowen 1984; Lear 1986), the Soil Survey (Bradley 1980) and the University of Liverpool (Crimes *et al.* 1992), the exact relationship between the Late Devensian Welsh and Irish Sea glaciers in this area remained very uncertain. Although recent mapping by the British Geological Survey, complemented by a series of deep boreholes and geophysical investigations, has revealed important new information regarding the glaciation of the Teifi valley, precise ice limits for the two ice masses still remain difficult to define. (Waters *et al.* 1997; British Geological Survey 1997, 2003; Heaven *et al.* 1999; Fletcher and Siddle 1998; Carruthers *et al.* 1997; Hambrey *et al.* 2001; Davies *et al.* 2003; Sheppard 2003; Etienne *et al.* 2006).

2.5.2.1 Glacial deposits and landforms of the Irish Sea glacier

The distribution and characteristics of Irish Sea till in the Cardigan area have long been a source of debate (Keeping 1882; Jehu 1904; Williams 1927; Jones 1965; Lear 1986; Eyles and McCabe 1989; Waters *et al.* 1997; Hambrey *et al.* 2001; Davies *et al.* 2003). Irish Sea till, distinguished from Welsh tills by its erratic content (sourced from Scotland and North Wales), calcareous character, abundant derived marine microfaunas and shell debris (Jehu 1904; Williams 1927; Hope MacDonald 1961; John 1970a; Davies *et al.* 2003), is found in coastal sections from Llanrhystud, Ceredigion, southward to Pembrokeshire. Although Eyles and McCabe (1989) interpreted the deposits on the Cardigan Bay coast (e.g. at Abermawr and Aberaeron) as subaquaeous debris flow facies and glaciomarine muds, it is now widely believed that these sediments are subglacially deposited tills that entrained and reworked marine sediments from the floor of the Irish Sea (McCarroll 2001; Hambrey *et al.* 2001; McCarroll and Rijsdijk 2003; Etienne *et al.* 2005). Striations indicate that the Irish Sea glacier overrode what is now the present coastline from northwest to southeast (Jehu 1904; Hicks 1885; Watson 1968; John 1970a; Hambrey *et al.* 2001). The age of this advance is constrained by Irish Sea till overlying the raised beach ($\delta^{18}O$ Stage 5.5) at Poppit Sands (Jones 1965; John 1970a; Bowen 1973b, 1977; Bowen and Lear 1982; Lear 1986; Campbell and Bowen 1989).

Charlesworth (1929) postulated that as the Irish Sea glacier advanced onshore it impounded the drainage of the Cardigan Bay coast, leading to the development of

pro-glacial ice-dammed lakes in several of the catchments (Lake Teifi, Lake Manorwen, Lake Nevern, Lake Aeron, plus numerous smaller lakes including Lake Moylgrove and Lake Mydroilyn). Whilst no geological evidence (e.g. shorelines, deltas or lake deposits) has been found to support the existence of Lakes Newquay, Aberporth, Nevern, Moylgrove, Gwaun, Mydroilyn or Manorwen (Bowen and Gregory 1965; Gregory and Bowen 1966; Bowen 1967; John 1970a; Watson 1970), abundant evidence for Lake Teifi, originally proposed by O.T. Jones in a series of lectures in Aberystwyth in 1928, has been recorded. Laminated clays, first identified in a small gravel pit near Llechryd (Jones 1965; Bowen 1967; Lear 1986), are widespread throughout the Teifi valley and have been mapped upvalley to Mackwith, 2 km east of Llandysul, and up to elevations of 130 m OD (Price 1976; Lear 1986; British Geological Survey 1997; Waters *et al.* 1997). Several of the Teifi's drift-plugged pre-glacial meanders have been the subject of geophysical investigations, which suggested thick fills of unconsolidated materials (Allen 1960; Francis 1964; Nunn and Boztas 1977; Carruthers *et al.* 1997; Heaven *et al.* 1999). Recent borehole investigations have proved that sequences of structureless and silt-laminated (varved) clay and laminated silt up to 75 m thick extend to depths of -37 m OD beneath these abandoned meanders and buried valleys (Fletcher and Siddle 1998; Hambrey *et al.* 2001; Davies *et al.* 2003; Etienne *et al.* 2006). Sand and gravel deposits interpreted as possible deltas, with upper surfaces or prominent benches between 120-130 m OD, have been identified at Rhuddlan, Llanybydder, Llanwnnen, Pencarreg and Lampeter (Charlesworth 1929; Watson 1965, 1970; M.S. Parry *unpublished* in Bowen 2005; Lear 2003), Pentrecwrt (Jones 1965; Lear 2003), Craig Gwtherym (Jones 1965) and at Llanllwni (Price 1976) (Figure 2.19). The 'delta' at Banc-y-warren, however (Jones 1965; Helm and Roberts 1975; Fletcher and Siddle 1998), is now widely recognised as fluvioglacial outwash or dead-ice deposits (Williams 1927; Mitchell 1960; Gregory and Bowen 1966; Allen 1982; Worsley 1984; Lear 1986; Hambrey *et al.* 2001; Etienne *et al.* 2006).

Prior to recent work, the lack of modern systematic mapping by the British Geological Survey (BGS) in the area to the north of Carmarthen had prohibited the use of the spatial extent of near continuous glacial and fluvioglacial deposits to define the extent of Devensian ice. As a result, despite observations of Irish Sea till near Llwynduris, in the Teifi valley 4 km northwest of Cenarth (Jones 1965) and in a

borehole at Henllan (Lear 1986), the extent to which the Irish Sea glacier extended into the Teifi valley has not yet been determined accurately. Jones (1965) believed that the likely ice margin (Irish Sea and Welsh ice) at the time of the development of Lake Teifi ran between Cardigan and Llanybydder, within the northern tributaries of the Teifi. This view is supported by recent BGS mapping (British Geological Survey 1997), which suggests that it is highly unlikely that the northern tributaries of the Teifi were ice-free during the existence of Lake Teifi.

Although Irish Sea till is seen to overlie Welsh glacial deposits on the coast at Llan-non (Watson 1976; Campbell and Bowen 1989; Harris 2001a), the stratigraphical relationship between Irish Sea till and Welsh glacial deposits inland has remained obscure. Boreholes drilled by the BGS, however, have demonstrated that Irish Sea till overlies the thick sequences of glaciolacustrine sediments in the lower Teifi valley (Waters *et al.* 1997; Fletcher and Siddle 1998; Hambrey *et al.* 2001; Davies *et al.* 2003; Etienne *et al.* 2005), confirming Charlesworth's (1929) and Bowen's (1967) suggestions that proglacial deposition in Lake Teifi occurred in front of an advancing Irish Sea ice margin. This further complicates mapping of glacial limits as a calving margin means that till and erratics could be deposited at localities beyond the ice margin from debris within icebergs.

2.5.2.2 Glacial deposits and landforms of the Teifi glacier

Charlesworth (1929) placed the limit of Welsh ice in the Teifi valley at the Tregaron moraine (Figure 2.19), based on the absence of any clear evidence for end-moraines further downvalley. Jones (1929 *in Charlesworth 1929*, 1965) however criticised Charlesworth's limit in the upper Teifi valley, referring to the kettle-holes and extensive glacial deposits between Llanybydder and the moraine at Tregaron. Although Charlesworth (1929) had described extensive sand and gravel deposits between Tregaron and Lampeter, these were attributed either to an earlier glaciation, or to glacial meltwater streams draining from the ice margin at Tregaron. Although Griffiths (1940) described halt stage moraines throughout the Teifi valley from Tregaron to Newcastle Emlyn, inferring a more extensive ice limit than Charlesworth, these 'end-moraines' were later reinterpreted as ice-marginal accumulations against downwasting ice (Watson 1970). Glaciofluvial sediments derived from Welsh ice dominate the superficial deposits of the middle Teifi valley, particularly between

Lampeter and Llandysul (Watson 1970; Price 1976; M.S. Parry *unpublished* in Bowen 2005; Waters *et al.* 1997; British Geological Survey 1997). It is believed that significant thicknesses of Welsh tills underlie these sand and gravel sequences (Waters *et al.* 1997). Upstream, the upper Teifi and Dulais valleys between Lampeter and Tregaron contain a landsystem of ice-contact landforms and sediments providing key evidence for the nature of late Devensian deglaciation (Sheppard 2003). This area, briefly described by Charlesworth (1929) and identified as an area with significant potential sand and gravel resource (Crimes *et al.* 1992), is characterised by kame terraces, glacio-fluvial outwash sheets, kettle holes and numerous moraine complexes (Sheppard 2003).

Based on borehole evidence for till and outwash material at Llangeler (Lear 1986), and abundant evidence for Welsh tills throughout the middle Teifi valley between Pentrecwrt and Llanybydder (Jones 1965; Price 1976; Bowen 1999), a westward limit of Welsh ice has been suggested between Llangeler and Henllan (Figure 2.19) (Lear 1986). Recent BGS mapping has shown that Welsh ice of Devensian age spread across the high ground both to the north and south of the Teifi valley (Waters *et al.* 1997). In the Teifi valley, Welsh tills and ice-contact glaciofluvial sands and gravels deposited at this time extend as far west as Llandysul, but more extensive spreads of tills are found east of Maesycrugiau (Figure 2.19) (Waters *et al.* 1997). Glaciofluvial ice-contact deposits suggest that this westward flowing ice extended to the area between Henllan and Llandysul, where it overrode and displaced Lake Teifi (Waters *et al.* 1997). This ice is believed to have receded only after drainage of Lake Teifi, suggesting that the barrier of Irish Sea ice in the Lower Teifi valley retreated more rapidly than the Welsh ice (Waters *et al.* 1997). It has been suggested that during ice wastage temporary dams made of glacial debris and/or stagnating ice may have ponded several smaller, temporary lakes upstream of Llandysul (Price 1976; Waters *et al.* 1997; Bowen 2005). If this model is correct, then logically the deltas at Llanllwni, Rhuddlan, Llanybydder, Llanwnnen, Pencarreg, and Lampeter (Figure 2.19) may not have been deposited in Lake Teifi, but may instead be related to the development of smaller lakes developed during deglaciation (Waters *et al.* 1997). Lake Teifi was perhaps not therefore as extensive as has been suggested by some (Charlesworth 1929; Lear 1986; Etienne *et al.* 2006). A thickness of at least 12 m of glaciolacustrine silts and clays has been proved beneath 8 m of glaciofluvial deposits

46

in a 20 m deep borehole located on the alluvial plain north of the river at Lampeter however (Heaven *et al.* 1999).

2.6 Hydrogeology of the Welsh Basin area

Because of the low permeability of the mudstones and fine sandstones of the Silurian and Ordovician bedrock, and the fine-grained nature of most of the superficial deposits, groundwater potential in the areas underlain by rocks of the Welsh Basin (e.g. Ceredigion and northern Carmarthenshire) is limited (Robins *et al.* 2000; Hiscock and Paci 2000). Currently, groundwater throughflow in bedrock is small; the baseflow component in the Afon Teifi is mainly derived from local recharge and lateral flow direct to the river (Robins *et al.* 2000). This is because, although subordinate units of siltstone and sandstone through which groundwater flow might occur are present, these units are thin and the bedrock succession is dominated by thick sequences of marine mudstones.

Groundwater flow in the Teifi catchment currently occurs through four main pathways. These are: i) within granular superficial deposits (e.g. fluvioglacial sediments); ii) through minor, dilated cracks and joints within the shallow, weathered and highly permeable upper zone of bedrock (10-20 m thick in many areas); iii) in interconnected deep-seated fractures and faults in 'fresh' bedrock; and iv) seepage along geological boundaries (both at the contact between the Quaternary sediments and bedrock, and at boundaries between bedrock formations) (Robins *et al.* 2000; Hiscock and Paci 2000). Unlike areas with similar geological terrains in Ireland and southern Scotland, where groundwater is found mainly within Quaternary deposits, in west Wales the bedrock is also an important aquifer. This may be because of a thicker weathered zone caused either by a longer period of periglacial weathering or as a result of less glacial erosion in this area (Robins *et al.* 2000). Whilst the complexity of the Quaternary sequences may inhibit vertical connectivity, it also increases the likelihood of confined seepage along contacts between granular and clay-rich sediments. There is little reason to believe that during the Late Pleistocene the hydrogeology of the area was very much different, although higher groundwater pressures would be expected as a result of glacial meltwaters and the presence of permafrost.

3 Research Methods

3.1 Introduction to near-surface geophysics

High-resolution near-surface geophysical techniques are highly effective tools for characterising lateral and vertical changes in the physical properties of the terrestrial subsurface. Shallow geophysical techniques are widely utilised in engineering, environmental and archaeological surveys and for offshore marine studies, but have so far had limited use in investigations of terrestrial Quaternary deposits in the British Isles, although notable exceptions occur (e.g. Harris *et al.* 1997; Brabham *et al.* 1999). Geophysical surveys provide important geological information that would not be available using only boreholes and outcrop. As well as being cost-effective and rapid techniques to use, a significant advantage of geophysical methods is that most techniques are non-invasive and therefore have a low environmental impact, ideal for vulnerable sites or sites with conservation designations. Geophysics should be perceived as a complementary tool and should be used in conjunction with borehole and exposure data. It can also be used to target boreholes and trial pits as well as to correlate between them. Ideally, geophysical surveys should integrate a suite of complementary methods (e.g. Slater and Reeve 2002; Aaltonen 2003; Comas *et al.* 2004; Turesson and Lind 2005).

Geophysical techniques are divided into two categories, those which make passive measurements of naturally occurring fields (e.g. gravity, magnetics, self potential (SP)) and those which make active physical measurements (e.g. seismics, electrical resistivity, electromagnetics, ground penetrating radar (GPR)). No passive geophysical techniques were used in surveys undertaken as part of this project. This section will briefly outline the techniques and methods used for site investigations in Wales (electrical resistivity tomography, seismic refraction, induced polarisation, GPR) and in Svalbard (GPR, electrical resistivity tomography).

3.2 Electrical resistivity tomography

3.2.1 Introduction

Resistivity is a fundamental parameter of materials that describes how effectively a material can transmit an electrical current (the flow of free electrons between atoms in a material). The difference in electrical energy between two points in a circuit is called the potential difference and is measured in volts. By measuring the current and the voltage, the resistance (R) of a material can be calculated using Ohm's law by dividing the potential (ΔV) by the current (I).

$$R = \frac{\Delta V}{I}$$
(1)

Resistivity measurements can provide information on the electrical properties of the subsurface. In electrical resistivity surveys an electrical current is induced into the ground through a pair of metal electrodes (current electrodes) by connection to a DC power source (battery). Measurements of the electrical potential (voltage) are then made across a second pair of electrodes (potential electrodes) (Figure 3.1a). However, as resistivity is the resistance per unit of volume, the resistance must be multiplied by an appropriate geometrical factor, dependent on the measurement geometry, to calculate the apparent resistivity (ρa) (Reynolds 1997) (Figure 3.1b).

Current typically flows along arc-shaped paths between two current electrodes. Therefore, by increasing the spacing between the electrodes, the depth of investigation can also be increased, as the injected current will flow to greater depths. However, the increase of electrode spacing results in a loss of near surface information, a decrease in resolution with depth (Griffiths and Turnbull 1985) and a loss of lateral resolution (Scott *et al.* 1990). The conductivity ($1/\rho$) of the ground also modifies the current paths so a standard relationship between path depth and electrode spacing cannot be assumed. As the measured potential difference will fall as the electrode spacing is increased, there is also a requirement for a larger electrical current to get a measurable voltage. The maximum depth is therefore partly determined by the size of the current source (battery).

a)

I

↓ Current Electrodes
↓ Potential Electrodes

ΔV

a

b

c

d

Distance
measurements
(metres)

Measurement point

b)

$$\rho_a = 2.\pi.\frac{\Delta v}{I} . \left[\frac{1}{\left[\frac{1}{a} - \frac{1}{b} - \frac{1}{c} + \frac{1}{d}\right]} \right]$$

Geometrical Factor
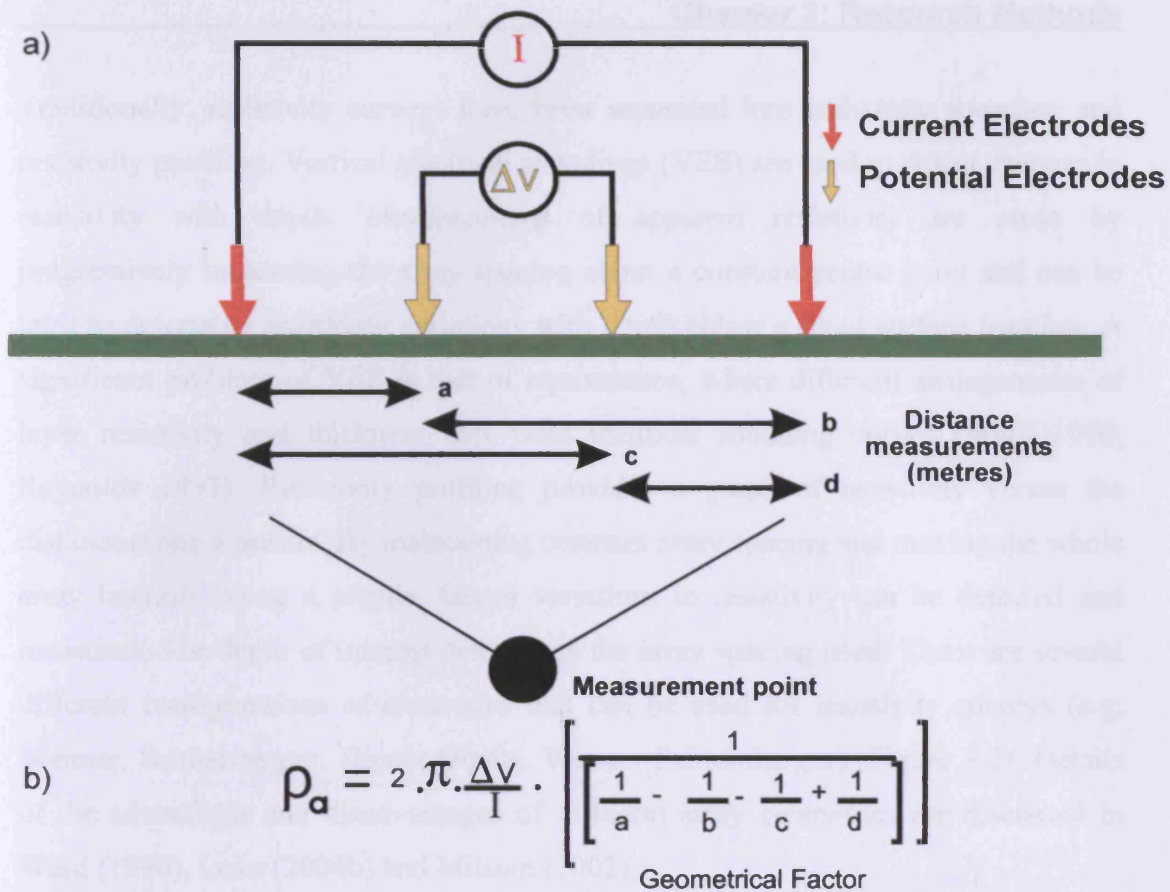
Figure 3.1: (a) Array of four electrodes used to make measurements of voltage associated with a given current; (b) Equation to calculate apparent resistivity of a volume of material between pairs of electrodes.

a) Wenner array

b) Schlumberger array

n = 1

a   a   a

2a   2a   2a

n = 2

3a   3a   3a

n = 3

a   a   a

2a   a   2a

3a   a   3a
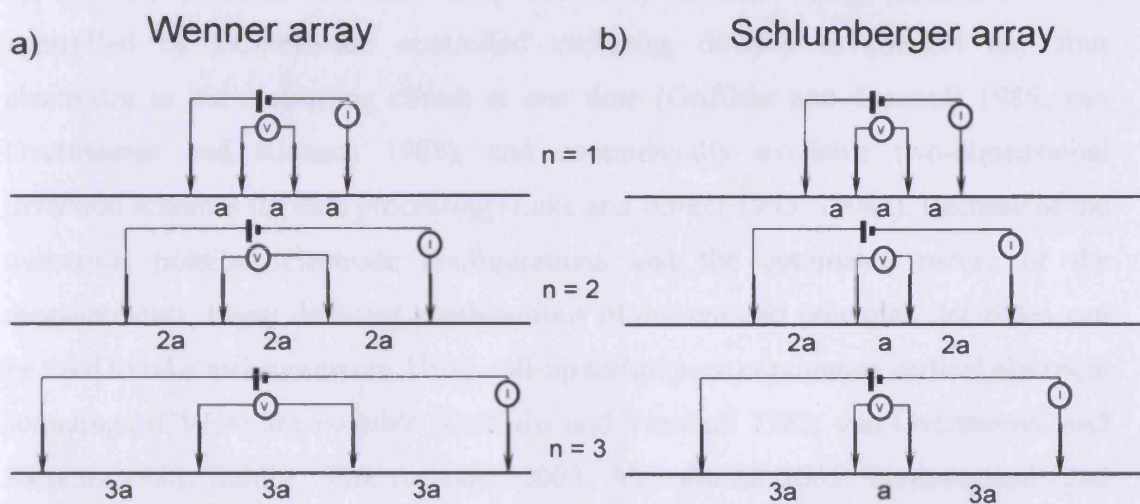
Figure 3.2: (a) Wenner electrode array; (ii) Schlumberger electrode array (adapted from Loke 2004b). By increasing the spacing between electrodes (n), the depth of measurement increases enabling measurements of resistivity at greater depth to be recorded.

Traditionally, resistivity surveys have been separated into resistivity sounding and resistivity profiling. Vertical electrical soundings (VES) are used to detect changes in resistivity with depth. Measurements of apparent resistivity are made by progressively increasing the array spacing about a constant centre point and can be used to determine resistivity variations with depth below a fixed surface location. A significant problem of VES is that of equivalence, where different arrangements of layer resistivity and thickness will yield identical sounding curves (Ward 1990; Reynolds 1997). Resistivity profiling provides a graph of resistivity versus the distance along a profile. By maintaining constant array spacing and moving the whole array laterally along a profile, lateral variations in resistivity can be detected and measured. The depth of interest determines the array spacing used. There are several different configurations of electrodes that can be used for resistivity surveys (e.g. Wenner, Schlumberger, Dipole-Dipole, Wenner-Schlumberger) (Figure 3.2). Details of the advantages and disadvantages of different array geometries are discussed in Ward (1990), Loke (2004b) and Milsom (2002).

Recent advances in data acquisition and geophysical inversion techniques have enabled the integration of the sounding and profiling techniques, leading to the development of electrical resistivity tomography (Figure 3.3). This has been driven by the use of multi-electrode array resistivity systems using multicore cables controlled by PC-software controlled switching devices to connect any four electrodes to the measuring circuit at one time (Griffiths and Turnbull 1985; van Overmeeren and Ritsema 1988), and commercially available two-dimensional inversion schemes for data processing (Loke and Barker 1995, 1996a). Because of the numerous possible electrode configurations and the automated nature of the measurements, many different combinations of current and potential electrodes can be used to take measurements. Using roll-up techniques, continuous vertical electrical soundings (CVES) are possible (Griffiths and Turnbull 1985; van Overmeeren and Ritsema 1988; Dahlin 1996; Aaltonen 2003; Wisen et al. 2005; Turesson and Lind 2005). These developments have enabled the rapid collection of resistivity measurements, using a combination of sounding and profiling techniques, to produce contoured "images" (pseudo-sections) of the electrical characteristics of the subsurface (Figure 3.4). As these images are distorted by the electrode geometry and resistivity variations in the ground it is necessary to process such data using inversion
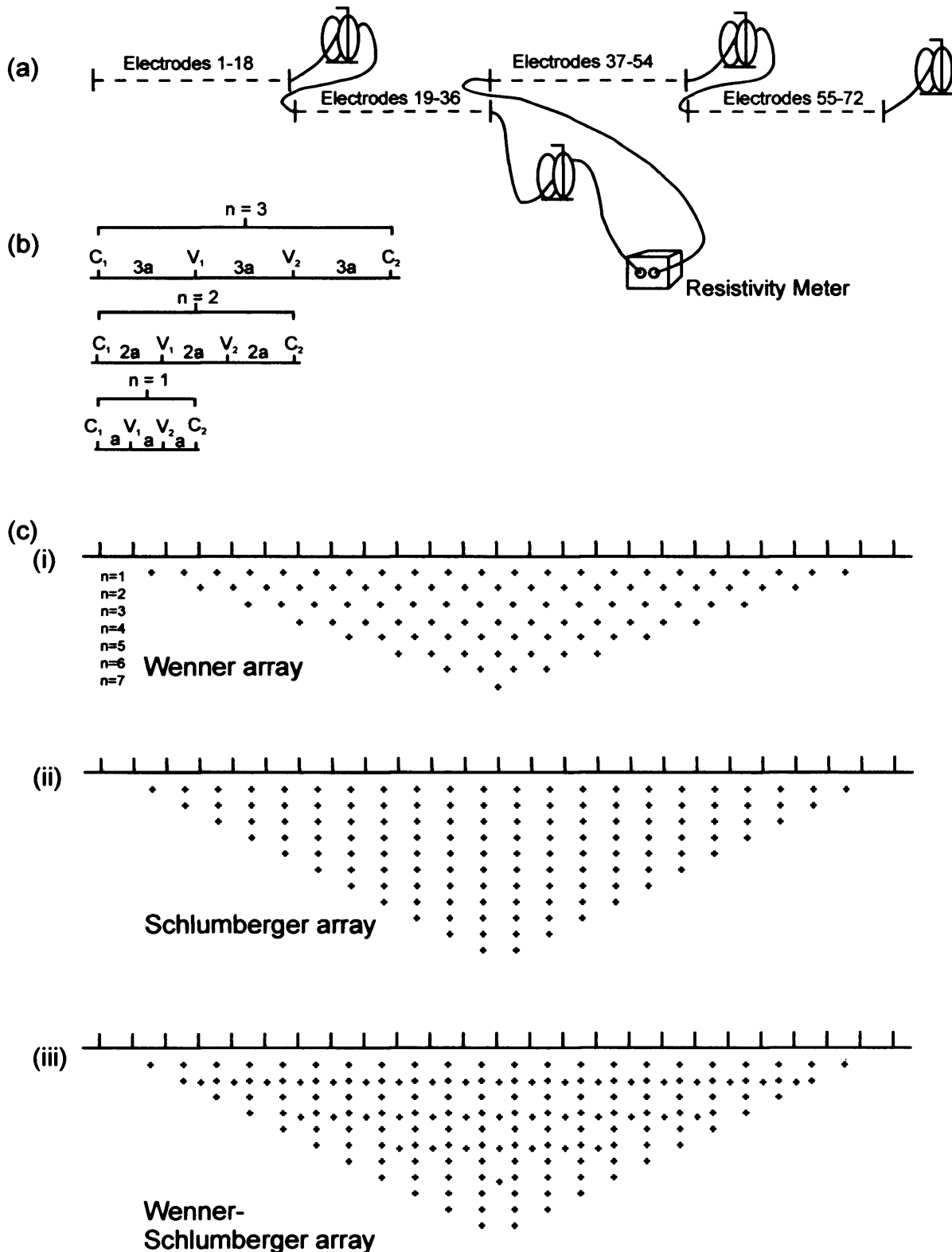
Figure 3.3: Multi-electrode electrical resistivity tomography system (a) Field setup using four multicore cables (adapted from van Overmeeren and Ritsema 1988, Dahlin 1996). (b) Sequence of electrode spacings for Wenner array (adapted from Loke and Barker 1996a, Loke 2004a). (c) Points of measurement (pseudosection data pattern) for (i) Wenner, (ii) Schlumberger and (iii) Wenner-Schlumberger tomographic arrays (adapted from Loke 2004b).
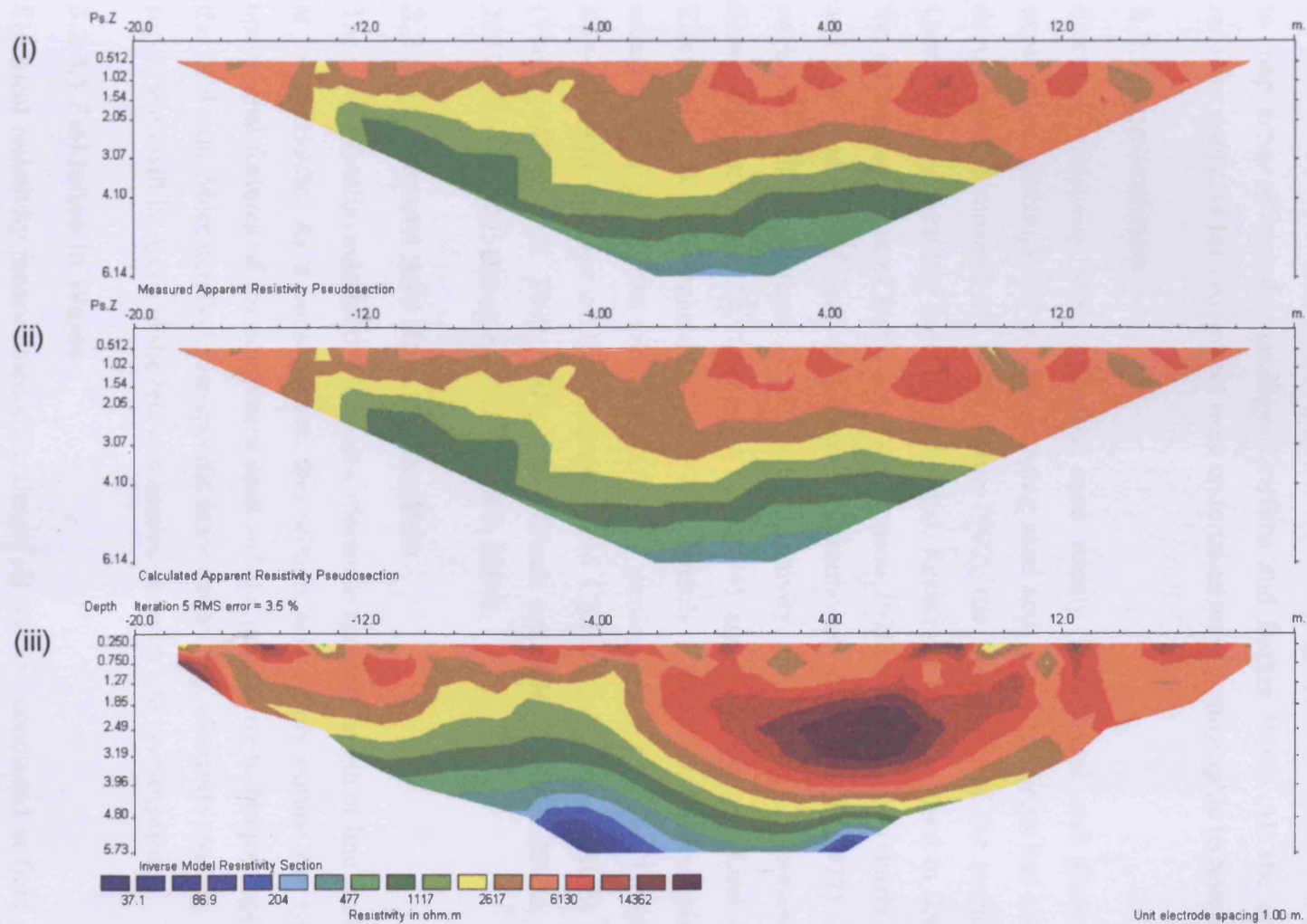
Figure 3.4: Example of (i) measured apparent resistivity pseudo-section; (ii) calculated apparent resistivity pseudo-section; and (iii) inverted model resistivity section. Dataset from resistivity survey from the area of ground between the SAS Radisson hotel and the UNIS building Longyearbyen, Svalbard.

modelling packages to create a more geometrically and quantitatively true representation of the subsurface (Loke and Barker 1995, 1996a). Processing techniques for 3D electrical resistivity surveys have also been developed (Loke and Barker 1996b). Tomography surveys have wide ranging applications and can be used to map areas of complex geology (Griffiths and Barker 1993). All the electrical resistivity surveys for this project were undertaken using tomographic techniques.

3.2.2 Applications

Electrical resistivity was originally used widely for mineral and groundwater exploration. Although its use for mapping sand and gravel resources has also been documented (Crimes *et al.* 1994; Auton 1992), the application of the technique in Quaternary research has been rather limited. Resistivity has been used to determine the internal structure of kettle holes (Thompson 1978), relict pingos (Harris 2001b) and the presence of ice wedge casts (Greenhouse and Morgan 1977). Recent environmental applications of electrical resistivity tomography are presented by Slater and Reeve (2002), Comas *et al.* (2004) and Turesson and Lind (2005). Electrical resistivity techniques have been widely applied for the mapping and monitoring of permafrost (Scott *et al.* 1990), particularly during the 'Geophysical Survey' work package of the Permafrost and Climate in Europe (PACE) project (Vonder Mühll *et al.* 2000, 2001, 2002; Hauck and Vonder Mühll 2003a, 2003b, 2003c; Hauck 2002; Hauck *et al.* 2001, 2003, 2004).

3.2.3 Equipment and data acquisition

The survey details (number of electrodes, electrode spacing, length of line etc.) varied at each fieldsite. As a consequence, this section will simply outline the type and operational features of the equipment used and the processing techniques applied to the field data. More detailed, site-specific information (e.g. electrode spacing, date of survey etc.) will be given in the relevant section for each site investigation.

3.2.3.1 Fieldsites in Wales

Electrical resistivity measurements for almost all surveys conducted at field sites in Wales were conducted using an IRIS Instruments SYSCAL Junior Switch 72 (Figure 3.5). The only exception was the original profile at 'Pingo L' in the Cledlyn valley for which an ABEM SAS 4000 with an ES464 electrode selector was used (Section 7.2).

Figure 3.5: Electrical resistivity tomography system: (a) IRIS Systems SYSCAL Junior Switch 72 resistivity meter; (b) Multicore cable, steel electrodes and copper electrode jumpers. This equipment was used for the majority of surveys undertaken at field sites in Wales. Photo (b) by P.J. Brabham.

For surveys conducted in 2004, the IRIS resistivity meter was borrowed from Terradat UK, but following the purchase of identical equipment by Cardiff University in early 2005, all surveys after this date were conducted using this system. The SYSCAL Junior Switch 72 system uses a multi-channel switching unit and data logger to control the selection of steel electrodes (up to 72 not using roll-up methods) and to record voltage measurements. Current is induced by a 12V DC power supply. Electrodes were inserted into the ground at regular spacings, varying between 1 and 5 m, depending on the resolution and depth of survey required. The multi-core cable was connected to the steel electrodes with copper electrode jump leads. Measurements were made using Wenner-Schlumberger arrays (Figure 3.3c), with multi-combinations of pairs of current and potential electrodes used to take as many measurements along as many different paths as possible. Although it has a slightly lower signal to noise ratio than a standard Wenner array, the Wenner-Schlumberger array provides better horizontal coverage, enhanced sensitivity to vertical and horizontal structures, and a greater maximum depth of survey (Loke 2004a, 2004b). The protocol file for the Wenner-Schlumberger array was uploaded from a PC to the SYSCAL Junior Switch using the Electre II program.

To minimise the effects of electrical noise or poor electrical contact, prior to measurement the SYSCAL Junior Switch undertakes a resistance (RS) check to assess the quality of ground contact for each electrode. Poor ground contact can occur in dry, stony conditions or in areas with a highly resistive substrate (e.g. aeolian sands). However, this was not considered a significant problem for the field sites in Wales due to the typically saturated, clay- and silt-rich nature of the superficial deposits. Where RS check values were above 2 kΩm, normally due to direct contact with large clasts, attempts were made to improve ground contact by repositioning electrodes.

3.2.3.2 Fieldsites in Svalbard

Electrical measurements conducted for investigations in Svalbard used an ABEM SAS 300C Terrameter instrument with an ES464 electrode selector (Figure 3.6) supplied by the Institute for Geography, University of Oslo. The SAS 300C uses a PC-controlled (via the program ERIC) 4 x 64 channel relay-matrix electrode selector between the multicore cable and the resistivity meter. All survey lines used 2 cables

with 20 electrodes takeouts each and electrode spacing of between 4 m and 5 m (cable length of 156 m or 195 m), with measurements on the multi-electrode array made using the Wenner fast array. This array was used to optimise battery life under cold conditions. To avoid the costs of transporting heavy electrodes to Svalbard, steel electrodes were custom built on-site in Longyearbyen, Svalbard.

There were surprisingly few practical problems in achieving good ground contact with the electrodes in the frozen ground. Warm air temperatures during the period of survey (19th to 23rd April 2005) and the fine-grained nature of the substrate at all three field sites allowed electrodes to be inserted into the ground quite easily. However, problems were experienced achieving ground contact where deep snow had drifted on the leeward side of pingos and snowpits had to be dug to reach ground level (Figure 3.7). In some cases electrode contact was not possible where snow depths were in excess of 2 m. Unlike the SYSCAL Junior Switch 72 used for surveys in Wales, the current induced into the ground with the SAS 300 can be manually altered during the course of the surveys. Due to the limited problems with ground contact, the current used in the surveys was generally between 10-100 mA. On average three measurements of the voltage between electrode pairs were used to calculate the average ground resistivity value during surveys.

3.2.4 Processing

The raw data from the surveys in Wales were uploaded from the IRIS SYSCAL Junior Switch 72 using the PROSYS program. In PROSYS, the correct array type, electrode spacings and topography were assigned to the raw data. The quality of the data was assessed using the filtering option before exporting the data as a .dat file for processing. Resistivity data collected in Svalbard was imported directly into Res2DINV for processing. Processing of the resistivity measurements used Res2DINV (Loke and Barker 1995, 1996a; Loke 2004a, 2004b). This program uses a 2D smoothness constrained inversion algorithm to produce 2D vertical subsurface models displaying contoured resistivity values of apparent resistivity. The inversion divides the subsurface into a cell-based model of fixed rectangular blocks. During the inversion process the resistivity of each cell is varied until the modelled resistivity of the blocks that best reproduces the measured apparent resistivity values is determined.
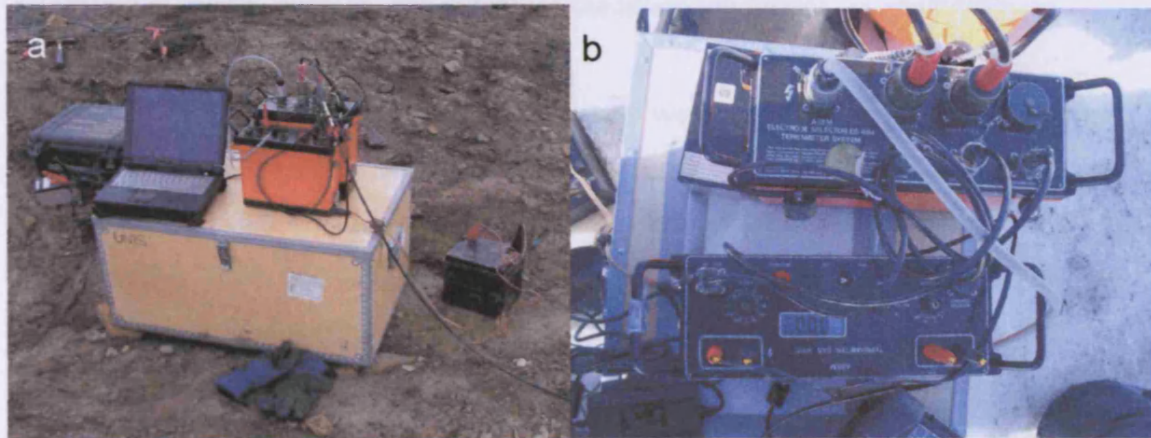
Figure 3.6: ABEM SAS 300C terrameter resistivity meter with ES464 electrode selector used for resistivity surveys in Svalbard. Photo (a) by H.H. Christiansen.
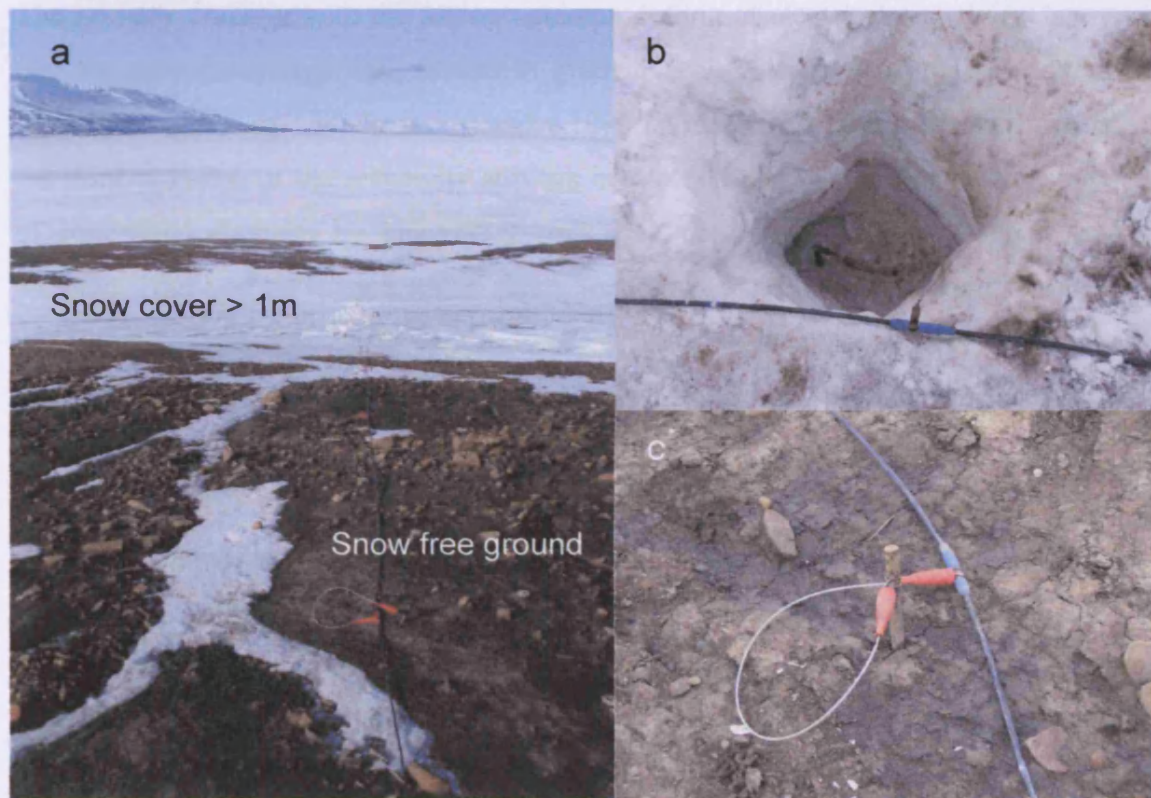
Figure 3.7: Examples of ground contact locations for electrodes at Longyear and Hytte pingos, Adventdalen. Problems were experienced with placing electrodes on the lee side of pingos, where deep snowdrifts had accumulated (b), where snow depth was greater than 1.5 m. Photo (b) by L. Kristensen. Photo (c) by H.H. Christiansen.

The root mean square (RMS) error between the observed resistivity and modelled resistivity is used to evaluate the quality of the inversion model.

Prior to the inversion of resistivity data, datasets were evaluated for noisy data points caused by random or systematic noise (e.g. the result of bad electrode contacts). Any obviously noisy data was removed using the 'exterminate bad datum points' function in Res2DINV (Loke 2004a). Because of the 'clean' nature of the majority of the data from surveys in Wales (high signal to noise ratio) a low damping factor was used for each inversion (normally the default value of 0.16). Where there was significant variability in the near-surface resistivity, the inversion model mesh was refined by assigning a finer mesh (half the electrode spacing), creating apparent resistivity measurements that were more reliable (Loke 2004a).

The primary problem with the tomographic modelling of electrical resistivity data is that the smoothing algorithm results in gradual layer interfaces even if geological boundaries are sharp and distinct (Dahlin 1996; Wišen et al. 2005). Because one of the principal aims of the resistivity surveys in Wales was to determine the thickness of superficial deposits by identifying rockhead, the robust inversion option was selected. This method is used where sharp boundaries are expected in the datasets, to minimise the smearing effect of the smoothness-constrained least-squares inversion method and produce sharp boundary interfaces between geological materials (Loke 2004a).

All data were adjusted for topographic effects by inputting data derived from EDM surveying or from LiDAR datasets supplied by the Environment Agency. The topography was incorporated directly into the inversion model using a uniformly distorted finite element grid with no damping. This method shifts all the subsurface nodes vertically by the same amount as the surface node and is acceptable for moderate topographic variation (Loke 2000, 2004a, 2004b).

Because the model with the lowest RMS error is not necessarily the most accurate resistivity model, the model at the iteration after which the RMS error did not change significantly was chosen, as recommended by Loke (2004a). To enable comparison between surveys, all electrical resistivity survey lines from sites in Wales are

60

presented using a common contouring scale (user defined logarithmic contour intervals: minimum contour value 36.2, user defined contour increase factor 1.23).

3.3 Induced polarisation

Where geological materials are capable of storing electrical charge they are described as capacitors. The induced polarisation (IP) method is used to measure the capacitance effect of a given geological material. Measurements of capacitance are undertaken with time domain IP instruments, which measure the decay of a voltage for a short period after an applied current is switched off (Figure 3.8). The degree to which a material is able to store charge by capacitance is known as its chargeability, measured in millivolt per volt (mV/V). Mineral deposits (e.g. metal sulphides), volcanic tuffs and clays are characterised by high chargeability values. The IRIS SYSCAL Junior Switch 72 is able to make IP measurements whilst undertaking resistivity measurements. IP is not routinely used in commercial surveys for geological surveys (Turesson and Lind 2005). However, because of the clay-rich substrate at many of the sites surveyed, time domain chargeability surveys were undertaken in addition to the electrical resistivity tomography surveys at fieldsites in Wales to assess whether the values of chargeability could be used to distinguish between superficial sediments of differing character. Inversion of the IP data was undertaken simultaneously with the inversion of the resistivity data in Res2DINV. Due to a lower signal to noise ratio, the IP data normally required a greater level of editing to remove noisy data points prior to inversion. To enable comparison between surveys, all IP survey lines from sites in Wales are presented using a common contouring scale (user defined contour intervals: minimum contour value 0, contour spacing value 0.6).

3.4 Seismic refraction

3.4.1 Introduction
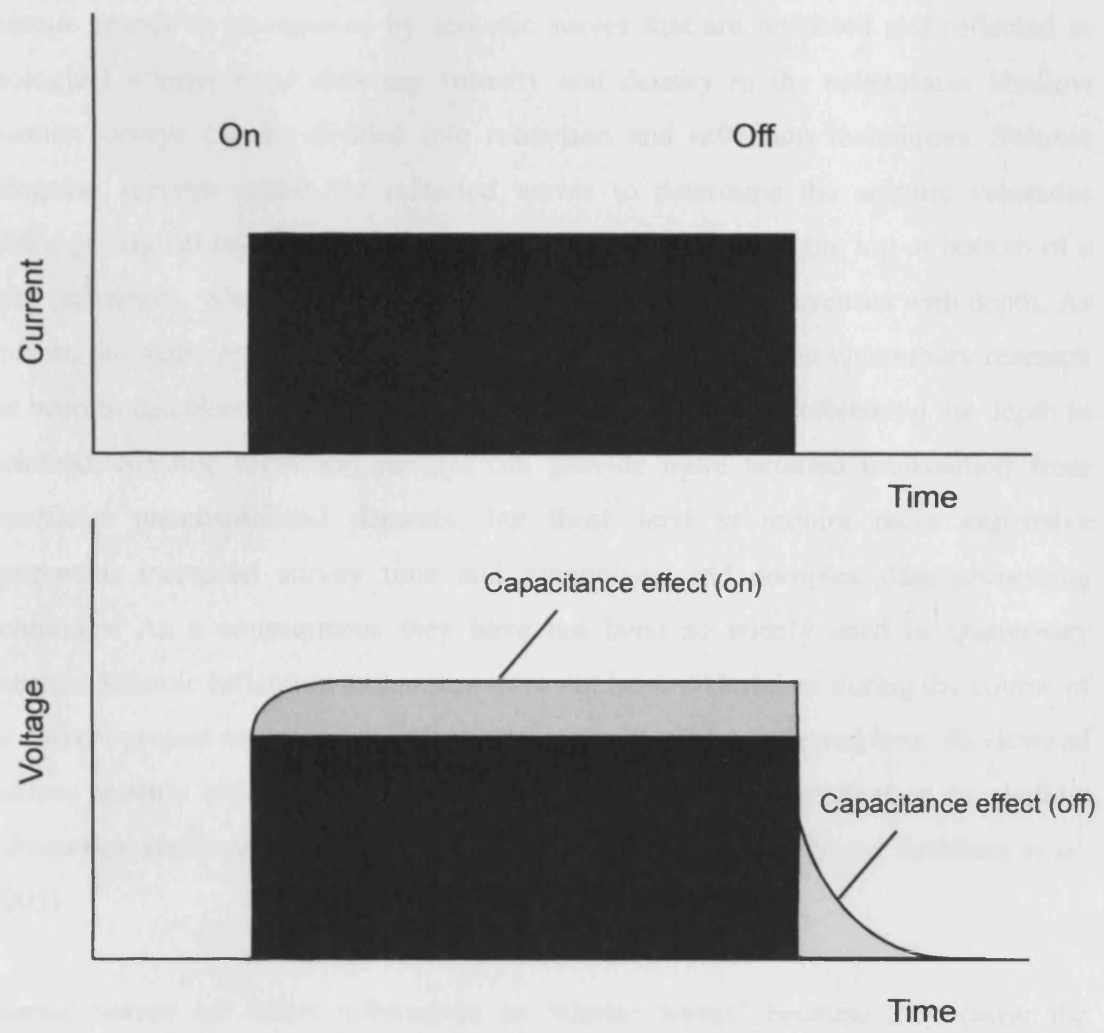
Figure 3.8: Voltage measurements of a geological material acting as a capacitor. The gradual decay of the voltage over a fixed time period after the current is switched off is measured using time domain induced polarisation (IP) methods. The degree of chargeability is proportional to the area under the curve of the decay of the capacitance effect.

3.4 Seismic refraction

3.4.1 Introduction

Seismic energy is transported by acoustic waves that are refracted and reflected at geological interfaces of differing velocity and density in the subsurface. Shallow seismic surveys can be divided into refraction and reflection techniques. Seismic refraction surveys utilise the refracted waves to determine the seismic velocities within geological layers and identify and measure the depth of the top or bottom of a layer (refractor), where the velocity of each successive layer increases with depth. As a result, the main application of the seismic refraction method in Quaternary research has been to calculate the thickness of superficial deposits by establishing the depth to rockhead. Seismic reflection surveys can provide more detailed information from superficial unconsolidated deposits, but these tend to require more expensive equipment, increased survey time and manpower, and complex data processing techniques. As a consequence they have not been so widely used in Quaternary research. Seismic reflection techniques have not been undertaken during the course of the current project and as a result the technique will not be reviewed here. Reviews of shallow seismic reflection methods and examples of their application to shallow sedimentary environments can be found in Roberts *et al.* (1992) and Brabham *et al.* (2005).

Seismic waves are often referred to as 'elastic waves' because they cause the deformation of the material in which they propagate. P-waves (primary or pressure waves) are compressional waves that result in dilation and shear of the material. As the wave travels through a material, particles oscillate backwards and forwards linear to the direction of wave propagation. S-waves (secondary or shear waves) cause shear of the material where particles vibrate at right angles to the direction the wave is travelling. Energy from a seismic source can also generate surface waves (ground roll) known as Rayleigh waves (P-wave ground roll) and Love waves (S-wave ground roll). These travel at much slower rates to standard P- and S- waves.

The seismic refraction method conventionally uses compressional (P-) waves, although S-wave offer theoretical advantages in shallow Quaternary sediments. The

internal structures of unconsolidated superficial deposits tend not to be detected using seismic refraction as the P-wave velocities of different units are not contrasting enough to produce observable refraction events. Because of the usual significant P-wave contrast between superficial sediments and rockhead however, this boundary is usually recognisable using seismic refraction. Where the bedrock is a weathered sedimentary rock, the contrast between the compressional waves of some superficial deposits (e.g. till) and bedrock can be small. Velocity contrasts are greater using shear waves (S-waves) making it theoretically easier to obtain first arrivals from rockhead (Brabham and Goulty 1988). Additionally, S-waves are not affected by water in pore spaces and are therefore not affected by the presence of the water table. The production, recording and processing of S-waves is however more complex because they arrive later than P-waves and for these reasons are not regularly employed.

Seismic refraction is based on the principle that seismic ray paths behave in accordance with Snell's Law. Refraction of a wave occurs at the interface of two layers of different velocities. Where a low velocity layer overlies one of higher velocity (Figure 3.9a), the wave is refracted along the interface between the two layers. This critically refracted wave travels along the boundary of the two layers, at the higher propagation velocity of the lower layer, causing oscillating stress which results in the production of a wavefront (head wave), which is refracted back towards the ground surface through the overlying layer (Figure 3.9a). At a given distance along the ground surface, offset from the seismic source, the refracted raypaths that travelled at greater velocities through deeper layers (refracted waves) will reach the surface faster than the direct wave, which has travelled a shorter distance through shallower, lower velocity materials. By measuring, offset from the seismic source, the arrival time of the return of energy from the direct and refracted raypaths, the point at which the arrival of the refracted wave overtakes the direct wave (cross-over) can be measured. By plotting the first breaks on an offset distance vs. time graph, the distance from the shot point to the break in the gradient of the velocity graph can be defined (Figure 3.9b). By calculating the gradient of the two lineations in the graph on either side of the crossover distance, the velocities of the two layers can be determined from the direct and refracted waves respectively.
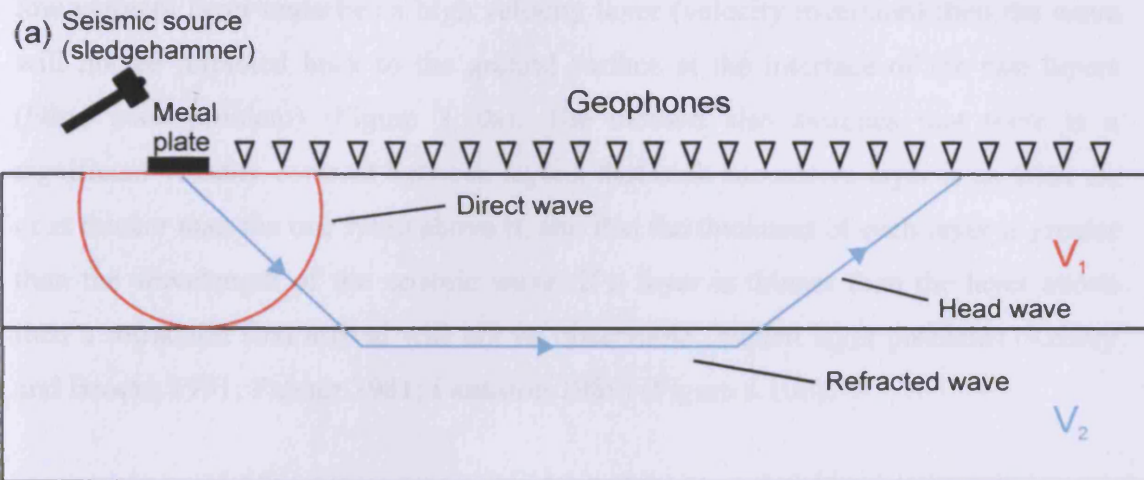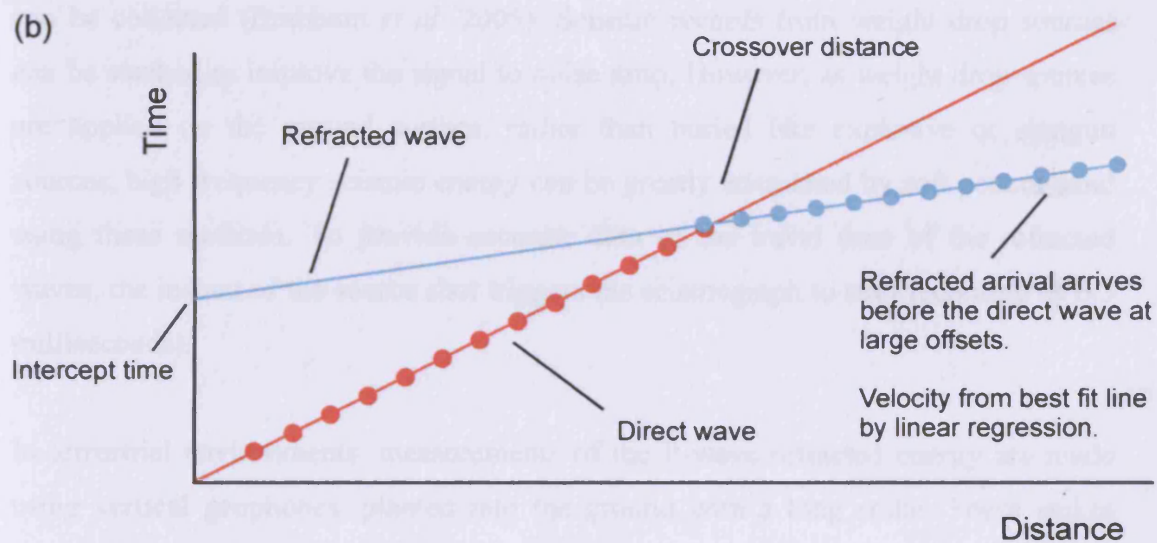
Figure 3.9: (a) The behaviour of direct and refracted seismic waves where a lower velocity layer overlies a higher velocity layer (V = velocity); (b) An example of an offset distance vs. time (Traveltime) graph produced from this context.

The refraction method assumes that there is an increase in velocity with depth. If a low velocity layer underlies a high velocity layer (velocity inversion) then the wave will not be refracted back to the ground surface at the interface of the two layers (blind zone problem) (Figure 3.10a). The method also assumes that there is a significant velocity contrast between layers, that each successive layer is as thick as, or is thicker than the one lying above it, and that the thickness of each layer is greater than the wavelength of the seismic wave. If a layer is thinner than the layer above then a refraction first arrival will not be observable (hidden layer problem) (Kearey and Brooks 1991; Palmer 1981; Lankston 1989) (Figure 3.10b).

The high frequency acoustic energy (>30 Hz) required for seismic surveys at, or near the ground-surface, can be generated by explosives, shotgun sources or weight drops (sledge hammers, large weights dropped from several metres or an accelerated mass) (Brabham *et al.* 2005). Weight drops tend to be the most rapid and cheapest techniques to utilise providing that good quality data with a high signal to noise ratio can be collected (Brabham *et al.* 2005). Seismic records from weight drop sources can be stacked to improve the signal to noise ratio. However, as weight drop sources are applied on the ground surface, rather than buried like explosive or shotgun sources, high frequency seismic energy can be greatly attenuated by soft peat or sand using these methods. To provide accurate data of the travel time of the refracted waves, the instant of the source shot triggers the seismograph to start recording (± 0.5 milliseconds).

In terrestrial environments, measurements of the P-wave refracted energy are made using vertical geophones, planted into the ground with a long spike. These spikes couple with the ground, producing an electrical signal proportional to the velocity, or rate of displacement, of ground movement. This electrical signal is recorded by a seismograph, which measures the geophone output as a function of time. The data is presented as a seismic trace (amplitude vs. time). The number of signals that can be recorded by a seismograph is dependent on its number of recording channels (normally 24- or 48-channel).
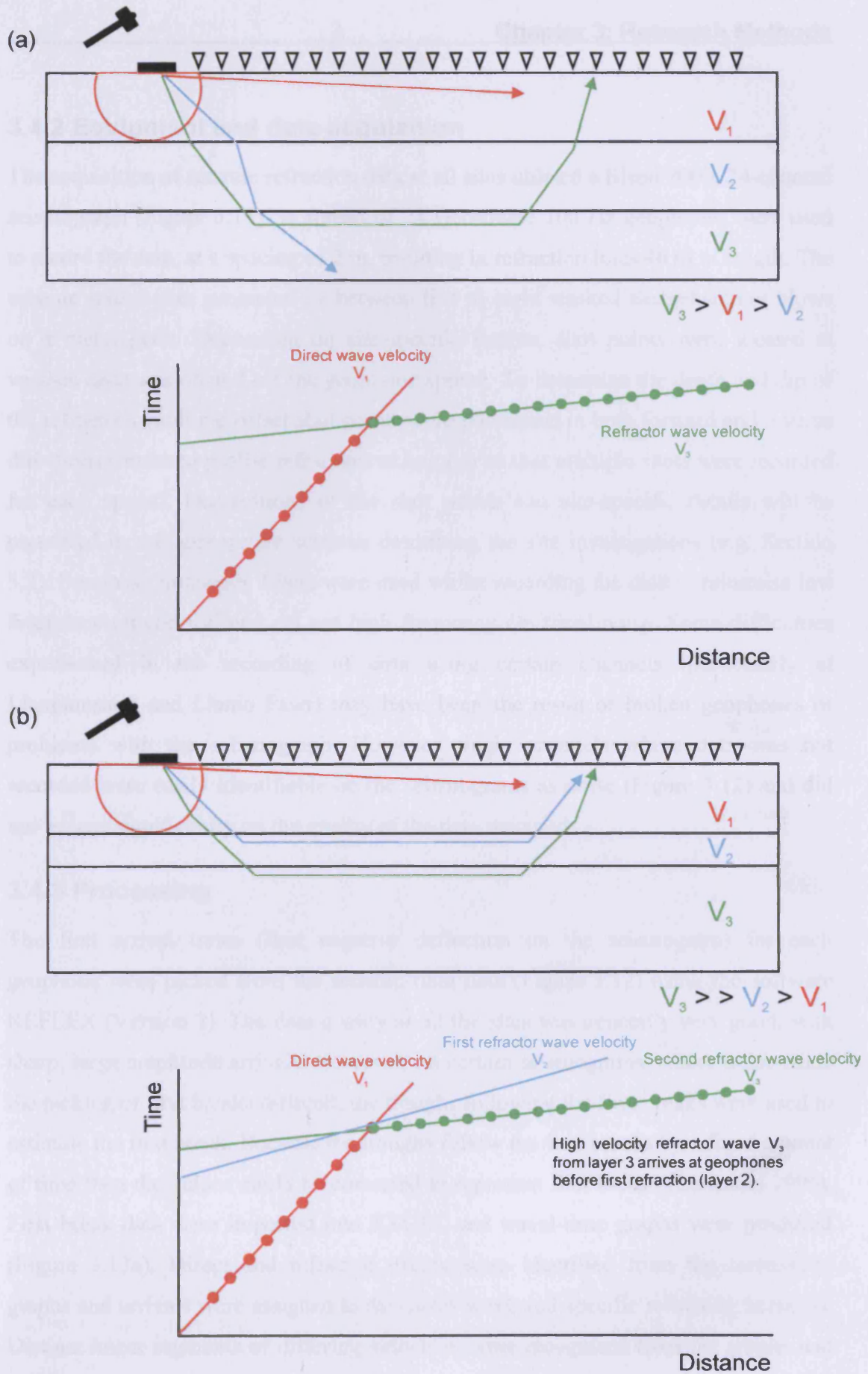
Figure 3.10: (a) Blind zone refraction model where no refraction is generated by the low velocity layer 2. (b) Hidden layer refraction model where layer 2 is too thin for the refraction to be identified at the geophones.

3.4.2 Equipment and data acquisition

The acquisition of seismic refraction data at all sites utilised a Bison 9000, 24-channel seismograph (Figure 3.11). A spread of 24 Geosource 100 Hz geophones were used to record the data, at a spacing of 2 m, resulting in refraction lines 46 m in length. The seismic source was generated by between five to eight stacked sledgehammer blows on a metal plate. Depending on site-specific factors, shot points were located at various distances on and off the geophone spread. To determine the depth and dip of the refractors, multiple offset shot points were positioned in both forward and reverse directions (reversed profile refraction technique) so that multiple shots were recorded for each spread. Descriptions of the shot points and site-specific details will be presented in the appropriate sections describing the site investigations (e.g. Section 5.2). Bandpass frequency filters were used whilst recording the data to minimise low frequency ground roll and cut out high frequency electrical noise. Some difficulties experienced in the recording of data using certain channels (particularly at Llanpumsaint and Llanio Fawr) may have been the result of broken geophones or problems with the seismograph. However single channels where data was not recorded were easily identifiable on the seismograms as noise (Figure 3.12) and did not impact significantly on the quality of the data recorded.

3.4.3 Processing

The first arrival times (first negative deflection on the seismogram) for each geophone were picked from the seismic field data (Figure 3.12) using the software REFLEX (Version 3). The data quality at all the sites was generally very good, with sharp, large amplitude arrivals. However, on certain seismograms, where noise made the picking of first breaks difficult, the troughs following the first breaks were used to estimate the first break. Because the troughs follow the first breaks by a fixed amount of time then the values could be corrected to represent first breaks (Lankston 1990). First break data were imported into EXCEL and travel-time graphs were produced (Figure 3.13a). Direct and refracted events were identified from the travel-time graphs and arrivals were assigned to the direct wave and specific refracting horizons. Distinct linear segments of differing velocities were recognised from the graphs and best-fit lines were produced for each velocity segment by linear regression (Figure 3.13b).
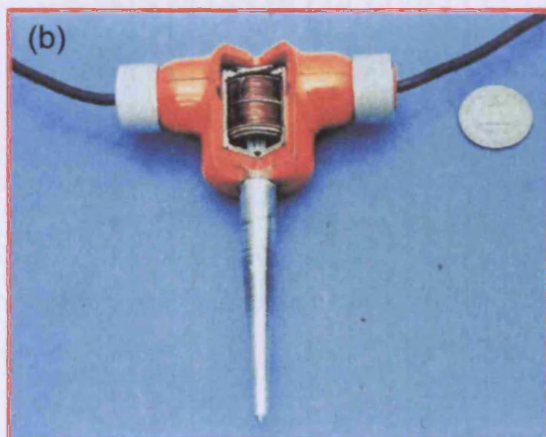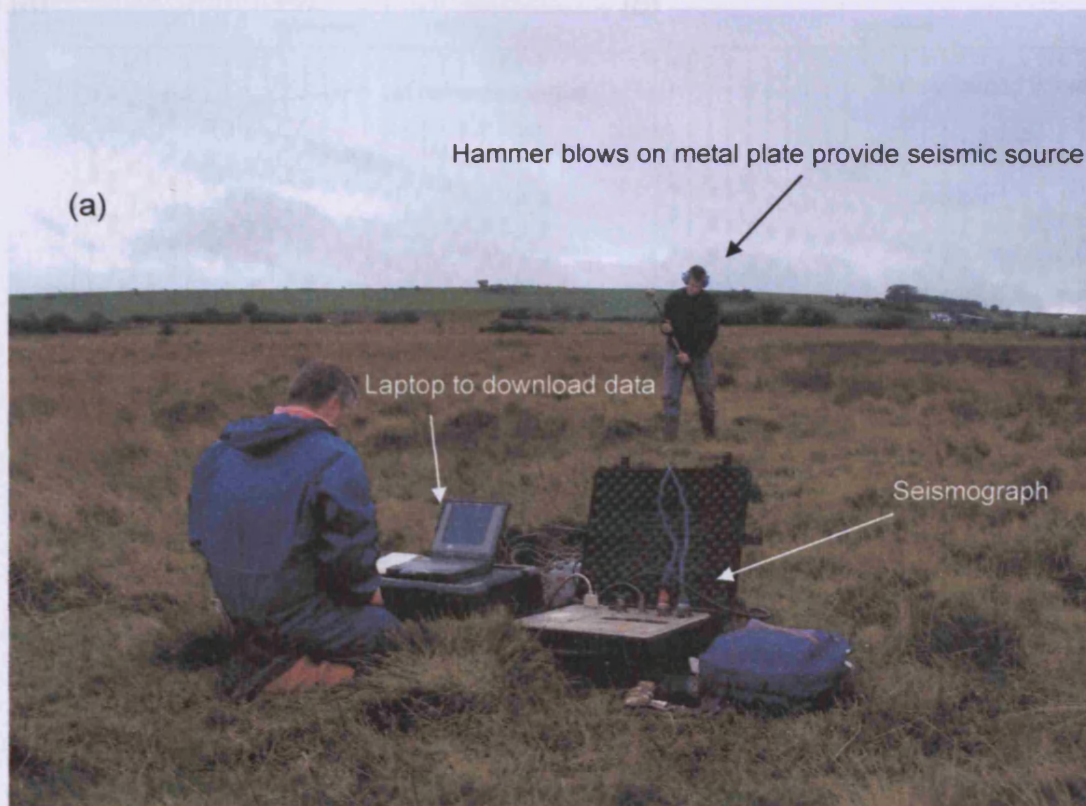
Figure 3.11: (a) Seismic survey setup for seismic refraction surveys in Wales. The seismic source was provided by between five to eight stacked sledgehammer blows on a metal plate; (b) Example of geophone used for recording ground movement; (c) Bison 9000 24-channel seismograph. Photo (c) by C. Harris.
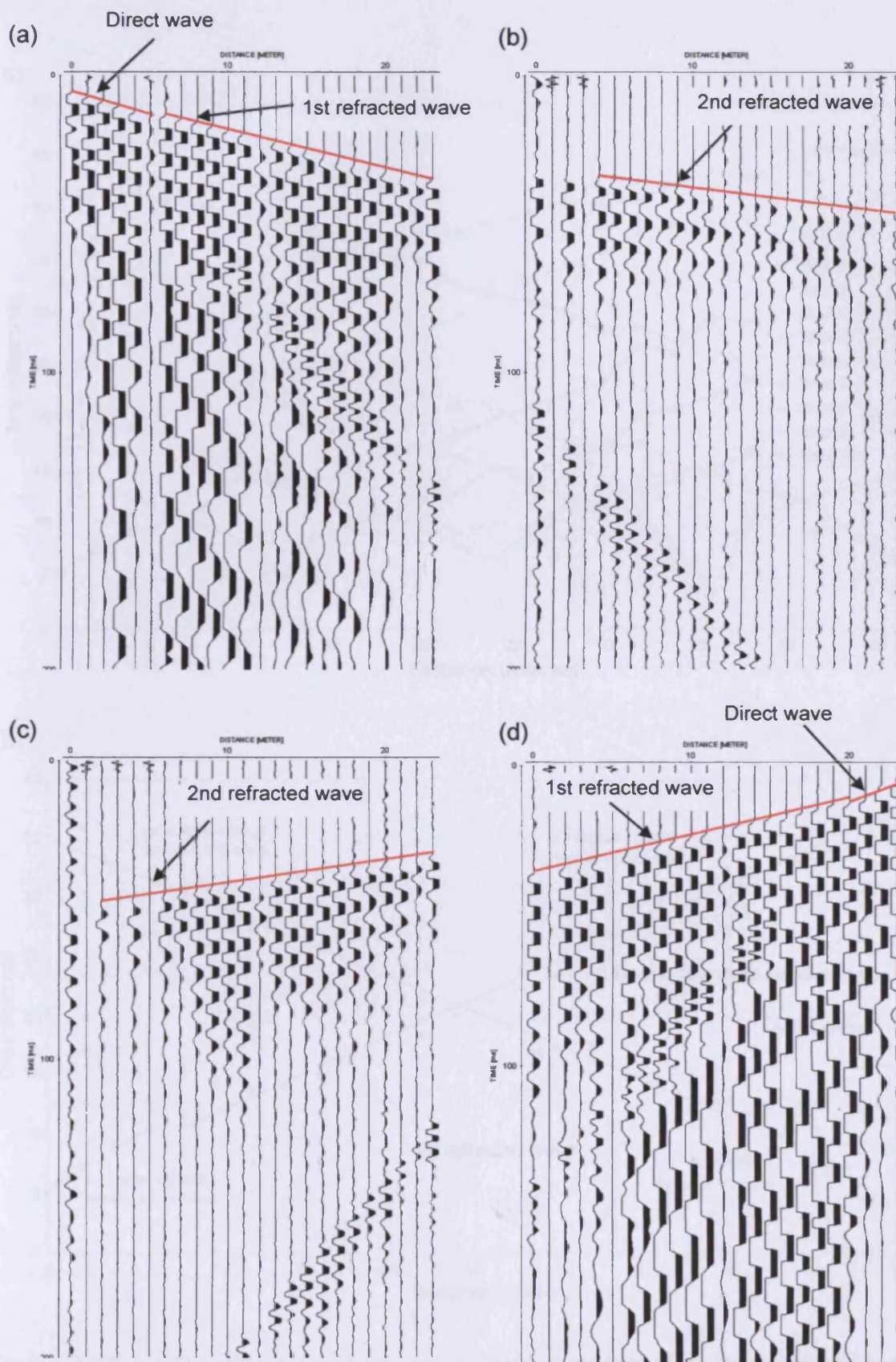
Figure 3.12: Seismograms from field data collected at Rhos Llawr Cwrt, Cletwr Fawr valley, displaying direct wave and first refracted wave (Shot 1 (a) Shot 2 (d)) and a second refracted wave (Shot 7 (b) Shot 6 (c)).
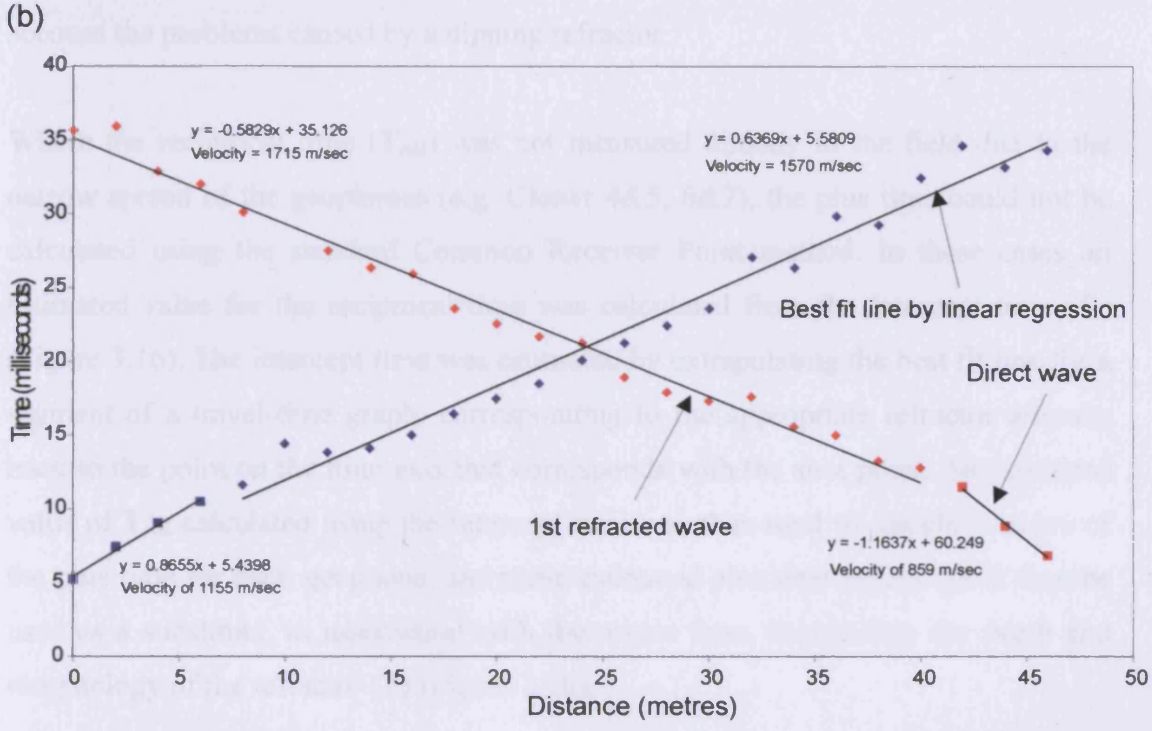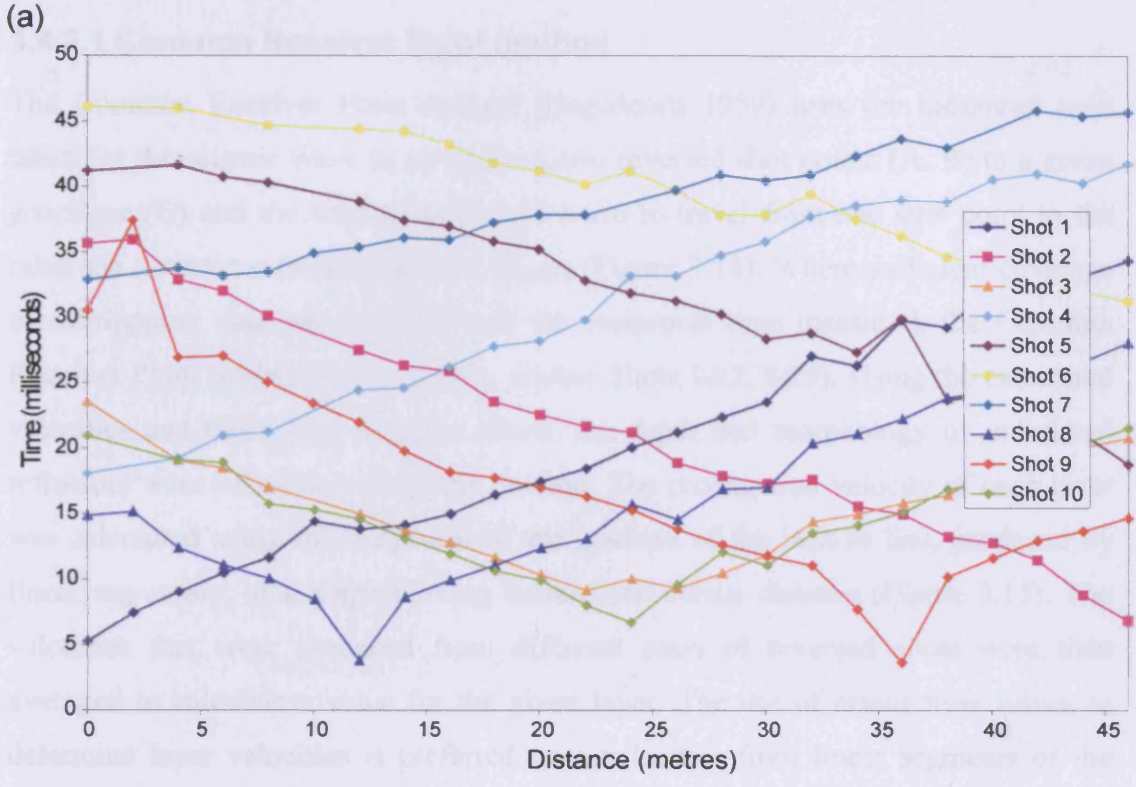
Figure 3.13: (a) Traveltime graph of seismic refraction data from Rhos Llawr Cwrt, Cletwr Fawr valley; (b) Example of linear segments established for direct and refracted waves recognised from traveltime data (Shots 1 and 2), Rhos Llawr Cwrt, Cletwr Fawr valley.

3.4.3.1 Common Receiver Point method

The Common Receiver Point method (Hagedoorn 1959) uses the measured time taken for the seismic wave to travel from two reversed shot points (A, B) to a given geophone (G) and the time taken for the wave to travel from one shot point to the other via a refractor (reciprocal time (T_{AB})) (Figure 3.14). Where sufficient coverage of overlapping data was recorded and the reciprocal time measured, the Common Receiver Point method was used (e.g. Cletwr Shots 1&2, 8&9). Using the calculated velocities and the minus and plus times, the depth and morphology of individual refractors were calculated using this method. The propagation velocity of each layer was calculated using the reciprocal of the gradient of the best-fit line, produced by linear regression, of a graph plotting minus time versus distance (Figure 3.15). The velocities that were produced from different pairs of reversed shots were then averaged to calculate a value for the given layer. The use of minus time values to determine layer velocities is preferred over velocities from linear segments of the travel-time graphs as the averaging technique of the minus time calculation takes into account the problems caused by a dipping refractor.

Where the reciprocal time (T_{AB}) was not measured directly in the field due to the narrow spread of the geophones (e.g. Cletwr 4&5, 6&7), the plus time could not be calculated using the standard Common Receiver Point method. In these cases an estimated value for the reciprocal time was calculated from the intercept time (T_i) (Figure 3.16). The intercept time was estimated by extrapolating the best fit line for a segment of a travel-time graph, corresponding to the appropriate refractor arrivals, back to the point on the time axis that corresponds with the shot point. An estimated value of T_{AB} calculated using the intercept time was then used to calculate values of the plus time for each geophone, and these estimated plus time values could then be used as a substitute, in association with the minus time, to calculate the depth and morphology of the refractor (Z) (Figure 3.16).

Because the calculated reciprocal time is an approximation rather than a direct field measurement then this method is not as accurate a method to calculate the plus time as the standard Common Receiver Point method. Using the intercept time to calculate a substitute for a direct measurement of the reciprocal time was therefore used only
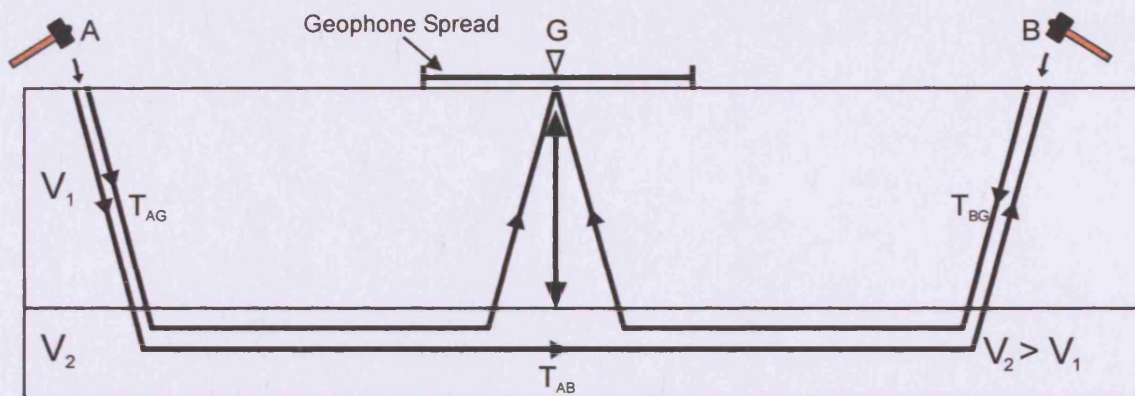
Minus Time = $(T_{AG} - T_{BG}) / 2$

Plus Time = $T_{AG} + T_{BG} - T_{AB}$

Depth (z) = $0.5 \times$ Plus Time $\times (V_2 \times V_1)/(V_2^2 - V_1^2)^{0.5}$

Figure 3.14: Common Receiver Point Method, used to calculate the depth of a refractor (G = geophone; V = velocity; T_{AB} = reciprocal time).
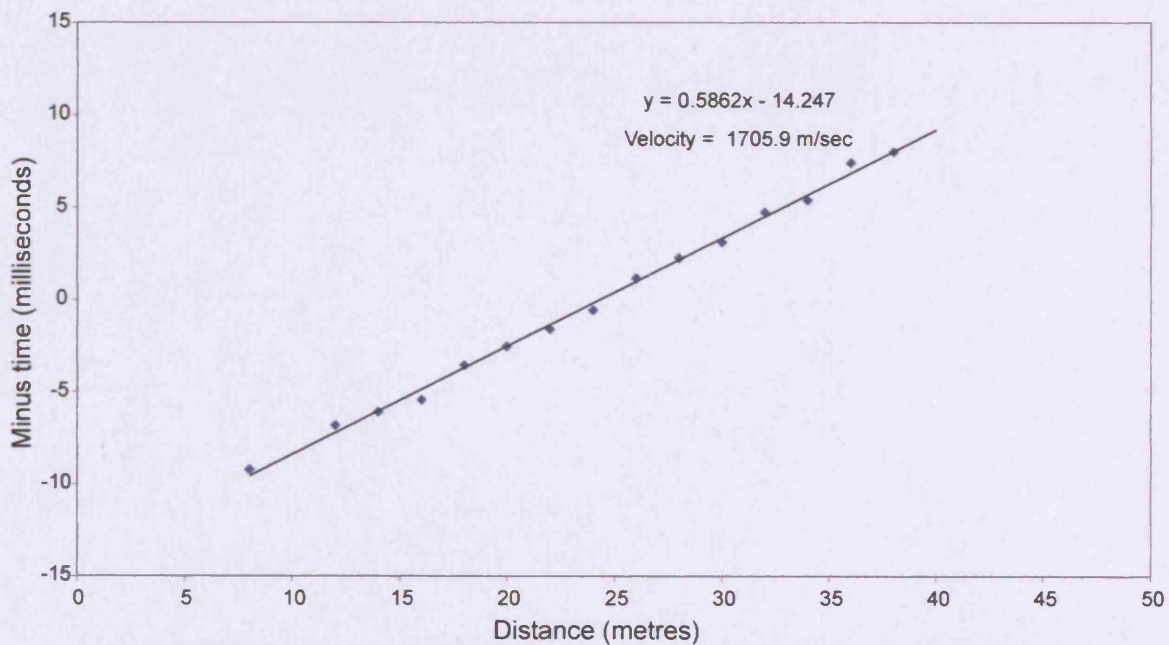
Figure 3.15: Minus graph produced from Shots 1 and 2 from reversed seismic refraction survey, Rhos Llawr Cwrt, Cletwr Fawr valley. This method of calculating velocity is more accurate than that calculated in Figure 3.13 where velocity is derived from the gradient of the best fit line for each shot.
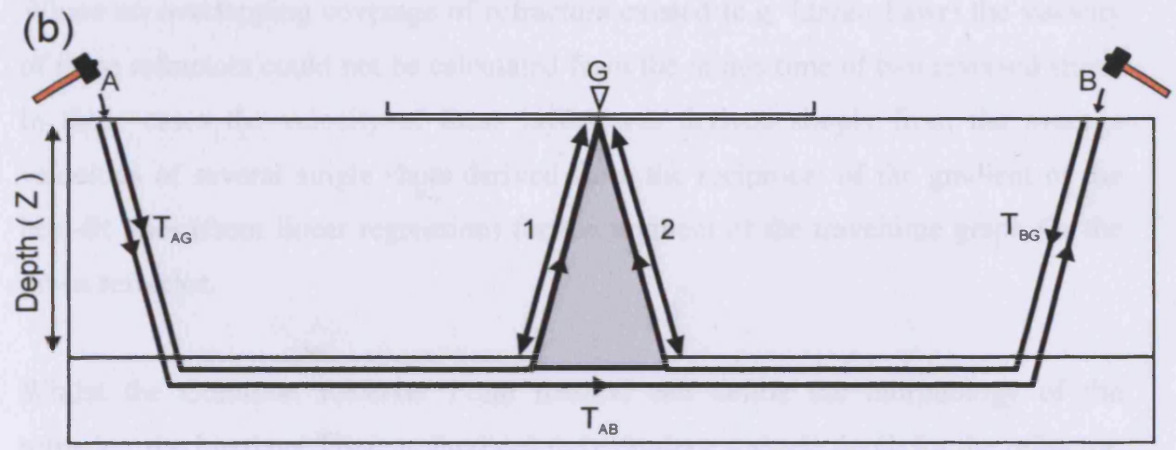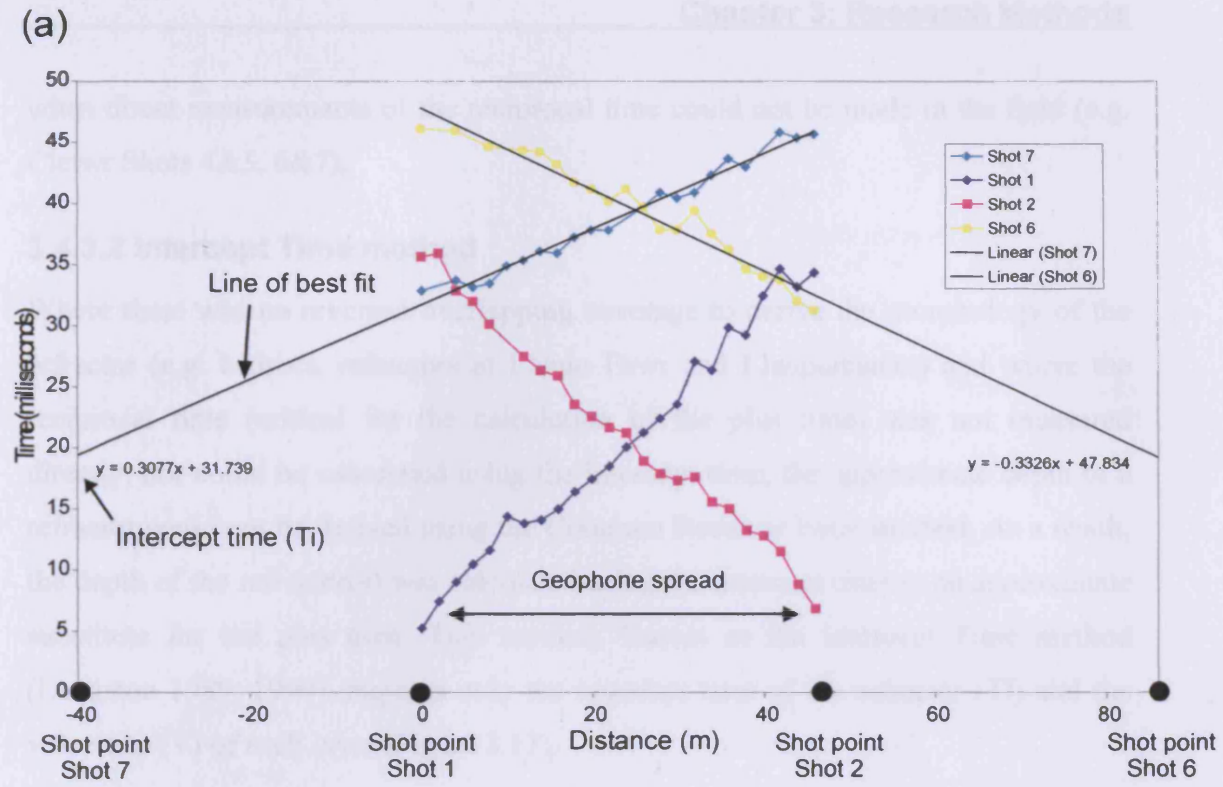
Figure 3.16: (a) Traveltime graph with best fit lines for Shots 6 and 7 extrapolated back to the shotpoints to demonstrate the intercept time for each shot. Data from Rhos Llawr Cwrt, Cletwr Fawr valley. (b) How the intercept time can be used to calculate the reciprocal time (T_{AB}) for use in the Common Receiver Point method.

when direct measurements of the reciprocal time could not be made in the field (e.g. Cletwr Shots 4&5, 6&7).

3.4.3.2 Intercept Time method

Where there was no reversed overlapping coverage to derive the morphology of the refractor (e.g. bedrock refractors at Llanio Fawr and Llanpumsaint) and where the reciprocal time (critical for the calculation of the plus time) was not measured directly, nor could be calculated using the intercept time, the approximate depth to a refractor could not be derived using the Common Receiver Point method. As a result, the depth of the refractor(s) was calculated using the intercept time as an approximate substitute for the plus time. This method, known as the Intercept Time method (Lankston 1989, 1990), requires only the intercept time of the refractor (Ti) and the velocities (V) of each layer (Figure 3.17).

Where no overlapping coverage of refractors existed (e.g. Llanio Fawr) the velocity of these refractors could not be calculated from the minus time of two reversed shots. In these cases the velocity of these layers was derived simply from the average velocities of several single shots derived from the reciprocal of the gradient of the best-fit lines (from linear regression) for the segment of the traveltime graph for the given refractor.

Whilst the Common Receiver Point method can define the morphology of the refractor, the Intercept Time method can only produce a single depth for the refractor. The Intercept Time method assumes planar and horizontal boundaries, increasing velocity with depth and that each layer is sufficiently thick (Lankston 1989). By shooting reversed refraction data and averaging the velocities, a dipping refractor model can be identified from the two intercept times. However, even with reversed data all that can be achieved is a straight line between the two calculated depths (Lankston 1989). If the refractor is undulating or its lateral velocity varies then the intercept time method will produce a model that oversimplifies the true geology. However, as the aim of the seismic refraction investigations undertaken in this project was simply to estimate the thickness of superficial geology to calibrate the interpretation of the resistivity data, rather than characterise the morphology of rockhead, then the use of the Intercept Time method is still valid.

Figure 3.17: Intercept Time method of establishing the depth of a refractor. The intercept time (T_i) is used as a substitute for the plus time in calculations of the depth of the refractor when the plus time cannot be calculated using the Common Receiver Point method.

3.5 Ground penetrating radar

3.5.1 Introduction

Ground penetrating radar (GPR) uses high frequency electro-magnetic pulses (1-1000 MHz) to detect variations in the dielectric properties of subsurface materials, with the potential to provide high-resolution images of the shallow subsurface (0-40 m) (Davis and Annan 1989). GPR is based on the measurement of the travel time of a transmitted electromagnetic (EM) wave (generated by a transmitter antenna), which is reflected from various subsurface interfaces and detected by a receiver antenna, producing a reflection (Figure 3.18). Where transmitter antennae are unshielded, direct EM waves are transmitted both through the air and through the ground (air and ground waves). In the ground the signal is either reflected or scattered by changes in the electrical properties (electric permittivity, conductivity and magnetic permeability) or absorbed (Davis and Annan 1989). Where significant changes in the dielectric properties and velocity occur, as a result of changes in material, temperature, moisture and density, part of the wave is reflected back to the surface from boundaries between materials of varying electrical properties. The electrical properties of unconsolidated Quaternary geological materials are mainly controlled by the fresh water content. Changes in water content are important for producing radar reflections because the dielectric permittivity (ε_r) of water is much greater than most dry geological materials (Davis and Annan 1989). Ideal conditions for GPR surveys are resistive sediments and materials such as sands, gravels, peat, limestone and ice (Scott *et al.* 1990; Jol and Bristow 2003). These materials are characterised by low permittivity, which causes high velocities, and/or low conductivity (high resistivity), which results in lower attenuation (Table 3.1). GPR surveys typically work poorly in areas of fine-grained sediments (silts and clays) of low resistivity and in areas of saline or contaminated groundwater where the radar signal is rapidly attenuated, causing limited penetration depths (Table 3.1). As higher frequencies are preferentially attenuated to some degree as waves propagate through the earth regardless of the material, the return centre frequency of the waves at the receiver is always lower than the frequency of the transmitted wave.

Figure 3.18: Ground penetrating radar data acquisition using the common offset profiling setup (adapted from Jol and Bristow 2003, Neal 2004).

There is a trade off between the range and resolution of GPR surveys (Davis and Annan 1989). Attenuation decreases as the frequency is lowered, but at the same time vertical resolution also decreases (Davis and Annan 1989; Jol 1995; Smith and Jol 1995) (Table 3.2). Low frequency antennae (10-50 MHz) have longer wavelengths that yield greater penetration depths (Smith and Jol 1995). High frequency antennae (400-1000 MHz) have shorter wavelengths that yield high-resolution data but shallower penetration depths. Radar systems with centre frequencies of around 100 MHz provide the best compromise between the depth of penetration, the vertical resolution and the portability of the equipment (Davis and Annan 1989). The transmitter power is also important, greater output resulting in a greater depth of penetration (Jol 1995; Smith and Jol 1995). Where possible, all antennae frequencies and transmitter powers should be tested at a site prior to extensive surveys being undertaken (Jol 1995; Jol and Bristow 2003).

Reflections are only generated by reflectors where the thickness of the vertical change in physical properties is greater than or equal to the wavelength of the radar signal. If the wavelength is greater than the thickness of individual beds then individual reflections may represent composites of interference from several layers (Vaughan *et al.* 1999; van Dam *et al.* 2003). The greatest vertical resolution that can be theoretically expected is ¼ of the wavelength (Jol and Bristow 2003) although in most surveys the vertical resolution is found to be two to three times the theoretical value (Schwamborn *et al.* 2002).

If the dielectric permittivity of the materials above a reflector is known, then the two-way travel time (TWT) to that reflector can be converted to depth estimates (Scott *et al.* 1990; Annan and Cosway 1992). Measurements of the signal velocity in the ground can be determined using common midpoint (CMP) surveys or wide-angle reflection and refraction (WARR) sounding. Once average velocities have been obtained then the TWT can be converted to depth estimates. In CMP surveys the transmitter and receiver antennae are first placed at the minimum spacing separation. The antennae spacing is gradually increased by moving them apart along a line at intervals of 5-10 cm (total separation 10-20 cm) around a centre point (Figure 3.19). The direct airwave and ground wave can be observed from this data, followed by other reflected and refracted waves (Figure 3.19). By measuring the time move out

versus the antennae separation for the various wavefronts, the radar propagation velocity versus depth can be estimated. The groundwave can be used to calculate the velocity of the material.

Table 3.1: Electrical properties of common geologic materials at 80-120 MHz (Davis and Annan 1989; Reynolds 1997; Neal 2004)

Medium	Relative dielectric permittivity (ε_r)	Electromagnetic -wave velocity (V) (m/ns)	Conductivity (σ) (mS/m)	Attenuation (α) (dB/m)
Air	1	0.3	0	0
Fresh water	80	0.033	0.5	0.01-0.1
Distilled water	80	0.033	0.01	0.002
Seawater	80	0.01	30,000	1000
Unsaturated sand	2.55-7.5	0.1-0.2	0.01	0.01-0.14
Saturated sand	20-31.6	0.05-0.08	0.1-1	0.03-0.5
Unsaturated sand and gravel	3.5-6.5	0.09-0.13	0.007-0.06	0.01-0.1
Saturated sand and gravel	15.5-17.5	0.06	0.7-9	0.03-0.5
Unsaturated silt	2.5-5	0.09-0.12	1-100	1-300
Saturated silt	22-30	0.05-0.07	100	1-300
Unsaturated clay	2.5-5	0.09-0.12	2-20	0.28-300
Saturated clay	15-40	0.05-0.07	20-1000	0.28-300
Unsaturated till	7.4-21.1	0.1-0.12	2.5-10	-
Saturated till	24-34	0.1-0.12	2-5	-
Freshwater peat	57-80	0.03-0.06	<40	0.3
Limestone	4-8	0.12	0.5-2	0.4-1
Shales	5-15	0.09	1-100	1-100
Silts	5-30	0.07	1-100	1-100
Clays	5-40	0.06	2-1000	1-300
Granite	4-6	0.13	0.01-1	0.01-1
Dry salt	5-6	0.13	0.01-1	0.01-1
Ice	3-4	0.16	0.01	0.01
Permafrost	1-8	0.106-0.3	-	-

Table 3.2: Theoretical resolutions of GPR surveys for particular sediments and antennae frequencies (from Jol and Bristow 2003):

Antenna frequency	Lithology		
	Saturated sand (V = 0.06 m/ns)	Damp sand (V = 0.1 m/ns)	Dry sand (V = 0.15 m/ns)
50 MHz	0.3-0.6 m	0.5-1.0 m	0.75-1.5 m
100 MHz	0.15-0.3 m	0.25-0.50 m	0.375-0.75 m
200 MHz	0.075-0.15 m	0.125-0.25 m	0.1875-0.375

3.5.2 Applications

GPR is now a commonly utilised tool for modern stratigraphic and sedimentary investigations, particularly of aeolian sands and fluvioglacial sand and gravel deposits (Bristow and Jol 2003a, 2003b; Neal 2004). The method has also had wide application in studies of peatland thicknesses and stratigraphy (Warner *et al.* 1990; Theimer *et al.* 1994; Jol and Smith 1995; Völkel *et al.* 2001; Slater and Reeve 2002; Leopold and Völkel 2003; Comas *et al.* 2004, 2005) and for glaciological investigations (Plewes and Hubbard 2001). GPR is a particularly suitable technique for the investigation of frozen ground (Annan and Davis 1976; Davis *et al.* 1976; Dallimore and Davis 1987, 1992). This is because frozen soils are highly resistive as porewaters are frozen, minimising signal attenuation. The electrical properties of frozen soils indicate that radar signals should be capable of penetrating to depths of 3-30 m with more resolution than other techniques (Annan and Davis 1976). Dallimore and Davis (1987) demonstrate that under favourable site conditions (ice-rich permafrost with high impedances) reflectors at 60 m depth can be detected with 30 MHz antennae. The resolution of GPR surveys is also enhanced in permafrost. For example, a 500 MHz antenna will have a resolution of 24 cm in dense snow, 20 cm in ice and less in permafrost (Arcone *et al.* 1995).

The application of GPR to permafrost research was pioneered by the Geological Survey of Canada (Scott *et al.* 1974; Annan *et al.* 1975; Davis *et al.* 1976; Annan and Davis 1976; Dallimore and Davis 1987). Since then it has been utilised for a wide variety of frozen ground investigations (Vonder Mühll *et al.* 2001; Moorman *et al.* 2003), including the thickness of the active layer, groundwater and bedrock profiling (Arcone *et al.* 1998), the position of the permafrost table and ice wedges (Hinkel *et al.* 2001), mapping contamination (Pettersson and Nobes 2003), the internal structure
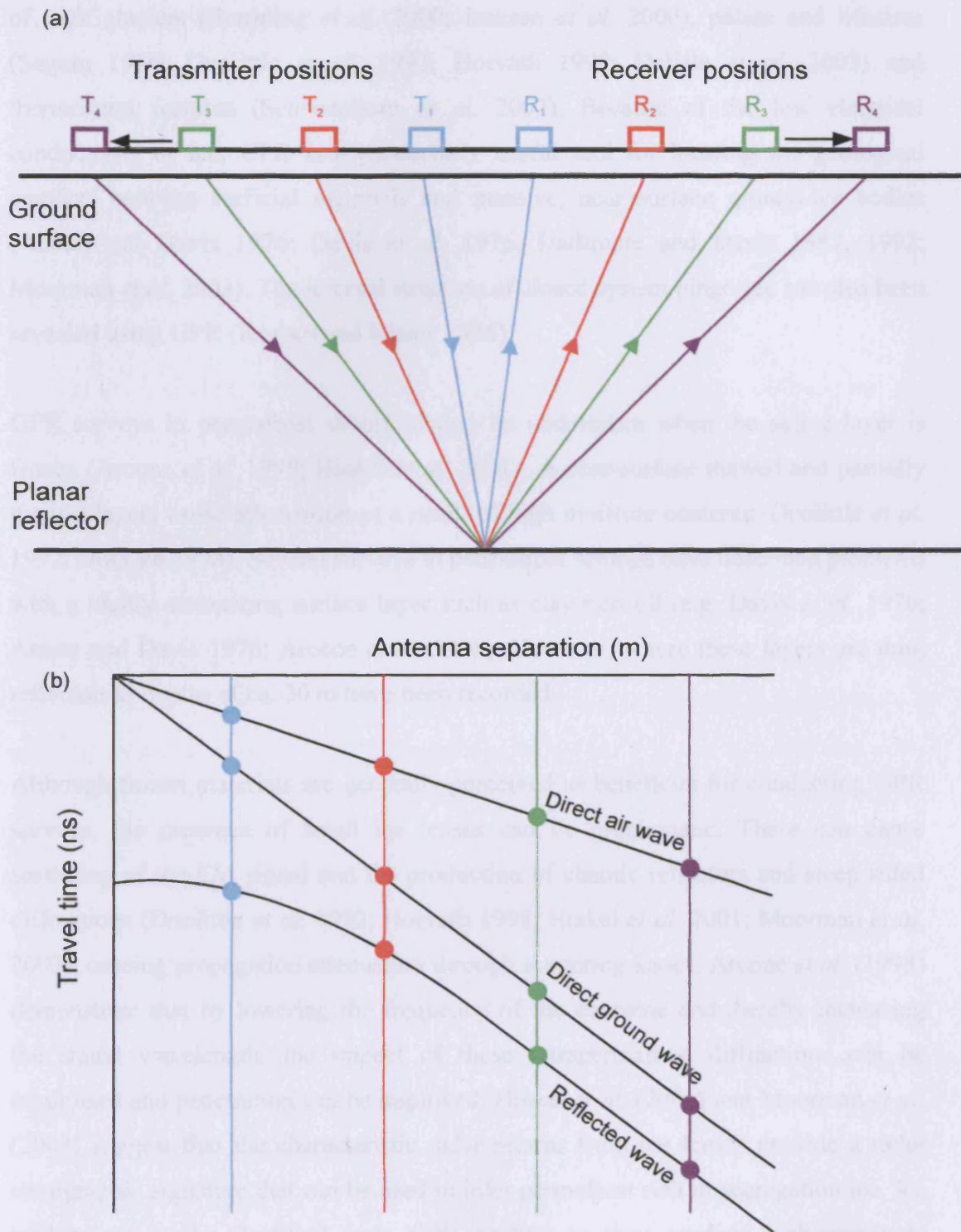
Figure 3.19: (a) Standard setup for common midpoint (CMP) survey, used to establish EM wave velocity; (b) Theoretical example of data acquired (separation vs traveltime plot) (adapted from Jol and Bristow 2003, Neal 2004).

of rock glaciers (Berthling *et al.* 2000; Isaksen *et al.* 2000), palsas and lithalsas (Seguin 1986; Doolittle *et al.* 1992; Horvath 1998; Delisle *et al.* 2003) and thermokarst features (Schwamborn *et al.* 2002). Because of the low electrical conductivity of ice, GPR is a particularly useful tool for locating the geological contacts between surficial materials and massive, near surface ground-ice bodies (Annan and Davis 1976; Davis *et al.* 1976; Dallimore and Davis 1987, 1992; Moorman *et al.* 2003). The internal structure of closed system pingo-ice has also been revealed using GPR (Kovacs and Morey 1985).

GPR surveys in permafrost should always be undertaken when the active layer is frozen (Arcone *et al.* 1998; Hinkel *et al.* 2001), as near-surface thawed and partially thawed layers cause attenuation as a result of high moisture contents (Doolittle *et al.* 1992; Horvath 1998). Several surveys in permafrost settings have described problems with a highly attenuating surface layer such as clay-rich till (e.g. Davis *et al.* 1976; Annan and Davis 1976; Arcone *et al.* 1998). However, where these layers are thin, reflectors at depths of ca. 30 m have been recorded.

Although frozen materials are generally perceived as beneficial for conducting GPR surveys, the presence of small ice lenses can be problematic. These can cause scattering of the EM signal and the production of chaotic reflectors and steep sided diffractions (Doolittle *et al.* 1992; Horvath 1998; Hinkel *et al.* 2001; Moorman *et al.* 2003), causing propagation attenuation through scattering losses. Arcone *et al.* (1998) demonstrate that by lowering the frequency of the antennae and thereby increasing the signal wavelength, the impact of these intrapermafrost diffractions can be minimised and penetration can be improved. Hinkel *et al.* (2001) and Moorman *et al.* (2003) suggest that the characteristic radar returns from ice lenses provide a radar stratigraphic signature that can be used to infer permafrost rich in segregation ice. Ice wedges are easily identified from GPR profiles as they produce high-amplitude hyperbolic reflections (Hinkel *et al.* 2001). Despite the advantages that the ice-content of permafrost has for the GPR method, GPR signals still attenuate significantly in frozen clays and silts (Hoekstra and Delaney 1974; Davis *et al.* 1976; Delaney and Arcone 1984; Arcone and Delaney 1989). Despite being below zero, these materials contain unfrozen absorbed water that significantly affects relative permittivity (ε_r) (Delaney and Arcone 1984).

3.5.3 Equipment and data acquisition

GPR was chosen as a suitable geophysical technique for the investigation of the internal structures of active open system pingos in Svalbard. The target depths of pingo ice-cores are within the potential depth of investigation of GPR and the electrical properties (permittivity, conductivity) of the pingo ice would be expected to have strongly contrasting electrical properties to the host geological materials, thereby enabling the geometry of the pingo ice to be defined.

A Sensors and Software, Pulse EKKO 100 GPR system was utilised for the investigations (Figure 3.20). To optimise the conditions for the surveys, fieldwork was conducted during April 2004, before thaw of the active layer (Arcone *et al.* 1998; Hinkel *et al.* 2001). Survey lines were conducted in common-offset reflection profiling step mode using unshielded 50 or 100 MHz antennae in a perpendicular broadside setup. The use of the step-mode should have resulted in more coherent and higher amplitude reflections than would be achieved in a continuous profiling mode, as the antennae are stationary, therefore enabling better antennae-ground coupling and trace stacking (Neal 2004). Antennae separations of 2 m and 1 m and step sizes of 0.5 m and 0.25 m were used in combination with the 50 and 100 MHz antennae respectively. These are in accordance with recommendations (Annan and Cosway 1992; Jol and Bristow 2003), and do not exceed Nyquist sampling intervals. The pulser voltage was 400 volts and the time window was 600 ns (100 MHz antennae) or 860 ns (50 MHz antennae). The traces were stacked 32 times to reduce the signal-to-noise ratio. The sampling rate was 1600 ps for surveys conducted at 50 MHz and 800 ps at 100 MHz. Preliminary CMP surveys were also undertaken using the 100 MHz antennae with antennae separations of 10 cm and 20 cm. However, due to operational problems with the GPR system no CMP surveys with total separations of greater than 5.9 m could be performed.

3.5.4 Processing

Following data editing (correction and merging of lines, deletion of traces etc.), the GPR survey lines were processed using the REFLEX (Version 3) processing package. Processing involved application of the following steps a) move start time (time zeroed), b) subtract mean (dewow), c) gain function, d) time cut, e) bandpass frequency, f) static correction (topographic adjustment) (Figure 3.21).

3. Information travels to computer via fibre-optic cables

2. EM waves reflect off underground layers and are received by the receiver antenna

1. Transmitter antenna sends EM waves into the ground
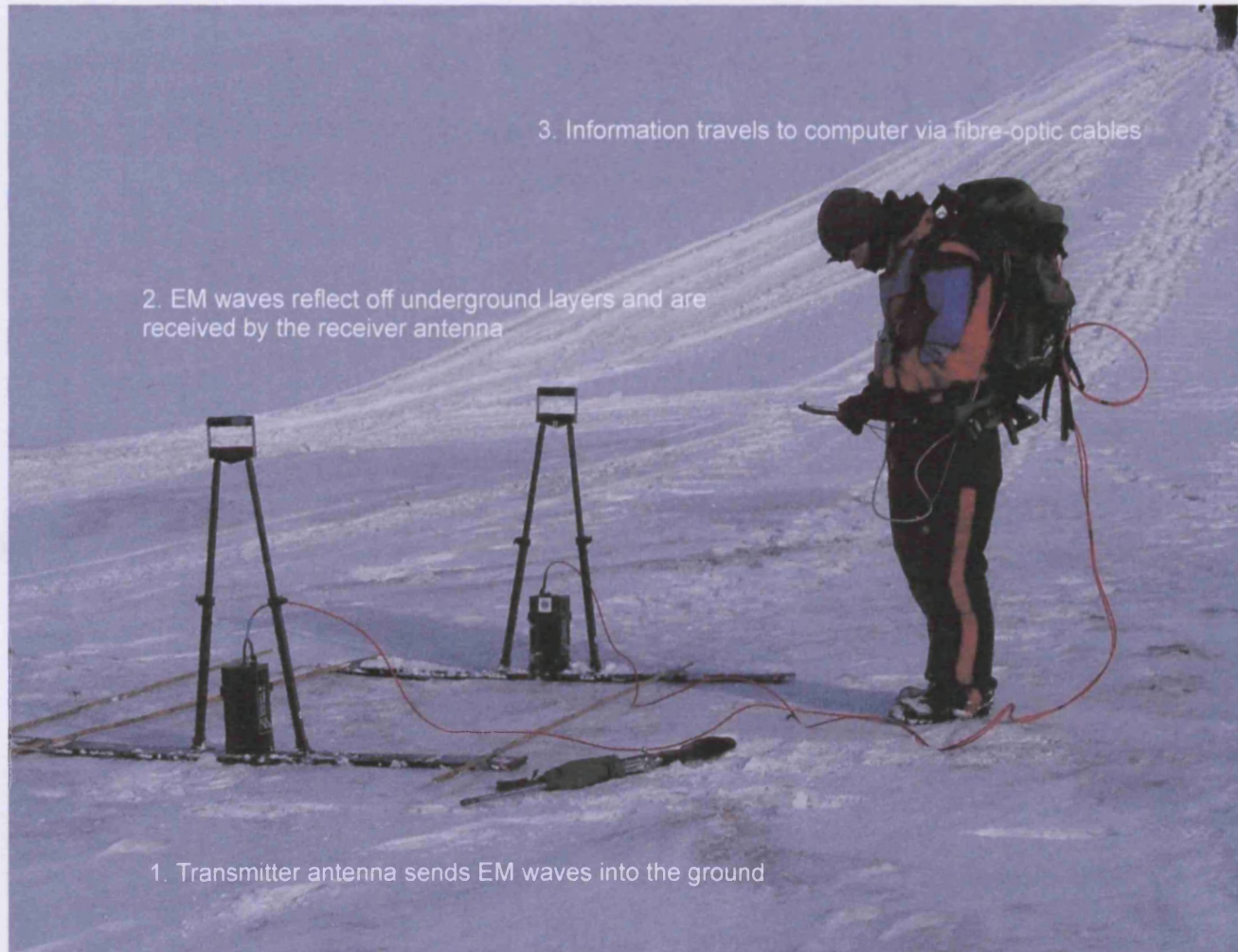
Figure 3.20: Pulse Ekko 100 GPR system used for field surveys in Svalbard (Photo: H. H. Christiansen).
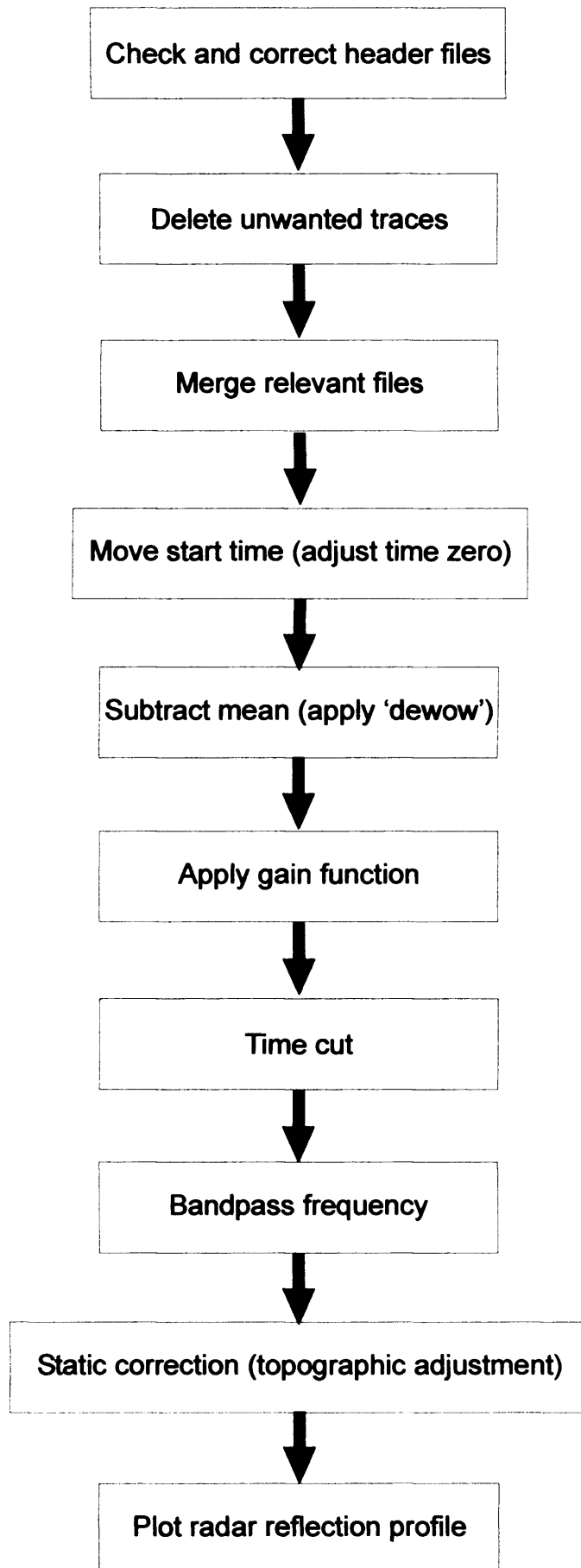
Figure 3.21: Flow diagram of processing sequence applied to GPR surveys conducted for this project.

The dewow filter applied removed very low-frequency components ('wow') of the data which were superimposed on higher frequency reflections. The very low frequency components are caused by the short period between repeated shots causing signal saturation of the receiver from energy input from airwave, groundwave and near-surface reflectors. The low frequency signals are caused by inductive phenomena or possible instrumentation dynamic range limitations (Annan 1999).

The time gain function was applied to the GPR sections to amplify the radar signal amplitude at depth, which falls off with time. In materials of high attenuation, depths of only 1 or 2 metres can be penetrated, even with low frequency antennae, due to conductivity losses in the sediment (Jol and Bristow 2003). A spherical and exponential gain compensation (SEC) was applied to the data to correct for the decrease in the signal amplitude at depth/with time. This was preferred over automatic gain control (AGC), which calculates the average signal over a time window and then amplifies or attenuates the radar signal to equalise all signals. Where signals are weak the gain is large and where the signal is strong the gain is small or attenuated. Therefore AGC can destroy any information on reflection amplitude and amplify both reflections and noise. However, this is not important for many sedimentological studies where continuity of reflections is the main aim of the surveys. The SEC gain instead attempts to maintain the variation of signal amplitude as it propagates downwards, preserving the amplitude fidelity (Annan 1999). This is a linearly increasing time gain combined with an exponential increase to compensate for spherical spreading losses and exponential dissipation of energy.

A timecut was used to truncate the lower parts of the GPR profiles that contained no data as they were below the depth of maximum penetration of the radar signal. To reduce random and high frequency noise, a bandpass frequency filter was applied to remove low and high frequency bands from the data set. This should improve the signal-to-noise ratio and enhance the visibility and lateral continuity of the primary reflections. Bandpass frequency filters are deemed better than horizontal running-average filters, which emphasise horizontal or gently dipping reflections and remove more steeply dipping ones (Neal 2004). Running averages reduce horizontal and vertical resolution and can distort or remove important reflections.

The final step applied to the data was a topographic correction. The topographic data were collected using an EDM survey. The static corrections applied to the TWT of the GPR profiles were based on this data and on the published velocities of EM waves through permafrost and the preliminary velocities estimated from the CMP surveys.

3.6 Sedimentological techniques

3.6.1 Vibro-coring

An Atlas Copco Cobra vibro-coring system was utilised to drill boreholes for sedimentological analysis (Figure 3.22). The system uses a two-stroke percussion drill that drives an open-window core-barrel, connected via extension rods, into the ground. Once the 1 m long core barrel is filled with sediments, the barrel is jacked out of the ground by hand using a leverage jacking system. The depth of penetration depends on the nature of the substrate, but in silts and clays is generally up to around 10 m. The vibrocorer technique is normally relatively ineffective in sands and gravels. Use of progressively smaller diameter core barrels with increasing depth increases the range of the equipment. A 0.5 m long, 95 mm diameter barrel was used for the uppermost metre of sediments. At greater depths, 1 m long barrels with diameters of either 65 mm or 40 mm were utilised depending on ground conditions. The cores were logged in the field through the open windows of the core barrels following British Standard 5930 (1999), using a Munsell chart to describe the colour of the sediments. Representative disturbed samples were collected in sealable airtight plastic sample bags for later laboratory analysis.

3.6.2 Clast fabric analysis

Clast fabric measurements from sections exposed by trenching and trial pitting of ramparts of landforms in the Hirwaun and Cledlyn valleys were collected using a compass clinometer. Measurements of the dip and orientation of at least 25 clasts were measured from each trial pit, whilst trenches were divided into subsamples (e.g. 2 m wide sections) from which at least 25 clasts could also be measured. The presentation and eigenvalue analysis of clast fabric data was undertaken using StereoWin v1.2. The data was plotted (scatter plots and contour diagrams of linear data) as lower hemisphere equal area stereonets and contoured using the 1% area contour method. The eigenvalues (normalised to 1) and corresponding eigenvectors were calculated using a Bingham Axial Distribution statistical analysis and were summarised on standard graphs (Dowdeswell and Sharp 1986) and triangular fabric shape diagrams (Benn 1994a).

Figure 3.22: Atlas Copco Cobra vibro-coring system used to drill boreholes at sites in Wales. (a) two-stroke percussion drill in operation; (b) 0.5 m long, 95 mm diameter open window core barrel used for the upper 1 m of sediment; (c) 1 m long, 40 mm diameter open window core barrel used for drilling to depth. Photo (a) by P.J. Brabham.

3.6.3 Grain-size analysis

Samples were analysed for grain-size properties in the laboratory following British Standard 1377 (1990) for dry and wet sieving, using a Sedigraph to analyse the fraction <63µm. The minimum sample size analysed was, where possible, >100 g for sand or smaller and >200 g for fine gravel. Samples were oven dried at 60°C for 24 hours, unless they had a significant clay content, in which case they were air dried for 1 week. Dried samples were disaggregated using a rubber bung and mortar.

500 ml of water and 25 ml of Calgon dispersant were added to a large sub-sample (where possible at least >100 grams) of sediment. This mixture was allowed to stand for at least 1 hour before being washed through a 2 mm and 63 µm sieve. Material from both sieves was collected into an evaporating dish and dried in the oven overnight at 100°C before being sieved through a standard nest of sieves on a mechanical sieve shaker. The fraction retained on each sieve was weighed and cumulative percentage passing curves were plotted in EXCEL for the fraction > 63 µm.

A small subsample (<20 grams) of the original dried and disaggregated material was dispersed in Calgon and washed through a 63 µm sieve. The washings were collected in a tray and then dried in an oven at 100°C. This dried fraction was disaggregated using a rubber bung and mortar. Two grams of this disaggregated sediment was added to 40 ml of Calgon and passed through a sedigraph. This data was then combined with the analysis of the fraction >63 µm to plot a cumulative percentage passing curve for the entire sample in EXCEL.

3.7 Topographical surveying

At sites where high-resolution LiDAR data were not available, site surveys, utilising a Topcon EDM theodolite, target prism and the triangulation of ground stations (including borehole locations), were undertaken to produce digital terrain models of the landforms under investigation and the surrounding topography. Accuracy is estimated to within ± 50 mm, limited by repeatability in target location rather than instrument error. The EDM surveys and the locations of boreholes, trenches, trial pits and geophysical surveys were georeferenced using a handheld Garmin GPS system (nominal accuracy ± 10 m).

3.8 Geographical information systems (GIS) techniques

Identification of sites in Wales was performed throughout the research period using a wide array of literature resources in association with the application of several GIS techniques (see Ross *et al.* 2005a for more details). The most important for remote confirmation of sites identified from the literature was the Countryside Council for Wales Getmapping© aerial photographic resource for Wales. The entire resource, north of a west-east line between 169000.200000 and 305000.200000, was examined through the ERMapper interface software. As well as confirming the positions of several sites recorded in the published literature, new sites were also discovered (e.g. near Bodowen). The selection of sites for geological investigation was undertaken through a programme of preliminary field surveys during summer 2003 (Ross *et al.* 2005a).

Geomorphological mapping of sites was performed using Getmapping© aerial photography in ArcView Version 3.2, supplemented by stereoscopic aerial photography resources provided by the Central Register of Air Photography for Wales (National Assembly for Wales) and by LiDAR digital terrain data provided to the project by the Environment Agency. Field mapping of landforms was not possible over such a large area due to financial constraints and access difficulties, so remotely sensed mapping was not ground truthed, as recommended even for sites with LiDAR coverage (Smith *et al.* 2006). Nevertheless, confidence in the mapping of those sites with LiDAR data is high given the high-resolution nature of this datasets, the use of which has been recommended as a base map for high-resolution geomorphological mapping and for evaluating the accuracy of field mapping (Smith *et al.* 2006).

Mapping was also supported by lower-resolution digital terrain model datasets. NEXTMap digital terrain data was supplied from the British Geological Survey (BGS) for areas within the Cardiff University-BGS collaborative project 2K03E024. Where sites were beyond the boundaries of interest for this project (e.g Crychell Moor), Ordnance Survey products (OS Panorama® and OS Profile®) were used to provide coarse-resolution digital terrain model data (Table 3.3). The Ordnance Survey historical map derived datasets perform extremely poorly for the visualisation of even large-scale glacial landforms (Smith *et al.* 2006), but do provide a representation of

the general context of the large-scale geomorphology. Geomorphological maps were produced in ArcView Version 3.2 using the Ordnance Survey LANDLINE 1:10,000 dataset as a base layer. 'Raw' digital terrain model data were presented as shaded relief images in SURFER©.

Table 3.3: Horizontal and vertical resolution of digital terrain model (DTM) datasets used in this project (From Smith *et al.* 2006).

Digital Terrain Model	Nominal horizontal resolution (m)	Relative vertical accuracy (m)
LiDAR	2	0.25
NEXTMap	5	1
OS Panorama ®	50	5
OS Profile ®	10	5

4 Hirwaun Valley

4.1 Introduction

Numerous linear ridges, interspersed with occasional enclosed circular forms, are located across the upper Afon Hirwaun valley at altitudes of 110-130 m OD (Figures 4.1, 4.2 and 4.3). Originally interpreted as relict open system pingos by Watson (1972), these landforms were first mapped by Bradley (1980). The site is located 4.5 km inland of the village of Aberporth and 7 km east of the extensive glaciofluvial sand and gravel deposits at Banc-y-warren and Penparc (Williams 1927; Helm and Roberts 1975; Allen 1982; Etienne *et al.* 2006).

Calcareous Irish Sea till of the St Asaph Formation (Bowen 1999, 2005), deposited by the Irish Sea glacier and containing erratic clasts from Scotland and Llŷn, north Wales, is found along the Cardigan Bay coast southwards from Llanrhystud into Pembrokeshire, and inland within the upper reaches of the northern tributary valleys of the Lower Teifi (e.g. Hirwaun and Ceri valleys) (Williams 1927; Waters *et al.* 1997; British Geological Survey 1997). Although primary fabrics within this deposit are frequently disturbed by post-depositional modification by periglacial processes, where undisturbed clast fabrics do occur they indicate an orientation of ice flow from north-northwest (315° to 355°N) (Jehu 1904; Watson 1968; John 1970a; Lear 1986; Hambrey *et al.* 2001). At its maximum extent, the Irish Sea glacier obstructed the drainage of the lower Teifi valley causing the development of a large ice-dammed lake known as Lake Teifi (Charlesworth 1929; Jones 1965; Bowen 1967; Price 1976; Bowen and Lear 1982; Lear 1986; Fletcher and Siddle 1998; Hambrey *et al.* 2001; Davies *et al.* 2003; Etienne *et al.* 2006). Glaciolacustrine deposits associated with Lake Teifi have been mapped in the lower reaches of all the north bank tributaries of the lower Teifi, including the Hirwaun valley (Lear 1986), eastwards as far as Llandysul (Waters *et al.* 1997; British Geological Survey 1997). The upper altitudinal limit of this proglacial lake is estimated at 120-125 m OD, based on the presence of deltas at Llanllwni, Rhuddlan, Pentrecwrt, Llanwnnen, Llanybydder, Pencarreg and Lampeter, (Charlesworth 1929; Jones 1965; Watson 1965, 1970; M.S. Parry *unpublished* in Bowen 2005). The landforms in the Hirwaun valley, and less well-defined features in the adjacent Ceri valley (Watson 1972), are located at altitudes of

90-130 m OD. Although originally interpreted as open system pingos (Watson 1972; Bradley 1980), it has been alternatively suggested that the Hirwaun valley landforms may have formed as a consequence of downwasting of the Irish Sea glacier rather than as a result of periglacial processes (Hambrey *et al.* 2001). If it is the case that these landforms have glacial origins then they may have the potential to provide key information on the nature of the Irish Sea glacier at the time of its maximum extent and during the initial stages of its retreat. Given the altitude of the landforms and the distribution of glaciolacustrine deposits in the Hirwaun and adjacent Ceri valley (Waters *et al.* 1997; British Geological Survey 1997), a possible link with Lake Teifi must also be considered.

The bedrock geology of the Hirwaun valley is dominated entirely by mudstones of the Nantmel Mudstones Formation of Ashgill Series (Ordovician) age (Figure 4.4). A prominent west-southwest to east-northeast trending fault has been mapped just to the south of the majority of the landforms at the site (Figure 4.4; BGS Sheet 194: Llangrannog, *unpublished map*). A bedrock exposure in small quarries at SN 28117.48003 and at Fronlas shows that bedrock is at, or near, the surface on the valley sides above an altitude of about 135-140 m OD. This is confirmed by the distribution of superficial deposits in the valley mapped by the BGS (British Geological Survey 1997; Hambrey *et al.* 2001; BGS Sheet 194: Llangrannog, *unpublished map*).
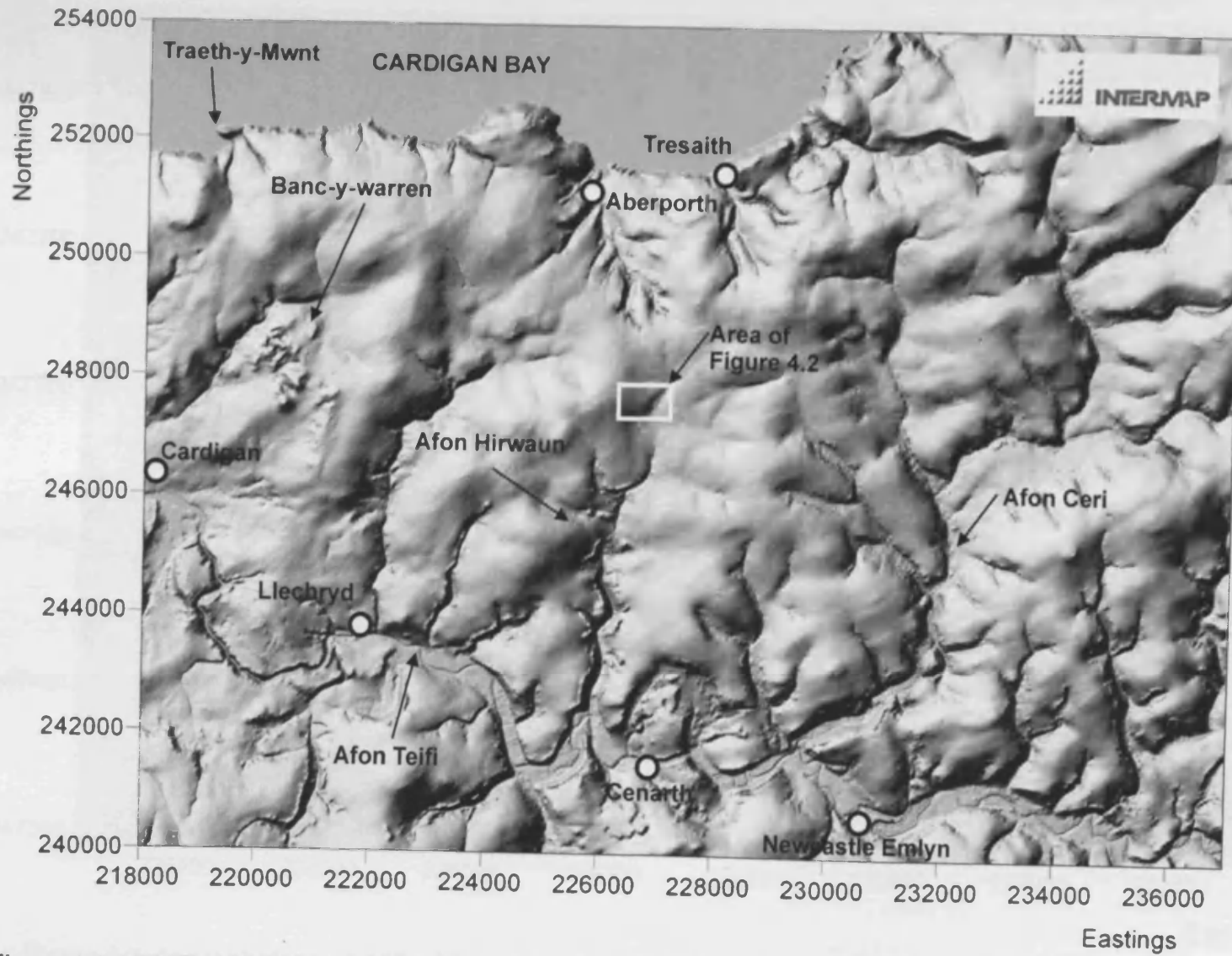
Figure 4.1: NEXTMAP digital terrain model (DTM) of the Hirwaun, Ceri and Teifi valleys (© Intermap Technologies Inc).
Area of Figure 4.2 indicated.

Figure 4.2: Aerial photograph of the Hirwaun valley with the locations of specific landforms and key farms labelled (© Getmapping Plc 2006). The Trench and Trial Pit 1 are located at Site A, and Trial Pit 2 at Site B.
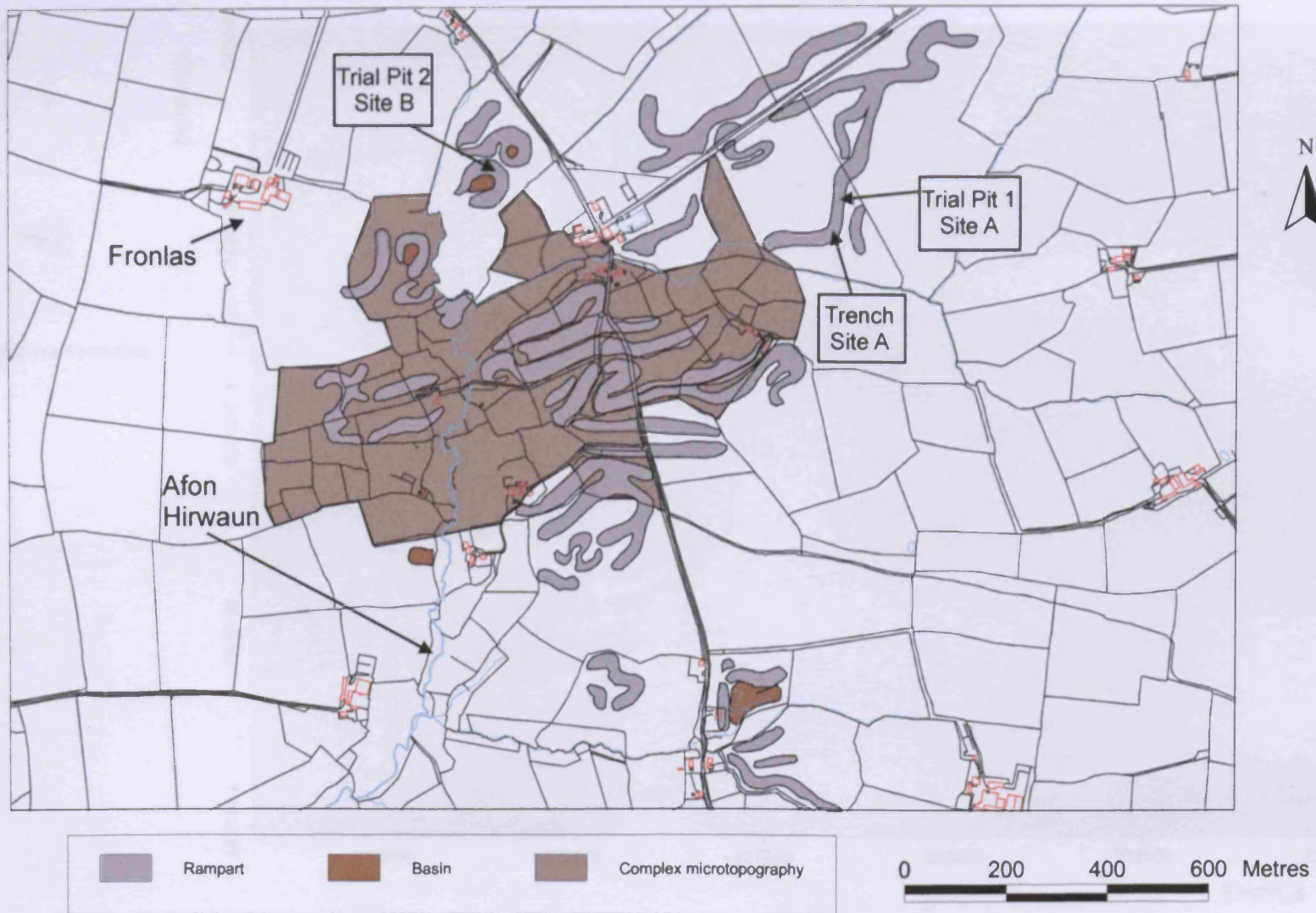
Figure 4.3: Geomorphological map of the Hirwaun valley landforms (SN 27175.47275), based on mapping from stereoscopic aerial photographs, and indicating the locations of the landforms investigated. LANDLINE data © Crown Copyright/database right 2005. An Ordnance Survey/(Datacentre) supplied service.
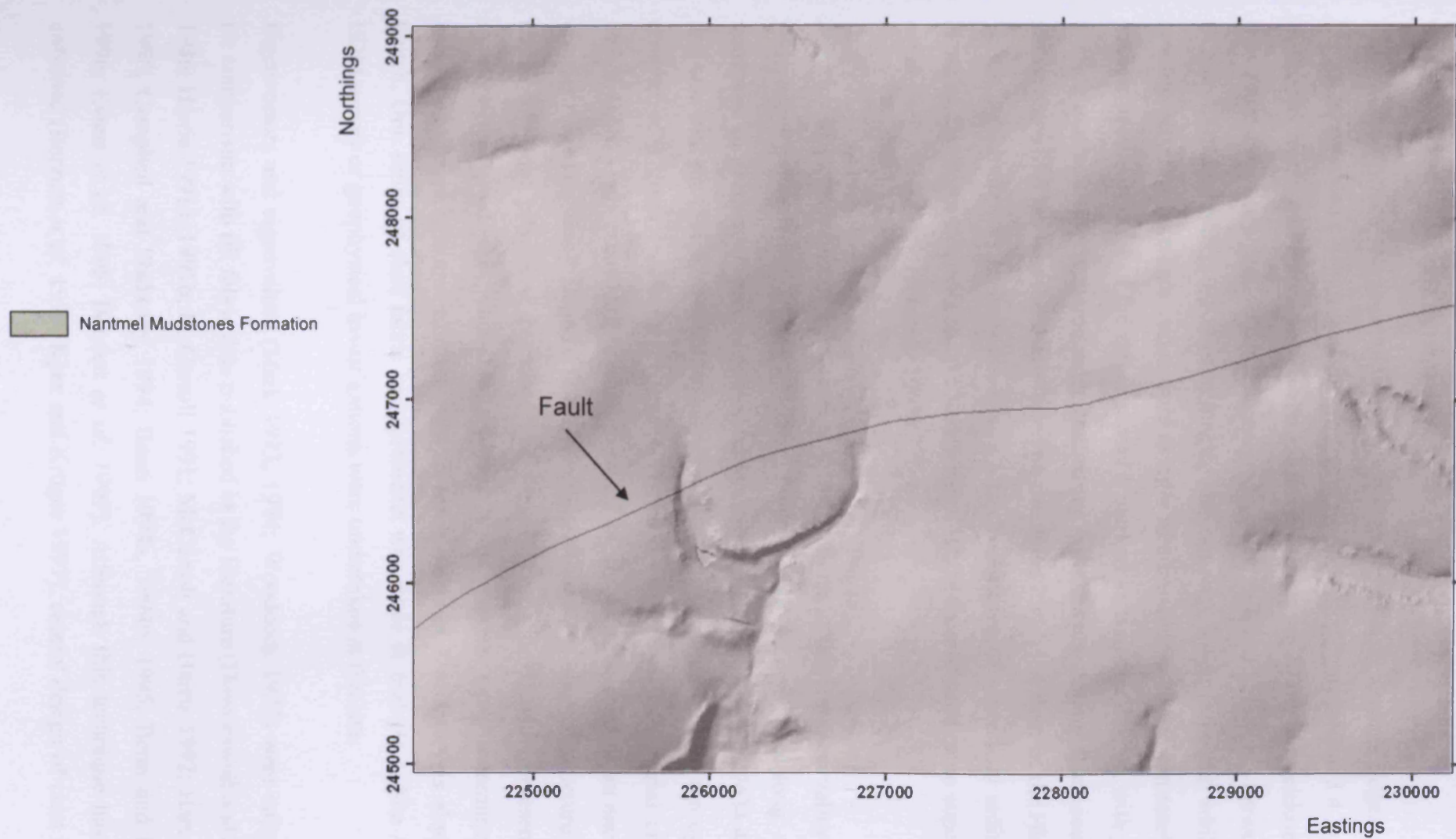
Figure 4.4: Bedrock geology of the Hirwaun Valley (© British Geological Survey) draped on the surface of a NEXTMAP digital terrain model (DTM) with 3 x vertical exaggeration (© Intermap Technologies Inc.). Note that this map is adapted from unpublished, unchecked, draft mapping by the British Geological Survey and may therefore contain some inaccuracies.

4.2 Site description and survey

The Hirwaun valley site is dominated by elongate, esker-like, sinuous ridges, which have a pronounced east-northeast to west-southwest trend (Figures 4.2 and 4.3). Only to the northwest of Penlon are circular ridges (diameter 40-75 m) that enclose what may have once been peat-filled depressions found. The linear ridges are between 20 m and 45 m in width, 50-500 m in length, and between 1-4 m in height, whilst the spacing between the ridges varies from as little as a few metres to approximately 150 m. The profile of most of the ridges shows a marked asymmetrical form, with gently sloping north-northwest facing sides contrasting with steeply sloping south-southeast facing sides. All the landforms are found on the wide, low-lying floor of the Hirwaun valley, which appears to be infilled with a thick sequence of superficial sediments. None of the ridges extends onto the valley sides, where there is little or no superficial cover (British Geological Survey 1997).

A series of excavations of landforms at two locations in the Hirwaun valley were undertaken between the 5th and 7th July 2004. At Site A, one 34 m long, north-northwest to south-southeast orientated trench (SN 27618.47384 to SN 27634.47351) and one trial pit (SN 27654.47420) were excavated, to a depth of 2 m, through the rampart of a linear landform (Figures 4.5a and 4.6). At Site B, one trial pit (SN 26976.47485) was excavated, to a depth of 2.3 m, through the crest of an enclosed, circular ridge (Figures 4.5b and 4.6c). The sedimentology and internal structure of the trench and trial pits were described and logged in the field, with representative samples recovered for grain-size analysis. Clast fabrics were determined by measuring the plunge and azimuth of >25 large clasts at 2 m intervals along the trench. One series of clast fabric measurements was made in trial pit 1, Site A. No EDM survey or geophysical investigations were undertaken at this site.

Eigenvectors and eigenvalues (Mark 1973, 1974; Woodcock 1977) were calculated for comparison with till fabric data published in the literature (Dowdeswell and Sharp 1986; Harris 1991a, 1991b; McCarroll 1991; McCarroll and Harris 1992; Hart 1994, 1995; Campbell and Shakesby 1994; Benn 1994a, 1994b, 1995; Benn and Evans 1996; Evans et al. 1995; Bennett et al. 1999). Although this technique has been criticised (Bennett et al. 1999; Kjær and Krüger 1997), careful design of clast fabric

data collection can ensure that results provide useful information on stress history and depositional process (Benn 2004). Presentation and eigenvalue analysis of clast fabric data was undertaken using StereoWin v1.2 (see Section 3.6.2). Data are presented as contoured, equal area projection stereonets (Figure 4.7).
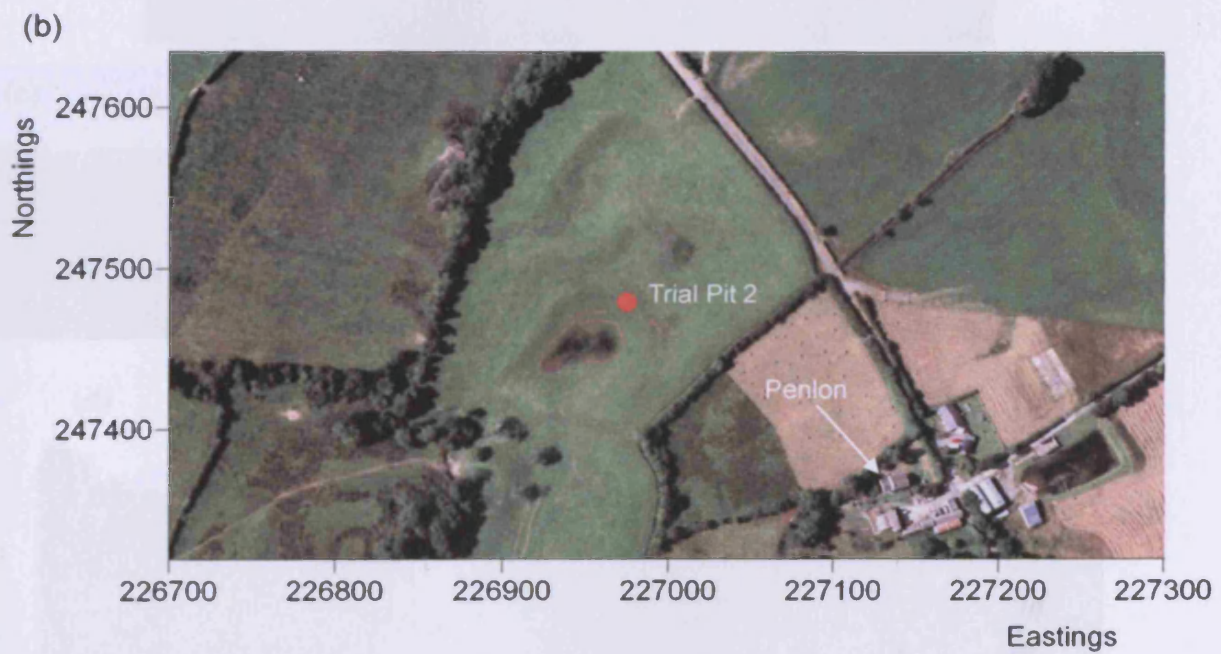
Figure 4.5: Locations of sedimentological investigations in the Hirwaun valley (a) Site A: Penlon; (b) Site B: Fronlas (aerial photographs © Getmapping Plc 2006).

(a)

↑ West

(b)

North →

(c)

↑ North

(d)

↑ West

Figure 4.6: Photographs of landforms in the Hirwaun valley: (a) Distal slope of ridge at Site A; Note the asymmetry of the 'rampart', with steep, south-facing slopes; (b) Trench at Site A, Hirwaun valley; (c) Overview of circular, ramparted landform investigated at Fronlas (Site B) in the Hirwaun valley. The peat-filled basin that is visible in earlier aerial photographs of the site has been removed as a result of agricultural improvement. Location of trial pit apparent to right of photograph; (d) View looking west along a linear ridge at Hirwaun to the west of Site A.

4.3 Results of sedimentological investigation

4.3.1 Trench

The trench at Site A was almost entirely dominated by a homogenous, matrix-supported, silty clayey diamict containing occasional large (up to cobble size), striated, subangular to subrounded clasts of mudstone and sandstone (Figures 4.7 and 4.8). This diamict was consolidated and calcareous at depths below the current soil profile, reacting strongly with 10% HCl acid. Evidence for re-precipitation of carbonate was apparent at 28.1 m along the trench, where small pedogenic nodules were developed. Fragments of shell debris were evident in samples collected from 17.5 m and 22.8 m along the trench. A >20 cm thick unit of silty, sandy, fine-gravel was seen to underlie the diamict at the proximal side of the rampart (30-31 m) but due to the limitations of the excavating equipment the total thickness of this unit could not be established. No evidence for glaciotectonism was observed in the section.

The grain-size data highlight the low clast content and homogenous properties of the diamicton (Figure 4.9). The diamicton is dominated by fine-grained sediments, with clays and silts comprising 55-80% of the total weight. There is little variation between the diamict samples analysed for grain-size, the variations in the gravel-sized content mainly reflecting the size of the occasional gravel-sized clasts measured. The sample from 30.4 m along the trench was taken from the thin unit of poorly sorted, silty, sandy, fine-gravel recorded at the base of the trench (Figure 4.7).

Although measurements of clast plunge and azimuth were made at sixteen 2 m intervals along the trench (e.g. 0-2 m, 2-4 m, 4-6 m etc.), for simplicity the data have been collated into three zones with distinct fabric signatures (0-18 m, 18-24 m and 24-32 m) (Figures 4.7 and 4.10). The eigenvalues of the summary zones are tabulated (Table 4.1), whilst the eigenvalues of the original 2 m spacing data are presented on a standard graph (Dowdeswell and Sharp 1986) and as a fabric shape diagram (Benn 1994a) to display the range of eigenvalues within each summary zone (Figure 4.11).

The first 18 m of the trench (0-18 m) was characterised by a strong unimodal and clustered clast fabric (S1 = 0.71, S3 = 0.12), with a NNW trend, perpendicular to the

106

axis of the ridge (Figure 4.7, Table 4.1). The fabric shape (the 3D distribution of the orientations of the sampled clasts) (Benn 1994a, Benn 2004) was characterised by low isotropy and high elongation (Figure 4.11b). The dip of the clasts was relatively shallow (78% of clasts dipping less than 40°) (Figure 4.10). The clast fabric measurements made beneath the crest of the ridge (18-24 m) differed markedly from those between 0-18 m. They had a weaker, more random fabric (S1 = 0.49, S3 = 0.14), with a greater proportion of clasts dipping at greater angles (38% of clasts dipping at greater than 40°) (Figure 4.10). However, the principal eigenvector was still orientated NNW, perpendicular to the ridge axis (Figure 4.7, Table 4.1). The fabric shape showed higher isotropy and lower elongation for clasts between 18-24 m (Figure 4.11b). Clast fabrics on the southeast facing side of the ridge were again characterised by greater fabric strength (S1 = 0.6, S3 = 0.18), shallow dip angles (73% dipping at angles less than 30°) and a strong NNW trend, perpendicular to the ridge axis (Figure 4.7, Table 4.1). A significant proportion of the clasts between 24-32 m do not therefore lie parallel to the southeastwardly dipping slope of the ridge, but instead dip to the north-northwest. Clasts measured between 18-24 m showed a similar fabric shape to those between 0-18 m, but with a slightly higher degree of isotropy and lower degree of elongation (Figure 4.11b)

Table 4.1: Eigenvalues, eigenvectors and plunge of clasts from Site A in the Hirwaun valley.

	S1	S3	V1 (trend) (°)	Plunge (°)
Trench 0-18 m	0.71	0.12	338.2	22.5
Trench 18-24 m	0.49	0.14	333.5	11.2
Trench 24-32 m	0.6	0.18	331.2	0.7
Trial Pit 1	0.66	0.11	316.6	5.3

4.3.2 Trial pits

Trial pit 1 was excavated into the crest of the linear rampart at Site A (Figure 4.5), perpendicular to the trench. The trial pit was dominated by the same homogenous matrix-supported diamict observed throughout the trench. Clast fabric measurements of the matrix-supported diamiction were undertaken and showed a similar fabric to those within the trench (Figure 4.12). The clasts had a slightly more northwesterly

trend (316.6°) compared to the orientation of clasts measured in the trench, but were still perpendicular to the ridge axis (Figure 4.12a). The diamicton was characterised by high fabric strength (S1 = 0.66, S3 = 0.11) and very shallow dip angles (100% less than 40°) (Table 4.1, Figures 4.11a and 4.12b). The fabric shape was characterised by low isotropy and high elongation (Figure 4.11b).

A second trial pit, excavated into the rampart of the circular feature at Site B (Fronlas, Figure 4.5), again revealed a thick sequence of consolidated, calcareous, matrix-supported diamicton (Figure 4.13). Between 48 and 64 cm a thin lens of poorly sorted clayey, sandy, rounded gravel was apparent, similar to that found at the base of the trench at Site A. No clast fabric measurements were made in this trial pit due a scarcity of clasts within the diamict.
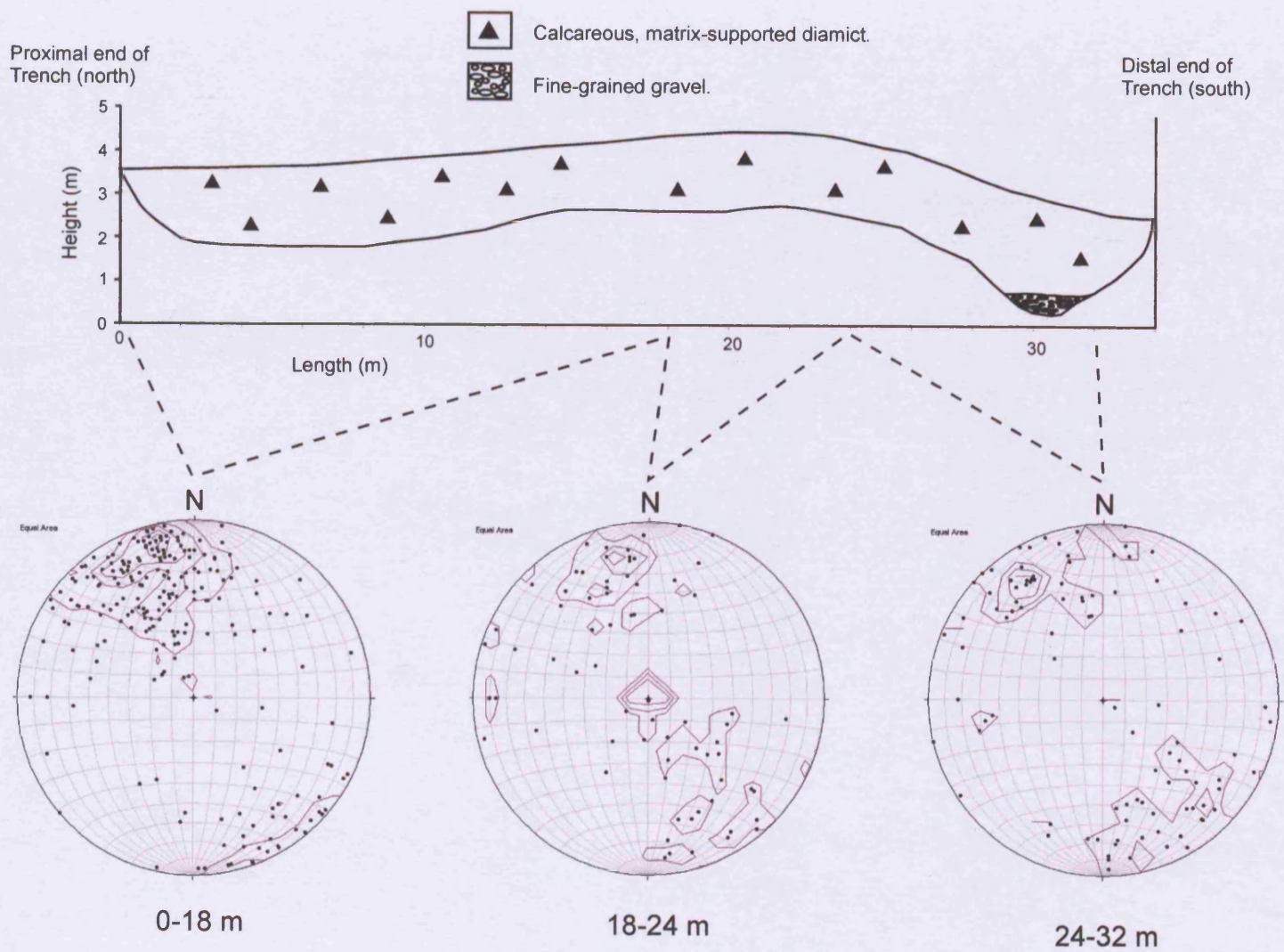
Figure 4.7: Trench section, Hirwaun valley, Site A, with summary of clast fabric data from the Hirwaun valley trench section. Results displayed as equal-area projection stereonets.
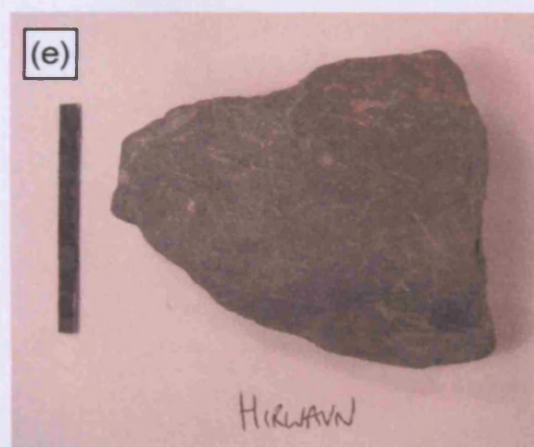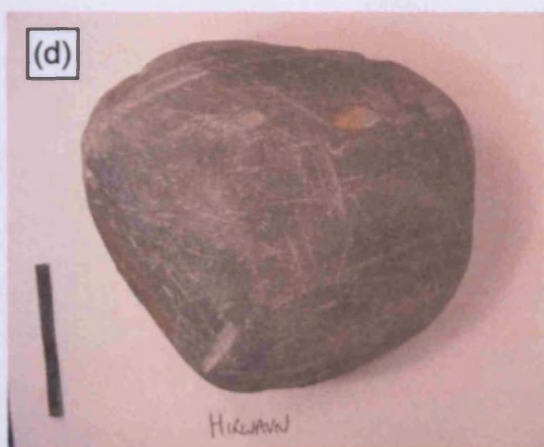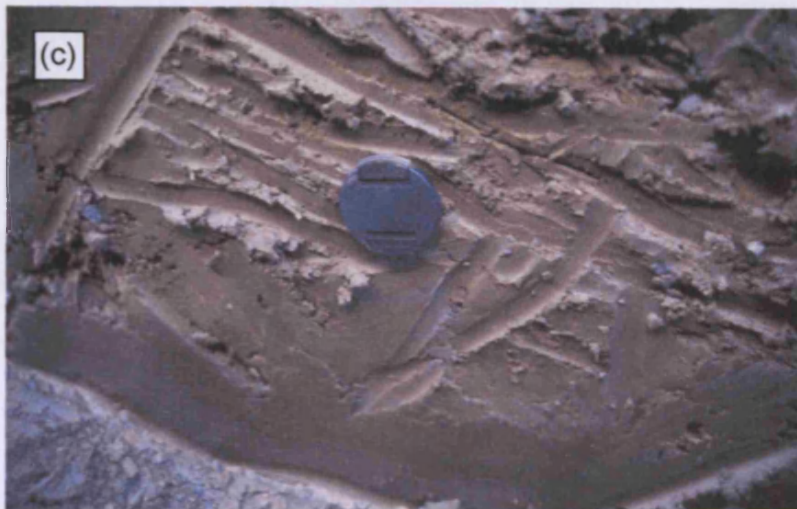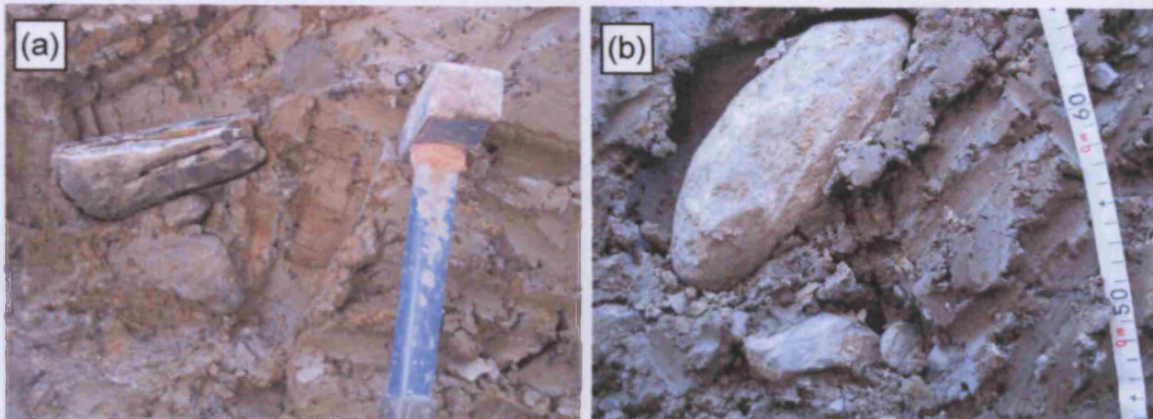
Figure 4.8: Photographs of sediments from the trench section (Site A) in the Hirwaun valley: (a&b) Northwards (up-glacier) dipping clasts within calcareous clayey silt matrix, near the proximal end of the trench; (c) Homogenous clayey silt matrix typical of trench section (Photo: C. Harris); (d&e) Examples of heavily striated clasts sampled from within the clayey silt matrix (black bar is 5 cm long).
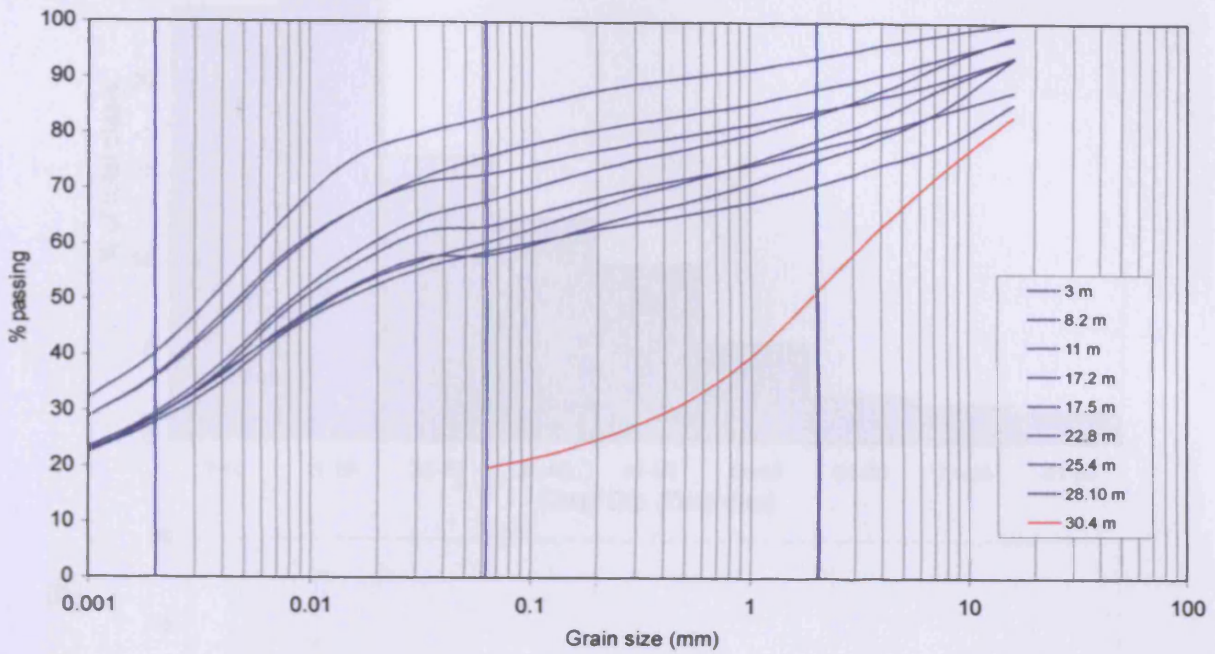
Figure 4.9: Grain-size analysis of sediments from the trench at Site A, Hirwaun valley. Samples taken from positions along the trench wall.
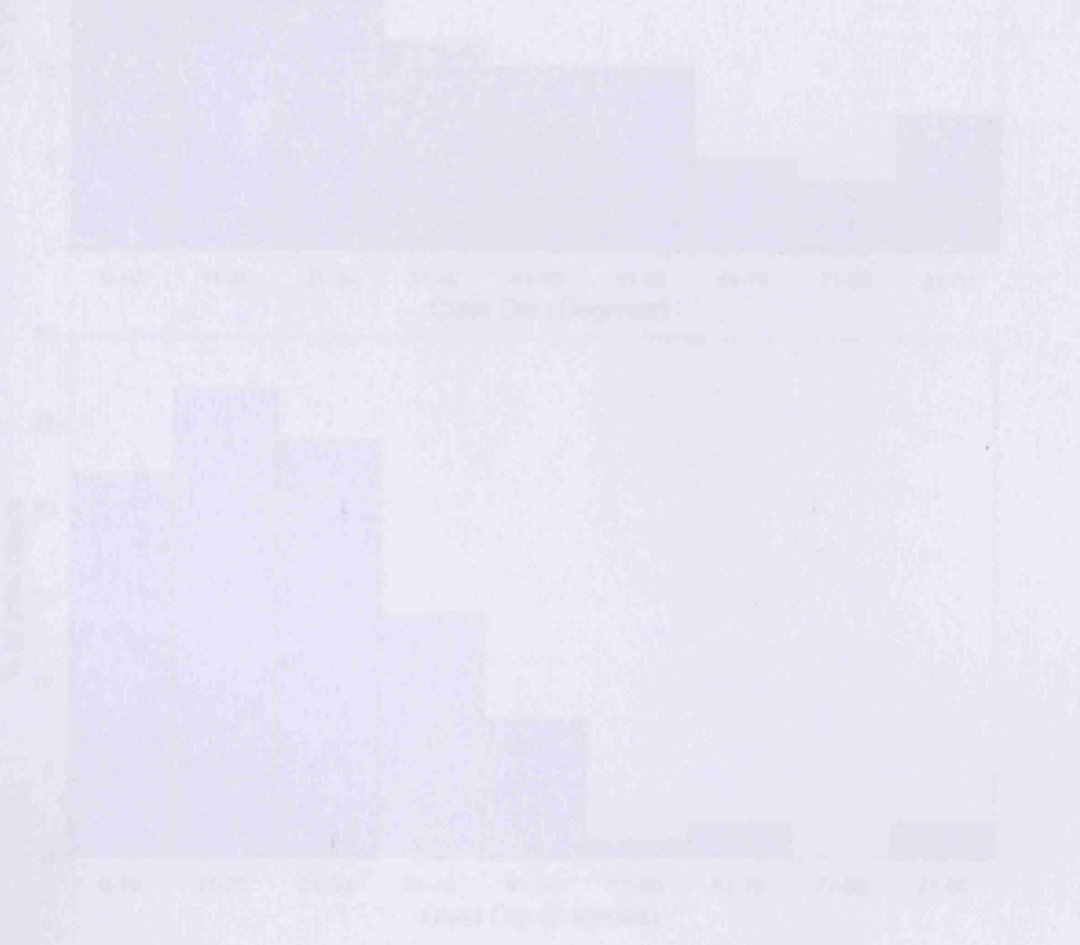
Figure 4.10: Dip angle of clasts from the trench at Site A, Hirwaun valley: (a) 0-18 m; (b) 18-24 m; (c) 24-32 m.

(a)

(b)
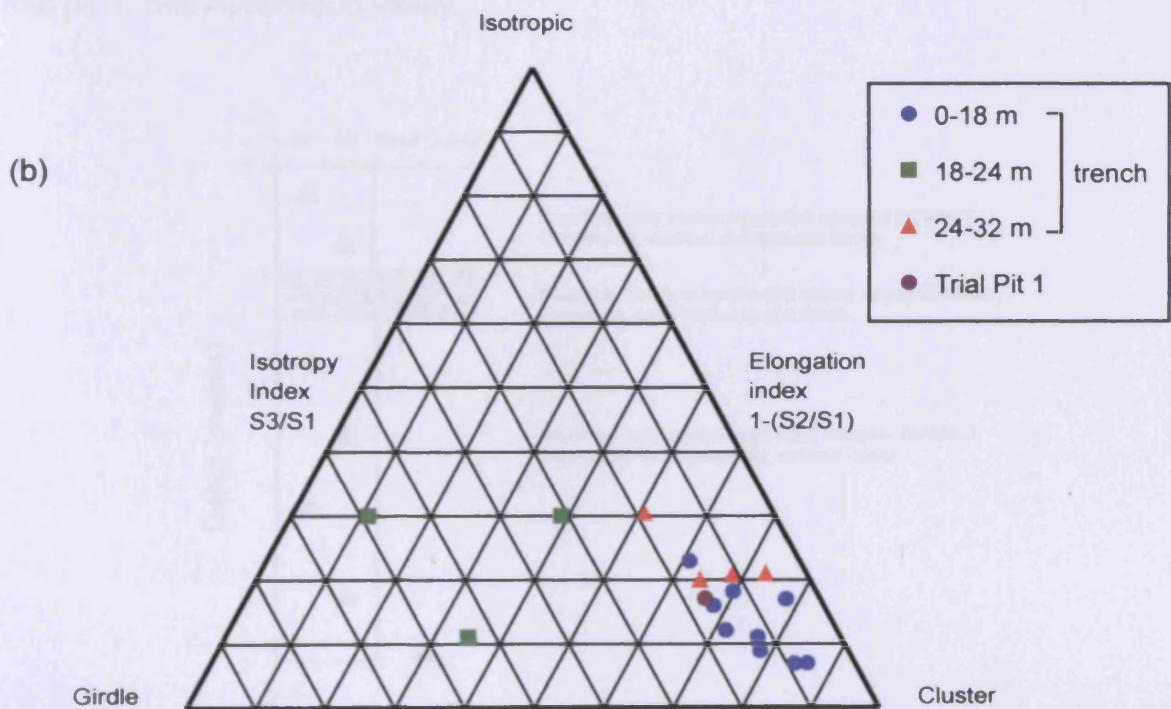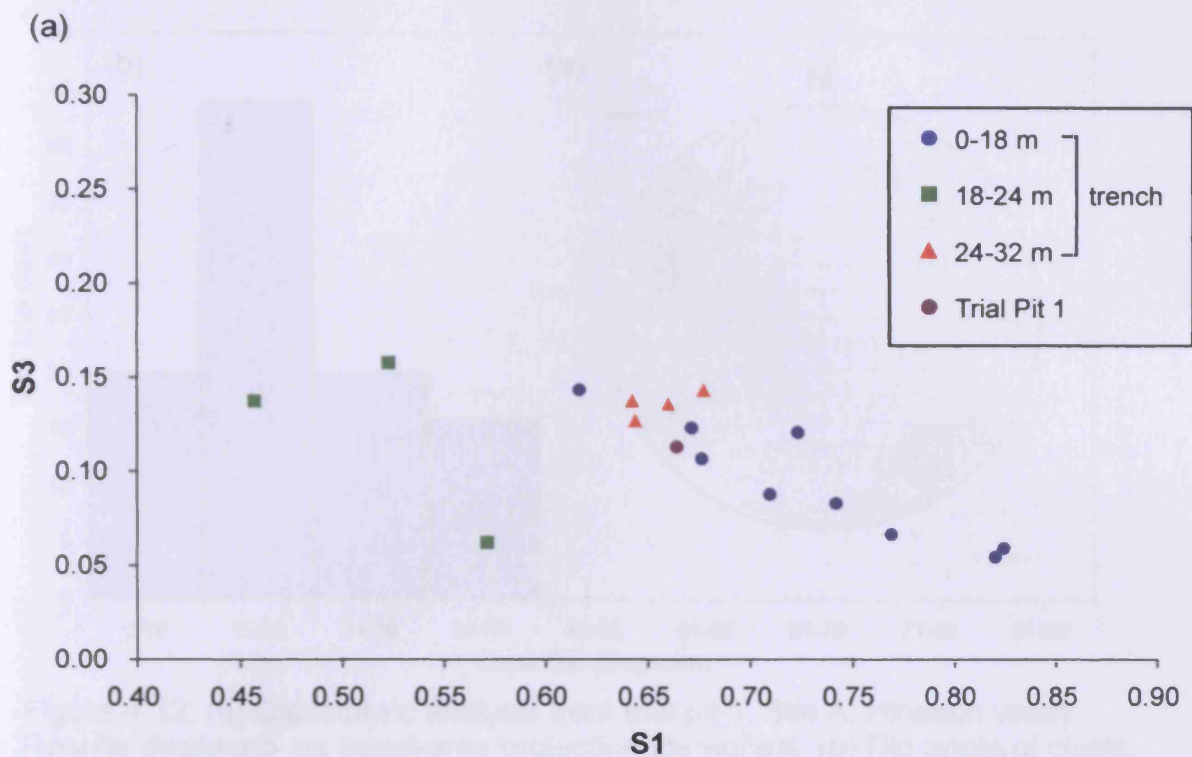
Figure 4.11: Eigenvalue analysis of clast fabric data from the Hirwaun valley trench section (Site A) at 2 m intervals and trial pit 1 (Site A). Data plotted as (a) a standard graph Dowdeswell *et al*. 1986); and (b) as a fabric shape diagram (Benn 1994a).
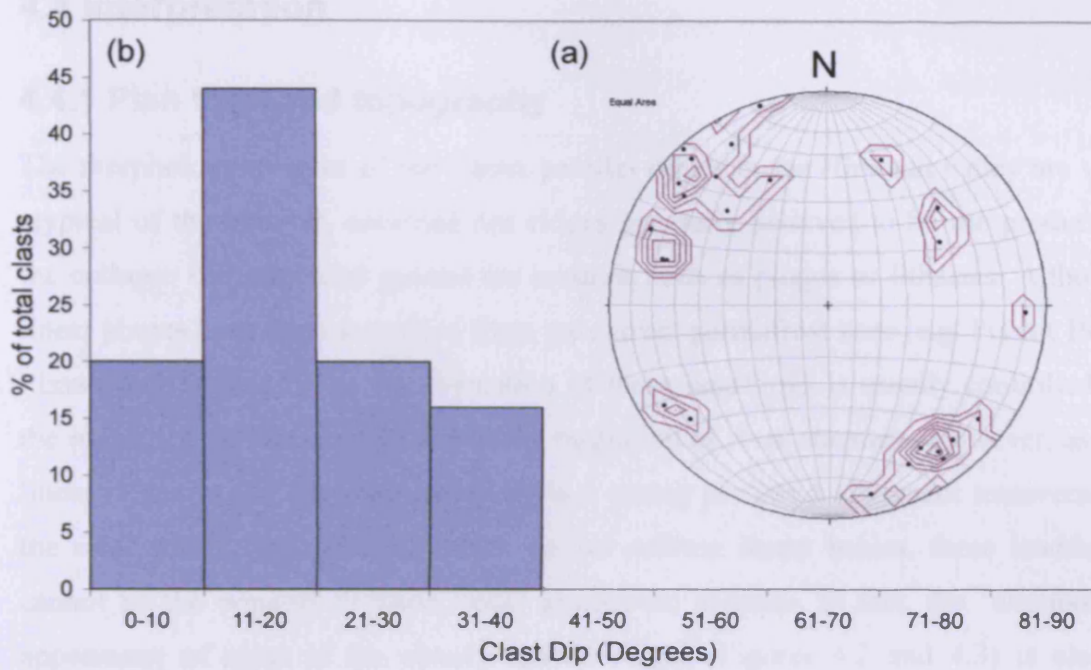
Figure 4.12: (a) Clast fabric analysis from trial pit 1, Site A, Hirwaun valley. Results displayed as equal-area projection stereonets. (b) Dip angle of clasts, trial pit 1, Site A, Hirwaun valley.
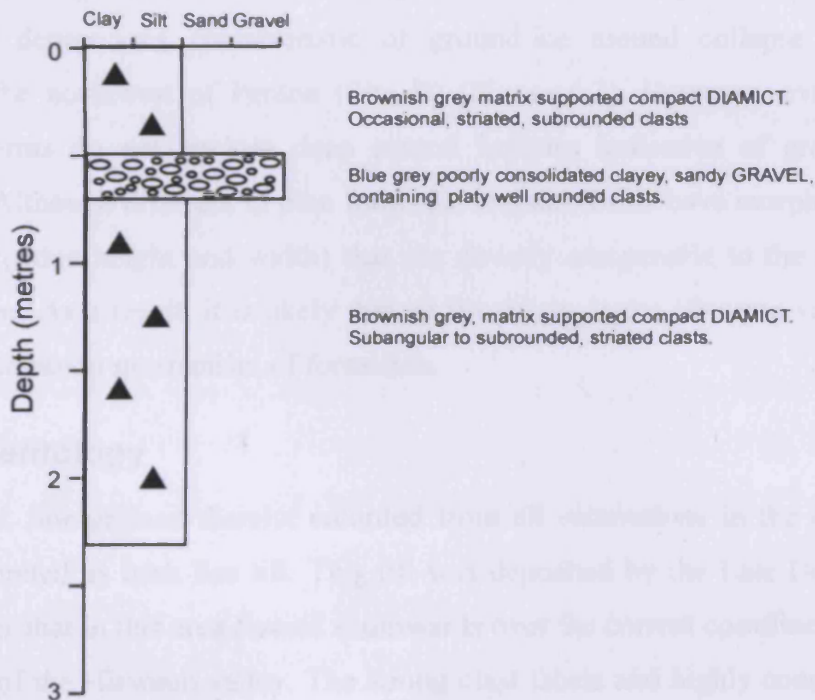
Figure 4.13: Sedimentary log of the Hirwaun trial pit 2 within the rampart of the circular landform (Site B).

4.4 Interpretation

4.4.1 Plan form and topography

The morphology of most of the linear, parallel ridges in the Hirwaun valley are very atypical of the circular, enclosed rim ridges generally believed to be the product of the collapse of periglacial ground-ice mounds such as pingos or lithalsas. Although linear pingos have been described from the current permafrost zone (e.g. Pissart 1967; Pissart and French 1976), the formation of these landforms is usually controlled by the refreezing of linear taliks due to the migration of river channels. However, as the linear ridges in the Hirwaun valley show a strong preferred alignment transverse to the river valley, and pairs of ridges do not enclose linear basins, these landforms cannot be the remains of these linear ground-ice mounds. In fact, the 'washboard' appearance of most of the closely spaced ridges (Figures 4.2 and 4.3) is clearly inconsistent with any landforms produced by the growth of ground-ice in current permafrost environments.

The only circular ridges in the Hirwaun valley that have morphological similarities to the ramparted depressions characteristic of ground-ice mound collapse are the landforms to the northwest of Penlon (Site B) (Figure 4.2). However, even these circular landforms do not enclose deep central hollows indicative of ground-ice development. Although different in plan form, the circular forms have morphological characteristics (ridge height and width) that are directly comparable to the adjacent linear landforms. As a result, it is likely that all the ridges in the Hirwaun valley are the result of a common mechanism of formation.

4.4.2 Sedimentology

The calcareous, fine-grained diamict recorded from all excavations in the Hirwaun valley is interpreted as Irish Sea till. This till was deposited by the Late Devensian Irish Sea glacier that in this area flowed southwards over the current coastline into the upper reaches of the Hirwaun valley. The strong clast fabric and highly consolidated nature of the diamicton, as well as the presence of heavily striated clasts, suggest that this deposit was transported subglacially before deposition at the ice-bed interface. The eigenvalues of the majority of the trench (high S1, low S3) are characteristic of

meltout tills, undeformed lodgement tills, or deformation tills (Dowdeswell and Sharp 1986; Bennett *et al.* 1999). The low angle dips of the clasts and the strong clustering are not consistent with a glaciomarine model of deposition, as ice-rafted diamictons have elongate clasts with dips in excess of 45° and isotropic fabrics with no relationship to the direction of ice flow (Domack and Lawson 1985). Furthermore, the altitude of the till (ca. 130 m OD) is inconsistent with deposition in a glaciomarine setting. The evidence from the Hirwaun valley is therefore consistent with the prevailing model of terrestrial subglacial deposition in southwest Wales (McCarroll 2001; Hambrey *et al.* 2001; McCarroll and Rijsdijk 2003). In the artificial exposures created in this investigation, the till displays no evidence of post-depositional disturbance. There is no evidence for reworking through periglacial or paraglacial slope processes or ground-ice development. As a result, it is believed that the ridges in the Hirwaun valley are primary landforms that developed contemporaneously with till deposition. These landforms therefore have subglacial, rather than periglacial (e.g. from the collapse of open system pingos), origins.

Tills, deposited by the Irish Sea glacier are found at various sites along the Cardigan Bay coast from Pembrokeshire to Llanrhystud (e.g. Traeth-y-Mwnt, Newquay, Aberaeron, Llan-non) (Jehu 1904; Williams 1927; John 1970a; Watson 1970; Bowen 1974; Campbell and Bowen 1989). The clast fabric data from the Hirwaun valley demonstrates a strong consistent fabric with a marked north-northwesterly (upglacier) dip, characteristic of basal tills (Dowdeswell and Sharp 1986; Bennett *et al.* 1999). This orientation is consistent with clast fabric measurements made from Irish Sea till and with striae recordings in the vicinity of Cardigan and from coastal sites around Cardigan Bay that indicate that the Irish Sea ice mass flowed onshore from a north to northwesterly direction (Jehu 1904; Watson 1968; John 1970a; Lear 1986; Hambrey *et al.* 2001; Hiemstra *et al.* 2005). The clast fabrics reported by Hambrey *et al.* (2001) from massive diamictons near Cardigan and at Gwbert display weak or girdle fabrics (S1 eigenvalues between 0.507 to 0.661), compared to the stronger range of fabrics recorded from 0-18 m and 24-32 m in the trench in the Hirwaun valley (Figure 4.11a). Based on the evidence for foreign erratics and broken shells, these diamictons were interpreted as subglacial tills derived from the Irish Sea. Hambrey *et al.* (2001) argue that the primary fabric has been modified by cryoturbation, resulting in the absence of a strong fabric, but that there is a weakly developed northwest to southeast

116

orientation (V1 = 315-343°). This is consistent with the orientation of the clasts in the Hirwaun valley and with striae at Gwbert (Hambrey *et al.* 2001). In the western end of the buried Nawmor meander of the Teifi at Cenarth, east of the mouth of the Afon Hirwaun, Lear (1986) recorded a NNW trending (355°) clast fabric from a fine-grained (63% clay), highly calcareous, Irish Sea till, indicating ice flow from north to south. Lear (1986) also identified a second ice flow direction however, with ice flowing west to east up the Teifi valley.

At Traeth-y-Mwnt on the Cardigan Bay coast, 8 km northwest of the Hirwaun valley site (Figure 4.1), a matrix-supported, clast-poor, grey, clayey, Irish Sea till, rich in shell debris and with a low clast content is found (Williams 1927; Campbell and Bowen 1989; Rijsdijk 2001). Deformation structures at Mwnt, previously interpreted as the result of glaciotectonic deformation (Campbell and Bowen 1989) or glaciomarine subaqueous deposition (Eyles and McCabe 1989), have now been re-interpreted as the result of post-depositional density-driven vertical deformation of flow tills originally deposited by stagnant, debris-rich ice or in a small proglacially ponded lake (Rijsdijk 2001; Hambrey *et al.* 2001; McCarroll and Rijsdijk 2003; Hiemstra *et al.* 2005). Clast fabric data collected from this site is randomly distributed, reflecting post-depositional modification of clast fabric. As a result, the dataset from Mwnt cannot be utilised for regional studies of the direction of ice flow and to inform the interpretation of the Hirwaun site as they represent a complex, highly localised depositional environment possibly controlled by palaeoslopes and sediment density. The physical properties of the till at Mwnt therefore differ significantly from the till in the Hirwaun valley. In contrast to the low density till at Mwnt, the Hirwaun valley till was not subject to any post depositional modification, its sedimentary properties reflecting subglacial deposition beneath an actively moving warm-based glacier.

Although the structures at Traeth-y-Mwnt are no longer believed to represent glaciotectonic deformation, it is widely acknowledged that subglacial deformation of Irish Sea till is common at other sites in the southern sector of the Irish Sea basin (McCarroll 2001; McCarroll and Rijsdijk 2003). Thrust faults, fractures and shear planes within Irish Sea till, interpreted as regional evidence for intensive subglacial deformation in the direction of ice flow (Rijsdijk and McCarroll 2001; McCarroll and

117

Rijsdijk 2003), have been observed in southwest Wales at Gilfach-yr-Halen, Gwbert, Abermawr and Druidston (John 1970a; Campbell and Bowen 1989; Rijsdijk 2000; Hambrey *et al.* 2001; McCarroll and Rijsdijk 2003; Hiemstra *et al.* 2005; Etienne *et al.* 2005) and on the southeastern coast of Ireland (Rijsdijk *et al.* 1999; Ó Cofaigh and Evans 2001). Structures associated with glaciotectonic deformation in North Wales (Harris 1991a; McCarroll and Harris 1992; McCarroll 1995; Harris *et al.* 1997; Thomas *et al.* 1998) suggest that terrestrial subglacial conditions were also common throughout the southern half of the Irish Sea basin during deglaciation. This is in direct contrast to the basin-wide model of deep glaciomarine conditions proposed by Eyles and McCabe (1989). Several authors have recently suggested that because of its deformable bed of saturated fine-grained marine sediments, the Irish Sea ice mass was unstable and highly dynamic, reaching far south into the Celtic Sea during the Late Devensian (Scourse and Furze 2001; Ó Cofaigh and Evans 2001; Hiemstra *et al.* 2006).

Deformation of subglacial sediment occurs in response to ice overriding weak, water-saturated sediment. High pore-water pressures in unconsolidated sediments (determined by the matrix characteristics and water availability) reduce the effective normal pressure at the glacier sole, reducing the frictionally-derived resistance of the material to the shear stress applied by the ice, enabling flow by ductile shear deformation of the water-saturated sediment layer (Boulton and Jones 1979; Boulton and Hindmarsh 1987). Because of low basal shear stresses, glaciers on soft deforming beds are characterised by low-angled surface profiles (Boulton and Jones 1979; Boulton and Hindmarsh 1987). A deformation till (the product of deforming bed conditions) implies that at the time of its deposition the base of the glacier was at the pressure melting point and underlain by an unfrozen, saturated, soft, easily deformable material. The sedimentary end product of pervasive deformation of soft sediment is a completely homogenised, usually diamictic, material (Hart and Boulton 1991; Benn and Evans 1998; Piotrowski *et al.* 2002). Based on this definition, the evidence presented from the Hirwaun valley is entirely consistent with an interpretation of the Hirwaun sediments as a homogenised deformation till. However, entirely undeformed lodgement tills also share many of the characteristics of highly deformed tills and may therefore appear no different (Hart 1994, 1995). Therefore, whilst it is easy to identify glaciotectonites, where deformation has not been

118

pervasive and which therefore display tectonic structures, the interpretation of massive homogenised tills is more difficult, in that may have either undergone pervasive deformation, or alternatively no deformation whatsoever.

The clast fabric analysis from the Hirwaun valley cannot be used to assist in the identification of the depositional setting of the till (deformation or lodgement). This is because although it was originally believed that deformation tills were characterised by relatively weak isotropic clast fabrics and that basal meltout, lodgement and ploughed tills had strong clustering fabrics with low isotropy (Dowdeswell and Sharp 1986; Hart 1994, 1995; Benn 1994b, 1995), this has since been shown not to be the case (Bennett *et al.* 1999). The eigenvalue envelopes derived for diffent types of glacial deposits overlap significantly and cannot therefore provide a means of unambiguous discrimination for sediments of unknown origins (Bennett *et al.* 1999). Laboratory experiments have suggested that highly strained deformation tills have strong fabrics orientated parallel to the flow direction (Hooyer and Iverson 2000). It is now suggested that unremoulded basal melt-out tills are actually quite rare and that tills with weak fabrics are not deformation tills. As a result there are significant problems associated with the use of clast fabric analysis as a technique to help discriminate the depositional setting of individual till units.

Many of the physical properties and characteristics (e.g. grain-size, texture, strength) of Irish Sea tills in west Wales were determined during primary deposition by marine sedimentation prior to cannibalisation by the Irish Sea glacier (McCarroll and Rijsdijk 2003). This further complicates the interpretation of the Hirwaun valley till, as the original sequence of marine muds from which the till was generated was presumably rather homogenous making it difficult to recognise evidence for deformation in the reworked deposit. Therefore, although the Hirwaun valley till does share many physical properties (high strength, subglacially compacted) with Irish Sea till at other sites along the Cardigan Bay coast, it does not display any structural evidence for glaciotectonism. Elsewhere in Wales, strong clast fabrics with low angle dips similar to those in the Hirwaun valley have been reported from other sites where ice masses have advanced over fine-grained marine sediments, cannibalising them and redepositing them onshore (Harris 1991a, 1991b; McCarroll and Harris 1992;

Campbell and Shakesby 1994; McCarroll and Rijsdijk 2003). These have been variously interpreted as deformation, basal meltout or lodgement tills.

One of the most important characteristics of the onshore area between the Afon Teifi and Cardigan Bay is the juxtaposition between drift-filled valleys, and low hills with very little or no superficial cover. Such a setting, compounded by the influence of the steep bedrock cliffs, would have had a significant impact on the glaciological and hydrological systems of the Irish Sea glacier as it advanced. It is no coincidence that the Irish Sea ice advanced further inland where high cliffs are absent (e.g. the mouth of the Afon Teifi and the relatively low relief inland of Aberporth). In North America, fast flow of the Laurentide Ice Sheet appears to have occurred where the margin overrode fine-grained beds such as proglacial lake sediments, but flow was inhibited by permeable bedrock (sticky spots) in areas of discontinuous till (Hicock and Dreimanis 1992; Clark 1994). If the Irish Sea ice mass was characterised by rapid flow in the current offshore zone, then the discontinuous superficial drift cover of southwest Wales, in combination with the influence of the rapidly rising topography, would have severely inhibited flow. This may have resulted in a shift from deposition primarily by deformation of basal till to deposition by lodgement processes. At Wylfa Head, Anglesey, basal till derived from reworking of marine sediments from the Irish Sea Basin had very high values of S1 (0.79-0.869, average 0.81). The exposures of inland deposits on Anglesey may provide a better analogue than the coastal sites along the Cardigan Bay coast, as Anglesey provided a significant bedrock obstruction to the southward flow of the Irish Sea glacier leading to compressional deformation of the ice, increased basal stress and till deposition by lodgement (Harris 1991a, 1991b).

4.4.3 Model of landform formation

The predominantly unidirectional, shallowly dipping clast fabrics observed in this study are entirely inconsistent with the interpretation of these landforms as relict ground-ice mounds. The orientation of clast fabrics displays no evidence of reworking by mass movement processes or by deformation as a result of ground-ice development. Instead, clast fabrics are consistent with regional orientation data from glacial deposits and striae, indicating that these fabrics were developed during primary deposition at the bed of the Irish Sea glacier as it advanced onshore from

Cardigan Bay. The ridges in the Hirwaun valley must therefore have developed at the glacier bed contemporaneously with the deposition of sediments. The sedimentary evidence from the Hirwaun valley therefore strongly indicates that these landforms are glacially derived, representing a subglacially derived or ice-contact landform.

A complex diversity of landforms has been attributed to development at the subglacial bed (Menzies and Shilts 2002). Many can be viewed as part of a subglacial landform continuum, with very different landforms having clear spatial relationships to each other. Transitions between such bedforms, dependent on sub-ice terrain, ice thickness and the rate of ice movement are well documented. Rogen or ribbed moraine (Hoppe 1959; Lundqvist 1981, 1989a) are large-scale subglacial diamict ridges orientated transverse to the direction of ice flow. They are frequently associated with drumlin fields, and tend to be located in the core areas of former ice sheets, rarely being found within 200-300 km of the ice margin (Menzies and Shilts 2002). They are common in areas glaciated by the Laurentide and Fennoscandinavian ice sheets during the last Glaciation and are thought to be the result of brittle fracture of superficial deposits under an extensional flow regime during the transition from a frozen to unfrozen bed during deglaciation (Hättestrand and Kleman 1999). Rogen moraines have been identified as an integral component of Irish geomorphology (Knight and McCabe 1997; McCabe *et al.* 1999; Clark and Meehan 2001). Although these moraines develop transverse to ice flow they are much larger in scale and less elongate (lower length/width ratio) than the landforms in the Hirwaun valley. The main line of evidence against a Rogen moraine interpretation however is the proximity of the landforms in the Hirwaun valley to the maximum extent of late Devensian ice in west Wales. Rogen moraines are not found in ice-marginal zones and must therefore be rejected as a possible analogue for the landforms in the Hirwaun valley.

In terms of marginal moraines, however, the ridges in the Hirwaun valley are not significant landforms. They are narrow, relatively small in scale (<5 m high) and are not visible on digital terrain models derived from NEXTmap datasets. The suggestion by Hambrey *et al.* (2001) that the Hirwaun ridges represent the results of ice wastage processes is deemed unlikely given the strong evidence for subglacially formed clast fabrics. An ice wastage model for the development of these landforms would require

121

an inexplicably high level of englacial debris within the Irish Sea ice mass. Rather, it appears that the Irish Sea glacier appears to have deposited fine-grained tills cannibalised from shallow marine sediments. The dominance of these tills suggests relatively low englacial debris contents, which may be the reason for the subdued nature of the ice-marginal landforms in the north-bank tributaries of the Teifi valley. The paucity of englacial debris has previously been attributed to the steepness of the coastal cliffs, which prevented debris-rich basal ice from penetrating inland (Charlesworth 1929; Bowen 1981). Given the clear evidence for reworked marine sediments in the Hirwaun valley however, this argument is clearly invalid.

The morphology and sedimentological composition of the ridges and their association with glaciolacustrine deposits down valley (British Geological Survey 1997) suggests that De Geer moraines (also known as "washboard or cross-valley moraines") might be appropriate analogues for the Hirwaun valley ridges. De Geer moraines form at the interface between the subglacial and subaquatic environments, close to local grounding lines. Sedimentological evidence indicates that De Geer moraines are ice-marginal landforms associated with the deformation of sediment at the grounding-line and the calving of ice blocks into proglacial water bodies (De Geer 1940; Sollid and Carlsson 1984; Larsen *et al.* 1991; Blake 2000; Lindén and Möller 2005). Alternatively however, some authors have suggested that they are sub-marginal crevasse-fill ridges associated with extensional flow (Hoppe 1957, 1959; Strömberg 1965; Mickelson and Berkson 1974; Zilliacus 1989; Beaudry and Prichonnet 1991; Lundqvist 1981, 1989b, 2000), perhaps associated with fracturing of the ice due to seismic activity (De Geer 1940; Lundqvist 2000). De Geer moraines are hundreds of metres in length, 10-20 m broad and less than 5 metres high, occurring in swarms or clusters perpendicular to ice flow, although they may be winding or anastomosing (Lundqvist 1981, 2000; Zilliacus 1989; Blake 2000; Lindén and Möller 2005). They usually occupy a low point in the terrain and "...commonly occur in fields of closely spaced ridges in association with subaqueous sediments, and mark the intermittent retreat of water terminating glaciers." (Benn and Evans 1998, pg 512). They are deposited transverse to the direction of ice flow with a slightly arcuate down-ice plan form and are asymmetrical in profile, with a steep distal and a lower gradient proximal slope (Zilliacus 1989; Menzies and Shilts 2002; Lindén and Möller 2005). Although generally associated with former tidewater conditions, De Geer moraines

associated with ice-dammed lakes have also been reported (Borgström 1979). As they develop at the interface between the subglacial and subaqueous environment, De Geer moraines are characterised by a wide variety of sediments (Mickelson and Berkson 1974; Zilliacus 1989; Larsen *et al.* 1991; Beaudry and Prichonnet 1991; Blake 2000; Lindén and Möller 2005). Extensive evidence for shearing and deformation has been reported from some De Geer moraines (Larsen *et al.* 1991; Blake 2000; Lindén and Möller 2005).

Clast fabrics within De Geer moraines display strong preferred orientations perpendicular to the ridge crest, with the proximal sediments characterised by up-ice dips and the distal fabrics dipping down-glacier (Hoppe 1957; Zilliacus 1989; Larsen *et al.* 1991; Blake 2000; Menzies and Shilts 2002; Lindén and Möller 2005). This is explained by subglacial deposition of sediments on the proximal side of the ridge, up-glacier from the grounding-line, and subaqueous sedimentation by sediment gravity flows on the distal side, beyond the grounding-line (Blake 2000; Lindén and Möller 2005). Glaciofluvial deposits found within some De Geer moraines (Larsen *et al.* 1991; Blake 2000; Lindén and Möller 2005) represent localised outwash fans. Many of the characteristics of De Geer moraines listed above are also common to the ridges in the Hirwaun valley (ridge dimensions and asymmetry; arcuate down-glacier plan form; strong clast fabrics perpendicular to the ridge axis and dipping up-glacier; glaciofluvial deposits). As well as explaining the strong NNW orientated clast fabrics between 0-18 m and 24-32 m in the trench at Site A (subglacial deposition), the interpretation of these landforms as De Geer moraines is consistent with the random clast fabrics recorded between 18-24 m. Deposition at a subaquaeous margin is characterised by a complex array of processes, including sediment gravity flows and glaciofluvial deposition. The random fabric distribution between 18-24 m is therefore interpreted as the result of subquaeous deposition at the ice-margin during northwards recession.

The Hirwaun valley landforms, and possibly other ridges present in the adjacent Ceri valley (Watson 1972), may therefore represent the geomorphological response of a lobe of Irish Sea ice that terminated in Lake Teifi. Their distribution is consistent with this hypothesis, as they are found altitudes of 90-130 m OD (Figure 4.14), below the
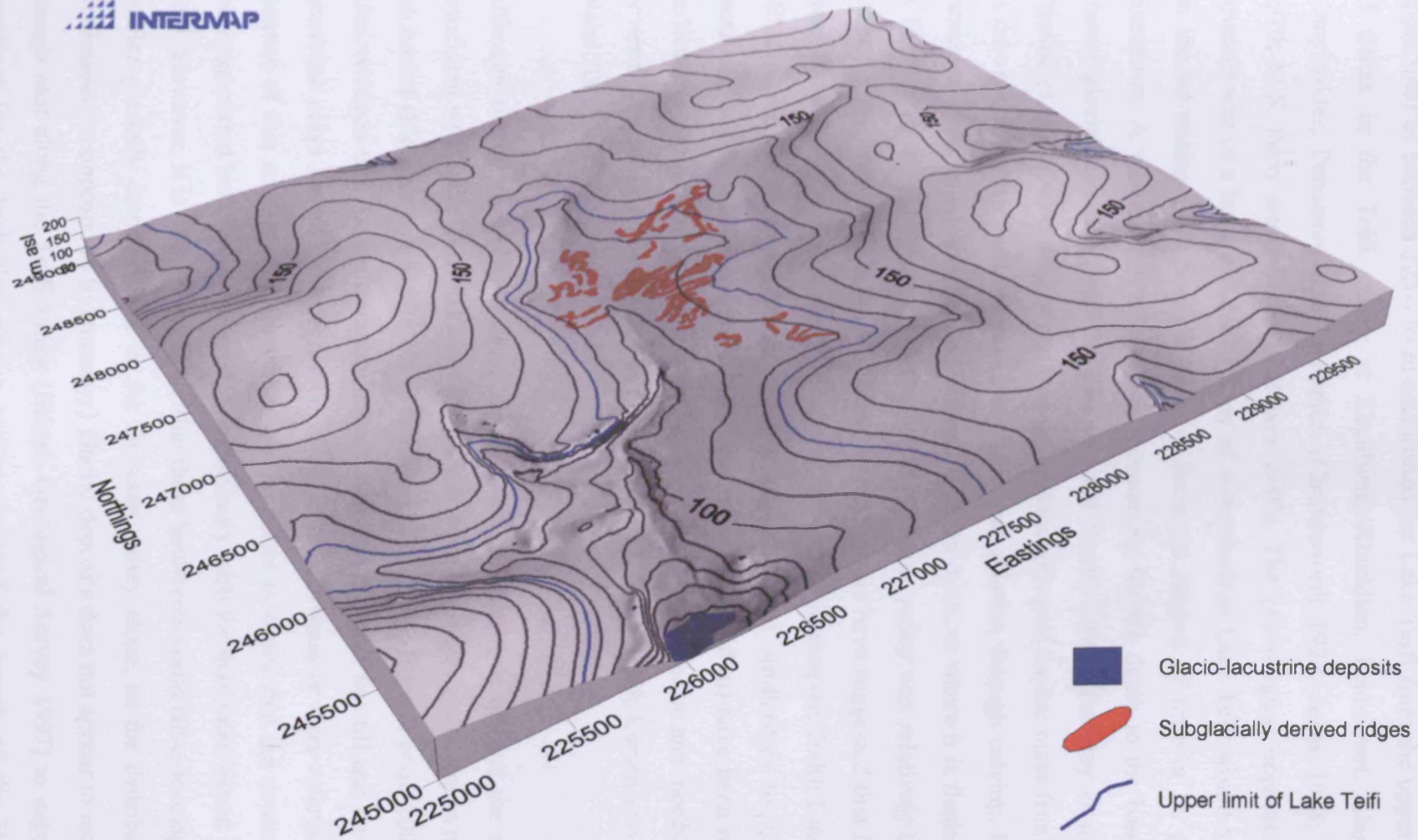
Figure 4.14: Digital terrain model (DTM) of the Hirwaun valley displaying the relationship of the landforms to the upper limits of Lake Teifi (ca. 126 m), and to its associated deposits. Contours at 10 m intervals. Terrain data © Intermap Technologies Inc. Distribution of glaciolacustrine deposits after British Geological Survey (1997).

upper limit of between 125-130 m established for Lake Teifi from the upper surface of deltas in the Teifi valley at Llanllwni, Rhuddlan, Pentrecwrt, Llanwnnen, Llanybydder, Pencarreg and Lampeter, (Charlesworth 1929; Jones 1965; Watson 1970; M.S. Parry *unpublished* in Bowen 2005). The glaciological impacts that the development of a large proglacial body of water such as Lake Teifi would have had on the advancing Irish Sea glacier have been the subject of little or no previous discussion. A water depth of >125 m (accounting for the depth to the base of the known glaciolacustrine deposits, Fletcher and Siddle 1998; Hambrey *et al.* 2001; Etienne *et al.* 2006) probably resulted in the decoupling of the ice mass from its bed in the mouth of the Teifi, resulting in significant ablation through calving. De Geer moraines however, cannot develop where ice is too thick, or where it is floating, so it is likely that the ice thickness in the upper Hirwaun valley was relatively thin and water depths relatively shallow (<30 m). Some authors have suggested that De Geer moraines form in water depths in excess of 70-100 m (Lundqvist 2000; Lindén and Möller 2005). However, moraines with morphological similarities to De Geer moraines, and which formed in shallow water depths (25-30 m) have been reported, particularly from more mountainous areas in northern Sweden and northern and western Norway (e.g. Borgström 1979; Sollid and Carlson 1984; Larsen *et al.* 1991; Blake 2000).

Although the stratigraphic relationship between the Irish Sea till and the deposits associated with Lake Teifi has been discovered from boreholes elsewhere in the Teifi catchment (Fletcher and Siddle 1998; Hambrey *et al.* 2001; Etienne *et al.* 2006), it is acknowledged that the stratigraphic contact between the Irish Sea till and the glacio-lacustrine clays has not yet been recognised in the Hirwaun or Ceri valleys. In the absence of this relationship, there is as yet no direct evidence that the deposition of these ramparted landforms occurred synchronously with the maximum extent of Lake Teifi. However, it is believed unlikely that these landforms could have developed in a smaller glacially dammed lake in the Hirwaun valley alone, as the distribution of continuous (as opposed to fragmentary) glacial deposits does not appear to extend far enough east along the Teifi valley (British Geological Survey 1997) to support the argument for the Irish Sea glacier having dammed the mouth of the Hirwaun, inhibiting drainage. Therefore, if these landforms are De Geer moraines, then they probably developed in Lake Teifi. Given the evidence for southward-orientated ice

flow at Nawmor, near Cenarth (Lear 1986), the Hirwaun valley landforms probably developed during the recession of this southward flowing component of the Irish Sea glacier. The circular ridges at Fronlas, which have morphologies uncharacteristic of the majority of the landforms in the Hirwaun valley, may have formed by the downwasting of blocks of ice that became stranded as the ice margin retreated into increasingly shallower water conditions in the upper parts of the valley.

If the linear ridges of the Hirwaun valley are not De Geer moraines, then they could alternatively represent the arcuate belts of hummocky topography that can develop at the margins of surging glaciers, particularly where they have advanced over fine-grained marine sediments (Boulton and Paul 1976; Solheim 1986; Boulton *et al.* 1996). Terrestrial ice-marginal ridges associated with proglacial squeezing of dilatant tills and networks of sub-marginal crevasse-fill ridges are widely associated with the stagnation and *in situ* downwasting of dead ice following glacier surges (Lamplugh 1911; Sharp 1985, Eyles *et al.* 1994; Boulton *et al.* 1996; Evans and Twigg 2002). Although an interpretation of the ridges in the Hirwaun valley as crevasse-fill ridges is consistent with the model of a thin surging lobe of ice, with a low-gradient surface profile, in the Irish Sea Basin (Boulton and Jones 1979; O Cofaigh and Evans 2001), the shallowly dipping, northwards dominated trend of the clast fabrics within the Hirwaun valley ridges are not indicative of such landforms (Sharp 1985).

5 Llanio Fawr

5.1 Introduction

Linear to chaotically orientated ridges, in places enclosing occasional shallow depressions, are found near Llanio Fawr in the upper Teifi valley, at a site 2.5 km northwest of Llandewi-Brefi, just north of the rock gorge at the head of the Afon Dulais at Cockshead (Figure 5.1). The landforms are developed on a terrace of the upper Afon Teifi, where a tributary stream called the Nant Brynmaen joins the main channel. The majority of features at this locality have elongate ridges and are almost esker-like, with a northeast-southwest orientation (Figures 5.2, 5.3 and 5.4). Although most landforms at this site are not characterised by circular ramparts, and deep peat-filled depressions have not been identified, these features have been interpreted as the remains of open system pingos (Watson and Watson 1974; Sheppard 2003; Etienne *et al.* 2005).

The bedrock geology around the site is dominated by the Devils Bridge Formation, which comprises interbedded mudstones and sandstones of mid Llandovery Series (early Silurian) age (Figure 5.5). These rocks dominate the upper Teifi valley west of the Teifi Escarpment (Davies *et al.* 1997; British Geological Survey 1994a; BGS Sheet 195: Lampeter, *unpublished map*). North of the majority of the landforms at Llanio Fawr (Figure 5.3), rocks belonging to the Cwmystwyth Grits Group (Rhuddnant Grits Formation and Blaen Myherin Mudstones Formation) have been mapped (Figure 5.5). The rocks of the Cwmystwyth Grits Group are roughly the same age as the Devils Bridge Formation (late Llandovery Series, Silurian), and are lithologically similar (interbedded mudstones and sandstones). Preliminary mapping by the British Geological Survey has not identified any faults or major discontinuities near the site (Figure 5.5) (BGS Sheet 195: Lampeter, *unpublished map*), but this could be a result of the poor level of bedrock exposure in the area.

The site is within the late-Devensian limit of the Welsh ice mass (Jones 1965; Lear 1986, Waters *et al.* 1997), and the Teifi and Dulais valleys between Tregaron and Lampeter are dominated by landforms and sediments deposited by a northeastward retreating ice margin. Recessional moraine complexes, large kettle holes (e.g. Pant

Farm SN 66055.56342, Llyn Pencarreg SN 53729.45599), ice-contact gravels, kamiform benches, glaciofluvial outwash sheets and glaciolacustrine basins are common (Charlesworth 1929; Jones 1965; Crimes *et al.* 1992; Sheppard 2003). Oscillations of the retreating ice-margin are suggested by evidence for glaciotectonic structures, exposed in sand and gravel deposits south of Tregaron (SN 66740.58040) (Davies *et al.* 1997; Sheppard 2003).
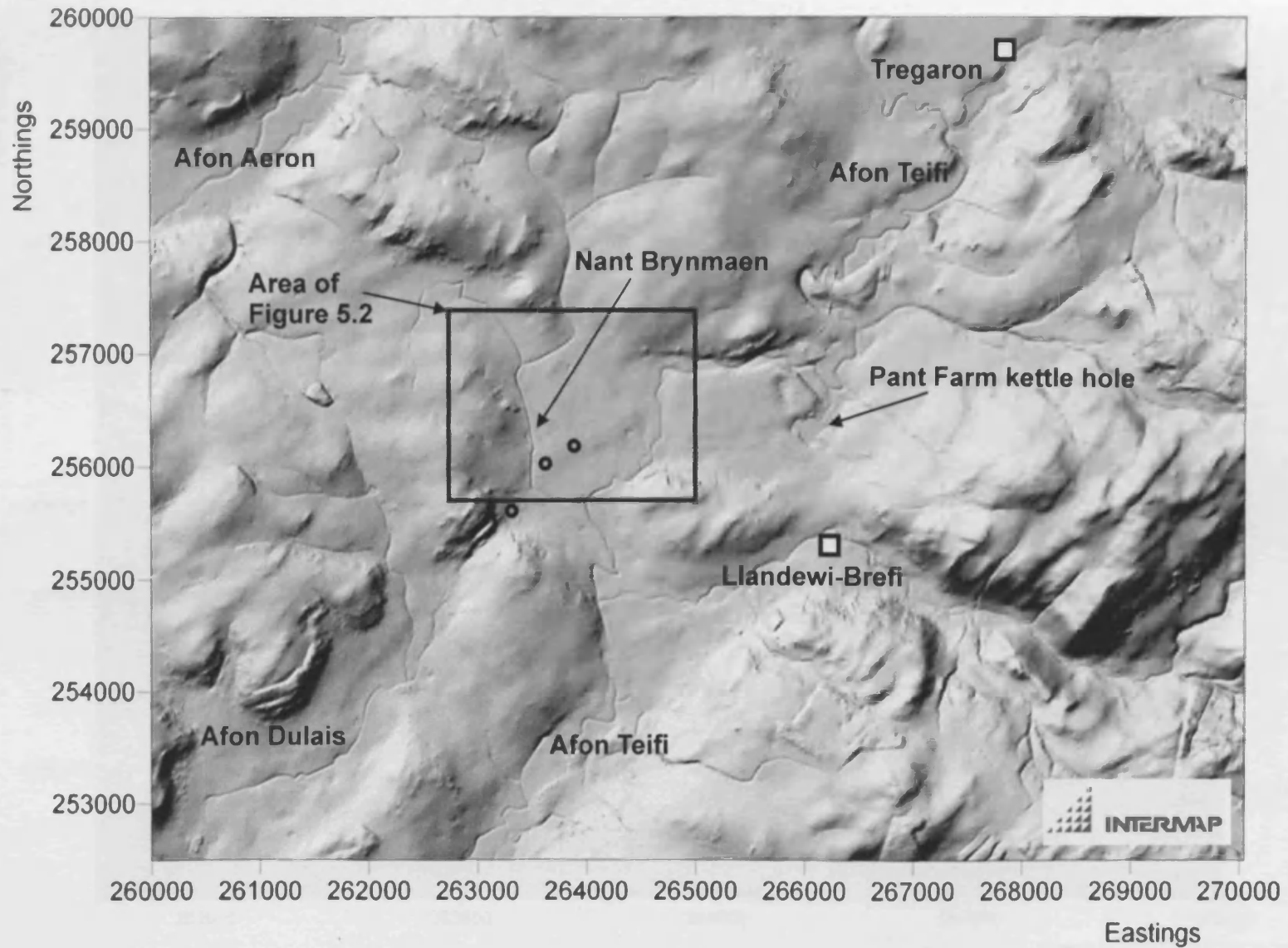
Figure 5.1: NEXTMAP digital terrain model (DTM) of the Teifi and Dulais valleys southwest of Tregaron (© Intermap Technologies Inc). Area of Figure 5.2 and locations of Dyfed County Council boreholes (black circles) indicated.

Figure 5.2: Aerial photograph of the Llanio Fawr site (© Getmapping Plc 2006). Area of Figure 5.3 indicated.
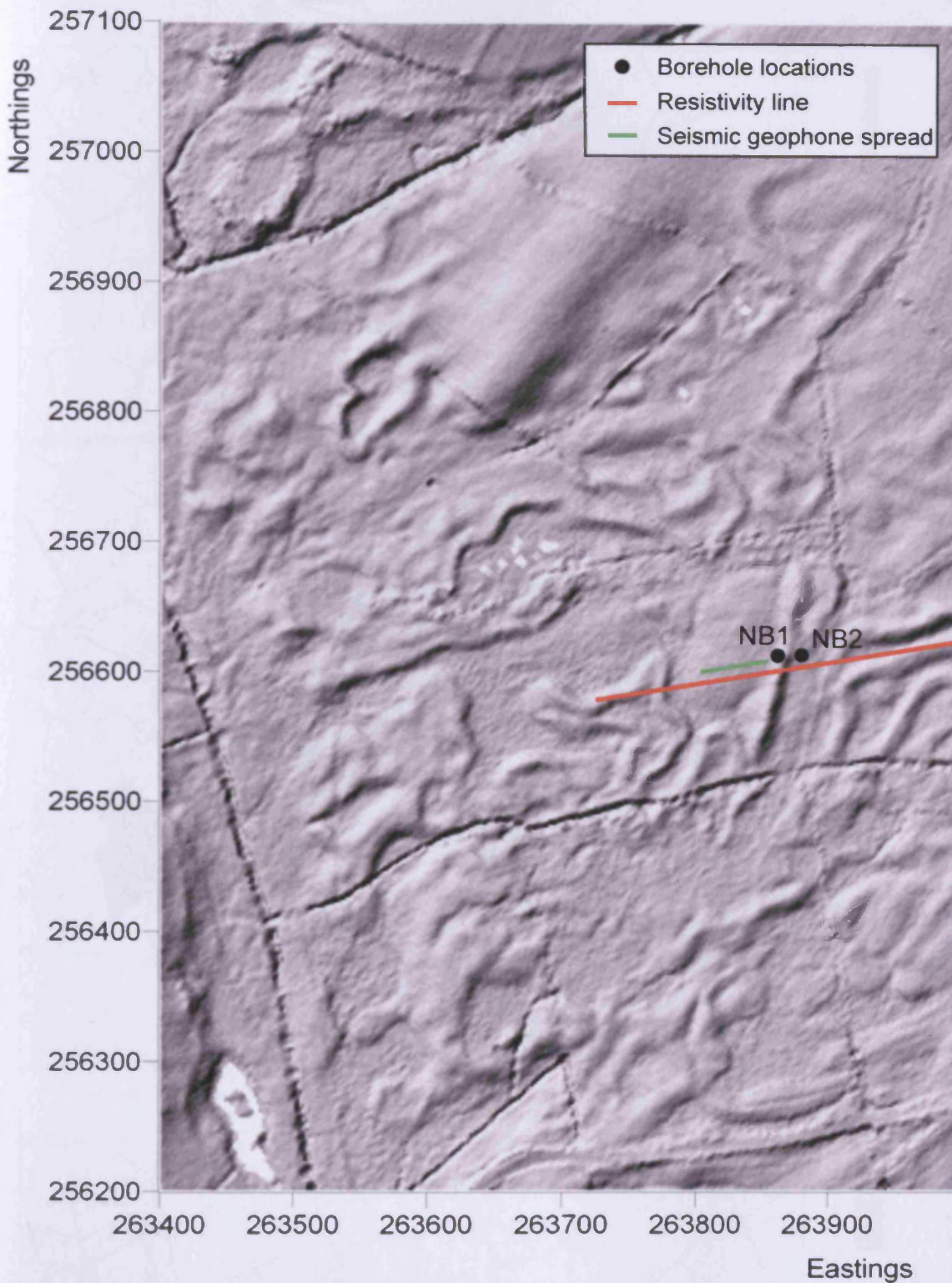
Figure 5.3: Shaded relief Digital Terrain Model (DTM) of landforms at Llanio Fawr, in the Nant Brynmaen valley, derived from LiDAR airborne surveying (© Environment Agency copyright and/or database right 2006). The locations of boreholes and geophysical surveys referred to in the text are indicated.
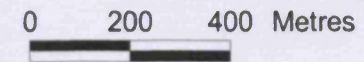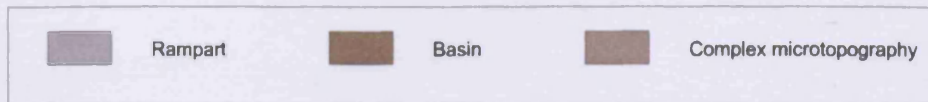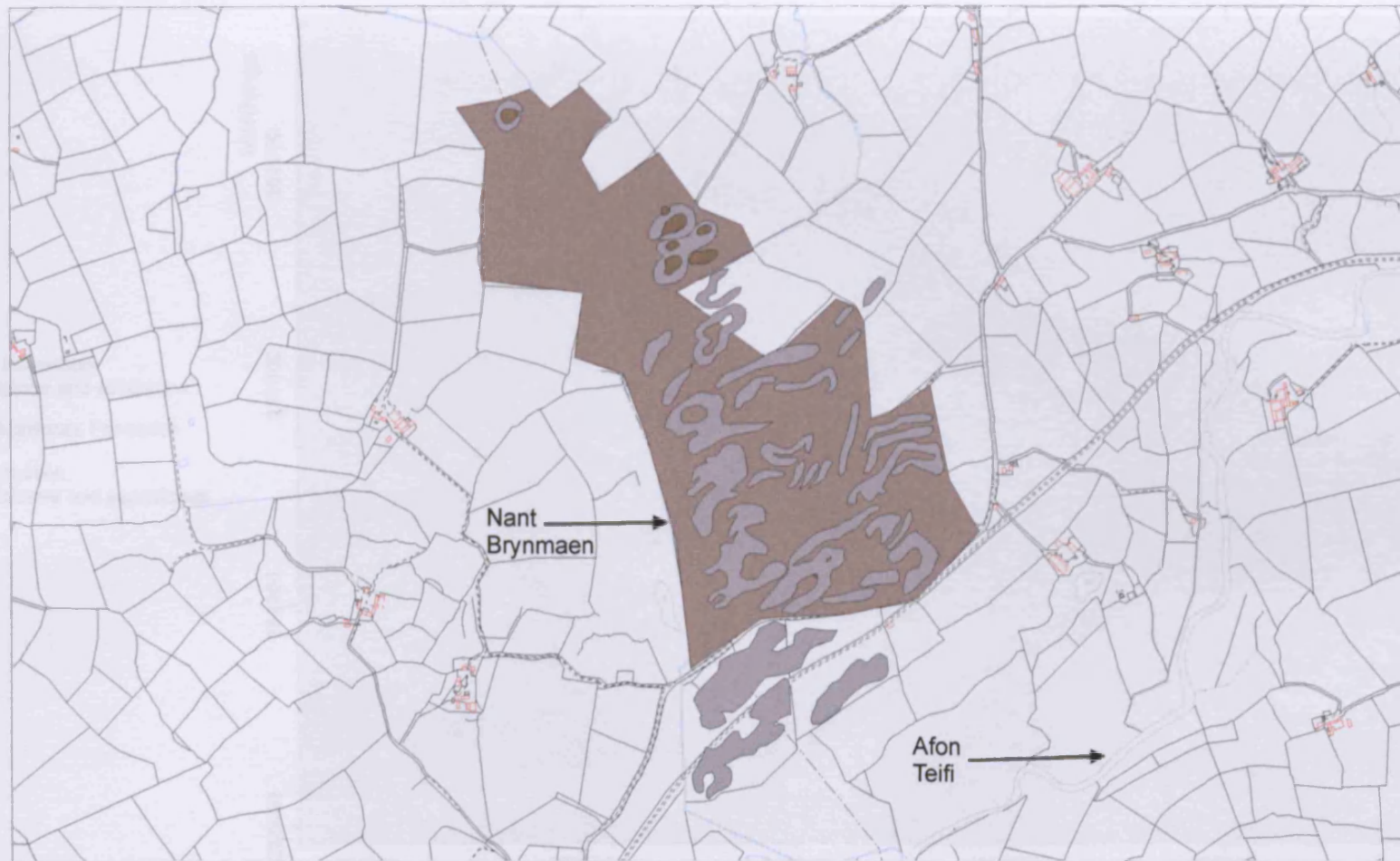
Figure 5.4: Geomorphological map of the Llanio Fawr ramparted ground-ice depressions, based on mapping from stereoscopic aerial photographs. LANDLINE data © Crown Copyright/database right 2005. An Ordnance Survey/(Datacentre) supplied service.

Silurian

Rhuddnant Grits Formation, interbedded mudstone and sandstone

Blaen Myherin Mudstones Formation

Devils Bridge Formation, interbedded mudstones and sandstones

Nant Brynmaen

Afon Teifi
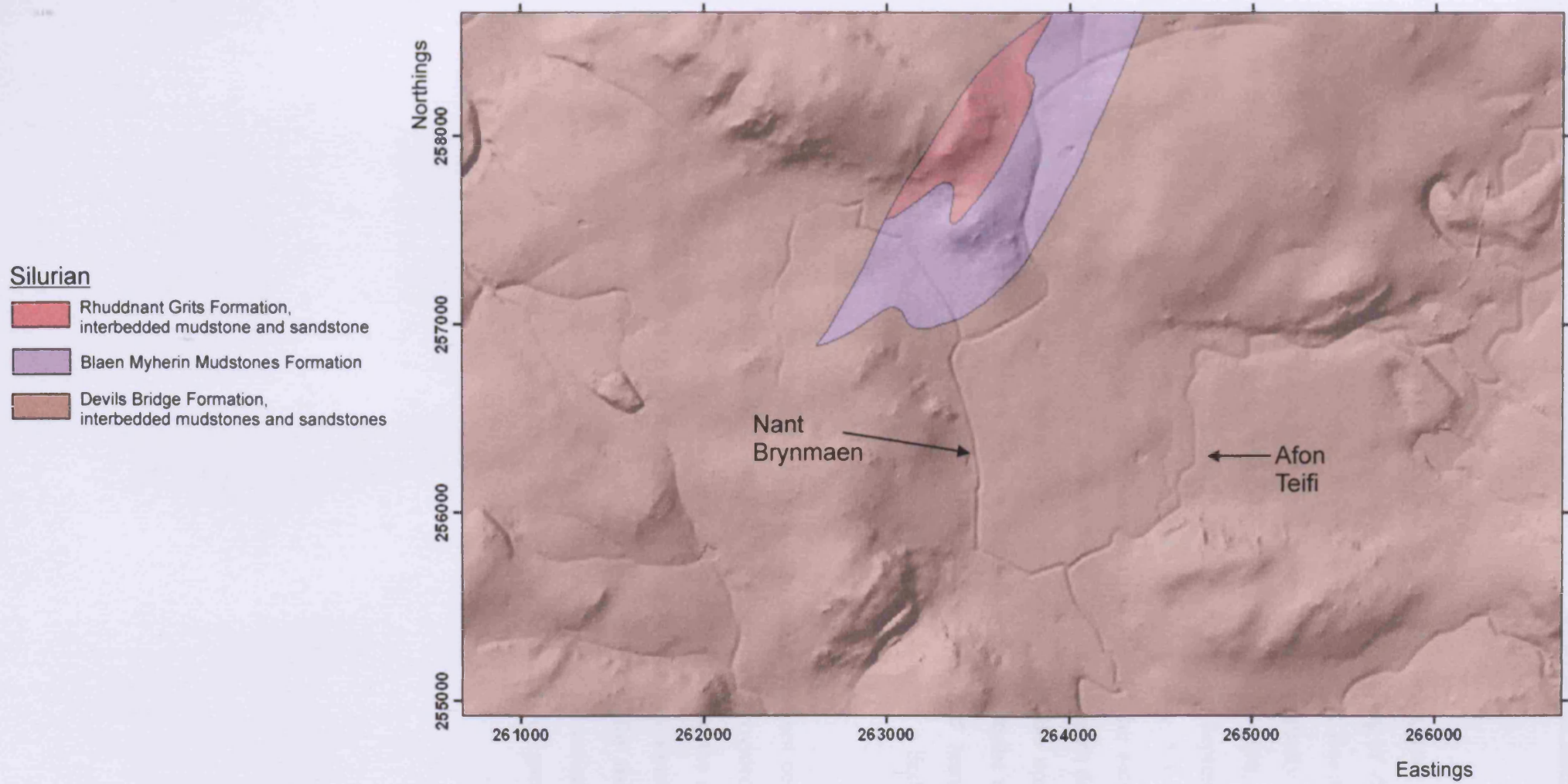
Figure 5.5: Bedrock geology of the Nant Brynmaen valley (© British Geological Survey) draped on the surface of a NEXTMAP Digital Terrain Model (DTM) with 3 x vertical exaggeration (© Intermap Technologies Inc.). Note that this map is adapted from unpublished, unchecked, draft mapping by the British Geological Survey and may therefore contain some inaccuracies.

5.2 Site description and survey

The site investigations at Llanio Fawr consisted of two boreholes, one east-west resistivity line (265 m in length, 3 x 18 electrode cables, 5 m spacing of electrodes) and a short reversed P-wave seismic refraction survey (Figure 5.3). Borehole NB1 (SN 63866.56604, beginning at 140 m from the east end of the resistivity line) was drilled through an elongate ridge, whilst Borehole NB2 (SN 63879.56598, at 120 m from the east end of the resistivity line), was located in an adjacent depression, at a height 1.13 m below, and 14.3 m east of Borehole NB1 (Figure 5.3 and 5.6). Problems with the recovery of the drilling equipment prohibited the recording of detailed sedimentological information on the superficial sequence beneath depths of 3 m. Cores were logged in the field through the open windows of the core barrels following British Standard 5930 (1999), using a Munsell chart to describe the colour of the sediments. Grain-size analysis of representative disturbed samples was undertaken in accordance with British Standard 1377 (1990), using a Sedigraph to analyse the fraction <63 μm.

Topographical data necessary to process the resistivity profile were not collected in the field, but were instead derived from a LiDAR dataset provided by the Environment Agency (Figure 5.3). The locations of the boreholes and the resistivity profiles were georeferenced using a handheld GPS system (nominal accuracy ± 10 m). The geophone spread (24 geophones at a spacing of 2 m) for the seismic refraction survey corresponded to 140-186 m from the east end of the resistivity line, beginning at the western foot of the ridge drilled by Borehole NB1 (Figure 5.3 and 5.6).
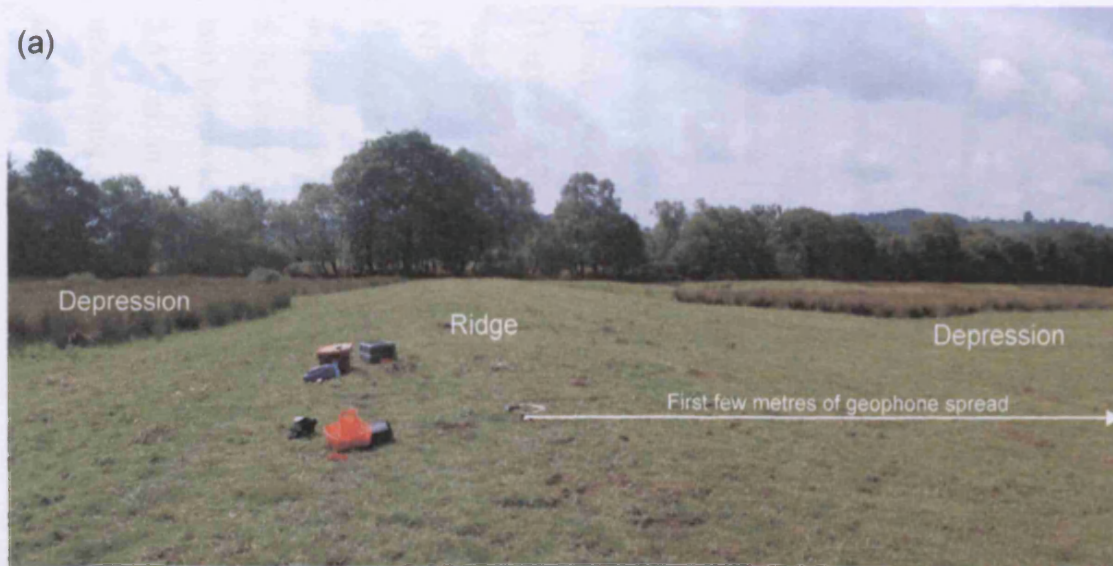
Figure 5.6: Overview of the Llanio Fawr site demonstrating gently undulating elongate ridges and shallow depressions: (a) ridge extending southward from borehole 1; (b) view west from borehole 1 along the resistivity and seismic refraction lines.

5.3 Results

5.3.1 Sedimentology

The upper 2.5 m of Borehole NB1 was dominated by a sequence of relatively poorly sorted, massive sandy fine-gravels with subangular to rounded, platy, elongate and disc-shaped clasts up to 6 cm in length (Figures 5.7a, 5.8a and 5.9a). The unit of silty, sandy gravel between 1.25-1.6 m was particularly poorly sorted and could be defined as a thin unit of diamict (Figure 5.9a). The lower 1.6-3 m of Borehole NB1 was characterised by a fining downward sequence, with a thin unit of well-sorted, clast-free, gravelly silty sand between 1.9-2 m and a unit of fine sand between 2.55-2.9 m, which graded into a thin (0.1 m) unit of laminated sandy silt at the base of the borehole (2.9-3 m) (Figures 5.8a and 5.9a). Core retrieval problems terminated the borehole at 3 m depth so the thickness of the laminated unit could not be established.

A fining downward sequence was also recovered from Borehole NB2, with 1.4 m of poorly sorted, silty, sandy gravel overlying 1.2 m of well-sorted gravelly sand (Figures 5.7b and 5.8b, 5.9b). Unfortunately the bottom 0.4 m of the core (2.6-3 m) was lost during drilling. The grain-size distribution of the upper 1.4 m of Borehole NB2 overlaps the distribution of the diamict unit found between 1.25-1.6 m in Borehole NB1 (Figure 5.9). When the boreholes are presented on a common scale, adjusted for the height difference between the two boreholes (ca. 1.13 m) (Figure 5.7c), there is good correlation between the upper contacts of both diamict units in the two boreholes. In addition, the contact between the gravel and the underlying sand at 2.55 m in NB1 correlates with the contact between the diamict unit and the underlying gravelly sand at 1.4 m in NB2, although the basal sand in NB1 is much finer in grain-size than the respective unit in NB2 (Figure 5.7c and 5.9).

5.3.2 Electrical resistivity tomography

The resistivity profile (Figure 5.10) is characterised by three zones with different electrical properties. The near surface has a laterally continuous, highly resistive layer (230-2300 Ωm) (NB Zone 1) that varies between 2-7.5 m in thickness. A marked and relatively abrupt decrease in resistivity with depth is apparent right across the profile beneath this upper zone, with a thick, homogenous layer of low resistivity (90-230

(a)

Very dry, light brown sandy TOPSOIL

Very dry orange stained light brown sandy fine GRAVEL with subangular to subrounded small clasts to 2 cm

S 5Y 4/1 dark grey very dry sandy GRAVEL, with subangular to subrounded platy, elongate and disc shaped clasts.

S 10 YR 5/6 yellowish brown dry silty sandy GRAVEL with subrounded clasts to 4 cm and some iron staining.

S 5Y 5/1 grey fine sandy GRAVEL with clasts to 5 cm.

S 10 YR 4/3 brown sandy GRAVEL with angular to subrounded clasts.

S 5Y 5/1 grey clast free silty gravelly fine SAND.

S 5Y 4/2 olive grey sandy GRAVEL with clasts to 3 cm, fining downwards into fine gravel.

S 5Y 4/1 dark grey fine SAND with coarser dark sand between 275-280 cm.

S 5Y 4/2 olive grey sandy coarse SILT with no clasts.

(b)

Dark brown silty sandy TOPSOIL

S

2.5Y 5/2 greyish brown to 5Y5/2 olive grey moist silty sandy GRAVEL with elongate subangular clasts to 8 cm. Fines downwards into a gravelly silty sand.

S

S

5Y 3/12 very dark grey to 5Y 5/1 grey gravelly SAND with occasional clasts below 220 cm.

S

(c)

Figure 5.7: Sedimentological logs of (a) Borehole NB1; (b) Borehole NB2; (c) fence diagram of Boreholes NB1 and NB2. 'S' marks sampling locations for grain-size analysis.

Figure 5.8: Core photographs, Llanio Fawr: (a) Borehole NB1: (i) poorly sorted sandy gravels and diamict units (1-2 m) (left hand core) grading downwards to well sorted fine sand (2-2.9 m) (right hand core); (ii) poorly sorted sandy gravel (2-2.5m); (iii) well-sorted sand and sandy silt (2.7-3 m); (b) Borehole NB2: (i) poorly sorted sandy gravel/diamict (1-2 m) (left hand core) grading downwards into a gravelly sand (2-2.6 m) (right hand core); (ii) well sorted gravelly sand (1.5-2 m); (iii) well sorted gravelly sand (2-2.6 m).
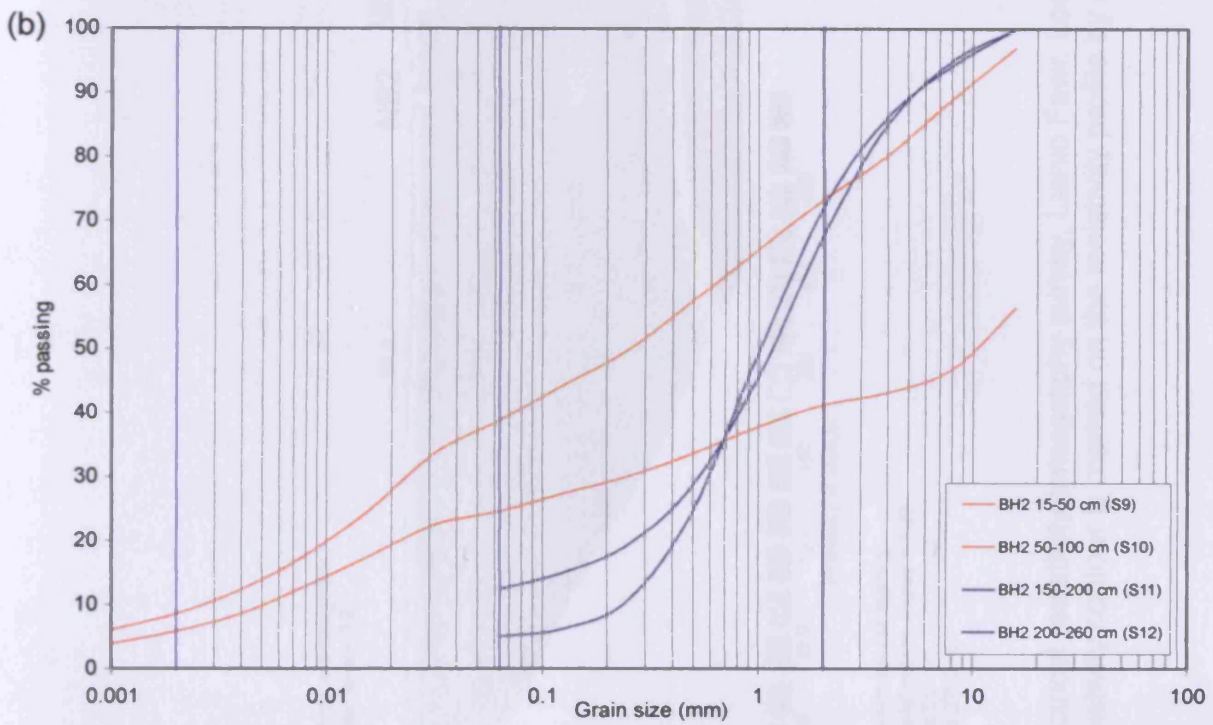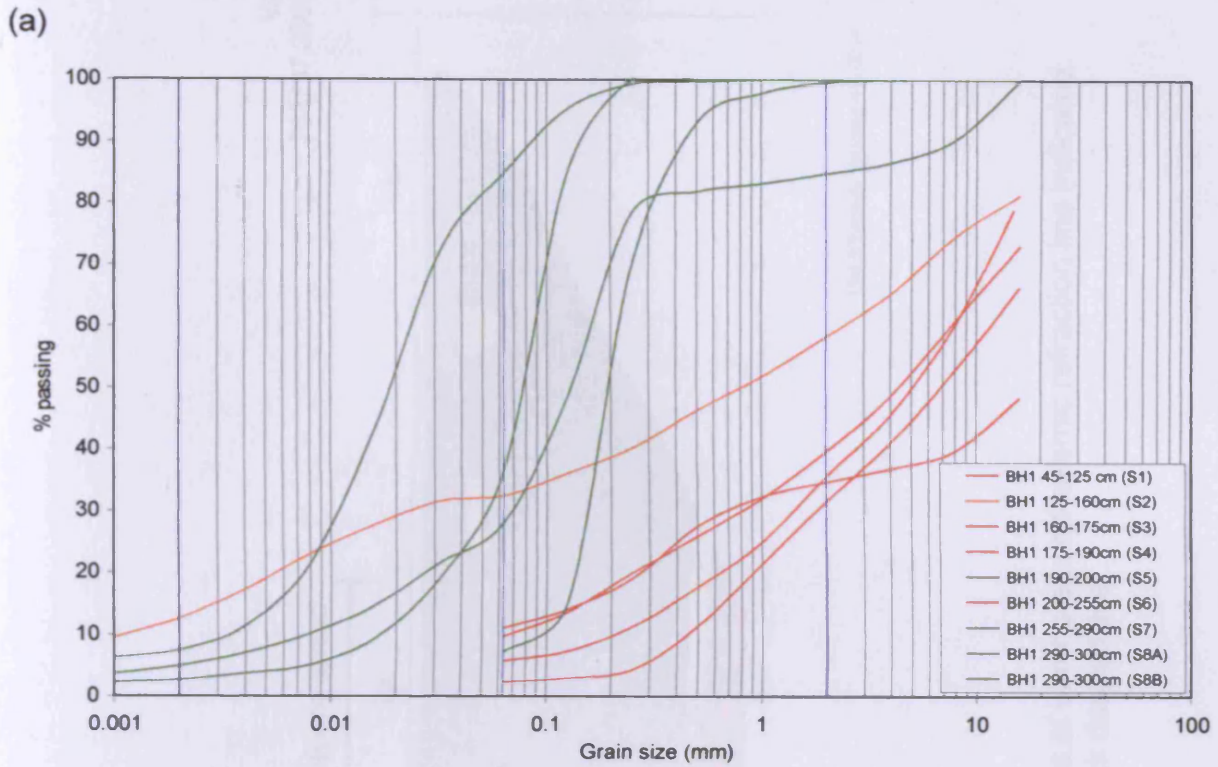
Figure 5.9: Grain-size analysis of sediments, Llanio Fawr (a) Borehole 1; (b) Borehole 2.
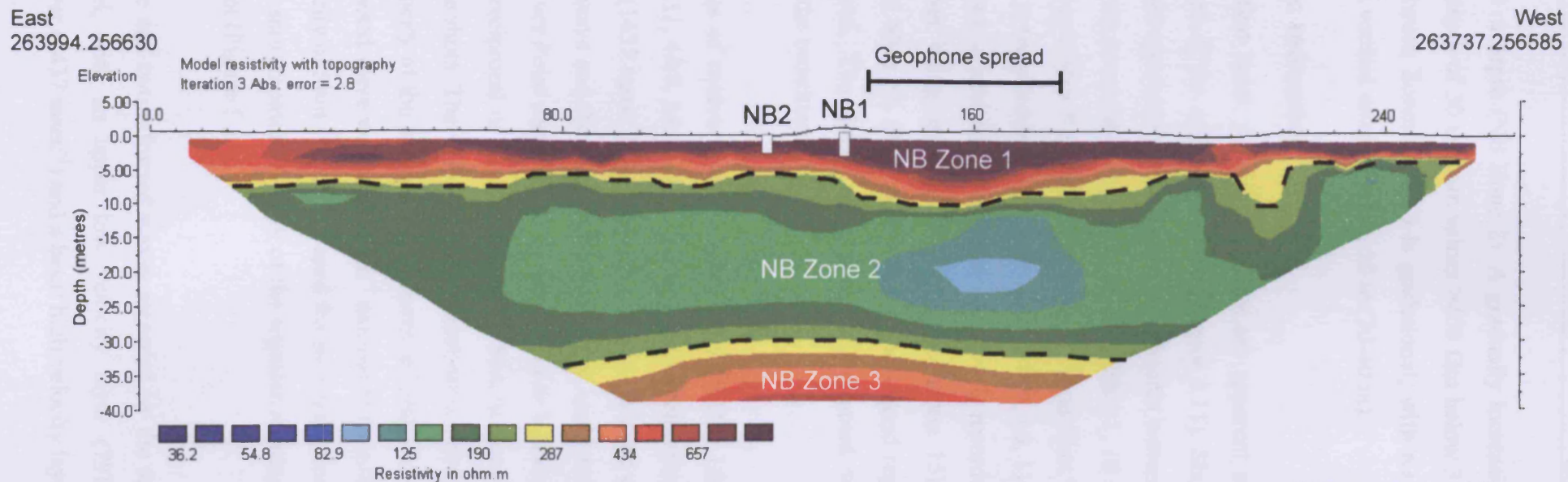
Figure 5.10: Electrical resistivity tomography survey, Llanio Fawr. Locations of boreholes and seismic refraction line indicated. The 230 Ωm resistivity contour is marked on the resistivity profile by a black dashed line.

Ωm) from 5-30 m depth (NB Zone 2). A gradually increasing zone of resistivity is found below a depth of 30 m, with values >400 Ωm below 35 m depth (NB Zone 3). The contact between Zones 2 and 3 is gradational, with resistivity increasing (190-500 Ωm) over a vertical distance of ca. 10 m (30-40 m).

5.3.3 Seismic refraction

Three P-wave first break velocity segments are apparent in both the forward and reverse directions of the traveltime graph (Figure 5.11). Shots 1, 8 and 9 have two velocity segments representing the direct and refracted waves. The crossover point of the refracted wave occurs at 6 m (geophone 4) on Shot 1, 18 m (geophone 10) and 28 m (geophone 15) on Shot 8 and 40 m (geophone 21) on Shot 9 (Figure 5.11). The first refracted wave is recorded by Shots 1, 2, 3, 4, 5, 8, 9, 10, 11 and 12, which all show strong parallelism. A second faster refracted wave is recorded by Shots 5, 6, 7, and 12, the crossover being apparent at 28 m (geophone 15) on Shot 5 and 16 m (geophone 9) on Shot 12. Shots 6 and 7, and the second segment of Shot 5 display strong parallelism. The direct wave and two refracted waves can therefore be identified from the traveltime graph.

The minus times of twelve reversed shots (1&9, 1&10, 1&11, 2&9, 2&10, 2&11, 3&9, 3&10, 3&11, 4&9, 4&10, 4&11) were used to determine the velocity of the first refracted wave (1437 msec^{-1}). Because of a lack of reversed coverage, the velocity of both the direct wave and the second refracted wave could not be calculated using the Common Receiver Point method and therefore had to be calculated from the average velocity of the reciprocal of the gradient of the best fit lines (from linear regression) of several single shots. The velocity of the direct wave was 791 msec^{-1} derived from the average velocity of the appropriate segments of Shots 1, 8 and 9. The velocity of the second refracted wave was 4151 msec^{-1} calculated from the average of Shots 5, 6 and 7. The velocity of Shot 12 was not used for the calculation of the second refracted wave due to the short measured length of the segment relating to the second refracted wave on this shot (Figure 5.11).

The direct wave and two refracted waves recorded by the seismic survey indicate a three-tier model, with an upper low velocity layer (791 msec^{-1}) overlying an intermediate layer (1437 msec^{-1}) and a basal high velocity layer (4151 msec^{-1}) (Figure

5.12). Using the Common Receiver Point method the depth and morphology of the first (upper) refractor was defined. The morphology of the first refractor was derived from Shots 1&9, 2&10 and 3&11. Whilst the plus time could be calculated for Shots 1&9 as the reciprocal time was directly measured, to calculate the plus time for Shots 2&10 and 3&11 the reciprocal time had to be estimated using the intercept time (see Section 3.4.3.1). Given the close correspondence of the depth and morphology of the refractor (Figure 5.12), the use of this estimated value was appropriate to extend the refractor laterally from that derived from Shots 1&9 alone, thereby enabling comparison with the electrical resistivity data over a longer section. Based on the depth of the refractor derived from Shots 1&9 the average depth of the first refracted horizon is 4.88 m, but the morphology of the refractor varies from 5.72 m to 4.24 m, generally dipping eastward. This observation is also supported by the morphology of the refractors derived from Shots 2&10 and 3&11 (Figure 5.12).

Due to the lack of reversed coverage and the absence of a direct reciprocal time measurement, the depth and morphology of the second (lower) refractor could not be calculated using the Common Receiver Point method. Instead, the depth to the refractor was calculated using the Intercept Time method (see Section 3.4.3.2). The calculated depths for the second refractor varied between 41-50 m (ca. 90-100 m OD) but with an average of 44 m. This may represent variation in the morphology of the refractor, but could also reflect lateral or vertical changes in velocity or the increased errors margins associated with the use of the intercept time as a substitute for the plus time.
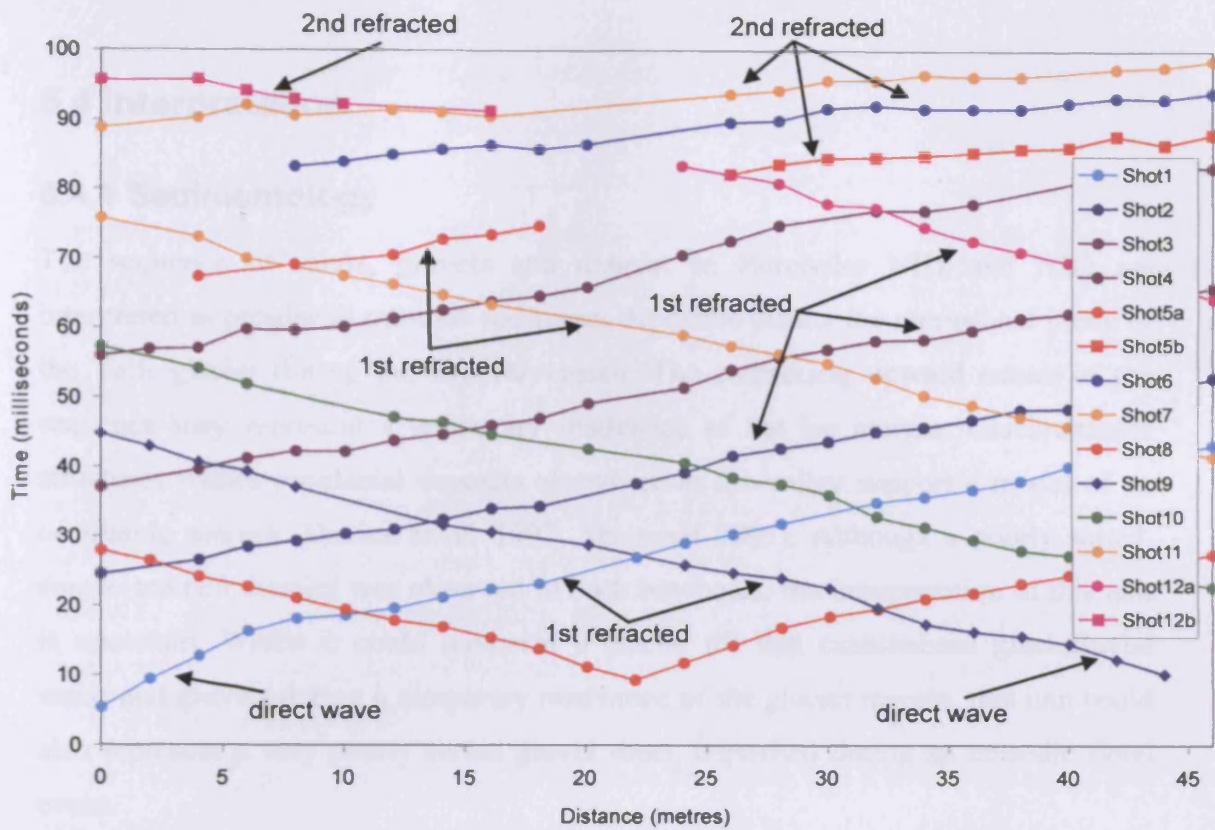
Figure 5.11: P-wave seismic refraction traveltime graph, Llanio Fawr.
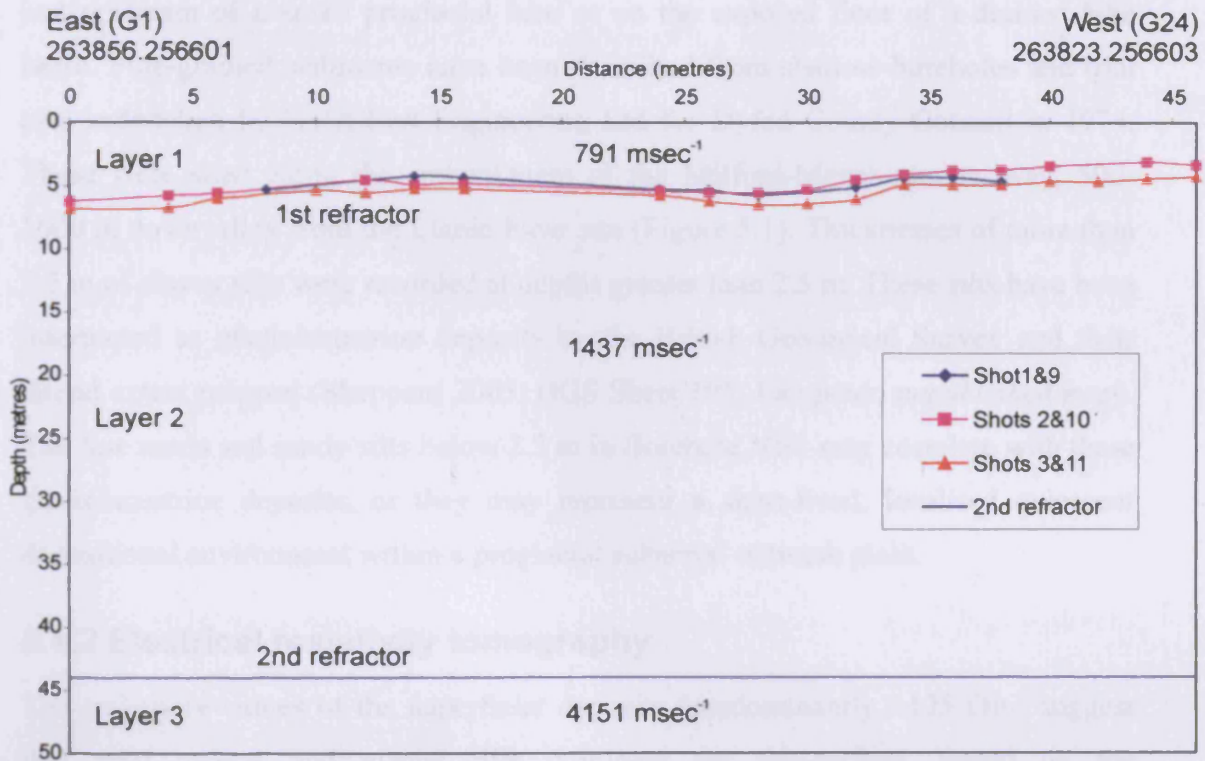
Figure 5.12: Model of seismic refraction data, Llanio Fawr. The 46 m long geophone spread corresponds to approximately 140-186 m on the resistivity profile.

5.4 Interpretation

5.4.1 Sedimentology

The sequence of sands, gravels and diamict in Boreholes NB1 and NB2 are interpreted as proglacial outwash sediments deposited during the recessional phase of the Teifi glacier during the late Devensian. The coarsening upward nature of the sequence may represent a temporary readvance of the ice margin. Glaciotectonic structures within proglacial deposits elsewhere in the valley support a model of an oscillating margin (Davies *et al.* 1997; Sheppard 2003). Although a poorly sorted, coarse-grained diamict was observed in both boreholes, the interpretation of this unit is uncertain. Whilst it could represent a glacial till that cannibalised glaciofluvial sands and gravels during a temporary readvance of the glacier margin, this unit could also represent a very poorly sorted gravel sheet, deposited during an episodic flood event.

Deposition of the glaciofluvial sediments at Llanio Fawr appears to have taken place just upstream of a small proglacial lake or on the exposed floor of a drained lake basin. Fine-grained sediments have been described from shallow boreholes and trial pits undertaken by Holst Soil Engineering Ltd for Dyfed County Council in 1974. These were sited along the embankment of the Milford-Manchester railway, 500-1000 m downvalley from the Llanio Fawr site (Figure 5.1). Thicknesses of more than 2.5 m of clayey silts were recorded at depths greater than 2.5 m. These silts have been interpreted as glaciolacustrine deposits by the British Geological Survey and their lateral extent mapped (Sheppard 2003; BGS Sheet 195: Lampeter, *unpublished map*). The fine sands and sandy silts below 2.5 m in Borehole NB1 may correlate with these glaciolacustrine deposits, or they may represent a short-lived, localised quiescent depositional environment within a proglacial subaerial outwash plain.

5.4.2 Electrical resistivity tomography

The resistivity values of the superficial deposits (predominantly >125 Ωm) suggest that sand, gravel and glacial tills dominate the sub-surface. Based on the sedimentology of the boreholes, the high resistivity zone in the near surface (NB Zone 1) is interpreted as a layer of unsaturated superficial deposits above the water

table. The lower resistivity zone at depths below 5 m (NB Zone 2) is unlikely to represent an extensive thickness of glaciolacustrine clays or silts. The resistivity of this zone (predominantly 125-190 Ωm) is not consistent with very fine-grained sediments, but is within the range of measured values for saturated sands and gravels, or tills. The high resistivity zone at depth (NB Zone 3) is interpreted as bedrock. On the basis of the resistivity data, the depth to bedrock at Llanio Fawr is therefore estimated to be between 30-40 m.

Complex variations in the superficial geology, including localised lenses of fine-grained clays or silts, may exist. However, due to the coarse resolution of the resistivity survey and the averaging and smoothing processes required during tomographic processing, they would not be identified using this technique unless they were of a significant lateral and vertical thickness. Given the very high resistivity values of NB Zone 1, and the absence of similar deposits in Borehole NB2, the thin unit of sandy silt at the base of Borehole NB1 (2.9-3 m) is unlikely to be of considerable vertical thickness or lateral extent. Although the depth to bedrock indicates a significant thickness of superficial deposits, the resistivity profile provides little unequivocal evidence for a thick glaciolacustrine succession at Llanio Fawr.

5.4.3 Seismic refraction

The two seismic refractors identified in this survey are interpreted as a) the boundary between unsaturated and saturated superficial sediments (water table) (upper refractor); and b) the superficial-bedrock boundary (lower refractor). The three layers defined by the P-wave velocities are therefore interpreted as Silurian mudstones and sandstones (Devils Bridge Formation or the Cwmystwyth Grits Groups), overlain by a thick succession of sand and gravels, and till, that can be divided into saturated and unsaturated zones. The calculated depth of rockhead is 44 m.

The velocity of the uppermost layer above the first refractor (791 msec^{-1}) is consistent with P-wave velocities for dry unsaturated sands and gravel (Reynolds 1997). This is supported by the high resistivity of NB Zone 1 (400-2300 Ωm). This near-surface layer is not interpreted as a weathered zone due to its thickness (>5 m), and the sedimentological evidence from the two boreholes, which indicate a thin zone of weathering (< 1m). Both the depth and morphology of the first refractor identified in

the seismic survey correlate well with the lower boundary of the high resistivity near-surface zone (NB Zone 1). The seismic velocity (1437 msec^{-1}) and the resistivity (90-230 Ωm) of the materials below the first refractor (NB Zone 2) are consistent with saturated unconsolidated sands and gravels or till (Reynolds 1997). This boundary, between materials of contrasting physical properties, is therefore believed to represent the water table rather than a true geological boundary. However, saturated sediments were encountered at very shallow depths in the boreholes (<1 m) indicating a high, or perched water table. This apparent contradiction is probably because the geophysical surveys were undertaken on the 26th July 2005, following an extended period of very dry weather, whilst the boreholes were drilled on the 13th October 2005, following a day of exceptionally high levels of rainfall in the upper Teifi valley, when a raised water table would be expected. As a result, the apparent boundary within the superficial deposits defined by the geophysical surveys may represent a lowered water table during the dry summer months. Given the highly resistive near-surface layer at Llanio Fawr, the application of ground penetrating radar (GPR) could be a very useful geophysical tool to use at this site to identify both the depth of the water table and to investigate the internal structure of the glaciofluvial sediments.

The velocity of the layer below the second P-wave refractor in the seismic survey (4151 msec^{-1}) is well in excess of the velocities of unconsolidated superficial deposits (normally <2000 msec^{-1}). The second refractor is therefore interpreted as representing the contact between the superficial geology and unweathered Silurian bedrock. Depending on the thickness of bedrock weathering however, the second P-wave refractor could alternatively represent a boundary between weathered and unweathered bedrock. The high velocity of the refractor is within the range established for unweathered shales, and is comparable to measured values from Lower Palaeozoic mudstones and sandstones elsewhere in the Teifi valley (Allen 1960; Francis 1964). Rockhead, based on the seismic survey, is therefore estimated at approximately 44 m (ca. 90-100 m OD). The depth to bedrock established from the seismic survey is therefore slightly more than the depth inferred from the resistivity profile (30-40 m). However, this may be the result of experimental errors associated with calculating P-wave velocities (ca. 10 % error margin), or because the resistivity survey is mapping a contact between superficial sediments and weathered bedrock, rather than a deeper boundary of unweathered bedrock below a thick layer of

weathered bedrock, which the seismic survey could be mapping. The smoothness algorithms used in 2D resistivity inversion models can also cause problems for accurately detecting the depth of sharp boundary interfaces (Wisén *et al.* 2005). Changes in seismic velocity associated with a lower velocity layer (blind zone) in the superficial geology could also affect the calculations of depth derived from the seismic refraction survey however, resulting in an overestimation of depth. Regardless, the geophysical surveys indicate a significant thickness of superficial deposits at this site (>30 m).

The geophysical methods applied in this study have, in comparison to previous studies (Harris 2001b), provided rather limited data regarding the internal structure and possible origins of these landforms. However, they have provided key information regarding both the physical properties of the sediments below the limited depth of investigation provided by drilling methods at this site, which can be used to infer lithology, and the depth to bedrock. When combined with the large-scale geomorphology of the area, the geophysical evidence is consistent with the suggestion that this part of the valley represents a meander loop formed during pre- or early-Quaternary incision of the Teifi valley that may later have been modified by glacial erosion (Sheppard 2003). Significant thicknesses of superficial deposits have also been recognised in similar buried meander loops in the lower reaches of the Afon Teifi (Allen 1960; Francis 1964; Jones 1965; Nunn and Boztas 1977; Hambrey *et al.* 2001; Etienne *et al.* 2006). Elsewhere in the upper Teifi, a borehole at Olwen in the Dulais valley just north of Lampeter recorded a thickness of sand and gravel greater than 27 m (Crimes *et al.* 1992; Robins *et al.* 2000). Depth to rockhead in the upper- to mid-Teifi valley, estimated from resistivity soundings, gravity surveys and a single borehole, is up to 45 m (70 m OD) near Lampeter, and approximately 50 m (45 m OD) near the mouth of the Cledlyn valley at Rhuddlan (Heaven *et al.* 1999). The upper Teifi valley therefore represents a significant sedimentary sink of the western sector of the Welsh ice mass during the late Quaternary and represents a potentially important palaeoenvironmental record of the glaciation and deglaciation of this area. These observations may contradict the view that the intensity of glacial erosion associated with the Welsh ice mass was limited and was unable to erode deep valley basins (Watson 1968).

5.4.4 Model of landform formation

The linear, orientated morphology of the ridges at Llanio Fawr (Figure 5.3) is puzzling. Although there is clear evidence that the mid Wales uplands were subject to significant periglacial activity after deglaciation (Watson 1965, 1981; Potts 1971) the morphology and sedimentology of the landforms described in this article are not consistent with a model that interprets them as the remains of periglacial ground-ice mounds. Because the surface ridges at this site formed through glaciofluvial deposition rather than through post-depositional ground-ice disturbance, they are superficial landforms that have no genetic relationship with the sediments below the very near surface. Neither the sedimentological or geophysical data provides any evidence for deep silt- or clay-filled basins beneath these landforms, such as those found in association with ramparted depressions in the Cledlyn valley (Watson and Watson 1972), nor any evidence for the extensive glaciolacustrine deposits necessary for lithalsa development (Gurney 1995). These are almost certainly not therefore the remains of open system pingos, and are considered unlikely to be lithalsa remnants. The geomorphology and sedimentology of these landforms instead suggests that their formation is the result of proglacial outwash deposition. However, although they are orientated downstream, presumably in the direction of downvalley flow, the linear ridges do not appear to be longitudinal bars associated with the braided channel systems of an outwash plain (Miall 1983). Possible alternative processes for the development of these landforms could be i) glaciofluvial sedimentation around and above melting blocks of buried glacier ice (Price 1973; Maizels 1992); or ii) glaciofluvial deposition on the surface of proglacial icings (also known as naledi or aufeis) (Åkerman 1982).

The melting of masses of glacier ice buried by glaciofluvial deposition (Price 1973) could explain the formation of the landforms at Llanio Fawr. Glaciofluvial sediments dominate the superficial geology of the mid- to upper-Teifi valley between Llanybydder and Tregaron (Waters *et al.* 1997). Under rapid rates of sedimentation during the Late-Devensian, burial of stagnant parts of the ice margin by glaciofluvial sedimentation clearly took place, as evidenced by the large kettle hole at Pant Farm, only 2 km due east of Llanio Fawr (Figure 5.1). As well as kettle hole development, the melt out of extensive bodies of stagnant ice can also cause kettled-outwash, with a

complex, chaotic assemblage of ridges, mounds and hollows, when buried by rapidly deposited sands and gravels (Price 1973). Ramparted depressions can also occur at significant distances from the ice margin due to the burial of ice blocks transported by jökulhaup events (Price 1973; Maizels 1992). Whilst the more circular enclosed depressions within the complex of landforms at Llanio Fawr could represent the deposition of proglacial outwash above blocks of buried glacier ice deposited by catastrophic drainage, the elongate morphology of the majority of ridges at Llanio Fawr is clearly distinct from the circular examples described from Iceland (Maizels 1992), and the evidence presented here from this site cannot be used to justify such an analogy. Although catastrophic drainage of the Lateglacial moraine-dammed lake at the current site of Tregaron Bog (northeast of Tregaron) could potentially have transported ice blocks downvalley to Llanio Fawr, there is currently no evidence that this lake drained catastrophically.

In Svalbard, esker-like landforms (<2 m in height, up to several tens of metres in length) form as a result of glaciofluvial sedimentation in the meandering drainage channels incised into the surface of ephemeral proglacial icings (Åkerman 1982). Because of favourable localised hydrogeological conditions, icings frequently develop in the same place each winter. As icings tend to aggrade passively on top of the ground surface (Worsley 1997), a series of superimposed, crosscutting ridges could develop as glaciofluvial sediments, annually deposited in meltwater channels incised into the surface of the icing, collapse when the icing melts during late spring or early summer. Over a period of several years this could result in a complex assemblage of superimposed, chaotic to linear, esker-like landforms composed of glaciofluvial sediments developing, such as observed at Llanio Fawr. During the early summer melt season, proglacial icings commonly disintegrate into a chaotic series of ice blocks and sheets dissected by meltwater channels (Åkerman 1982) and sedimentation around such bodies of ice could explain the more circular depressions at Llanio Fawr. The long-term preservation potential of aggradational landforms associated with icing development is rather limited however (Coxon 1978; Worsley 1997). Furthermore, as the evidence for these landforms is ambiguous, we follow Worsley's (1997) advice that a cautious approach to the interpretation of these landforms should be exercised. Nevertheless, proglacial icing development is a possible mechanism for the development of the ramparted depressions at Llanio

Fawr, although the current evidence does not enable a more specific interpretation regarding the origins of these landforms to be made.

It is quite clear that the morphology and sedimentological composition of the ridges at Llanio Fawr indicate that these landforms are probably not the remains of periglacial ground-ice mounds. This conclusion has implications for the interpretation of ramparted depressions elsewhere in the British Isles. Many landforms, particularly those within the Devensian glacial limits, which have previously been interpreted as the remains of open-system pingos or lithalsas, may also have alternative origins, kettled outwash or esker-like landforms associated with proglacial icings being only two of several possible mechanisms for their development.

6 Crychell Moor

6.1 Introduction

A high-density concentration of small, enclosed, shallow, circular peat-filled depressions is located at Crychell Moor, 4 km west of Llanbister, Powys (Figures 6.1, 6.2, 6.3 and 6.4). First identified by the Soil Survey, these landforms were interpreted as the remains of open system pingos (Rudeforth *et al.* 1984). The nearest known sites where ramparted depressions, interpreted as relict ground-ice mounds, have been identified are at Llangurig 20 km to the west (Pissart 1963) and at Owlbury, Shropshire 30 km to the northeast (Gurney and Worsley 1996). The Crychell Moor site is situated in the catchment of the River Ithon, in the valleys of the Crychell Brook and Ffrwd Wen (Figures 6.1 and 6.3). Glaciers in this area, east of the watershed of the Cambrian Mountains of mid-Wales, fed the south and eastward flowing Wye glacier during the last glaciation (Dwerryhouse and Miller 1930; Lewis 1970; Luckman 1970; Richards 2005; Lewis and Thomas 2005). Ice flowed into the Wye and the Ithon-Irfon Depression through the Ithon valley and eastwards into Herefordshire through the Teme, Lugg, Hindwell and Arrow valleys.

During late Devensian deglaciation of the mid-Wales uplands and the Cambrian Mountains, downwasting of debris-rich ice took place in the main valley systems. The Wye valley north of Builth Wells and the Irfon-Ithon depression (e.g. around Llandrindod Wells) are dominated by hummocky glacial sediments and landforms deposited during this phase (Lewis 1966, 1970). Stagnation of *in situ* ice also occurred in the smaller Lugg, Arrow and Hindwell valleys (Luckman 1970). More recent mapping of the Wye, Ithon and Severn valleys has identified broad tracts of hummocky glacial sediments and ice-contact glaciofluvial deposits (Crimes *et al.* 1992; British Geological Survey 1993, 1994b, 2005; Davies *et al.* 1997; Cave and Hains 2001; Schofield *et al.* 2004), supporting this model of deglaciation.

The bedrock geology of the area around the Crychell Moor site is characterised by sandstones and mudstones of Ordovician and Silurian age (Figure 6.5; British Geological Survey 1993). The site is underlain by mudstones of the Dolgau Mudstones Formation of Llandovery Series (Ordovician) age. The area is structurally

complex, but the feature of most significance is the north-south trending fault that directly underlies the site (Figure 6.5).
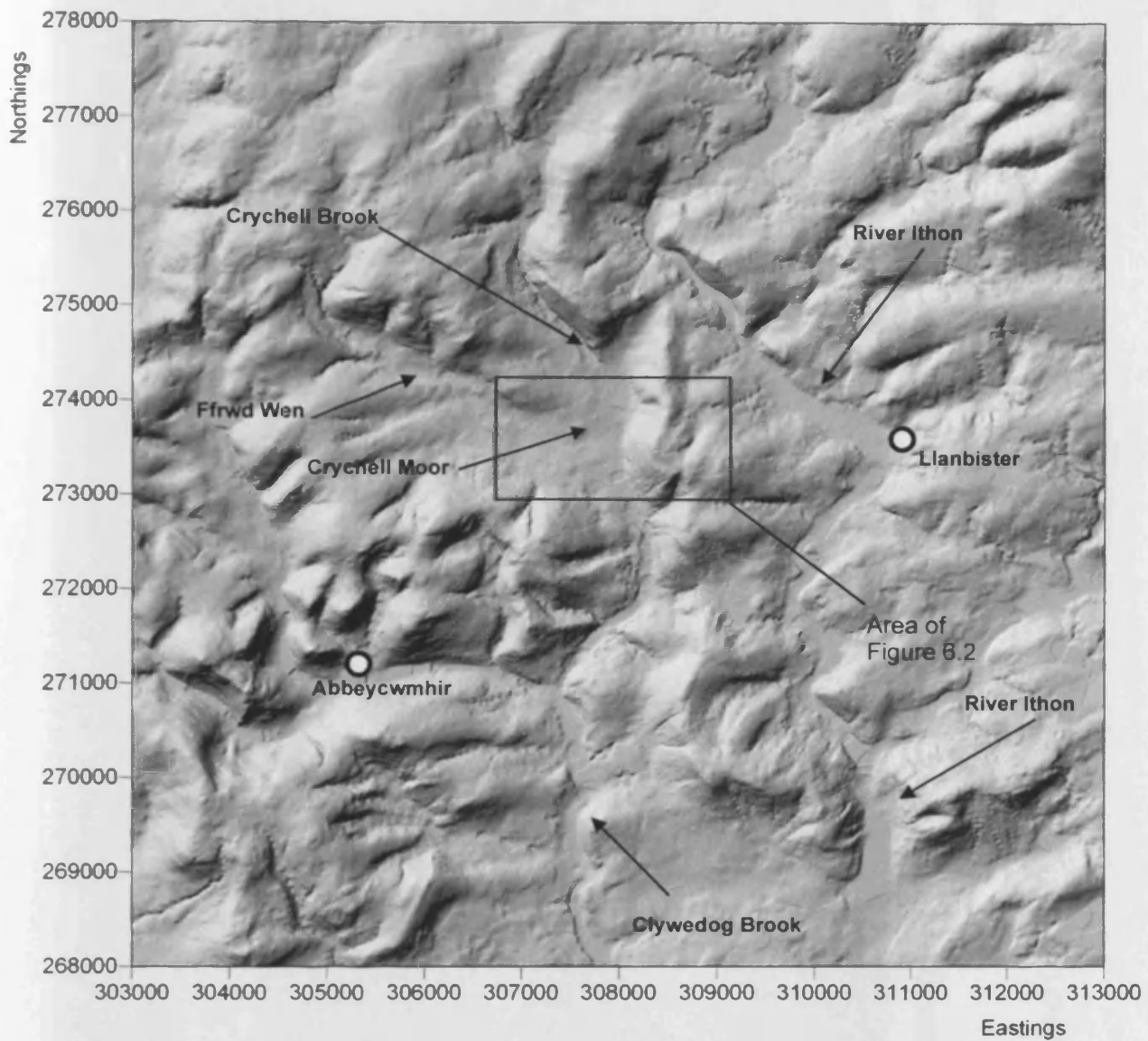
Figure 6.1: OS Profile® digital terrain model (DTM) of the Ithon and Crychell Brook valleys (OS Profile® data © Crown Copyright/database right 2006. An Ordnance Survey/(Datacentre) supplied service.
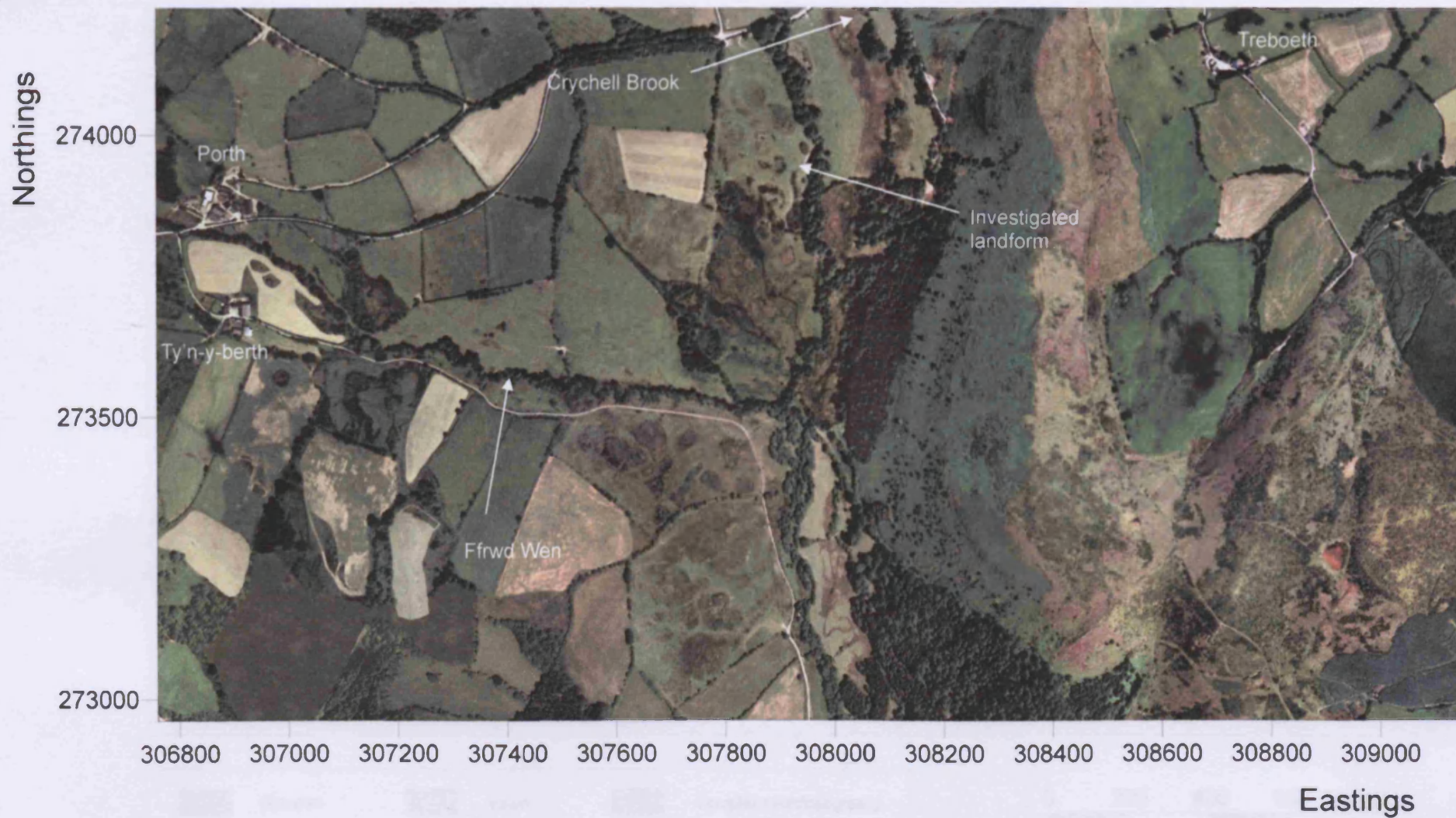
Figure 6.2: Aerial photograph of Crychell Moor, near Llanbister, Powys, taken in 2000 (© Getmapping Plc 2006).
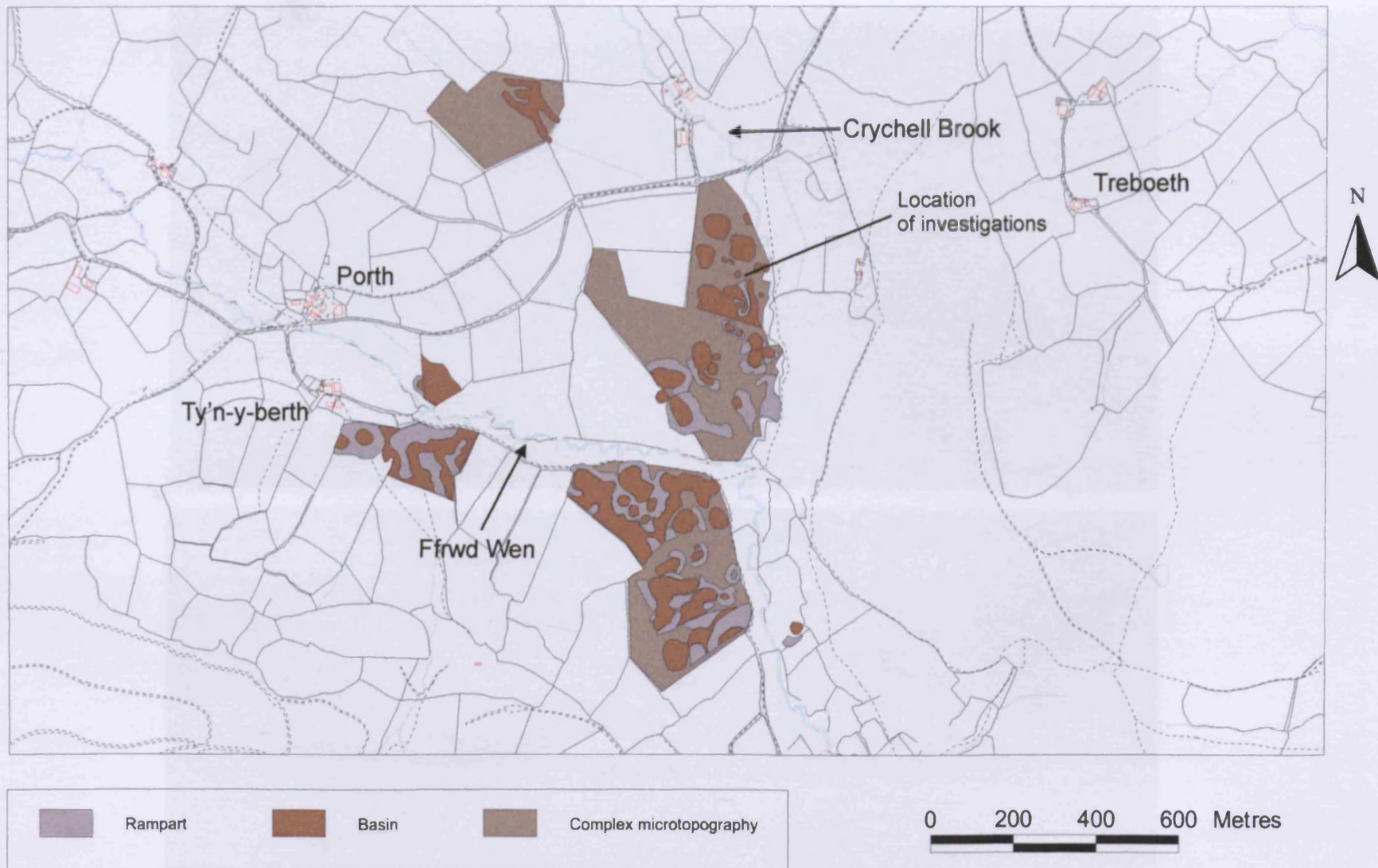
Figure 6.3: Geomorphological map of the Crychell Moor site. LANDLINE data © Crown Copyright/database right 2005. An Ordnance Survey/(Datacentre) supplied service.

Figure 6.4: Ramparted depressions, Crychell Moor, near Llanbister, Powys: (a) overview of site looking to the south with the investigated basin indicated; (b) example of small peat-filled depression lacking a pronounced rampart. Location of landform indicated in Figure 6.4a (Photo: C. Harris).

Legend:

Quaternary
- Alluvium
- Till

Silurian
- Penstrowed Grits Formation
- Nant-ysgollen Mudstone Formation
- Glanyrafon Formation
- Dolgau Mudstones Formation
- Dolgau Mudstones Formation

Ordovician
- Cwmcringlyn Formation
- Yr Allt Formation

Structure
- — — — Fault
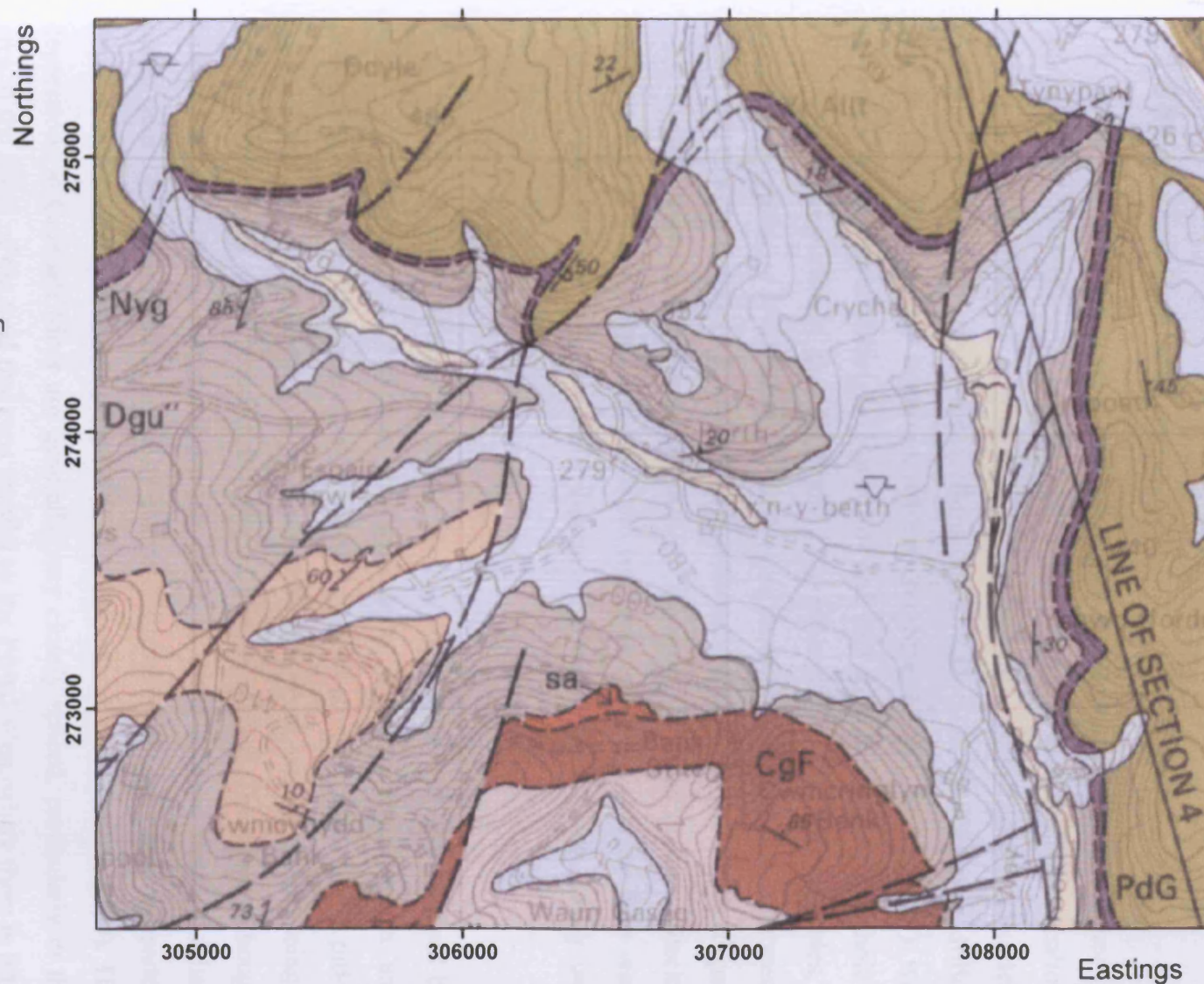
Figure 6.5: Drift and bedrock geology of the area around the Crychell Moor site (British Geological Survey 1993).

6.2 Site description and survey

One small, peat-filled, ramparted depression was investigated at Crychell Moor on the 29th June 2005 (Figures 6.4a and 6.6). The survey consisted of two shallow boreholes, which reached depths of <4 m, and two, perpendicular, electrical resistivity tomography survey lines. Borehole 1 (SO 07905.73930) was drilled through the ridge of the landform, whilst Borehole 2 (SO 07901.73953) was positioned in the central basin, 1.32 m below and 19.8 m to the north of Borehole 1 (Figure 6.6). The resistivity profiles (both 175 m in length, 2 x 18 electrode cables, 5 m electrode spacing of electrodes) ran from south-north (Line CM-1) and from west-east (Line CM-2). Borehole 2 marked the intersection point of the two cables (Figure 6.6). Topographical data necessary to process the resistivity profiles was collected using an EDM system. The locations of the boreholes and the resistivity lines were georeferenced using a handheld GPS system. No seismic refraction survey was undertaken at this site.

The majority of the landforms at the Crychell Moor site are not characterised by easily defined ramparts. Although the topography appears rather uneven and undulating, the general impression is of a relatively level ground surface that is pitted with depressions (a few metres to 50 m in diameter) (Figure 6.4a), rather than being a series of ridges that stand proud of the general ground surface. Therefore, although subdued ridges up to 1-2 m high are present, generally the area has a 'negative' relief, rather than the 'positive' relief normally characteristic of other sites where ramparted depressions are found in Wales (Watson 1971; Watson and Watson 1972, 1974). The depressions at Crychell Moor are generally very closely spaced, particularly in the area to the south of the road that runs parallel to the Ffrwd Wen, where there is little or no clear evidence for well defined, wide ramparts (Figures 6.2 and 6.3). In places, the ramparts are very narrow (ca. 10 m across). There are a few, more defined, circular features however, some with more substantial enclosing ridges (2-3 m high) (e.g. at 307789.273744, 307726.273711 and 307760.273636).
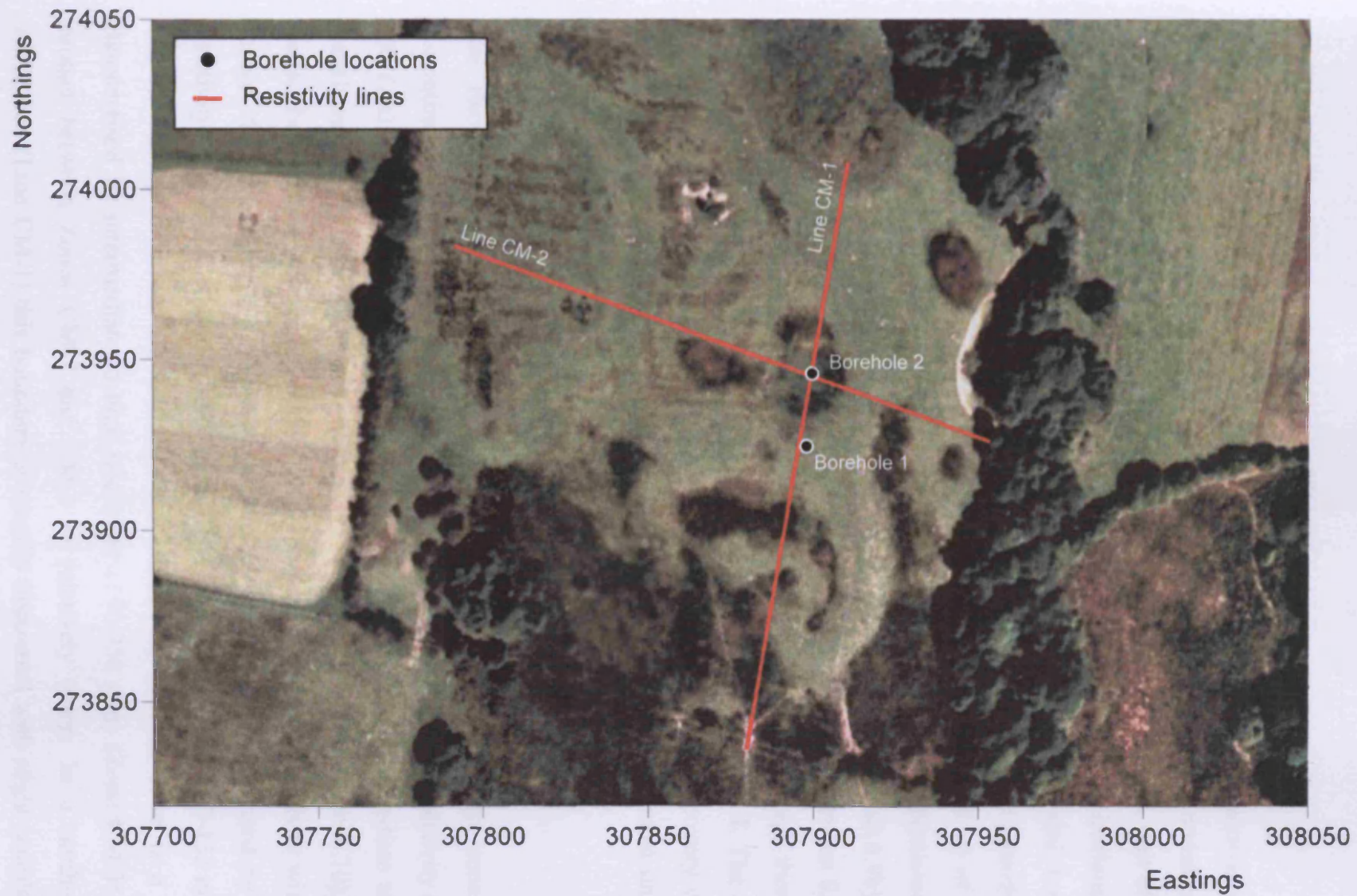
Figure 6.6: Locations of sedimentological and geophysical surveys at Crychell Moor, near Llanbister, Powys (aerial photograph © Getmapping Plc 2006).

6.3 Results

6.3.1 Sedimentology

The upper 0.3-2.1 m of Borehole 1 was composed of a clast-supported, sandy gravelly diamicton with subrounded to subangular platy to rod-shaped mudstone and sandstone clasts, up to 5 cm in length (Figures 6.7a, 6.8a and 6.9a). A unit of very poorly sorted, well-graded, silty gravelly clayey sand, with possible laminations, was incorporated within the diamicton between 1.3-1.65 m. Between 2.1 and 4 m the borehole was dominated by a firm, matrix-supported, poorly sorted, silty sandy fine gravelly diamicton (Figures 6.7a and 6.8b). Borehole 2 revealed 0.8 m of peat, overlying 0.1 m of gravelly clayey silt, 1.6 m of sandy fine gravelly diamicton and 1.5 m of stoneless, in parts laminated, clayey silt (Figures 6.7b, 6.8c and 6.9b). The sandy gravelly diamicton found between 0.3-4 m in Borehole 1 and between 0.9-2.5 m in Borehole 2 have similar grain-size distributions (Figure 6.9), although there is a slightly higher matrix component to those between 2.1-4 m in Borehole 1. The depth reached in both boreholes was restricted by the limits for the safe recovery of the coring equipment. As a consequence, the total thickness of the lowermost units in both boreholes is unknown.

6.3.2 Electrical resistivity tomography

The two resistivity profiles are characterised by three resistivity zones. A discontinuous, thin (0-5 m), near-surface zone of intermediate to high resistivity (190-500 Ωm) (Zone CM-1) overlies a laterally continuous zone of intermediate to low resistivity (50-190 Ωm), which is 5-10 m thick (Zone CM-2) (Figure 6.10). The contact between the two zones is sharp, with an abrupt change in resistivity within a vertical distance of ca. 2 m. Where the near-surface is not characterised by high resistivity, Zone CM-2 continues upwards to the ground surface (e.g. 110-135 m Line CM-1). At depths below 10 m across both resistivity profiles there is a zone characterised by intermediate to high resistivity (190-350 Ωm) (Zone CM-3). The contact between Zones CM-2 and CM-3 is relatively sharp. In a north-south orientation (Line CM-1) this boundary is roughly horizontal with slight undulations (Figure 6.10a). However, in an east-west orientation (Line CM-2), this contact dips eastwards between 80-125 m along the line, and appears to dip westward between 0-

80 m along Line CM-2, marking an apparent boundary between a lower resistivity zone upslope and the high resistivity zone at the east end of Line CM-2 (Figure 6.10b).

(a)

CLAY SILT SAND GRAVEL

Depth (metres)

2.5Y 5/3 Light olive brown sandy SILT

2.5Y 5/3 Light olive brown stony sandy SILT. Subrounded to subangular platy to rod-shaped clasts to 5cm.

2.5Y 5/4 Light olive brown sandy GRAVEL. Clasts subrounded.

2.5Y 6/2 Light brownish grey sandy GRAVEL. Subangular black Aberystwyth Grits to 4 cm.

2.5Y 6/1 Gray clayey gravelly silty SAND with 10YR 6/8 brownish yellow iron staining. Possible laminations.

5Y 4/1 Dark grey sandy fine GRAVEL. Subrounded clasts to 3 cm.

5Y 5/2 Olive grey stony silty sandy GRAVEL, becoming increasingly gravelly with depth. Subangular clasts to 3 cm.

(b)

CLAY SILT SAND GRAVEL

Depth (metres)

Very dark brown fibrous PEAT with roots.

5Y 7/1 Light grey gravelly clayey SILT with roots.

GLEY 1 5/N Grey sandy fine GRAVEL. Clasts rounded to subrounded. Clast size increasing with depth, long axes up to 10 cm.

GLEY 1 4/1 Dark grey stoneless clayey SILT. Laminated in places, particularly below 3 m.

Figure 6.7: Sedimentary logs of (a) Borehole 1; (b) Borehole 2; Crychell Moor, near Llanbister, Powys. 'S' marks the locations of sampling for grain-size analysis.
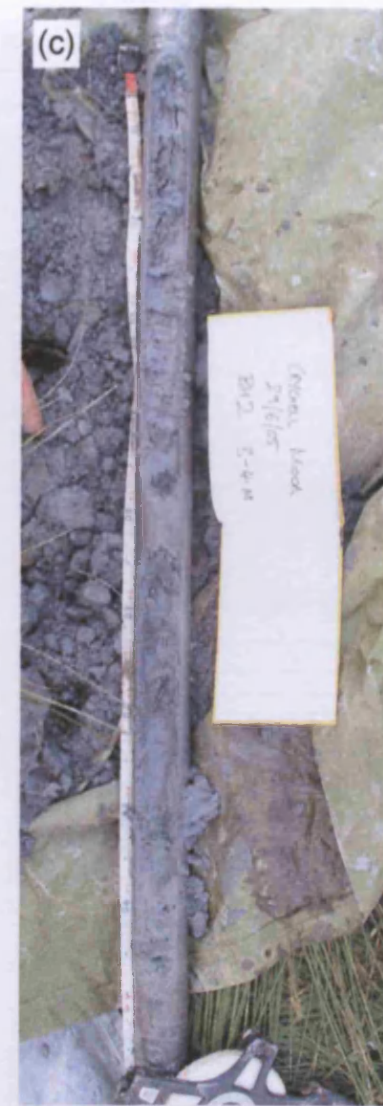
Figure 6.8: Photographs of sediments from Borehole 1 and Borehole 2, Crychell Moor: (a) Sandy fine gravel (diamict), with gravelly silty sand (1.3-1.65 m), 1-2 m, Borehole 1; (b) Silty sandy gravel (diamict), 3-4 m, Borehole 1; (c) Clayey silt, 3-4 m, Borehole 2.
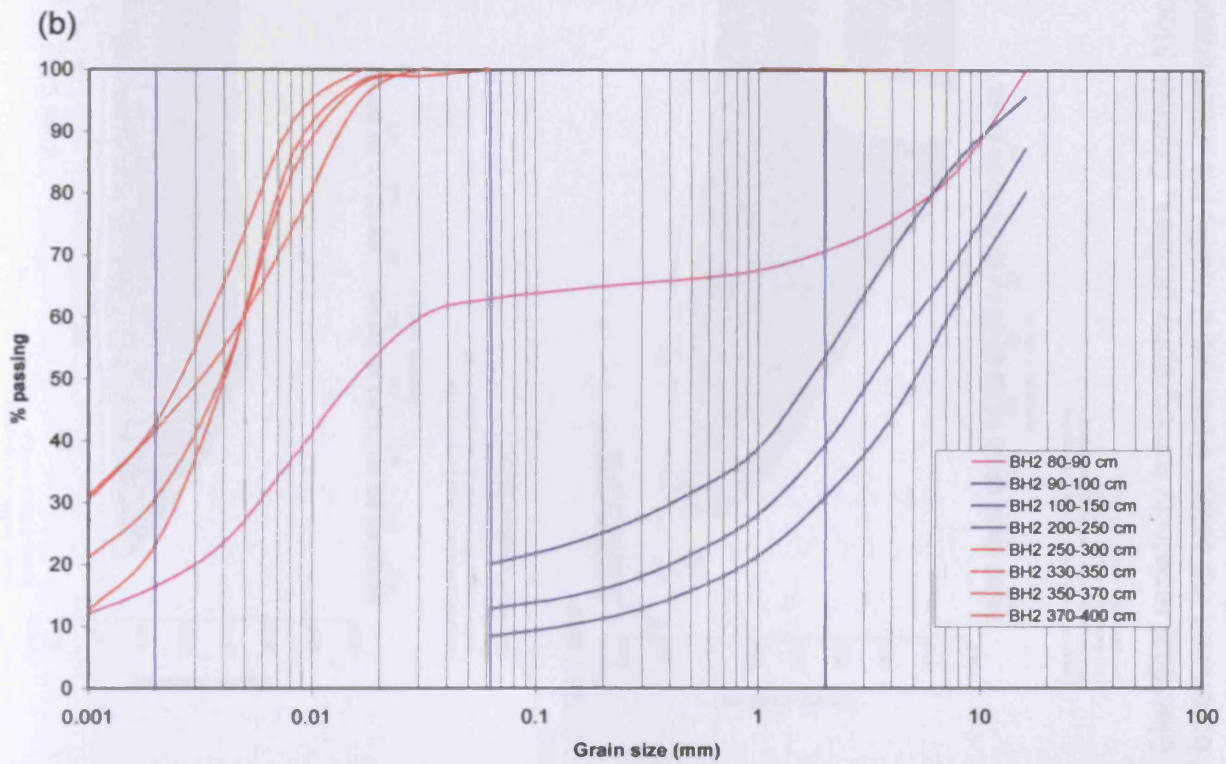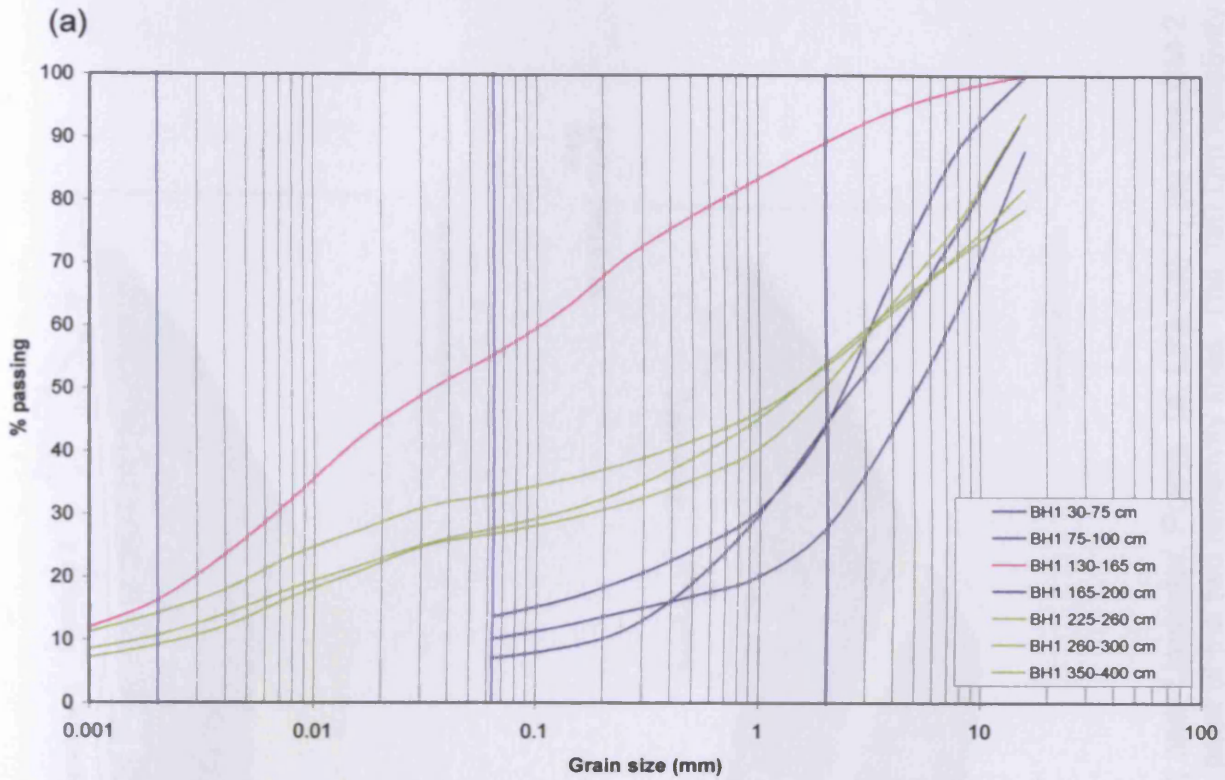
Figure 6.9: Results of grain-size analysis of samples from Crychell Moor, Powys: (a) Borehole 1; (b) Borehole 2.
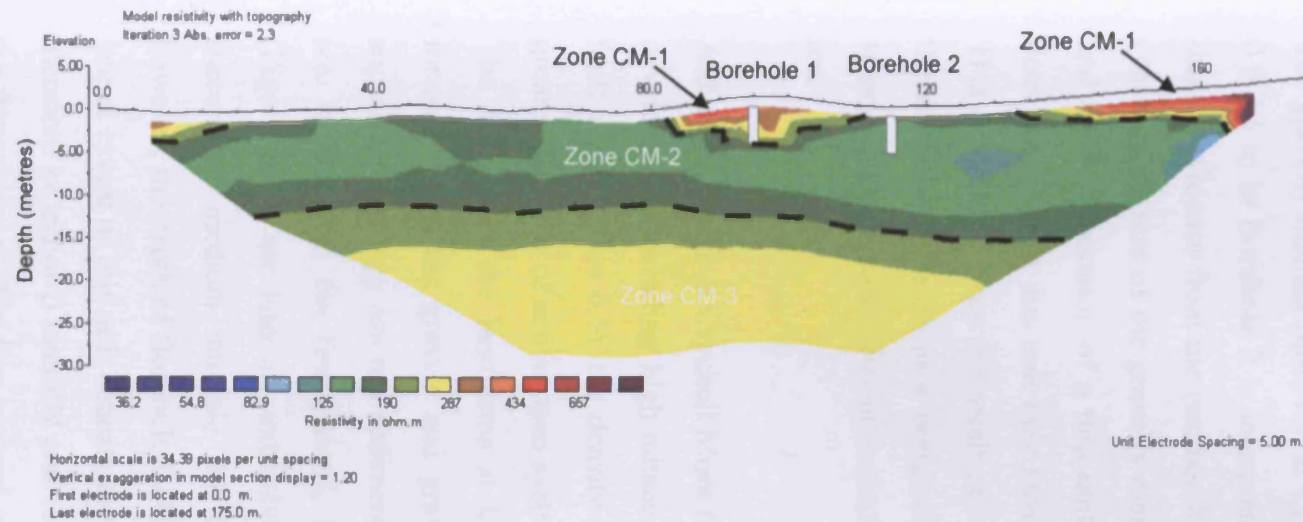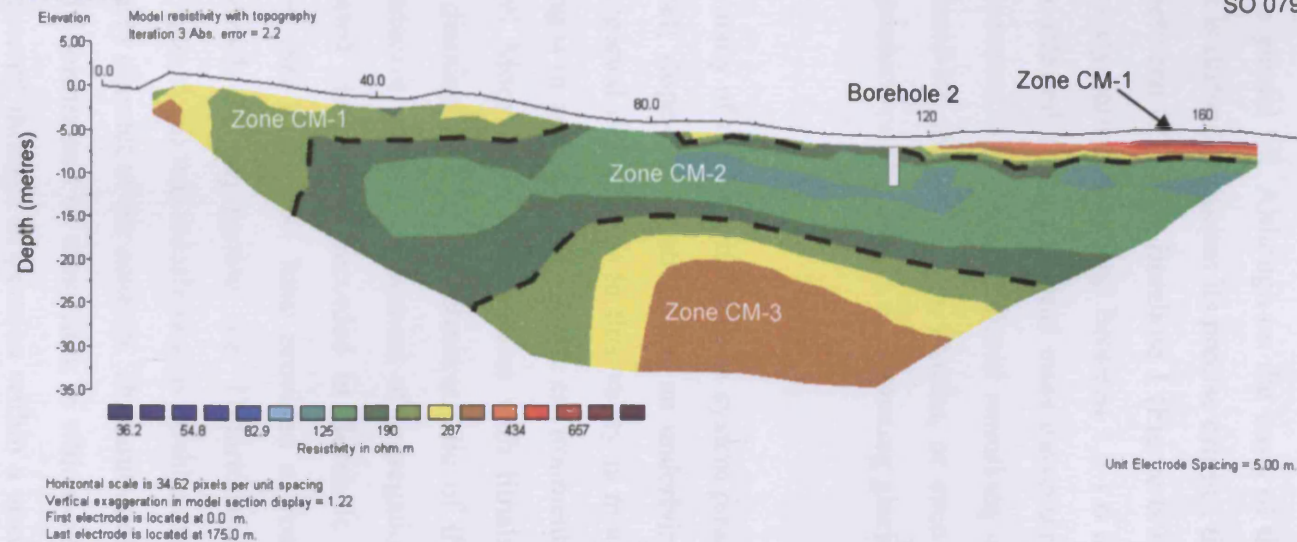
Figure 6.10: Electrical resistivity tomography profiles, Crychell Moor, near Llanbister, Powys: (a) Line CM-1; (b) Line CM-2. Locations of boreholes indicated. Borehole 2 marks the intersection point of the two resistivity lines. The 190 Ωm resistivity contour is marked by a black dashed line.

6.4 Interpretation

6.4.1 Sedimentology

The gravelly diamict observed at Crychell Moor throughout Borehole 1 and between 0.9-2.5 m in Borehole 2 is interpreted as a glacial till. Although on the basis of the limited evidence from the two boreholes it is difficult to assess its precise origins, the coarse grain-size of the gravelly diamict between 0.3-2.1 in Borehole 1 (Figure 6.9a) and the incorporation of a thin unit of poorly-sorted silty sand between 1.3-1.6 m, does suggest that this unit may have been affected by gravitational mass movement. This could have been the result of two processes: (i) post-depositional reworking on the steep-sided flanks of a periglacial ground-ice mound (pingo, lithalsa, or even a seasonal frost mound); (ii) supraglacial deposition on the surface of stagnating glacier ice.

Although the site at Crychell Moor fulfils many of the criteria for open system pingo development, including high adjacent relief; slope-foot location; and an underlying fault zone (Figure 6.5), the density of ramparted depressions in this valley is much greater than that of active open system pingos in contemporary Arctic environments. The density of the landforms at Crychell Moor is more consistent with lithalsa formation, but the gravels and gravelly diamicts that appear characteristic of the superficial geology are not sediments conducive to the development of segregation ice. If however, the fine-grained, laminated clayey silts recorded in Borehole 2 (Figure 6.7b) are laterally extensive, then this unit could have provided a frost-susceptible medium suitable for the growth of segregation ice. Unfortunately however, the depth of Borehole 1 (4 m) (Figure 6.7a) was insufficient to establish the lateral extent of this unit beneath the gravelly diamict of the rampart. This unit could therefore be either i) laterally and vertically constrained by diamicton, in which case the deposition of this fine-grained unit occurred through suspension within a small basin impounded by diamicton (Borehole 1: 0.3-4 m); or ii) laterally extensive, extending beyond the boundaries of the landforms basin, in which case development must have occurred in a larger body of water prior to the deposition of the diamicton. If the latter were the case, then this would strengthen any argument that these

landforms might be the remains of lithalsa-like periglacial ground-ice mounds, as it would provide a frost-susceptible medium suitable for their development.

Supraglacial deposition onto the surface of a debris-covered glacier pitted with small thaw lakes probably best explains the current sedimentological evidence however. The diamict recorded in Borehole 2 (0.9-2.5 m) and in Borehole 1 (0.3-2.1 m) (Figure 6.7) could be interpreted as supraglacial till deposited by the flow and mass movement of saturated supraglacial sediment and the meltout of glacier ice (Boulton 1972; Paul 1983). An alternative possibility however is that the diamict-cored rampart was formed by the slumping of overburden material down the steep flanks of a ground-ice mound, whilst the 1.6 m thick unit of diamict in Borehole 2 was later deposited by the slumping of the walls of the enclosing rampart into the central basin during the final stages of ground-ice mound collapse. However, given the thickness of this unit (1.6 m) and the apparent absence of bedding within the unit this possibility is thought unlikely. Rather than being the result of the slopewash and mass wasting of the sandy, gravelly diamict within the ramparts from the collapse of a ground-ice mound (which would probably produce a less homogenous, fine-grained grain-size distribution), the laminated clayey silts in Borehole 2 (2.5-4 m) are more easily explained by deposition from meltwater accumulating in a depression on the surface of debris-covered stagnant ice. The deposition of the overlying unit of diamicton that is found between 0.3-2.1 m in Borehole 2 could be explained by the flow of water-saturated diamict in the later stages of the meltout of the buried ice. The presence of the 1.6 m thick unit of coarse-grained diamict resting upon the >1.5 m thick unit of clayey silt in Borehole 2 makes this landform unique in Wales, as the fine-grained minerogenic-fill of all the other ramparted depressions so far investigated is directly overlain by peat.

Differential melting of a buried, stagnating ice mass, resulting in the slumping and deposition of supraglacial diamict into topographical lows, is widely recognised in supraglacial environments, and commonly leads to the development of a complex geomorphology characterised by hummocks and depressions (Price 1973), similar to that recognised at Crychell Moor. Supraglacial sedimentation may not explain the complete sequence of sediments observed at Crychell Moor however. The increased proportion of fine-grained material within the matrix of the diamict between 2.1-4 m

in Borehole 1, and its more compact nature compared to the overlying unit, could reflect deposition under subglacial conditions.

The chaotic, complex nature of supraglacial environments makes interpretation of their sedimentary product exceptionally difficult, particularly when such interpretation is restricted by a limited number of shallow boreholes and exposures. Nevertheless, although by no means entirely diagnostic, the association of sediments recorded at Crychell Moor (coarse-grained tills and stoneless clayey silts) appears characteristic of deposition within a predominantly supraglacial environment (Paul 1983; Johnson and Menzies 2002). Additional boreholes between Boreholes 1 and 2, near to the edges of the central basin, would clarify the relationship between the diamicton in both boreholes and the lateral extent of the clayey silt, thereby testing whether the correlation of units between the boreholes, which is key to the interpretation of these landforms, is valid.

On the basis of the current sedimentological evidence and the density and morphology of the ramparted depressions at Crychell Moor, a model of glacigenic sedimentation (widespread burial and meltout of downwasting glacier ice) is favoured over one of periglacial ground-ice development as a result of permafrost aggradation after deglaciation. The most likely explanation for the entire sequence of minerogenic deposits in Boreholes 1 and 2 is their deposition in a complex supraglacial environment characterised by the slumping and flow of saturated till, the meltout of buried ice and the development of thaw lakes on the glacier surface. As the meltout of the buried ice took place, the overlying sediments collapsed, resulting in the formation of the ramparted depressions. This interpretation is consistent with the regional evidence for the downwasting of debris-rich stagnant ice in mid Wales (Lewis 1966, 1970; Luckman 1970; Crimes *et al.* 1992; British Geological Survey 1993, 1994b, 2005; Davies *et al.* 1997; Cave and Hains 2001; Schofield *et al.* 2004).

6.4.2 Electrical resistivity tomography

The high resistivity of the rampart (Zone CM-1) is consistent with the gravel and clast-rich diamicton in Borehole 1. Resistivity Line CM-1 suggests that this zone is no more than 5 m thick and that there is an abrupt and marked decrease in resistivity below this (Zone CM-2). In contrast, the central basin of the landform is not

characterised by a thick (>2 m) near-surface high resistivity zone. Instead the low resistivity Zone CM-2 approaches the ground surface. As the resistivity of a material is strongly influenced by the porewater content of the material, the marked boundary in resistivity between Zone CM-1 and Zone CM-2 probably represents the change from saturated and unsaturated sediments, marking the location of the water table, rather than a geological contact. The difference in water saturation can be seen from the photographs of the boreholes (Figure 6.8), which show unsaturated sediments between 1-2 m underlain by saturated sediments between 3-4 m in Borehole 1.

Alternatively, Zone CM-2 could be interpreted as representing the extent of fine-grained materials. If this was the case then the near-surface resistivity data suggests that the clayey silts in Borehole 2 are laterally extensive, and that Zone CM-2 extended beneath the gravels in Borehole 1 at depths below 5 m. However, the electrical properties of the sediments (predominantly 100-190 Ωm) suggest that sand and gravel and/or clast-rich till, rather than silts or clays are likely to dominate the near-surface zone (<10 m). This supports the theory that the clayey silts found in Borehole 2 are not laterally or vertically extensive. However, without better geological control from additional, deeper boreholes, the resistivity data cannot be used to characterise individual units within the superficial geology at this site.

The apparent absence of a marked high resistivity zone at the base of both resistivity lines means that defining rockhead is difficult at this site based on the resistivity data. It may be that the depth to bedrock exceeds the vertical limits of the survey (>30 m). However, it is thought more likely that electrical definition of this boundary is difficult because of only a small contrast in resistivity between the superficial deposits and bedrock. If this is the case, the higher resistivity zone (>190 Ωm) below a depth of 10 m (Zone CM-3) may be interpreted as representing bedrock, with the upper boundary of this zone (Figure 6.10) representing a minimal rockhead depth. If this is correct, then Line CM-2 suggests that there may be evidence for rather abrupt undulations in rockhead morphology at this site (Figure 6.10b). However, if the depth to bedrock does exceed the vertical limits of the resistivity survey then Zone CM-3 may represent a very thick unit of sand and gravel rather than bedrock. A deep borehole and/or seismic refraction survey would be required to test these hypotheses.

7 Cledlyn valley

7.1 Introduction

The most remarkable landforms interpreted as open system pingos by E. Watson are those found in the upper part of the Cledlyn valley, 0.5 to 2 km west of Cwrt Newydd at 165-215 m OD (Watson 1971, 1972, 1975; Watson and Watson 1972) (Figures 7.1 and 7.2). Ramparts, 6.5 m high and composed of till, have been recognised (Watson 1971). The majority are oval or elongate rather than circular in form, rarely surrounding their depression entirely (Figures 7.3 and 7.4). Complete ramparts form the minority and tend to be located only on the valley bottoms where slopes are less than 2°. Upslope ramparts are frequently absent. The ramparts generally suggest that the original ground-ice mound morphologies were round to oval, with the latter generally elongated perpendicular to the slopes. An often-quoted characteristic of open system pingos is that they cluster in geologically and hydrogeologically favourable localities. This certainly appears true of the landforms of the Cledlyn valley (Figures 7.3 and 7.4), which appear to have many generations of features, and have been described as 'mutually interfering' (Watson 1971). This characteristic makes identification of individual forms extremely difficult due to their topographical setting and gregarious nature (Watson and Watson 1974). Watson argued that some rampart-basin complexes suggest compound development, attributed to the simultaneous development of more than one ice core. Commonly, the upslope section of many ramparts appears to be cut by the rampart of a landform that developed later on the upslope side, a characteristic that has been attributed to upslope migration of the point of water injection (Watson 1971).

Extensive mapping, levelling and augering of six of the Cledlyn valley depressions ('Pingos': W, U, M, R, A and X) (Figure 7.3) revealed a remarkable variation in their depth and basal profile (Watson 1972; Watson and Watson 1972). All basins show some degree of asymmetry, with the deepest point near to the downslope rampart. This has been attributed to the collapse of the upslope rampart and overburden material into the basin following ground-ice decay (Watson and Watson 1972) and is more pronounced where the valley slope exceeds 3-4° ('Pingos': U, M, and R). No rampart exists upslope of 'Pingo' A, located on a slope of 5-6°. Those on slopes of 1-

2° (e.g. 'Pingos' X and W) tend to have more symmetrical basins, with near-complete, or entire, rampart enclosure (Figure 7.3).

Large variation is recognised in the depth of the basins, a characteristic that appears unrelated to the external form of the landforms. The depth of basin infill sediments varies between <2.5 m to >11 m. Augering of 'Pingos' W and U reached depths of 10.13 m and 11.77 m below the surface without reaching the base of each depression (Watson and Watson 1972). In all basins augered, three types of deposit occur, with the uppermost peat and organic units overlying a smooth, structureless grey silty clay unit, which in turn overlies unsorted gravelly clay (Watson and Watson 1972). Within U, 2.54 m of peat overlies at least 9.23 m of blue-grey, structureless, clayey silt. This is in contrast to 'Pingo' M, where the thickness of clayey silt did not exceed 18 cm (Watson and Watson 1972). The grain-size distribution of the silt analysed at various depths in 'Pingo' U showed consistently more than 90% less than 65 µm (Watson 1975). Two groups of ramparted ground-ice depressions can therefore be recognised from the Cledlyn valley. Those that are relatively shallow, with basal gravelly silt found 3-4 m below the surface (e.g. 'Pingos' A and M), and those where the bottom is much deeper, (e.g. 'Pingos' U, W and R). Watson and Watson (1972) suggested that this reflects the amount of mineral material within the ground-ice mound, with shallower forms originally having a higher segregated ice content, and the deeper types comprising largely clear injection ice.

Radiocarbon dating of the basal peat in 'Pingo' U provided uncalibrated ages of 10,080± 320 yrs BP and 10,060±380 yrs BP (Shotton et al. 1975), which have been supported by pollen analysis of the basin infill (Handa and Moore 1976; Walker and James 2001). Comparable radiocarbon ages were also derived from the base of the peat infill within 'Pingos' M and W (Shotton and Williams 1973; Shotton et al. 1975). Watson (1975, 1982) argued that the regular boundary between the base of this organic deposit and the underlying grey clay indicated that the ground ice had melted out before the end of the Younger Dryas (12,500-11,000 cal yrs BP).

Based on surface mapping of the distribution and nature of the superficial geology in the Cledlyn valley, Gurney (1994, 1995) proposed a local stratigraphy. This

171

comprised a sequence of till, resting on bedrock, overlain by glaciolacustrine clays and then head. The clays were interpreted as being deposited prior to ground-ice formation, and Gurney (1994, 1995) suggested that the frost-susceptible nature of these clays promoted the development of segregation ice. As a result, the landforms in the Cledlyn valley were reinterpreted as the remains of collapsed lithalsas, rather than open system pingos. In this model, the thick sequences of fine-grained sediments within the basin-fill of some landforms were also interpreted as being deposited during extensive glacio-lacustrine sedimentation prior to ground-ice formation, rather than during collapse of the landforms (Gurney 1994, 1995, 2000). The inference from this model is that similar thicknesses of silt are present between the basins of the ramparted depressions, as well as within them. However, it remains unclear how laterally or vertically extensive these fine-grained sediments within the Cledlyn valley actually are. Recorded observations outside the confines of the landforms were only made at a few locations in stream sections within a very localised area. Furthermore, with the exception of the thin unit of clay in the section through the rampart of 'Pingo' R (Watson 1971), the proposed stratigraphy was not observed in section, and nowhere was the clay seen to stratigraphically overlie the till.

Mudstones of Ordovician age characterise the bedrock geology of the Cledlyn valley (Figure 7.5) (BGS Sheet 194: Llangrannog, *unpublished map*). The section of the valley where all the ramparted depressions are found is underlain by silty mudstones of the Yr Allt Formation of Ashgill Series (Ordovician) age. Two northeast to southwest trending faults have been mapped just downvalley, but these are not directly associated with the distribution of ramparted depressions (Figure 7.5). It is possible however that thin units of sandstone, as well as minor faults and other discontinuities underlie the ramparted depressions in the Cledlyn valley. Because of the poor level of exposure in the valley however, this cannot currently be established with any degree of confidence.
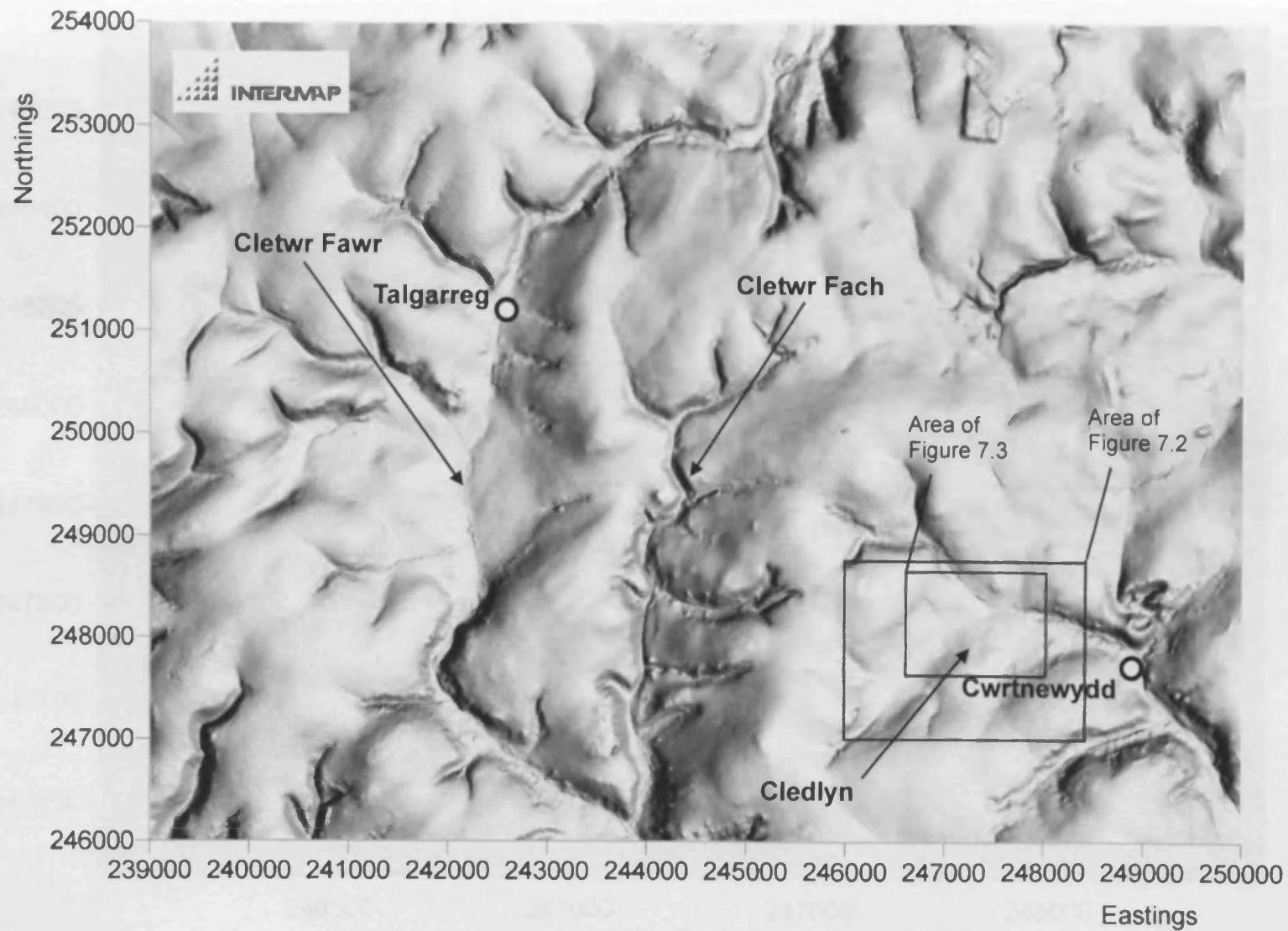
Figure 7.1: NEXTMAP digital terrain model (DTM) of the Cledlyn and Cletwr valleys (© Intermap Technologies Inc.). Note the contrast between the deeply incised valleys (e.g. Cletwr Fach) and the drift-filled Cledlyn and Cletwr Fawr valleys. Extent of Figures 7.2 and 7.3 indicated.

Figure 7.2: Aerial photograph of the Cledlyn valley taken in 2000 (© Getmapping Plc 2006) with the locations of specific landforms and key farms labelled.
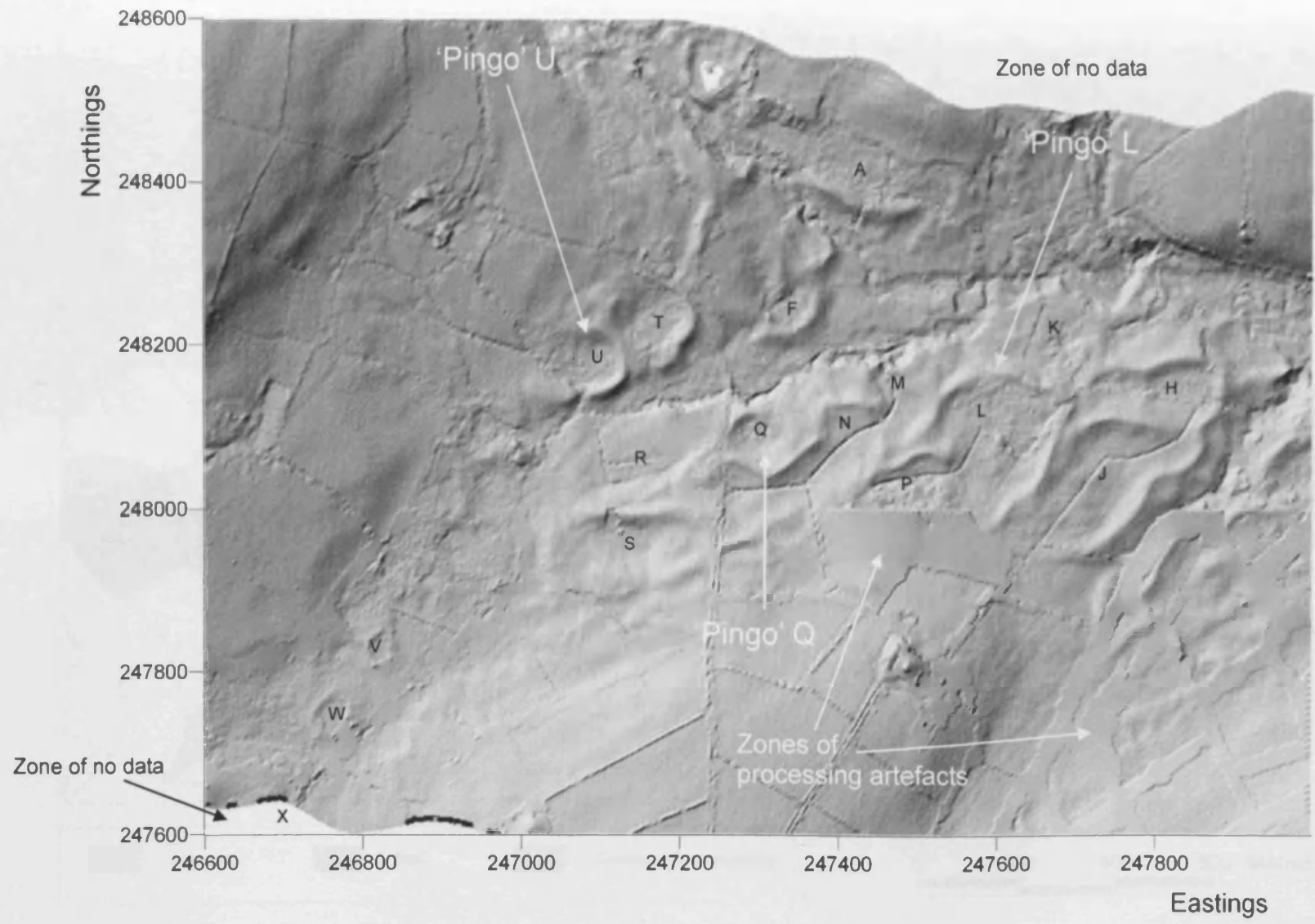
Figure 7.3: Digital terrain model (DTM) of ramparted depressions in the Cledlyn valley, derived from LIDAR airborne surveying (© Environment Agency copyright and/or database right 2006). Individual landforms annotated after Watson (1971) and Gurney (1995).
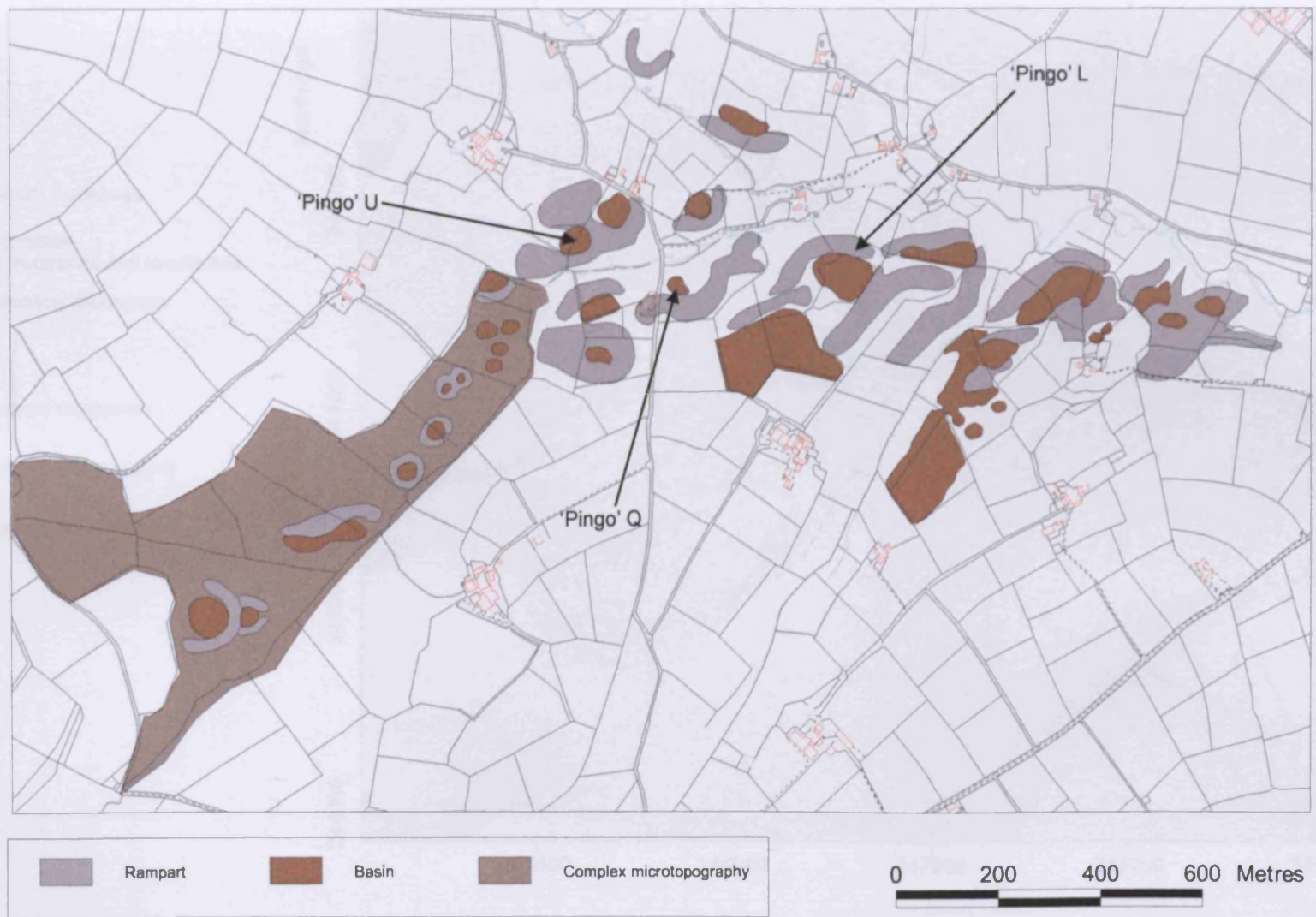
Figure 7.4: Geomorphological map of the Cledlyn valley site (SN 47398.48063), based on mapping from stereoscopic aerial photographs. LANDLINE data © Crown Copyright/database right 2006. An Ordnance Survey/(Datacentre) supplied service.

Silurian
- Claerwen Group, mudstones
- Rhyddlan Formation, interbedded mudstones and sandstones
- Cwmere Formation, mudstones

Ordovician
- Yr Allt Formation, sandstones
- Yr Allt Formation, silty mudstone
- Nantmel Mudstones Formation

Faults
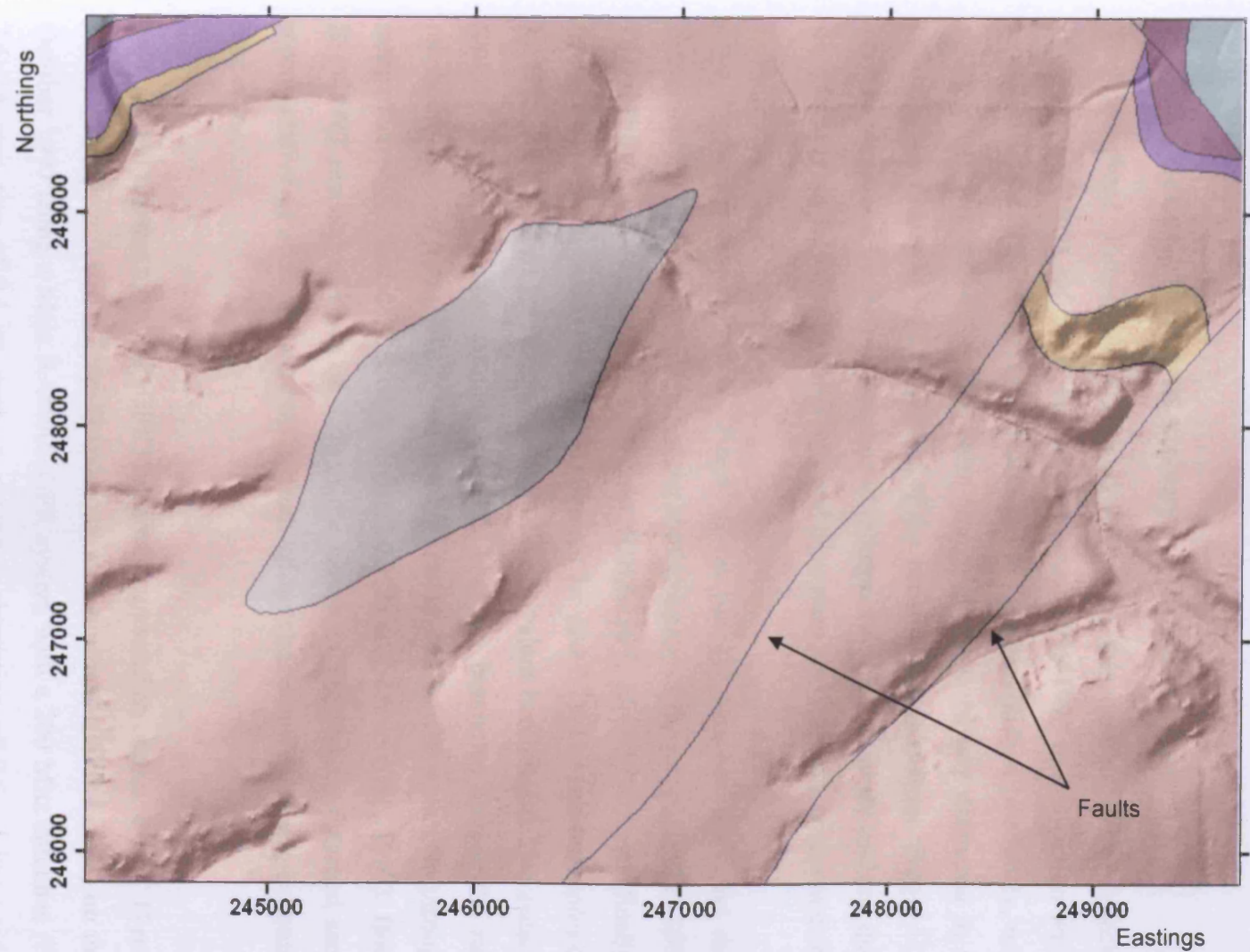
Figure 7.5: Bedrock geology of the Cledlyn Valley (© British Geological Survey) draped on the surface of a NEXTMAP digital terrain model (DTM) with 3 x vertical exaggeration (© Intermap Technologies Inc.). Note that this map is adapted from unpublished, unchecked, draft mapping by the British Geological Survey and may therefore contain some inaccuracies.

7.2 Site description and survey: 'Pingos' U and L

The data from 'Pingos' U and L, described in this section, were collected by Professor C. Harris and Dr P. Brabham between 1996-1998 in association with staff from Terradat UK. This processed data has not been published previously, with the exception of a resistivity profile from 'Pingo' U reported and discussed in Harris (2001b). All data, with the exception of the resistivity profile from 'Pingo' U, have been re-processed by the author prior to incorporation in this study and the majority of sample grain-size distributions reported here were also analysed by the author.

Five boreholes were drilled at 'Pingo' U on the 31st October 1997 and the 17th September 1998. Two were drilled at the southern base of the rampart (BH1-1997 and BH1-1998), two into the rampart crest (BH2-1997, BH2-1998) and finally one through the central basin (BH3-1997) (Figures 7.6 and 7.7). The two boreholes drilled in 1998 penetrated to greater depths than the equivalent boreholes drilled outside the rampart and through the rampart in 1997. The two boreholes outside the rampart reached depths of 5 m (BH1-1998) and 2 m (BH1-1997), whilst the two through the rampart crest reached depths of 4 m (BH2-1998) and 2.6 m (BH2-1997). Borehole BH3-1997 reached a depth of 7 m in the centre of the basin. Disturbed samples, representative of all units, were taken from all boreholes and analysed for grain-size properties.

Two ground penetrating radar (GPR) lines were undertaken across 'Pingo' U running southeast-northwest (GPR Line 1) and southwest-northeast (GPR Line 2) on the 31st October 1997 using a Mala RAMAC GPR system with a 200 Mhz antennae (Figure 7.6). A step size of 0.1 m, with an antennae separation of 0.6 m was used. The velocity was not measured in the field using a common midpoint survey (CMP) survey but was estimated on the basis of previous coring (Watson and Watson 1972; Gurney 1994) and on the basis of the depth of the interface between peat and mineral sediment in BH3-1997. A velocity of 0.038 mns^{-1} was found to best fit the geological data, and this is in accordance with measurements made for peat elsewhere (Theimer *et al.* 1994; Jol and Smith 1995; Slater and Reeve 2002; Comas *et al.* 2004, 2005). The following processing steps were used: 1) subtract mean (dewow); 2) gain function; 3) static correction; 4) time cut. Elevation corrections, based on EDM

survey data, were applied to compensate for the significant topographic variation along the length of both survey lines. GPR Line 1 was 138 m long and GPR Line 2 was 72 m long. The maximum investigation depth did not exceed 3 m.

A short reversed seismic refraction line (24 geophones, 2 m spacing, 46 m in length), running northeast to southwest was undertaken to the south of the enclosing rampart of 'Pingo' U on the 17th September 1998 (Figure 7.6). A second very high-resolution (24 geophones 0.25 m spacing, 5.75 m in length) reversed line was also undertaken at the centre of the first geophone spread (19.25-25 m) to establish the properties and depth of any near-surface layers.

A 300 m long electrical resistivity tomography line, collected using an ABEM LUND SAS 4000 resistivity meter with an ES464 electrode selector on the 19th September 1996, was aligned northwest-southeast across 'Pingo' L (Figure 7.6). These resistivity data (Line CL-L1) therefore represent the only survey line from Wales presented in this thesis that was collected with equipment other than the IRIS Instruments Junior Switch 72 resistivity meter (see Section 3.2.3.1). A second resistivity profile (150 m long) was also undertaken at 'Pingo' U on the 31st October 1997 also using the same ABEM system (Figure 7.6), but unfortunately the raw data for this survey have now been lost. However, the results of the survey at 'Pingo' U are presented in Harris (2001b), where they are mislabelled as 'Pingo' L. The actual data from 'Pingo' L has been reprocessed using the common scale chosen for sites in Wales (see Section 3.2.4), to enable comparison with other resistivity data collected in the Cledlyn valley and at other sites.
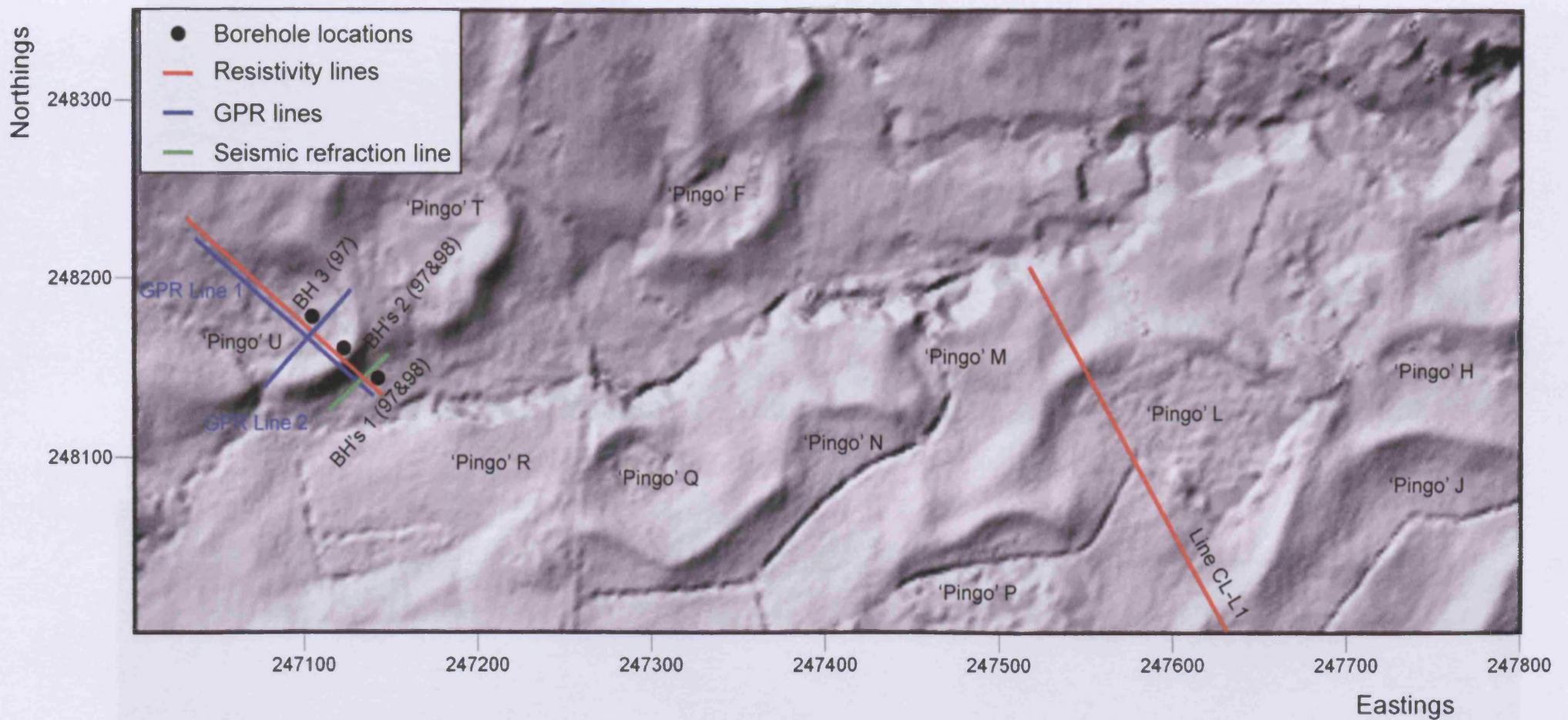
Figure 7.6: Locations of sedimentological and geophysical surveys at 'Pingos' U and L, Cledlyn valley. Digital terrain model (DTM) data derived from LIDAR airborne surveying (© Environment Agency copyright and/or database right 2006). The raw data from the resistivity survey from 'Pingo U' has now been lost, but see Harris (2001b) for a processed section.

Figure 7.7: (a) Rampart crest, inner rampart and basin of 'Pingo' U, Cledlyn valley; (b) South facing ramparts of 'Pingos' U and T Cledlyn valley. Note horse for scale in both photographs.

7.3 Results: 'Pingos' U and L

7.3.1 Sedimentology

The two boreholes drilled outside the rampart of 'Pingo' U (BH1-1997, BH1-1998) were both dominated by a 2.5Y 5/2 greyish brown, poorly sorted, well-graded silty sandy gravel (diamict) with subangular to subrounded clasts (Figures 7.8a and 7.9). The upper 50 cm of both boreholes were composed of a dark brown to yellowish brown (10YR 3/4 to 10YR 5/4) silt with occasional clasts and greyish brown (2.5Y 5/2) mottling. In BH1-1998 the silty sandy gravel was matrix-supported between 0.5-2.5 m and at depths between 4.2-5 m, but between 2.5-4.2 m the gravel content increased (Figures 7.8a and 7.9). However, it was generally difficult to subdivide the deposit and it should be viewed as a single homogenous unit with a varying content of gravel-sized material (Figure 7.9).

The two boreholes drilled from the crest of the rampart (BH2-1997, BH2-1998) were also characterised by a matrix-supported silty sandy clayey gravel (diamict) that was very similar in grain-size to the materials sampled throughout the boreholes outside the landform (Figures 7.8b and 7.9). The upper 30 to 50 cm of both boreholes was darker in colour compared to the sediments at depth (10YR 4/4 compared to 2.5Y 6/2), and had fewer clasts. In comparison to the majority of samples analysed from BH1-1998 and BH1-1997, the grain-size of the rampart sediments (Figures 7.8 and 7.9) was characterised by a reduction in the gravel-sized component. This may not be significant however, and is likely to simply be a function of localised variations in the amount of gravel-sized materials in the sediment. Only one sample (at 3 m) was recovered and analysed from BH2-1998 and this may not be representative of the entire borehole. The sediments that comprised the entirety of BH2-1997 and BH2-1998 should be viewed as part of the same unit as the sediments beyond the ramparts. None of the boreholes displayed clear evidence for stratification or sorted layers within the diamict.

The sole borehole within the central basin of the landform (BH3-1997) was characterised by 3 m of peat overlying at least 4 m of homogenous clayey silt to silty clay with occasional gravel-sized clasts (Figure 7.8c), extending to a depth greater

(i) Borehole 1-1997

CLAY SILT SAND GRAVEL

Depth (metres)

Dark brown organic SILT 10YR3/4. Dark yellowish brown. Soft friable slightly platy structure.
Firm moist, blocky mottled 10YR4/4 dark yellowish brown SILT.

Moist strong 10YR 5/4 yellowish brown SILT with subangular fine sandstone clasts.
Grey mottling 2.5Y 5/2 greyish brown.

2.5Y 5/2 greyish brown moist firm silty sandy GRAVEL. Subangular to subrounded clasts.

(ii) Borehole 1-1998

CLAY SILT SAND GRAVEL

Depth (metres)

Brown silty DIAMICT, crumb structure.

Becomes slightly more strong at depth. Sub-rounded clasts. Very fine dark grey blue sandstones. Gravelly sandy SILT.

Brownish orange becoming light yellow silty sandy GRAVEL. Very firm non plastic.

Reddish brown-mottled gravelly sandy SILT. Hard dry.

Hard dry-slightly moist gravelly sandy clayey SILT. Sub-rounded to rounded clasts smooth polished surfaces.

Damp grey silty sandy GRAVEL slightly plastic firm.

NCR

Very wet grey strong silty sandy GRAVEL. Sticky plastic firm. Rounded-subrounded siltstone, grey. Some angular broken clasts. Clasts mainly 2-3cm diameter, but smaller and larger present.

NCR

Very wet silty sandy GRAVEL. Gravel rounded-subrounded some large stones. Clasts mainly 0.5-3 cm diameter. Sample of bluish grey silty clayey gravel taken.

Dark grey very wet sandy GRAVEL containing large clasts. Rounded to subrounded with interstitial silty fines.

Blue grey coarse sandy GRAVEL.

Blue grey silty sandy GRAVEL. Wet soft. Flakey subangular mudstone also very well rounded and striated mudstone clasts.

Very dense hard moist but not wet very plastic brown silty sandy GRAVEL with rounded clasts.

(iii)

Figure 7.8a: Borehole logs from 'Pingo' U, Cledlyn valley: (i) Sedimentological log of Borehole 1-1997; (ii) Sedimentological log of Borehole 1-1998 ('S' marks the locations of sampling for grain-size analysis, NCR = no core recovery); (iii) Example of the homogenous, massive silty/gravelly diamict that dominates boreholes 1-97, 1-98, 2-97 and 2-98.

(i)   Borehole 2-1997

CLAY SILT SAND GRAVEL

Depth (metres)

0

1

2

3

S

S   2.5Y 6/2 light brownish grey firm moist grey-brown mottled gravelly sandy clayey SILT to silty sandy clayey GRAVEL (180-200 cm). Subrounded to subangular clasts up to 4 cm.

10YR 4/4 dark yellowish brown, firm moist stony sandy SILT. Organic rich top to merging lower boundary. Subangular-angular fine sandstone clast.

S

S   2.5 Y 6/4 light yellowish brown dry firm silty sandy GRAVEL. Hit boulder. 5Y 7/1 light grey to2.5Y 6/4 light yellowish brown mottling.

(ii) Borehole 2-1998

CLAY SILT SAND GRAVEL

Depth (metres)

0

1

2

3

4

Silty brown TOPSOIL, organic brown earth, moist.

Grey silty GRAVEL. Subrounded to subangular stones up to 3cm wet.

Brown/grey mottled gravelly sandy clayey SILT to silty GRAVEL.

S

Figure 7.8b: Borehole logs from 'Pingo' U, Cledlyn valley: (i) Borehole 2-1997; and (ii) Borehole 2-1998 ('S' marks sampling locations for grain-size analysis).

Borehole 3 -1997

(i)

CLAY   SILT SAND GRAVEL

Depth (metres)

0

1

2

3

4

5

6

7

S

S

Wet sphagnum MOSS.

5YR 2/2. Dark reddish brown PEAT. Bottom 10 cm (290-300 cm) slightly silty clay.

2.5Y 6/2, light brownish grey, very wet, very soft clayey SILT to silty CLAY with occasional gravel sized clasts and granules.

(ii)

3 m

4 m
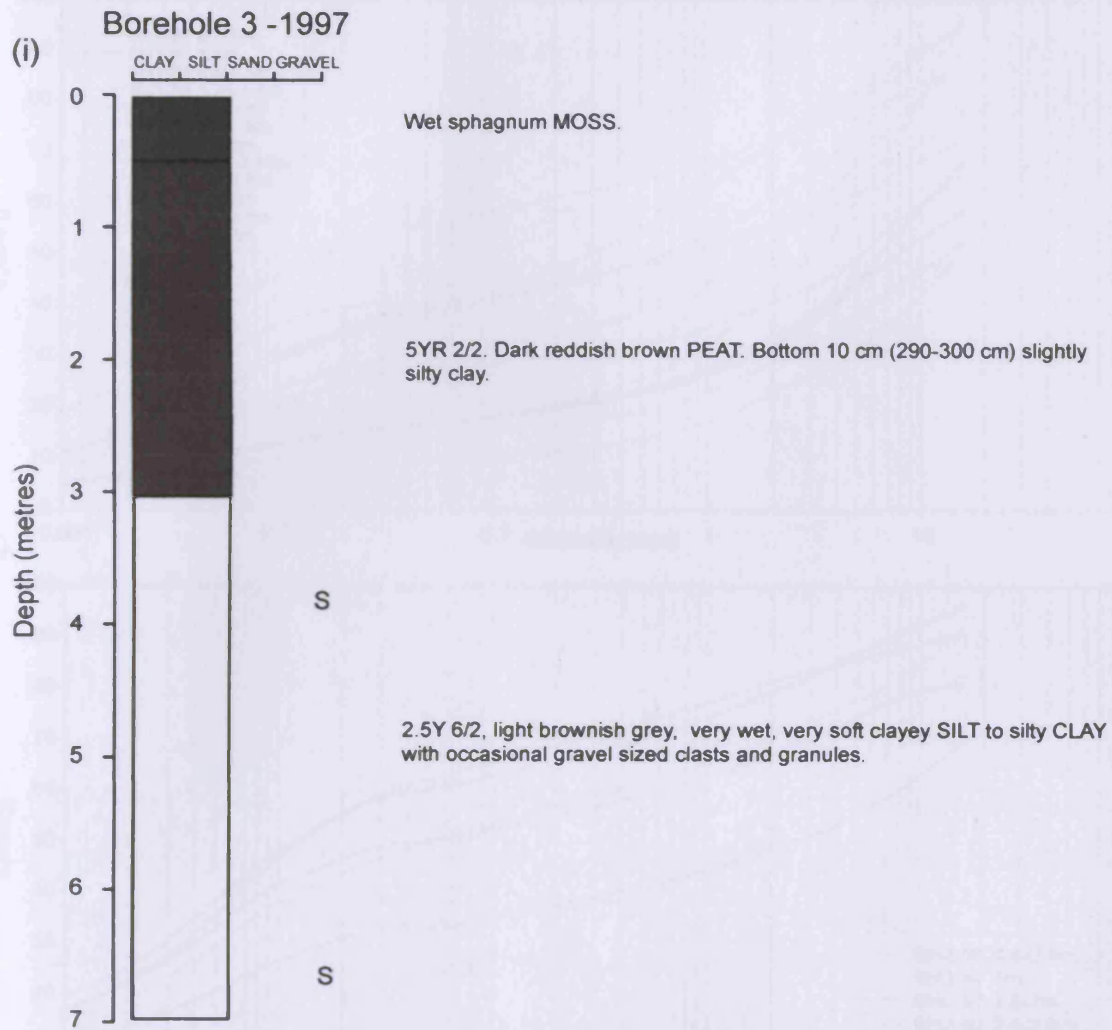
Figure 7.8c: Borehole logs from 'Pingo' U, Cledlyn valley: (i) Sedimentological log for Borehole 3-1997 ('S' marks sampling locations for grain-size analysis; (ii) Core photograph of clayey silt (Borehole 3-1997: 3-4 m) (Photo: C. Harris).
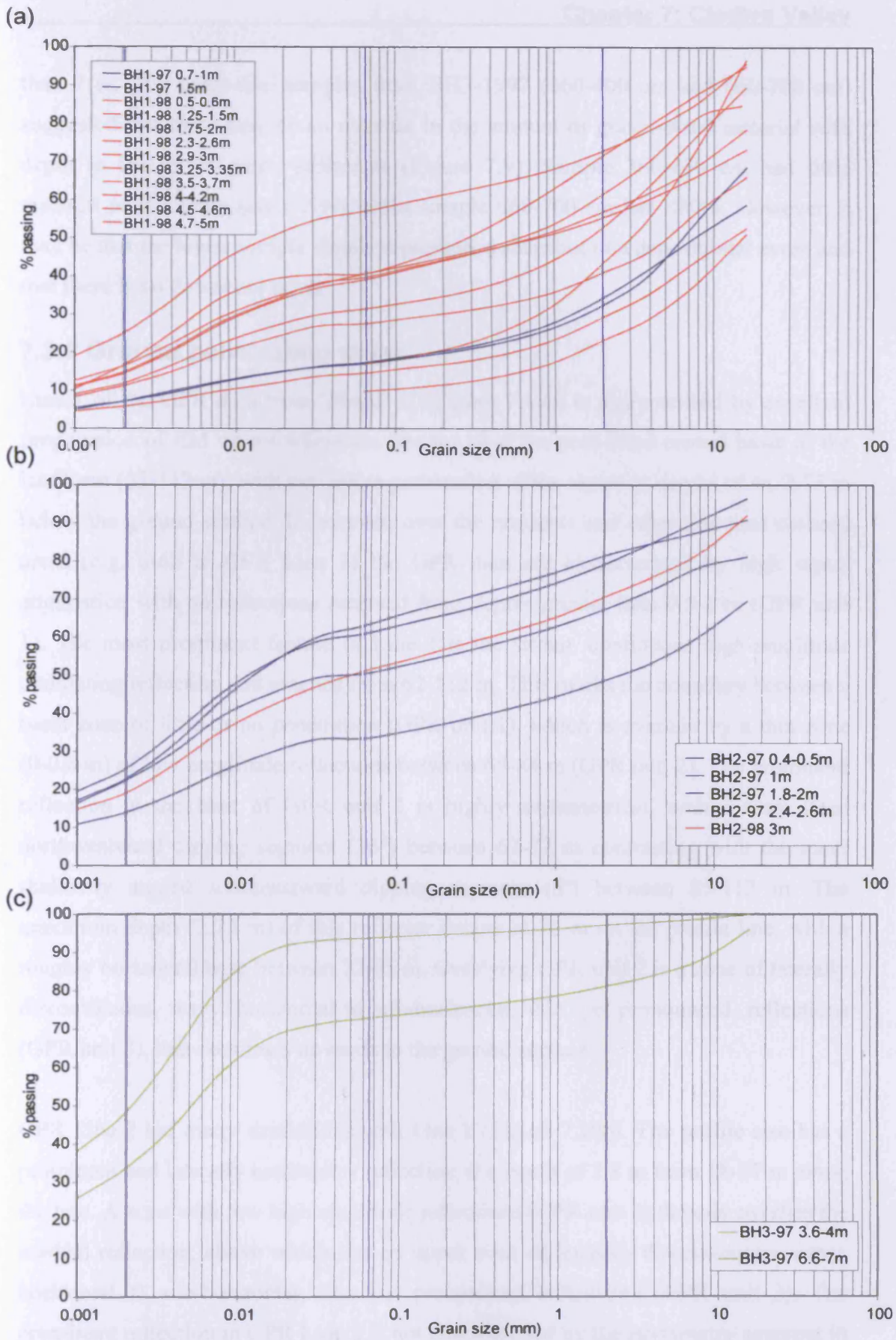
Figure 7.9: Grain-size analysis of sediments sampled from 'Pingo' U, Cledlyn valley: (a) Boreholes: 1-1997, 1-1998; (b) Boreholes: 2-1997, 2-1998; (c) Borehole 3-1997.

than 7 m. The grain-size samples from BH3-1997 (360-400 cm and 660-700 cm) suggested that there may be an increase in the amount of gravel-sized material with depth in the minerogenic sediments (Figure 7.9). Sample 360-400 cm had little material of this grain-size (<5%) whilst sample 660-700 cm has <30%. However, it may be that the lower sample simply represents a snapshot of a depositional event and that there is no downcore trend.

7.3.2 Ground penetrating radar

Line 1 of the GPR data from 'Pingo' U (Figure 7.10a) is characterised by excellent propagation of EM waves where the line ran over the peat-filled central basin of the landform (62-112 m), with maximum penetration of the signal to depths of ca. 2.75 m below the ground surface. In contrast, over the ramparts and other non-peat covered areas (e.g. 0-62 m GPR Line 1) the GPR data are characterised by high signal attenuation with no reflections received from depths greater than 0.5-1 m (GPR unit 1). The most prominent feature of Line 1 is the strong, continuous high-amplitude undulating reflection that extends from 62-112 m. This marks the boundary between a basal zone of little or no penetration (GPR unit 1), which is overlain by a thin zone (0-0.6 m) of low-amplitude reflections between 65-84 m (GPR unit 2). The prominent reflection at the base of GPR unit 2 is highly asymmetrical, with a very steep northwestward dipping segment (16°) between 62-72 m contrasting with the more shallowly angled southeastward dipping segment (6°) between 85-112 m. The maximum depth (2.75 m) of this reflector occurs at 72 m on the profile line, with a roughly horizontal base between 72-85 m. Overlying GPR unit 2 is a zone of laterally discontinuous, wavy, horizontal to sub-horizontal, thin, yet pronounced, reflections (GPR unit 3), that continues upwards to the ground surface.

GPR Line 2 has many similarities with Line 1 (Figure 7.10b). The profile also has a prominent and laterally continuous reflection at a depth of 2.8 m from 18-57 m along the line. A zone with few high amplitude reflections (GPR unit 2) directly overlies the marked reflection, above which lies an upper zone of laterally discontinuous, wavy, horizontal to sub-horizontal, thin yet pronounced reflections (GPR unit 3). The prominent reflection in GPR Line 2 is not characterised by the asymmetry apparent in GPR Line 1, and is roughly horizontal between 28-48 m.
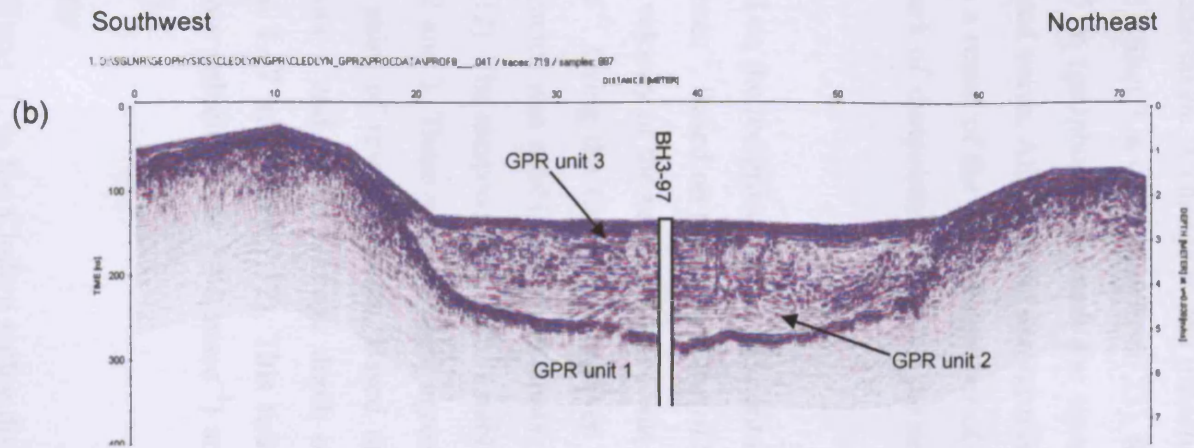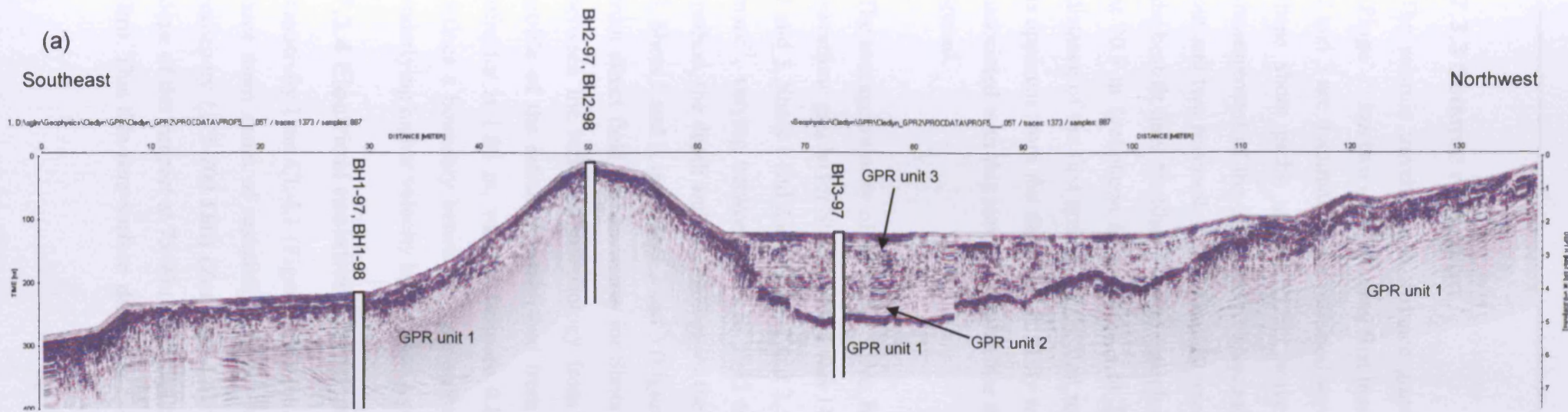
Figure 7.10: Ground penetrating radar profiles of 'Pingo' U, Cledlyn valley (a) GPR Line 1; (b) GPR Line 2. Data acquired using a Mala RAMAC GPR system with 200 MHz antennae. Locations of boreholes indicated.

7.3.3 Seismic refraction

The seismic traveltime vs distance graph for the line shot outside the rampart of 'Pingo' U has two clear P-wave, first break velocity segments (Figure 7.11). Shots 1, 2 and 3 are dominated by a refracted wave, but the initial few geophones of each of these shots picks up the direct wave. To improve the error margins in the measurement of the direct wave a second, very short spread of geophones was laid out and two reversed shots (6 and 8) were undertaken. A change in the inflection of the best-fit lines for Shot 1 at 4 m (geophone 3), Shot 3 at 44 m (geophone 23), Shot 6 at 20.5 m (geophone 6) and Shot 8 at 23.75 m (geophone 19) mark the crossover distance of the first arrivals of the first refracted wave. Although no second refractor is apparent from the data, this is likely to be a result of the limited number of shots associated with this survey, in particular the lack of shotpoints offset from the seismic spread.

The average velocity of the direct wave, based on the reciprocal of the gradient of the traveltime graphs for Shots 6 and 8 was 140 msec^{-1}. Based on the minus time of Shots 1 and 3, Shots 1 and 2 and Shots 2 and 3, the velocity of the refracted wave was 1886 msec^{-1}, varying between 1814 to 1945 msec^{-1}. Using the Common Receiver Point method, the depth and morphology of the refractor was established from Shots 1 and 3, Shots 1 and 2, and Shots 2 and 3 (Figure 7.12). The reciprocal time was established from direct field measurements for Shots 1, 2 and 3. There was excellent agreement between the refractor morphology from all pairs of reversed shots. Based on the profile of the refractor established from Shots 1 and 3, the average depth of the refractor is 1.08 m, varying between 0.81 to 1.47 m (Figure 7.12). This refractor defines a boundary between a near-surface low velocity layer (140 msec^{-1}) and an underlying higher velocity layer (1886 msec^{-1}).

7.3.4 Electrical resistivity tomography

Resistivity Line CL-L1 (Figure 7.13), from 'Pingo' L in the Cledlyn valley displays three main zones of resistivity values. A thin (<5 m) zone of intermediate to high resistivity (125-700 Ωm) (Zone CL-L1) is apparent between 0-100 m. The outside slope of the rampart at 75-90 m is characterised by particularly high resistivity (>400 Ωm). This thin near-surface zone may extend across the profile, intermediate values

are observed between 110-210 m. A laterally and vertically continuous zone of low resistivity (mainly 40-100 Ωm) extends throughout the profile (Zone CL-L2), beneath and through the rampart and the central basin of the feature. The upper contact of Zone CL-L2, with Zone CL-L1, is abrupt. This is particularly marked beneath the rampart. A zone of high resistivity (Zone CL-L3) underlies Zone CL-L2 with values increasing gradually with depth to values exceeding 230 Ωm (green/yellow boundary on scale) at 25 m depth at the southeastern end of the profile and 5-10 m depth at the northwestern end. The contact between Zones CL-L2 and CL-L3 (taken as the 230 Ωm contour) appears to be undulating and displays a clear northwestward dip. Zone CL-L2 is relatively thin upslope from the landform, its maximum thickness being found at approximately 160 m along the resistivity profile.
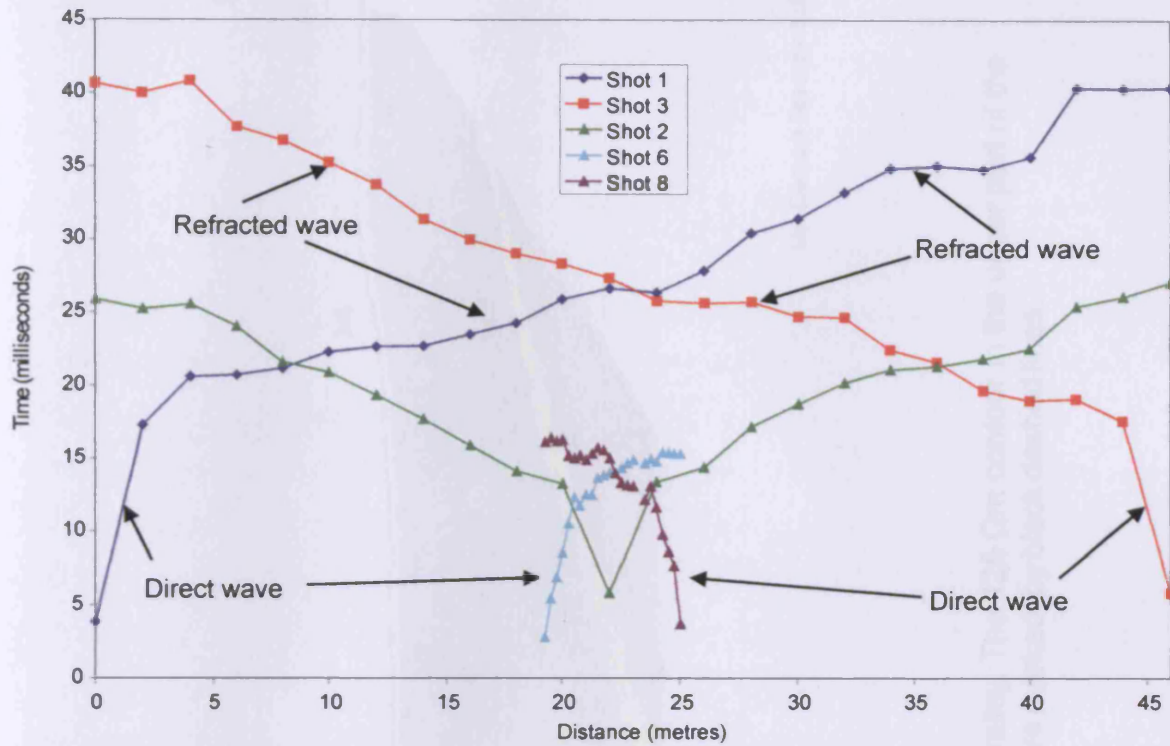
Figure 7.11: Traveltime graph of seismic refraction data collected from 'Pingo' U, Cledlyn valley.
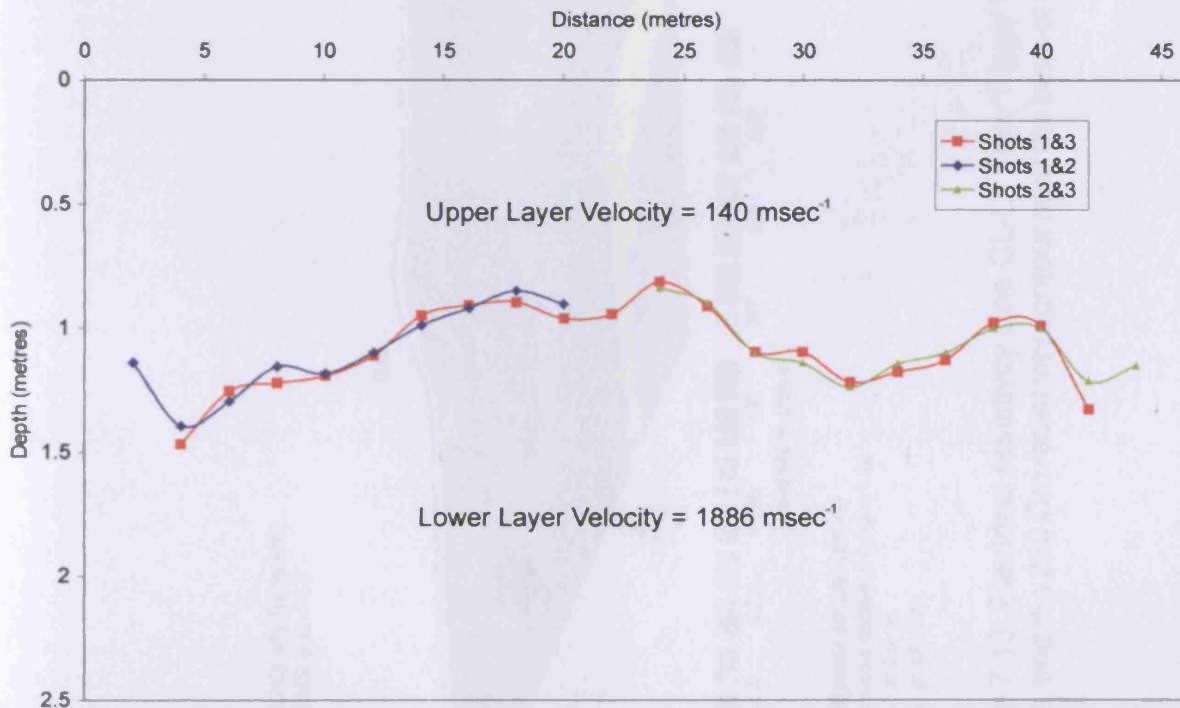
Figure 7.12: Depth and morphology of refractor calculated from seismic refraction survey at 'Pingo' U, Cledlyn valley.
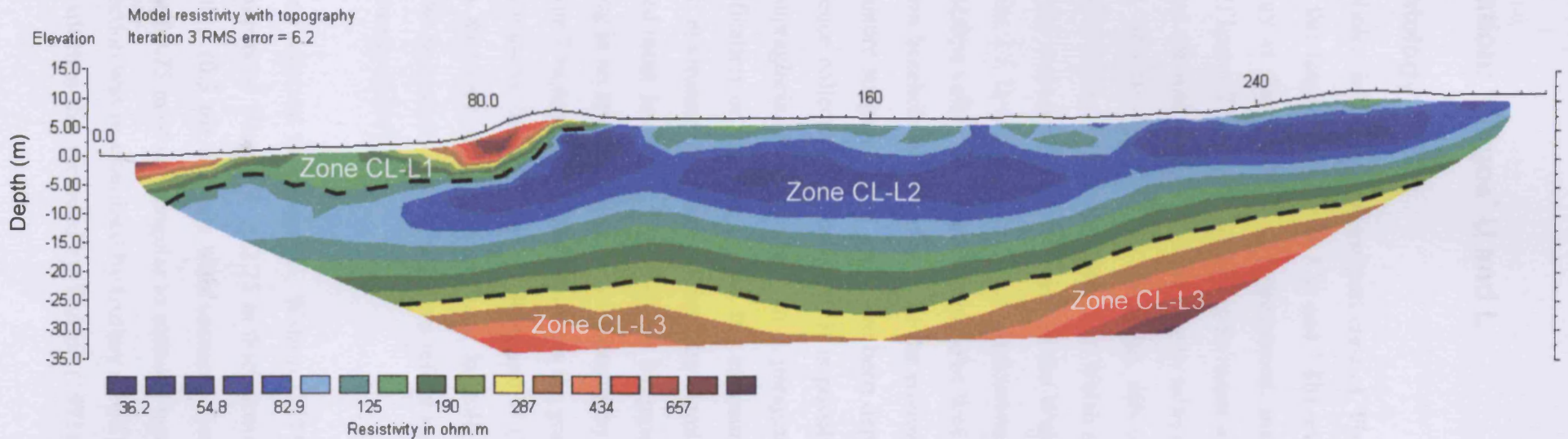
Figure 7.13: Electrical resistivity Line CL-L1 from 'Pingo' L, Cledlyn valley. The 125 Ωm contour in the upper part of the profile, and the 230 Ωm resistivity contour near the base of the profile are marked by black dashed lines.

7.4 Interpretation: 'Pingos' U and L

7.4.1 Sedimentology

The shallow boreholes drilled into the rampart crest of 'Pingo' U and around the edge of the rampart of this landform (Figures 7.8a and 7.8b) reveal that the upper 4-5 m of superficial geology is dominated by a homogenous, matrix-supported, silty sandy gravel (diamict) (Figures 7.9a and 7.9b). Given its massive, structureless and compact characteristics, and the wide range of subangular to subrounded clasts, this diamict is interpreted as till. Matrix-supported, but clast-rich, tills of this type are common in deposits associated with the Teifi valley glacier of Welsh origins (Waters *et al.* 1997). In the context of the current view of the extent of the Welsh and Irish Sea ice masses in the area (Section 2.5.2) and the absence of a calcareous matrix or erratics of Irish Sea origin, the Cledlyn valley till is believed to be of Welsh origins. It is difficult, on the basis of shallow borehole data, to determine the environment of deposition of this till. Its compact nature suggests that it may have been deposited subglacially. On the basis of the evidence collected here however, it is possible that this till could have been deposited supraglacially or reworked in a paraglacial setting. However, the absence of stratification or layering within the exposures of till observed is not indicative of such environments of deposition. The diamict is not head however, as the volume of sediment involved is unlikely to be produced by periglacial slope processes operating in an area of such subdued topography. The grain-size analysis of the deposit (Figures 7.9a and 7.9b) closely matches the grain-size distribution of both basal and rampart material from 'Pingos' U, R, A and W (Watson and Watson 1972). This deposit can therefore be interpreted as a laterally extensive till within the Cledlyn valley. The rampart sediments therefore reflect the general superficial cover, as suggested by Gurney (1995).

In a stream cutting adjacent to 'Pingo' U, Watson (1971) described a section that intersected the rampart of 'Pingo' R. A 2.25 m thick gravelly diamict, interpreted as head, overlay a thin (0.3 m) clay-silt with scattered fine gravel. The base of the sequence comprised 0.75 m of silty angular to rounded gravel, interpreted as fluvially deposited. This section was re-examined by Gurney (1994) who emphasised a greater thickness of clay-silt than that recorded by Watson (1971), and he also noted similar

193

deposits in stream sections near 'Pingos' R, T and F and the site of the former footbridge at SN 476483. Gurney (1994, 1995) believed that the presence of these fine-grained sediments provided proof of the presence of a glacially dammed lake. Whilst localised pockets of lacustrine deposits clearly exist, it is clear from the borehole data and shallow sections within the Cledlyn valley (e.g. in the rampart of 'Pingo' M), that at least the upper few metres of superficial deposits are dominated by a matrix-supported diamict that has been interpreted as head (Watson 1971) and glacial till (Gurney 1994, 1995). The latter interpretation is favoured, although localised reworking of this diamict was likely to have occurred. The highly consolidated and matrix-dominated nature of the deposit and the frequent striated subangular to subrounded clasts are not consistent with the interpretation of this diamict as head, derived from the solifluction of frost shattered waterlain gravels and bedrock (Watson 1971). The ramparts are also composed of this diamict.

The thickness of peat (3 m) and of clayey-silt (>4 m) from the infill of the central basin of the ramparted depression (BH3-1997) (Figure 7.8c) supports the observations and grain-size analysis of Watson and Watson (1972) and Gurney (1994). Radiocarbon dating and palaeoecological analysis of the peat has revealed that it is early Holocene in age (Handa and Moore 1976; Shotton et al. 1975; Walker and James 2001). On this basis therefore, no organic deposits of pre-Holocene age were recovered from BH3-1997. The clayey silt from BH3-1997 (Figure 7.8c) does display clear evidence for the input of coarser clastic material, however, with a sample from 6.6-7 m containing 30% gravel by weight. The absence of significant volumes of clastic material in the basin-infill of the landform has always been acknowledged as a problem (Watson and Watson 1972; Watson 1976; Gurney 1995; Watson 1996). The thick sequence of fine-grained material (>8 m in 'Pingo' U) was believed to originate from sedimentation by suspension within the collapsing pond of the pingo, the sediment source being the ramparts, which were eroded by mass wasting (Watson and Watson 1972). However, if this was the case, then the grain-size of the basin-infill should be comparable to that of the ramparts. The absence of the coarse material in the basin is therefore inconsistent with derivation of basin fill sediments from the covering layer of either a pingo or a palsa (Watson 1996). Derivation of the thick basin-infill sequence from mass wasting of the ramparts alone appears unlikely (Gurney 1994). Apart from "infinitesimal traces" (p. 221 Watson

and Watson 1972) of sand and gravel there is little evidence of the coarse gravel that is common within the rampart sediments. To counter this problem Gurney (1994) proposed that the fine-grained basin infill existed prior to the development of ground-ice, and that segregation ice formed within these frost-susceptible fine-grained materials, resulting in the growth of lithalsas. Unfortunately the boreholes at 'Pingo' U were unable to penetrate to the depths required to test the hypothesis that glaciolacustrine deposits underlie the ramparts. A low resistivity zone measured at 'Pingo' U extended through the proven silt-clay basin-infill of the landform into the unproven sediments that extend beneath the ramparts and upslope of the feature (Harris 2001b). However, since different sediments with similar moisture contents might display similar electrical properties, it is not necessarily the case that glaciolacustrine deposits are more laterally extensive than those recorded by Watson and Watson (1972), as was suggested by Gurney (1994, 1995). Unpublished microgravity data is consistent with the basin structure indicated by coring (Harris 2001b).

7.4.2 Ground penetrating radar

The interpretation of the GPR data is dependent upon the interpretation of the strong, high-amplitude, laterally continuous reflection that underlies the central basin of the landform in both GPR Lines 1 and 2 (Figure 7.10). Fortunately, this landform has been intensively explored using coring techniques (Watson and Watson 1972; Handa and Moore 1976; Gurney 1994; Walker and James 2001), which have provided important controls on the depth and interpretation of this reflector, and BH3-1997 (this study), which has provided additional borehole information for geological control. The maximum depth of the reflector (2.75-2.8 m), determined from the known velocity at which EM waves travel through peat (0.038 mns^{-1}) (Theimer et al. 1994; Comas et al. 2005), correlates well with the depth of the base of the peat recognised from augering and boreholes (Watson and Watson 1972; Gurney 1994). Prominent reflectors have been reported from peat-clay/silt boundaries in other GPR surveys (Warner et al. 1990; Theimer et al. 1994; Jol and Smith 1995; Slater and Reeve 2002; Comas et al. 2004, 2005). The reflections above the prominent reflector therefore represent the stratigraphy and internal structure of the organic infill (peat and lacustrine sediment) of the basin, but the GPR data does not provide any information regarding the mineral infill of the landform. The absence of reflections

195

from below this peat-mineral sediment boundary is in accord with knowledge of the rapid attenuation of EM waves by clay- or silt-rich sediments, particularly at the base of peat (Warner *et al.* 1990; Theimer *et al.* 1994; Jol and Smith 1995; Slater and Reeve 2002; Comas *et al.* 2004). As peat is 80-95% water (Hobbs 1986) the fluid conductivity of the pore waters is important for geological interpretation of GPR surveys of peat deposits. Increased fluid conductivity of pore waters at the base of peat deposits can attenuate EM wave propagation, reducing penetration depth of a GPR survey (Theimer *et al.* 1994; Slater and Reeve 2002) but this problem is thought unlikely to produce an abrupt change in a radar profile, such as the prominent reflector interpreted as the base of the peat (Comas *et al.* 2004).

The morphology of the peat-clay interface based on the GPR data matches the profile that was established by coring (Watson and Watson 1972; Gurney 1994). The profile of the interface in GPR Line 1 confirms the asymmetrical profile established for the base of the peat by Watson and Watson (1972). The prominent hump at 96 m in GPR Line 1 (Figure 7.10a) corresponds to a similar feature recorded by Watson and Watson (1972). The base of this peat was radiocarbon dated to 10,080±320 yrs BP and 10,060±380 yrs BP (Shotton *et al.* 1975) and it is believed that the buried ice had melted out before peat development because of the undisturbed contact between the peat and mineral soil (Watson 1975, 1982).

The basal 0.5 m of the organic infill in both GPR lines is characterised by a homogenous zone (GPR Zone 2) with few high amplitude reflections. This zone may represent a layer of organic material deposited in open water conditions (gyttja), prior to the initiation of peat development. Watson and Watson (1972) did not subdivide the organic infill of the basin of 'Pingo' U, but both Handa and Moore (1976) and Walker and James (2001) describe a unit of detritus mud or gyttja (30-75 cm thick) overlying the basal clay. Both palynological studies reported the presence of aquatic taxa indicative of an open water habitat within this unit. A radar unit with similar features (lack of prominent reflections) was observed at Caribou Bog, Maine, USA although a distinct reflection was also observed between the peat and lake sediments (Slater and Reeve 2002; Comas *et al.* 2004). Such a reflection is absent from both GPR lines at 'Pingo' U.

As the GPR signal is primarily controlled by the water content of a material through the relative dielectric permittivity (ε_r), the strong reflections of the upper 2-2.25 m of the organic infill represent distinct stratigraphical changes associated with the physical properties of the peat that influence the moisture content (e.g local moisture content, bulk density, type and properties of organic matter content) (Theimer *et al.* 1994). These reflections may be due to changes in the bulk density or organic content of the sediment due to variations in vegetation type or local groundwater levels. These may reflect key Holocene palaeoenvironmental events, perhaps associated with regional changes in moisture availability.

7.4.3 Seismic refraction

Given that BH1-1998 reached a depth of 5 m through unconsolidated sediment, the shallow refractor at a depth of ca. 1 m observed in the seismic refraction data (Figure 7.12) must represent an internal division of the unconsolidated, superficial geology. Given its shallow depth, this refractor is thought to represent the boundary between the shallow weathered zone and the underlying diamict recorded at the top of each borehole. Although the depth derived from the seismic refraction survey appears to be significantly greater than that apparent from the boreholes, this may simply reflect the error margin of the layer velocity as it was calculated from the reciprocal of the gradient of the traveltime graphs of Shot 6 and Shot 8, rather than from a minus graph. A velocity of 140 msec^{-1} is extremely low for weathered unconsolidated deposits (Brabham *et al.* 1999), and is in fact less than the speed of sound in air (330 msec^{-1}).

The higher velocity layer (1886 msec^{-1}) underlying the weathered zone (Figure 7.12) corresponds to the unweathered till that was recorded in BH1-1998 and BH1-1997. The P-wave velocity is comparable to seismic velocities for unconsolidated glacial deposits in North Wales (MacDonald 1994; Harris *et al.* 1997; Brabham *et al.* 1999). Unfortunately, as a result of geographical constraints, the lack of shots far offset from the geophone spread meant that it was not possible to determine the depth to bedrock from this survey.

7.4.4 Electrical resistivity tomography

A preliminary interpretation of the resistivity data from 'Pingo' U has been presented by Harris (2001b), but the processed data from 'Pingo' L (Figure 7.13) has not previously been presented. In the absence of direct sedimentological evidence from 'Pingo' L the following interpretation relies heavily on boreholes, exposures and trial pits from elsewhere in the Cledlyn valley. Despite being the largest landform in the Cledlyn valley (210 x 140 m) and having steep rampart slopes (ca. 18°), the basin of 'Pingo' L is shallow like 'Pingo' M, with only a thin (5 cm) infill of grey clay (Watson 1975).

Zone CL-L1 represents the unsaturated matrix-supported gravelly diamict that has been extensively recorded throughout the Cledlyn valley. The compact, silty matrix of the sediment does limit the interstitial water-bearing capacity of this sediment, but the particularly high resistivity zone in the rampart is believed to be a function of lateral seepage of groundwater to the north, draining the rampart sediments. The laterally extensive, underlying zone of low resistivity (Zone CL-L2) may also represent the same lithological unit, but in a water-saturated state. However, within such a thick sequence of unconsolidated glacial deposits (>25 m), sedimentological heterogeneity is commonplace, and units of sands and gravels or clays are believed likely. However, given the thin minerogenic infill within the basin of 'Pingo' L it is not believed that Zone CL-L2 represents a thick laterally extensive sequence of glaciolacustine silts and clays within the valley, as suggested by Gurney (1994, 1995).

The high resistivity zone (Zone CL-L3) at the base of the resistivity profile (>230 Ωm) is interpreted as bedrock. Although the resistivity values of this zone are quite low for bedrock, nearby resistivity values derived from bedrock are between 468 Ωm (at Lampeter) to 610 Ωm (at Cornel) (Heaven *et al.* 1999). A gradual decrease in the bedrock resistivity from the mouth of the Teifi upvalley has been observed (values ca. 5000 Ωm having been reported near Cenarth), and this has been attributed to an increase in the sandstone component of the rock eastward (Carruthers *et al.* 1997; Heaven *et al.* 1999). In the Cledlyn valley, rockhead is near to, or at the surface above 215-245 m OD (Watson 1971) and bedrock with no superficial cover is apparent in

198

exposures at Coedlanau-Fach (SN 469487) and Cathal (SN 468474) (Figure 7.2) (Gurney 1994). Despite the large ramparts just downslope, bedrock is also exposed at the surface behind the house at Llwynfallen (SN 471485) (Gurney 1994, 1995). The morphology of the contact between resistivity Zones CL-L2 and CL-L3 is consistent with these observations, as it clearly dips northwards beneath 'Pingo' L, the superficial deposits apparently thickening towards the centre of the Cledlyn valley. The resistivity profile from 'Pingo' U also indicates a thick sequence of unconsolidated deposits (>15 m) beneath 'Pingo' U (Harris 2001b), in accordance with observations from augering (Watson and Watson 1972).

7.5 Site description and survey: 'Pingo' Q

A third ramparted depression was investigated in the Cledlyn valley on the 3rd March 2005. This landform corresponds to 'Pingo' Q, which was mapped, but not investigated, by Watson (1971). It is located on the southern slopes of the Cledlyn valley, to the east of Rhydnis (Figure 7.2). 'Pingo' Q is a peat-filled basin enclosed by a large rampart on its upslope side that extends west from 'Pingo' N and by a subdued rampart downslope (Figures 7.3 and 7.4). Figure 7.14 shows the locations of three trial pits, excavated, along a transect, across the enclosing ridge of the landform. Clast fabrics based on more than 25 clasts were measured and two grain-size samples (one from a depth of ca. 1 m and one at the base, ca. 2 m) were recovered from each trial pit. Two resistivity lines were also undertaken on the same day as the trial pitting, using an IRIS instruments Syscal Junior Switch 72. Line CL-Q1 ran north-northeast to south-southwest across the landform (140 m in length, 2 x 18 electrode cables, 4 m spacing of electrodes), intersecting the peat-filled basin. Line CL-Q2 (180 m in length, 2 x 18 electrode cables, 5 m spacing of electrodes) ran east-northeast to west-southwest, just inside the upslope rampart of the feature (Figure 7.14 and 7.15). Due to the availability of the LiDAR data supplied by the Environment Agency (Figure 7.3 and 7.14) no EDM derived DTM of the landform was produced, but topographical profiles were measured in association with the resistivity profiles.
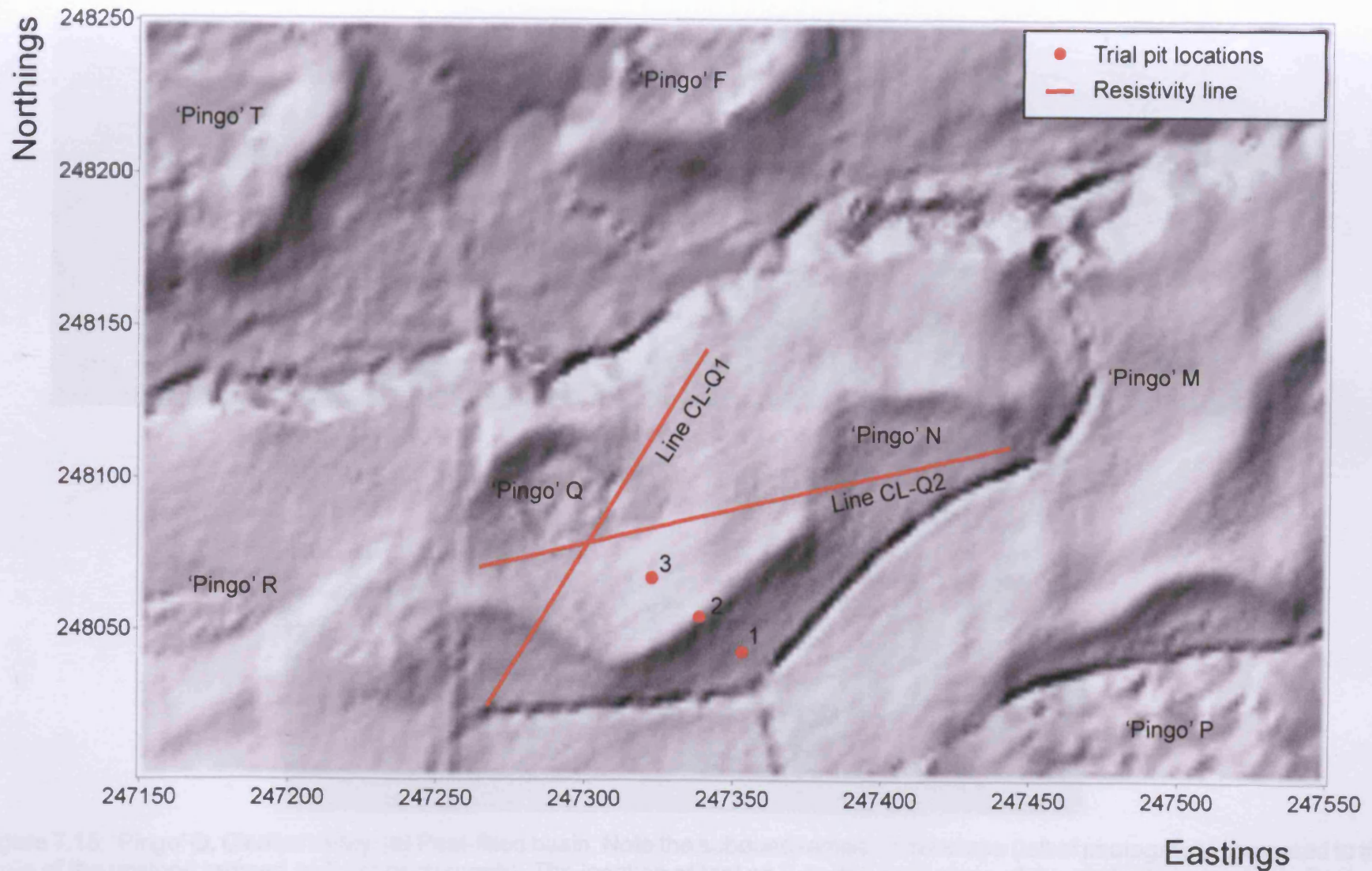
Figure 7.14: Locations of sedimentological and geophysical surveys at 'Pingo' Q, Cledlyn valley. Digital terrain model (DTM) data derived from LiDAR airborne surveying (© Environment Agency copyright and/or database right 2006).

Figure 7.15: 'Pingo' Q, Cledlyn valley. (a) Peat-filled basin. Note the subdued rampart downslope (left of photograph) compared to the large scale of the upslope rampart (right of photograph). The location of trial pit 3 on the inner slope of the upslope rampart is indicated by the position of the mini digger. The resistivity line 2 ran eastwards from the point where this photo was taken through the EDM station on the rampart in the far distance; (b) 'Pingo' Q from the east. Basin is located out of the line of sight, between the large rampart in the middle distance and the house.

7.6 Results: 'Pingo' Q

7.6.1 Sedimentology

The three trial pits excavated into the rampart of 'Pingo' Q were dominated entirely by a homogenous, hard and compact 2.5Y 5/3 light olive brown, orange mottled, well-graded, poorly sorted matrix-supported silty sandy clayey gravel diamict (Figures 7.16a-d and 7.17). The diamicton contained subangular to subrounded, highly striated clasts of fine sandstone and mudstone (Figures 7.16e and 7.16f), and occasional subangular clasts of quartz.

The diamicton of trial pit 1 (southern rampart slope) has a strongly preferred south to southeastward dipping clast fabric (high fabric strength, S1 = 0.74, S3 = 0.09), roughly perpendicular to the ridge trend and parallel to the local slope azimuth, the eigenvector of maximum clustering trending 157°, and dipping 22° (Figure 7.18 and 7.19). The vast majority of clasts measured in trial pit 1 had gently dipping a-axes (>80% 0-40°) with a clear peak between 11-20°. However, 16% of a-axes did have dips of 50-80°, with 8% of clasts having dips of 71-80° (Figure 7.18). Trial pit 2 (rampart crest) has a weaker clast fabric than pit 1 (S1 = 0.58, S3 = 0.15) with a NW-SE preferred orientation (approximately perpendicular to the ridge crest trend), the eigenvector of maximum clustering trending 328°, dipping 0.1°. Gently dipping a-axes were dominant (85% <30°) and no measured clasts had a-axes dips of >52°. The clasts did not have a preferred direction of dip however, with a roughly even distribution of clasts dipping northward and southward (Figure 7.18). The clasts from trial pit 3 (northern rampart slope) have a stronger clast fabric than pit 2, but weaker than pit 1 (S1 = 0.63, S3 = 0.14), the eigenvector of maximum clustering trending 318° (approximately perpendicular to the ridge crest and parallel to the slope azimuth), dipping 40.7°. Trial pit 3 was characterised by a much wider and even distribution of a-axes dip angles in contrast to trial pits 2 and 3 (Figure 7.18) but was marked by a strongly preferred dip direction to the northwest. The fabric shape diagram (Figure 7.19) indicates that all three clast fabric sample sets have a clustering fabric shape, characterised by high elongation and low isotropy. All samples are dominated by a SE-NW orientation of clasts, although the preferred dip direction on either side of the rampart is in the direction of the rampart slope.
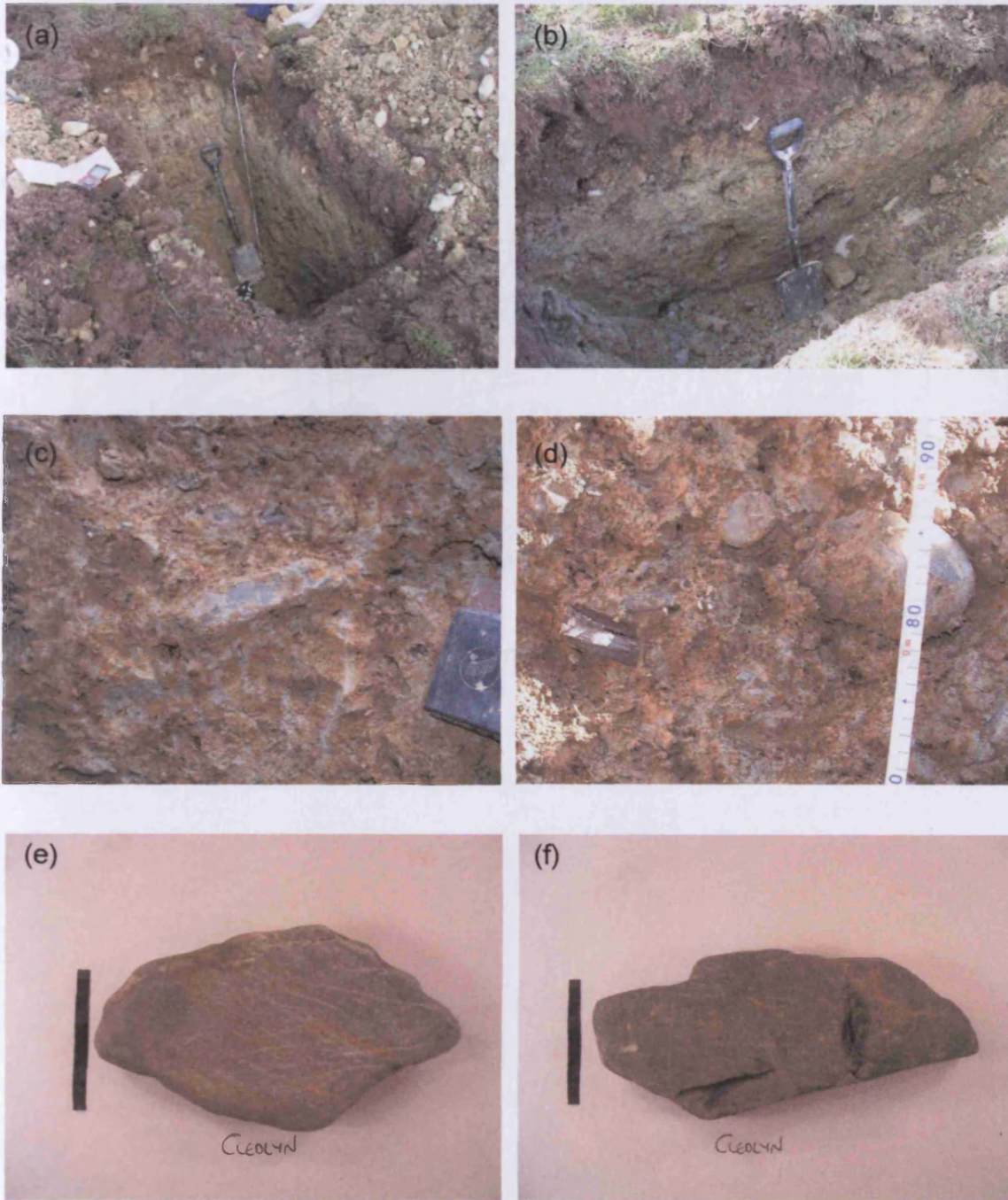
Figure 7.16: Excavations of the rampart of 'Pingo' Q, Cledlyn valley: (a) Trial pit 1, 'Pingo' Q; (b) Trial pit 2, 'Pingo' Q; (c) Matrix-supported diamict, trial pit 2; (d) Matrix-supported diamict, trial pit 2; (e) Striated clast, rampart of 'Pingo' Q, scale bar 5 cm; (f) Striated clast, rampart of 'Pingo' Q, scale bar 5 cm.
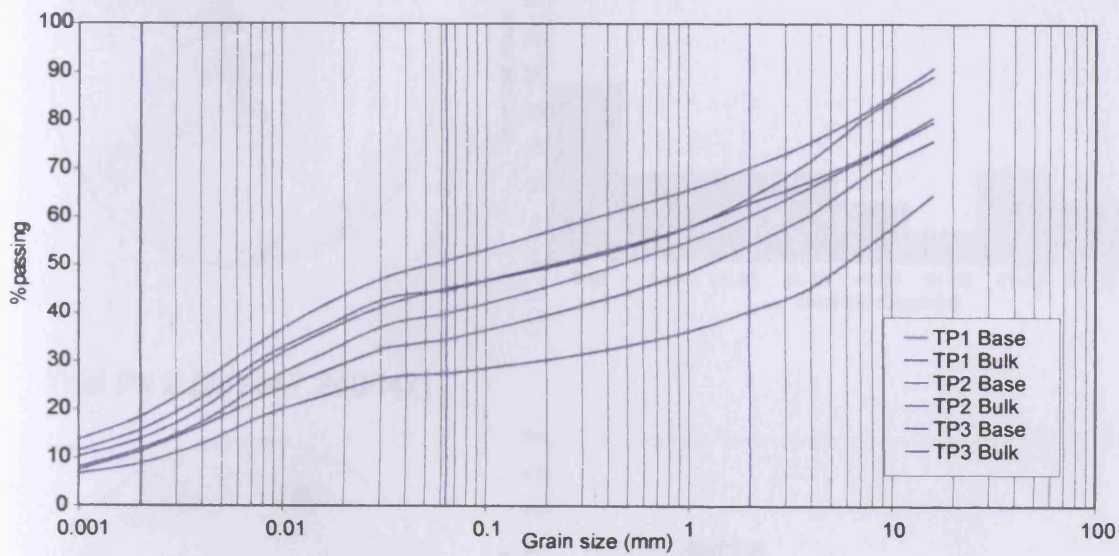
Figure 7.17: Grain-size analysis of sediments sampled from trial pits (TP) 1, 2 and 3, 'Pingo' Q, Cledlyn valley.

Trial Pit 3 (247319.248070)
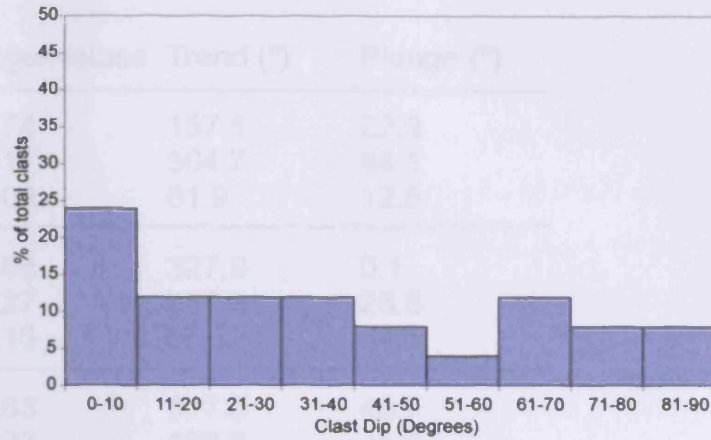
Trial Pit 2 (247347.248047)
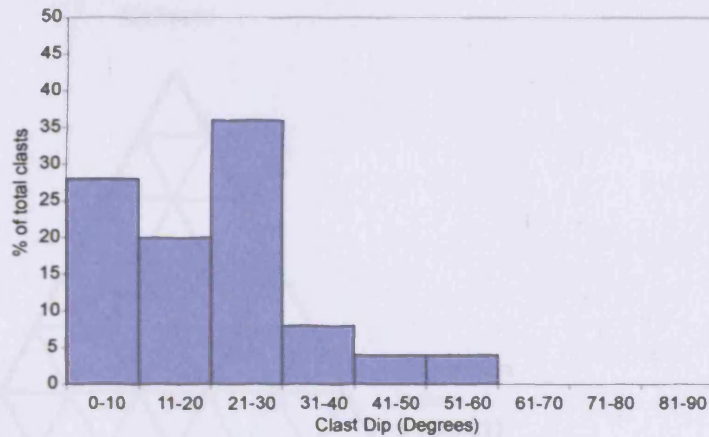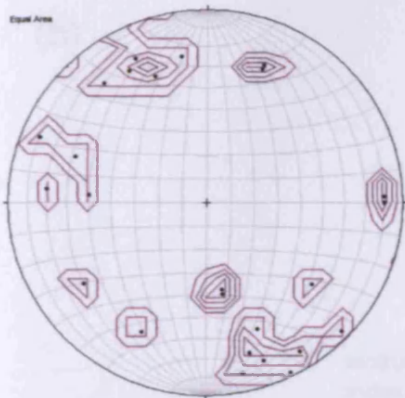
Trial Pit 1 (247351.248045)
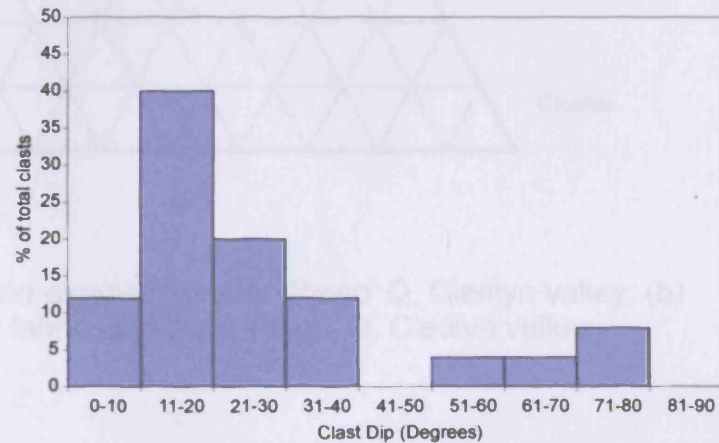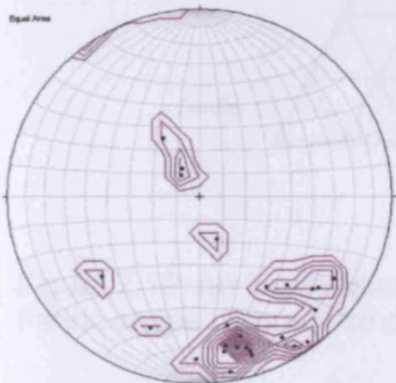
Figure 7.18: Clast fabric analysis and clast dip data from 'Pingo' Q trial pits 1-3: Clast fabric data displayed as equal-area projection stereonets, presented in sequence from north to south across the rampart.

(a)

		Eigenvalues	Trend (°)	Plunge (°)
Pit 1	S1	0.74	157.1	22.3
	S2	0.17	304.7	64.1
	S3	0.09	61.9	12.5
Pit2	S1	0.58	327.9	0.1
	S2	0.27	237.9	25.5
	S3	0.15	58.1	64.5
Pit3	S1	0.63	317.8	40.7
	S2	0.23	169.8	44.6
	S3	0.14	62.7	16.6

(b)
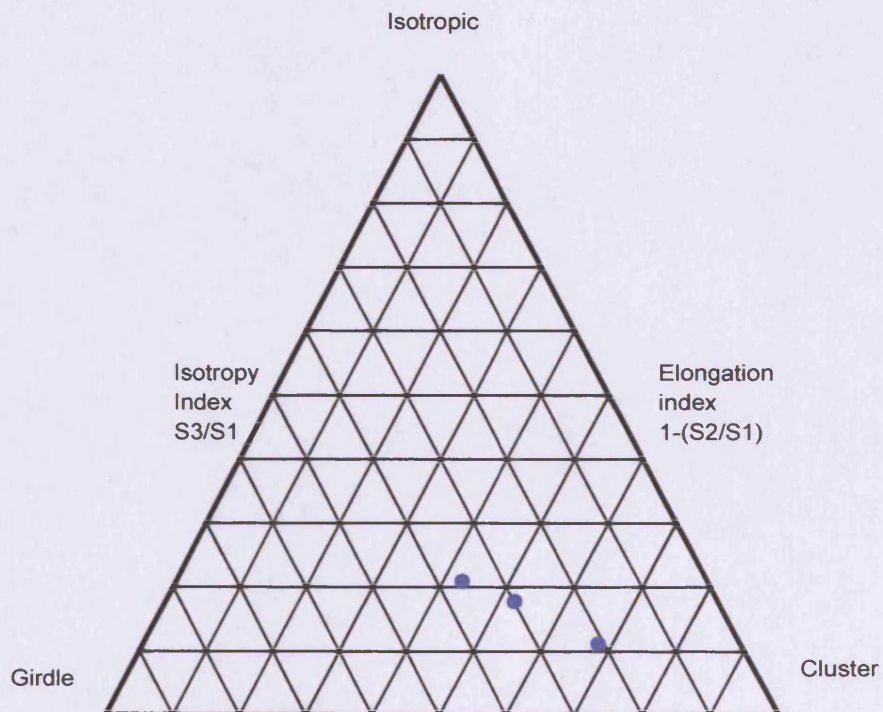
Figure 7.19: (a) Eigenvalues and eigenvectors for 'Pingo' Q, Cledlyn valley; (b) Fabric shape diagram for clast fabric data from 'Pingo' Q, Cledlyn valley.

7.6.2 Electrical resistivity tomography

Resistivity Line CL-Q1 has three distinct zones of differing resistivity values (Figure 7.20a). The near surface (including the ramparts and the central basin) is characterised by a 2-5 m thick zone of intermediate resistivity, generally 125-300 Ωm from 0-110 m (Zone CL-Q1). At 65-85m however, there is a localised but marked high resistivity zone of >700 Ωm. Beneath the near-surface Zone CL-Q1 there is a thick (15-20 m) zone of very low resistivity (mainly 30-100 Ωm) (Zone CL-Q2) that between 110-134 m extends upwards to the ground surface. At the base of the profile, underlying Zone CL-Q2, the resistivity increases to higher values (230-400 Ωm) at depths of 25-30 m below the ground surface (Zone CL-Q3). The boundary between Zones CL-Q2 and CL-Q3 in Line CL-Q1 has a slight north-northeastward dip.

Line CL-Q2 (Figure 7.20b) has very similar characteristics to Line CL-Q1. The uppermost, near-surface zone is characterised by intermediate resistivity (125-300 Ωm) (Zone CL-Q1). This zone is thicker in Line CL-Q2 than Line CL-Q1, extending to a depth of 7.5 m at the east-northeastern end of the profile (0-40 m). Below Zone CL-Q1 is a laterally continuous zone of low resistivity (30-230 Ωm, but predominantly 30-100 Ωm) (Zone CL-Q2) that is 15-20 m thick, underlain by an intermediate to high resistivity zone (230-600 Ω) (Zone CL-Q3). The boundary between Zones CL-Q1 and CL-Q2 is gradational in nature, the resistivity of Zone CL-Q3 increasing rapidly with depth. However, resistivity values do not change laterally, suggesting a horizontal boundary between Zones CL-Q2 and CL-Q3.
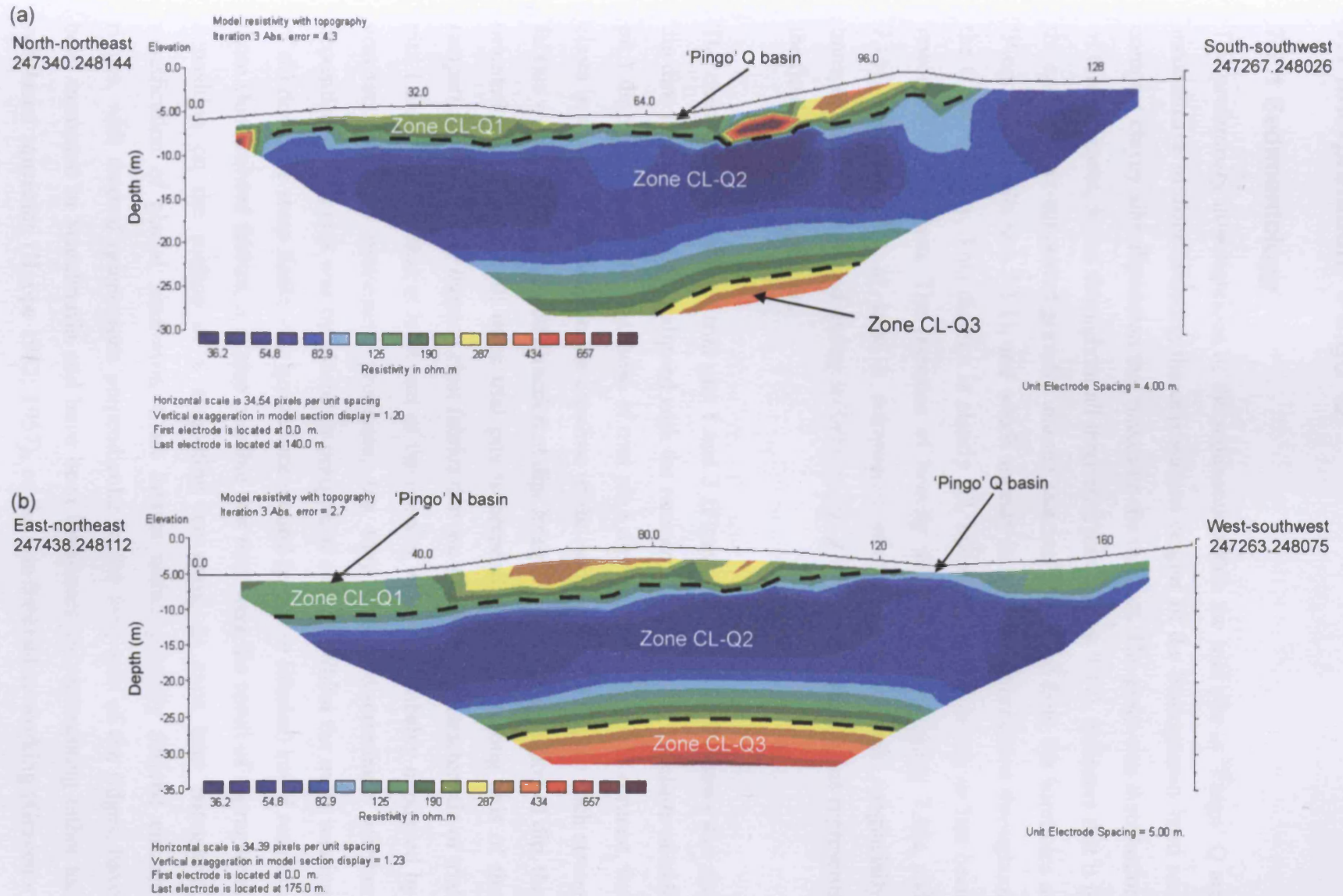
Figure 7.20: Electrical resistivity Lines (a) CL-Q1 and (b) CL-Q2, 'Pingo' Q, Cledlyn valley. The 125 Ωm contours in the upper parts of the profiles, and the 230 Ωm resistivity contours near the base of the profiles are marked by black dashed lines.

7.7 Interpretation: 'Pingo' Q

7.7.1 Sedimentology

The preliminary investigations of the sediments within the trial pits at 'Pingo' Q are inconclusive in discriminating the depositional origins of the homogenous hard and compact clayey silty diamicton that makes up the rampart. The grain-size distribution of this sediment, found throughout all three trial pits (Figure 7.17), indicates that it is the same matrix-supported gravelly diamict that was recovered from the boreholes at 'Pingo' U (see Section 7.3.1), and which appears to be widely distributed throughout the Cledlyn valley. This diamict is clearly till, but whether it is *in situ* or has been reworked is uncertain. The presence of heavily striated clasts (Figures 7.16e and 7.16f) indicates that at least a component of this sediment was subglacially transported at some period during its history, but it is unclear whether this represents the final stage of deposition.

The clast fabric analysis of trial pits 1 and 3 (Figures 7.18 and 7.19) shows that the dip direction of the clasts is aligned with the rampart slope azimuth, the clasts of trial pit 1 dipping southwards, and those of trial pit 3 dipping to the north. In contrast, the clasts in trial pit 2, located on the crestline of the rampart do not display such strong fabrics with no clear preferred direction of dip. Irrespective of the direction of dip, the orientation of clasts in all three trial pits is perpendicular to the long axis of the rampart. The shallowly dipping clast fabrics that are particularly characteristic of trial pits 1 and 2 suggest that at least part of the diamict was most probably deposited by gravitational mass movement processes, but they cannot discriminate whether deposition of this unit was by glacial or periglacial origins. Whilst the mass wasting of till down the steep flanks of a ground-ice mound (pingo or lithalsa) could result in these slope-related fabrics, it is also possible that they were the result of supraglacial deposition on the surface of a stagnating ice mass, or even later paraglacial modification of glacial landforms. Clast fabrics within glacially derived circular ridges, with marked orientations perpendicular to the long axis of the ridges, have been measured in Scandinavia and have been interpreted as representing either the subglacial squeezing (Hoppe 1952; 1957), or the gravitational re-working (Gravenor and Kupsch 1959; Knudsen et al 2006), of till. If the ridges in the Cledlyn valley are

of glacial origins, then the latter is the most likely explanation for the shallowly dipping clast fabrics from the three trial pits. However, this does not mean that the primary formation of these ridges could not have been the result of subglacial processes; the reworking of the diamict may have been post-formational. This suggestion is supported by the heavily striated clasts, which indicate the influence of subglacial processes, and the absence of even crude stratification within the rampart sediments, which would have provided independent evidence for the reworking of sediment by slope processes. The more steeply dipping distribution of clasts within trial pit 3 could have been the product of the collapse of sediments through the meltout of buried ice (either ground-ice or stagnating glacier ice), or post-depositional frost sorting (Watson and Watson 1971).

7.7.2 Electrical resistivity tomography

The resistivity surveys do not provide clear information on the internal structure of landform 'Pingo' Q. However, both lines indicate the nature and thickness of the superficial valley-fill deposits within which the landform (and the adjacent 'Pingo' N) is developed. The upper resistivity zones (CL-Q1 and CL-Q2) are interpreted as unconsolidated glacial deposits. Whilst the boundary between the two zones may reflect a lithological contact (e.g. glacial till overlying glaciolacustrine clay), alternatively it may simply represent a change in the pore-water content of a single lithological unit, perhaps due to the level of the water table. The apparent homogeneity of resistivity Zone CL-Q2 may mask significant complexity in the superficial sequence, different lithologies may result in similar electrical properties, or the resolution of the survey may mask laterally or vertically restricted sedimentary units. Water-saturated silty diamicts at depth that are less consolidated than those at the surface could have similar resistivity values to fine-grained glaciolacustrine deposits.

The marked high resistivity zone at the base of both profiles (Zone CL-Q3) is interpreted as bedrock. The gradational nature of the contact between Zones CL-Q2 and CL-Q3 can be explained by either i) a layer of superficial deposits of intermediate resistivity (e.g. sand and gravel) resting on bedrock; ii) a weathered layer of bedrock; or iii) the coarse resolution of points of measurement at the base of the resistivity profile resulting in average resistivity values that are intermediate between the low

resistivity unconsolidated deposits and the high resistivity bedrock. In any case, the resistivity values below a depth of 25 m are comparable to those interpreted as bedrock in the resistivity profile from 'Pingo' L (Figure 7.13) and from resistivity soundings in the Teifi valley near Lampeter and at Cornel (Heaven *et al.* 1999). The depth of bedrock indicated by the two resistivity lines at 'Pingo' Q is therefore in accordance with the depth suggested by the resistivity line undertaken at 'Pingo' L. The interpretation that Zone CL-Q3 represents bedrock is supported by the morphology of the boundary between Zones CL-Q2 and CL-Q3. In Line CL-Q1 the boundary dips northwards, towards the centre of the Cledlyn valley, whilst it is horizontal in Line CL-Q2, which runs parallel to the axis of the valley. At 'Pingo' L this boundary also dipped northwards, again towards the centre of the valley. The morphology of the upper contact of the high resistivity layer at the base of all resistivity profiles from the Cledlyn valley therefore suggests that this boundary may represent a palaeo-surface of the pre-glacial (pre-late Devensian?) river valley. The data presented here and from 'Pingo' U (Harris 2001b), indicate that there is a thick valley-fill sequence of unconsolidated materials (ca. 20-25 m) in the centre of the Cledlyn valley. Additional seismic surveys should be employed to verify the interpretation derived from the resistivity data. However, only a deep borehole to bedrock would clarify the internal composition of the unconsolidated deposits (Watson 1996).

8 Cletwr Valley

8.1 Introduction

Like those of the Cledlyn valley (Chapter 7), the ramparted depressions of the Cletwr Fawr basin (Figure 8.1) have a 'mutually interfering' character with a complex arrangement of superimposed forms (Watson and Watson 1974). Two groups of landforms with different characteristics have been identified in the Cletwr Fawr valley: i) round and oval forms (Llawr Cwrt group); ii) linear or very elongate forms (Glan-rhyd-y-dre (Glantre) and Darren Fawr groups) (Watson and Watson 1974) (Figures 8.2, 8.3 and 8.4). Although morphologically very different, and segregated in terms of their distribution, Watson and Watson (1974) believed that both groups in the Cletwr valley were the result of a common process (open system pingo development), and that the variance in morphology may have been a response to different groundwater conditions. Parallels have been drawn between the elongate features and linear landforms reported from the Hautes Fagnes, Belgium (Pissart 1963) and from the Hohe Venn region of Germany (Mückenhausen 1960).

The bedrock of the Cletwr Fawr valley is characterised by mudstones and sandstones of Ordovician and Silurian age (Figure 8.5) (BGS Sheet 194: Llangrannog, *unpublished map*). Most of the valley where ramparted depressions are situated (e.g. around 241000.250000 and 242400.248900) is underlain by mudstones of the Claerwen Group and Cwmere Formation, both of Llandovery Series (Silurian) age. Mudstones and sandstones of the Yr Allt Formation of Ashgill Series (Ordovician) age underlie these Silurian rocks at depth and outcrop to the southeast and southwest of the river valley (Figure 8.5). A series of west-southwest to east-northeast trending faults have been mapped across the area (Figure 8.5), but these do not directly underlie any of the ramparted depressions. Seepage of groundwater is likely through these faults (and numerous smaller, unmapped discontinuities), and through the more permeable sandstone units within the Allt Goch Sandstone Formation, the Rhyddlan Formation and parts of the Yr Allt Formation.

Watson and Watson (1974) conducted a series of investigations of the internal structure of the enclosed basins at Rhos Llawr Cwrt ('Pingos' 1 and 3) and at Glan-

rhyd-y-dre (Glantre) ('Pingo' 5 and rampart 'a') (Watson and Watson 1974; Watson 1975, 1976). The peat-filled basins of 'Pingos' 1 and 3 (Llawr Cwrt group) (Figures 8.2 and 8.6) were underlain by a well-sorted, dark grey clay (<0.2 m thick), containing scattered gravel (mostly <2 cm), and incorporating small amounts of plant debris and pollen (Watson and Watson 1974). Beneath this deposit was a gritty, gravelly, dark grey clay greater than 1.55 m in thickness (Watson and Watson 1974). Based on a transect of auger points, the basins of both 'Pingos' 1 and 3 appeared to have an asymmetrical form (Watson and Watson 1974), the maximum depth of 'Pingo' 1 being ca. 4 m and the smaller 'Pingo' 3 ca. 2.5 m. Pollen analysis of the peat infill of 'Pingo' 1 was conducted by Handa and Moore (1976), whilst two radiocarbon dates of 10,170±220 yrs BP and 8,260±300 yrs BP from the lowermost peat within the basin were provided by Shotton *et al.* (1974). 'Pingo' 2 (Watson and Watson 1974) at Rhos Llawr Cwrt was augered by Gurney (1994, 1995). This revealed that the contact between the mineral soil (smooth, structureless, plastic, blue grey (5B 7/1) silty-clay) and the overlying peat infill in the central basin was at a depth of less than 4.1 m (Gurney 1994).

The linear rampart of 'Pingo' 5 at Glan-rhyd-y-dre (Figure 8.3b) impounded a 3.3 m sequence of peat within an asymmetrical basin (Watson and Watson 1974), but more detailed investigations of the basins of these linear landforms have not been undertaken. A section through linear rampart 'a' (Watson and Watson 1974) of the Glan-rhyd-y-dre group (Figure 8.3b) was provided by the construction of a drainage ditch in the early 1970s. The section displayed a zone of interbedded silts and fine gravels, alongside a zone of deformation with upturned beds, and vertical clast fabrics. Watson (1975) argued that this section provided evidence for deformation from outward ice expansion, alongside evidence for pingo collapse and related mass movement processes (Watson 1975; 1976). Similar features have been recorded in rampart sections from Llangurig (Pissart 1963), the Hautes Fagnes, Belgium (see Section 2.3.1) (Bastin *et al.* 1974; Pissart 1983, 2000; Pissart *et al.* 1981; Pissart and Juvigne 1980), and in active pingos in the Canadian Arctic (Pissart 1967; Pissart and French 1976).
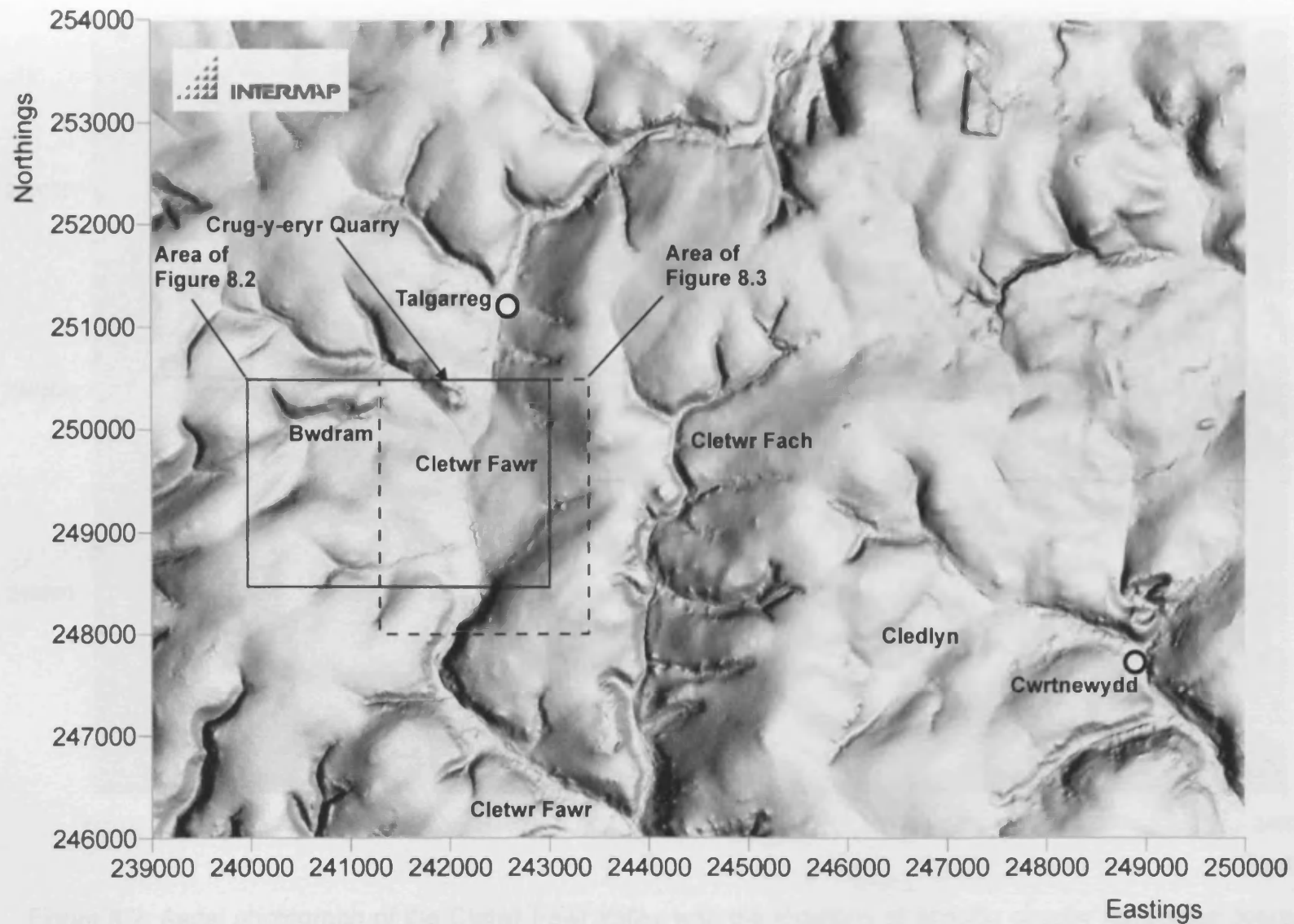
Figure 8.1: NEXTMAP digital terrain model (DTM) of the upper reaches of the Cletwr and Cledlyn valleys (© Intermap Technologies Inc). Areas of Figures 8.2 and 8.3 indicated.

Figure 8.2: Aerial photograph of the Cletwr Fawr valley with the locations of specific circular ramparted depressions ('Pingos' 1, 2, and 3), zones of linear 'pingos' ('Pingo' 5, and rampart 'a') and key farms labelled (© Getmapping Plc 2006).
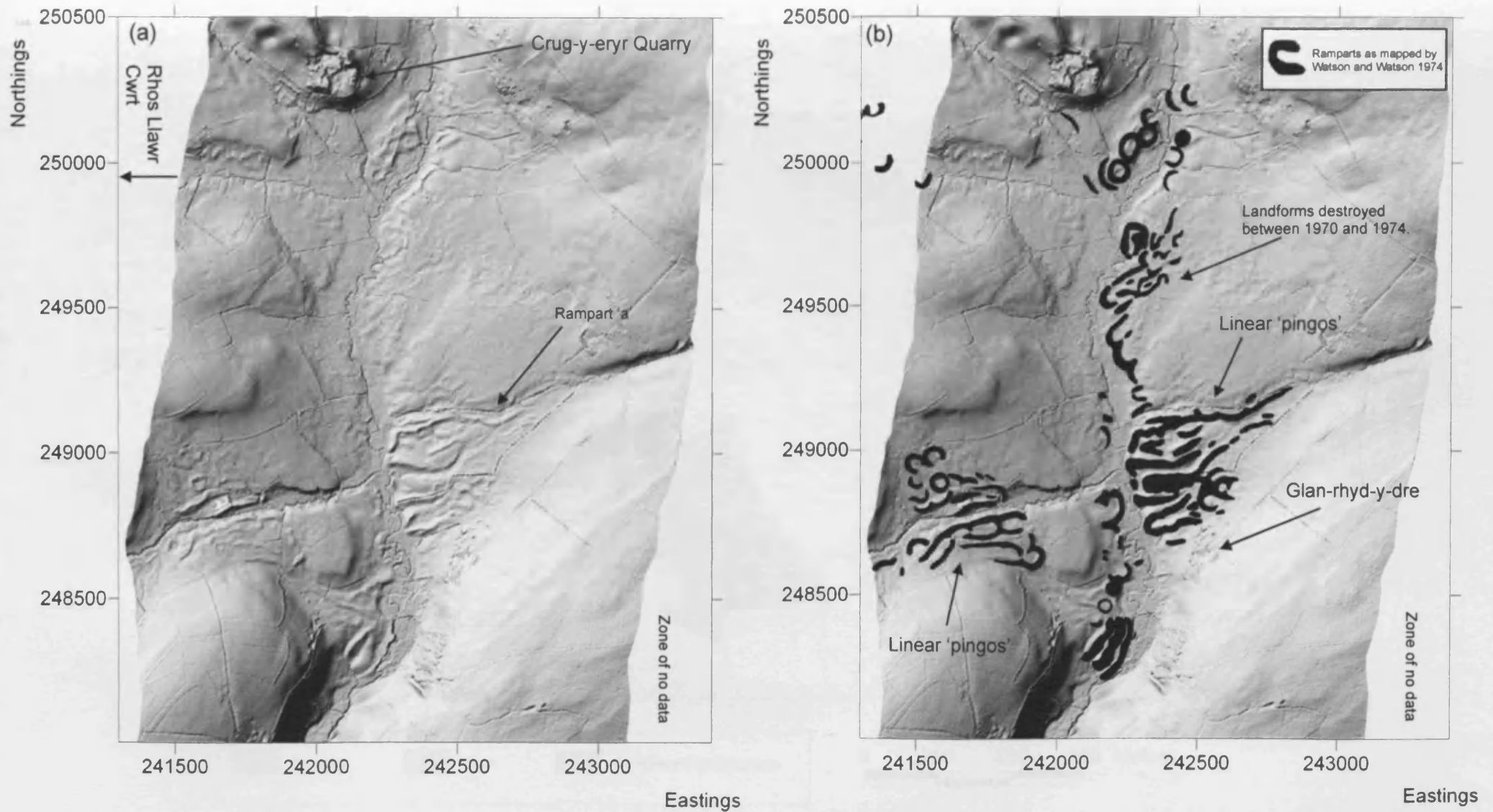
Figure 8.3: Shaded relief Digital Terrain Model (DTM) of landforms in the Cletwr Fawr valley, derived from LiDAR airborne surveying (© Environment Agency copyright and/or database right 2006). (a) LiDAR DTM data with 4 x vertical exaggeration; (b) LiDAR DTM data with 4 x vertical exaggeration with geomorphological mapping of Watson and Watson (1974) overlaid.

Figure 8.4: Geomorphological map of the Cletwr Fawr valley ramparted depressions (SN 41080.49977), based on mapping from stereoscopic aerial photographs. LANDLINE data © Crown Copyright/database right 2006. An Ordnance Survey/(Datacentre) supplied service.
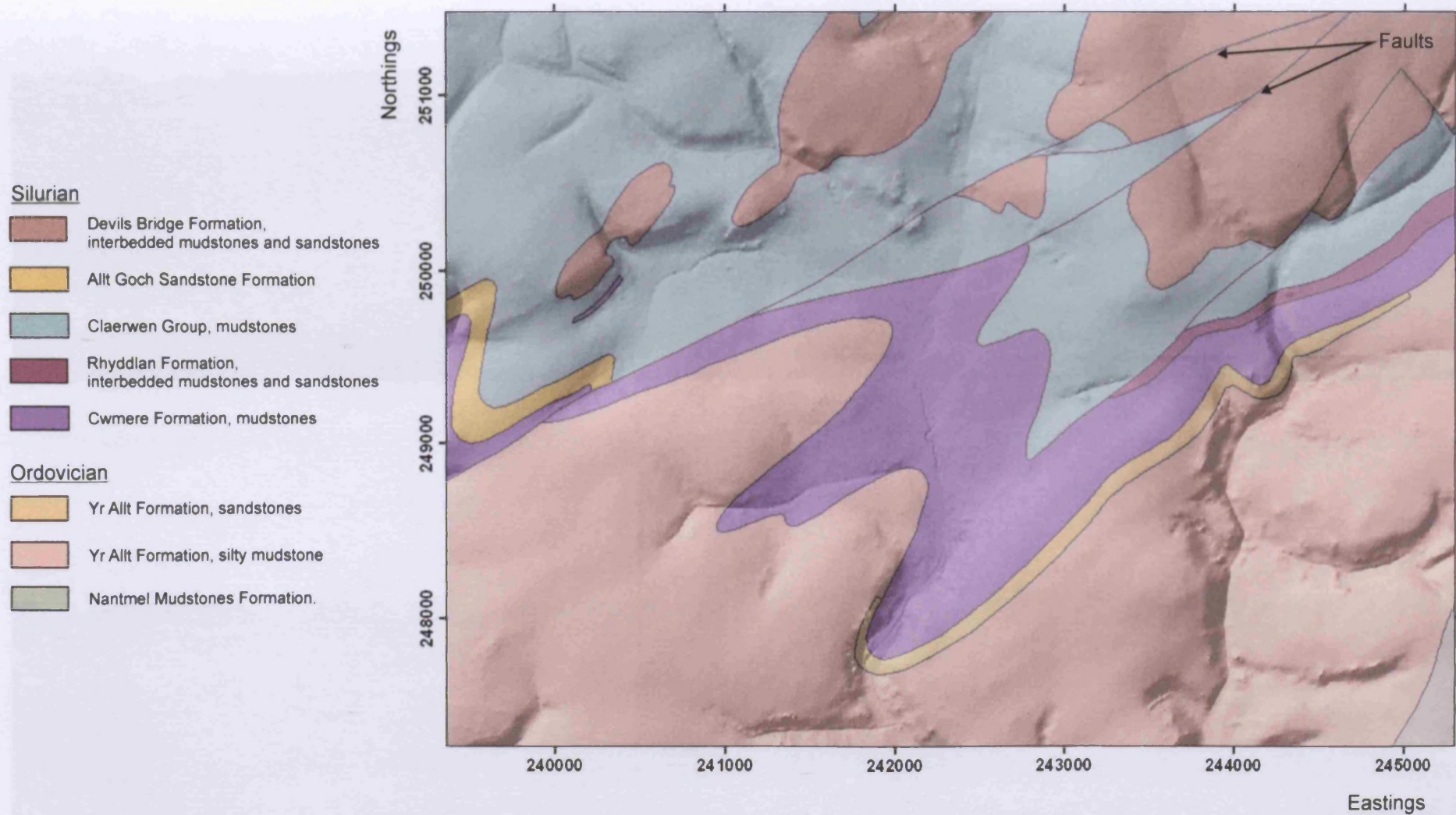
Figure 8.5: Bedrock geology of the Cletwr Fawr Valley (© British Geological Survey) draped on the surface of a NEXTMAP digital terrain model (DTM) with 3 x vertical exaggeration (© Intermap Technologies Inc.). Note that this map is adapted from unpublished, unchecked, draft mapping by the British Geological Survey and may therefore contain some inaccuracies.
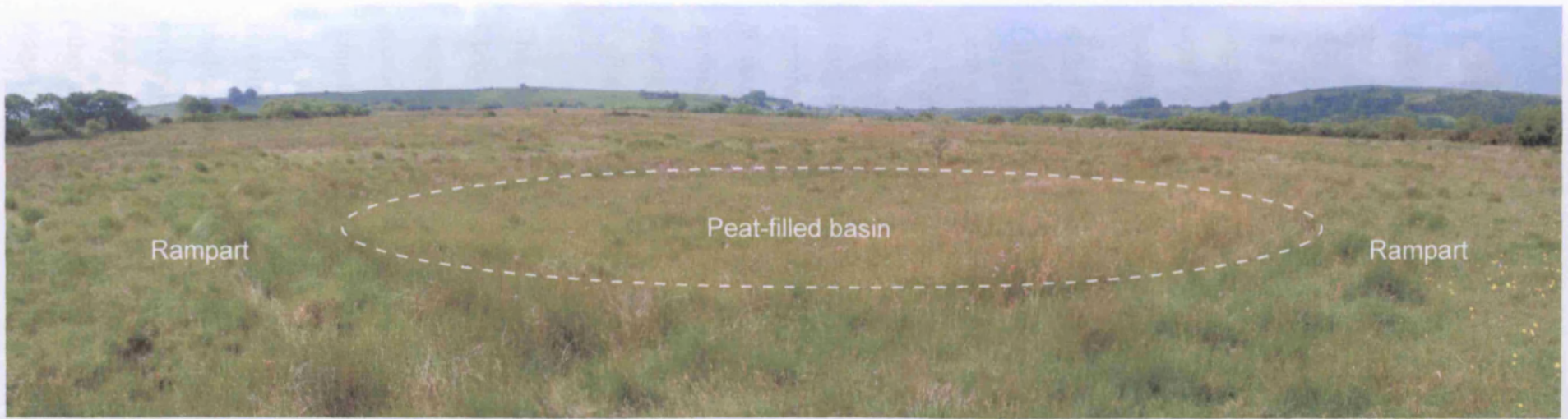
Figure 8.6: Ramparted depression ('Pingo' 3) at Rhos Llawr Cwrt, Cletwr Fawr. The boreholes were drilled in a transect across the subdued rampart of the landform.

8.2 Site description and survey

The linear ridges near Glan-rhyd-y-dre and Darren Fawr were not investigated during this research project. Instead, geological and geophysical investigations were concentrated on the round and oval forms of the Llawr Cwrt Group. However, as these two groups are considered by Watson and Watson (1974) to have common origins, and because LiDAR data are available for the linear ramparts (Figure 8.3), a brief outline and discussion of the geomorphology and possible origins of the linear landforms is also provided in this section.

8.2.1 Glan-rhyd-y-dre and Darren Fawr groups

LiDAR-derived digital terrain model data (Figure 8.3) show that the geomorphological mapping of the landforms near Glan-rhyd-y-dre and Darren Fawr by Watson and Watson (1974) was highly accurate (Figure 8.3b). Many of the landforms originally mapped by Watson and Watson (1974) were not recognised using modern aerial photographic resources (Figures 8.2 and 8.4), but are clearly apparent in the LiDAR data (Figure 8.3). The absence of some ramparts mapped by Watson and Watson (1974) in the LiDAR dataset (e.g. around 242250.249500) is probably the result of agricultural improvements during the late 20th Century. For example, several landforms at Glan-rhyd-y-dre (Glantre) were bulldozed flat in the 1970s (Watson and Watson 1974, Sybil Watson *pers comm.*) (Figure 8.3).

The LiDAR data however, does indicate that the morphology of the landforms in the Cletwr Fawr valley is rather more complex than the well-defined, linear, sinuous ramparts of collapsed permafrost ground-ice mounds suggested by the geomorphological map produced by Watson and Watson (1974) (Figure 8.3b). This complexity of "..close-set ridges, sometimes forming irregular "plateaus".." (Watson and Watson 1974, pg. 219) (e.g. around Glan-rhyd-y-dre), was attributed to the repetitive, cyclic development of linear pingos (Watson and Watson 1974), but it is unclear from the LiDAR data how such an interpretation can be justified. With the exception of 'Pingo' 5, investigated by Watson and Watson (1974), there are no other examples of linear, enclosed depressions in the Cletwr valley. Instead, many of the other linear ridges appear to be solitary landforms that cannot be grouped with other ridge fragments to form enclosed rampart forms (Figure 8.3a). As a result, these

ridges do not impound central basins (Figure 8.3a). On the basis of the LiDAR data therefore, these landforms do not appear to fulfil the basic criteria necessary to enable their classification as ramparted ground-ice depressions. The suggestion that clearly defined, linear ramparted depressions can be identified from the complex association of ridges is therefore somewhat misleading. On the basis of the geomorphology alone, several of the linear ridges could have formed as the result of alternative processes unrelated to the development of permafrost ground-ice mounds. Given that the Cletwr Fawr valley was glaciated during the late Devensian (see Section 2.5.2.2), the stagnation and meltout of glacier ice could provide an alternative hypothesis for the origins of many of the linear sinuous ridges near Glan-rhyd-y-dre and Darren Fawr. In at least one case, the depressions between long sinuous ridges mapped as ramparts by Watson and Watson (1974), could have been the result of fluvial (meltwater?) incision of a thick sequence of superficial sediments by tributary streams of the Cletwr Fawr, rather than the development of ground-ice (Figure 8.3a).

8.2.2 Rhos Llawr Cwrt group

One ramparted depression was investigated at Rhos Llawr Cwrt in the Cletwr valley. This subdued landform corresponds to 'Pingo' 3 investigated by Watson and Watson (1974) (Figure 8.6). It is situated on the north-facing slope of the Bwdram valley, a tributary of the Cletwr Fawr, at an altitude of approximately 195 m OD. Rhos Llawr Cwrt was selected as an appropriate site for geological and geophysical investigation because the model of open system pingo development in west Wales, proposed by Watson and Watson (1974), was developed at this site. 'Pingo' 3 was selected from the numerous landforms at Rhos Llawr Cwrt because the morphology of the peat-filled basin was already known (Watson and Watson 1974), physical access to the landform was straightforward, and because the basin had not been affected by historical peat cutting (Watson and Watson 1974), which made 'Pingos' 1 and 2 unsuitable for the safe deployment of drilling and geophysical equipment.

Figure 8.7 shows the locations of the investigations described below. Three boreholes were drilled on the 28th and 29th September 2004. Borehole 1 was drilled directly through the rampart crest (Figure 8.7), and reached a depth of 5.5 m. The second, Borehole 2, was drilled into the peat-filled basin, just inside the inner edge of the rampart (Figure 8.7), and reached a depth of 3 m. A third borehole, Borehole 3, was

drilled just beyond the outer edge of the rampart (Figure 8.7), and reached a depth of 5 m. Thirteen representative disturbed samples were extracted from the cores and later subjected to grain-size determination in the laboratory. The three boreholes were supplemented by three electrical resistivity and induced polarisation (IP) surveys, and a seismic refraction line.

Three resistivity and IP surveys (Lines RLC-1, RLC-2 and RLC-3) were undertaken utilising an IRIS instruments Syscal Junior Switch 72. Line RLC-1 (106 m in length, 3 x 18 electrodes cables, 2 m spacing of electrodes) and Line RLC-2 (140 m in length, 2 x 18 electrode cables, 4 m spacing of electrodes) both ran north-northwest to south-southeast across the landform, orientated so they were aligned through all three boreholes (Figure 8.7). Lines RLC-1 and RLC-2 overlapped; electrode 1 (0 m) is common to both Lines RLC-1 and RLC-2, so Line RLC-2 simply extends the survey to the north by 34 m (Figure 8.7). Compared to Line RLC-1, Line RLC-2 extends the maximum depth of survey from 17 m to 25 m, but provides a lower resolution 2D profile as a result of the larger spacing between the electrodes (4 m rather than 2 m for Line RLC-1). Line RLC-3 (105 m in length, 2 x 18 electrode cables, 3 m spacing of electrodes) was perpendicular to Lines RLC-1 and RLC-2, running east-northeast to west-southwest.

One short, reversed, P-wave seismic refraction line was shot along the northern rampart of the landform, intersecting the location of Borehole 1 (Figure 8.7). Geophone 1 was located on the westernmost end of the spread with geophone 24 to the east. A 2 m spacing between geophones was deployed resulting in a 46 m long spread. The seismic line was orientated roughly parallel to resistivity/IP Line RLC-3, but was offset 20 m to the north of the resistivity/IP profile. Borehole 1 was located approximately at the centre of the geophone spread.

A site survey utilising an EDM theodolite was undertaken to produce a digital terrain model of the landform and its surrounding topography (Figure 8.7). The boreholes and geophysical surveys were georeferenced by correcting the EDM data using handheld GPS data and Getmapping aerial photography. LiDAR data of the Cletwr valley (Figure 8.3a) does not provide coverage of these landforms.
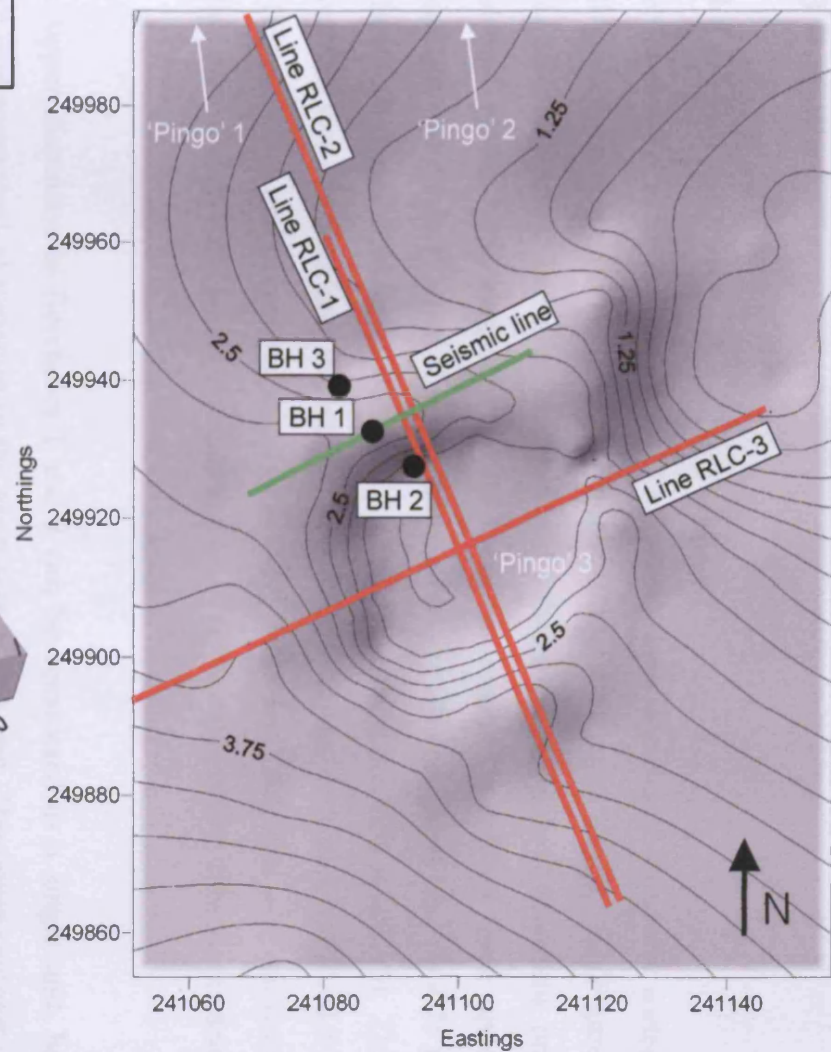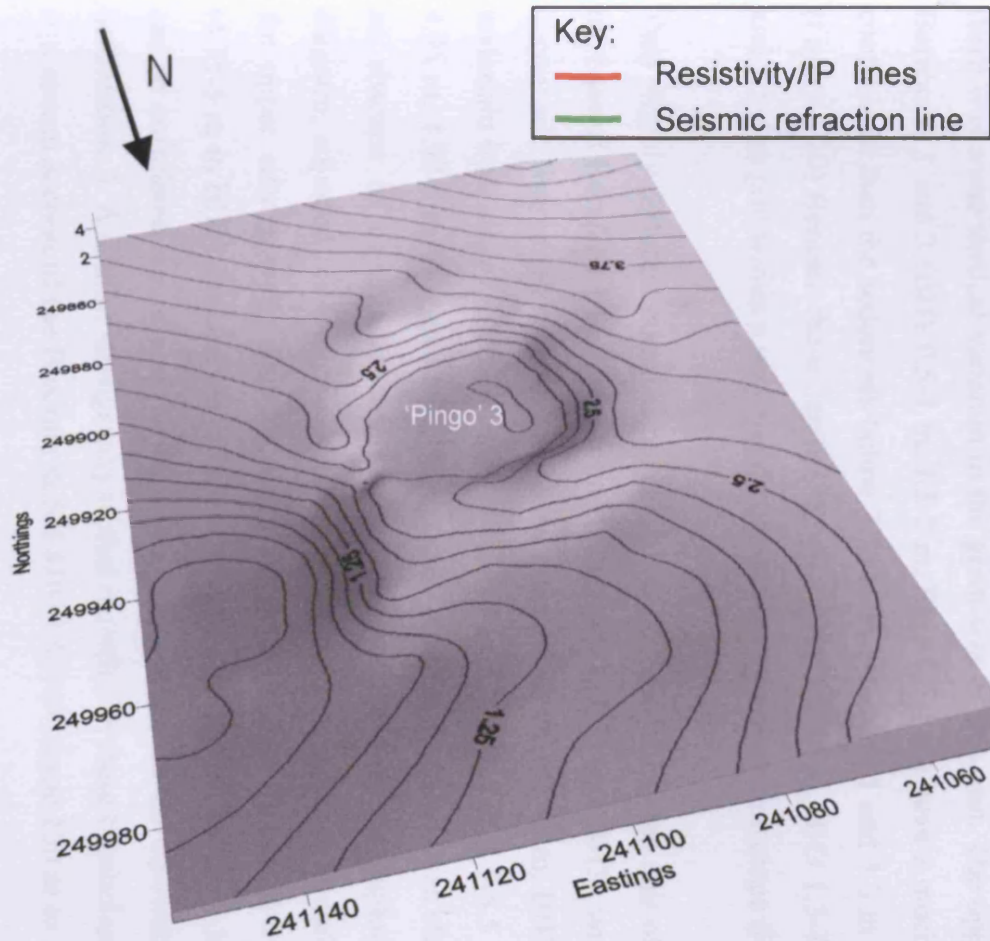
Figure 8.7: Digital Terrain Model (DTM) of ramparted depression 'Pingo' 3 at Rhos Llawr Cwrt, Cletwr Fawr derived from EDM surveying. Locations of boreholes, electrical resistivity, induced polarisation (IP) and seismic refraction survey lines indicated. Contours at intervals of 0.25 m.

8.3 Results

8.3.1 Sedimentology

The upper 4-4.5 m of Borehole 1 and Borehole 3 were dominated by poorly sorted, well-graded, compact, non-calcareous gravelly silt to silty gravel diamictons (Figures 8.8a, 8.8c and 8.9a). The gravels comprised subangular to rounded mudstone and sandstone clasts, with long axes up to 7 cm in length. Underlying these upper sediments, more than 0.5-1 m of non-calcareous clayey silt was found beneath 4.75 m in Borehole 1 and 3.91 m in Borehole 3 (Figures 8.8a, 8.8c, 8.9a and 8.9b). This lower unit was characterised, in parts, by very fine, faint laminations (e.g. BH3 4.5-5 m) (Figure 8.9b) and occasional small clasts (e.g. BH1 5-5.5 m). The total thickness of this unit of clayey silt is unknown as neither of the boreholes was able to penetrate it.

The upper diamicton in Boreholes 1 and 3 can be considered as a single unit, but there was some vertical variation in the grain-size of this unit. The upper samples of Boreholes 1 and 3 (BH1 0.5-1 m, 1.5-2 m, BH3 0.5-1 m) have a much lower gravel component than the sediments below 2.75 m in Borehole 1 and 1.3 m in Borehole 3 (Figure 8.10) Beneath these depths, samples BH1 2.75-3 m, BH3 1.3-1.5 m, 1.5-2 m and 3.5-4 m plot within a very tightly constrained grain-size envelope (Figure 8.10).

Two slightly different components can be recognised within the unit of clayey silt at the base of Borehole 1 (4.75-5.5 m) and Borehole 3 (3.91-5 m BH3), with a laminated clayey silt, free of gravel and sand-sized material (BH1 4.75-5 m, BH3 4.5-4.75 m), underlain by a clayey silt including occasional small clasts (BH1 5-5.5 m, BH3 4.75-4.95 m, 4.92-5 m) (Figures 8.8a, 8.8c and 8.10). The clayey silt was characterised by an absence of organic material and was non-calcareous throughout. The fence diagram, adjusted for topography (Figure 8.8d), shows that the boundaries between the upper silty gravelly diamicton (0-4.75 m in BH1), the gravel-free clayey silt (4.75-5 m in BH1), and the clayey silt with occasional small clasts (5-5.5 m in BH1), can be correlated laterally at the same relative height with the equivalent boundaries in Borehole 3. A similar stratigraphy to that recorded in these boreholes was observed in a stream section of the Bwdram at SN 41013.50069, some 150 m to the northwest,

225

(a)

CLAY SILT SAND GRAVEL

Depth (metres)

0

1

2

3

4

5

6

S Fm

Fm

S Dmm

S

Dcm

Dmm

Dcm

S Fm

S Fm

2.5YR 2.5/1 black organic topsoil (SILT)

10YR 6/2 light brownish grey orange mottled, gravelly slightly sandy clayey SILT. Subangular Silurian mudstone/sandstone 4-5cm.

7.5 YR 5/8 strong brown mottled slightly sandy clayey SILT, occasional small clasts.

10YR 5/2 greyish brown slightly mottled gravelly slightly sandy clayey SILT. Very compact, very hard and dry. Mudstone/sandstone subangular clasts up to 4 cm in length.

2.5Y 5/2 greyish brown slightly clayey silty GRAVEL. Occasional larger subangular clasts to 5 cm in length (Aberystwyth grits).

10YR 5/2 greyish brown slightly mottled slightly sandy clayey SILT. Very compact, very hard and dry. Mudstone/sandstone subangular clasts to 4 cm in length.

10YR 5/4 yellowish brown hard, wet to moist silty fine GRAVEL with occasional clasts to 7cm.
2.5YR 4/1 dark grey silty GRAVEL, clasts to 0.75 cm.
2.5 Y 5/2 bluish greyish brown moist firm clayey SILT.

2.5Y 5/2 bluish greyish brown moist firm clayey SILT with occasional fine clasts

(b)

CLAY SILT SAND GRAVEL

Depth (metres)

0

1

2

3

4

5

6

PEAT

S

Gley 1 5/N grey sandy silty clayey GRAVEL, wet, soft to very soft. Occasional subangular to subrounded occasional clasts to 4-5 cm in length.

Figure 8.8: Sedimentary logs of (a) Borehole 1; and (b) Borehole 2, 'Pingo' 3, Rhos Llawr Cwrt, Cletwr Fawr. 'S' marks sampling locations for grain-size analysis.

(c)

10YR 2/1 black peaty organic soft TOPSOIL.

10YR 4/2 dark greyish brown clayey SILT moist, firm to soft.

2.5Y 7/2 light grey sandy, clayey SILT with 10YR 6/8 brownish yellow orange mottling. Slightly moist, non plastic. Slightly sandier towards base.

10YR 5/2 greyish brown moist sandy gravelly clayey SILT. Rounded to subrounded clasts to 7 cm in length.

2.5Y 4/2 dark greyish brown to10YR 5/4 yellowish brown silty sandy GRAVEL, contains clasts up to 6-7cm.

10YR 5/1 grey moist firm SILT with occasional small clasts.

2.5Y 4/2 dark greyish brown, soft (finely laminated?) clayey SILT. Soft to firm.

Gley 1 5/10Y greenish grey firm to soft (laminated?) gravelly clayey SILT with occasional small clasts.

(d)

Figure 8.8 (cont): Sedimentary log of (c) Borehole 3; and (d) fence diagram of Boreholes 1-3, adjusted for topography, 'Pingo' 3, Rhos Llawr Cwrt, Cletwr Fawr. 'S' marks sampling locations for grain-size analysis.

Figure 8.9a: Photographs of borehole cores from 'Pingo' 3, Rhos Llawr Cwrt, Cletwr valley. Borehole 1: (i) gravelly, slightly sandy, clayey silt (1-2 m) (Photo: C. Harris); (ii) clayey silty gravel (3-4 m); (iii) silty fine gravel underlain by clayey silt (4.5-5 m); (iv) clayey silt with occasional clasts (5-5.5 m). Borehole 2: (v) sandy, silty clayey gravel (2-3 m). Borehole 3: (vi) peaty organic topsoil underlain by weathered sandy, clayey silt (0-0.5 m); (vii) silty sandy gravel (1-2 m) (Photo: C. Harris); (viii) finely laminated clayey silt (4.5-5 m) (Photo: C. Harris).
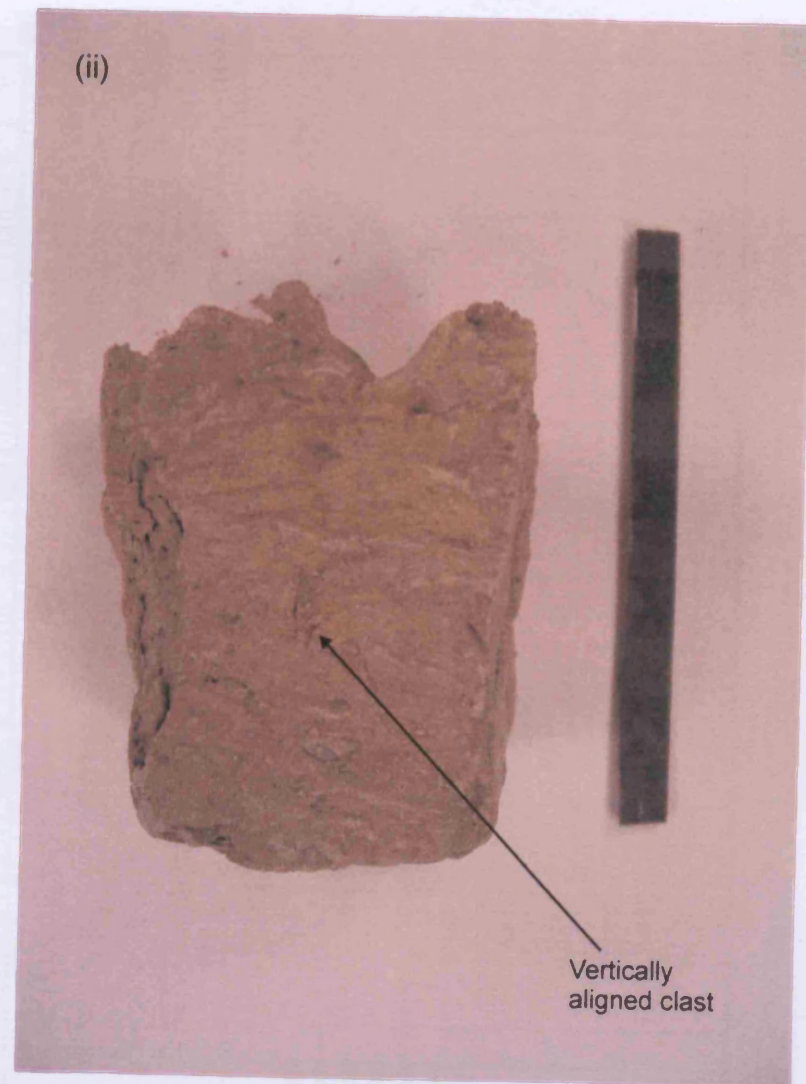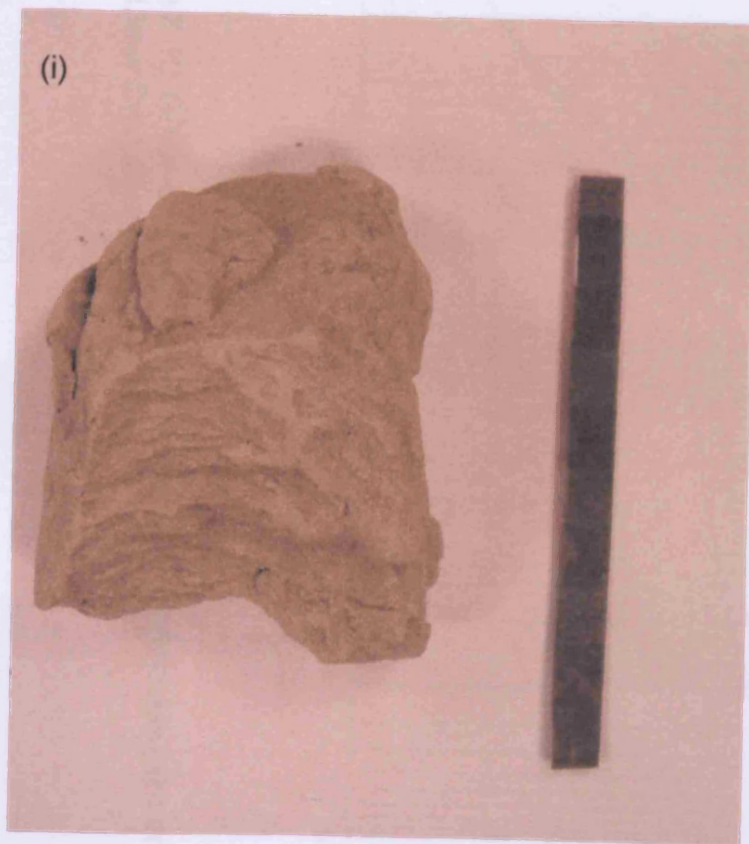
Figure 8.9b: Laminated clayey silts from Borehole 3, Rhos Llawr Cwrt, Cletwr Fawr. (i) Sample from unit 4.5-4.75 m; (ii) Sample from unit 4.75-5 m. Black scale bar is 5 cm long. Note the vertically orientated elongate gravel-sized clast in the centre of the sample from unit 4.75-5 m.
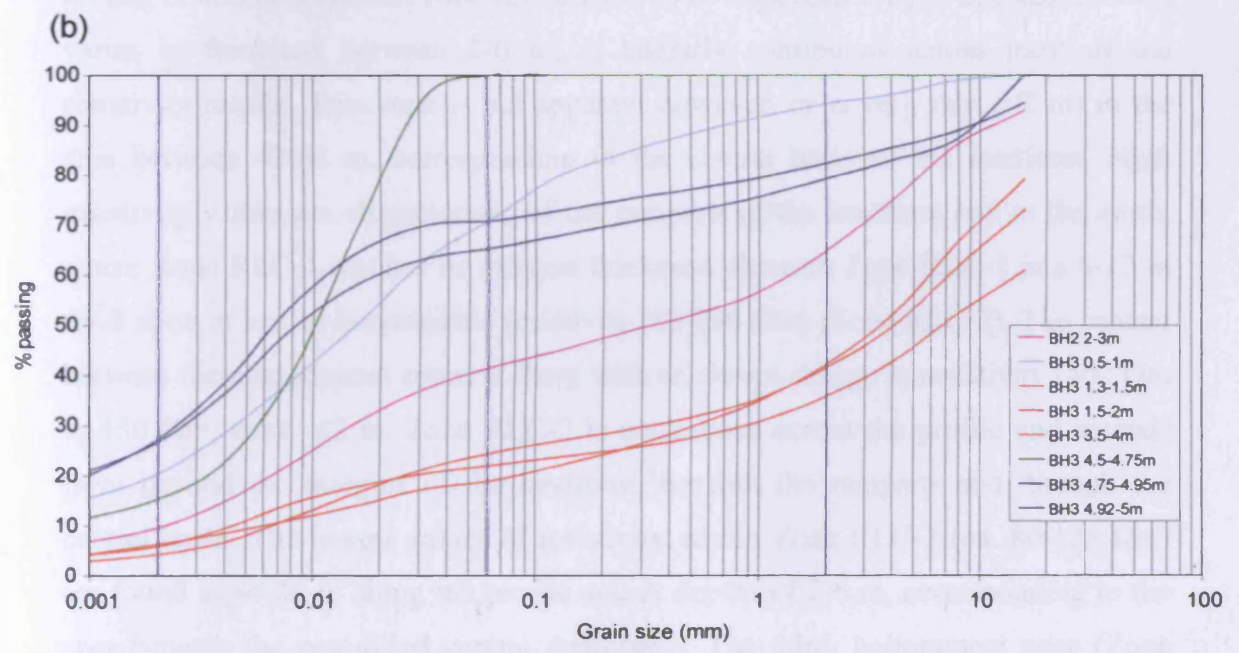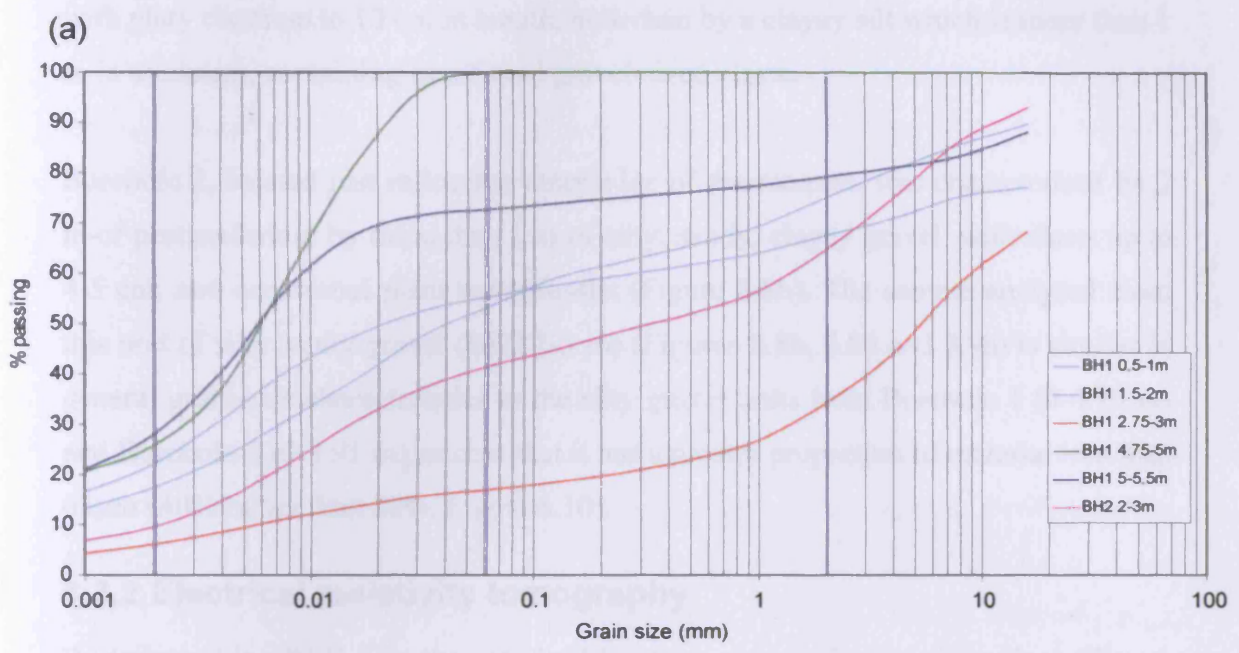
Figure 8.10: Grain-size analysis of samples from Boreholes (a) 1 and 2; (b) 2 and 3, Rhos Llawr Cwrt, Cletwr Fawr.

where a 1.25 m thick blue-grey silty diamict, overlies a thin gravelly unit (<10 cm), with platy clasts up to 10 cm in length, underlain by a clayey silt which is more than 1 m in thickness, containing occasional gravel-sized clasts.

Borehole 2, located just inside the inner edge of the rampart, was characterised by 2 m of peat underlain by more than 1 m of silty, sandy, clayey gravel, with clasts up to 4-5 cm, and occasional plant macrofossils (Figure 8.8b). The sample analysed from this unit of silty sandy gravel (BH2 2-3 m) (Figures 8.8b, 8.8d and 8.9a) is similar in general grain-size characteristics to the silty gravel units from Borehole 1 (0-4.75 m) and Borehole 3 (0-3.91 m), except that it has a greater proportion of material less than 63μm (40% rather than 20%, Figure 8.10).

8.3.2 Electrical resistivity tomography

Resistivity Line RLC-1 is characterised by three zones of resistivity values (Figure 8.11a). A thin near-surface zone (Zone RLC-1) of high resistivity (>230 Ωm), which varies in thickness between 2-6 m, is laterally continuous across most of the resistivity profile. This zone is not apparent however, or is very thin (<2 m) in the area between 42-68 m, corresponding to the central basin of the landform. High resistivity values are characteristic of the ramparts of the landform and to the north, where Zone RLC-1 reaches its greatest thickness. Beneath Zone RLC-1 is a 6-12 m thick zone of low to intermediate resistivity (80-230 Ωm) (Zone RLC-2). The contact between these uppermost zones is sharp with an abrupt change in resistivity (400 Ωm to 150 Ωm) over <2 m. Zone RLC-2 is continuous across the profile and extends from beyond the margins of the landform, beneath the ramparts and through the central basin. The lowest values of resistivity within Zone RLC-2 (ca. 80-125 Ωm) are found at 44-66 m along the profile and at depths of 2-6 m, corresponding to the area beneath the peat-filled central depression. The third, bottommost zone (Zone RLC-3) has intermediate to high resistivity values (230-400 Ωm). The contact between this zone and the overlying Zone RLC-2 is gradational in nature with resistivity values increasing over a vertical distance of 2-4 m. This contact is characterised by a marked south to north dip. Taking the 230 Ωm contour as the boundary between these two zones, the contact dips from a depth of 6 m in the south to 14 m at the north end of the profile. The internal resistivity of Zone RLC-3 shows little lateral variability, but an increase in resistivity is apparent with depth.

Line RLC-2 is characterised by the same three distinct zones of resistivity values as Line RLC-1 (Figure 8.11b). Due to the reduced resolution in comparison to Line RLC-1, the thin, near-surface Zone RLC-1 is not apparent to the south of the central basin in Line RLC-2, but is identified in the rampart to the north and extends continuously from here (68 m) to the end of the line (134 m). It is clear from Line RLC-2 that Zone RLC-1 is of greater thickness to the north of the central basin (5 m), compared to its thin vertical extent to the south of the landform. As in Line RLC-1, Zone RLC-2 extends throughout, but is marked by a decreasing resistivity from south to north. The contact between Zones RLC-1 and RLC-2 is again abrupt. Line RLC-2 provides additional information regarding the resistivity and lateral and vertical character of Zone RLC-3 and the morphology of the contact between this basal zone and the overlying Zone RLC-2. Line RLC-2 indicates that the thickness of Zone RLC-3 extends to depths in excess of 25 m and is characterised by relatively high resistivity values (up to 500 Ω m). Taking the 230 Ωm contour as the boundary between Zones RLC-2 and RLC-3, Line RLC-2 supports the observation that the contact dips northwards, but also suggests that this contact may be marked by a stepped profile, an observation that was not apparent from Line RLC-1.

Line RLC-3, also characterised by three zones of resistivity (Figure 8.11c), was run perpendicular to Lines RLC-1 and RLC-2, with the centre of the landform's basin marking the intersection point between the lines (Figure 8.7). The high resistivity near-surface zone (Zone RLC-1) is apparent, but is again absent over the central basin and is slightly thinner to the east of the profile (1 m) in comparison to its vertical thickness to the west (2-3 m). Zone RLC-2 is again characterised by relatively low resistivity values (80-230 Ωm), and is laterally continuous with little horizontal variation. Resistivity values increase with depth. At 12 m below the ground surface the 230 Ωm contour marks the upper contact of Zone RLC-3. The horizontal nature of the contact between Zones RLC-2 and RLC-3 in Line RLC-3 contrasts with the steeply dipping and/or stepped profile observed in Lines RLC-1 and RLC-2. Again, the contact between Zones RLC-2 and RLC-3 is marked by a gradational boundary of resistivity values in Line RLC-3.
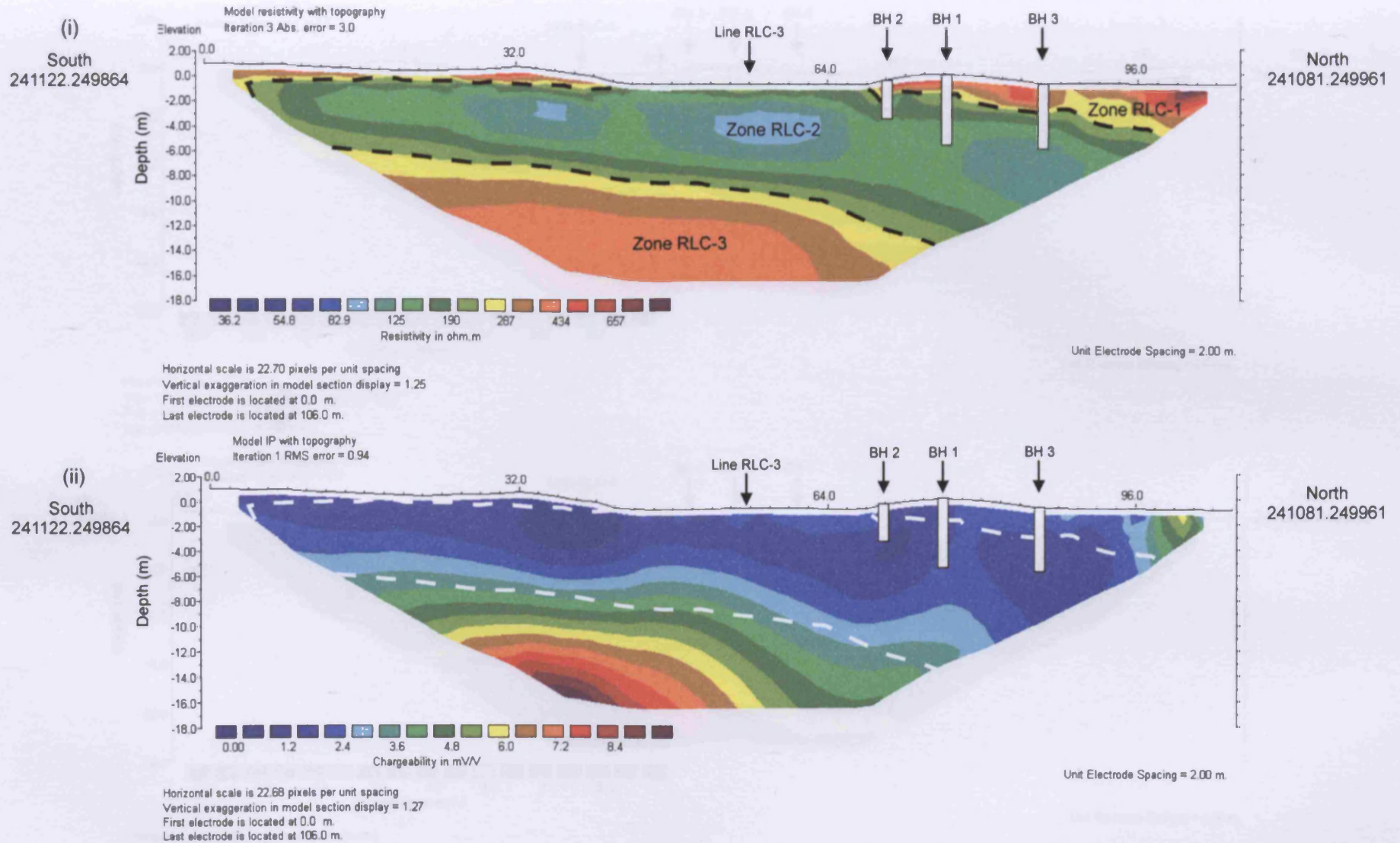
Figure 8.11a: (i) Electrical resistivity and (ii) IP profiles (Line RLC-1), 'Pingo' 3, Rhos Llawr Cwrt, Cletwr Fawr. Locations of boreholes and intersection points of other resistivity/IP lines indicated. The 230 Ωm resistivity contours are marked on the resistivity profile by black dashed lines and on the IP profile by dashed white lines. The seismic refraction profile ran perpendicular to this line, intersecting it at the location of Borehole 1.
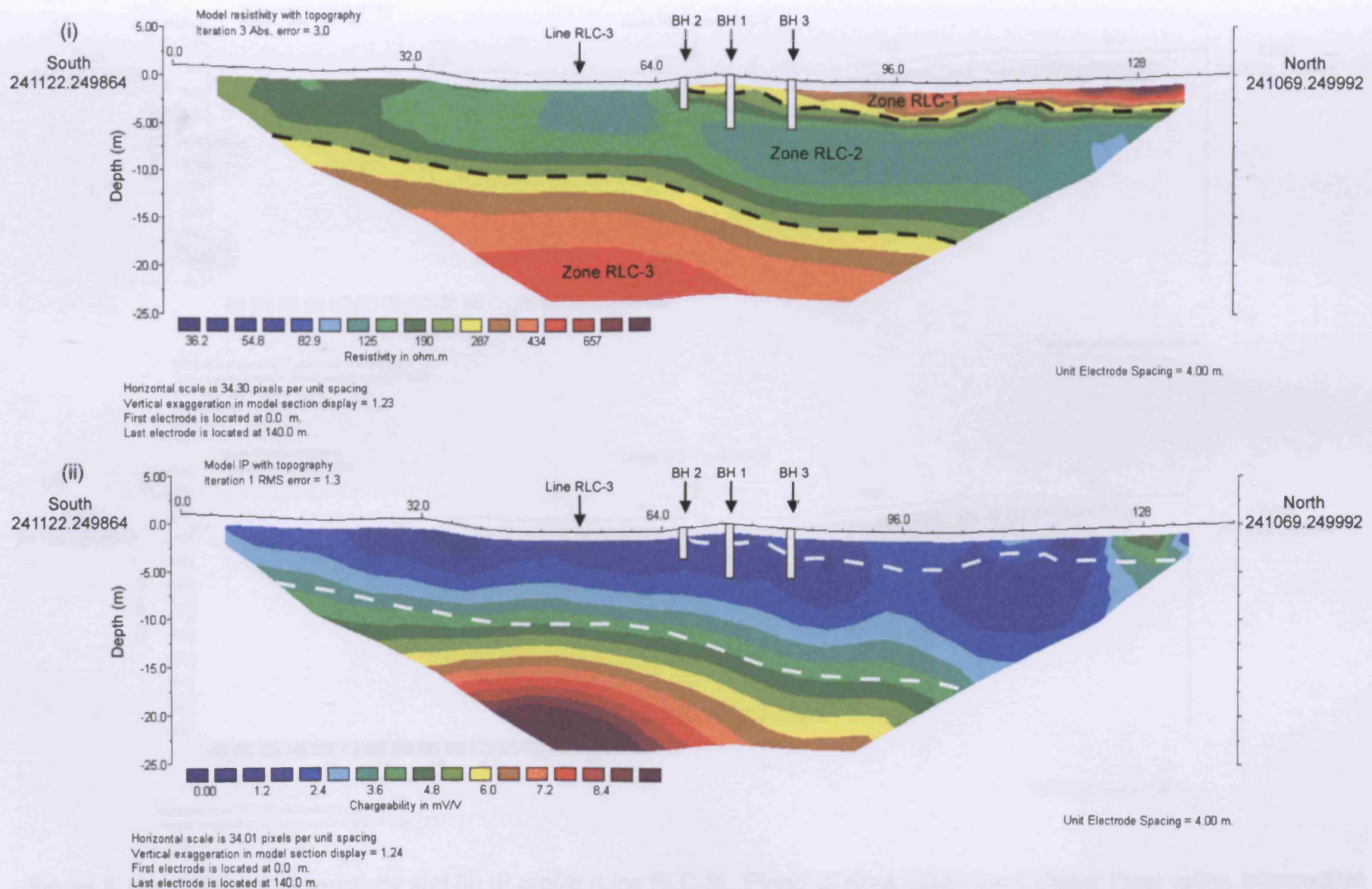
Figure 8.11b: (i) Electrical resistivity and (ii) IP profiles (Line RLC-2), 'Pingo' 3, Rhos Llawr Cwrt, Cletwr Fawr. Locations of boreholes and intersection points of other resistivity/IP lines indicated. The 230 Ωm resistivity contours are marked on the resistivity profile by black dashed lines and on the IP profile by dashed white lines. The seismic refraction profile ran perpendicular to this line, intersecting it at the location of Borehole 1.
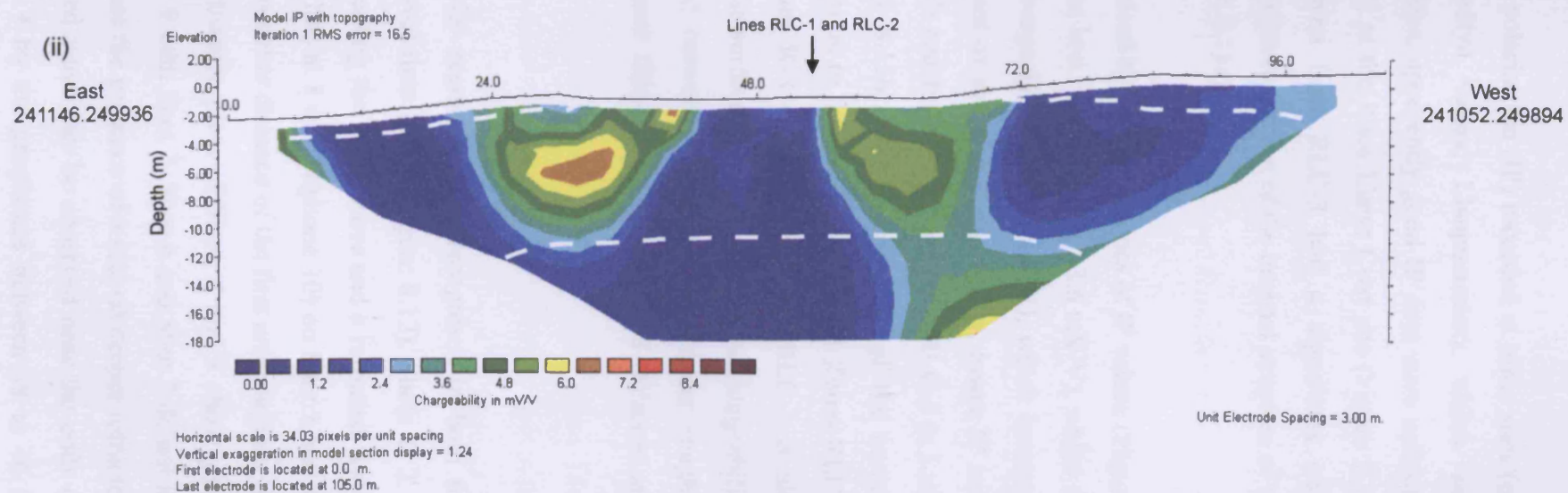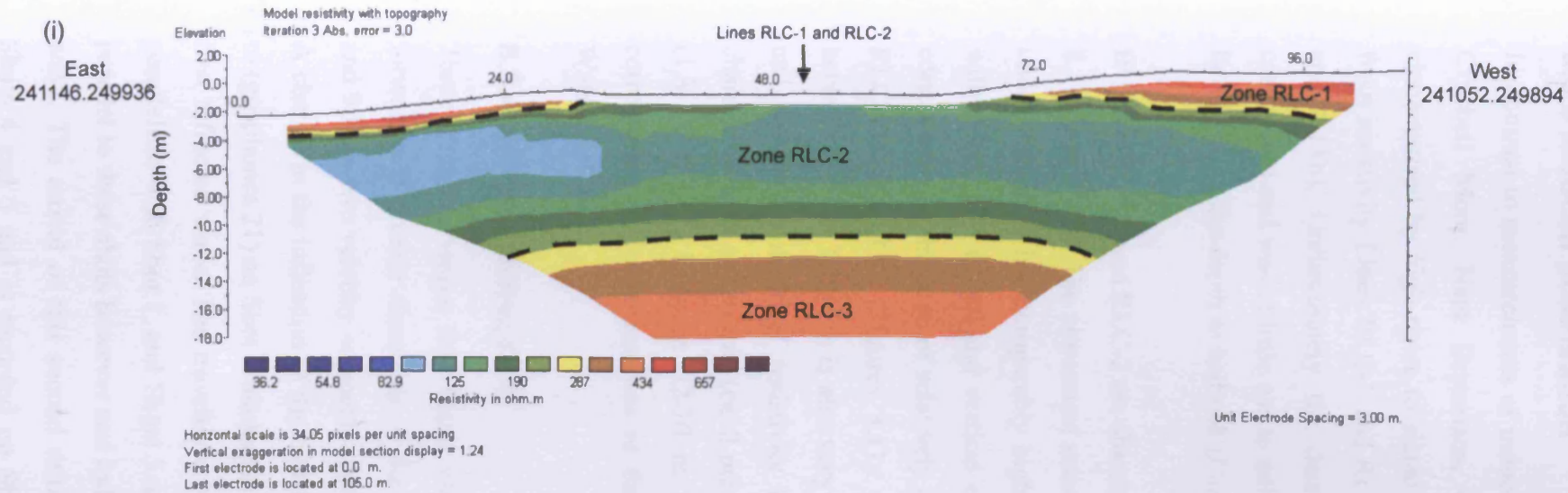
Figure 8.11c: (i) Electrical resistivity and (ii) IP profile (Line RLC-3), 'Pingo' 3, Rhos Llawr Cwrt, Cletwr Fawr valley. Intersection points of other resistivity/IP lines indicated. The 230 Ωm resistivity contours are marked on the resistivity profile by black dashed lines and on the IP profile by dashed white lines. Note high root mean square (RMS) error of IP data compared to Figures 8.11a (ii) and 8.11b (ii). The seismic refraction profile ran parallel to this line, offset 20 m to the north.

8.3.3 Induced polarisation

In contrast to measurements of induced polarisation (IP) recorded at other sites (e.g. Crychell Moor, Nant Brynmaen, Cledlyn valley, Llanpumsaint), which were characterised by high noise to signal ratios, apparently good IP data were collected from resistivity Lines RLC-1 and RLC-2 at the Rhos Llawr Cwrt site (Figure 8.11a and 8.11b). Unfortunately the data from Line RLC-3 had a significant noise component and was of little use to inform interpretation of the internal structure of the landform, or the depth to bedrock (Figure 8.11c).

IP Lines RLC-1 and RLC-2 are characterised by two main zones of IP values (Figures 8.11a and 8.11b). The uppermost zone has low chargeability (0-3.6 mV/V), whilst the underlying zone has comparably high chargeability (3.6-10 mV/V), which increases with depth. The lateral and vertical extent of the high-chargeability, lower IP zone corresponds to the zone of relatively high resistivity values of Zone RLC-3 in Lines RLC-1 and RLC-2 (Figures 8.11a and 8.11b). The morphology of the contact between the two IP zones is also very similar to the boundary between Zones RLC-2 and RLC-3 in electrical resistivity Lines RLC-1 and 2. IP Line RLC-1 is also characterised by a very thin (ca. 2 m) near-surface zone of intermediate chargeability (1.8-3.6 mV/V) between 52-70 m and between 78-96 m. The former roughly corresponds to the dimensions of the peat filled basin of 'Pingo' 3 (Watson and Watson 1974).

8.3.4 Seismic refraction

Three distinct P-wave first break velocity segments were recognised in both the forward and reverse directions of the travel-time graph (Figure 8.12). Shots 1, 2, 8 and 9 have two velocity segments representing the direct wave and a refracted wave. A change in the inflection of the best-fit line at 8 m (geophone 10) on Shot 1 and 40 m (geophones 21) on Shot 2 marks the crossover distance of the first arrivals from the first refracted wave. The traveltime vs distance plots of Shots 4 and 8 show good parallelism with Shot 1, and Shots 5 and 9 with Shot 2. Shot 6 and Shot 7 do not lie parallel to these shots however and indicate the presence of a second deeper refracted wave. The arrival of this second refracted wave can be observed near the ends of Shots 4 and 5 and is recorded on Shot 4 by the geophones between 38 to 46 m

(geophones 20-24) and on Shot 5 between 4 to 8 m (geophones 3-5). The direct wave and two refracted waves can therefore be identified on the basis of the traveltime graph (Figure 8.12).

The average P-wave velocity of the direct wave, calculated from the average velocity of Shots 1 and 2, was 1007 msec^{-1}. The P-wave velocity of the first refracted wave, calculated from the reciprocal of the gradient of the graph of the minus time vs. distance for Shots 1&2, 1&3, 2&3, 8&9, varied between 1705 to 1913 msec^{-1} (average of 1832 msec^{-1}). The second refracted wave, derived from the minus graph of Shots 6&7, has a velocity of 3146 msec^{-1}

The observation of two refracted waves from the first break data at Rhos Llawr Cwrt indicates a three-layer model. Using the Common Receiver Point method the depth and morphology of the two refractors were defined (Figure 8.13). For Shots 1&2, 1&3, 2&3, 8&9 (all Refraction 1), the reciprocal time was measured directly, but because the reciprocal time was not measured in the field for Shots 4&5 (Refraction 1) and Shots 6&7 (Refraction 2), an estimated value of the reciprocal time was calculated using the intercept time (see Section 3.4.3.1). Based on the depth of refractor 1 derived from Shots 1&2 the average depth to the first refracted horizon is 4.01 m, but the morphology of the refractor varies from a depth of 3.02 m to 6.18 m, with significant variation between 30-40 m (Geophones 16-21) (Figure 8.13). This observation is supported by the morphology of refractors derived from Shots 1&3, 2&3 and 8&9, which are also undulating between 30-40 m. The average depth to the lower refracted horizon, based on Shots 6&7, is 21.78 m, varying from 19.54 to 23.31 m (Figure 8.13).
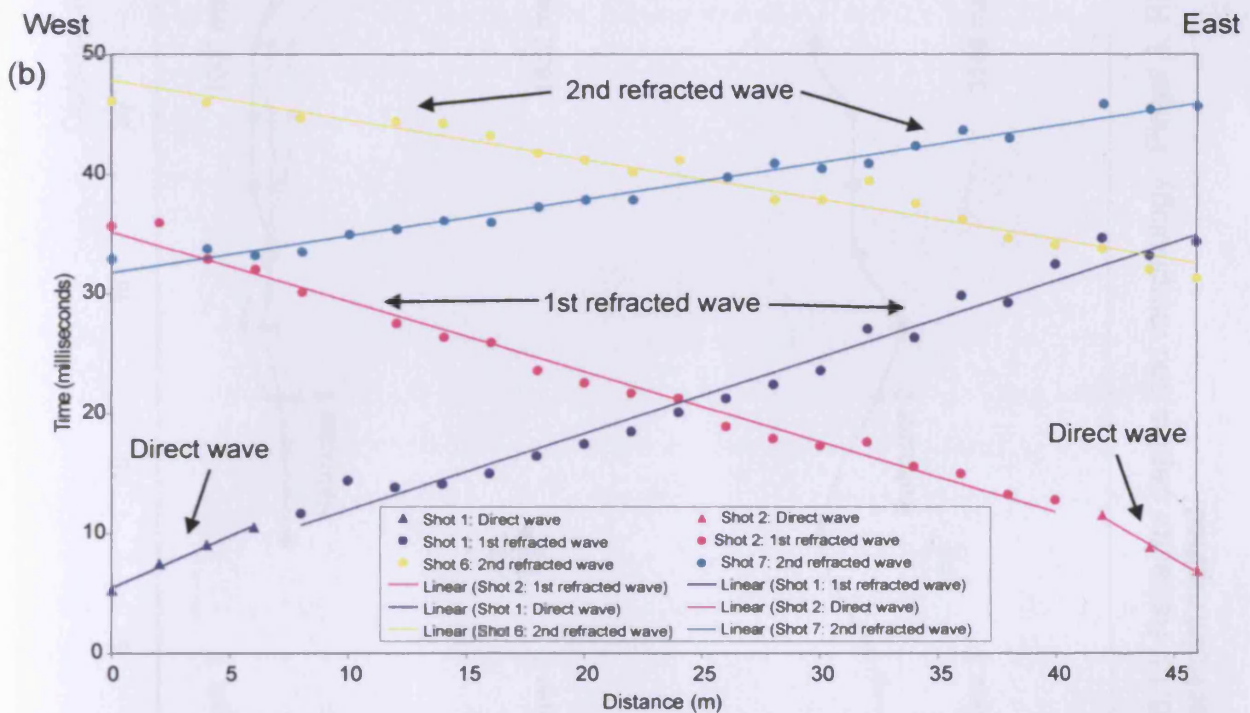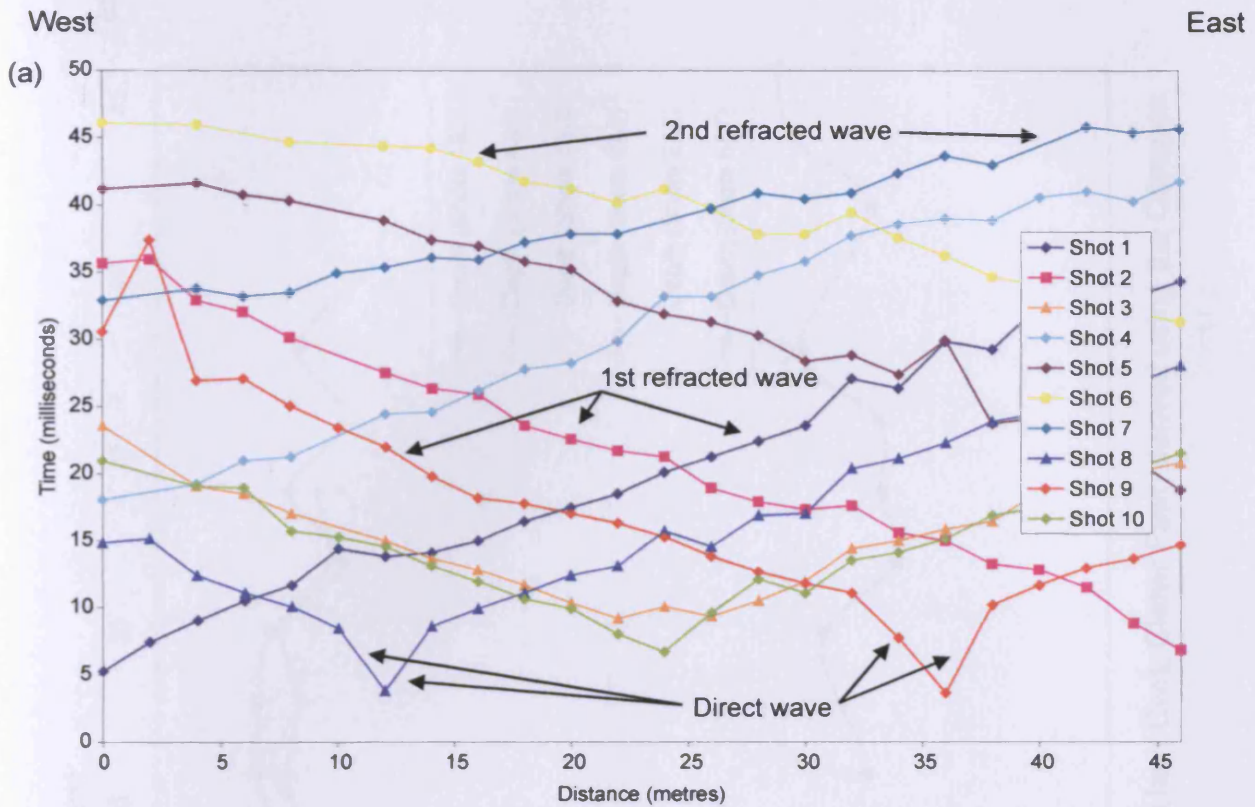
Figure 8.12: (a) Traveltime graph of seismic refraction data collected at 'Pingo' 3, Rhos Llawr Cwrt, Cletwr Fawr. (b) Traveltime graph of selected shots, to demonstrate the direct, first refracted and second refracted waves.
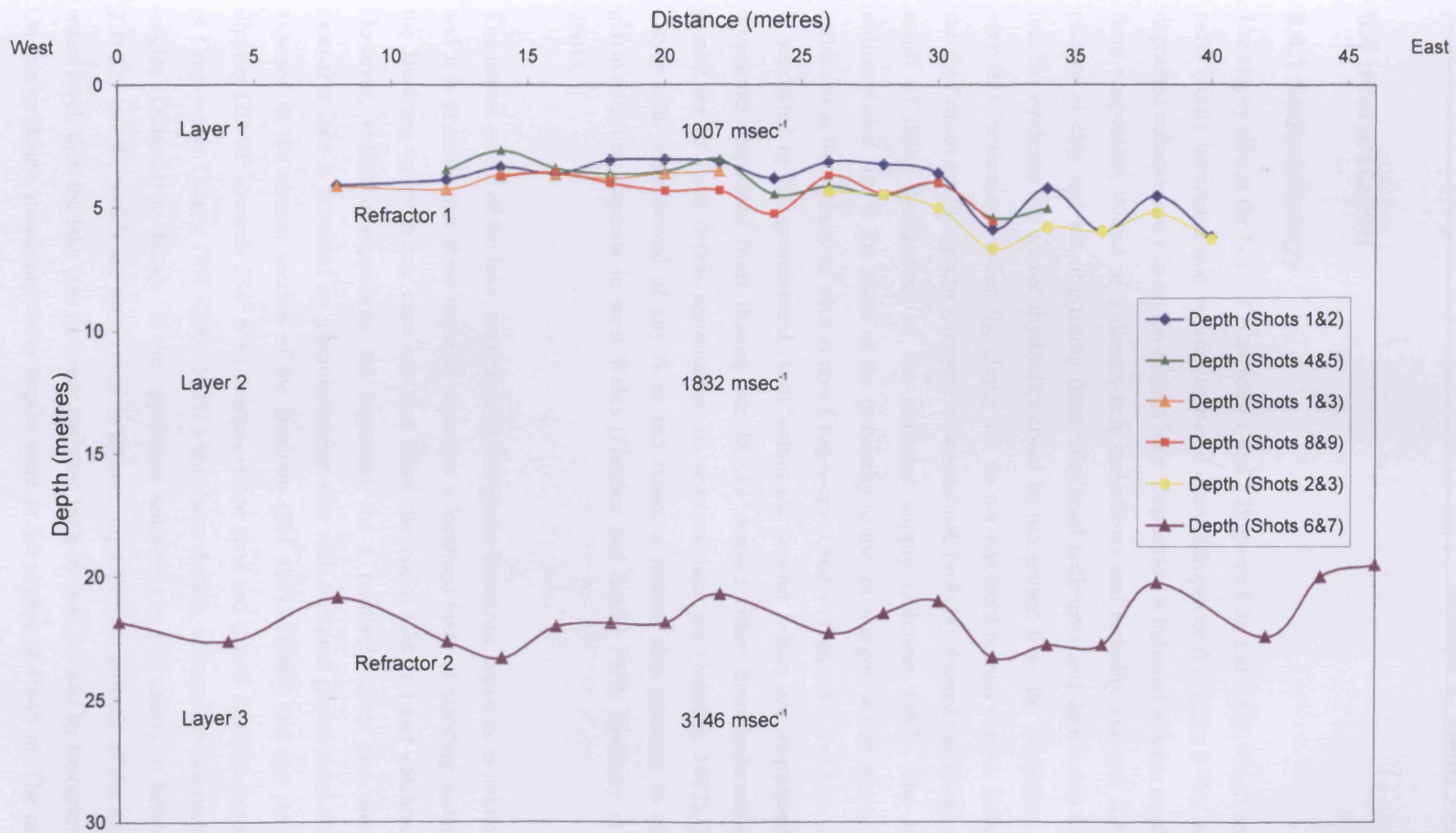
Figure 8.13: Refractor depths and morphology, 'Pingo' 3, Rhos Llawr Cwrt, Cletwr Fawr, derived using the Common Receiver Point method.

8.4 Interpretation

8.4.1 Sedimentology

The clayey silts at the base of Boreholes 1 and 3 (Figures 8.8a and 8.8c), which are in parts faintly laminated and contain scattered clasts (dropstones) (Figure 8.9b), were deposited subaqueously in an ice-contact lake. Deposition is believed to have resulted from suspension fallout of sediment-rich underflows and turbidity currents fed by plumes of clay and silt originating from subglacial sediments and debris-rich basal ice. No evidence for annual rhythmites could be recognised from the boreholes, the very fine laminations within the clayey silt do not represent annual varves. Instead, the rhythmites are thought to represent intra-seasonal, probably diurnal variations as a result of daily fluctuations of the sediment supply (Johnson 1997). The high sedimentation rate is the result of the proximity to the ice margin, which apparently stabilised in the vicinity of what is now Crug-y-eryr Quarry (Figure 8.1 and 8.3). This is supported by the gravel-sized clasts within the deposit, which are interpreted as dropstones deposited from floating ice blocks derived either from sediment-rich glacier ice or from debris accumulated on seasonal lake ice (Johnson 1997). The clayey silts were devoid of any flora and fauna, a feature also common to other glaciolacustrine deposits in west Wales (Fletcher and Siddle 1998; Hambrey *et al.* 2001).

The lateral extent of the lake, suggested by the glacio-lacustrine deposits, is unknown and it is possible that these deposits represent a localised body of standing water in the Bwdram valley rather than one that filled the entire Cletwr Fawr catchment. However, evidence supporting the argument for a relatively deep and areally extensive lake is provided by glaciolacustrine silts with scattered gravel-sized clasts exposed in the stream section of the Bwdram (SN 41013.50069) and the steeply dipping (20-40° towards 234° SW) coarse-grained sand and gravel deposits exposed at Crug-y-eryr Quarry (SN 42065.50311) that have deltaic, subaqueous ice-contact origins (Gilbert-type delta). If the uppermost sediments in this quarry at between 220-225 m OD, which are interpreted as topsets, represent the altitude of the upper water level, then the lake was probably dammed both by both ice and by topography. On this evidence, maximum water depths were in the region of 40-45 m. The delta

marks an ice-marginal position of a glacier flowing from the upper part of the Cletwr Fawr valley into the basin from the north or northeast. The presence of occasional erratics in the delta (Jerry Davies, *pers comm.*) suggests that this landform was fed by Irish Sea ice, or that Welsh ice was reworking pre-existing sediments derived from the Irish Sea.

The obvious drainage outlet for the lake was through the narrow lower reaches of the Cletwr Fawr at the southern end of the basin at 170-175 m OD (Figures 8.14 and 8.15). However, the altitude of the Gilbert-type delta at Crug-y-eryr suggests that for at least part of the lakes existence the lower part of the Cletwr Fawr was dammed with glacier ice. At the time of the development of the Cletwr Fawr lake and the Crug-y-eryr delta, ice masses must have been present in both the northern and southern parts of the Cletwr valley. Whether these were distinct ice masses, or simply different lobes of the same glacier is extremely difficult to establish. However, there remains the possibility that the lake could have been impounded between the westward flowing Teifi glacier of Welsh origins and the southward flowing Irish Sea glacier.

Given that the altitude of the cols between the Cletwr Fawr and the Cerdin valley (>250 m OD) and the Cletwr Fach (>240 m OD) are significantly greater than the altitude of the topsets at Crug-y-eryr Quarry (220-225m OD) (Figure 8.14), overspill drainage did not occur into these valleys during this phase of the lake, that is, when the lake level corresponded to the Crug-y-eryr delta. For overspill to occur into these valleys, the depth of the lake would have needed to be at least 60-65 m. The location of the Crug-y-eryr delta suggests that the Mydr was ice-filled at this time and drainage could not occur through the Cletwr-Mydr col (currently at ca. 245 m OD) (Figure 8.14). In contrast to the deep sequence of superficial deposits in the middle-reaches of the Cletwr Fawr valley, the lower reaches, south of Darren Fawr and Glan-rhyd-y-dre, are characterised by steep sided valleys with bedrock at the surface. This suggests that this route (Figure 8.15) may have been used as a spillway, with the superficial cover being removed by meltwater erosion during (catastrophic?) drainage of the lake.
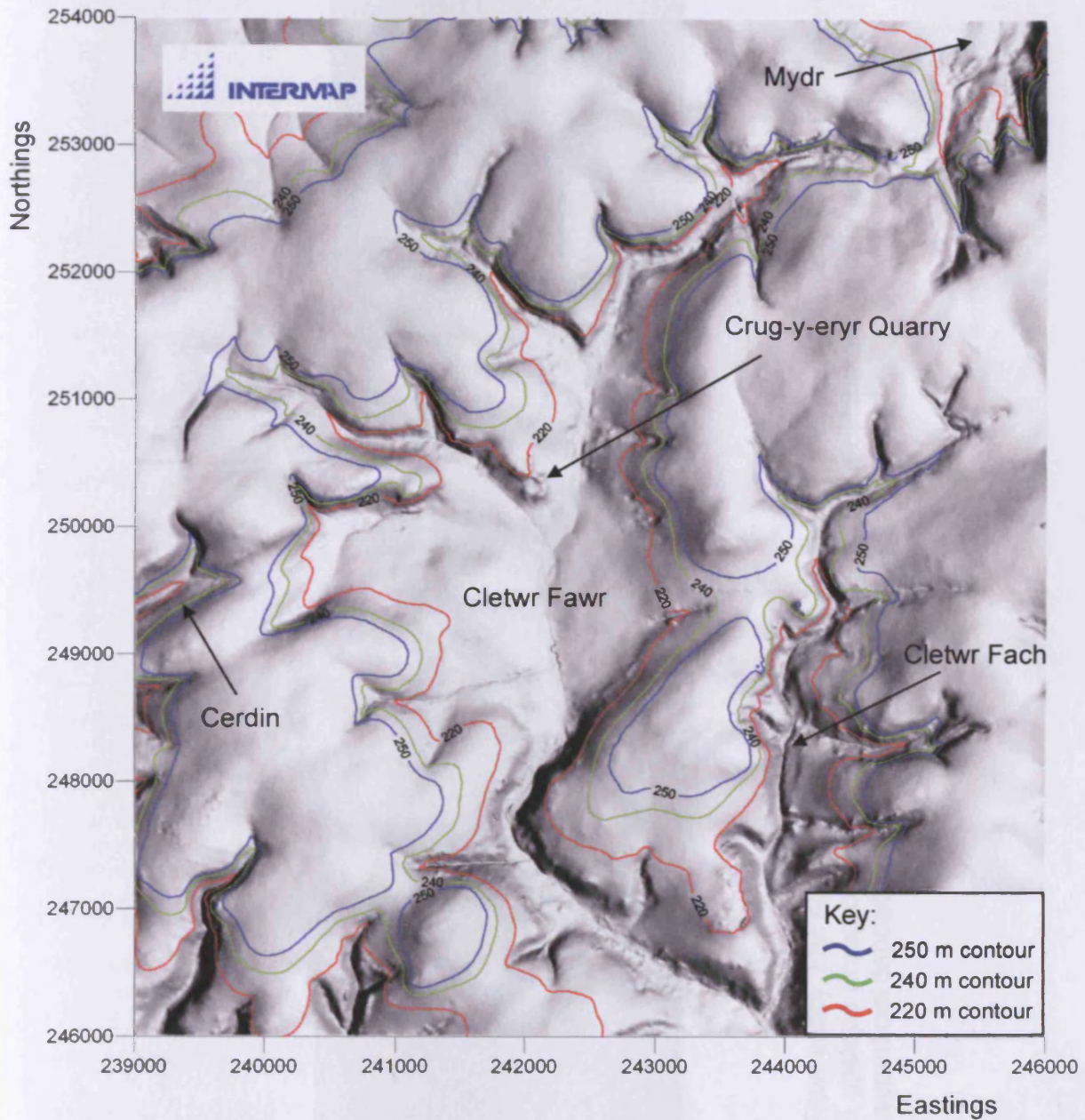
Figure 8.14: Nextmap digital terrain model (DTM) of the Cletwr Fawr basin displaying important contours. The 220 m contour marks the uppermost height of the delta topsets at Crug-y-eryr Quarry and therefore the uppermost evidence for postulated lake levels in the basin (© Intermap Technologies Inc).

Figure 8.15: Cletwr Fawr valley, just south of the linear 'pingos' at Darren Fawr and Glan-rhyd-y-dre. Compared to the wide, drift-filled basin upslope (foreground of photo), the lower part of the catchment (middle distance) is narrow and steep-sided with little superficial deposits in the floor of the channel.

The diamicton recorded in Boreholes 1 and 3 is very similar in physical properties to the 'gravelly clay' or 'clayey gravel' with angular to rounded clasts, that dominates the near-surface superficial geology of the lower slopes of the valley (Watson and Watson 1974). The deposition of this unit occurred either late in the existence of the ice-contact lake or after its drainage, as there is no evidence for glaciolacustrine sediments overlying the diamict. The interpretation of this deposit is critical. If it represents periglacial or paraglacial deposition or reworking, then the landforms at Rhos Llawr Cwrt cannot have glacial origins. However, if this diamict was subglacially or supraglacially deposited then their development may not be the result of periglacial processes.

Watson and Watson (1974) believed that the diamict represented reworked glacial deposits that had been removed from the upper slopes of the valley and the adjacent plateau by mass movement processes under extended periglacial conditions, although they did predict that *in situ* glacial deposits existed at depth in the valley bottom. In the model of open system pingo development proposed by Watson and Watson (1974), this unit was deposited before and/or during the period of pingo development, being reworked again during pingo growth and collapse (Watson and Watson 1974). Alternatively, the diamict could represent a high magnitude geomorphic event such as a mudflow or a debris-flow either into the lake or onto the exposed lake floor following drainage. The amount of sediment accumulated seems significant (up to 4 m), but at Morfa Bychan on the Ceredigion coast 45 m of sediments were deposited by rapid slumping and flow of water-saturated till under paraglacial conditions during deglaciation (Watson and Watson 1967; Harris 1998). However, based on the borehole data and the limited exposure in the stream section at Rhos Llawr Cwrt, there is no clear evidence for the reworking of the diamict by slope processes. This does not suggest a supraglacial or paraglacial origin for the diamict. This often-compact diamicton contains no evidence for sorting in either Borehole 1 or 3. Instead the sediment resembles an *in situ* glacial till. It is therefore believed possible that a short-lived readvance of glacier ice over the floor of the drained lake occurred during deglaciation, depositing the diamict subglacially onto the glaciolacustrine sequence. Although there is no clear evidence for glaciotectonism of the underlying clayey silts in Boreholes 1 and 3, deformation structures should also be present if the unit represented a large mass movement event, such as a large debris flow, which was

deposited onto water-saturated lacustrine deposits (Johnson 1997). Such structures were not observed. The absence of erratic clasts characteristic of Irish Sea ice and the absence of calcium carbonate in the samples from Rhos Llawr Cwrt suggests that this till was deposited by Welsh ice. Scattered erratics have been reported from the Cletwr valley however (Watson and Watson 1974; Watson 1976; Watson 1996; Jerry Davies, *pers comm.*), suggesting the influence of ice from an Irish Sea source. The grain-size of the till falls within the grain-size envelope of till from elsewhere in Cletwr Fawr and from the adjacent Cledlyn valley.

The sandy, silty clayey gravel infill of the basin that underlies the peat recorded in Borehole 2 is interpreted as a partially sorted component of reworked till slumped and washed from the ramparts into a central pond impounded by the rampart. The grain-size of this material overlaps with the grain-size envelope of both the sediments in the rampart of this landform (Figure 8.10) and till in the Cledlyn valley (Figures 7.9 and 7.17). The presence of organic fragments suggests that deposition of this unit occurred some time after formation of the rampart. The depth of this unit beneath the peat infill indicates that the inner slope of the rampart at the northern edge of the basin is quite steep, in accordance with the asymmetrical nature of the peat-filled depression presented by Watson and Watson (1974)

8.4.2 Electrical resistivity tomography

Based on the evidence from Boreholes 1 and 3, the base of the high resistivity near-surface zone (Zone RLC-1) at Rhos Llawr Cwrt correlates with the boundary between the diamict (till) and the underlying clayey silt. This boundary also appears to represent an important hydrogeological boundary, as there is a relationship between the lithology and the water content of the sediment (dry diamict vs. moist clayey silt) (Figures 8.8a and 8.8c). The water chemistry and water content of sediment are important factors determining the resistivity of unconsolidated superficial deposits. Because there is a close relationship between groundwater conditions and the near-surface sedimentary properties at Rhos Llawr Cwrt, Zone RLC-1 is believed to provide a reliable representation of the vertical and lateral extents of the diamict. The boundary between Zone RLC-1 and Zone RLC-2 therefore corresponds to the contact between the dry diamict (till) and the underlying water-saturated clayey silts observed in Boreholes 1 and 3. Zone RLC-1 cannot represent a near-surface weathering zone as

its thickness (2-6 m), is much greater than the depth of weathering observed in the boreholes (<1.5 m).

The thickness and distribution of Zone RLC-1 displays some degree of variability. The central basin of 'Pingo' 3 is not characterised by a high resistivity near-surface zone. This corresponds to the absence of the diamict unit in Borehole 3, which penetrated 2 metres of peat and a further metre of matrix-supported silty sandy gravel that had a higher silt-component compared to the diamict in Boreholes 1 and 3 (Figure 8.10). The resistivity and thickness of Zone RLC-1 is greatest to the north of 'Pingo' 3, where Line RLC-2 extends on to the eastern rampart of 'Pingo' 1 (Figures 8.4 and 8.7), and where a relatively thick sequence of diamict is predicted. The thickness of RLC-1 at this point may also be a function of the water table dipping downwards towards the Bwdram, and the northward dipping bedrock surface (see below). The apparent absence of Zone RLC-1 to the south of the landform in Line RLC-2 is a function of the resolution of the survey (electrode spacing of 4 m) compared to Line RLC-1 (electrode spacing of 2 m). Line RLC-1 however does suggest that the diamict is thinner to the south of landform.

The laterally extensive, low resistivity Zone RLC-2 is interpreted as saturated unconsolidated sediments. The low resistivity values beneath the ramparts appear to correlate with the clayey silt deposits that underlay the diamicton in the boreholes. There is some horizontal variation in the resistivity of Zone RLC-2. Line RLC-1 in particular demonstrates a zone of low resistivity (80-100 Ωm) beneath the peat-filled central basin of the landform to depths of ca. 7 m. This is likely to represent enhanced saturation of the underlying minerogenic sediments because of vertical migration of water from the water-saturated peat. Unfortunately, the current investigations were unable to drill to greater depths due to problems with the extraction of the coring equipment. Therefore, whilst the basal units of Boreholes 1 and 3 were composed of clayey silt greater than 1 m thick it was not possible to determine the vertical extent of these deposits. Without borehole control, the resistivity data alone cannot be used to confidently ascribe the lithology of the thick sequence (up to 15 m) of unconsolidated deposits. The resistivity of different unconsolidated sediments overlaps considerably depending on the water content (Loke 2004b), and it is likely that there will be some degree of variation within this sequence with depth. The

gradational boundary between Zone RLC-2 and Zone RLC-3 may represent a lithological change at the base of Zone RLC-2, perhaps to fluvioglacial deposits or till associated with higher resistivity values. Nevertheless, as there is little vertical variation for the majority of Zone RLC-2, it is also possible that the entirety of Zone RLC-2 represents glaciolacustrine clayey silts. The resistivity data, supported by the shallow boreholes, indicates a glaciolacustrine sequence capped by a thin (<4 m) unit of diamict. This diamict is not laterally contiguous and is apparently absent where peat-filled depressions occur.

Because the ramparts of this landform are more subdued than those in the Cledlyn valley and the area is generally less well drained, the ramparts are not characterised by high resistivity values of the type recorded in the nearby Cledlyn valley (see Sections 7.3.4 and 7.6.2). Overall, the general resistivity of the saturated unconsolidated materials (Zone RLC-2) at Rhos Llawr Cwrt tend to be higher than those measured in the Cledlyn valley (Figures 7.13 and 7.20). However, without deeper boreholes (10-20 m) at both sites it is difficult to assess the significance of these values. These differences may reflect variations in water content between the different seasons when these surveys were conducted, resulting from slight differences in the physical properties (e.g. density, void ratio) of the sediments. A higher void ratio would result in higher moisture contents in saturated soils and therefore lowering the resistivity of that material.

The basal high resistivity Zone RLC-3 (>230 Ωm) is interpreted as representing bedrock. Although these are relatively low resistivity values for bedrock, they are similar to values recorded by Carruthers *et al.* (1997) and Heaven *et al.* (1999) from resistivity soundings of Silurian and Ordovician mudstones and sandstones at nearby Lampeter and at Cornel. The resistivity data therefore indicate a thickness of superficial deposits of 10-15 m, although it is impossible to determine the composition or structure of these deposits without additional borehole control. Although the boundary between Zone RLC-2 and Zone RLC-3 appears gradational, this may be a function of the increased size of model blocks with depth used by the inversion of the resistivity data. The 230 Ωm contour, taken as the boundary between Zone RLC-2 and Zone RLC-3, has a marked northward dip in Lines RLC-1 and RLC-2. The data in Line RLC-2 suggest that this boundary may also be characterised

by a stepped profile. This is in contrast to the horizontal nature of the 230 Ωm contour in Line RLC-3. The 3D morphology of this boundary suggests that rockhead dips significantly to the north, towards the Bwdram (Figure 8.11).

8.4.3 Induced polarisation

The IP data (Lines RLC-1 and RLC-2) are characterised by a near-surface zone of low chargeability (<3.6 mV/V) underlain by a basal zone of higher chargeability (>3.6 mV/V) (Figure 8.11). The most significant feature of the IP data is the correspondence of the basal high chargeability zone with the high resistivity Zone RLC-3. The higher chargeability zone (>3.6 mV/V) is therefore interpreted as bedrock. Comparison of the measured values with recognised IP values indicate that the bedrock underlying the site is either sandstone or weathered shale. Thick sequences of weathered, mineralised bedrock have been recorded in the area near Ffostrasol (Huw Sheppard, *pers comm.*). The measured values are probably too low to represent unweathered shales, which have chargeability values of ca. 100 mV/V.

The slight near-surface increase in chargeability may represent peat. Peat is recognised as chargeable (Slater and Reeve 2002, Slater and Lesmes 2002), but the thin sequence of peat (<2 m) and the coarseness of the inversion model blocks makes it difficult to evaluate this hypothesis at this site. A slight increase in chargeability is apparent within the central basin of the landform and to its north in Line RLC-1 however, where peat thickness was greatest.

8.4.4 Seismic refraction

The two seismic refractors are interpreted as defining: a) the boundary between two layers of unconsolidated sediments (refractor 1); b) the superficial-bedrock boundary (rockhead) (refractor 2). The three layers defined by the seismic P-wave velocities are therefore Silurian bedrock (mudstone or sandstone) overlain by two distinct unconsolidated lithologies. The calculated depth of the upper bedrock boundary indicated by the seismic refraction survey is therefore approximately 22 m. Although the velocity contrast between superficial deposits and the solid geology is normally significant enough to define the boundary between the two, it is not as common to detect internal divisions within unconsolidated glacial materials, because the P-wave velocity contrast is not normally large enough (Brabham *et al.* 1999). The borehole

248

data supports the interpretation of an internal division within the superficial deposits at Rhos Llawr Cwrt however, as the depth derived from the first refracted arrivals (ca. 4 m) corresponds to the contact between the diamict (silty gravels to gravelly silts) and the underlying clast-poor clayey silts in Borehole 1. The thin, near-surface, low velocity layer therefore corresponds to the gravelly silty diamict found in the upper 4-4.5 m of Boreholes 1 and 3. Although the upper limit of the clayey silt found at the base of Boreholes 1 and 3 corresponds to the depth of the first refractor it is not necessarily the case that this lithology continues to rockhead. The sequence may be more complex, as P-wave velocity contrasts between individual units within the sequence may not be significant enough to produce refracted arrivals or the clayey silts may be underlain by a lower velocity zone from which a refracted wave would not be produced at the interface of the two layers (blind zone problem). However, it is clear from the P-wave velocities and the borehole data that the upper two layers are composed of unconsolidated materials.

The P-wave velocity of the upper diamict (interpreted as till) derived from the direct wave (1007 m sec^{-1}) is low in comparison to the velocity derived from saturated till in the adjacent Cledlyn valley (see Section 7.3.3), which ranged between 1814 to 1945 msec^{-1}. Near-surface Holocene weathering of the upper part of the till may have contributed to the low P-wave velocity derived from the direct wave at Rhos Llawr Cwrt. The measured P-wave velocity is comparable to values recorded from weathered glacial deposits in North Wales (Brabham *et al.* 1999). Mottling of the upper few metres of Borehole 1 (Figures 8.8a and 8.9a) and clear mottling (iron staining) of the upper 75 cm of the till exposed in the stream section at SN 41013.50069 demonstrates the existence of a near-surface weathering profile. Additionally, the velocity of the upper unit at Rhos-Llawr Cwrt was based on only a few data points and is therefore susceptible to a more significant error margin. The velocity may therefore be an underestimate of the true velocity. P-wave velocity measurements using a short geophone spread with a closer geophone spacing (e.g. 0.25 m) would be required to reduce the error margins and resolve this issue. However, the velocity of the upper layer (1007 msec^{-1}) is much greater than that measured for the weathered zone at 'Pingo' U in the Cledlyn valley (140 m sec^{-1}). This may be a result of different agricultural practices. It is unlikely that the field at Rhos Llawr Cwrt in which 'Pingo' 3 is located has been ploughed, although it is

thought that the fields in the Cledlyn valley have at some point in their history (Watson 1971).

The P-wave velocity of the first refractor (1705 to 1913 msec^{-1}), which corresponds to the contact between the overlying diamict and the clayey silts recorded in Borehole 1, is high in comparison to the velocities recorded for glacio-lacustrine deposits elsewhere in Wales (e.g. Camlad valley 1430-1500 msec^{-1}, Hussen 1998; Brabham *et al.* 2005) and at Llanpumsaint (1352-1441 msec^{-1}, see Section 9.3.4) Lateral and vertical variability in the superficial sequence is likely however and this could influence the measured seismic velocity. Furthermore, if the upper diamict represents a till then it is likely that deposition of that till was associated with consolidation of the underlying silts, which could increase their P-wave velocity.

The P-wave velocities of the superficial deposits and bedrock measured in the Rhos Llawr Cwrt survey are comparable to seismic velocities measured for similar materials in the abandoned meander of the Afon Teifi at Castle Malgwyn, south of Llechryd (blue clay 1524 msec^{-1}, Ordovician slates 3901 msec^{-1}) (Allen 1960), in the estuary mouth of the Teifi (till 1524 msec^{-1}, bedrock 4328 to 4999 msec^{-1}) (Allen 1960) and in an abandoned meander at Cenarth (overburden 1768 msec^{-1}, bedrock 4023 to 4053 msec^{-1}) (Francis 1964). The velocity of bedrock in the Cletwr valley is lower than the velocities derived by Allen (1960) and Francis (1964), but this may simply represent weathering of the bedrock in the Cletwr Fawr valley. Deep weathering of bedrock in the area is evident from exposures around Ffostrasol on the watershed between the Teifi valley and Cardigan Bay (Huw Sheppard, *pers comm.*). The velocity of refracted arrivals from Ordovician bedrock at Dinas Dinlle and Porth Neigwl in North Wales varies between 2915 to 4300 m sec^{-1}, with the low end of the range representing weathered bedrock (Harris *et al.* 1997; Brabham *et al.* 1999). These values are comparable to the 3146 m sec^{-1} derived for bedrock at Rhos Llawr Cwrt.

The rockhead depth established from the refraction survey supports the interpretation of the depth to bedrock derived from the electrical resistivity tomography surveys. The seismic line ran perpendicular to resistivity Line RLC-2, the intersection point being ca. 74 m on the resistivity line (Figures 8.7 and 8.11b). The 230 Ωm contour at

74 m in Line RLC-2 (15 m depth) (interpreted as the bedrock boundary) appears to underestimate the depth to bedrock derived from the seismic survey (22 m) however. This may be because the bedrock is characterised by a surface weathered zone, which has a seismic velocity similar to that of the overlying superficial deposits and therefore did not produce a refracted wave. Whilst the resistivity data define the upper limit of the weathered bedrock, the increasing resistivity with depth representing the change from weathered to unweathered bedrock, the refraction data may be defining the upper limit of unweathered bedrock. Alternatively, both data sets could be picking out the same boundary (rockhead), but the accepted error margins of the seismic refraction data (10%) and the resolution of the resistivity model blocks (3 m x 3 m) could be responsible for the apparent mismatch of depth between the two methods. A velocity inversion within the unconsolidated sequence (e.g. sands and gravels underlying the clayey silts) would also result in an overestimation of depth (blind zone problem) from the seismic data. Despite these uncertainties, both geophysical techniques indicate a significant thickness of superficial deposits (15-22 m) at this site. The morphology of the superficial-bedrock boundary derived from the refraction survey is in accordance with the horizontal nature of the 230 Ωm contour in Line RLC-3, supporting the interpretation that whilst the bedrock dips significantly from south to north, there is little vertical change in an east-west direction.

9 Llanpumsaint

9.1 Introduction

Relict pingos near Llanpumsaint, Pont-ar-sais (Figure 9.1) and at other sites in Carmarthenshire, were first reported by Bowen (1974), and Watson and Watson (1974), but no geological investigations or geomorphological maps of these landforms were ever published. Of the numerous landforms located over a wide area around Llanpumsaint (Ross *et al.* 2005a), perhaps the most impressive are those at Helfa Hall, south of Llanpumsaint, where six ring-like circular ramparted depressions are found at altitudes of 125-140 m OD. These landforms lie on a low-gradient, north-facing slope to the east of the Nant Cwm-cerwyni, a tributary of the Afon Gwili (Figures 9.1, 9.2, 9.3a and 9.4).

The bedrock geology of the area around the Helfa Hall site is characterised by interbedded mudstones, siltstones and sandstones of Silurian and Ordovician age (Figure 9.5). The contact between the Yr Allt Formation and the mudstones of the Cwmere Formation and the Claerwen Group that underlie the site also represents the boundary between rocks of late Ashgill Series (latest Ordovician) age (Yr Allt Formation), and Llandovery Series (early Silurian) age (Cwmere Formation and Claerwen Group) (BGS Sheet 211: Newcastle Emlyn, *unpublished map)*. This boundary is obliquely intersected by a prominent west-southwest to east-northeast trending fault (Figure 9.5) (BGS Sheet 211: Newcastle Emlyn, *unpublished map)* that underlies several of the landforms near Helfa Hall.

The Gwili valley lies in an unexplored part of Wales in terms of Quaternary research, roughly equidistant between the classic exposures of glacial deposits on Gower to the south and the Cardigan Bay coast to the north. No sites from this inland area are included within either the Quaternary of Wales Geological Conservation Review (GCR) volume (Campbell and Bowen 1989), or the Revised Correlation of Quaternary Deposits in the British Isles (Bowen 1999). The lack of research into the glacial history of the area is partly a result of very poor geological exposure, paucity of Quaternary deposits, and until very recently, the lack of basic geological mapping by the British Geological Survey. The site lies beyond the conjectural glacial limits

defined by the part of the South Wales End Moraine between Tregaron and Mynydd Du (Charlesworth 1929), but within the ice-margins proposed by Griffiths (1940) and Bowen (1970, 1973a, 1973b, 1974, 1981). The glacial deposits of the Llanpumsaint area, recently mapped by the British Geological Survey (BGS Sheet 211: Newcastle Emlyn, *unpublished map*), belong to the Elenid Formation of late Devensian age (Bowen 1999, 2005), and comprise materials derived from Lower Palaeozoic rocks. The very sparse distribution of tills and fluvioglacial deposits to the west and southwest of Llanpumsaint suggest that the landforms at Helfa Hall are found at, or very near to, the maximum extent of the Elenid glaciation in this area (BGS Sheet 211: Newcastle Emlyn, *unpublished map*).
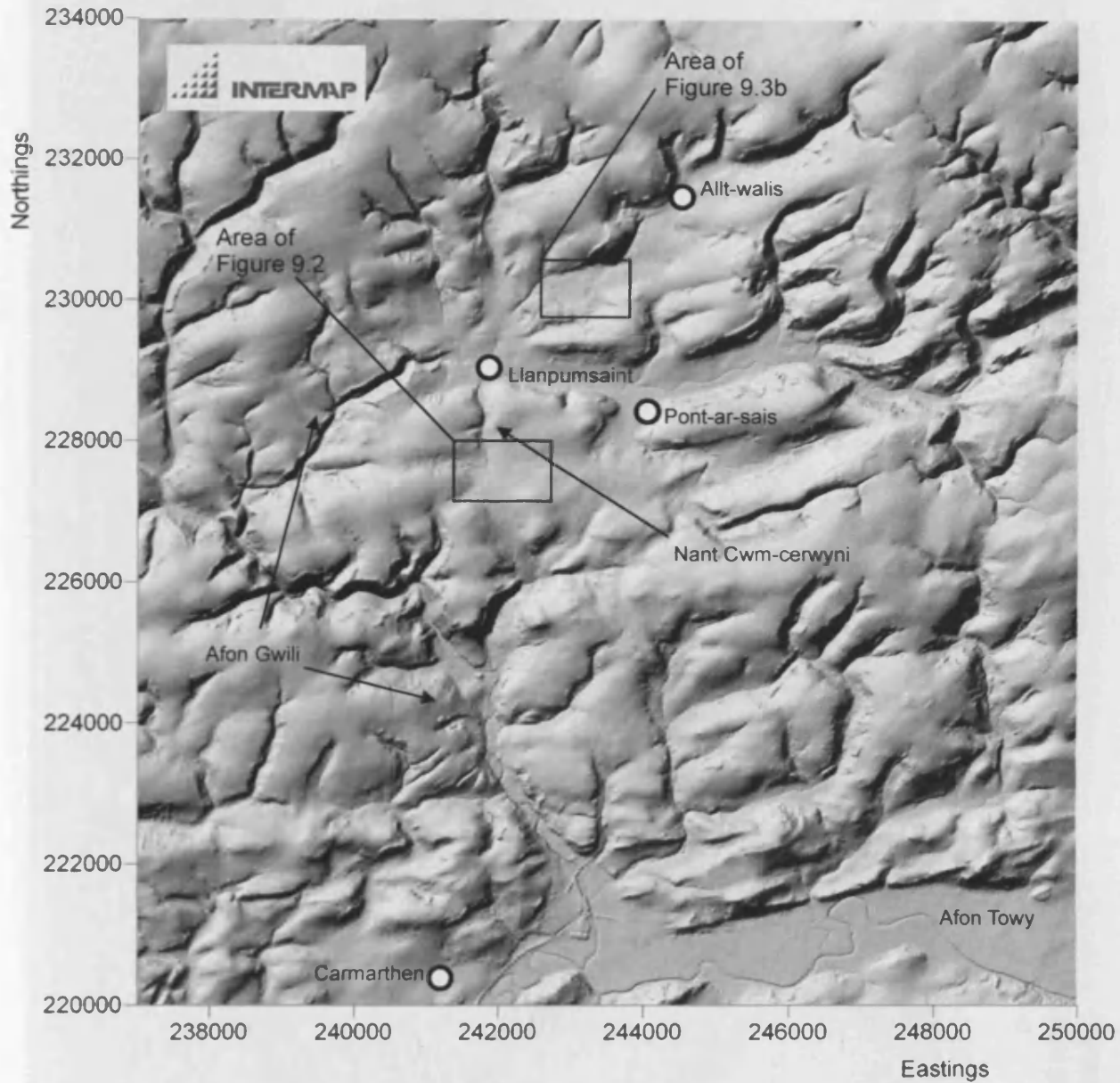
Figure 9.1: NEXTMAP digital terrain model (DTM) of the Gwili valley north of Carmarthen (© Intermap Technologies Inc). Areas of Figures 9.2 and 9.3b are indicated. For area of Figure 9.3a please see Figure 9.2.

Figure 9.2: Aerial photograph, Helfa Hall, Llanpumsaint, taken in 2000 (© Getmapping Plc 2006). Area of Figure 9.3a indicated.
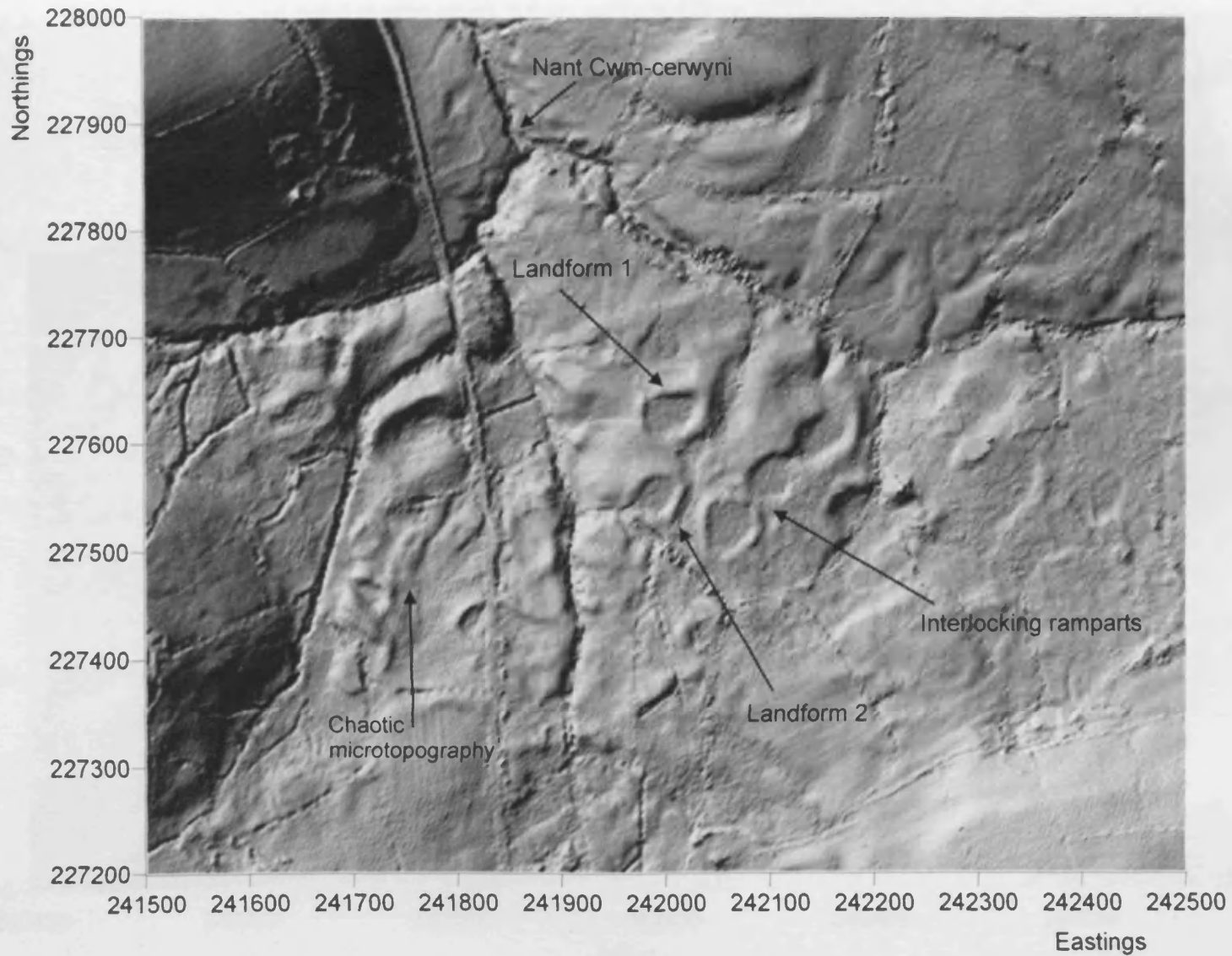
Figure 9.3a: Digital terrain model (DTM) of landforms at Helfa Hall, Llanpumsaint, Carmarthenshire, derived from LiDAR airborne surveying (© Environment Agency copyright and/or database right 2006).
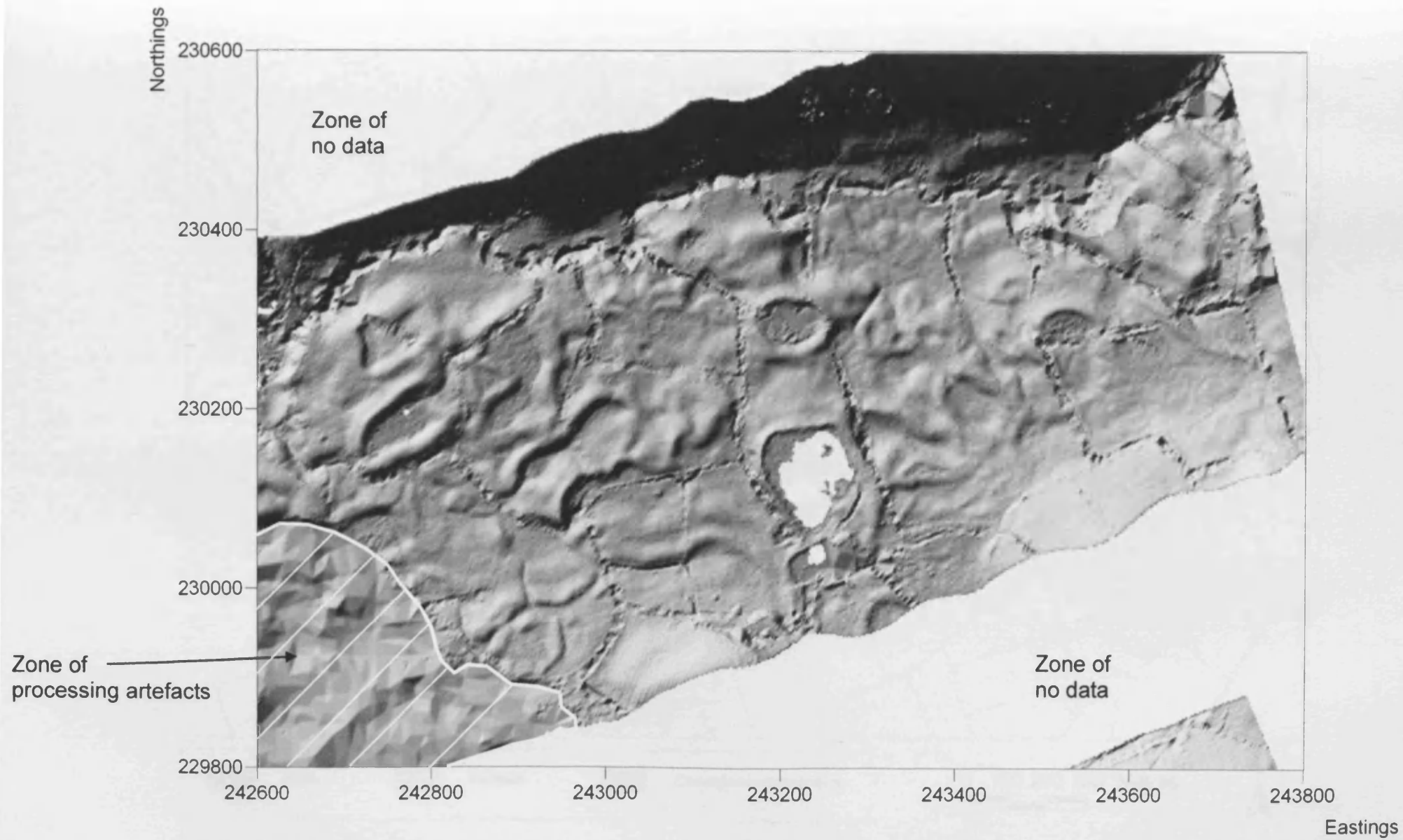
Figure 9.3b: Digital terrain model (DTM) of landforms north of Llanpumsaint, Carmarthenshire, derived from LiDAR airborne surveying (© Environment Agency copyright and/or database right 2006).

Figure 9.4: Geomorphological map, Helfa Hall, Llanpumsaint, based on mapping from stereoscopic aerial photographs. LANDLINE data © Crown Copyright/database right 2006. An Ordnance Survey/(Datacentre) supplied service.
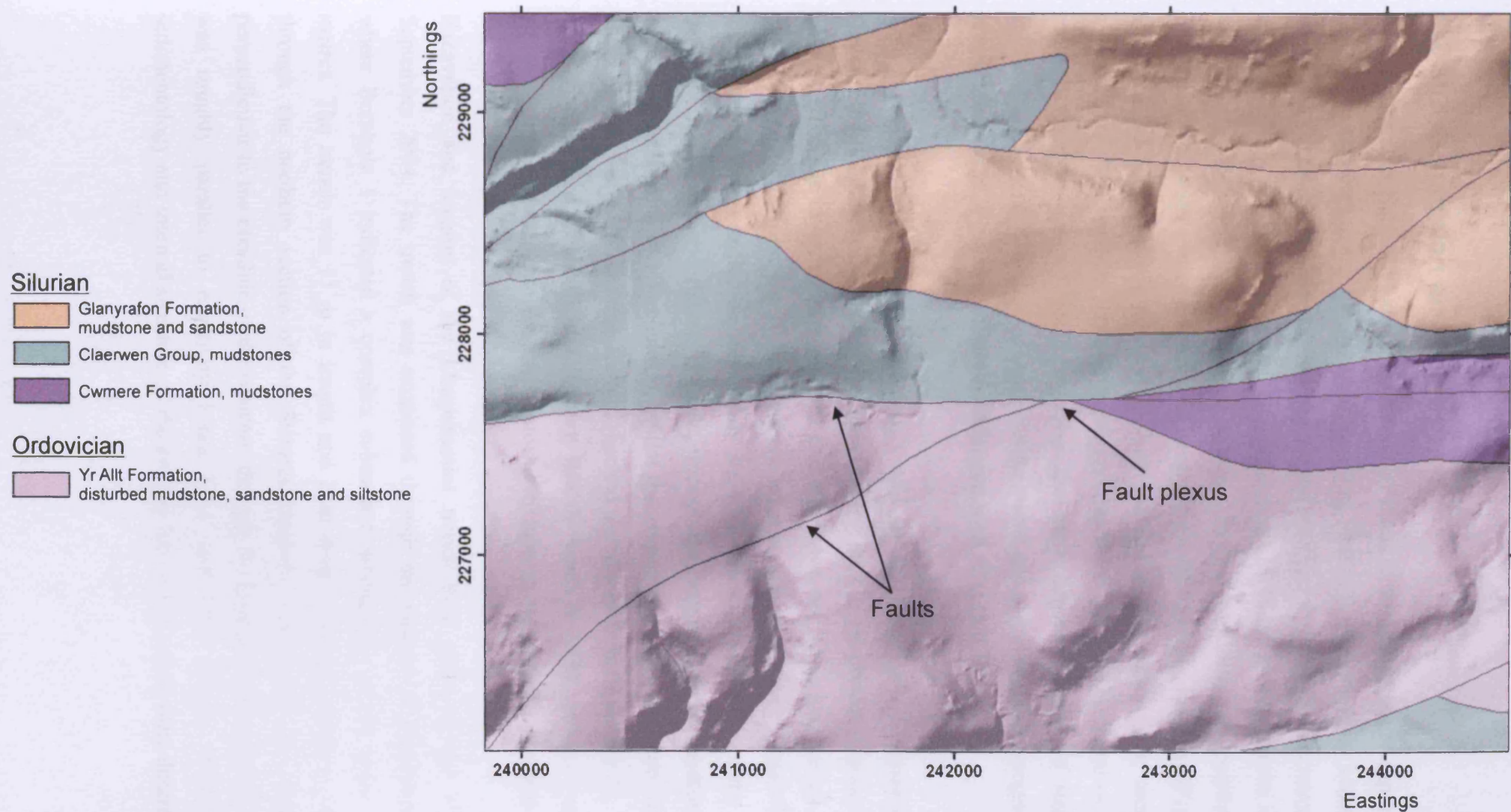
Figure 9.5: Bedrock geology of part of the upper Gwili Valley (© British Geological Survey) draped on the surface of a NEXTMAP Digital Terrain Model (DTM) with 3 x vertical exaggeration (© Intermap Technologies Inc.). Note that this map is adapted from unpublished, unchecked, draft mapping by the British Geological Survey and may therefore contain some inaccuracies.

9.2 Site description and survey

The landforms at Helfa Hall are characterised by circular, peat-filled basins (up to 45 m in diameter) impounded by low (less than 2 m high) circular ramparts, which in some cases stand proud of the surrounding ground surface by up to 4 m. The ramparts entirely encircle the basins, even on the upslope side. The width of the ramparts is up to 25 m, but most are less than 15 m across. Several landforms are positioned immediately adjacent to one another, and several have interlocking ramparts (Figure 9.3a). In addition to the prominent circular landforms, the surrounding area is characterised by a complex, chaotic microtopography (Figure 9.3a). Some of this more subdued topography could represent the more degraded forms of similar landforms. A similar variety of ramparted depressions and complex microtopography is also apparent in an area to the north of Llanpumsaint (Figure 9.3b).

Two ramparted depressions (Landforms 1 and 2) at Helfa Hall, Llanpumsaint (Figures 9.2, 9.3a, and 9.4) were investigated during the current project (Figures 9.6 and 9.7). The site investigations included two boreholes, one 15 m long trench, six electrical resistivity lines, four IP lines and one seismic refraction survey (Figure 9.6). Two boreholes were drilled on the 1st July 2004 to assess the suitability of the site before trenching was undertaken. The first, through the rampart crest of Landform 1 reached a depth of 8 m (Borehole 1), whilst the second, through the centre of the enclosed peat basin of the same feature, reached a depth of 5 m (Borehole 2). The cores were logged in the field following British Standard 5930 (1999). Twelve representative, disturbed samples were removed for laboratory grain-size analyses.

Excavation and logging of the Llanpumsaint trench took place on the 1st-3rd September 2004. The trench was excavated through the rampart of Landform 1, where Borehole 1 indicated a complex subsurface stratigraphy in the upper few metres. The trench was 15 m in length and 2 m deep, excavated north to south through the northern section of the features rampart. The trench was aligned perpendicular to the crestline of the rampart, through the location of Borehole 1 and was roughly parallel to resistivity Lines LP-1 and LP-2 (Figure 9.6). The sedimentology and internal structure of the eastern face of the trench were described

and logged in the field, with representative samples extracted from each key unit for grain-size analysis.

Four electrical resistivity surveys were undertaken at Llanpumsaint on the 30th July 2004 utilising an IRIS instruments Syscal Junior Switch 72. Lines LP-1 and LP-2 ran southwest to northeast through Landform 1. Line LP-1 extended across the entire landform (106 m in length, 3 x 18 electrode cables, 2 m spacing of electrodes), and ran roughly parallel to the line of the excavated trench, orientated so that it was aligned approximately through both boreholes (Figure 9.6). Line LP-2 (35 m in length, 2 x 18 electrode cables, 1 m spacing of electrodes) provided a higher resolution survey of the rampart than that given by Line LP-1, but with a shallower depth and shorter length of profile (Figure 9.6). Borehole 1 was located at the central point of Line LP-2, with Electrode 1 (0 m) of the line corresponding to Electrode 4 (6 m) of Line LP-1. Line LP-3 ran perpendicular to Line LP-1 (70 m in length, 2 x 18 electrode cables, 2 m spacing of electrodes), aligned southeast to northwest across Landform 1. Line LP-4 (79.5 m in length, 3 x 18 electrode cables, 1.5 m spacing of electrodes), ran southeast to northwest across Landform 2. Induced polarisation (IP) data was collected for Lines LP-1 and LP-4 only.

A further field visit was made to the site on the 25th July 2005 to undertake a seismic refraction survey and two supplementary electrical resistivity tomography profiles. The geophone spread for the short seismic survey was located between the two landforms, orientated northwest to southeast (Figure 9.6). The location was chosen to minimise the problems associated with the attenuation of high-frequency seismic energy by soft peat (Brabham *et al.* 2005), and thereby maximise the signal to noise ratio. One resistivity line (175 m in length, 2 x 18 electrode cables, 5 m spacing of electrodes) was positioned along the line of the geophone spread and the offset shots, to provide complementary information on the physical properties of the near-surface geology (Line LP-5). The second resistivity line (175 m in length, 2 x 18 electrode cables, 5 m spacing of electrodes) was approximately perpendicular to the first, through the central basin of Landform 1 and along the western rampart of Landform 2 (Line LP-6) (Figure 9.6). These two additional resistivity profiles were undertaken to provide information, additional to the seismic refraction survey, on the depth to

bedrock at Helfa Hall. Induced polarisation (IP) data was also collected for both Lines LP-5 and LP-6.

A site survey utilising an EDM theodolite, target prism and the triangulation of ground stations (including borehole locations) was undertaken to produce a digital terrain model of the landform under investigation and its surrounding topography. However, since the EDM survey, LiDAR data of the field area has been made available to the project by the Environment Agency, providing extensive, high-resolution terrain data of the site (Figure 9.3). This dataset has therefore been used for all terrain models of the site (e.g. Figure 9.6) and for providing the topography necessary for the processing of resistivity Lines LP-5 and LP-6. Topography data for Lines LP-1, LP-2, LP-3 and LP-4 were measured at the time of survey using the EDM system.
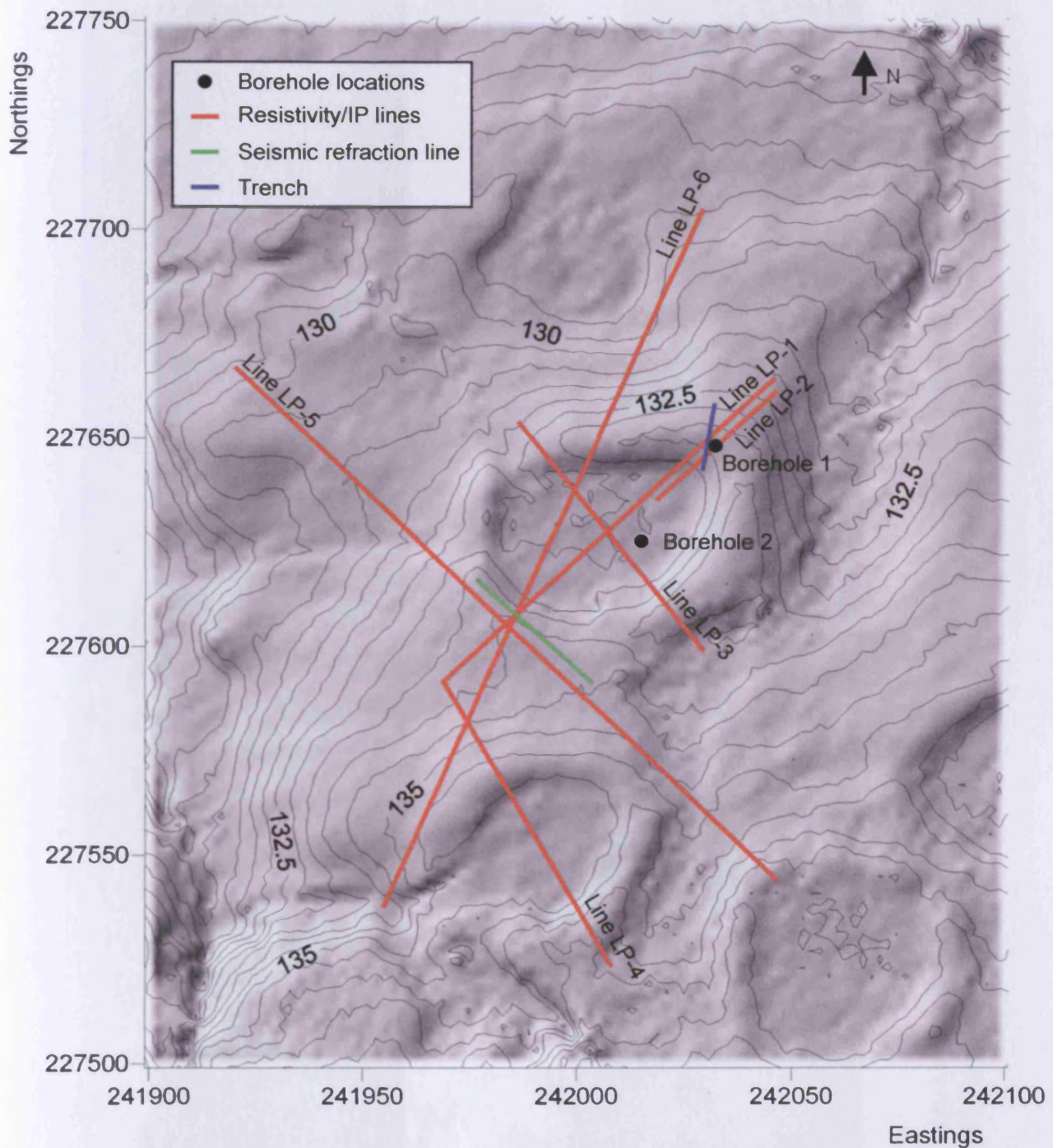
Figure 9.6: Locations of sedimentological and geophysical surveys at Helfa Hall, Llanpumsaint. Digital Terrain Model (DTM) data derived from LiDAR airborne surveying (© Environment Agency copyright and/or database right 2006). Contours at 0.5 m intervals.

Figure 9.7: (a) Landform 1, Helfa Hall, Llanpumsaint. Location of trench apparent to right of basin; (b) Landform 2, Helfa Hall, Llanpumsaint.

9.3 Results

9.3.1 Sedimentology

9.3.1.1 Boreholes

The upper 4 m of Borehole 1 (SN 42029.27658) were composed of silt and silty clay interspersed with thin (<0.20 m) units of silty, sandy gravel and silty sand between 1.82-2 m, 3.24-3.29 m, 3.74-3.81 m and 4-4.07 m (Figures 9.8a, 9.9, 9.10 and 9.11). The clayey silts that dominated the upper 1.5 m of the borehole were characterised by the presence of occasional subangular sandstone and quartzite clasts with long axes of 0.5-5 cm, which were particularly concentrated between 0.74-0.81 m. Although the clayey silt was generally massive, pale brown laminae were observed between 1.28-1.59 m (Figure 9.8a). The poorly-sorted, thin units of gravel between 1.82-2.00 m and 3.24-3.29 m contained platy, subrounded to rounded shale and sandstone clasts, up to 3 cm long, embedded in a fine gravel matrix. Precipitation of iron oxide from solution was apparent in the mottling throughout the uppermost 2-3 m of the borehole, but was particularly concentrated within the gravel units, in which there was also evidence for manganese precipitation. The beds of massive, silty, fine sands between 3.74-3.81 m and 4.00-4.07 m were separated and underlain by a moist, firm, silty clay which dominated the sequence between, and exceeding, 4.07-8.00 m. Laminations were apparent in the field between 5.00-5.50 m (Figure 9.8a), an observation verified in the laboratory following the drying of the samples which suggested laminations throughout the sequence from 5 m to the base of the borehole at 8 m depth. The borehole was terminated at this depth, so the total thickness of this unit could not be established.

Borehole 2 (SN 42018.27638) demonstrated a thick fill of dark, reddish-brown, fibrous peat, containing woody macrofossils, in the centre of the basin. This was underlain, below 4.07 m, by a unit of silty clay (Figure 9.8b), which was in parts laminated (Figure 9.10a), and was similar in grain-size to the sediments at the base of Borehole 1 (Figure 9.11a). Drilling to a depth greater than 5 m was inhibited by the thick peat fill, which posed problems for the safe retrieval of the coring equipment. The total thickness of the silty clay could not therefore be established.

9.3.1.2 Trench

The Llanpumsaint rampart section was dominated by a massive, structureless, light grey mottled clayey silt with occasional clasts (Unit M) (Figure 9.9). Interspersed within this 'matrix' were numerous units of iron and manganese stained, subrounded to rounded sandy gravels to silty sands (e.g. Units C, D and E) (Figure 9.10b). These units were exposed as asymmetrical antiforms; approximately horizontal to gently dipping between 0-8 m along the length of trench, and dipping at angles of up to 45° proximal to the central basin (e.g. 8-13.5 m) (Figure 9.9). Localised, dipping laminae within the light olive grey, clayey silt matrix of Unit M, where it was sandwiched between Units G and H at 9-11 m (Figure 9.10b), were similar to those observed within Borehole 1, between 1.28-1.59 m. These laminae dipped parallel to the angle of the contacts between the underlying units (Units E, F & G). Unit N corresponded to the concentration of gravel clasts recorded between 0.74-0.81 m in Borehole 1. Evidence for compressional deformation of the sequence was provided by the partial folding and buckling (reverse faulting) of Units D, E and H, particularly at 6 m and 8 m. Each of the sand and gravel units between 0-12 m thinned away from the central basin, tapering out on the downslope side of the rampart (Figure 9.9). This was mirrored by a fining of the grain-size, with poorly sorted sandy gravels becoming increasingly finer, gravelly, coarse sands (e.g. Samples LPT 10 and 11, and Samples LPT 4 and 7, Figure 9.11b). The poorly sorted gravel units had a comparable grain-size distribution to the gravel units between 1.82-2 m (Sample BH1-3) and 3.24-3.29 m (Sample BH1-6) in Borehole 1 (Figures 9.8a and 9.11a).

Units L and O, at the proximal end of the rampart section (13.5-15 m) were composed of gravelly to silty sands (Figures 9.9, 9.10b and 9.11b) that did not display a trend of decreasing grain-size towards the distal end of the trench. Unit L contained alternating beds of iron-stained and non iron-stained beds of silty sand, which dipped southwards towards the central basin of the landform (Figures 9.10b). Although they were dipping southwards, these thin beds did not display the arching structures that were apparent in the deformed gravel units (e.g. Units D, E and F). The unit of gravelly sand (Unit O) was horizontal and displayed no evidence for deformation.
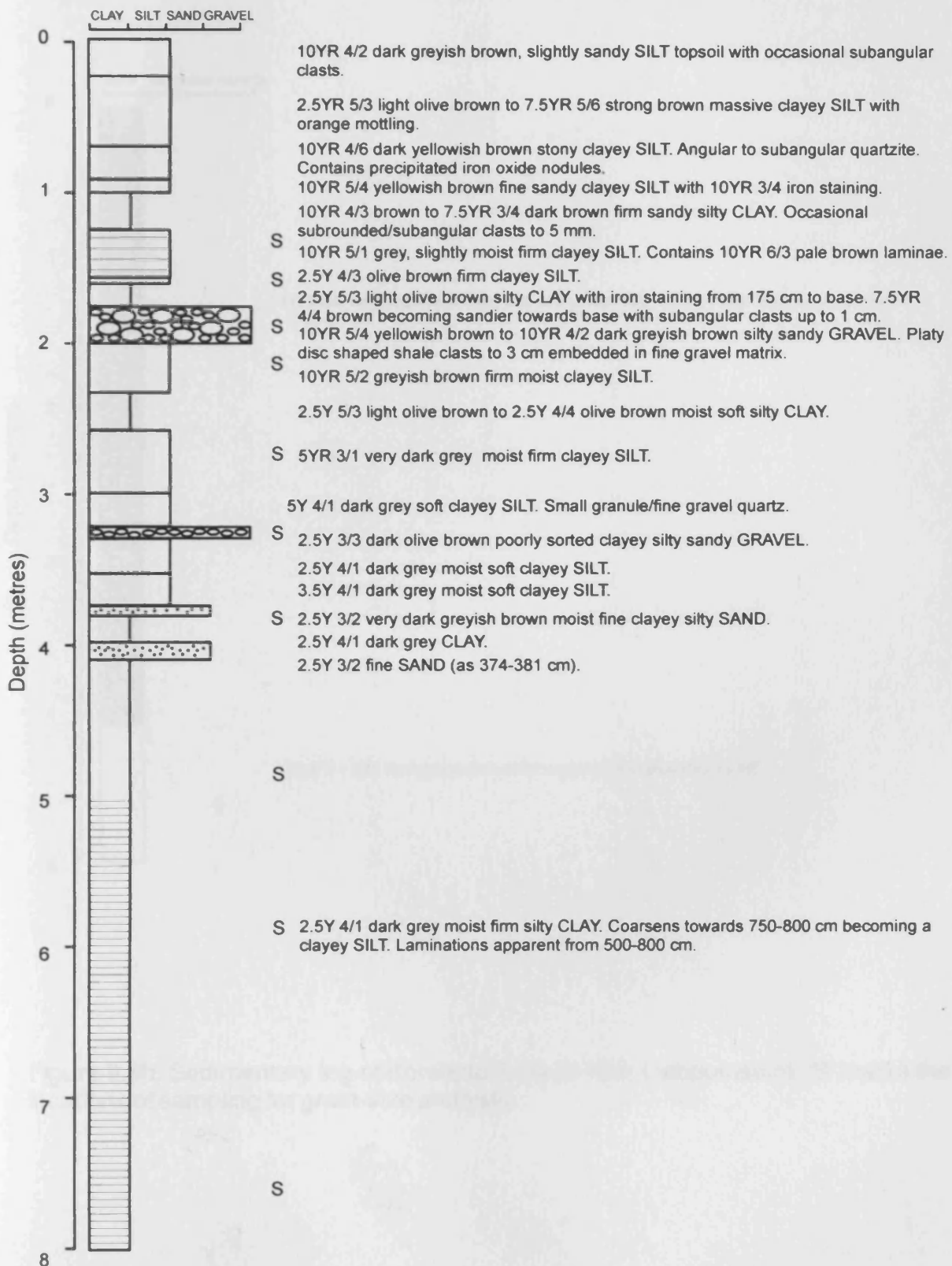
Figure 9.8a: Sedimentary log of Borehole 1, Helfa Hall, Llanpumsaint. 'S' marks the locations of sampling for grain-size analysis.
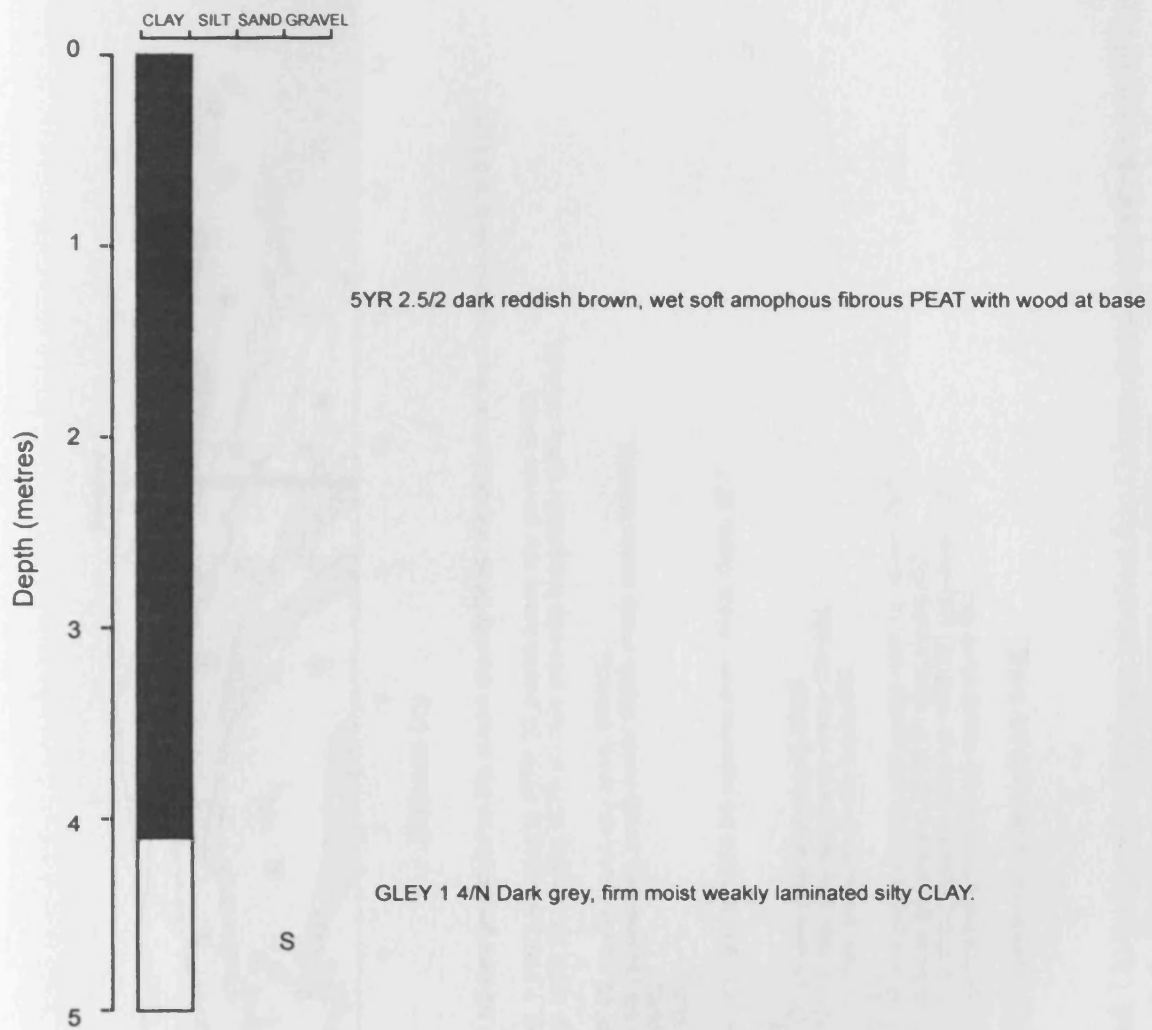
Figure 9.8b: Sedimentary log of Borehole 2, Helfa Hall, Llanpumsaint. 'S' marks the locations of sampling for grain-size analysis.
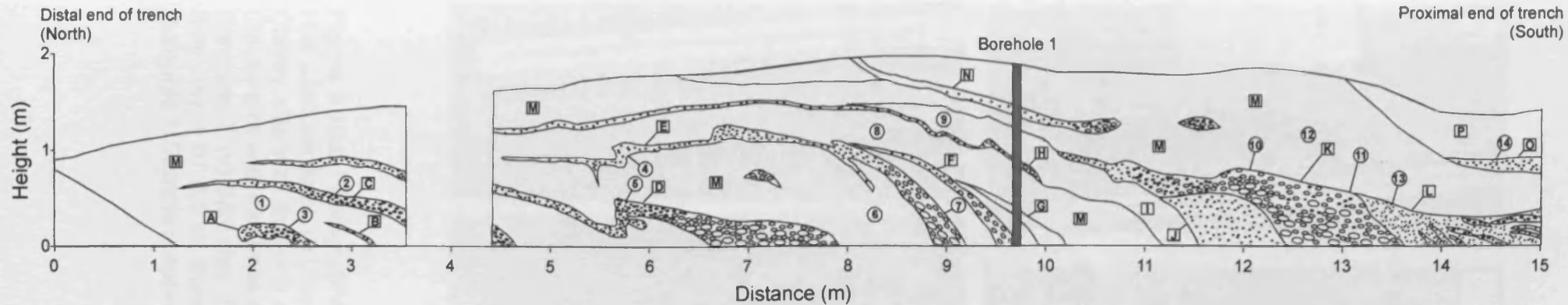
Unit A (Sample LPT 3): 10 YR 4/2 dark greyish brown silty coarse gravelly SAND with occasional large rounded clasts to 0.5 cm.
Unit B: Brown streak of SAND.
Unit C (Sample LPT 2): Mottled, 7.5YR 2.5/1 black to 10YR 5/2 greyish brown silty gravelly SAND.
Unit D (Sample LPT 5): Mottled 10YR 2/1 Black to 10YR 4/1 dark grey silty fine granule sandy GRAVEL.
Unit E (Samples LPT 4 & 7):
        Sample LPT 4 - 10YR 4/2 greyish brown silty sandy GRAVEL.
        Sample LPT 7 - 5YR 5/8 yellowish red, poorly sorted slightly sandy coarse GRAVEL.
Unit F: Orange silty sandy GRAVEL.
Unit G: Dark brown/black silty CLAY.
Unit H: Silty GRAVEL.
Unit I (Sample LPT 9): 2.5Y 4/1 dark grey to 10YR 5/6 yellowish brown sandy clayey SILT.
Unit J: Blue grey silty SAND.
Unit K (Samples LPT 10 & 11):
        Sample LPT 10 - 10 YR 4/1 dark grey, silty gravelly SAND.
        Sample LPT 11 - 10YR 4/1 dark grey, silty sandy coarse GRAVEL.
Unit L (Sample LPT 13): 10YR 4/1 dark grey uniform silty fine SAND.
Unit M (Samples LPT 1, 6, 8 & 12):
        Sample LPT 1 10YR 4/2 dark greyish brown, with orange mottling, clayey SILT.
        Sample LPT 6 10YR 6/6 brownish yellow to 10YR 6/1 grey, clayey SILT.
        Sample LPT 8 Mottled, 10YR 5/6 yellowish brown to 10YR 6/1 grey clayey SILT.
        Sample LPT 12 10YR 5/6 yellowish brown sandy clayey stony SILT.
Unit N: Light grey stony CLAY.
Unit O (Sample LPT 14): 10YR 2/2 dark brown, organic gravelly SAND.

Figure 9.9: Trench section, Helfa Hall, Llanpumsaint. Units are labelled A to O from distal to proximal ends of the trench. Locations of sampling for grain-size analysis indicated by annotations (LPT) 1-14.

Figure 9.10a: Photographs of sediments from Borehole 1 and Borehole 2, Helfa Hall, Llanpumsaint: (i) Clayey silts and silty, sandy gravels, 1.5-2 m, Borehole 1; (ii) Clayey silts with thin unit of clayey, silty, sandy gravel, 3-3.5 m, Borehole 1; (iii) Clayey silts with thin units of fine sand, 3.5-4 m, Borehole 1; (iv) Silty clay, 6.5-7 m, Borehole 1; (v) Silty clay, 7.5-8 m, Borehole 1; (vi) Peat, 3-3.5 m, Borehole 2; (vii) Silty clay, 4.07-4.5 m, Borehole 2; (viii) Laminated silty clay, sampled from 6-7 m, Borehole 1. Sample is approximately 8 cm long.
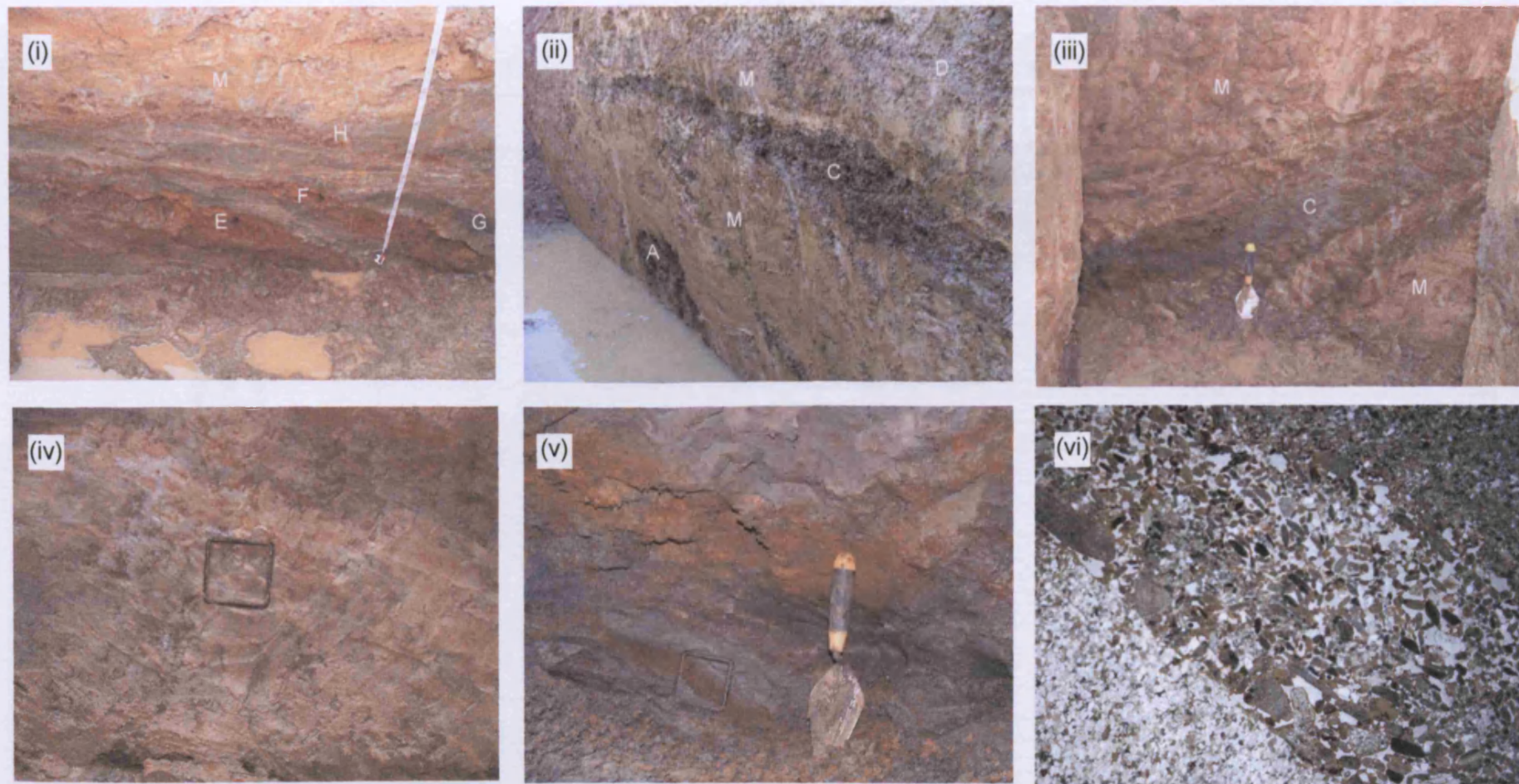
Figure 9.10b: Photographs of sediments and structures exposed in trench, Helfa Hall, Llanpumsaint: (i) Oblique photograph of trench, 8-10.5 metres from the distal end, taken from ground surface. Note steeply dipping iron-stained gravels (Units E & F) embedded within a clayey silt matrix (Unit M); (ii) Gravelly sands (Units A and C) within Unit M, 1-3.5 m from distal end of trench (Photo: C. Harris); (iii) Gravelly sand (Unit C), on west wall of trench (not logged), 3.5-4.5 m from distal end of trench; (iv) Laminated clayey silts within Unit M, at 9-11 m from distal end of trench (thin section block is 6 cm across); (v) Silty fine sand and sandy silt (Unit L), 14-15 m from distal end of trench (thin section block is 6 cm across); (vi) Thin section from Unit L displaying sand grains with southward dipping fabrics overlying clast of quartzite (bottom left of view). Field of view 17 mm across. Location of thin section shown in photo (v).
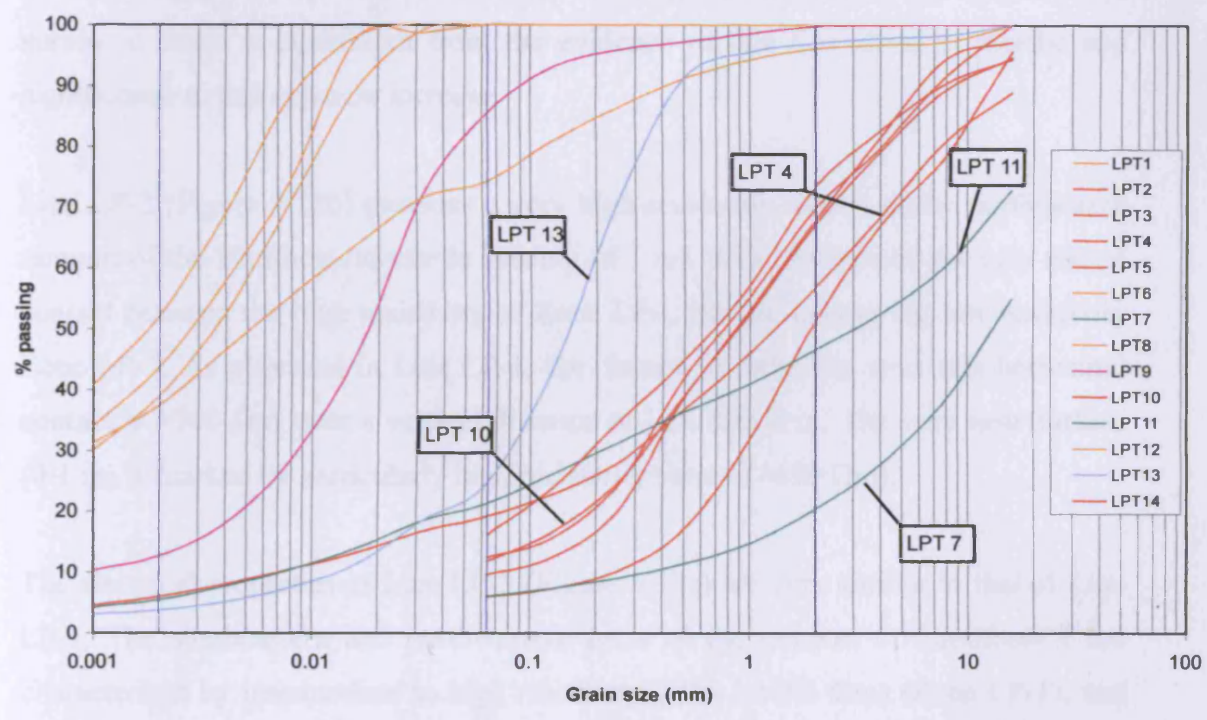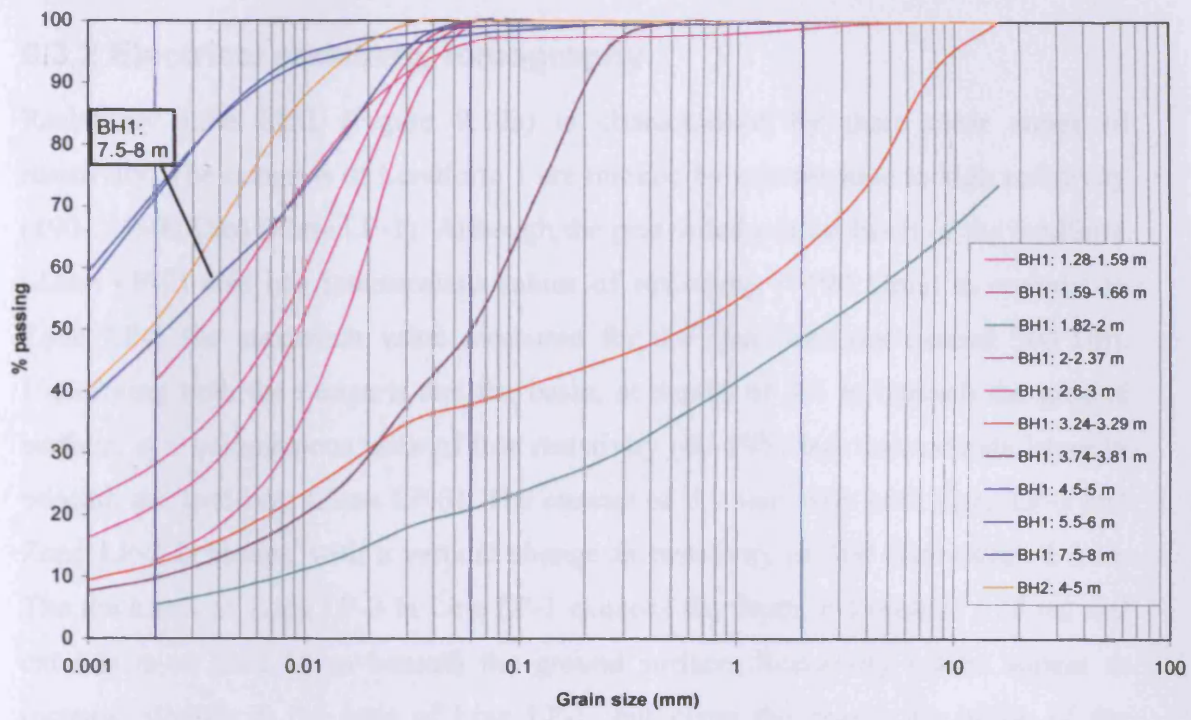
Figure 9.11: Results of grain-size analysis of samples taken from Landform 1, Helfa Hall, Llanpumsaint: (a) Boreholes 1 & 2 (BH1, BH2); (b) Trench section (LPT). For locations of samples see Figures 9.8 and 9.9.

9.3.2 Electrical resistivity tomography

Resistivity Line LP-1 (Figure 9.12a) is characterised by three clear zones of resistivity. The ramparts of Landform 1 are marked by intermediate to high resistivity (190- >1500 Ωm) (Zone LP-1). Although the peat-filled central basin of the landform (Zone LP-2) also has intermediate values of resistivity (>190 Ωm), in contrast to Zone LP-1 the maximum value measured for the peat does not exceed 500 Ωm. Underlying both the ramparts and the basin, at depths of 3-4 m beneath the ground surface, is a homogenous zone of low resistivity (40-190 Ωm) that extends laterally beneath the landform (Zone LP-3). The contact of this unit with both Zone LP-1 and Zone LP-2 is abrupt, with a vertical change in resistivity of 300 Ωm within 1-2 m. The thickness of Zone LP-3 in Line LP-1 exceeds the depth of Borehole 1 (8 m) and extends to at least 16 m beneath the ground surface. Resistivity values appear to increase slightly at the base of Line LP-1, but given the coarse resolution of the survey at depth it is difficult from the evidence of this line alone to ascribe any significance to this apparent increase.

Line LP-2 (Figure 9.12b) provides a very high-resolution survey of the northeastern rampart of the landform (electrode spacing of 1 m). This emphasises the very abrupt contact between the high resistivity of Zone LP-1 and the underlying low resistivity Zone LP-3. As observed in Line LP-1, the change in resistivity over this horizontal contact is >300 Ωm over a vertical distance of less than 2 m. The very near surface (0-1 m) is marked by particularly high resistivity values (>650 Ωm).

The electrical properties of Line LP-3 (Figure 9.12c) are very similar to that of Line LP-1. The southeastern and northwestern parts of the rampart of Landform 1 are characterised by intermediate to high resistivity (190- >1500 Ωm) (Zone LP-1), and intermediate resistivity (190-500 Ωm) again characterises the peat-filled depression at the centre of the profile (Zone LP-2). A homogenous layer of low resistivity materials (40-190 Ωm, although predominantly <100 Ωm) again underlies both these zones, extending laterally beneath the ramparts and the basin (Zone LP-3). As observed in Lines LP-1 and LP-2, the contact between the near-surface Zones LP-1 and LP-2 with Zone LP-3 is abrupt. The thickness of Zone LP-3 exceeds 8-10 m.
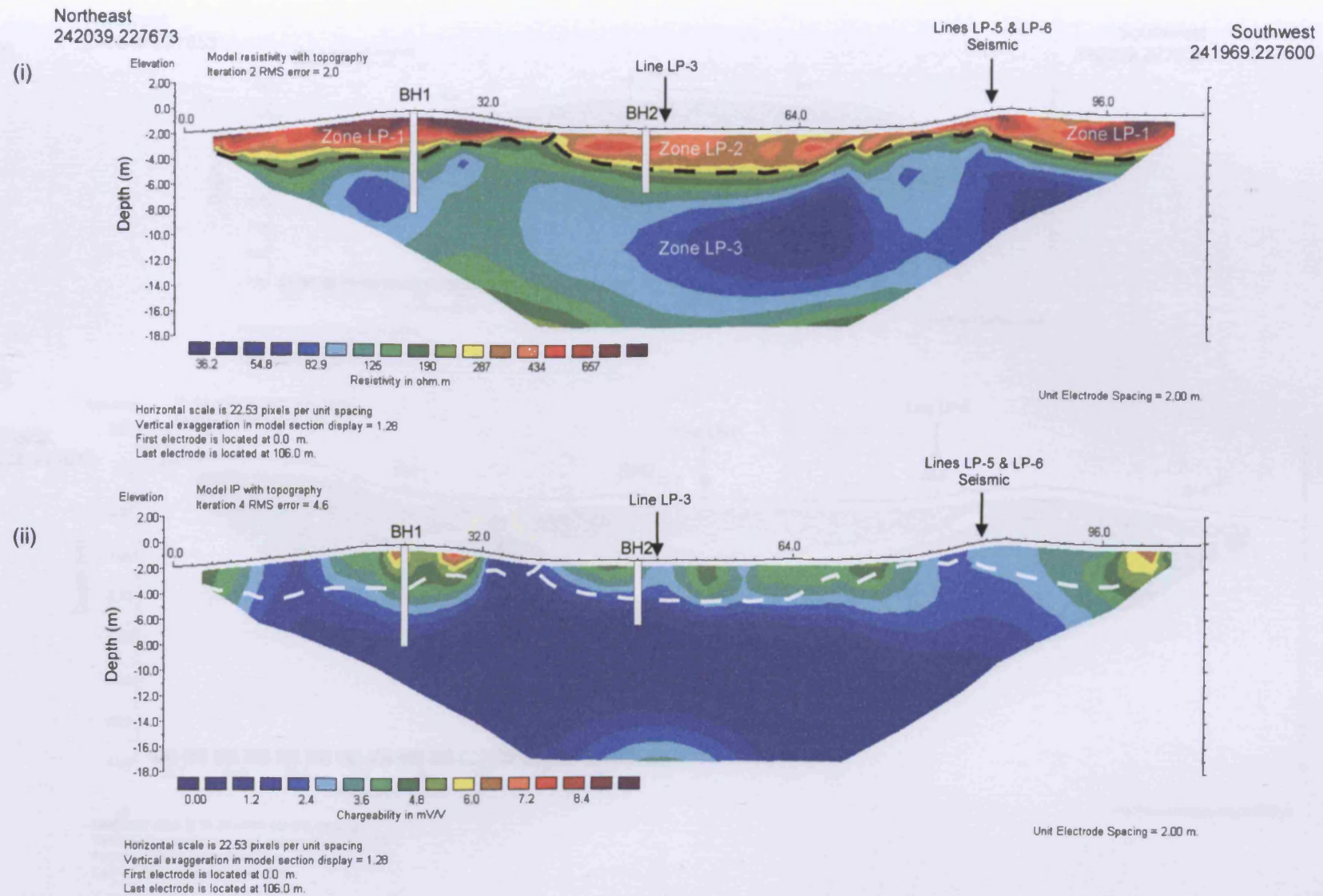
Figure 9.12a: (i) Electrical resistivity and (ii) IP profiles (Line LP-1), Helfa Hall, Llanpumsaint. Locations of boreholes and intersection points of other geophysical survey lines indicated. The 190 Ωm resistivity contour is marked on the resistivity profile by a black dashed line and on the IP profile by a white dashed line.

(b)

Northeast
242040.227653

Southwest
242009.227639

Model resistivity with topography
Iteration 3 RMS error = 2.6

BH1

Zone LP-1

Zone LP-3

Resistivity in ohm.m
36.2 54.8 82.9 125 190 287 434 657

Horizontal scale is 34.24 pixels per unit spacing
Vertical exaggeration in model section display = 1.24
First electrode is located at 0.0 m.
Last electrode is located at 35.0 m.

Unit Electrode Spacing = 1.00 m.

(c)

Southeast
242035.227613

Northwest
241988.227664

Model resistivity with topography
Iteration 2 RMS error = 3.8

Line LP-6

Line LP-1

BH2

Zone LP-1

Zone LP-2

Zone LP-1

Zone LP-3

Resistivity in ohm.m
36.2 54.8 82.9 125 190 287 434 657

Horizontal scale is 34.28 pixels per unit spacing
Vertical exaggeration in model section display = 1.23
First electrode is located at 0.0 m.
Last electrode is located at 70.0 m.

Unit Electrode Spacing = 2.00 m.

Figure 9.12: (b) Electrical resistivity Line LP-2, Helfa Hall, Llanpumsaint; (c) Electrical resistivity Line LP-3, Helfa Hall Llanpumsaint. Locations of boreholes and intersection points of other geophysical survey lines indicated. The 190 Ωm resistivity contour is marked on both resistivity profiles by a black dashed line.

Resistivity Line LP-4 (Figure 9.12d) ran southeast to northwest across Landform 2 (Figure 9.6). Although there is no sedimentological control for the interpretation of this landform from boreholes or trenching, the electrical properties of this landform are very similar to those observed from Landform 1 (resistivity Lines LP-1, LP-2 and LP-3). The ramparts are marked by very high resistivity (predominantly >650 Ωm) (Zone LP-1), the peat-filled basin by intermediate resistivity (190-500 Ωm) (Zone LP-2), both underlain by a low resistivity layer (<190 Ωm) that is more than 8 m thick (Figure 9.12d).

The depth of investigation of resistivity Lines LP-1, LP-2, LP-3 and LP-4 was limited (maximum depth of investigation 18 m) because of the narrow electrode spacings that were deployed (1-2 m). The additional resistivity surveys undertaken in July 2005 (Lines LP-5 and LP-6) utilised electrode spacings of 5 m in an attempt to provide additional information on the electrical properties at greater depths, and identify rockhead.

A thin (<3 m) layer of intermediate to high resistivity (190-1500 Ωm) (Zone LP-1) is apparent in the near-surface zone of resistivity Line LP-5 (Figure 9.12e). This is underlain by a 20-25 m thick layer of low resistivity (40-230 Ωm) that corresponds to resistivity Zone LP-3 observed in Lines LP-1, LP-2, LP-3 and LP-4. The modelled resistivity increases at the base of Line LP-5, with a layer of intermediate resistivity (230-450 Ωm) (Zone LP-4). If the 230 Ωm contour is selected as the boundary between Zones LP-3 and LP-4, then the contact between these two zones appears to dip southeastwards. This boundary appears to be gradational in nature, with resistivity values increasing from 100 Ωm at 15 m depth to 290 Ωm at a depth of 20-25 m. Line LP-5 did not intersect any peat-filled basins (Figure 9.6), and as a result, resistivity Zone LP-2 was not measured in this profile.

Resistivity Line LP-6 (Figure 9.12f), which ran perpendicular to Line LP-5, is also characterised by at least three resistivity zones. The survey line ran over the ramparts of both Landform 1 and Landform 2, as well as over the peat-filled basin of Landform 1 (70-105 m) (Figure 9.6). Where the profile ran over the ramparts and areas of high ground, the profile is characterised by intermediate to high resistivity (190->600 Ωm) (Zone LP-1). Because of the low resolution of resistivity Line LP-6, in comparison to

(i)

Model resistivity with topography
Iteration 3 RMS error = 1.2

Southeast
242018.227529

Elevation

Line LP-6

Northwest
241970.227605

Zone LP-1

Zone LP-2

Zone LP-1

Zone LP-3

Resistivity in ohm.m

36.2 54.8 82.9 125 190 287 434 657

Horizontal scale is 11.30 pixels per unit spacing
Vertical exaggeration in model section display = 1.23
First electrode is located at 0.0 m.
Last electrode is located at 79.5 m.

Unit Electrode Spacing = 0.750 m.

(ii)

Model IP with topography
Iteration 4 RMS error = 4.2

Elevation

Line LP-6

Chargeability in mV/V

0.00 1.2 2.4 3.6 4.8 6.0 7.2 8.4

Horizontal scale is 22.59 pixels per unit spacing
Vertical exaggeration in model section display = 1.28
First electrode is located at 0.0 m.
Last electrode is located at 79.5 m.

Unit Electrode Spacing = 1.50 m.

Figure 9.12d: (i) Electrical resistivity and (ii) IP profiles (Line LP-4), Helfa Hall, Llanpumsaint. Locations of boreholes and intersection points of other geophysical survey lines indicated. The 190 Ωm resistivity contour is marked on the resistivity profile by a black dashed line and on the IP profile by a white dashed line.
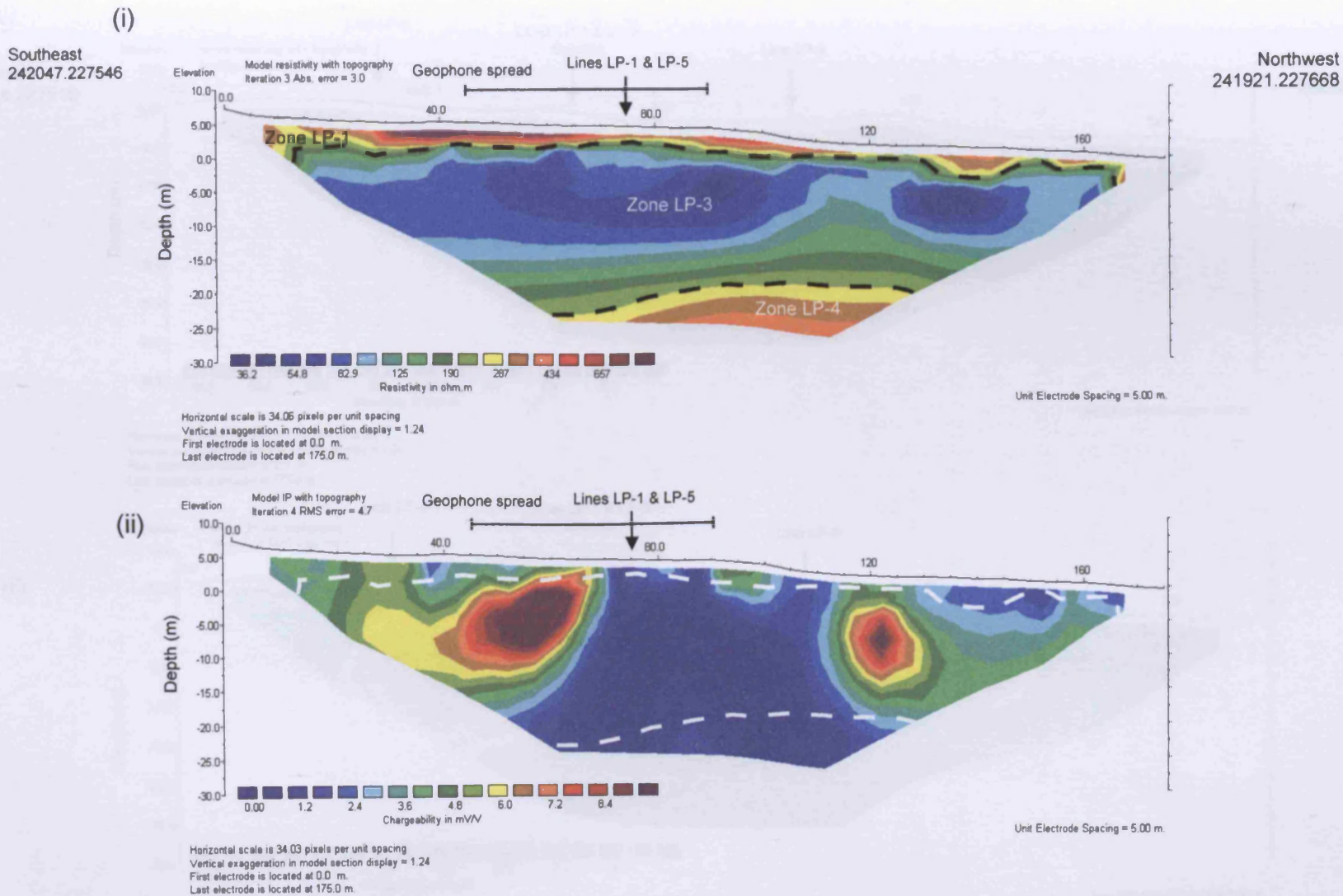
Figure 9.12e: (i) Electrical resistivity and (ii) IP profiles (Line LP-5), Helfa Hall, Llanpumsaint. Locations of boreholes and intersection points of other geophysical survey lines indicated. The 190 Ωm (upper part of profile) and 230 Ωm (lower part of profile) resistivity contours are marked on the resistivity profile by black dashed lines and on the IP profile by white dashed lines.
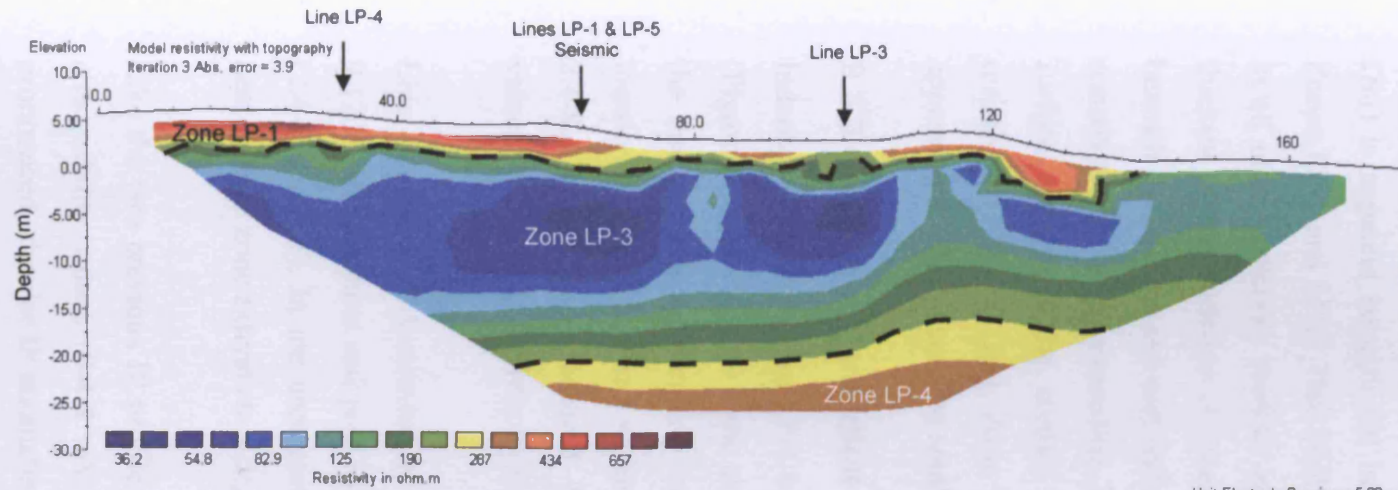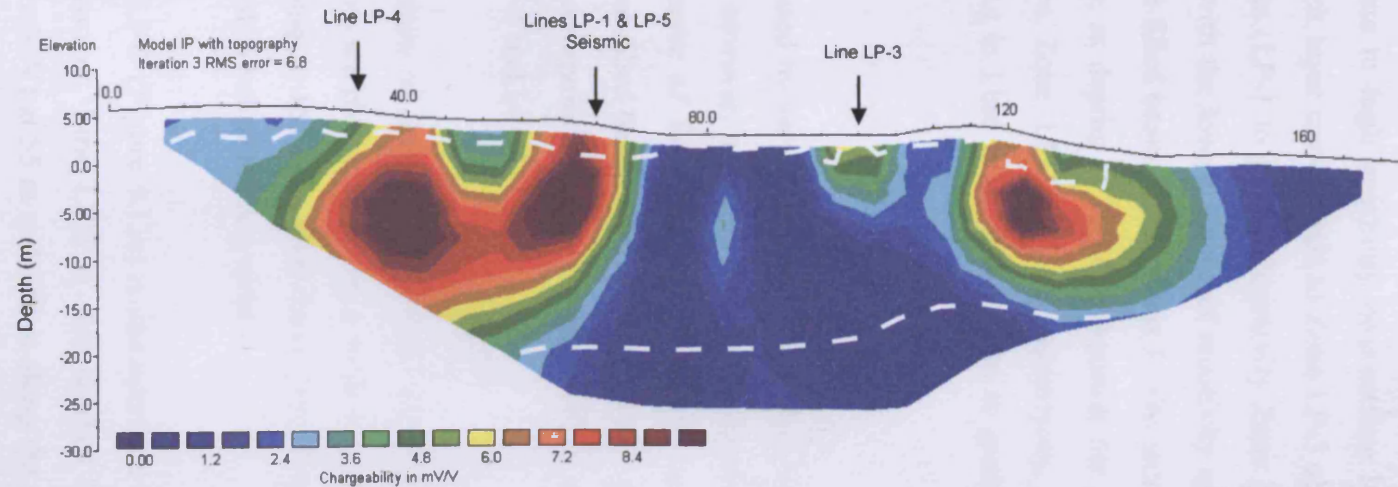
Figure 9.12f: (i) Electrical resistivity and (ii) IP profiles (Line LP-6), Helfa Hall, Llanpumsaint. Locations of boreholes and intersection points of other geophysical survey lines indicated. The 190 Ωm (upper part of profile) and 230 Ωm (lower part of profile) resistivity contours are marked on the resistivity profile by black dashed lines and on the IP profile by white dashed lines.

Lines LP-1 and LP-3, it is difficult to clearly define the peat-filled basin of Landform 1 (Zone LP-2). However, a slight decrease in resistivity is apparent in the near-surface zone between 70-105 m compared to where the profile ran over the landforms ramparts (0-70 m and 105-135 m). A laterally continuous low resistivity zone (40-230 Ωm) is apparent beneath the intermediate to high resistivity near-surface layer of Zones LP-1 and LP-2. This 20-25 m thick layer corresponds to Zone LP-3 observed in all other resistivity profiles at this site (LP-1 to LP-5). Resistivity Zone LP-3 is thickest to the southwest of Line LP-6, with the lowest values of resistivity apparent beneath the upslope rampart and the peat-filled basin of Landform 1. The increase in resistivity, to values exceeding 230 Ωm, at depths of 25-30 m beneath the ground surface, represents the contact between Zone LP-3 and the underlying, higher resistivity (230-350 Ωm), Zone LP-4. As in Line LP-5, this contact is gradational, appearing to dip towards the southwest.

9.3.3 Induced polarisation

Induced polarisation Line LP-1 is dominated by very low chargeability (0-3.6 mV/V) (Figure 9.12a). There is some evidence however, of slightly higher chargeability in the near surface, particularly in the centre of the northeastern rampart near the location of Borehole 1 and within the peat-filled basin, where chargeability values of 2.4-8.4 mV/V were measured. These correspond to zones of intermediate to high values of resistivity (resistivity Zones LP-1 and LP-2).

Line LP-4 is also dominated by low values of chargeability (0-3.6 mV/V) (Figure 9.12d). The ramparts and peat-filled basins are characterised by a weak chargeability (2.4-6.6 mV/V). In the area corresponding to the peat-filled basin (16-42 m), this near-surface zone extends to a depth of 3-4 m below the bog surface.

Like the two previous IP profiles, Line LP-5 (Figure 9.12e) is characterised by low chargeability values (0-4.8 mV/V). However, Line LP-5 is also marked by two pronounced, circular IP anomalies (>8.4 mV/V) at 55 m and 122 m along the profile, at a depth of approximately 10 m below the ground surface. Similar 'bulls eye' shaped anomalies are also apparent in Line LP-6 (Figure 9.12f), at 40 m, 60m and at 120 m.

9.3.4 Seismic refraction

Three first break velocity segments are apparent from the seismic P-wave travel-time graph (Figure 9.13). The direct wave, representing a very thin near-surface zone, is indicated by the low velocity gradients between 18-22 m and 22-24 m of Shot 2. The direct wave is not apparent in Shots 1 and 3 however, suggesting that this layer is very thin. For the purposes of this site investigation this layer has been ignored but is thought to represent a thin, near-surface, unsaturated, weathered zone. The first refracted wave is apparent on the traveltime vs distance plots of Shots 1, 2, 3, 5, 6, 7 and 13, which all show strong parallelism. Shots 9, 10, and 11 have two velocity segments representing two refracted waves. Shot 10 and Shot 11 display good parallelism. The arrival of the second refracted wave, indicated by the change in the inflection of the best-fit lines, occurs at 26 m (geophone 14) on Shot 9, 36 m (geophone 19) on Shot 10, and 28 m (geophone 15) on Shot 11. A total of two refracted waves are therefore identified from the traveltime graph.

The average velocity of the first refractor, derived from the reciprocal of the gradient of the minus graphs of eight pairs of reversed shots (1&3, 1&13, 3&6, 3&7, 5&3, 5&13, 6&13, 7&13) was 1395 msec^{-1}, varying from 1352 to 1441 msec^{-1}. The velocity of the second refractor (Shots 9, 10 and 11) could not be calculated using minus time values due to the lack of reversed coverage. The velocity of this refractor was therefore determined from the reciprocal of the gradient of the best-fit line for the appropriate segment of the traveltime graph for each shot. The calculated values were 3915 msec^{-1} (Shot 9), 4058 msec^{-1} (Shot 11) and 4335 msec^{-1} (Shot 10), averaging 4103 msec^{-1}.

The refracted waves identified from the first break data can be simply interpreted using a two-layer model with a low velocity (1395 msec^{-1}) layer overlying a higher velocity layer (4103 msec^{-1}). The depth of the refractor between these two layers was calculated using the Intercept Time method because of a lack of reversed coverage and the absence of a direct reciprocal time measurement (see Section 3.4.3.2). The calculated depths for the second refractor varied between 29-35 m, averaging 32 m (Figure 9.14).
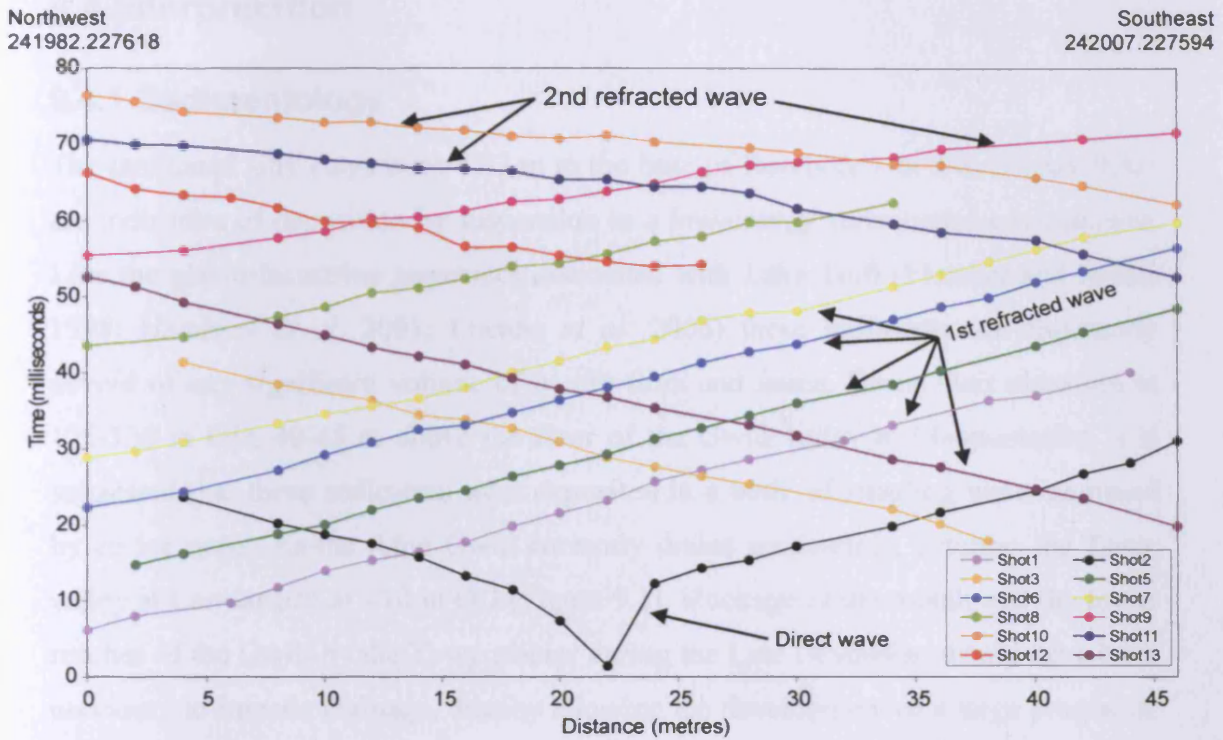
Figure 9.13: Traveltime graph of seismic refraction data collected at Helfa Hall, Llanpumsaint.
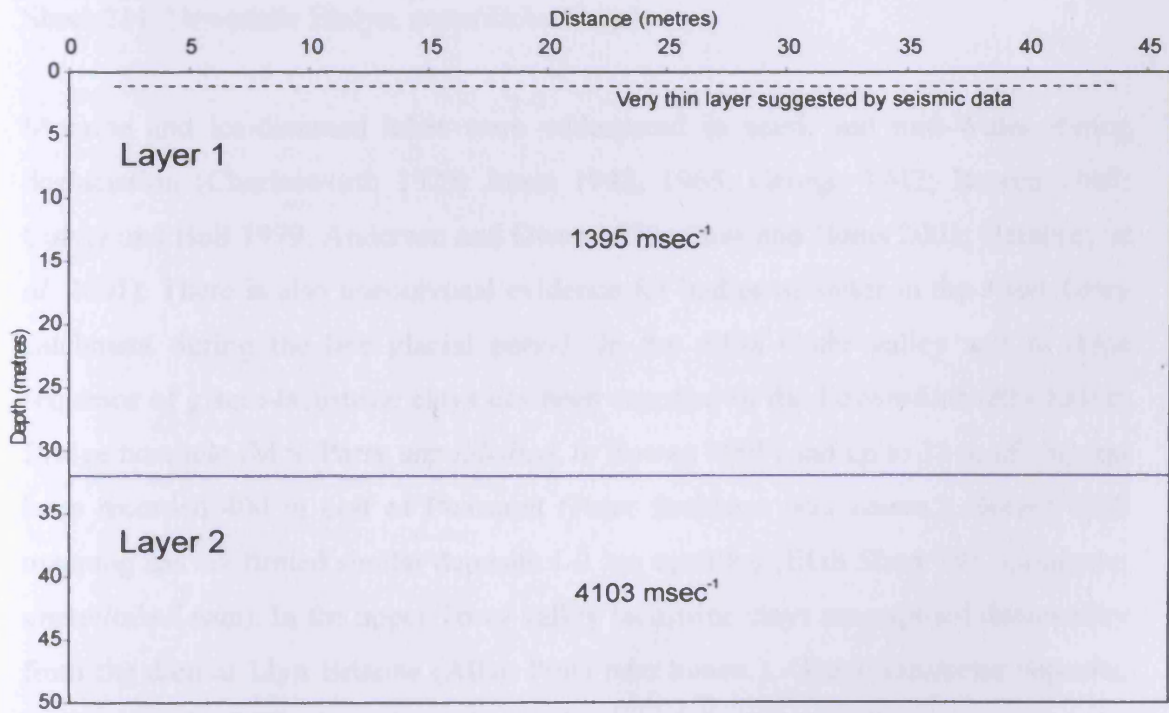
Figure 9.14: Model of refractor depth, Helfa Hall, Llanpumsaint, derived using the Intercept Time method.

9.4 Interpretation

9.4.1 Sedimentology

The laminated silty clays from 4.07 m to the base of Borehole 1 at 8 m (Figure 9.8a) are indicative of deposition by suspension in a low-energy subaqueous environment. Like the glacio-lacustrine sequences associated with Lake Teifi (Fletcher and Siddle 1998; Hambrey *et al.* 2001; Etienne *et al.* 2006) these sediments are apparently devoid of any significant volume of *in situ* flora and fauna. Given their elevation at 125-130 m OD, 40-45 m above the floor of the Gwili valley at Llanpumsaint, it is suggested that these sediments were deposited in a body of standing water dammed by an ice mass. As the Afon Gwili currently drains southwards, entering the Towy valley at Carmarthen at <10 m OD (Figure 9.1), blockage of the mouth and the lower reaches of the Gwili by the Towy glacier during the Late Devensian would have been necessary to impede drainage, thereby allowing the development of a large proglacial lake (Lake Gwili). Recent British Geological Survey (BGS) mapping in the area however does suggest that glaciers flowing from northeastern (Teifi glacier) or eastern (Cothi glacier) sources may also have influenced lake development (BGS Sheet 211, Newcastle Emlyn, *unpublished map*).

Moraine and ice-dammed lakes were widespread in south and mid-Wales during deglaciation (Charlesworth 1929; Jones 1942, 1965; George 1942; Bowen 1967; Culver and Bull 1979; Anderson and Owen 1979; Cave and Hains 2001; Hambrey *et al.* 2001). There is also unequivocal evidence for bodies of water in the Afon Towy catchment during the late glacial period. In the Afon Cothi valley a 5 m thick sequence of glacio-lacustrine clays has been reported in the Edwinsford (Rhydodyn) Bridge borehole (M.S. Parry *unpublished, in* Bowen 2005) and up to 11 m of clay has been recorded 400 m east of Pumsaint (Peter Brabham *pers comm.*). Recent BGS mapping has confirmed similar deposits 1-2 km upvalley (BGS Sheet 195, Lampeter, *unpublished map*). In the upper Towy valley lacustrine clays are exposed downvalley from the dam at Llyn Brianne (Allan Potts *pers comm.*). Glacio-lacustrine deposits, mapped by the BGS, throughout the catchment of the Afon Gwili suggest that Lake Gwili may have been relatively extensive (BGS Sheet 211, Newcastle Emlyn, *unpublished map*). The drainage of this lake presumably occurred following up-valley

retreat of the Towy glacier to the east. This event could have been responsible for the deposition of the large volumes of sand and gravels, composed predominantly of Palaeozoic shales and grits, which underlie Carmarthen, downstream of the confluence of the Afon Gwili and Afon Towy (Strahan *et al.* 1909; British Geological Survey 1967). Terraces of fluvioglacial sands and gravels at the mouth of the Afon Cothi (Strahan *et al.* 1909) may also represent a similar event associated with the deglaciation and drainage of the Cothi valley.

Following exposure of the glacio-lacustrine sediments deposited by Lake Gwili after lake drainage, permafrost aggradation, during the late Devensian and/or the Loch Lomond Stadial (Younger Dryas), is likely to have occurred. Ice-wedge casts developed within glaciofluvial ice-contact sands and gravels 3 km east of Helfa Hall at Lletty-tegan (SN 44896.27477) provide clear evidence for permafrost in the area after deglaciation and lake drainage (Figure 9.15). The clayey silts and silty clays throughout Borehole 1 and from Units M and I of the trench (Samples LPT 1, 6, 8, 9 and 12) (Figure 9.11) are highly frost susceptible (Beskow 1935). Following lake drainage, the high pore-water content of these sediments would have meant that the development of even a thin layer of permafrost within these glacio-lacustrine silts and clays would have resulted in ice segregation, and frost heave. Such conditions are characteristic of both lithalsa and open system pingo development within freshly exposed fine-grained sediments, such as marine clays, in actively uplifting arctic coastal zones (Svensson 1971; Åhman 1973; Pissart and Gangloff 1984; Allard *et al.* 1987, 1996).

The upper 4 m of Borehole 1 (Figure 9.8a) and the trench section (Figure 9.9) provide an important record of the development of the rampart of Landform 1 at Helfa Hall, Llanpumsaint. The units of rounded and sandy gravels within the trench represent sediments deposited, reworked and/or deformed during development of the circular rampart. The distal fining of grain-size and the abrupt tapering of Units E and K towards the outer slope of the rampart (Figure 9.9) indicates localised sedimentary events that resulted in deposition outwards from the central basin of the landform. These observations make it unlikely that the sediments that comprise the rampart were deposited before landform development and were simply heaved upward and deformed without remobilisation. If the ground was permanently frozen after the
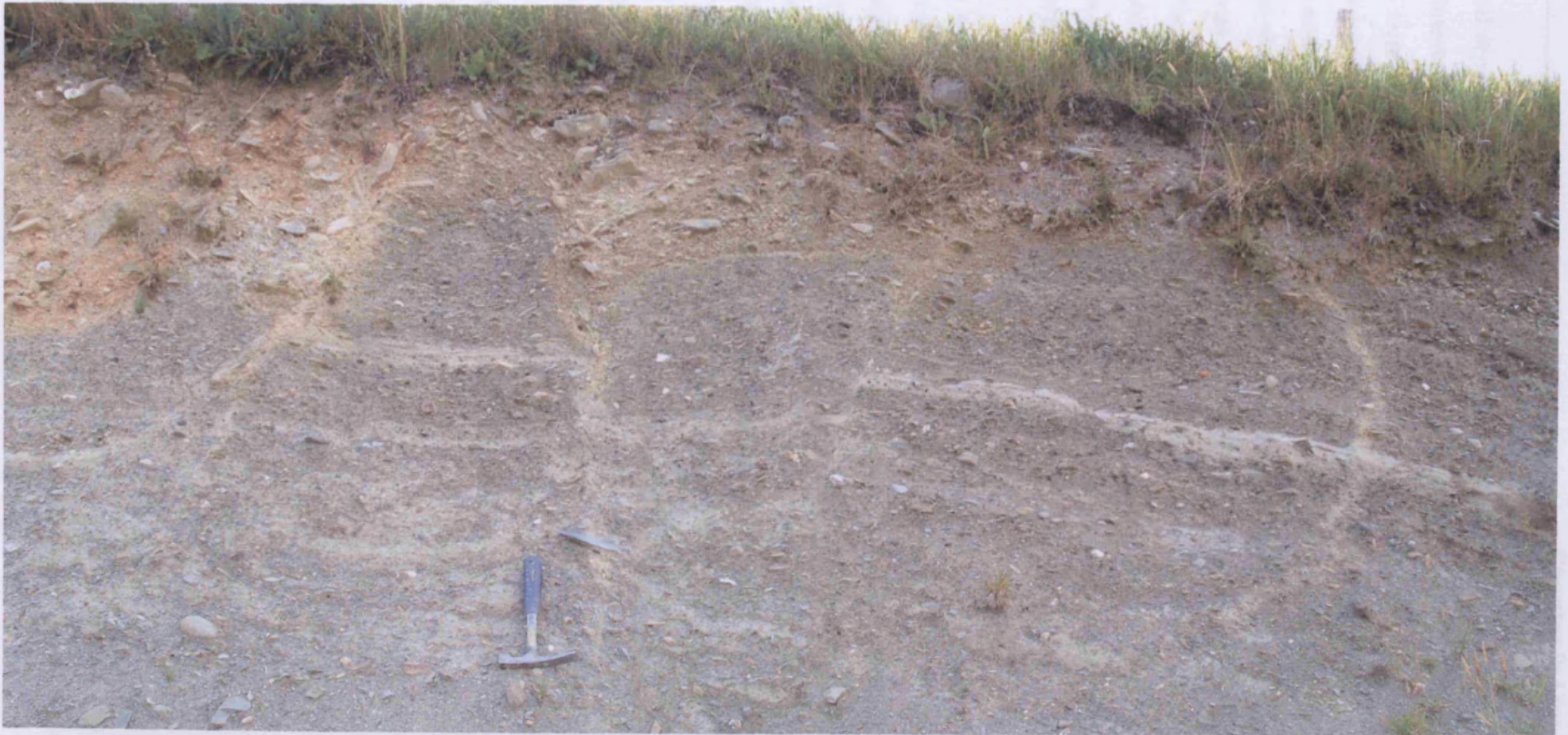
Figure 9.15: Ice-wedge casts developed within glaciofluvial ice-contact sands and gravels 3 km east of Helfa Hall at Lletty-tegan (SN 44896.27477).

initial deposition of glacio-lacustrine materials associated with Lake Gwili, then these sediments may have been extensively reworked and re-deposited by mass movement and slope wash processes associated with seasonal active layer thaw and melting of bodies of ground-ice or buried glacier ice. Given its generally massive, structureless nature and the occasional presence of larger clasts, Unit M was probably deposited by mass wasting (Harris 1981). The occasional laminae that are apparent in parts of Unit M may reflect deposition of material in small, localised bodies of standing water both on the surface of the landform and around its periphery or as the result of surface wash. The presence of bodies of standing water can be attributed to differential thaw consolidation processes during summer thaw of the active layer and during permafrost degradation.

The asymmetrical, anticlinal, arching structures seen in the rampart section suggest lateral deformation. Similar structures have been reported from sedimentological investigations of ramparted depressions in Wales near Llangurig (Pissart 1963) and in the Cletwr valley (Watson 1975, 1976), as well as at Clonroche, Co. Wexford, Ireland (Lewis 1985), in Belgium (Bastin *et al.* 1974; Pissart and Juvigne 1980; Pissart *et al.* 1981; Pissart 1983, 2000, 2003), Holland (De Gans 1981), and from degrading pingos in Canada (Mackay and Stager 1966; Pissart 1967; Pissart and French 1976; French and Dutkiewcz 1976; French *et al.* 1982). These structures are not diagnostic evidence for ground-ice mounds however, anticlinal structures have also been observed in sections through the ramparts of iceberg gravity craters (Longva and Bakkejord 1990). Irrespective of potential origins, the arching, partial folding and buckling of Units D, E and H must have occurred as a result of deformation and collapse associated with the gradual thaw of massive ground-ice, or buried glacier ice, at depth. The scale of deformation in the sequence suggests the meltout of a relatively significant body of ground ice. Massive ground-ice has been reported from beneath the periphery of Ibyuk Pingo, Canada (Rampton and Walcott 1974; Mackay 1988).

The lack of deformation and the shallowly dipping to horizontal beds of Units L, O and P (Figure 9.9) suggest that during the later stages of rampart development, sediment was redistributed back into the central basin by slumping and surface wash. The part of Unit M that overlies Units K and L was also redistributed back into the central basin following the deposition of Unit L. The sharp contact between Unit K

and Unit M suggests that the erosion of Unit K may have provided a sediment source for the deposition of Unit L. The 4.07 m thick sequence of peat in Borehole 2 is believed to be of Holocene age. The laminated clays that underlie this peat are interpreted as lacustrine sediments deposited within a pond confined by the encircling rampart, rather than during glaciolacustrine conditions associated with Lake Gwili prior to landform development. Depending on when the rampart was formed, deposition of these clays may have occurred either during the late Devensian, or during the Younger Dryas. No organic sediments that could be perceived as representing the Lateglacial Interstadial were found, although they may exist below the maximum depth of coring. The silty clay at the base of Borehole 2 was deposited either contemporaneously, or after, Units O and P.

9.4.2 Electrical resistivity tomography

Based on the geological evidence provided by the two boreholes and the trench, the interpretation of three of the four resistivity zones identified within the resistivity surveys (Zones LP-1, LP-2 and LP-3) can be constrained by direct observation. The upper 4 m of Borehole 1 and the section exposed by the trench indicate that the ramparts of these landforms are predominantly composed of unsaturated, massive clayey silts, interspersed with thin units of sand and gravels containing some precipitated iron and manganese (Figures 9.8, 9.9 and 9.10). The unsaturated nature of these sediments and the coarse-grained units of sand and gravel, are the result of the high values of resistivity characteristic of Zone LP-1. The very high resistivity values measured in the rampart of Landform 2 (Line LP-4, Figure 9.12d) suggest that this rampart may be characterised by a greater proportion of sand and gravel than the rampart of Landform 1.

Because peat is 80-95% water, the electrical resistivity of peat is fundamentally dependent on the solute content of its porewaters, which determines the waters conductivity (Theimer *et al.* 1994; Comas *et al.* 2004). The intermediate to high values of resistivity (190-500 Ωm) that characterise the peat-filled central basins of both landforms at Helfa Hall primarily reflect the low ionic concentrations of the porewaters of the peat at this site. The relatively high resistivity (low conductivity) of these peats compared to some other sites (Theimer *et al.* 1994; Comas *et al.* 2004) means that the peat-infill of the central basins would be highly suitable for ground

penetrating radar (GPR) surveys. Although previous studies have reported increases in the electrical conductivity of peat with depth due to the influence of inorganic solutes dissolved from mineral sediments underlying the peat (Theimer *et al.* 1994; Slater and Reeve 2002), this could not be confidently observed in the current surveys. The low solute content suggested by the intermediate to high resistivity of the peat-filled basin suggests that the porewaters are derived mainly from precipitation. These systems can therefore be classified as oligotrophic basin mires (bogs) rather than minerotropic fens, which at least partly source inorganic ions from groundwater sources (Lindsay 1995).

A significant contrast between the resistivity of the peat-filled basins and the underlying mineral soil is apparent from profiles LP-1, LP-3 and LP-4 (Figures 9.12a, 9.12c and 9.12d). This sharp boundary is a function of the markedly different physical properties of organic and non-organic sediments (Comas *et al.* 2004). The base of the peat in Borehole 2 (4 m) (Figure 9.8b) corresponds well with the lower boundary of Zone LP-2 in both Line LP-1 and LP-3 (Figures 9.12a, 9.12c), suggesting that the intermediate resistivity zone that characterises the peat-filled basins of the landforms (Zone LP-2) can be utilised to clearly define the lower and lateral boundaries of the peat. The vertical extent of Zone LP-2 in Line LP-4 suggests that a similar thickness of peat is present within the central basin of Landform 2. This observation was supported by preliminary augering of the basin, which recorded a 3.3 m thick layer of peat.

The low resistivity Zone LP-3 that extends laterally beneath the ramparts and the peat-filled basins in all resistivity lines corresponds to the saturated, laminated silty clays observed between 4.07-8 m in Borehole 1, and the fine-grained saturated sediments beneath the peat-filled basin between 4.07-5 m in Borehole 2 (Figure 9.8). The very low resistivity values measured for these sediments, relative to the clayey silts that comprised the upper 4.07 m of Borehole 1, are partly the result of a reduction in grain-size with depth, but are mainly a function of the saturated state of the sediments below 4 m in Borehole 1. Therefore, the boundary between Zones LP-1 and LP-3 primarily represents the location of the water table rather than a geological boundary. Clay minerals are naturally conductive because of their large surface area and cation exchange capacity (CEC), which enables surface chemical reactions.

Although this usually results in very low resistivity values, the resistivity of Zone LP-3 is relatively high for clay. This may be a result of the clay being relatively compact rather than being composed of disassociated particles, thereby restricting the CEC (Turesson and Lind 2005).

The increased resistivity at the base of Lines LP-5 and LP-6 (Zone LP-4) (Figures 9.12e and 9.12f) is interpreted as bedrock. Although resistivity values do increase from a depth of 15-20 m beneath the ground surface in both lines, the 230 Ωm contour is interpreted as representing the superficial-bedrock boundary. This contour is found at depths of 25-30 m in both Lines LP-5 and LP-6. The increase in resistivity at the base of resistivity Zone LP-3 apparent in Lines LP-1, LP-5 and LP-6 may represent a change in the lithology of the superficial deposits with depth (e.g. to till), but may alternatively be a function of the coarse resolution of the resistivity model blocks. Irrespective of the composition of Zone LP-3, Lines LP-5 and LP-6 indicate that the thickness of superficial deposits at Helfa Hall is >25 m. This is in accordance with resistivity Lines LP-1, LP-3 and LP-4, which suggest that the thickness of superficial sediments at this site exceeds at least 8 m, and the results of the seismic refraction survey (see Section 9.4.4).

9.4.3 Induced polarisation

The IP data from Line LP-1 and LP-4 (Figures 9.12a and 9.12d) suggest that the peat deposits within the central basins of the both Landform 1 and Landform 2 are chargeable. The chargeability of peat has been attributed to the high surface-charge density on partially decomposed organic matter (Hobbs 1986; Slater and Reeve 2002). As a result of this factor, the IP response of peat should contrast significantly with the IP response of mineral soil (Slater and Reeve 2002). As a consequence, IP surveys therefore provide a better technique for estimating the thickness of a peat deposit than electrical resistivity (Slater and Reeve 2002). Contrary to this conclusion, this study has found that IP surveys are not necessarily a suitable method for estimating the location of the peat-mineral soil boundary at all sites. Whilst the IP data at Helfa Hall does suggest that the peat at this site is chargeable, the high resistivity Zone LP-2 is more consistent with the direct geological sampling (Borehole 2) of peat thickness than the zone of high chargeability (e.g. Figure 9.12a). At Helfa Hall, electrical resistivity therefore provides a much better geophysical tool

for estimating the thickness of peat. This supports the argument that a suite of geophysical methods must be deployed during site surveys, as results for each technique can vary widely on a site-by-site basis depending on geological and hydrogeological conditions. Despite the positive results achieved from the resistivity method at Helfa Hall however, GPR will remain by far the best technique for estimating the thickness of peat deposits where the conductivity of peat is low (Theimier *et al.* 1994; Jol and Smith 1995).

The high chargeability 'bulls-eyed' shaped anomalies from IP Lines LP-5 and LP-6 (Figures 9.12e and 9.12f) are believed to be the result of noisy data. Although they partly correspond to the low resistivity Zone LP-3, the high values of chargeability do not extend throughout this layer. It is therefore likely that these high chargeability anomalies are the result of noisy data, perhaps caused by poor ground contact of electrodes. This interpretation is supported by the high root mean square (RMS) error of IP Line LP-6 (6.8%) (Figure 9.12f).

Although it is widely reported that the large surface area and cation exchange capacity of clays enables clay-rich deposits to store charge (e.g. Slater and Reeve 2002), this has not been observed, despite the high clay content of the glacio-lacustrine clays, at the Llanpumsaint site. IP data cannot always be used to reliably identify the presence of clay-rich materials, as the CEC is partly dependent on the density of the material (Turesson and Lind 2005). High densities of clay particles may reduce the CEC of a clay unit. Alternatively, ambiguous IP data may simply be a function of the insensitivity of raw chargeability measurements to lithological variation (Slater and Lesmes 2002), or noisy datasets (e.g. LP-5 and LP-6, Figures 9.12e and 9.12f). Calculation of the normalised chargeability, which is a direct measurement of surface polarisation processes, may improve the identification of clay-rich zones in IP data (Slater and Lesmes 2002).

9.4.4 Seismic refraction

The seismic refractor observed at a depth of 32 m is interpreted as rockhead. The two layers identified from the seismic survey at Llanpumsaint are therefore: i) a layer of unconsolidated superficial deposits; ii) bedrock (Figure 9.14). Based on the evidence from Borehole 1 (Figure 9.8a), the superficial deposits are dominated, at least in the

upper 8 m, by fine-grained silts and clays, interspersed with occasional thin units of sand and gravel. The velocity of the upper layer (1395 msec^{-1}) is consistent with P-wave velocities measured for similar glaciolacustrine sediments elsewhere in Wales (e.g. Camlad valley 1430-1500 msec^{-1}, Hussen 1998; Brabham *et al.* 2005). This layer corresponds with the very low resistivity zone (40-190 Ωm) of Zone LP-3.

The velocity of the second, high-velocity layer (4103 msec^{-1}) is greater than the recognised values for unconsolidated sediments (normally <2000 msec^{-1}). This layer must therefore represent unweathered bedrock, and the velocity is comparable to measured velocities for Silurian and Ordovician mudstones elsewhere in the region (see Section 5.4.3) and in previous studies (Allen 1960; Francis 1964). Rockhead is therefore interpreted at a depth of approximately 32 m (ca. 100 m OD). This corresponds with the depth of the high resistivity Zone LP-4 at the base of resistivity profiles LP-5 and LP-6 (Figures 9.12e and 9.12f), which was also interpreted as bedrock. Based on these two independent geophysical observations, a significant thickness of superficial deposits is interpreted to exist at this site (ca. 30 m).

The seismic data suggest that the velocity of the superficial deposits may increase at depth. Velocity calculations for the first refracted wave based on the reciprocal of the gradient of the best-fit lines for Shots 8, 9, 10, 11 and 12 varied between 1747 to 2451 msec^{-1} (average = 2065 msec^{-1}), compared to the average value of 1395 msec^{-1} calculated from minus graphs using Shots 1, 3, 5, 6, 7 and 13. This increase in velocity is not apparent on the traveltime graph (Figure 9.13) because the increase is not very pronounced (1395 msec^{-1} to 2065 msec^{-1}). This increase in velocity could represent a more consolidated superficial material (e.g. till or compacted clays) or a weathered bedrock layer between the glaciolacustrine deposits and unweathered bedrock. A higher P-wave velocity layer of this nature would result in an increase in the calculated depth to bedrock derived from the seismic survey. The presence of this layer is consistent with the increasing resistivity of Zone LP-3 at depth in resistivity lines LP-5 and LP-6.

10 Svalbard

10.1 Introduction: pingos and permafrost in Svalbard

To accurately classify relict forms interpreted as periglacial ground-ice mounds, modern analogue data on the internal structure (ground ice geometry and physical characteristics) of active pingos in the current permafrost zone are required (Pissart 1988). Studies of this type are rare however due to the lack of suitable exposures and the difficulties associated with the transportation and deployment of drilling equipment. This chapter presents results from ground penetrating radar (GPR) and electrical resistivity tomography surveys used to determine the internal structure (geometry and physical properties) of open system pingos on Svalbard. This research was primarily designed to provide reference data for the interpretation of relict landforms in Wales. Pingos in Svalbard were selected as suitable modern analogues because the current permafrost environment of the archipelago is comparable to that found in Western Europe during the late Pleistocene (Åkerman 1987), when permafrost aggraded on deglaciated terrain. The varied character and environmental contexts of Svalbard pingos means they have great potential to provide evidence for the origins and evolution of open system forms. Unfortunately however, previous investigations of pingos in Svalbard have focused primarily on their geomorphology and the geochemistry of the ground-ice or groundwaters (e.g. Orvin 1944; Piper and Porritt 1966; van Autenboer and Loy 1966; Svensson 1971; Åhman 1973; Liestøl 1977). With the exception of Yoshikawa (1993), detailed investigations of the internal structure remain rare.

Many open system pingos in Svalbard are located in areas where groundwater migration occurs through faults and other discontinuities (Orvin 1944; van Autenboer and Loy 1966; Liestøl 1977; Yoshikawa and Harada 1995). Liestøl (1977) proposed that groundwater supplying these open system pingos originated from meltwater at the base of polythermal glaciers. Downward flowing meltwaters from the glacier sole become confined within sub-permafrost bedrock aquifers below cold-based glacier margins and impermeable permafrost, where it may be forced down to significant depths and geothermally heated (Liestøl 1977) (Figure 2.5). Upwelling of this, frequently warm and mineralised groundwater, occurs preferentially through

292

geological structures in large, wide valleys, where the artesian head is greatest and the permafrost relatively thin, to form pingos. The flow path of this water will be strongly influenced both by permafrost and by geological structure (Liestøl 1977). Like open system pingos in Greenland (Müller 1959; Cruickshank and Colhoun 1965; O' Brien 1971; Allen at al 1976; Scholz and Baumann 1997; Worsley and Gurney 1996) a characteristic of many of these 'fault guided' pingos is the incorporation and heave of bedrock as well as superficial Quaternary sediments (van Autenboer and Loy 1966; Åhman 1973; Liestøl 1977). Many are also associated with perennial groundwater springs with high salt contents, which often form surface icings (Orvin 1944; Liestøl 1977).

It is also clear however, that the development of many pingos in Svalbard is also partly determined by changes in Holocene relative sea level. The lowermost pingos in Adventdalen, (Lagoon, Longyear and Hytte) (Figure 10.1) are found developed in highly frost-susceptible, saturated, fine-grained marine sediments, below the uppermost Holocene marine limit in inner Adventdalen at 62 m asl, where a raised beach is dated to 10,025±160 yrs BP (Lønne and Nemec 2004). As a consequence, it has been suggested that these pingos may be a derivative of the closed system type, caused by permafrost aggradation on isostatically uplifted marine sediments (Svensson 1971). However, these pingos have many features characteristic of the open system type, as they are clearly associated with groundwater seepage and surface icings (Orvin 1944; Liestøl 1977; Yoshikawa and Harada 1995). Other pingos located in similar settings elsewhere on Svalbard (e.g. Woodfjorden) may also be of a type related to the closed system model (Åhman 1973; Liestøl 1977; Pękala and Repelewska-Pękalowa 2004). Pingos developed within marine sediments of Holocene age or in nearshore settings have also been reported from the Canadian Arctic (Pissart 1967) and Greenland (Cruickshank and Colhoun 1965; O' Brien 1971; Yoshikawa 1991; Yoshikawa et al. 1996; Christiansen 1995). Because the overburden of many 'nearshore' pingos in Adventdalen (e.g. Longyear and Hytte), and in Reindalen and Grøndalen, does not incorporate evidence for terrestrial sedimentation, it has been suggested that many developed rapidly after glacio-isostatic emergence (Yoshikawa and Harada 1995). A number of these 'nearshore' pingos in Svalbard have been radiocarbon dated on the basis of material within or above the sediment covering the pingo surface (Svensson 1971; Åhman 1973; Yoshikawa and Nakamura 1996;

Humlum *unpublished*) but the majority are dated with less certainty, constrained by the timing of deglaciation and Holocene relative sea level curves (Landvik *et al.* 1998; Forman *et al.* 2004).

Permafrost in Svalbard is defined as continuous (Liestøl 1977; Åkerman 1987; Brown *et al.* 1997) but, due to the complexity of its glacial and sea level history, this definition disguises a great variability in permafrost thickness and distribution (Landvik *et al.* 1988; Humlum *et al.* 2003). Permafrost has been recorded by direct measurements at depths of 200-400 m below the ground surface in the mountains of Svalbard (Liestøl 1977; Christiansen *et al.* 2005). Based on the extrapolation of temperature profiles from boreholes, permafrost is 220 m thick at Janssonhaugen, inner Adventdalen (Figure 10.1) (Isaksen *et al.* 2001), and between 100-190 m thick in and around Longyearbyen (Gregersen and Eidsmoen 1988). 1D electrical resistivity surveys suggest that the thickness of permafrost varies between 3 m to 100 m in the nearshore area around Longyearbyen (Yoshikawa and Harada 1995; Harada and Yoshikawa 1996). Beneath the cold-based Foxfonna ice cap south of Adventdalen, permafrost is found at a depth of 290 m below rockhead (Christiansen *et al.* 2005). Generally, permafrost is estimated at 100 m thick beneath the floors of the major valleys (e.g. Longyearbyen and Reindalen) and up to 400-500 m below the high mountains (Orvin 1944; Liestøl 1977; Humlum *et al.* 2003).
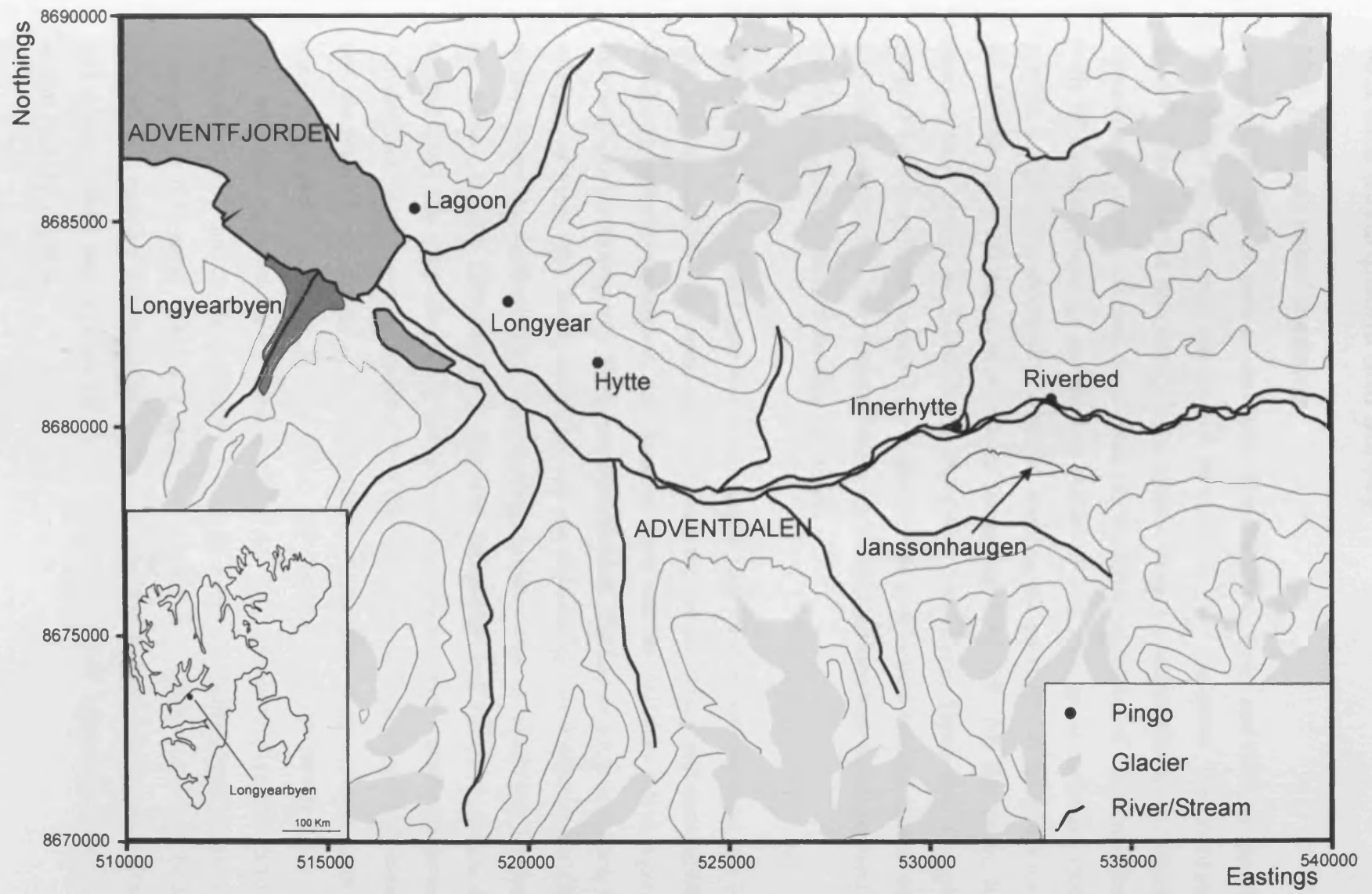
Figure 10.1: Location of Riverbed, Innerhytte, Hytte, Longyear and Lagoon pingos, Adventdalen, Svalbard. The location of the PACE borehole at Janssonhaugen is marked. Contours at intervals of 250 m.

10.2 Site descriptions and survey

10.2.1 Geophysical methods

Geophysical methods such as electrical resistivity tomography and GPR can provide key data on the geometry and internal structure of pingo ice-cores. The conceptual model of the internal structure of open system pingos assumes that they contain a simple plano-convex ice core. As a result, the electrical properties of a high resistivity body of massive pingo ice and the low resistivity host geological materials should provide a significant geophysical contrast, enabling the geometry of the pingo ice to be defined using 2D electrical resistivity tomography or GPR. For this study, four open system pingos in Adventdalen (Riverbed, Innerhytte, Hytte and Longyear pingos) were investigated using these methods. The geophysical method used at each site was determined by the substrate within which the landform was developed and by the degree of snow cover at the time of survey.

GPR surveys at Riverbed and Innerhytte pingos were undertaken between the 14th and 21st April 2004. This period was chosen as the use of sledges and snowmobiles facilitated equipment transport, and because there was no unfrozen active-layer to interfere with electromagnetic (EM) wave penetration. The key factor determining the selection of these sites for investigation was the well-recognised limitations of GPR at sites where the dominant superficial geology is silt or clay, or where groundwaters are saline (Jol and Bristow 2003). Because Innerhytte and Riverbed pingos are located above the upper altitudinal limit of fine-grained Holocene marine deposits in Adventdalen (which would significantly limit the penetration depth of EM waves) and are primarily developed in frozen Jurassic shales, these pingos were chosen as sites most suitable for GPR. A Pulse Ekko 100 GPR system with 50 Mhz and 100 Mhz antennae was used for the surveys (Section 3.5.3). Based on a limited common midpoint (CMP) survey, the propagation velocity of the electromagnetic waves was measured at 0.14 mns^{-1}. This is a relatively conservative estimate for both frozen bedrock and massive ice, which have values in the region of 0.13-0.16 mns^{-1} (Davis and Annan 1989), and is supported by velocity analysis of hyperbolic reflections within the GPR profiles.

The pingos located below the Holocene marine limit in lower Adventdalen (Longyear and Hytte), were deemed inappropriate for GPR survey because they are developed in, and uplift, fine-grained, saline marine clays. Electrical resistivity tomography was therefore selected as a suitable near-surface geophysical technique for the investigation of the internal structure of these landforms. All electrical resistivity tomography surveys in Svalbard were undertaken between 19th and 23rd April 2005, using an ABEM SAS 300C Terrameter instrument with an ES464 electrode selector (Section 3.2.3.2). In addition to surveys at Longyear and Hytte pingos, a single resistivity survey was also undertaken at Innerhytte pingo, but snow cover and topography restricted any other lines being acquired at this site. A planned survey of Riverbed pingo could not be performed because of the deep snow drifted against the pingo sides in April 2005. All resistivity survey lines used 2 cables with 20 electrodes takeouts each and an electrode spacing of either 4 m or 5 m (cable length of 156 m or 195 m), with measurements on the multi-electrode array made using the Wenner fast array. This array was selected because it is well adapted to highly resistive, heterogeneous materials with weak signal strengths (Vonder Mühll *et al.* 2001), and to optimise battery life under cold conditions.

10.2.2 Riverbed pingo

Riverbed pingo (Figure 10.2), located approximately 17.5 km east of Longyearbyen (Figure 10.1), is 12 m high (summit at 93 m asl), with dimensions of 90 m by 50 m. The pingo is developed in mid- to late Jurassic shales of the Agardhfjellet formation (Major *et al.* 2000), overlain by a superficial cover of alluvial gravels. An EDM derived map of Riverbed pingo shows that the landform is oval in plan, with an asymmetrical north-south profile resulting from fluvial incision on its southern flanks (Figure 10.3). Pronounced frost blisters were evident at the western end of the feature during March and April 2004 and to the south of the pingo in 2005. Piper and Porritt (1966) recorded massive, clean ice at depths of less than 1 m below the surface of the pingo, and further work by Yoshikawa (1993) has described the internal structure and crystallography of the ice core as revealed by a fluvially eroded section on the south side of the landform. Yoshikawa (1993) estimated a permafrost thickness of 15.5 m at Riverbed pingo based on 1D resistivity surveys, but this depth is likely to be a significant underestimate given that a permafrost depth of 22.8 m was also estimated
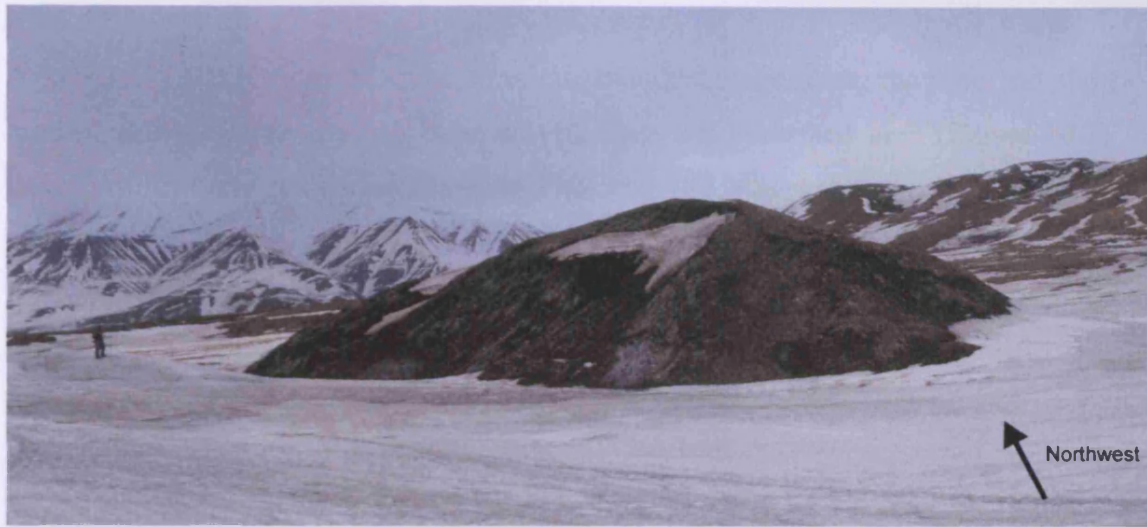
Figure 10.2: Riverbed pingo, Adventdalen, showing steep, fluvially incised southern flank. The person to the left of the photograph is standing on the surface of a seasonal frost blister.
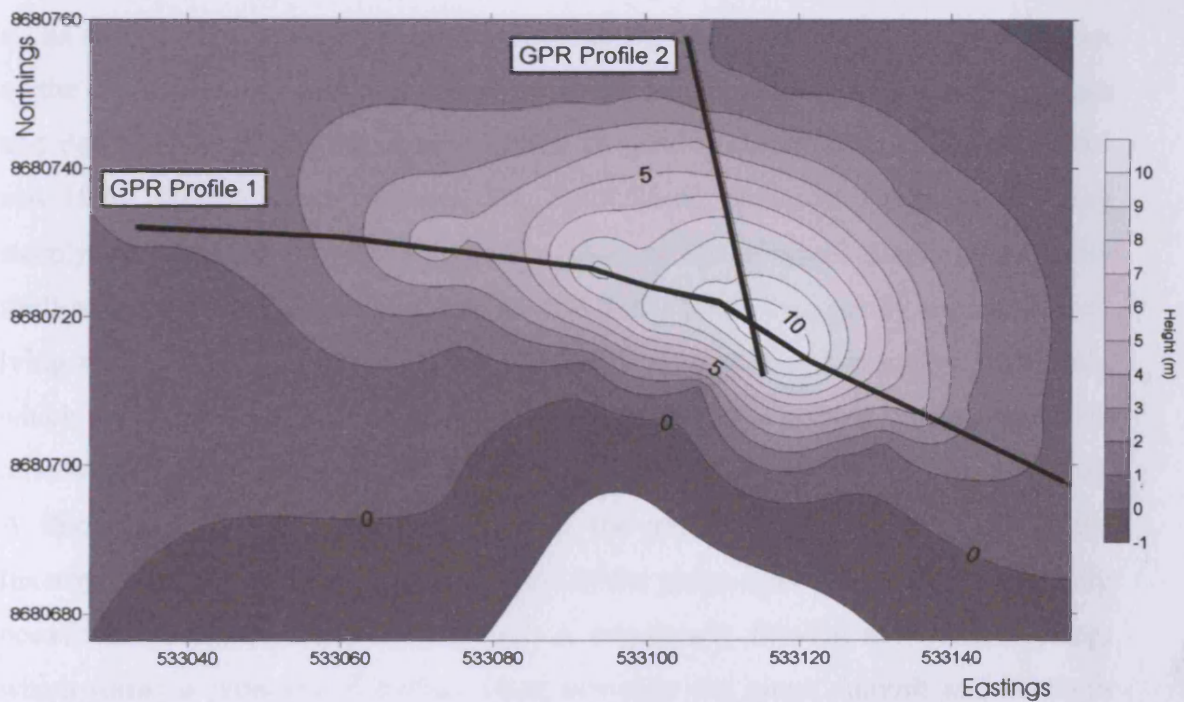
Figure 10.3: Map of Riverbed pingo, surveyed using an EDM. Contours at 1 m intervals. Locations of GPR survey lines (Profiles 1 and 2) indicated.

at Lagoon pingo near the shore of Adventfjord using the same technique (Yoshikawa and Harada 1995; Harada and Yoshikawa 1996).

A series of GPR profiles were measured at Riverbed pingo along the long and short axes of the landform. Two of these survey lines are presented here (Figure 10.3). Both profiles were completed using 50 Mhz and 100 Mhz antennae to evaluate the suitability of each frequency. As expected, the 100 Mhz antennae resulted in an increased resolution of survey. Surprisingly however, there was no apparent decrease in the depth of penetration between the 100 Mhz and 50 Mhz antennae. As a consequence, data from the higher frequency antennae are presented here.

10.2.3 Innerhytte pingo

Innerhytte pingo (Figure 10.4) (16 km east of Longyearbyen, dimensions 410 m by 200 m, 28 m in height, summit at 95 m asl), is located above the Holocene upper marine limit in inner Adventdalen (Figure 10.1) and is developed within, and uplifts, Jurassic shales of the Agardhfjellet formation (Major et al. 2000), which are exposed on its surface. The surface topography is complex, with the distinct, steep-sided apex of the pingo characterised by a crater containing several roughly concentric, ridges and depressions, displaying clear evidence for cryogenic disturbance (Figures 10.4 and 10.5). Due to fluvial incision, the south-facing flanks of the pingo dip very steeply down to the floodplain, but the slope of the northern flanks is markedly shallower. The main area of uplift is flanked to the north by a gently sloping, lower-lying zone (Figure 10.5), elevated only about 10 m above the Adventelva floodplain, which is characterised by ice wedge polygons or extensive tension cracks, but which otherwise displays little evidence for ground-ice disturbance (Piper and Porritt 1966). A thin cover of alluvial gravels overlies the gently sloping 'lower tier' of the Innerhytte feature, but this does not extend to the pingo apex where shales with only occasional sandstone clasts are exposed. A perennially flowing mineralised spring, which forms a pronounced surface icing covering the pingo summit and southern flank each winter (Figures 10.4 and 2.6), indicates that Innerhytte pingo is of the open system type (Orvin 1944; Liestol 1977). Piper and Porritt (1966) conducted the first investigations of Innerhytte pingo and produced a detailed topographic map of the landform. As at Riverbed pingo, massive, clean ice, which followed the surface
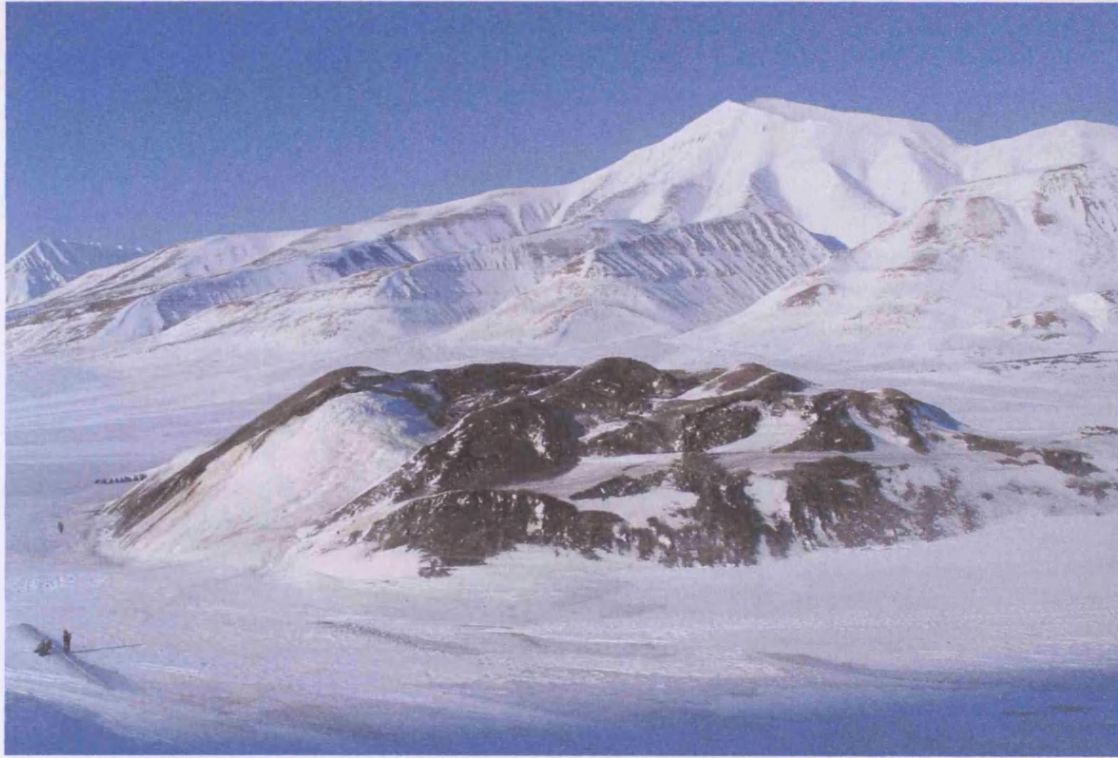
Figure 10.4: Innerhytte pingo, Adventdalen. Note the well developed surface icing on the southern flank of the pingo (left of photograph), the result of the perennial seepage of groundwater (see Figure 2.6), and the chaotic surface topography.
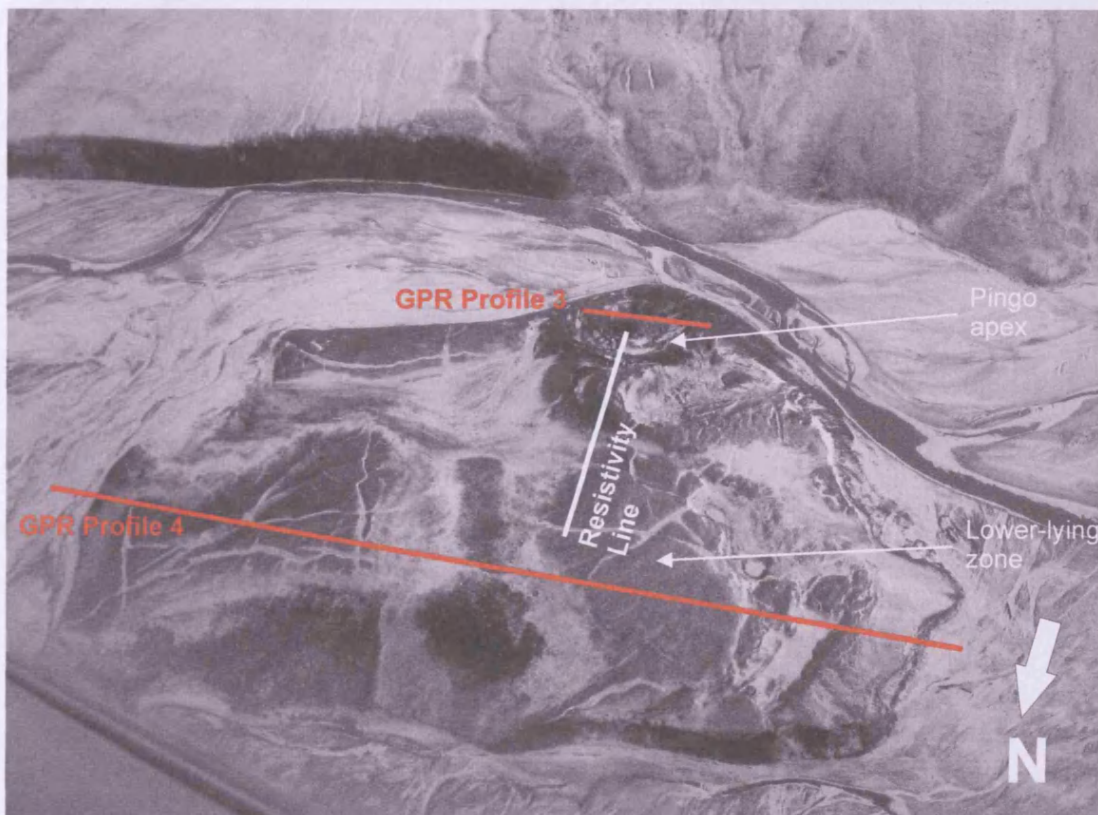
Figure 10.5: Oblique aerial photo of Innerhytte pingo, Adventdalen (Photo: I. Roer, September 2004). Locations of GPR and electrical resistivity lines indicated.

topography, was recorded at depths of less than 1 m below the surface of Innerhytte (Piper and Porritt 1966).

Two GPR survey lines are presented from Innerhytte pingo. Due to constraints on the survey time at Innerhytte, it was necessary to use different antennae depending on the length of the survey line. High-resolution 100 Mhz profiles were undertaken around the pingo apex and lower resolution 50 Mhz surveys over the lower gradient, lower tier zone (Figure 10.5). Because attenuation of the EM wave significantly limited the depth of investigation over much of the landform using radar techniques, the following year a complementary resistivity tomography survey was undertaken. This single survey line (4 m electrode spacing, 156 m long) ran roughly north to south from the gently sloping, flat lying area that characterises the northern part of the landform, up the north-facing flank and into the central crater at the pingo crest (Figure 10.5).

10.2.4 Hytte pingo

Hytte pingo (Figure 10.6) (dimensions 825 m long, 275 m wide and 20 m high), located 9 km to the west of Innerhytte pingo (Figure 10.1), is formed within marine muds deposited during early Holocene high relative sea levels. Shells from within these sediments have been radiocarbon dated to 6980±70 yr BP (Yoshikawa and Nakamura 1996) and 7405±65 yrs BP (AAR-7985) (previously unpublished date). Hytte pingo has a highly chaotic surface topography, with no clear pingo crest. The landform is composed of a series of small mounds and depressions, and is deeply incised by two southward flowing streams (Figure 10.7). Although apparently inactive since at least 1990 (Yoshikawa and Harada 1995), springflow and icing mound development were observed at Hytte pingo during 1924 (Orvin 1944) and 1971 (Liestøl 1977). A single resistivity survey tomogram (5 m spacing of electrodes, 195 m in length) was conducted at Hytte pingo, running roughly northwest to southeast, aligned along the long axis of the landform (Figure 10.7). Because the values of resistivity measured at this site are significantly lower than those recorded from Innerhytte pingo, the data are plotted using a different scale.

Figure 10.6: Hytte pingo, Adventdalen. Note the elongate form of this open system pingo, and its location on the valley floor at the base of a steep slope.

Figure 10.7: Oblique aerial photograph of Hytte pingo. The location of the electrical resistivity survey line is indicated.

10.2.5 Longyear pingo

Longyear pingo (Figure 10.8) is 300 m in diameter and about 15 m high. Like Hytte pingo, it is also developed within fine-grained marine sediments, but a radiocarbon age of 2650±55 yrs BP from driftwood within its overburden (Svensson 1971) and its location 3 km downvalley (Figure 10.1) suggests that it developed at a somewhat later stage. Longyear pingo has a much simpler morphology than Innerhytte and Hytte pingos, with a single rounded dome of uplifted material. The landform already displays initial evidence for decay, with an incipient crater developing at its crest and a well-developed drainage gully on its southeastern flank. Because Longyear pingo has a circular plan form, and has a less complex topography than Hytte pingo, it was possible to undertake two perpendicular survey lines at this site. Line 1 ran northwest to southeast and Line 2 ran from northeast to southwest (Figure 10.9). Both lines used electrode spacings of 4 m, but snow cover conditions on the pingo flanks meant that ground contact was not possible for all electrodes. As a result, Line 1 was 144 m long and Line 2 156 m long. The lines intersected at a distance of 76 m along line 1 and 84 m along Line 2. To facilitate easy comparison of the datasets, the resistivity tomograms from Longyear pingo are plotted using the same contour scale as Hytte pingo.

Figure 10.8: Longyear pingo, Adventdalen. This landform is positioned on the valley floor, at the base of a steep slope, a typical location for open system pingos development.
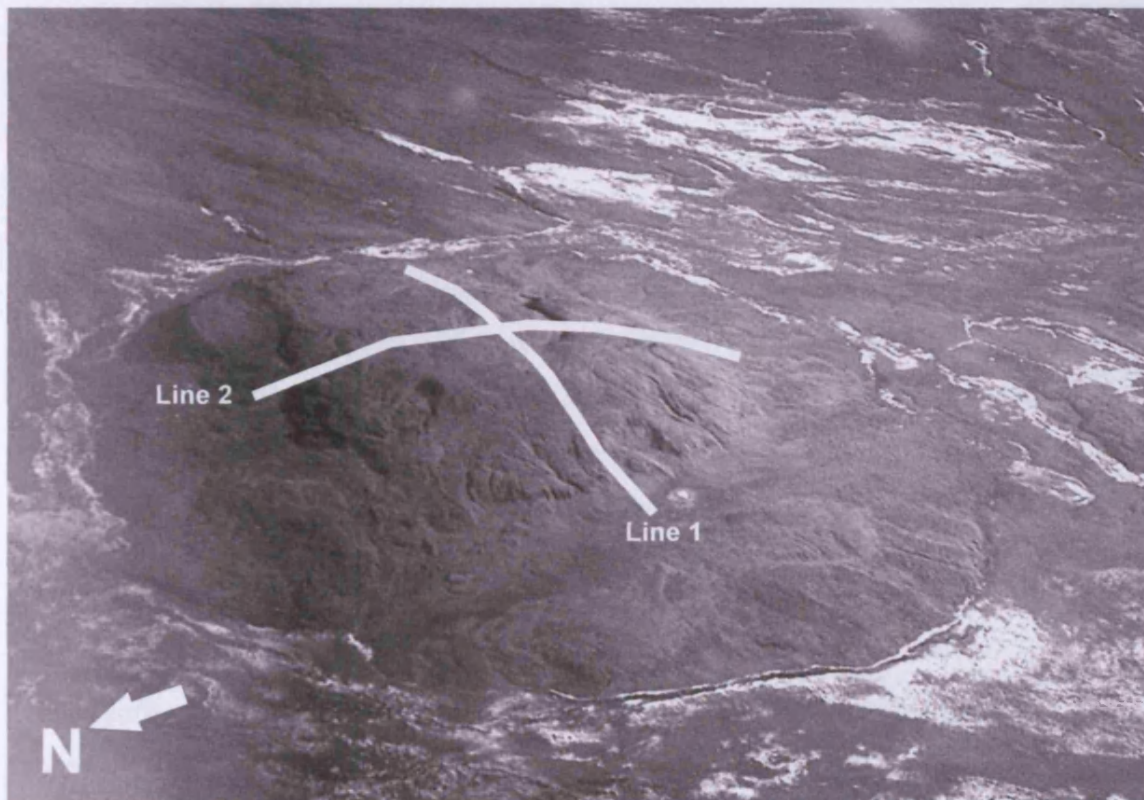
Figure 10.9: Oblique aerial photograph of Longyear pingo. The location of the electrical resistivity survey lines are indicated.

10.3 Results

10.3.1 Riverbed pingo: GPR surveys

GPR Profile 1 (Figure 10.10) was conducted from west to east along the length of Riverbed pingo (Figure 10.3). The profile is characterised by a high degree of variability in the depth of penetration of the radar signal, with up to 10 m of penetration on the western flank in contrast to approximately 5 m on the top of the feature. The central zone of the profile is characterised by complex chaotic reflections, with little or no lateral continuation. This is in contrast to the continuous planar horizontal sub-surface reflectors parallel to the valley floor adjacent to the pingo. The best example of these horizontal reflectors is between 0-45 m at the western-most edge of the landform. Between 25-45 m these reflectors appear to be uplifted, particularly beneath the surface icing whose surface form the reflectors parallel. Steeply dipping reflections (>45°) which are sub-parallel to the sides of the pingo are apparent within both flanks but are more markedly pronounced on the west side between 45-60 m. Between 60-70 m these reflections become less steeply dipping but due to the poor signal penetration around the centre of the pingo they cannot be traced across the landform.

More than five steeply dipping reflections are also apparent beneath the northernmost flank of the pingo in Profile 2 (Figure 10.11). Although they are roughly sub-parallel to the ground surface, these reflections are clearly more steeply dipping. Signal penetration is again relatively shallow beneath the top of the pingo where the reflections are characterised by complex chaotic reflections similar to those recorded in Profile 1. A GPR profile of the southern flank of Riverbed pingo could not be obtained due to its steep gradient.

10.3.2 Innerhytte pingo: GPR and resistivity surveys

GPR Profile 3 (Figure 10.12) crosses the apex of Innerhytte pingo (Figure 10.5), where thermokarst processes have resulted in the development of complex crater topography, suggesting ice near to the ground surface. The profile was only a few metres from a conspicuous surface icing. Like Riverbed pingo, the depth of penetration varied widely. Penetration was approximately 10 m between profile
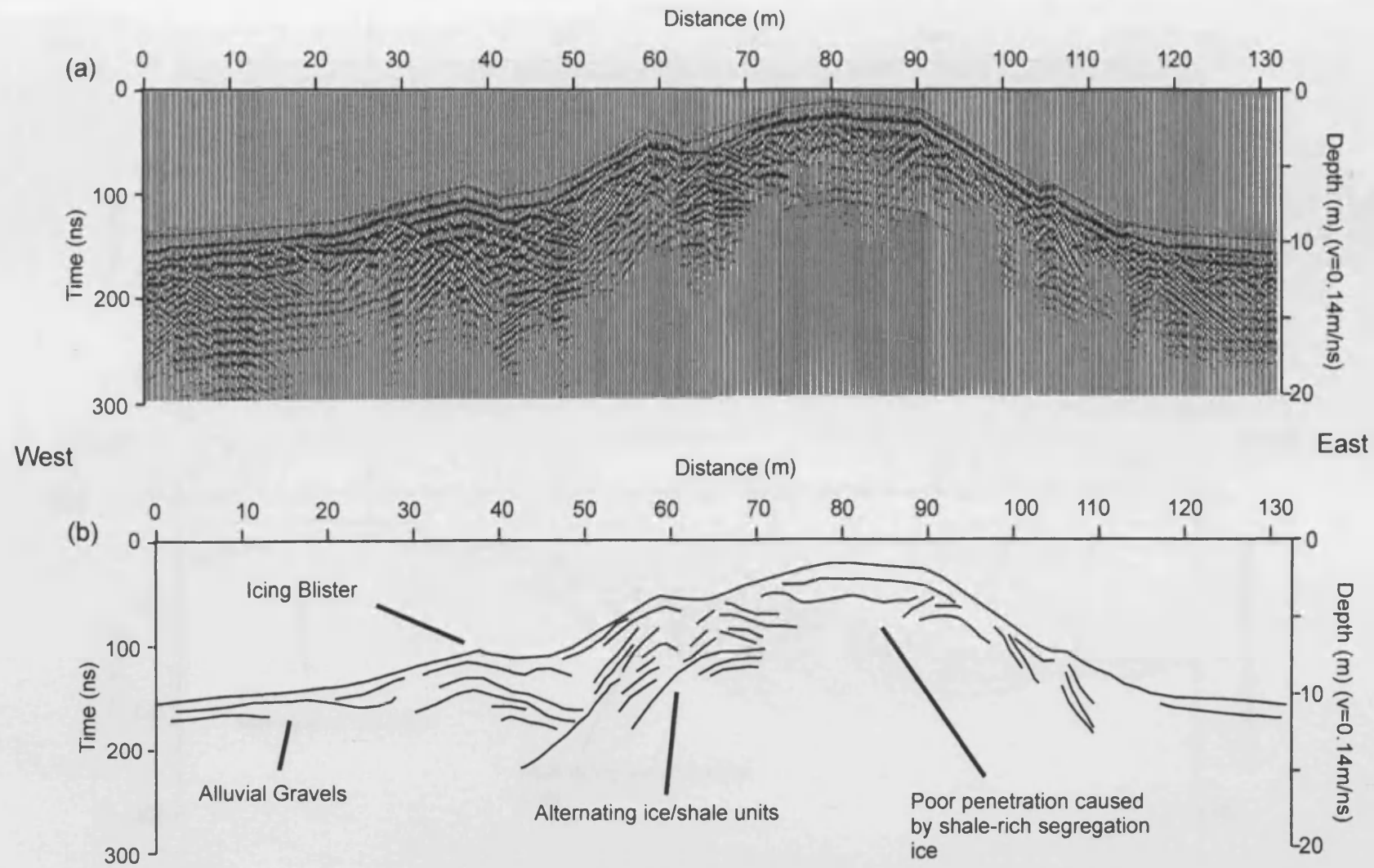
Figure 10.10: Ground penetrating radar Profile 1, Riverbed pingo, Adventdalen: (a) 100 MHz GPR data; (b) Interpretation.
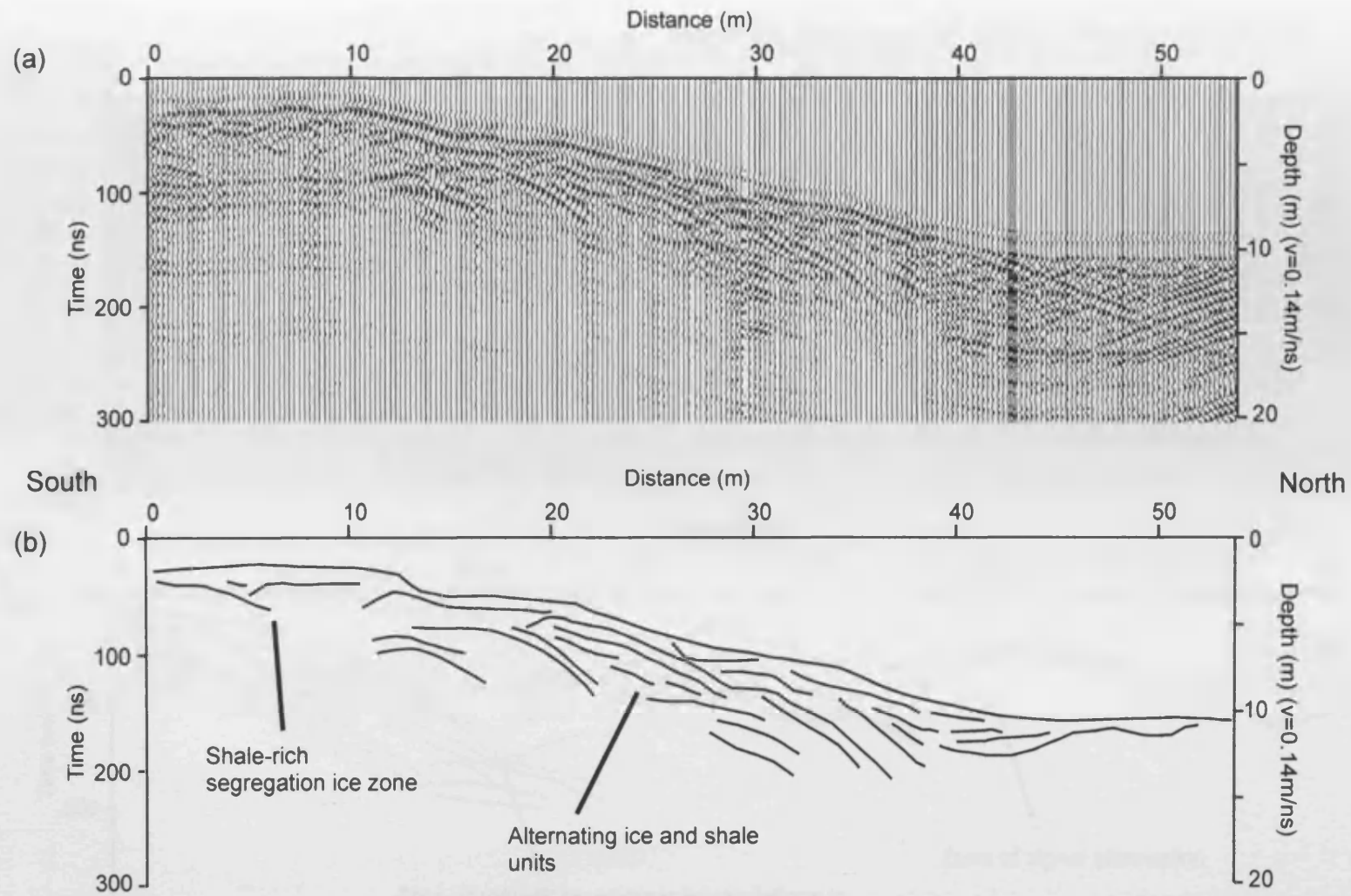
Figure 10.11: Ground penetrating radar Profile 2, Riverbed pingo, Adventdalen: (a) 100 MHz GPR data; (b) Interpretation.
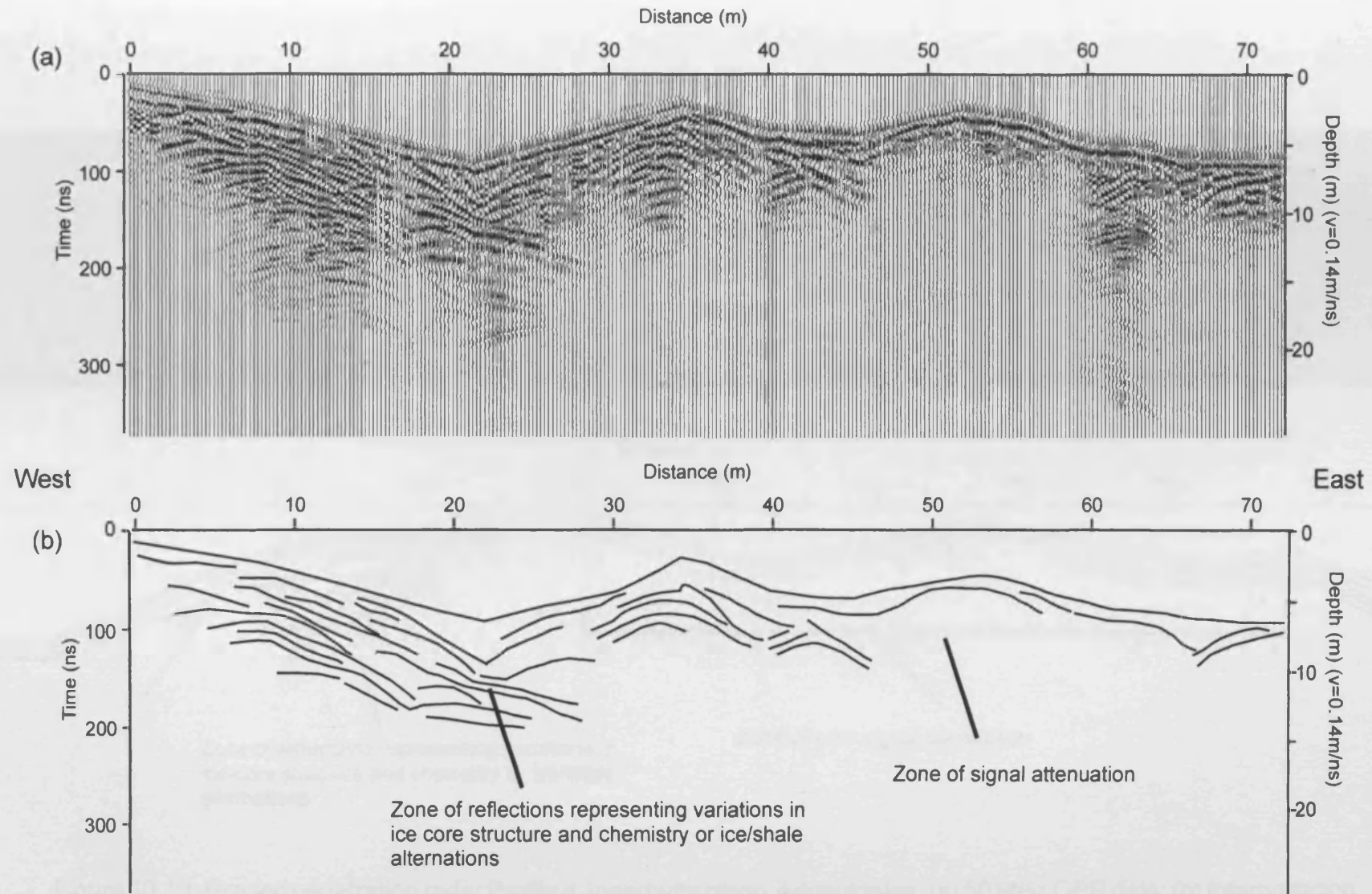
Figure 10.12: Ground penetrating radar Profile 3, Innerhytte pingo, Adventdalen: (a) 100 MHz GPR data; (b) Interpretation.
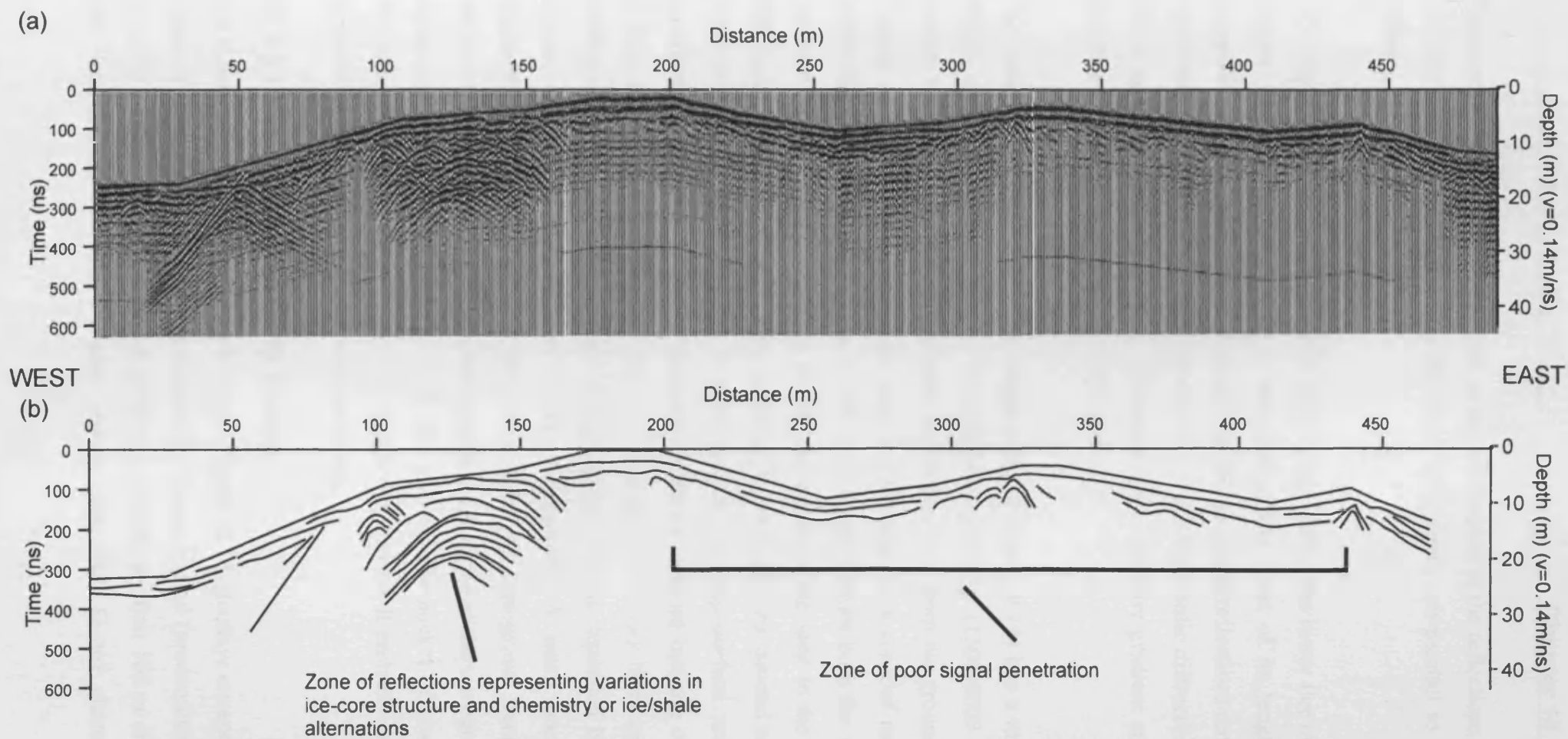
Figure 10.13: Ground penetrating radar Profile 4, Innerhytte pingo, Adventdalen: (a) 50 MHz GPR data; (b) Interpretation.

distances of 0 and 30 m. Although not as steeply dipping as the reflections recorded at Riverbed pingo, the reflections in this zone were again sub-parallel to the ground surface.

GPR Profile 4 (Figure 10.13) trended west to east across the lower tier of Innerhytte (Figure 10.5). Signal penetration is poor throughout most of its length with the exception of the western edge of the landform where strong reflections reminiscent of hyperbolic diffractions are located. In contrast to the hyperbolic diffractions at 45 m, 320 m and 440 m however, these reflections have very low gradient arms and are therefore more likely to be primary structures.

The resistivity tomogram from Innerhytte pingo (Figure 10.14) has a marked near-surface zone of relatively low to intermediate resistivity (1500-6000 Ω m) that extends laterally across the entire profile, and downwards from the ground surface to a depth of 3-4 m. This near-surface layer is underlain by a zone of much greater resistivity (6000-30,000 Ω m) that is well developed beneath both the steep upper flanks of the pingo and beneath the gently sloping flat-lying zone to the north. This high resistivity zone extends from a depth of 3-4 m below the ground surface, to a depth of at least 20-25 m. The contact between the near-surface zone and the underlying zone of high resistivity is relatively abrupt, with an increase of ca. >6000 Ω m in a vertical distance of less than 5 m. The high resistivity layer appears to be divided into two clear zones of very high resistivity that are separated by a vertical column with intermediate to high values of resistivity. A small pocket of low resistivity exists at the bottom right of the resistivity tomogram. Because of the uncertainty associated with the model blocks at the margins of the tomogram, and the coarseness of the model blocks used in this survey, this pocket of low resistivity should not be considered as geologically significant. Instead, it probably represents an anomalous value, associated with data processing.

10.3.3 Hytte pingo: resistivity survey

The resistivity tomogram from Hytte pingo (Figure 10.15) displays exceptionally low values of electrical resistivity for permanently frozen ground (predominantly 10-100 Ω m, but ranging up to 400 Ω m) at all depths beneath the first 100 m of the survey line. Intermediate to relatively high values (400-3000 Ω m) characterise the
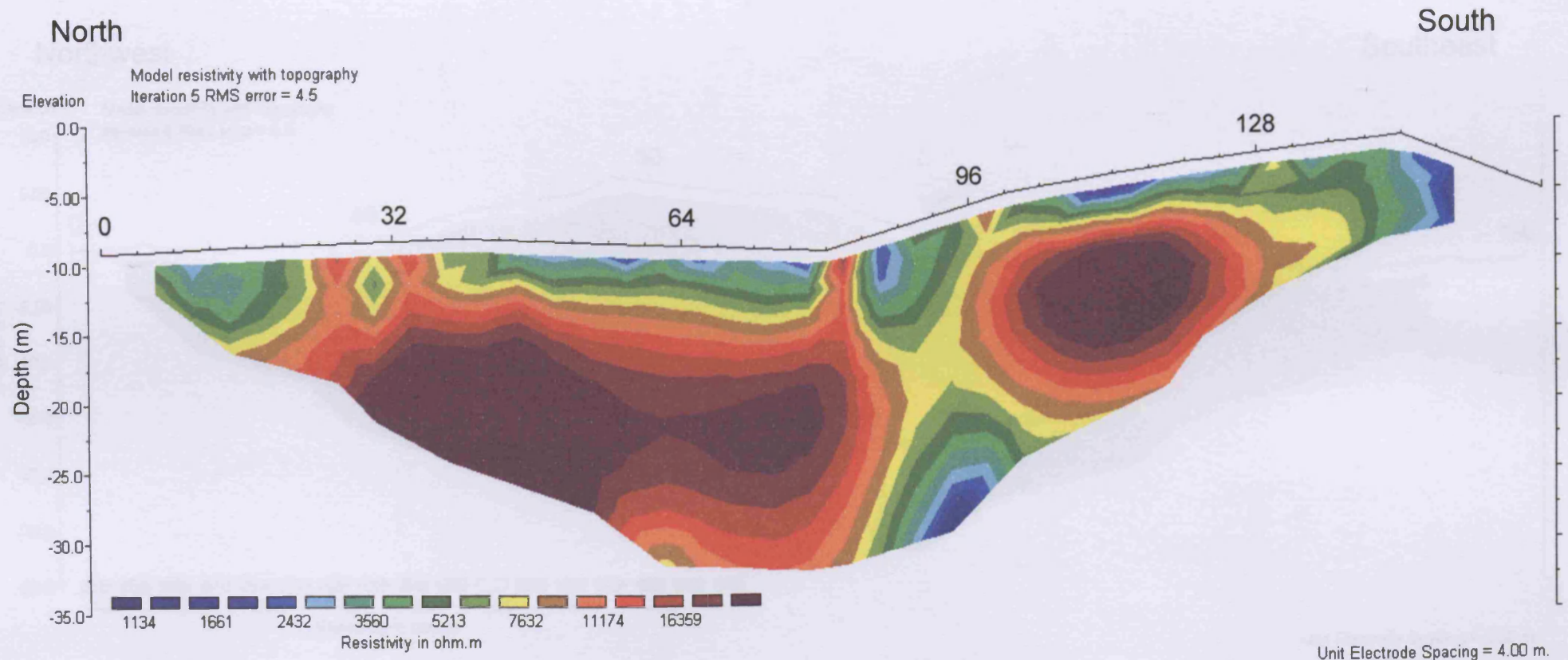
Figure 10.14: Electrical resistivity tomogram from Innerhytte pingo, Adventdalen. Data plotted using a different contouring scale to that of Hytte and Longyear pingos.
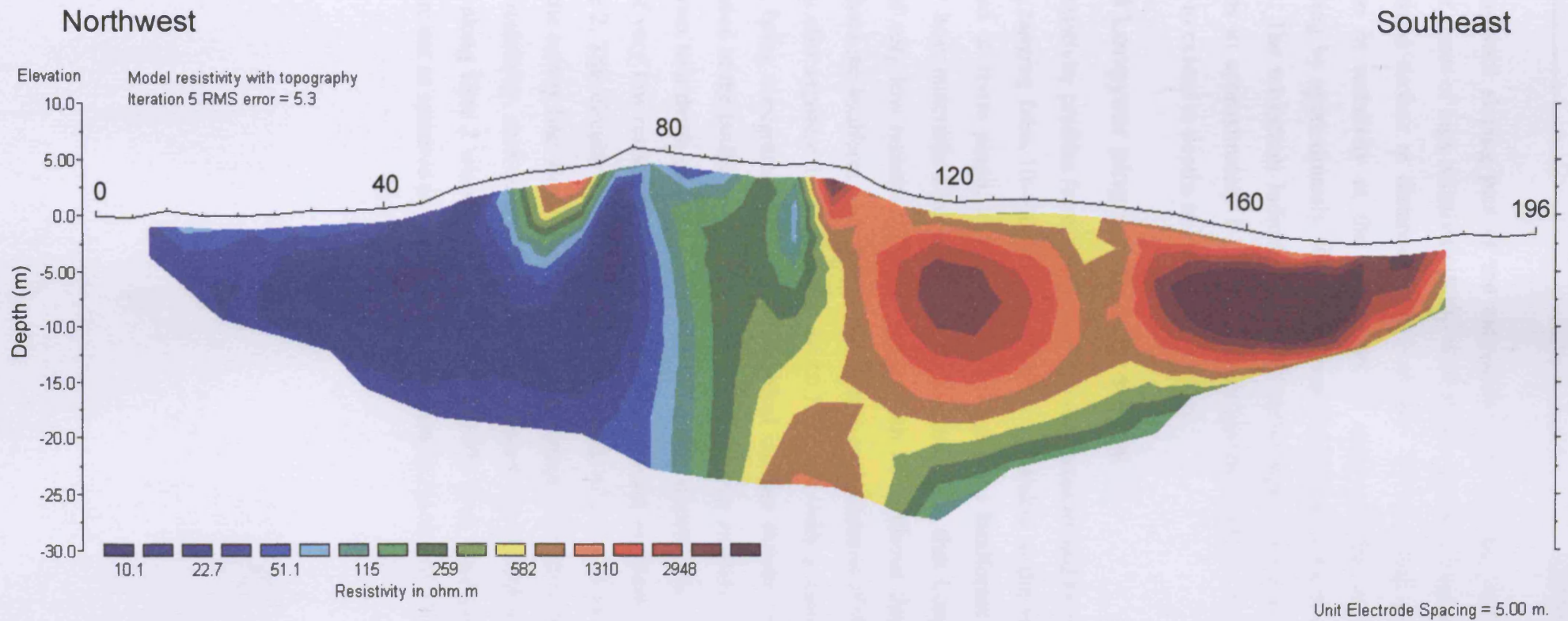
Figure 10.15: Electrical resistivity tomogram from Hytte pingo, Adventdalen. Data plotted using the same contouring scale as Figures 10.16a and 10.16b.

southeastward sloping part of the tomogram (100-196 m), with two pronounced circular zones of high resistivity (900->4000 Ω m) centred at depths of 5-10 m below the ground surface at distances of 120 m and 160 m along the tomogram. The increase in resistivity at the boundaries of these circular anomalies is abrupt, increasing by approximately 1000 Ω m over lateral and vertical distances of a few metres. The tomogram indicates that both these high resistivity anomalies extend upwards to approximately 1-2.5 m from the ground surface, but that they do not appear to extend to depths in excess of 15-20 m.

10.3.4 Longyear pingo: resistivity survey

Both resistivity profiles from Longyear pingo are characterised by very low resistivity values, ranging from 10-400 Ω m. These are comparable to the values of resistivity recorded at Hytte pingo, as might be expected from landforms developed within similar host materials. Line 1 (Figure 10.16a) indicates that Longyear pingo has a zone of very low resistivity (<50 Ω m) beneath its southeast flank, which extends throughout the landform from the ground surface to the bottom of the tomogram. This zone is also apparent in Line 2 (Figure 10.16b), but with a more restricted lateral extent, being concentrated in a narrow vertical column directly beneath the central depression of the landform. This plume of low resistivity extends from the base of the tomogram to a depth of 2.5-5 m beneath the central depression. A second, localised zone of very low resistivity is also apparent beneath the northeast flank of the pingo in Line 2. This circular anomaly is found at a depth of 2.5-12.5 m and from 24-40 m along the survey line. Both lines from Longyear pingo also have localised pockets of higher resistivity, such as at depths of 0-10 m beneath the ground surface between 96-136 m along Line 2 where resistivities of 250-1000 Ω m were measured. However, these are not as resistive as the anomalies apparent in the single tomogram from Hytte pingo.
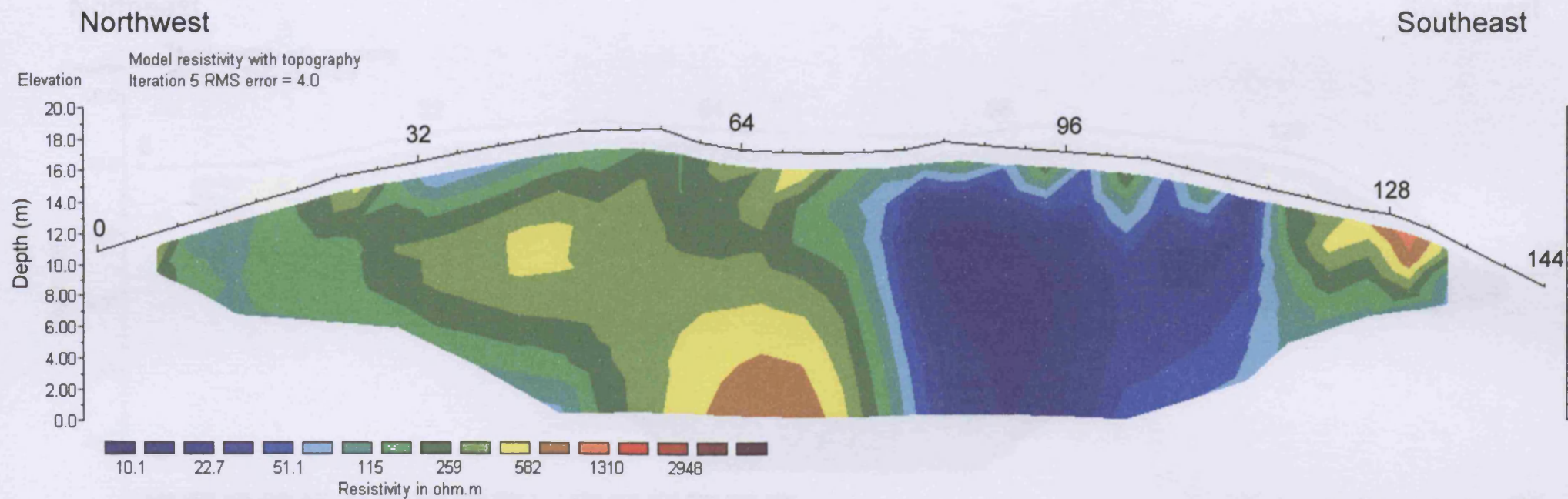
Figure 10.16a: Electrical resistivity tomogram Line 1 from Longyear pingo, Adventdalen. Data plotted using the same contouring scale as Figures 10.15 and 10.16b.
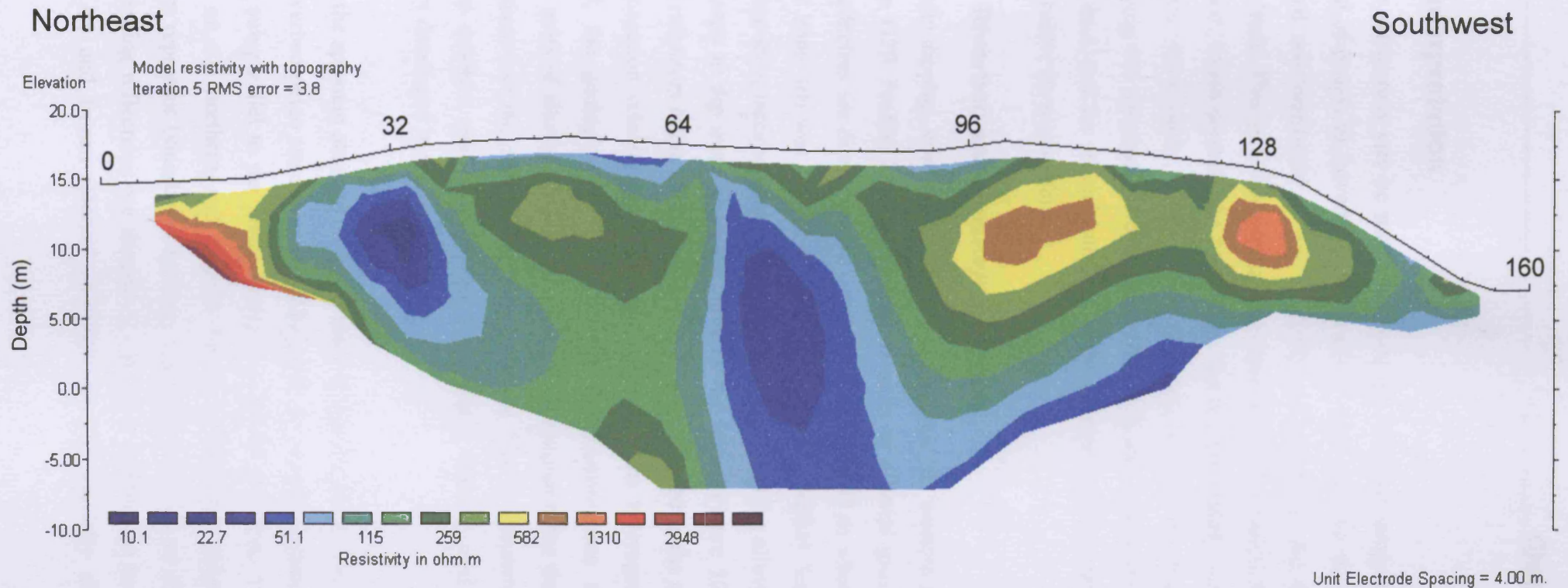
Figure 10.16b: Electrical resistivity tomogram Line 2 from Longyear pingo, Adventdalen. Data plotted using the same contouring scale as Figures 10.15 and 10.16a.

10.4 Interpretation

A clear distinction can be made between the physical properties of the internal structure of pingos in Adventdalen depending upon whether they are located above (Riverbed and Innerhytte) or below (Hytte and Longyear) the maximum Holocene marine limit. This is a function of the material within which these landforms are developed, which controls the type of ground ice responsible for the uplift of these landforms. As a result, this section is therefore divided into two sections, the first interpreting the geophysical data from Riverbed and Innerhytte pingos, above the marine limit, and the second interpreting the surveys of Hytte and Longyear pingos, located below the marine limit.

10.4.1 Riverbed and Innerhytte pingos

The gently dipping, continuous reflectors that drape the western margin of Riverbed pingo in GPR Profile 1 are interpreted as units of alluvial gravels (Figure 10.10). These reflectors are disturbed and uplifted between 30-45 m where they underlie the seasonal icing that was developed in the winter of 2003-2004. Exposures reveal that the surface icing incorporated thick bands of gravel from the alluvial cover. These are clearly seen to dip away from the apex of the icing (Figure 10.10). Although the uplifted reflectors in the GPR profiles could be interpreted as the result of a change in the propagation velocity of radar signal caused by the heterogeneity of subsurface material, the geological evidence favours the interpretation that they represent uplifted units of alluvial gravel. The GPR profiles suggest that these gravel bands do not continue into the core of the pingo however. This is supported by exposures on the steep southern side of the pingo, which show that the landform appears to be primarily developed in shales.

Despite the apparent absence of gravel units within the pingo core, both GPR profiles from Riverbed pingo are characterised by gentle to steeply dipping reflections that lie roughly sub-parallel to the pingo flanks (e.g. 45-60 m Figure 10.10). Most clearly defined on the northern and western flanks of Riverbed pingo, these onlapping reflectors represent boundaries between materials of different dielectric properties. These dipping reflections are thought to represent alternations between thin units of ground ice and frozen mineral material, probably partially disaggregated shale.

Although strong continuous reflectors can be generated by the dielectric contrast between zones of clear ice and ice with high air bubble content (Annan and Davis 1976; Moorman and Michel 2000), the evidence for units of segregation and injection ice alternating with units of shale observed by Yoshikawa (1993) at this site supports the former interpretation. Each of the 4-6 layers of ice described by Yoshikawa was approximately 0.5 m thick (Matsuoka *et al.* 2004). The strong dipping reflections apparent in GPR Profiles 1 & 2 (Figures 10.10 and 10.11) may therefore reflect the strong contrast between ice-rich layers, interspersed with units of shale, in the uppermost parts of Riverbed pingo. Alternating bands of ice and sediment have also been recorded above pure ice cores from sections and drill holes through pingos in Canada (e.g. Porsild 1938; Müller 1959, 1962; Mackay and Stager 1966; Rampton and Mackay 1971; Tarnocai and Netterville 1976; Pissart and French 1976).

The GPR surveys at Riverbed pingo were unable to image the geometry of a massive ice-core. Because massive ice has homogenous dielectric properties and is highly resistive, EM waves will propagate rapidly (0.16 mns^{-1}) through ground-ice without producing internal reflections (Moorman and Michel 2000). However, below the upper few metres of the GPR profiles, no reflections that might be interpreted as the base of a massive ice body were observed. Such reflections would be expected from a contact between ground-ice and bedrock, or between ground-ice and a sub-pingo water lens because of the contrasting dielectric properties of these materials. The lack of a basal reflection may be due to signal attenuation beneath the top of the pingo caused by a greater thickness of shale overburden and/or the absence of thin (0.5 m thick) units of massive ice within the shale. Signal attenuation can also be caused by intra-permafrost scattering of EM waves resulting from the presence of high concentrations of segregation ice (Arcone *et al.* 1998; Moorman *et al.* 2003). Such scattering of the GPR signal is suggested in the central zone of Profile 1 (70-90 m) where the data is characterised by complex chaotic reflections with little or no lateral continuation, and shallow signal penetration. These chaotic reflections are similar to those described by Moorman *et al.* (2003) as being produced by segregation ice. This is supported by the observations of Yoshikawa (1993) who describes segregation ice in the uppermost part of the section in the southern flank of the pingo. Whereas shale, rich in segregation ice, near the top of the pingo may have caused the observed signal attenuation with no clear reflectors, alternating units of injection ice and shale within

the flanks could result in the much clearer, stronger reflections apparent in GPR Profiles 1 and 2 (Figures 10.10 and 10.11).

GPR Profile 3 (Figure 10.12) displays reflections that are interpreted as representing the internal structure of the ice core at the apex of Innerhytte pingo. Given that Piper and Porritt (1966) record massive ice at a depth of 1 m, these reflections are likely to represent internal structures within the ice. These reflections may be due to the presence of units of shale interspersed with bodies of injection ice, similar to those described from Riverbed pingo. With the exception of the surface icings, ice was not visible at or near the surface of either pingo during the period in which the GPR surveys were conducted. The ground-ice described by Piper and Porritt (1966) at Innerhytte was found only beneath the area of the pingo apex, and followed the surface topography, contained air bubbles, but was free of rock debris. In the absence of observational evidence for rock debris within the ice core of Innerhytte pingo it is difficult to unequivocally argue that the internal reflectors recorded in Profile 3 represent such ice-shale alternations and it may be that variations in the chemistry, ice crystal properties or air content of the ice core may be the cause of these reflections. At Riverbed pingo, Yoshikawa (1993) described stratification of the basal pingo ice, interpreting these structures as the result of seasonal changes in the freezing of new ice onto the base of the ice body. The layering followed the shape of the pingo surface as it was uplifted by the freezing of water at the centre of the base of the ice body. Such variations in the structure of pingo ice have also been recorded from closed system pingos in Canada (Pissart and French 1976; Gell 1978; Mackay 1985, 1990) and in icing mounds (Pollard and French 1983, 1984, 1985), where they were due to variations in the content of air bubbles. Internal layering of subsurface ice has also been recognised from GPR surveys of several closed system pingos in Alaska (Kovacs and Morey 1985). Such reflections corresponded with units of sandy ice and layers of varying air bubble arrangements and geometries recorded from cores through the pingo ice. Variations of this nature could result in the apparent 'banding' of pingo ice suggested by the GPR reflections within Profile 3. However, without borehole control such interpretations should be regarded as preliminary in nature.

It is significant that Piper and Porritt did not locate ice within 1.2 m of the surface beneath the more gently sloping, flat-lying northern zone of Innerhytte pingo, which

they describe as "having little evidence for ice action" (p. 84). They did however believe that ice existed at depth, as the topography did not suggest that this sector was derived from slope processes on the pingo apex (Piper and Porritt 1966). GPR Profile 4 (Figure 10.13) was conducted across this intermediate level of the pingo. Between 90-160 m the depth of signal penetration is greater than 10 m. The arching layered reflections are similar in structure and in scale to those found around the pingo apex and may therefore suggest the presence of a buried ice mass. The poor depth of signal penetration and the absence of radar reflections in the area between 170-500 m on this profile (Figure 10.13) are interpreted as the result of a high degree of signal attenuation by shale with a low massive ice content. The lack of massive ice in this part of the pingo suggested by radar Profile 4 may be due either to an almost complete absence of ground-ice development in this area, or the absence of any significant volumes in the upper few metres, within the depth penetration range of the EM waves.

As was the case at Riverbed pingo, no clear reflection that could be interpreted as delimiting the base of the ice-core was recognised from either of the two GPR profiles from Innerhytte pingo. This is surprising given that GPR surveys of glacial ice masses commonly delimit the ice-bedrock interface (Plewes and Hubbard 2001). Although the presence of a body of highly conductive saline groundwater beneath the ice body at Innerhytte, as suggested by geochemical analysis of the spring waters (Orvin 1944; Liestøl 1977), could cause attenuation of the radar waves, a strong reflection from the interface between the pingo ice and such a body would be expected. Alternatively it could be that the boundary between the ice body and underlying shales is gradational, causing no clear reflections. Buried ice bodies, mapped from GPR profiles of the internal structure of the moraine of Scott Turnerbreen in Bolterdalen, a tributary valley of Adventdalen, also appear to have no clear basal reflections (Lønne and Lauritsen 1996). Determination of the basal geometry of pingo ice therefore awaits the application of further geophysical and/or borehole investigations at Riverbed and Innerhytte pingos.

Previous investigations of the north-facing flanks of Innerhytte pingo (Piper and Porritt 1966), and GPR Profile 4 suggest that ground ice is either found at significant depth below the ground surface, or that there is a complete absence of massive

ground ice development beneath that part of the pingo. Both interpretations may be consistent with the resistivity data (Figure 10.14). The high values of resistivity (5-25 kΩ m) that dominate the resistivity tomogram from Innerhytte pingo (Figure 10.14) could be interpreted either as ice-rich frozen bedrock or as large lenses of massive ice. However, without borehole calibration of the dataset it is very difficult to make an unequivocal interpretation. Although values of resistivity comparable to those at Innerhytte pingo have been measured from ground-ice bodies (see Haeberli and Vonder Mühll 1996) these values are exceptionally low for massive ground ice, most measurements being greater than 1 MΩ m. The resistivity measurements at Innerhytte pingo are also within the range of frozen bedrock. 1D resistivity soundings and profiling at the nearby PACE drillsite at Janssonhaugen (Figure 10.1), where the bedrock is a relatively homogenous sandstone, gave a range of apparent resistivity values from 8 kΩ m to 30 kΩ m in the upper 20-30 m (Ketil Isaksen *personal communication*). Although the bedrock type is shale rather than sandstone, the high values of resistivity at Innerhytte pingo could also represent ice-rich permanently frozen bedrock. It is widely acknowledged that high resistivity anomalies in permafrost environments are not always the result of the presence of ground ice. Ice, air and certain rock types can have very similar high resistivities because they all act as electrical insulators. Therefore, without additional information from complementary geophysical methods or borehole control, distinguishing between these very different materials can be difficult (Hauck and Vonder Mühll 2003a, 2003c). Deriving the P-wave velocity of the high resistivity zone at Innerhytte pingo using seismic refraction tomography could therefore assist in distinguishing whether this unit is composed of massive ice or ice-rich frozen bedrock.

Because the resistivity surveys at Innerhytte pingo were undertaken during the late winter period, the near-surface layer of low to intermediate resistivity (Figure 10.14) cannot represent a thawed active layer. As a result, this uppermost zone must represent frozen bedrock. The relatively low resistivity of this layer, in comparison to the values at depth, is likely to be a function of weathering of the upper few metres of bedrock. Weathering of bedrock in this environment is evident from the highly friable pieces of shale that scatter the surface of this and other pingos developed in bedrock in Svalbard. The depth of weathering may be related to the depth of summertime active layer processes. During the summers of 1998 and 1999, the depth

of the active layer at Janssonhaugen was 1.54 m and 1.42 m respectively (Isaksen *et al.* 2001).

10.4.2 Hytte and Longyear pingos

At both Longyear and Hytte pingos (Figures 10.15 and 10.16), resistivity values were exceptionally low for permanently frozen ground (<2000 Ω m), apparently inconsistent with the presence of a large body of massive ground ice. These low values of resistivity cannot be attributed to warm permafrost however. Although air temperatures were relatively high during the period of survey, ground temperatures (and therefore ground resistivity) within permafrost should be at their lowest in early spring (Hauck and Vonder Mühll 2003b). This is particularly true of pingos, where deflation results in snow-free conditions throughout the winter on the summit and upper flanks. Even at the end of summer, the unfrozen active layer at both Hytte and Longyear pingos will be less than 2 m and resistivity values at depths below this should not vary significantly, if at all, during the course of the year.

An alternative explanation is that a plano-convex lens of massive ice does not exist beneath Hytte or Longyear pingo. Instead, the internal structure of these landforms may be dominated by segregation ice and possibly small, localised pockets of massive ice. Segregation ice plays an important role in the heave of a variety of ground-ice mounds such as palsas and lithalsas (Åhman 1976; Allard *et al.* 1987; Seppälä 1988b; Allard and Rousseau 1999; Pissart 2002) and has been recorded within many pingos (Müller 1959; Pissart and French 1976; Mackay 1973, 1998). In Adventdalen, segregation ice has been observed within both Lagoon and Riverbed pingos (Åhman 1973; Yoshikawa 1993). Because Hytte and Longyear pingos are developed within highly frost-susceptible marine muds, then the development of segregation ice during permafrost aggradation following subaerial exposure of the materials is probable. If the uplift of these landforms is the result of lenses of segregation ice, then a significant proportion of their internal structure will be composed of minerogenic sediments, which might explain both the complex distribution of resistivity and the apparently uncharacteristically low values.

Because of the contrast in electrical properties of ice and water, the resistivity of frozen ice-rich materials (both superficial sediments and bedrock) is significantly

higher than the same material in its unfrozen state (Hoekstra *et al.* 1975; King *et al.* 1988; Scott *et al.* 1990; Hauck and Vonder Mühll 2003c). This increase in resistivity is more pronounced in coarse-grained sediments however. Fine-grained sediments such as clays can have very low resistivity (100-1000 Ω m) even when frozen at temperatures below –5°C (Scott *et al.* 1990) because of their high, unfrozen water contents. Films of unfrozen, adsorbed water enable electrolytic conduction through ionic transport in solution, giving anomalously low resistivity measurements (King *et al.* 1988). The high levels of dissolved salts recorded within marine muds in lower Adventdalen (Humlum *et al.* 2003) could further influence the electrical properties of Hytte and Longyear pingos by further depressing the soil water freezing point (Anderson and Morgenstern 1973; Furuberg and Berggren 1988; Scott *et al.* 1990; Brouchkov 2002). Because of solute rejection during freezing, the concentration of dissolved ions in the pore waters will increase as the pore water gradually freezes, further depressing the freezing point of the remaining liquid. For highly saline soils, pore waters can remain almost entirely unfrozen at temperatures of –2 °C to –3 °C (Gregersen *et al.* 1983) and, given the right material, unfrozen water can be present within unconsolidated permafrost at temperatures of -5°C (Anderson and Morgenstern 1973; Scott *et al.* 1990).

Saline permafrost is characterised by a highly complex heterogenous composition, with frozen zones containing ice lenses interspersed with zones of unfrozen porewaters and sediment (Brouchov 2002). Because current will preferentially flow through materials of low resistivity, the current induced into a subsurface containing unfrozen saline pore waters will flow through this matrix, rather than through highly resistive lenses of ice. The effect will be apparently low values of resistivity, particularly where the grain-size of the material is very fine. Laboratory analysis of marine clays from lower Adventdalen have revealed that even with low volumetric water contents (12%), the electrical resistivity of these sediments is low (<100 Ω m) at temperatures as low as -8°C, as a result of the relatively high salinity of the pore waters (ca. 5‰) (Harada and Yoshikawa 1996).

Although theoretically the development of segregation ice within fine-grained saline sediments can explain the low values of resistivity measured within Hytte and Longyear pingos, whether this process can account for the significant amount of

heave (>20 m) associated with the growth of these landforms is less certain. Low resistivity does not preclude high ground ice contents however, resistivity values of 1000-3000 Ω m have been observed from permanently frozen silts with a measured volumetric ice content of 60-70% (Delaney *et al.* 1988). In other frost mounds generated predominantly by segregation ice, however, such as lithalsas, it is rare to find mounds greater than 7 m in height (Pissart 2002). The pockets of high resistivity beneath the southeastern end of the resistivity tomogram from Hytte pingo (Figure 10.15), and the circular zones of higher resistivity within Longyear pingo (Figure 10.16), could be interpreted as larger lenses of massive ice or localised high volume concentrations of segregation ice. The heterogeneity that is characteristic of saline permafrost means that a mixture of segregation and massive ice, even within one landform, is possible.

The zones of very low resistivity (<100 Ω m) recorded at both Hytte and Longyear pingos could potentially represent zones of saturation caused by the build-up of upwelling groundwaters. Although it has been suggested that these landforms are of the closed system type (Svensson 1971) groundwater flow has been documented at Hytte pingo (Orvin 1944; Liestøl 1977), and the well developed drainage channel on the southeast flank may be evidence for past groundwater seepage at Longyear pingo. This evidence points to at least some influence for groundwater under hydraulic pressure influencing the development of these landforms. Potentially, the plumes of very low resistivity may indicate zones of groundwater seepage within the internal structure of these pingos. Although the regional groundwater has a high dissolved salt concentration (Orvin 1944; Liestøl 1977), this concentration is lower than would be expected within the pore waters of the marine clays following relative sea level fall. Seepage of "fresh" groundwater through partially frozen, highly saline marine clays at temperatures several degrees below zero could promote localised ice segregation. Preferential ground-ice development would occur in sediments saturated by the seepage of less saline groundwater from depth, because they would have a higher freezing point than the surrounding sediments containing highly saline pore waters. Where groundwater seepage was concentrated, such as at fault intersections, mounds of ice-rich relatively low salinity soils, surrounded by highly saline clays, could develop.

Traditional classifications of ground-ice mounds discriminate between mounds that are formed by the growth of segregation ice (palsas, minerogenic palsas and lithalsas), and those that result from the development of massive injection ice (pingos). If the landforms in lower Adventdalen are predominantly the result of segregation ice yet display evidence for groundwater seepage, then they appear to represent a transitional landform between these two extremes. This is not unique, examples of minerogenic palsa or lithalsa development in areas of groundwater seepage or incorporating units of injection ice have been documented (e.g. Worsley *et al.* 1995; Coultish and Lewkowicz 2003) and segregation ice has been observed in many pingos (e.g. Mackay 1973; Yoshikawa 1993).

10.5 Summary

Ground penetrating radar investigations of the internal structures of Innerhytte and Riverbed pingos suggest that the core of these landforms are not composed entirely of pure, massive ice, although ice bodies have been recorded at both pingos (Piper and Porritt 1966; Yoshikawa 1993). Steeply dipping radar reflections in the upper few metres of Riverbed pingo are likely to represent alternating units of ice and shale. Such banding of materials with strong dielectric properties may also be responsible for similar reflections in the GPR profiles from Innerhytte pingo. In the absence of geological, or crystallographic control however, the possibility that variations in the chemistry, ice crystal properties or air content of the pingo ice core might also be responsible for such reflections cannot be discounted.

Where pingos are developed within bedrock (e.g Innerhytte pingo), interpretation of electrical resistivity tomography data is complicated by the high resistivity characteristics of both frozen bedrock and massive ice. The resistivity from the northern part of Innerhytte pingo is therefore consistent with both the suggestion that a massive ground-ice body exists at depth (Piper and Porritt 1966) or that part of the pingo is a bedrock remnant without a body of massive ice (Ross et al. 2005b).

Electrical resistivity tomography surveys of Hytte and Longyear pingos show that these landforms have an internal structure characterised by relatively low resistivity. This is entirely inconsistent with the presence of a large body of massive ground-ice and suggests that the uplift of these landforms was generated by the development of a mixture of segregation ice and localised, discontinuous pockets of massive ice within a matrix of partially frozen fine-grained, saline marine muds. This contradicts the conceptual model of open system pingo development, but is in line with field observations from other pingos and ground-ice mounds.

The investigations described in this chapter merely provide basic geophysical data on open system pingos in Svalbard. Future work investigating open system pingos should concentrate on drilling boreholes for improved geological control, and the monitoring of air and ground temperatures and snow cover conditions. As well as providing information on the geomorphological processes related to the development

and evolution of these landforms, this monitoring would also improve interpretation of the geophysical data. This work should be complemented by more detailed geophysical surveys and by the establishment of fixed geophysical installations (e.g. Delisle *et al.* 2003; Hauck and Vonder Mühll 2003b) for long-term observations to monitor and evaluate future climatically driven changes (Vonder Mühll *et al.* 2001). The application of a variety of complementary geophysical techniques (e.g. seismic refraction tomography) would reduce ambiguity of interpretation (Scott *et al.* 1990; Vonder Mühll *et al.* 2001; Yoshikawa *et al.* 2006), particularly where the electrical contrast between massive ice and the host geological material (e.g. Innerhytte pingo) is not pronounced.

11 Discussion: Possible Mechanisms of Formation

This section aims to outline and evaluate the geomorphological processes that may have been responsible for the development of ramparted depressions in Wales. Four possible mechanisms that could account for the development of the landforms are identified. These are broadly divided into two categories: i) periglacial origins, incorporating pingo and lithalsa formation; and ii) glacial origins, including the stagnation, burial and meltout of glacier ice, and the meltout of grounded icebergs

11.1 Periglacial origins

11.1.1 The open system pingo model

Based on their location at the foot of valley slopes, Watson and Watson (1974) suggested that the model of development for open-system pingos of the Yukon Basin, (Canada and central Alaska) (Holmes *et al.* 1968; Hughes 1969), could also be used to explain the growth of ground-ice mounds in mid and west Wales during the late Pleistocene. Although applied specifically to the Cletwr valley, with minor modification this model may also be applicable to other sites in west Wales where the geology (both the type and distribution of bedrock and superficial sediments) and geomorphology are similar (e.g. in the Cledlyn and Grannell valleys and around Llanpumsaint). The pingos of the Yukon basin were selected as suitable modern analogues because they are concentrated on the lower slopes of minor river valleys in upland areas with discontinuous permafrost (Holmes *et al.* 1968; Hughes 1969) rather than on the alluvial plains of broad valleys in the continuous permafrost zone (e.g. Greenland and Svalbard) (Watson and Watson 1974).

Watson and Watson (1974) argued that during the Devensian, limited recharge of sub-permafrost groundwaters may have occurred on the valley interfluves and steep valley sides where permafrost was discontinuous and superficial deposits thin or absent (Figure 11.1). In contrast, groundwater flow would have been impeded beneath the lower slopes due to the thick sequences of impermeable fine-grained sediments, and the possibility of aspect-related deeper permafrost. Sub- and intra-permafrost groundwater migration could have occurred only in higher permeability zones, determined by the presence of gravel units or fractured bedrock. If
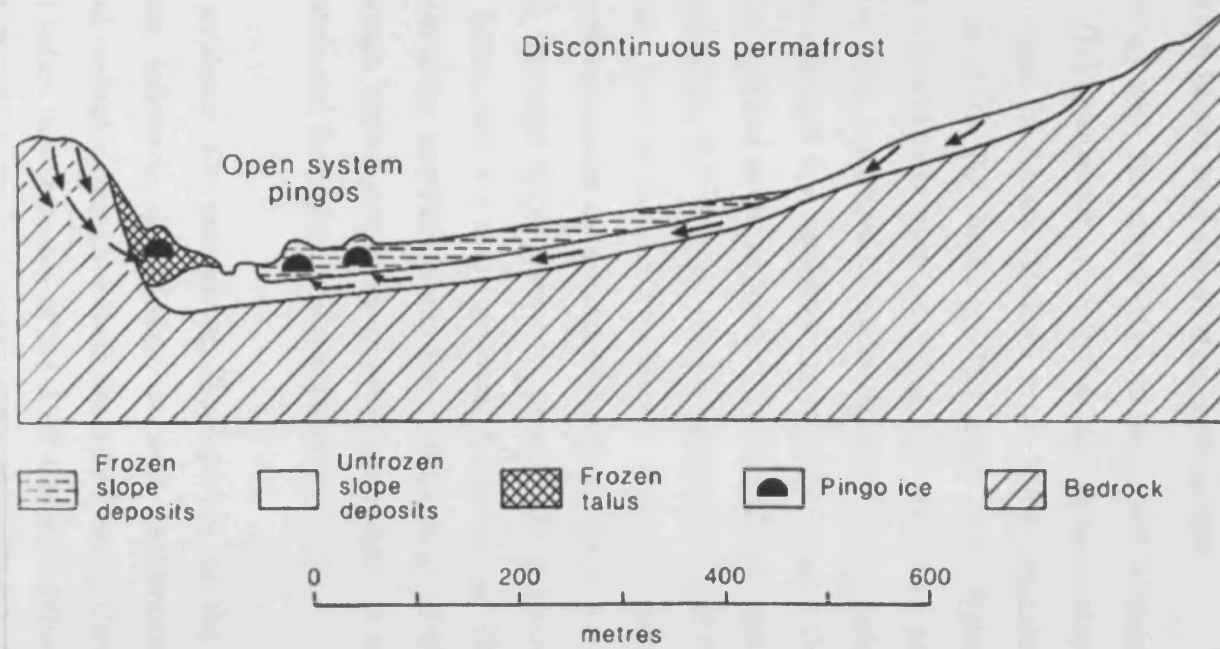
Figure 11.1: Model of the possible formation of open system pingos in Wales, leading to the formation of ramparted depressions (Ballantyne and Harris 1994, after Watson and Watson 1974).

groundwater was confined by an impermeable, permanently frozen near-surface layer of unconsolidated materials, high hydrostatic pressures conducive for the development of open system pingos might result (Figure 11.1) (Watson and Watson 1974).

11.1.1.1 Permafrost hydrogeology: the role of groundwater seepage through faults and other discontinuities

Whilst the analogy with the central Alaskan pingo belt is broadly acceptable, Watson and Watson (1974) ignored the key role that fault systems play in the development of open system pingos in Alaska (Holmes *et al.* 1968; Hamilton and Obi 1982) and elsewhere in the world (O' Brien 1971; Liestøl 1977; Babinski 1982; Wang and French 1995). Groundwater seepage along fracture zones associated with faulting could also have been important in west and mid Wales during the late Pleistocene since the mudstones and fine sandstones of the Silurian and Ordovician bedrock, and the resultant fine-grained nature of most of the superficial deposits have generally low primary permeabilities. Robins *et al.* (2000) and Hiscock and Paci (2000) have shown that groundwater flow in the Teifi catchment currently occurs through four main pathways: i) within granular superficial deposits; ii) through a shallow 10-20 m thick weathered and fractured upper zone of bedrock; iii) in interconnected deep-seated fractures and faults; and iv) along geological boundaries. There is little reason to believe that during the late Pleistocene the hydrogeology of the area was very much different, although higher groundwater pressures might be expected as a result of glacial meltwaters and the presence of permafrost.

Unequivocal evidence for permafrost development in the Teifi catchment and adjoining areas following deglaciation is well documented. Ice wedge casts, involutions and vertical stones have been described on the Cardigan Bay coast and in the main Teifi valley just upstream of the Teifi-Cletwr confluence, as well as around Lampeter and Tregaron (Watson 1965, 1981; Price 1976). A well-developed ice-wedge cast observed in sands and gravels at Crug-y-eryr Quarry provides evidence for the previous existence of permafrost in the Cletwr basin after lake drainage. There is no direct evidence for the thickness of permafrost that developed in the area after deglaciation, but the development of ice wedge casts suggests at least some time periods with significant winter cooling (Mackay 2000). The analogy with the Yukon

Basin (30-45 m) (Holmes *et al.* 1968; Watson and Watson 1974) may in this case be appropriate. The depth of rockhead indicated by the geophysical surveys conducted during this project, suggest that significant thicknesses of superficial sediments (e.g. 15-22 m at Rhos Llawr Cwrt, Cletwr valley) underlie most of the investigated sites. Under permafrost conditions during the late Devensian, these unconsolidated Quaternary sediments were likely to have been permanently frozen throughout. Lateral groundwater migration would therefore have been significantly impeded, except along unfrozen sub-permafrost geological boundaries, through deep-seated faults or in a fractured upper zone of bedrock. Under these conditions high hydrostatic pressures could have developed, increasing the probability of open system pingo development. Poor exposure in the study area means that knowledge of the distribution of faults and other geological structures is limited. However, fault-related fracture zones have been mapped beneath ramparted depressions near Llanpumsaint and at Crychell Moor in mid-Wales (Figures 6.5 and 9.5) (BGS Sheet 211: Newcastle Emlyn, *unpublished map*; British Geological Survey 1993). Given the degree of structural deformation of the Welsh Basin rocks (Anketell 1987; Craig 1987), it is also probable that numerous small-scale faults coincide with the zones of ramparted depressions in the Cletwr and Cledlyn valleys. Groundwater seepage through such faults may have promoted pingo development (Figure 11.1).

11.1.2 Problems associated with the pingo origin model

Whilst the preceding section has suggested that the geological and hydrogeological context of the ramparted depressions could support the interpretation of these landforms in mid and west Wales as the remains of open system pingos, there are a number of factors which are not consistent with this interpretation. These are discussed within this section.

11.1.2.1 The density and distribution of ramparted depressions in Wales

One of the major criticisms of the pingo model is that active open system pingos are not found in the same high densities as clusters of collapsed Pleistocene landforms (Sparks *et al.* 1972; Worsley *et al.* 1995; Matthews *et al.* 1997; Pissart 2000, 2003). Although there are numerous examples of gregarious, clustering groups of open system pingos in modern Arctic environments (e.g. Müller 1959; Holmes *et al.* 1968; Hughes 1969; Liestöl 1977; Worsley and Gurney 1996; Gurney 1998), it has been

acknowledged that the density and widespread distribution of ramparted depressions in Wales is much greater (Watson and Watson 1974). It is therefore something of a myth that the distribution and concentration of ramparted depressions in Wales is comparable to that of active open system pingos. To counter this problem, Watson and Watson (1974) argued that given an extended period of time and the "continuance of open system conditions" (Watson and Watson 1974, p. 224) the density of pingos in Alaska would approach the densities in Wales. However, the period when permafrost could have developed following deglaciation in west Wales (ca. 5000 years) was actually considerably shorter than the period available for pingo development in the Yukon basin (20-40,000 years). Even if the period of time was long enough, the rather uniform state of preservation of the ramparted depressions suggests that the development of these landforms occurred within a relatively short period of time. In fact, these landforms do not actually overlap as much as suggested in the literature. For example, at Rhos Llawr Cwrt, Cletwr valley, there are more than six landforms in extremely close proximity but, with the exception of the hour-glass form of 'Pingo' 1, these landforms do not impinge greatly on one another. This is also the case in the Cledlyn valley and is not consistent with suggestions that only one or two pingos were supported at any one time (Watson and Watson 1974; Watson 1977). A greater degree of disturbance of earlier forms would be expected if this were the case. The lack of overlapping forms is in direct contrast to images of clustering open system pingos in Greenland (Müller 1959), which demonstrate significant disturbance of collapsing landforms by newly growing pingos, the mass movement of material and fluvial erosion. This suggests that rather than being the result of repetitive pingo development over an extended period of time at a geologically favourable site with only one or two active landforms existing at any one time (Watson and Watson 1974; Watson 1977), the ramparted depressions in the Cletwr and Cledlyn valleys were formed roughly contemporaneously.

11.1.2.2 Linear pingos and elongated ramparted depressions

It has been suggested that the linear pingos resembling eskers, described from Alaska (Porsild 1938), the Mackenzie Delta (Mackay 1962) and Prince Patrick Island (Pissart 1967), may provide appropriate analogues for the linear, very elongate ramparted depressions in the Cledlyn (e.g. 'Pingos' X, Y, R, S and A) and Cletwr (e.g. Darren Fawr and Glan-rhyd-y-dre) valleys (Watson 1971; Watson and Watson 1974)

(Figures 7.3 and 8.3). These analogies may be misplaced however, since linear pingos in the Arctic have very specific modes of formation involving the aggradation of permafrost within taliks associated with either lateral migration of river channels (Pissart and French 1976; French and Dutkiewcz 1976; Gurney and Worsley 1997) or the aggradation of permafrost in sediments infilling nearshore gullies and marine inlets that have been exposed by falling relative sea level (Pissart 1967). Such mechanisms cannot be applied to the elongate landforms of the Cletwr valley however as they are situated on a slope perpendicular to the current drainage channel and there is no reason to believe that any significant palaeo-drainage would have been located here. Although the elongate landforms in the Cledlyn valley are aligned parallel to the current drainage, the small catchment of the Cledlyn precludes the likelihood of significant palaeo-drainage on the valley sides where the landforms are located. Also, as Watson and Watson (1974) acknowledged, accounts of elongate pingos in Arctic environments have not yet documented examples of these landforms on sloping valley sides, all so far having been described from flat locations. Linear pingos are therefore probably inappropriate analogues for the elongate, ramparted depressions in Wales. The very linear morphology of the landforms on the north-facing slopes of the Cledlyn valley (Figure 7.3), suggests that the ridges impound peat-filled hollows because they are orientated perpendicular to the slope rather than because of the formation of an oval rampart from the meltout of a large ground-ice body associated with a linear pingo.

11.1.2.3 The duration of late Devensian permafrost and pingo growth

Pissart (2000, 2003) believed that the Younger Dryas was too short a period for the apparent extent of open system pingo development suggested by the number of ramparted depressions in Wales and on the Hautes Fagnes plateau of Belgium. This observation is certainly true given that evidence from active pingos in the Arctic suggests that the time taken for a pingo to grow large enough to form a sizeable rampart upon its collapse is in the order of hundreds to thousands of years (Mackay 1986, 1988). Although pingo uplift is rapid during the first few years of growth, the rate of uplift declines rapidly thereafter (Mackay 1981). Unlike the ramparted depressions in Belgium however, the chronological control of the landforms in Wales is not robust enough to date either the initiation of these landforms, nor the period of their development. However, it is possible that these landforms could have developed

in the late Devensian during and/or after deglaciation, but before the Lateglacial. The climate and environment of this period was certainly suitable for the development of ground-ice mounds, following withdrawal of glacier cover, with extensive, probably discontinuous, permafrost. If this was the case then a period of about 5000 years, rather than 1500 years was available for pingo growth.

11.1.2.4 The permeability of superficial sediments in west Wales

Mackay (1978b) suggested that although pingos are developed in a variety of substrates, these substrates must be characterised by some degree of permeability, and that there are few examples of active pingos developed in thick sequences of impermeable materials such as clays. Relict landforms in the British Isles however are commonly found developed in areas of silt or clay-rich till or lacustrine deposits (Bryant and Carpenter 1987), and those in Wales are no exception. It is initially difficult to comprehend how groundwater flow can be maintained through the significant thicknesses of low permeability clayey-silt tills and glaciolacustrine deposits that dominate the sites where ramparted depressions are found (e.g. Llanpumsaint, Cletwr and Cledlyn valleys). However, numerous examples of active pingos in Svalbard associated with groundwater seepage are developed in nearshore areas where Holocene permafrost has aggraded into fine-grained sediments exposed by glacio-isostatic uplift, demonstrating that the development of large ground-ice mounds can occur even within apparently low permeability substrates.

11.1.2.5 Regional topography and groundwater flow

The topography at several ramparted depression sites in Wales also appears to undermine an open-system pingo interpretation. At sites elsewhere in Wales such as Crychell Moor, Llangurig and Bwlch Derwin, high groundwater pressures could be generated by the high surrounding relief. However, in the tributary valleys of the Afon Teifi, despite the observed concentration of ramparted depressions, there is a lack of significant relief from which such pressures could be generated. Although Pissart (2000, 2003) argues that an impervious bedrock and a lack of relief precludes open system pingo development, if groundwater seepage is restricted to deep-seated faults and other discontinuities within otherwise impermeable bedrock, then seepage may occur due to regional scale groundwater gradients at specific locations. This would favour open system pingo development under permafrost conditions even on

plateau locations (e.g. Pissart 1967). Although inter-granular flow is restricted through the mudstones and sandstones of the Welsh Basin area, where fractured, these rocks have high secondary permeability (Watson 1996; Robins *et al.* 2000).

11.1.2.6 Depth of depressions

One issue that has been previously overlooked is the shallow nature of several basins, particularly in the Cledlyn valley. Previous studies and review papers have focused on the more spectacular depressions (e.g 'Pingo' U). However, the basins of several landforms in the Cledlyn valley (e.g. 'Pingos' A, M, L, N and Q) appear to be too shallow to be the remains of open system pingos. In addition, many of the landforms have an apparent surplus of material within their ramparts. In these cases, the question arises, how can a large volume of rampart sediments be generated from such shallow depressions? Whilst the depth to bedrock, indicated by resistivity data, is significant in the centre of the Cledlyn valley, the superficial sediment is thin on the upper slopes (e.g. below 'Pingo' A) (Watson 1971; Gurney 1994, 1995). Whilst this might explain why 'Pingo' A has a shallow basin, 'Pingos' M and L are developed above a thick superficial sequence and still only have shallow basins. Furthermore, if the superficial sediments are thin beneath 'Pingo' A, it is difficult to explain the mechanism by which the well defined rampart of this landform could be generated by the collapse of an open system pingo which has upheaved so little sediment.

11.1.3 The re-interpretation of ramparted depressions as relict lithalsas

On the basis of the density and morphology of the ramparted depressions in Wales, it has been suggested that the ramparted depressions of the Cletwr and Cledlyn valleys are the remains of lithalsas (no peat cover) or minerogenic palsas (thin peat cover) which developed from the growth of segregation ice in fine-grained sediments (Pissart and Gangloff 1984; Gurney 1994, 1995; Pissart 2000, 2003). This revised interpretation has been supported by evidence from active examples in North America and in Scandinavia (Pissart and Gangloff 1984; Worsley *et al.* 1995; Matthews *et al.* 1997). Lithalsas and minerogenic palsas normally develop from the growth of segregation ice within fine-grained, frost-susceptible silts and clays (Svensson 1969; Matthews *et al.* 1997), but can also develop in coarser material and the internal structure can contain units of massive ice (Allard *et al.* 1987; Lagerbäck

and Rodhe 1986; Worsley *et al.* 1995) (see Section 2.2.1). There is now widespread evidence that lithalsas produce encircling rim-ridge ramparts during their collapse (Svensson 1969; Lagerbäck and Rodhe 1985, 1986; Åkerman and Malström 1986; Worsley *et al.* 1995; Matthews *et al.* 1997; Allard *et al.* 1987; Pissart 2000, 2003) but the exact mechanisms responsible for the development of ramparts remain unclear.

There are significant morphological similarities between some of the landforms in Wales (e.g. in the Cletwr valley and near Llanpumsaint), and collapsed or collapsing modern-day landforms in Scandinavia (Svensson 1964b, 1969; Seppälä 1972b). The relict forms in the Hautes Fagnes, Belgium, which have been interpreted as lithalsas or minerogenic palsas by Pissart (2000, 2003) also show striking morphological similarities to some of the Welsh features discussed in this thesis (e.g. Rhos Llawr Cwrt and Llanpumsaint). Intriguingly, although Watson and Watson (1974) interpreted the landforms at Rhos Llawr Cwrt in the Cletwr valley as the relict form of open-system pingos, they did suggest that the amount of clear ice within the landforms was probably limited and that it was likely that the ice contained lenses of sediments.

A critical argument used to support the re-interpretation of ramparted depressions in Wales as the remains of lithalsas was the presence of highly frost-susceptible fine-grained substrates, which are necessary for the development of these ground-ice mounds, at Llangurig, and in the Cletwr and Cledlyn valleys (Gurney 1994, 1995; Gurney and Worsley 1996). Similar sediments have also been recognised in association with ramparted depressions at Bwlch Derwin in north Wales (Moore 1980) and at Owlbury, just over the English border in Shropshire (Gurney and Worsley 1996). During the current investigation highly frost-susceptible silts and clays were found both within and beneath the ramparts at Llanpumsaint, at Rhos Llawr Cwrt and within the basin fills at four of the six sites investigated. If permafrost developed following deposition, these silts would have supported extensive ice segregation during ground freezing in such poorly drained settings. However, demonstrating the presence of these sediments alone does not provide unequivocal evidence that these landforms are the remains of lithalsas or minerogenic palsas.

11.1.4 Problems associated with the lithalsa origin model

In the Cledlyn valley, the main location used to support the re-interpretation of the Welsh landforms, the current investigation has provided little or no evidence that the ramparted depressions are the remains of lithalsas or minerogenic palsas. This hypothesis was based on the premise that a significant thickness of frost-susceptible sediments existed in the valley, within which ice segregation, and ground-ice mound development, had occurred. The evidence previously presented in support of extensive glaciolacustrine deposition however is limited to only thin units of this deposit observed in the few available, poorly exposed stream sections (Watson 1971; Gurney 1994, 1995), and the assumption that the thick basin infills of 'Pingos' U and W were deposited prior to ground-ice development. Gurney (1994, 1995) believed that extensive glaciolacustrine sediments overlay till in the Cledlyn valley. To the author's knowledge however, nowhere outside the basins of the ramparted depressions, is there a section that provides unequivocal stratigraphical evidence that extensive deposits of clay or silt overlie till. During the current investigations no glaciolacustrine deposits overlying the glacial till were observed. In fact, the current study found no evidence for lacustrine clays or silts at all (except within the basin of 'Pingo' U), in any of the boreholes or trial pits, although such deposits could exist at depth. The low resistivity zones beneath 'Pingos' L, M, N, Q and U may represent the presence of fine-grained sediments, but it is impossible from the geophysical evidence alone to define lithology. As Watson (1996) pointed out, only a deep bore to bedrock would finally prove the presence or absence of extensive glaciolacustrine deposits. However, neither the boreholes nor the trial pits from the ramparts of 'Pingo' U and 'Pingo' Q support a stratigraphy of till overlain by glaciolacustrine silts and clays and head.

The current evidence therefore appears to suggest that the unit of glaciolacustrine sediments in the Cledlyn valley is not laterally or vertically extensive and that there is little evidence for a widespread proglacial lake and extensive glaciolacustrine sedimentation (see also Watson 1996). It is instead possible that the fine-grained glaciolacustrine sediments observed by Gurney were deposited in a series of small lakes that developed either on the valley floor, where they could have been impounded by topography, or supraglacially. Even if extensive fine-grained

glaciolacustrine deposits existed (outside the landform infill), it is difficult to understand how large ramparts, composed of a matrix-supported, but clast-rich diamict could be produced. If the lithalsas were generated within a thick lacustrine succession overlying the till, then the ramparts would be expected to be mainly composed of fine-grained silts and clays. Furthermore, these ramparts far exceed the scale of any ramparts likely to be produced by the collapse of a lithalsa less than 10 m in height.

Simply interpreting landforms as the product of the collapse of lithalsas on the basis of the presence of fine-grained glaciolacustrine deposits (e.g. Gurney 1994, 1995; Worsley *et al.* 1995, Gurney and Worsley 1996) is misleading. There are a number of alternative mechanisms by which rim ridges can be produced, in association with fine-grained sediments, by processes associated with glacial lakes and glacial processes. Therefore, where these landforms are developed in glaciolacustrine clays and silts a segregation ice origin should still be considered a possible option, but the substrate alone is not necessarily an unequivocal indicator of the origins of these landforms.

11.1.5 Periglacial origins: a summary

Whilst the geomorphological setting, and the regional hydrogeology and permafrost history are consistent with a pingo origin for the ramparted depressions found throughout parts of mid and west Wales, the density of these landforms in particular makes it very unlikely that they are the remains of open system pingos. Whilst the mechanism by which open system pingos form does cause these landforms to congregate at localities where groundwater seepage favours their development (e.g. Müller 1959; Holmes *et al.* 1968; Worsley and Gurney 1996), this phenomena is not as common as widely believed. Most open system pingos have a very scattered distribution (Pissart 2000, 2003) and are not found in the densities characteristic of the Welsh landforms. This is in direct contrast to lithalsas, which are concentrated in low-lying areas, underlain by water-saturated, frost-susceptible fine-grained sediments (Pissart 2000, 2003). In terms of their density therefore, the ramparted depressions of Wales are more consistent with the interpretation of these landforms as the collapsed forms of late Pleistocene lithalsas (Pissart and Gangloff 1984; Gurney

337

1995; Pissart 2000, 2003) rather than open system pingos (Watson 1971; Bryant and Carpenter 1987; Ballantyne and Harris 1994).

Another possibility for the origins of ramparted depressions does exist however. A variety of glacial processes can also produce ramparted depressions, which, morphologically, can be very similar to those produced by periglacial processes. Although in terms of their density and morphology the Welsh landforms are very similar to the relict lithalsas of Belgium, because the Hautes Fagnes area was not glaciated during the late Pleistocene any possible glacial origins for the landforms in Belgium can be easily dismissed. This is not the case for the ramparted depressions in Wales however, which are all located within areas affected by glaciation during the late Pleistocene. As a result, these glacial mechanisms of formation must be incorporated within any evaluation of the possible origins of the Welsh landforms. This is the case even for the classic site of the Cledlyn valley, where the re-interpretation of these landforms as relict lithalsas (Gurney 1995) is undermined by the apparent absence of an extensive frost-susceptible, fine-grained substrate.

11.2 Possible glacial origins

11.2.1 Ice stagnation origins

11.2.1.1 Ice stagnation landforms in North America and Scandinavia

In North America and Scandinavia, complex till-cored hummocky topography, including a variety of ice-contact hummocks, rims, ridges, and moraine, interspersed with dead-ice hollows (kettle holes), have been reported from areas glaciated during the Late Pleistocene (Hoppe 1952; Gravenor and Kupsch 1959; Stalker 1960; Parizek 1969; Clayton and Moran 1974; Aartolahti 1974; Lundqvist 1981; Mollard 1983, 2000; Lagerbäck 1988; Eyles et al. 1999; Menzies and Shilts 2002; Knudsen et al. 2006). Of this collection of glacial landforms, which includes Veiki moraine (Hoppe 1952; Lagerbäck 1988), those of most relevance are the circular "closed disintegration ridges" (Gravenor and Kupsch 1959) or "rimmed kettles" (Parizek 1969). These ring-, or doughnut-shaped ridges range from 10-300 m in diameter and 1-7 m in height, and impound central depressions 0.5-3 m deep (Gravenor and Kupsch 1959; Mollard 2000), dimensions that are directly comparable with the ramparted depressions of Wales.

Two mechanisms by which these landforms could develop have been proposed: i) the irregular mass movement of supraglacial debris (flow tills) into crevasses and sinkholes around wasting ice blocks during the meltout of stagnant, dead ice (Gravenor and Kupsch 1959; Parizek 1969; Clayton and Moran 1974); and ii) the squeezing of saturated, plastic, subglacial till into basal crevasses and cavities during the stagnation and disintegration of glacier ice resting on fine-grained, water-saturated deformation till (Hoppe 1952; Gravenor and Kupsch 1952; Stalker 1960; Eyles et al. 1999; Boone and Eyles 2001). The two models of formation (supraglacial and subglacial) are not mutually exclusive however, and many studies have described very compact subglacial till, underlying supraglacial tills and glaciolacustrine deposits, within the internal structure of these landforms (e.g. Gravenor and Kupsch 1959; Parizek 1969; Aartolahti 1974). As the stagnating ice melts out small supraglacial lakes can develop, and fine-grained sedimentation in these lakes (dammed both by ice and by ridges of sediment) can result in the formation of a till

ridge ring surrounding a basin filled with glaciolacustrine clays (Eyles *et al.* 1999). Regardless of the exact mechanisms responsible for their development, there is widespread acceptance that these rim-ridge landforms have glacial origins, and that they formed as a result of the widespread regional stagnation, disintegration and melt-out of an ice mass (Gravenor and Kupsch 1959; Stalker 1960; Parizek 1969; Lundqvist 1981; Lagerbäck 1988; Eyles *et al.* 1999). The similarities in terms of the depositional environments indicated by their sedimentological composition (till and glaciolacustrine sediments) and their geomorphology (form, density etc.) means that they offer a possible analogue for the landforms of the Cledlyn (Chapter 7), Cletwr (Chapter 8) and Grannell (not investigated during this project) valleys. The following section presents a landsystem model that suggests how the ramparted depressions in the Afon Teifi-Cardigan Bay area could have formed by the meltout of stagnant glacier ice.

11.2.1.2 The Afon Teifi-Cardigan Bay area: a landsystem of glacier stagnation?

Supraglacial landforms and sediments are frequently associated with escarpments, where ice flow becomes compressional due to some topographic obstruction (Paul 1983; Eyles *et al.* 1999; Johnson and Menzies 2002). The uplands of Ceredigion provide an environment conducive for compressional flow and ice stagnation because both the Irish Sea and Teifi glaciers flowed uphill onto this upland area from lower ground to the north and the east respectively. The marginal zones of both these ice masses would therefore have experienced significant basal resistance from the rigid-bed zones ("sticky spots") associated with the upland areas free of superficial sediments. During deglaciation it is highly unlikely that any ice that had flowed onto the upland area would have retreated actively. Instead, parts of the ice masses probably became isolated, with *in situ* stagnation and downwasting taking place. The Irish Sea glacier in particular would have been strongly affected by this process, as the ice mass had flowed inland over the steep cliffs of what is now the current coastline and up the steep rise in topography from the coast (a vertical relief of up to 250 m). This probably explains the significant number of ridges and hummocks, originally interpreted as the remains of open system pingos (Watson 1972) that are developed in the northward draining valleys between Mydroilyn and Llwyncelyn that flow down to Cardigan Bay (Watson 1972, 1977; Ross *et al.* 2005a).

In the parts of the Afon Teifi-Cardigan Bay watershed area associated with deposition from the Teifi glacier, geomorphological and sedimentological evidence for ice stagnation may be limited to the valley floors and lower valley sides because ice persisted longer in the steeply incised tributary valleys of the Afon Teifi (e.g. Cledlyn, Cletwr and Grannell valleys). Whilst downwasting of this ice occurred, supraglacial and paraglacial processes could have reworked sediment, concentrating it on the surface of any remnant ice masses within the valleys. As melt-out proceeded, then the irregular mass movement of supraglacial till into crevasses, meltwater channels and depressions in the ice could have led to the accumulation of a significant thickness of supraglacial sediment within the steep sided valleys, and the formation of ramparted depressions. However, if this was the case, then the sediments associated with the landforms in the Cletwr and Cledlyn valleys should be dominated with supraglacial flow tills, fluvioglacial and mass movement sediments. The fine-grained, homogenous and massive nature of the till observed within the ramparted depressions of the Cledlyn valley (both 'Pingos' U and Q) however, is not indicative of supraglacial facies associations, which are normally composed of complexly-interbedded, coarse-grained flow and meltout tills, and glaciofluvial and glaciolacustrine deposits (Paul 1983; Eyles *et al.* 1999). The highly compact nature of the till in the Cledlyn valley in particular is instead suggestive of subglacial origins. Although there is some evidence for localised reworking of this till, the heavily striated clasts found from the trial pits excavated within the ridges at 'Pingo' Q in the Cledlyn valley certainly indicate subglacial transport at some stage during its formation (Section 7.7.1).

An alternative explanation for these landforms, consistent with the evidence for subglacial till, was that sediment was already concentrated within the "pre-glacial" valleys prior to deglaciation and that debris-poor ice stagnated across the entire landscape. Where the stagnating ice rested on saturated unconsolidated materials, subglacial sediments could be deformed and remobilised by differential overburden pressures, causing the development of "squeeze-up structures" analogous to the processes inferred to have formed ring-ridges in North America and Scandinavia (Hoppe 1952; Stalker 1960; Eyles *et al.* 1999). On the interfluves however, the thin superficial cover meant that the downwasting ice had little or no unconsolidated

material available for deformation, and ramparted depressions were unable to form. Geomorphological evidence (ramparted depressions) for ice stagnation would therefore only have been generated, and preserved, in the valleys where there were thick sequences of superficial sediments to deform (e.g. Cledlyn and Cletwr valleys), explaining the current distribution of these landforms. As well as being applicable to the Cledlyn and Cletwr valleys, this model is also relevant to the formation of ramparted depressions in the adjacent Grannell valley, not investigated during the current research programme. If regional stagnation simply modified existing (subglacial) sediments, then the model that valley infills in southwest Wales (Pembrokeshire) are comprised of flow tills and paraglacially modified sediments (McCarroll and Rijsdijk 2003) may not be appropriate throughout the region.

11.2.1.3 Implications of the glacial landsystem model

As well as being consistent with the available field evidence, a glacial origin for many ramparted depressions in the Afon Teifi-Cardigan Bay watershed area can also resolve the apparently intractable problems relating to the origins and thickness of the sequences of fine-grained sediment which infill the basins of some of the ramparted depressions in the Cledlyn valley (Section 7.4.1) (Watson and Watson 1972; Gurney 1994, 1995; Gurney and Worsley 1996). Although Gurney (1994, 1995) and Gurney and Worsley (1996) believe that these sediments could have been deposited in an extensive proglacial lake prior to landform (lithalsa/minerogenic palsa) formation, there is no evidence for a thick sequence of such sediments beyond the confines of the landforms' central depressions. Thick sequences of fine-grained silts and clays deposited under quiet-water conditions are characteristic of areas of hummocky moraine in North America and Scandinavia (e.g. Stalker 1960; Eyles et al. 1999; Mollard 2000). Many rim-ridge landforms in these areas are infilled with thick (up to tens of metres) accumulations of glaciolacustrine sediments (Stalker 1960; Lagerbäck 1988; Eyles et al. 1999; Mollard 2000). These sediments were deposited either within supraglacial lakes, or within ice walled meltwater channels (moulins or dolines). Stratified lacustrine sediments more than 7 m in thickness are also associated with the De Kalb mounds of Illinois (Flemal et al. 1973; Flemal 1976). Although originally interpreted as the remains of pingos, these landforms probably have glacial origins (Menzies and Shilts 2002; Iannicelli 2003). The current evidence for the distribution of glaciolacustrine sediment in the Cledlyn valley is more consistent with a model of

localised deposition in association with the stagnation of glacier ice, rather than widespread proglacial deposition followed by lithalsa formation. A glacial model addresses the problems associated with the previous interpretations of these landforms as either relict pingos (Watson 1971; Watson and Watson 1972) or relict mineral palsas (lithalsas) (Gurney 1994, 1995; Gurney and Worsley 1996), because the sediment infilling the central basins of these landforms is not derived from the ramparts. As a result, there is no need to explain why the gravel-sized material found in the ramparts is a rare component within the sedimentary infill of the central basins, nor how such thick sequences of fine-grained deposits were derived purely from the mass wasting of the compact till-cored ramparts (Watson and Watson 1972; Gurney 1994, 1995; Gurney and Worsley 1996).

11.2.1.4 Problems associated with the glacial model

One significant problem that contradicts the glacial model is the apparent absence of organic deposits from the Lateglacial Interstadial (Handa and Moore 1976; Walker and James 2001). This evidence appears to directly contradict the model of glacial origins as it suggests that the infilling of the central depressions of these landforms began no earlier than at the end of the Younger Dryas (Loch Lomond Stadial). If the landforms were formed by glacial processes during the Devensian glaciation, then their central depressions should contain organic deposits dating to the Lateglacial Interstadial. There are a number of reasons why this might not be the case however. Adapted from Ballantyne and Harris (1994), these include: i) the survival of subsurface ice during the interstadial; ii) the non-accumulation of interstadial organic deposits; and iii) the burial of interstadial deposits beneath minerogenic sediments during the Younger Dryas. In southwest Norway the infill of some glacial moraine rim ridges (Veiki or Pulju moraines) contain full Lateglacial sequences, whilst adjacent landforms contain only organic-rich gyttja, believed to be Holocene in age, indicating that the absence of Lateglacial sediments does not necessarily preclude a glacial origin for ramparted depressions (Knudsen *et al.* 2006).

11.2.2 Glaciolacustrine origins

Whilst the glacial (supraglacial or subglacial) model could be used to explain the origins of those landforms composed of till in the tributary valleys of the Afon Teifi, or those in the upland areas of mid-Wales (e.g. Crychell Moor), it cannot explain the

formation of the ramparted depressions at Llanpumsaint which are developed entirely within a thick sequence of glaciolacustrine deposits, beyond the late Devensian ice margin (BGS Sheet 211: Newcastle Emlyn, *unpublished map*). The hypothesis that many of the ramparted depressions in Wales are the remains of lithalsas rather than open system pingos (Gurney 1994, 1995; Gurney and Worsley 1996) appears strengthened by the borehole evidence presented in this thesis for fine-grained lacustrine deposits beneath the till-cored ramparts at Rhos Llawr Cwrt (Section 8.3.1) and the significant thickness of frost-susceptible glaciolacustrine silts and clays recorded from the deep borehole at Helfa Hall, near Llanpumsaint (Section 9.3.1.1). However, as previously discussed, the simple presence of frost-susceptible materials in association with ramparted depressions does not automatically mean that these landforms developed through ice segregation. There are several other mechanisms through which ramparted depressions can develop in extensive proglacial lacustrine depositional environments. It is acknowledged however that the exposure of water-saturated, fine-grained frost susceptible sediments by changes in lake level or catastrophic lake drainage is highly conducive to the formation of lithalsas. Excellent examples of collapsing lithalsas, with similar morphologies to those at Rhos Llawr Cwrt and Helfa Hall have been observed around shallow lake margins in Quebec (Pissart 2000, 2003).

Masses of stagnant debris-rich glacier ice can melt very slowly when buried beneath glacial debris and/or lake clays on the floors of glacial lakes (Mollard 1983). In a lake basin dammed by the Kaskawulsh Glacier, southwest Yukon, circular kettle holes, enclosed by ramparts and up to 100 m in diameter, were revealed after lake drainage, indicating extensive stagnant ice and ice-cored debris beneath the lake (Johnson 1997). Similar ice-stagnation kettle lakes have been reported from ice-marginal lakes in Alaska (Ashley 2002). Circular depressions surrounded by rim ridges have also been shown to result from the grounding of floating blocks of ice during the sudden or catastrophic drainage of ice-dammed lakes (Mollard 1983, 2000; Longva and Thoresen 1991; Maizels 1992). Such landforms are very similar in morphology and scale to the circular ramparted depressions at Rhos Llawr Cwrt, in the Cletwr valley and around Llanpumsaint. Their formation occurs through two different processes associated with the settlement ("let down") of ice blocks: i) grounded icebergs deform underlying soft, water-saturated, plastic lacustrine clays

and silts, displacing the substrate sideways towards the margins of the ice block to form 'boulder-ring' structures (Mollard 1983; Longva and Thoresen 1991); and ii) slumping of sediment from the *in situ* meltout of debris-rich ice blocks grounded by waning flow regimes, leading to the development of diamict cored ramparts (Maizels 1992).

Whilst the grounding of icebergs has been widely used to explain landforms that developed within the fine-grained sediments deposited by Lake Agassiz following the retreat of the Laurentide ice sheet in North America (Mollard 1983, 2000), evidence for ramparted depressions attributed to catastrophic lake drainage events during the late Pleistocene are rare in Europe. A notable exception is the drainage of an ice-dammed lake (jökulhaup) into a shallow fjord in southeastern Norway during the early Holocene, where Longva and Thoresen (1991) have described 'iceberg gravity craters' with pressure ridges developed in glaciomarine silts and clays. Although the majority of craters are 15 m to 30 m in diameter, some landforms up to 100 m in diameter have been recognised. Concentrations of these landforms are found in locations thought to represent immobile backwater positions during drainage (Longva and Bakkejord 1990; Longva and Thoresen 1991), and near drainage outlets, where flow is constricted (Longva and Thoresen 1991). In North America, similar doughnut-like rings are frequently found in association with lake shorelines (Mollard 2000).

11.3 Summary of the genetic interpretation of ramparted depressions in Wales

The preceding discussion has indicated that the precise interpretation of the origins of many of the ramparted depressions found at localities throughout Wales remains somewhat uncertain and that a single model cannot explain the development of all the landforms. Based on the evidence presented within this thesis however, this section aims to briefly summarise the most likely origins for these landforms. The origins of two of the Welsh sites (Hirwaun valley and Llanio Fawr) have already been discussed in their relevant chapters (Chapters 4 and 5) as the landforms at both of these sites have unequivocal glacial origins. The Hirwaun valley ridges are a form of subglacially derived or ice-marginal landform (possibly De Geer moraines) (Section 4.4.3), whilst the landforms near Llanio Fawr were deposited by proglacial fluvioglacial sedimentation onto the surface of either a stagnating ice margin, or a proglacial icing (Section 5.4.4). As they are clearly not the remains of periglacial ground-ice mounds, further discussion of their origins is not therefore necessary, and this section will focus on the landforms at Helfa Hall near Llanpumsaint, at Crychell Moor, and in the Cledlyn and Cletwr valleys.

11.3.1 Llanpumsaint

Of all the landforms investigated during this project, the ramparted depressions situated around Llanpumsaint (Chapter 9) are the most likely to represent the remains of periglacial ground-ice mounds. This interpretation is based on the morphology of the landforms (closely spaced ramparted depressions), the fine-grained, frost-susceptible substrate within which they are developed (glaciolacustrine silts and clays), and the presence of deformed units of mass movement and fluvial sediments described from the internal structure of the rampart. The close spacing of many of these landforms is similar to active lithalsas from the current permafrost zone, suggesting that these ground-ice mounds may provide the most appropriate modern periglacial analogue. Whilst the density of these ramparted depressions makes it is unlikely that they represent the remains of open system pingos, their development may have been at least partly controlled by fault-guided groundwater seepage. The landforms investigated near to Helfa Hall, south of Llanpumsaint, are clearly developed directly above the intersection of two faults (Figure 9.5), and groundwater

346

seepage through these faults may have influenced their development by maintaining a high moisture content within the overlying glaciolacustrine sediments, providing a potentially unlimited supply of water for ground-ice formation. In this sort of setting, it is possible that whilst some ground-ice mounds formed exclusively by ice segregation, immediately adjacent landforms may have been directly associated with points of groundwater seepage, and injection ice, as well as segregation ice, could have formed beneath the mound.

Given the possible influence that groundwater seepage could have played in controlling the location of their development, these landforms may represent a transitional form between pingos and lithalsas. It is clear from studies of active periglacial ground-ice mounds that a continuum of landforms between these two classifications exists, with the internal structure of some palsa and lithalsas containing units of injection ice (e.g. Åhman 1973; Allard *et al.* 1987, 1996; Coultish and Lewkowicz 2003), and many closed and open system pingos containing segregation ice (Sections 10.4.1 and 10.4.2) (e.g. Mackay 1973, 1979; Yoshikawa 1993). The possibility that the formation of some lithalsas and palsas is controlled by groundwater seepage has also been suggested (Worsley *et al.* 1995; Coultish and Lewkowicz 2003). This highlights the difficulties associated with the categorical definition of active periglacial ground-ice mounds within the current permafrost zone, let alone those formed during the late Pleistocene. Many existing classification schemes are too rigid to accommodate the continuum of landforms that exists.

The ramparted depressions at Llanpumsaint are situated in a hydrogeological setting highly conducive for the development of 'transitional' ground-ice mounds, with groundwater seepage through faults and other discontinuities potentially feeding the growth of segregation ice lenses within fine-grained, frost-susceptible sediments. However, without better knowledge of the current hydrogeological regime in the area, let alone during the late Devensian, precisely interpreting these ramparted depressions is virtually impossible. Nevertheless, the small- to medium-sized ground-ice mounds and ground-ice depressions found in parts of Scandinavia (Svensson 1969; Lagerbäck and Rodhe 1985, 1986; Åkerman and Malmström 1986), which contain a mixture of segregation ice lenses and units of massive injection ice, probably provide a more

appropriate modern periglacial analogue for the landforms at Llanpumsaint than the larger open system pingos on Svalbard for example.

Because they appear to be developed entirely within a glaciolacustrine sequence of sediments, the ramparted depressions at Helfa Hall cannot be the result of supraglacial or subglacial deposition during ice stagnation. However, there remains the possibility that these landforms could be a type of iceberg gravity crater, which formed when drainage of Lake Gwili occurred (Section 9.4.1). If this was the case, then the sediments and structures within the rampart could have formed either through the deformation of pre-existing sediments, or by deposition from the meltout of a debris-rich ice block, with deformation occurring when ice, buried by sediment released from within the iceberg, melted. Sedimentary beds deformed into an anticline within the ramparts of iceberg gravity craters have been reported (e.g. Longva and Bakkejord 1990), and these appear similar in gross form to those observed from the rampart at Llanpumsaint.

LiDAR data from the area around Llanpumsant (Figure 11.2) reveals many unusual elongate mounds that may have formed as a result of erosion (gullying) during the drainage of Lake Gwili. If these landforms do indeed represent this process, then they could support an iceberg gravity interpretation for the ramparted depressions around Llanpumsaint, including those at Helfa Hall. Similar elongate mounds are found in close proximity to ramparted depressions associated with catastrophic lake drainage in southwest Norway and in North America, and are also believed to be the result of current erosion (Longva and Thoresen 1991; Mollard 1983). Features that may have similar origins have also been observed developed in glaciolacustrine clays within the buried meander loops of the Afon Teifi (Bradley 1980; Lear 1986; Waters *et al.* 1997).

Whilst the alternative "grounded iceberg" model is possible on the basis of the existing evidence, the preferred explanation for the ramparted depressions around Llanpumsaint is that they are a type of periglacial ground-ice mound. The growth of ground-ice responsible for the development of these landforms may have been fed by the fault-guided seepage of groundwater. If these landforms are the result of the collapse of periglacial ground-ice mounds, given the complexities associated with
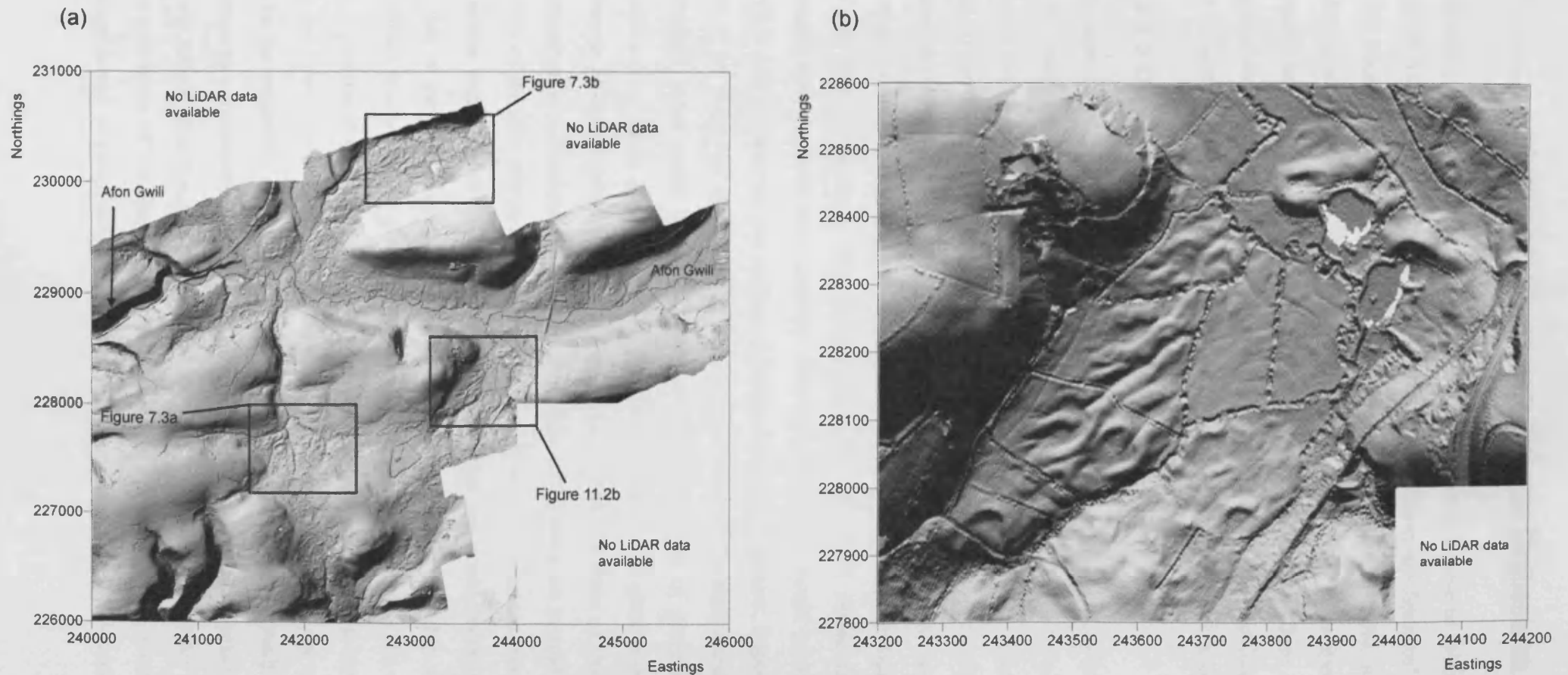
Figure 11.2: LiDAR derived digital terrain model (DTM) of the area around Llanpumsaint (© Environment Agency copyright and/or database right 2006): (a) Areas of Figures 7.3a, 7.3b and 11.2b indicated; (b) Elongate landforms near Pont-ar-sais that may have been formed by erosion (gullying) during the drainage of Lake Gwili.

accurately interpreting the origins of such landforms it is wise to follow the approach of Sparks *et al.* (1972), and refer to them as 'ground-ice features' or 'ground-ice depressions', or perhaps more specifically 'ramparted ground ice depressions' (Bryant and Carpenter 1987). These terms are preferred to more specific terms with genetic connotations, such as 'pingo scars', (Flemal 1976; De Gans 1988). Where a ground-ice origin for relict landforms cannot be confidently established, then the use of the simple, purely morphological term 'ramparted depressions' is advocated.

11.3.2 Crychell Moor

Because the investigations of the ramparted depressions at Crychell Moor (Chapter 6) were relatively limited compared to the study of other sites contained within this thesis, the origins of these landforms are very uncertain. As the internal structure of the ramparts is dominated by till, the ramparted depressions at Crychell Moor could have developed through the chaotic deposition of supraglacial sediments on the surface of an ice mass that downwasted on the floor of the steep sided valley within which they are located. The fine-grained silts and clays within the basin of the investigated landform are consistent with this model, and could have been deposited within a small lake on the surface of the downwasting glacier, impounded either by ice or by ridges of sediment. Alternatively however, the ramparted depressions at Crychell Moor could equally be the remains of a type of periglacial ground-ice mound. Like those at Llanpumsaint, they are found in too great a density to be the remains of open system pingos, and are most probably a form of smaller ground-ice mound such as lithalsas, or perhaps even seasonal ground-ice mounds. As the lateral extent of the silts within the basin of these landforms is uncertain (Section 6.4.1), it is possible that this unit extends beyond the landform and could underlie the entire site. If this is the case, then this deposit may have provided a highly frost-susceptible medium favourable for ground-ice mound development. Because the site is underlain by a prominent fault (Section 6.1), groundwater seepage may also have played a role in their development, by providing a constant supply of water for ice lens growth. Like the ramparted depressions at Llanpumsaint therefore, these landforms could also represent a transitional form of ground-ice mound, with internal structures containing a mixture of injection and segregation ice depending on groundwater availability and the proximity of the landform to faults and other discontinuities. Currently however, the preferred origin of these landforms is the stagnation and meltout of glacier ice.

11.3.3 Cletwr valley

Morphologically, the landforms at Rhos Llawr Cwrt in the Cletwr valley are very similar to the ramparted depressions at Llanpumsaint, as well as the relict landforms described from Scandinavia and Belgium (Svensson 1964b, 1969; Seppälä 1972b; Pissart 2000, 2003). In combination with the evidence for frost-susceptible, fine-grained silts at depth beneath their ramparts (Section 8.3.1), there is therefore a strong case that these landforms represent the remains of periglacial ground-ice mounds such as lithalsas (Gurney 1994, 1995; Gurney and Worsley 1996). These silts would have supported extensive ice segregation during ground freezing in a poorly drained environment such as in the Cletwr valley. Although it is accepted that the high density of these ramparted depressions is inconsistent with the interpretation of these landforms as open system pingos (Pissart 2000, 2003), it still remains possible that groundwater seepage may have contributed to their development. Numerous faults and discontinuities characterise the local bedrock, although unlike the sites at Llanpumsaint and Crychell Moor no significant faults have yet been mapped in direct association with the Rhos Llawr Cwrt site.

There is however, an equally plausible alternative explanation for these landforms: the stagnation and meltout of glacier ice. The ramparts of the landform investigated at Rhos Llawr Cwrt are composed of a compact, matrix-supported diamict. If this unit represents an *in situ* till, then the meltout of debris-rich glacier ice, or subglacial squeezing of sediment, rather than ground-ice mound development, may have been responsible for the development of the landforms at Rhos Llawr Cwrt.

Although the topography in the Cletwr basin would be highly suitable for the isolation of bodies of downwasting ice buried beneath the floor of a proglacial lake, the stratigraphy from the boreholes at Rhos Llawr Cwrt does not support this possibility. Because the till found in the rampart of 'Pingo' 3 overlies the silts in Boreholes 1 and 3 (Section 8.3.1), deposition of the silts must have occurred before the till was emplaced. This till could therefore only have been deposited after glaciolacustrine deposition, either by ice that overran the lake (followed either by glacier ice stagnation or by the formation of periglacial ground-ice mounds), or by the meltout of debris-laden icebergs that were stranded following lake drainage (cf.

351

Maizels 1992). The latter possibility is thought unlikely however, as the unit of till is widely distributed across the valley floor, rather than locally concentrated around the enclosed depressions. Furthermore, the boreholes at this site did not appear to demonstrate any evidence for mass movement processes. However, it is accepted that an excavated section would be far more likely to reveal such structures associated with slope processes than borehole cores of diameter 100 mm or less.

It is unlikely that the formation of the elongate landforms near the farms at Glan-rhyd-y-dre and Darren Fawr (Section 8.2.1), originally interpreted as collapsed linear pingos (Watson and Watson 1974), was entirely unrelated to the formation of the landforms at Rhos Llawr Cwrt. As discussed in Section 11.1.2.2 however, a pingo origin for the linear ridges is unlikely. Because the area was glaciated during the Devensian (Jones 1965; Price 1976; Lear 1986; Waters *et al.* 1997), glaciotectonism or deformation caused by the meltout of buried ice cannot be dismissed as possible causes for the deformed silts and steeply dipping and vertical clasts observed in the exposure through the rampart of linear landforms at Glan-rhyd-y-dre (Watson 1975, 1976). The elongate ridges at Glan-rhyd-y-dre might therefore be explained as a form of constructional morphology associated with glacier ice, and the chaotic overlapping forms the result of sediment mass movement and burial of glacier ice during decay of a stagnant ice margin. It is possible that the linear landforms were the result of sediment deformation (squeezing) into basal crevasses. Such an interpretation provides a model (ice stagnation) that can explain the origins of both the linear landforms and the more circular enclosed depressions within the Cletwr valley.

On the present evidence from the Cletwr valley, therefore, it can be argued that the ramparted landforms at Rhos Llawr Cwrt, and the linear ridge structures at Glan-rhyd-y-dre and Darren Fawr, were derived from glacial- rather than permafrost-related processes. This is currently the preferred interpretation of these landforms, although it is accepted that a periglacial ground-ice mound origin is also possible.

11.3.4 Cledlyn valley

Like those in the Cletwr valley, the ramparted depressions in the Cledlyn valley have previously been interpreted as the remains of open system pingos (Watson 1971; Watson and Watson 1972) or lithalsas (Gurney 1994, 1995; Gurney and Worsley

1996; Pissart 2000, 2003). The concentrated density of these landforms is incompatible with the former however (Gurney 1995; Pissart 2000, 2003), whilst the size of the ramparts (up to 5 m in height), and the lack of clear evidence for a widespread frost-susceptible substrate (Section 11.1.4) mean that the latter interpretation is also unlikely. Surprisingly, although the ramparts of these landforms are composed of till (Sections 7.3.1 and 7.6.1) (Gurney 1994, 1995), previous studies have never seriously considered the role that glacial processes might have had in generating these landforms. Although Watson (1971, 1972) acknowledged that rampart-like ridges can be found between some kettle holes, this possibility was simply dismissed because "....they are very localized, and they lack the level, nearly horizontal crestline of the pingo ramparts." (Watson 1972).

Both the large sinuous, elongate, esker-like ridges and the more circular enclosed ramparted depressions within the Cledlyn valley (Figure 7.3) have analogues, in terms of their distribution, morphology and sedimentary composition, in the glacial landforms of North America (Gravenor and Kupsch 1959; Stalker 1960; Parizek 1969; Eyles et al. 1999). These ridges, which are also intimately associated with dead-ice hollows, are believed to have formed either by the supraglacial sedimentation of flow tills and glaciolacustrine deposits above and between blocks of stagnating ice (Gravenor and Kupsch 1959; Parizek 1969), or by the squeezing of water-saturated subglacial till into air-filled cavities and voids (e.g. crevasses, dolines and meltwater channels) on the underside of a stagnant, disintegrating ice mass (Stalker 1960; Eyles et al. 1999). The till-cored linear ridges and ramparted depressions of the Cledlyn valley may also have similar origins. The compact, massive till, characterised by a lack of structures indicative of mass movement processes, that dominated the three trial pits from 'Pingo' Q (Section 7.6.1), and the numerous striated clasts support a subglacial origin for these landforms. The steeply dipping clast fabrics from these trial pits however could equally be interpreted as originating either from the mass movement of supraglacial sediment into depressions on the surface of a stagnating ice mass, or alternatively from the subglacial squeezing of water-saturated till combined with later gravitational reworking of sediment (or perhaps even from the redistribution of sediment down the flanks of a periglacial ground-ice mound). Therefore, although the current sedimentological and geomorphological evidence clearly supports a glacial origin for these landforms,

353

whether these ridges formed supraglacially or subglacially cannot be established on the basis of the current evidence. Nevertheless, the stagnation and meltout of glacier ice is currently the most favoured interpretation for these landforms, as well as those ramparted depressions in the adjacent Cletwr and Grannell valleys, which although in places morphologically slightly different, are also likely to have related genetic origins.

11.4 Implications

The results presented in this thesis demonstrate that the superficial geology underlying many of the ramparted depressions in Wales is commonly characterised by fine-grained sediments such as silts and/or clays. These fine-grained sediments are found not only within the central, enclosed depressions of many landforms (e.g. Cledlyn valley, Crychell Moor, Llanpumsaint, Cletwr valley), but are also an important component of the surrounding superficial geology at some sites (e.g. Llanpumsaint, Cletwr valley). Elsewhere in the British Isles, clusters of ramparted depressions developed within extensive fine-grained glaciolacustrine sediments are known at Bwlch Derwin in North Wales (Moore 1980), Owlbury in Shropshire (Gurney and Worsley 1996), and in the Whicham valley in Cumbria (Bryant et al. 1985).

The presence of such fine-grained, frost-susceptible sediments has been viewed as important evidence used to argue that such landforms are the collapsed forms of mineral palsas (lithalsas) (Gurney and Worsley 1996). However, the possibility that at least some of the ramparted depressions investigated during this project could be glacially derived landforms rather than the relict forms of periglacial ground-ice mounds, does undermine this argument. This conclusion has significant implications for the identification and interpretation of ramparted depressions in all formerly glaciated areas upon which late Pleistocene permafrost aggraded. These implications will be discussed in the context of the possible re-interpretation of ramparted depressions at localities elsewhere in the British Isles.

11.4.1 Implications for other landforms in the British Isles

11.4.1.1 Owlbury

At Owlbury in the Camlad valley, Shropshire, where enclosed ramparted depressions occur across a flat valley floor, Gurney and Worsley (1996) argued that the frost-susceptible fine-grained substrate (glaciolacustrine deposits), which underlies all the ramparted depressions, would have developed segregation ice during freezing, supporting the hypothesis that these landforms were the result of the collapse of mineral palsas (lithalsas) (Gurney 1994; Gurney and Worsley 1996). Based on

355

sedimentological and geomorphological comparisons, this interpretation was also extended to the ramparted depressions at Rhos Llawr Cwrt in the Cletwr valley, as well as those near Llangurig and in the Cledlyn valley (Gurney 1994, 1995; Gurney and Worsley 1996), simply because frost-susceptible, fine-grained glaciolacustrine sediments were also present at these sites.

Like the ramparted depressions at Llanpumsaint however, the ramparted depressions at Owlbury could also be the remains of iceberg gravity craters that formed when blocks of floating ice became grounded during lake drainage. The lake clays in the Camlad valley have a tendency to become plastic (Cave and Hains 2001), and would therefore deform quite easily if subjected to downward pressure from the load of a grounding iceberg when water-saturated. Gurney and Worsley (1996) did report that the Camlad valley is characterised by the presence of a number of kettle holes, some greater than 100 m in diameter, which made identifying ramparted depressions difficult. These were believed to have formed as a result of the slow meltout of buried glacial ice, which may have persisted throughout the existence of the proglacial lake by becoming buried by glaciolacustrine sediments. Whilst Gurney and Worsley (1996) believed that kettle holes and the scars of periglacial ground-ice mounds can be discriminated at Owlbury on the basis of the presence or absence of a rampart, in reality this is a highly simplistic diagnostic method. Several of the landforms interpreted as the remains of mineral palsas (lithalsas) have very subdued, "barely discernable" ramparts, between 0.4-1 m high (Gurney and Worsley 1996 pg. 16). The extremely close proximity of the kettle holes and ramparted depressions suggests that these landforms could have common origins. Furthermore, seismic and gravity surveys in the Camlad valley suggest that the thickness of Quaternary sediments may be up to 100 m thick, and boreholes indicate that a continuous sequence of gravel-free, grey, silt and silty clay extends to depths in excess of 12 m (MacDonald 1994; Hussen 1998; Brabham et al. 2005). Therefore, for glacier ice to form these kettle holes it must have been buried at a significant depth (at least >12 m) beneath the ground surface. An alternative possibility is that the kettle holes, and perhaps also the ramparted depressions, formed as a result of the grounding of icebergs associated with fluctuating lake levels, perhaps during lake drainage. This is feasible, as the lake was of a proglacial type, impounded within the Camlad valley by the retreating ice

margin to the west, and an accumulation of morainic material to the east (Gurney and Worsley 1996; Cave and Hains 2001).

11.4.1.2 Whicham valley

In the Whicham valley, Cumbria, a series of enclosed hollows developed in thick sequences of clayey silts (>4 m) were interpreted as the remains of pingos (Bryant *et al.* 1985). Although they were believed to be of the open system type fed by groundwater flowing through underlying units of sand, Bryant *et al.* (1985), and Bryant and Carpenter (1987), also suggested that there was a possibility that these landforms could have developed as a result of ground-ice development from pore-water expulsion due to permafrost aggradation in water-saturated sediments exposed by lake drainage. This model has been described as a modified version of the closed system pingo model (Bryant and Carpenter 1987). However, given that the ramparts of the landforms in the Whicham valley are composed of frost-susceptible, fine-grained sediments, it is equally likely that these landforms could be the remains of lithalsas.

As continuous permafrost would be required for closed system pingo development, lithalsa development is probably the most likely permafrost-related model. Like the ramparted depressions at Llanpumsaint and at Owlbury however, a further possibility is that the landforms in the Whicham valley could be a type of iceberg gravity crater caused by the grounding of icebergs on fine-grained, water-saturated sediments within an ice-dammed glaciolacustrine basin. Without further investigation of these landforms however, it is difficult to evaluate the likelihood of these alternative possibilities. However, the gully systems described in association with the ramparted depressions (Bryant *et al.* 1985) do suggest modification of the lake basin floor during lake drainage. Furthermore, a possible relationship between the ramparted depression and the lake margin has been suggested (Bryant *et al.* 1985). A similar relationship between doughnut-shaped rings formed by the grounding of icebergs and lake shorelines has been documented in North America (Mollard 1983, 2000). Lakeshores are also highly suitable localities for the development of lithalsas however (Pissart 2000, 2003), because even slight changes in water level will enable rapid permafrost aggradation on frost-susceptible sediments with a ready supply of water available for ice segregation.

11.4.1.3 Bwlch Derwin

Ramparted depressions at Bwlch Derwin on Llŷn, North Wales (Watson 1977; Moore 1980; Rogers 1998a, 1998b; Ross *et al.* 2005a) are developed within a thick sequence of laminated fine sands and silts deposited within a large ice-contact lake that formed between Bwlch Mawr and Mynydd Craig Goch in the Pant Glas col during the late Devensian (Thomas *et al.* 1998). Originally interpreted as the relict form of open system pingos (Watson 1977; Moore 1980), like the ramparted depressions at Owlbury and in the Whicham valley, these landforms could also have formed through the collapse of lithalsas that developed in frost-susceptible sediments after lake drainage, or as a result of the meltout of grounded icebergs. The latter possibility is supported by evidence for iceberg dump structures within these sediments (Thomas *et al.* 1998).

11.4.1.4 Ireland

In Ireland, a very high number and density of landforms, interpreted as the remains of open system pingos, were identified in the unglaciated southeastern parts of the country, beyond the maximum limits of both the Irish and Irish Sea ice masses during the last glaciation (Mitchell 1971, 1973; Coxon and O'Callaghan 1987) (Figure 2.13b). Since these landforms were identified however, it has become clear that the glacial limits in southern Ireland probably require significant modification, and that the Southern Irish End Moraine is no longer believed to mark the limit of the last glaciation (Warren 1991; Ó Cofaigh and Evans 2001; Bowen *et al.* 2002). Given that the density of these landforms (over 200 identified in an area of 5.75 km^2 (Mitchell 1973)) appears to be fundamentally incompatible with an open system model (Pissart 2000, 2003), the alternative origins proposed for the ramparted depressions in Wales are also applicable to similar landforms found in southern Ireland. Because they are not associated with glaciolacustrine deposits, the Irish landforms cannot be iceberg gravity-craters but, as they are normally developed in diamicton (Coxon and O'Callaghan 1987), they could have formed by the stagnation and meltout of glacier ice. Mitchell (1973) acknowledged that caution must be exercised in the interpretation of ramparted depressions in areas where ice-disintegration has taken place, but he did not believe that such processes were important in the region across which ramparted depressions were recorded in southern Ireland. As a more extensive glaciation in southern Ireland is now thought likely during the last glaciation however, there is a

distinct possibility that the ramparted depressions in Ireland could also have glacial origins. Like the ramparted depressions associated with the Welsh and Irish Sea ice masses in west Wales, the Irish landforms may therefore have the potential to provide important information concerning the basal regime and behaviour of the Irish ice sheet, and perhaps also the Irish Sea glacier, during the initial phase of deglaciation after the Last Glacial Maximum.

It does remain possible however that a model of ground-ice mound formation fed by sub-permafrost groundwater seepage through bedrock discontinuities, similar to that suggested for the landforms at Llanpumsaint, could also be applicable to the formation of some of the ramparted depressions in southern Ireland. Although they are found above a wide variety of bedrock types (Bryant and Carpenter 1987), at least some ramparted depressions in Ireland are developed in superficial sediments overlying Ordovician slates and sandstones, which were strongly modified by Caledonian deformation (Mitchell 1973). Direct analogy can therefore be made between the bedrock lithology and structure underlying both the Welsh and Irish landforms. Therefore, it is not unreasonable to assume that the hydrogeological systems in both areas are also similar. Many ramparted depressions in Ireland are located along spring-lines at the foot of south-facing slopes (Coxon and O'Callaghan 1987). This does not necessarily mean that these landforms are the remains of open system pingos however; in fact their density makes such an interpretation highly unlikely. It has been suggested that the smaller ramparted depressions could represent collapsed seasonal frost mounds or mineral palsas (lithalsas) (Coxon and O'Callaghan 1987) but, as some of the ramparts are up to 7 m in height (Coxon and O'Callaghan 1987), it is apparent that the formation and decay of these smaller ground-ice mounds cannot explain all the ramparted depressions in Ireland.

11.4.2 Implications for the interpretation of relict ground-ice features

Diagnostic criteria created for the identification and definition of "pingo scars" have been proposed (e.g. Flemal 1976; De Gans 1988; Mackay 1988). Several of these criteria however cannot even be used to discriminate between relict pingos and landforms created by glacial deposition, let alone between relict pingos and other types of ground-ice mounds. For example, sedimentary deposits associated with mass

wasting, stream deposition and debris flow, plus the presence of normal faults in ramparts (Mackay 1988) are likely both as the result of the meltout of ground-ice, and the meltout of glacier ice.

Flemal (1976) suggested that the following lines of evidence were suggestive of ramparted depressions formed by periglacial ground-ice development rather than those formed by glacial processes: i) development outside the limits of glaciation, or over pro- or postglacial deposits; ii) independent evidence for the existence of permafrost in the surrounding area at the time the ramparted depression formed; iii) an absence of till in the structure, except from within the rampart. Flemal (1976) argued that the differentiation of ramparted depressions formed by the thaw of different ground-ice mounds was much more difficult however. Nevertheless, numerous, overlapping landforms with deformed sediments within their ramparts were believed to be indicative of a pingo origin (Flemal 1976). It is apparent from the ramparted depressions of the Hautes Fagnes Plateau that, rather than supporting an open system pingo origin (Flemal 1976; Ballantyne and Harris 1994), the high density of interfering and superimposed characteristic of many ramparted depressions, particularly in the British Isles, is instead probably more indicative of collapsed lithalsas (Pissart 2000, 2003). Deformation of rampart sediments is also common within the ramparts of relict lithalsas (Pisssart 2000, 2003), as such structures simply indicate the growth of an ice core, rather than the precise origin of the ice (Ballantyne and Harris 1994).

The present study has shown that in areas glaciated during the late Pleistocene, it is extremely difficult to distinguish between ramparted depressions formed by periglacial processes and those that developed through the stagnation and meltout of glacier ice. Using geological and geomorphological evidence to distinguish between landforms that developed from the meltout of buried ice in proglacial lakes (kettle holes) from landforms that developed from the growth of ground-ice under permafrost conditions after lake drainage (e.g. pingos or lithalsas) is extremely difficult. Both mechanisms can produce high-density clusters of ring-ridge landforms (ramparted depressions) of similar morphology and scale, the deformation of soft sediments and the deposition of sediments by mass movement and fluvial processes. Both types of landforms are located in the bottoms of wide valleys with thick

sequences of water-saturated glaciolacustrine deposits. As a consequence, there appears to be little or no unequivocal diagnostic evidence that can be utilised to discriminate between landforms that could be the result of these very different processes.

11.4.3 Geophysical investigations of open system pingos in Svalbard: implications for ramparted depressions

The geophysical investigations undertaken on open system pingos in Svalbard during this project have provided further evidence that the upper few metres of some pingos are composed of alternating units of sediment and ice (Mackay and Stager 1966, Tarnocai and Netterville 1976, Yoshikawa 1993). The observation of alternating units of mineral material and ice has important implications for the generation of ramparts during pingo decay. The alternating ice units inferred from Innerhytte and Riverbed pingos may represent segregation ice rather than injection ice, and during pingo decay may generate episodic gravity-driven mass movement events on the pingo sides. Accumulation of such mass movement deposits has been suggested as a major mechanism of rampart formation (Mackay 1988).

The investigations of pingos in Svalbard have also demonstrated that the conceptual model that assumes pingos contain a simple plano-convex clear ice core is not necessarily the most appropriate. The heave of both Hytte and Longyear pingos appears to have been caused predominantly by the development of segregation ice. Many studies of the internal structure of pingos have emphasised the presence of segregated ice, even in medium-grained sands (Mackay and Stager 1966, Mackay 1973, 1979, Tarnocai and Netterville 1976; Yoshikawa 1993). It is therefore difficult to utilise the presence or absence of a particular ground-ice type (injection ice or segregation ice) to distinguish between pingos, lithalsas and other related active ground-ice mounds. A more realistic approach is to view ground-ice mounds as a continuum of landforms varying in scale, relief and composition of their cores. Unfortunately however, such a conclusion clearly makes the precise interpretation of relict forms even more difficult.

Although the fieldwork programme in Svalbard was designed to provide reference data for the interpretation of relict forms in Wales, it is concluded from the current

investigations that the open system pingos of Svalbard may not provide the most suitable analogue for ramparted depressions in Wales. Throughout Svalbard, the density of pingos is low, with clustering of several landforms only taking place in a few selected localities in nearshore settings (e.g. Woodfjorden). This is in direct contrast to the recognised concentrations of ramparted depressions in Wales and elsewhere in the British Isles. Permafrost in Svalbard is probably too thick (Liestøl 1977) to provide the most appropriate analogue for those parts of the British Isles glaciated during the late Pleistocene. Nevertheless, the current investigations have highlighted the variety of ground-ice types found even within individual open system pingos fed by groundwater seepage, providing further evidence supporting the argument for a continuum of ground-ice mounds.

12 Conclusions and future research

12.1 Main conclusions

12.1.1 The internal structure and origins of ramparted depressions in Wales

The results presented in this thesis do not support the interpretation that all the ramparted depressions of mid and west Wales formed either as a result of the collapse of open system pingos (Watson 1971, 1972, 1977; Watson and Watson 1972, 1974) or lithalsas (mineral palsas) (Pissart and Gangloff 1984; Gurney 1994, 1995; Gurney and Worsley 1996). It is clear that the density of the ramparted depressions at all sites in Wales is much greater than that of active open system pingos in the current permafrost zone. Whilst the groups of ramparted depressions at Llanpumsaint, Crychell Moor and the Cletwr valley could represent the remains of late Pleistocene lithalsas (mineral palsas), each could alternatively have formed as the result of processes associated with the meltout of glacier ice.

- In the Hirwaun valley, linear elongate ridges cored with compact, calcareous, homogenous fine-grained Irish Sea till (with a strongly preferred clast fabric orientation, and containing numerous striated clasts) are either subglacially derived, or ice-marginal landforms. These ridges could represent De Geer moraines, which formed subaqueously where the Irish Sea glacier calved into Lake Teifi.

- Fluvioglacial outwash sediments deposited by the retreating Teifi glacier dominate the internal structure of the linear to chaotic esker-like ridges at Llanio Fawr in the upper Teifi valley. The low ridges and shallow depressions at this site probably reflect deposition of these sediments onto the surface of either stagnating glacier ice, or an extensive proglacial icing.

- The preferred interpretation for the small, enclosed depressions at Crychell Moor is one of supraglacial sedimentation associated with the meltout of stagnating glacier ice. The site investigations at this locality were limited however, and it is

363

possible that the fine-grained clayey silt found within the investigated basin may represent only part of a laterally extensive frost-susceptible medium, highly conducive to the development of periglacial ground-ice mounds. If this were the case, groundwater seepage through an underlying fault zone may have promoted their development by providing a constant water supply to feed the growth of segregation ice.

- This study found no evidence supporting the argument that the ramparted depressions of the Cledlyn valley are the remains of open system pingos or lithalsas. No evidence for extensive glaciolacustrine sediments, as postulated by Gurney (1994, 1995) was found beyond the confines of the central basins of the landforms. The ramparts are cored with a homogenous, matrix-supported, compact till containing striated clasts, suggesting that glacial processes have played a role in their development. Without further investigations however, unequivocal interpretations of these ramparted depressions are difficult. For example, it is difficult to establish on the basis of the current sedimentological evidence whether this till has been reworked or is *in situ*. These landforms are unlikely to represent the remains of either open system pingos or lithalsas however, and probably resulted from the meltout of stagnating glacier ice.

- The ramparted depressions of the Cletwr valley are also cored with till. This suggests that these landforms may also be the result of sedimentary deposition associated with the meltout of stagnating glacier ice. The presence of glaciolacustrine sediments at depth beneath the rampart do however provide a substrate suitable for the development of segregation ice, and the possibility that these landforms represent relict ground-ice mounds therefore remains valid.

- The ramparted depressions at Llanpumsaint are the most likely, of all the sites investigated during this project, to represent the remains of periglacial ground-ice mounds. They are developed within frost-susceptible, fine-grained glaciolacustrine sediments, and groundwater seepage from an underlying fault zone may have provided a supply of water sustaining segregation ice development. Although on the basis of the current evidence this is the preferred interpretation of these landforms, it is also possible that the ramparted depressions

could be iceberg gravity craters formed by the grounding of icebergs during drainage of an ice dammed lake (Lake Gwili). Arching sedimentary structures within the rampart of one ramparted depression at Llanpumsaint, as revealed by trenching, are consistent with both interpretations.

• The precise origins of the ramparted depressions in Wales therefore remain uncertain. Whilst several groups of landforms (Llanpumsaint, Crychell Moor and Cletwr valley) could be interpreted as the remains of periglacial ground-ice mounds, each could just as convincingly be interpreted as the result of the stagnation of glacial ice. Other groups of landforms (Cledlyn valley, Hirwaun valley, Llanio Fawr) are almost certainly of glacial origins. These conclusions have clear implications for the interpretation of all ramparted depressions located in formerly glaciated areas (e.g. in the western and northern parts of the United Kingdom, and in southern Ireland). It is therefore essential that all potential glacial origins can be dismissed before firm conclusions can be made that such landforms represent the remains of periglacial ground-ice mounds. There are currently few, if any, diagnostic criteria that can distinguish between the landforms and sediments produced by these quite different processes.

• This study indicates that ramparted depressions should not be interpreted as relict lithalsas (mineral palsas) simply on the basis of the presence of sediments that have frost-susceptible properties which *could* make them suitable materials for the development of segregation ice through cryosuction (e.g. Gurney 1995; Gurney and Worsley 1996). There are many different processes (both periglacial and glacial) that can explain the origins of ramparted depressions developed in such sediments. The substrate alone is not an unequivocal indicator of the origins of ramparted depressions.

• Groundwater seepage through faults and other discontinuities can play a key role in the development of periglacial ground-ice mounds, whether they are lithalsas, open system pingos or transitional landforms between these two classification types. Future investigations of both relict and active periglacial ground-ice mounds should pay close attention to the hydrogeological regime where such landforms are located.

12.1.2 The internal structure of active open system pingos and other periglacial ground-ice mounds

The geophysical investigations of active open system pingos in Svalbard presented in this thesis have made a significant contribution to our understanding of the physical characteristics of the internal structure of these landforms.

- Although they were unable to delimit the geometry of the ice-core within Innerhytte and Riverbed pingos, ground penetrating radar investigations of these landforms have suggested that the upper parts of the internal structure of these landforms are cored with alternating units of injection ice, and sediments or disaggregated bedrock rich in segregation-ice.

- The electrical resistivity of Hytte and Longyear pingos is inconsistent with the presence of a body of massive ground ice, suggesting that the internal structures of these landforms do not follow the classic model of a plano-convex pingo-core of massive injection ice. Instead, the internal structure of these landforms may be dominated by segregation ice and localised pockets of massive ice within a matrix of partially frozen, fine-grained, isostatically uplifted marine muds.

- Although the pingos in the lower parts of Adventdalen, Svalbard are associated with groundwater seepage and are clearly of the open system type, geophysical surveys indicate that the internal structure of these landforms may be cored with a mixture of massive injection ice and lenses of segregation ice. These landforms may therefore represent a transitional ground-ice mound that lies on a continuum of landforms between open system pingos and lithalsas. However, without detailed borehole information on ground-ice conditions within the cores of a range of ground-ice mounds from a variety of environmental settings, plus knowledge of local and regional hydrogeology at each site, such a hypothesis is extremely difficult to test.

12.2 Future research

12.2.1 The formation of ramparts and their internal structures

Little observational evidence is currently available from contemporary studies in permafrost regions regarding the mechanisms of rampart formation by active periglacial ground-ice mounds. In particular, there is a distinct lack of observational data assessing the processes of open system pingo decay and collapse. Future work should therefore be directed at monitoring and modelling the geomorphological and sedimentological processes by which pingos and other ground-ice mounds create ramparts. As well as observing the decay phase of ground-ice mounds, observations and modelling of the growth phase may also be important for understanding rampart formation. For example, although ramparts form predominantly as a result of gravitational mass movement processes and slopewash during landform collapse, oblique heaving and lateral displacement during growth also contribute to rampart formation (Svensson 1969; Pissart 2000, 2003). Understanding the role played by these processes during ground-ice growth should therefore be a priority. Such investigations will provide a greater understanding of the mechanisms of rampart formation, and assist in the accurate identification and classification of relict Pleistocene ramparted ground ice depressions.

12.2.2 Important sites identified for future work

Of all the sites presented in this thesis, the clear uncertainties regarding the interpretation of the landforms of the Cledlyn valley and the possibility that they could be the result of glacial processes means that this site is particularly worthy of more detailed future investigations. The superficial geology of the Cledlyn valley is obviously highly complex (Chapter 7) and the boreholes and trial pit data presented in this project simply represent spot data within a very localised area, and to limited depths. Only a systematic series of deep boreholes throughout the Cledlyn valley, integrated with extensive geophysical surveys, would provide sufficient data to enable a comprehensive understanding of the internal structure and cryogenic origins of these landforms. Such a project should be viewed as a clear research priority. As the Cledlyn ramparted depressions can be viewed as a component of a wider landsystem of similar landforms in the adjacent Grannell and Cletwr valleys, clarification of the

processes responsible for their formation may provide key information on the nature and behaviour of the Welsh ice mass during and following the Last Glacial Maximum.

12.2.3 Dating the formation of ramparted depressions

Whilst it is clear that the majority of ramparted depressions in Wales and the rest of the British Isles date to the late Devensian period, it has been assumed by many that the landforms in Wales are Loch Lomond Stadial in age on the basis of radiocarbon dates and pollen analysis which date the initiation of organic sedimentation within basin fills (e.g. Watson 1977; Shotton *et al.* 1974, 1975; Handa and Moore 1976; Walker and James 2001; Harris 2001b). This may not be the case however; so far it has proven impossible to quantitatively date the formation of these features, primarily because of the lack of exposed rampart sections. The reinvestigation of previously identified sites for dateable material beneath enclosing ramparts has been proposed as a primary research objective (Bryant and Carpenter 1987), and this suggestion is supported by this author. The application of optically stimulated luminescence dating may have considerable potential in any future investigations, particularly at sites where units of sand are found within the ramparts (e.g. Llanpumsaint). Luminescence dates constraining the deposition of these units of sand, and therefore the timing of rampart formation, could play an important role in the interpretation of these landforms. For example, if sediments within the ramparts are dated to the end of the Younger Dryas or early Holocene, then these landforms cannot have glacial origins.

A

Åhman, R. (1973) Studier av pingos I Adventdalen och Reindalen på Spetsbergen. *Lund Universitets Naturgeografiska Institution, Rapporter och Notiser*, **15**, 27-44.

Åhman, R., (1976). The structure and morphology of minerogenic palsas in northern Norway. *Biuletyn Peryglacjalny*, **26**, 25-31.

Åkerman, J., (1982). Studies on naledi (icings) in west Spitsbergen. *Proceedings of the 4ᵗʰ Canadian Permafrost Conference, Calgary 1982*, 189-202.

Åkerman, J., (1987). Periglacial forms of Svalbard: a review. In Boardman, J., (ed) *Periglacial Processes and Landforms in Britain and Ireland*, Cambridge, Cambridge University Press, 9-25.

Åkerman, H.J., & Malmström, B., (1986). Permafrost mounds in the Abisko area, northern Sweden. *Geografiska Annaler*. **68A**, 155-165.

Aaltonen, J., (2003). The combination of GPR and CVES measurements. *Near Surface Geophysics*, **1**, 195-199.

Aartolahti, T., (1974). Ring ridge hummocky moraines in northern Finland. *Fennia*, **134**, 22 pp.

Allard, M., Seguin, M. K. and Lévesque, R. (1987). Palsas and mineral permafrost mounds in northern Québec. In Gardiner, V., editor, *International Geomorphology. Part II*. Chichester: J. Wiley and Sons Ltd, 285–309.

Allard, M., Caron, S., & Bégin, Y., (1996). Climatic and ecological controls on ice segregation and thermokarst: the case history of a permafrost plateau in northern Quebec. *Permafrost and Periglacial Processes*, **7**, 207-227.

Allard, M., & Rousseau, L., (1999). The internal structure of a palsa and a peat plateau in the Rivière Boniface region, Quebéc: inferences on the formation of ice segregation mounds. *Géographie physique et Quaternaire*, **53**, 373-387.

Allen, A., (1960). Seismic refraction investigations of the pre-glacial valley of the River Teifi near Cardigan. *Geological Magazine*, **97**, 276-282.

Allen, C.R., O'Brien, R.M.G., & Sheppard, S.M.F., (1976). The chemical and isotopic characteristics of some northeast Greenland surface and pingo waters. *Arctic and Alpine Research*, **8**, 297-317.

Allen, J.R.L., (1982). Late Pleistocene (Devensian) glaciofluvial outwash at Banc-y-Warren, near Cardigan (west Wales). *Geological Journal*, **17**, 31-47.

An, W., & Allard, M., (1995). A mathematical approach to modelling palsa formation: Insights on processes and growth conditions. *Cold Regions Science and Technology*, **23**, 231-244.

Anderson, D.M., & Morgenstern, N.R., (1973). Physics, chemistry, and mechanics of frozen ground: a review. Proceedings of the 2nd International Conference on Permafrost, Yakutsk, Washington DC. National Academy of Science, 257-288.

Anderson, J.G.C., & Owen, T.R., (1979). The late Quaternary history of the Neath and Afan valleys, South Wales. *Proceedings of the Geologists Association*, **90**, 203-211.

Anketell, J.M., (1987). On the geological succession and structure of South-Central Wales. *Geological Journal*, **22**, 155-165.

Annan, A.P., (1999). *Practical Processing of GPR Data*. Proceedings of the Second Government Workshop on Ground Penetrating Radar. Sensors and Software Inc. 16 p.

Annan, A.P., & Cosway, S.W., (1992). *Ground Penetrating Radar Survey Design*. Paper Prepared for the Annual Meeting of SAGEEP, Chicago, April 26-29, 1992. Sensors and Software Inc. 12 p.

Annan, A.P., & Davis, J.L., (1976). Impulse radar sounding in permafrost. *Radio Science*, **11**, 383-394.

Annan, A.P., Davis, J.L., & Scott, W.J., (1975). Impulse radar wide angle reflection and refraction sounding in permafrost. *Geological Survey of Canada Paper*, **75-1C**, 343-351.

Arcone, S.A., & Delaney, A.J., (1989). Investigations of dielectric properties of some frozen materials using cross-borehole radiowave pulse transmission: U.S. Army Cold Regions Research and Engineering Lab. CRREL Report 89-4.

Arcone, S.A., Tobiasson, W., & Delaney, A.J., (1995). *Ground-Penetrating Radar Investigation of the Proposed Dome - CARA Tunnel Route and Utilities at South Pole Station, Antarctica*. US Army Corps of Engineers. CRREL Report 95-24. 24 p.

Arcone, S.A., Lawson., D.E., Delaney, A.J., Strasser, J.C., & Strasser, J.D., (1998). Ground-penetrating radar reflection profiling of groundwater and bedrock in an area of discontinuous permafrost. *Geophysics*, **63**, 1573-1584.

Ashley, G.M., (2002). Glaciolacustrine environments. *In* J. Menzies (ed.), *Modern and past glacial environments*. Butterworth-Heinemann, Oxford, pp. 335-359.

Atkinson, T.C., Briffa, K.R., & Coope, G.R. (1987). Seasonal temperatures in Britain during the past 22,000 years, reconstructed using beetle remains. *Nature*, **325**, 587-592.

van Autenboer, T., & Loy, W., (1966). Pingos in north-west Spitsbergen. *Norsk Polarinstitutt, Årbok* 1965. 75-80.

Auton, C.A., (1992). The utility of conductivity surveying and resistivity sounding in evaluating sand and gravel deposits and mapping drift sequences in northeast Scotland. *Engineering Geology*, **32**, 11-28.

B

Babiński, Z., (1982). Pingo degradation in the Bayan-Nuurin-Khotnor Basin, Khangai Mountains, Mongolia. *Boreas*, **11**, 291-298.

Ballantyne, C.K., & Harris, C., (1994). *The Periglaciation of Great Britain*. Cambridge University Press, Cambridge, 330 pp.

Bastin, B., Juvigné, E., Pissart, A., & Thorez, J., (1974). Étude d'une coupe dégagée a travers un rampart d'une cicatrice de pingo de la Brackvenn. *Annales de la Société Géologique de Belgigue*, **97**, 341-358.

Beaudry, L.M., & Prichonnet, G., (1991). Late Glacial De Geer moraines with glaciofluvial sediment in the Chapais area, Québec (Canada). *Boreas*, **20**, 377-394.

Benn, D.I. (1994a). Fabric shape and the interpretation of sedimentary fabric data. *Journal of Sedimentary Research*, **A64**, 910-915.

Benn, D.I., (1994b). Fluted moraine formation and till genesis below a temperate valley glacier: Slettmarkbreen, Jotunheim, southern Norway. *Sedimentology*, **41**, 279-292.

Benn, D.I., (1995). Fabric signature of subglacial till deformation, Breidamerkurjökull, Iceland. *Sedimentology*, **42**, 735-747.

Benn, D.I., (2004). Macrofabric. *In* Evans, D.J.A & Benn, D.I., (eds). *A Practical Guide to the Study of Glacial Sediments*, 93-114, Arnold, London

Benn, D.I., & Evans, D.J.A., (1996). The interpretation and classification of subglacially-deformed materials. *Quaternary Science Reviews*, **15**, 23-52.

Benn, D.I., & Evans, D.J.A. (1998). *Glaciers and Glaciation*. Arnold, London.

Bennett, M.R., Waller, R.I., Glasser, N.F., Hambrey, M.J., & Huddart, D., (1999). Glacigenic clast fabrics: genetic fingerprint or wishful thinking? *Journal of Quaternary Science*, **14**, 125-135.

Berthling, I., Etzelmüller, B., Isaksen, K., & Sollid, J.L., (2000). Rock glaciers on Prims Karls Forland. II: GPR soundings and the development of internal structures. *Permafrost and Periglacial Processes*, **11**, 357-369.

Beskow, G., (1935). Tjäbildningen och tjällyftningen med särskild hänsyn till vägar och jarnägar. *Sveriges Geologiska Undersökning*. Arsbok 26, Ser. C, No. 375.

Blake, K.P., (2000). Common origin for De Geer moraines of variable composition in Raudvassdalen, northern Norway. *Journal of Quaternary Science*, **15**, 633-644.

Boone, S.J., & Eyles, N., (2001). Geotechnical model for great plains hummocky moraine formed by till deformation below stagnant ice. *Geomorphology*, **38**, 109-124.

Borgström, I., (1979). De Geer moraines in a Swedish mountain area? *Geografiska Annaler*, **61 A**, 35-42.

Boulton, G.S., (1972). Modern Arctic glaciers as depositional models for former ice sheets. *Quarterly Journal of the Geological Society of London*, **128**, 361-393.

Boulton, G.S., & Hindmarsh, R.C.A., (1987). Sediment deformation beneath glaciers: rheology and sedimentological consequences. *Journal of Geophysical Research*, **92**, B9, 9059-9082.

Boulton, G.S., & Jones, A.S., (1979). Stability of temperate ice caps and ice sheets resting on beds of deformable sediment. *Journal of Glaciology*, **24**, 29-43.

Boulton, G.S., & Paul, M.A., (1976). The influence of genetic processes on some geotechnical properties of tills. *Journal of Engineering Geology*, **9**, 159-194.

Boulton, G.S., van der Meer, J.J.M., Hart, J., Beets, D., Ruegg, G.H.J., van der Wateren, F.M., & Jarvis, J., (1996). Till and moraine emplacement in a deforming bed surge – an example from a marine environment. *Quaternary Science Reviews*, **15**, 961-987.

Bowen, D.Q., (1967). On the supposed ice dammed lakes of south Wales. *Transactions of the Cardiff Naturalists Society*, **93**, 4-17.

Bowen, D.Q., (1970). South-east and central South Wales. In: Lewis, C.A., (ed.) *The Glaciations of Wales and Adjoining Regions*. Longman, London, 197-228.

Bowen, D.Q., (1973a). The Pleistocene history of Wales and the Borderland. *Geological Journal*, **8**, 207-224.

Bowen, D.Q., (1973b). The Pleistocene succession of the Irish Sea. *Proceedings of the Geologists Association*, **84**, 249-272.

Bowen, D.Q., (1974). The Quaternary of Wales. In Owen, T.R. (ed), *The upper Palaeozoic and post-Palaeozoic rocks of Wales*. University of Wales Press, Cardiff, 373-426.

Bowen, D.Q. , (1977). The coast of Wales. In: Kidson, C. & Tooley, M.J. (eds). *The Quaternary History of the Irish Sea*. Geological Journal Special Issue No. 7. Seel House Press, Liverpool, 223-256.

Bowen, D.Q., (1981). The 'South Wales end-moraine': fifty years after. In: Neale, J., & Flenley, J. (eds.) *The Quaternary of Britain*. Pergamon Press, Oxford, 60-67.

Bowen, D.Q., (1999). Wales. In: Bowen, D.Q., (ed.) *A Revised Correlation of Quaternary Deposits in the British Isles. Geological Society of London Special Report No. 23*, 79-90.

Bowen, D.Q., (2005). South Wales. *In* Lewis, C.A., & Richards, A.E., (eds.), *The Glaciations of Wales and Adjoining Areas*, Logaston Press, Bristol, 145-164.

Bowen, D.Q., & Gregory, K.J., (1965). A glacial drainage system near Fishguard, Pembrokeshire. *Proceedings of the Geologists' Association*, 74, 275-281.

Bowen, D.Q., & Lear, D.L., (1982). The Quaternary Geology of the lower Teifi Valley. In: Bassett, M.G. (ed.). *Geological Excursions in Dyfed, south-west Wales*. National Museum of Wales, Cardiff, 297-302.

Bowen, D.Q., Phillips, F.M., McCabe, A.M., Knutz, P.C., & Sykes, G.A. (2002). New data for the Last Glacial Maximum in Great Britain and Ireland. *Quaternary Science Reviews*, 21, 89-101.

Brabham, P.J., & Goulty, N.R., (1988). Seismic refraction profiling of rockhead in the Coal Measures of northern England. *Quarterly Journal of Engineering Geology*, 21, 201-206.

Brabham, P.J., McDonald, R.J., & McCarroll, D., (1999). The use of shallow seismic techniques to characterize sub-surface Quaternary deposits: the example of Porth Neigwl (Hells Mouth Bay), Gwynedd, N. Wales. *Quarterly Journal of Engineering Geology*, 32, 119-137.

Brabham, P.J., Thomas, J., & McDonald, R.J. (2005). The terrestrial shallow seismic reflection technique applied to the characterization and assessment of shallow sedimentary environments. *Quarterly Journal of Engineering Geology and Hydrogeology*, 38, 23-38.

Bradley, R. I. (1980). Soils in Dyfed V: Sheet SN24 (Llechryd). Record No. 63, Soil Survey of England and Wales, Harpenden.

Bristow, C.S., & Jol, H.M., (2003a). (eds.) *Ground Penetrating Radar in Sediments*. Geological Society, London, Special Publications, 211. 327 p.

Bristow, C.S., & Jol, H.M., (2003b). An introduction to ground penetrating radar (GPR) in sediments. In Bristow, C.S., & Jol, H.M., (eds.) *Ground Penetrating Radar in Sediments*. Geological Society, London, Special Publications, 211, 1-7.

British Geological Survey Sheet 194: *Llangrannog, England and Wales Sheet 194*, 1:50,000 unpublished geological map, British Geological Survey, Keyworth.

British Geological Survey Sheet 195: *Lampeter, England and Wales Sheet 195*, 1:50,000 unpublished geological map, British Geological Survey, Keyworth.

British Geological Survey Sheet 211: *Newcastle Emlyn, England and Wales Sheet 211*, 1:50,000 unpublished geological map, British Geological Survey, Keyworth.

British Geological Survey (1967). *Carmarthen, England and Wales Sheet 229: Drift Geology, 1:50 000* British Geological Survey, Keyworth.

British Geological Survey, (1993). *Rhayader. England and Wales Sheet 179. Solid and Drift Geology.* 1:50,000. Keyworth, Nottingham.

British Geological Survey, (1994a). *Llanilar. England and Wales Sheet 165. Solid and Drift Geology.* 1:50,000. Keyworth, Nottingham.

British Geological Survey, (1994b). *Montgomery. England and Wales Sheet 165. Solid and Drift Geology.* 1:50,000. Keyworth, Nottingham.

British Geological Survey (1997). *Geology of the Afon Teifi Catchment, Map 1: Drift Deposits, 1: 50,000.* British Geological Survey, Keyworth.

British Geological Survey (2003). Cardigan and Dinas Island. England and Wales Sheet 193. Solid and Drift Geology. 1:50 000. British Geological Survey, Keyworth, Nottingham.

British Geological Survey, (2005). Builth Wells. *England and Wales Sheet 196. Solid and Drift Geology.* 1:50,000. Keyworth, Nottingham.

British Standard Institution (1990). *Methods of Test of Soil for British Civil Engineering Purposes,* no. 1377, BSI London. HMSO.

British Standards Institution (1999). *Code of practice for site investigations,* no. 5930. BSI London. HMSO.

Brouchkov, A., (2002). Nature and distribution of frozen saline sediments on the Russian Arctic Coast. *Permafrost and Periglacial Processes,* 13, 83-90.

Brown, J., Ferrians Jr, O.J., Heginbottom, J.A. and Melnikov, E.S. (1997). Circum-Arctic map of permafrost and ground-ice conditions. Circum-Pacific map series -45, U.S. Geological Survey 1/10 000 000.

Brown, R.J.E., & Péwé, T.L., (1973). Distribution of permafrost in North America and its relationship to the environment: a review 1963-1973. In *Permafrost, North American Contribution to 2nd International Conference on Permafrost.* National Academy of Science, Washington, D.C., 71-100.

Brown, J., Nelson, F., Brockett, B., Outcalt, S.I., & Everett, K.R., (1983). Observations on ice-cored mounds at Sukakpak Mountain, South Central Brooks Range, Alaska. *Proceedings, Fourth International Permafrost Conference, National Academy Press, Washington* DC, 91-96.

Bryant, R.H., & Carpenter, C.P. (1987). Ramparted ground ice depressions in Britain and Ireland. In Boardman, J., (ed.). *Periglacial processes and landforms in Britain and Ireland.* Cambridge University Press, Cambridge, 183-190.

Bryant, R.H., Carpenter, C.P., & Ridge, T.S., (1985). Pingo scars and related features in the Whicham Valley, Cumbria. In Boardman, J., (ed.) *Field Guide to the*

Periglacial Landforms of Northern England. Quaternary Research Association, Cambridge, 47-53.

C

Campbell, S., (1984). The nature and origin of the Pleistocene deposits around Cross Hands and on west Gower, South Wales. *Unpublished Ph.D. thesis, University of Wales.*

Campbell, S., & Bowen, D.Q., (1989). *Quaternary of Wales.* Geological Conservation Review Series, 2. Nature Conservancy Council, Peterborough.

Campbell, S., & Shakesby, R.A., (1994). Late Pleistocene deposits at Broughton Bay, Gower, South Wales: evidence for deposition at a non-marine Devensian ice margin. *Proceedings of the Geologists Association,* **105,** 167-185.

Carpenter, C.P., & Woodcock, M.P., (1981). A detailed investigation of a pingo remnant in Surrey. *Quaternary Studies,* **1,** 1-26.

Carruthers, R.M., Chacksfield, B.C., Heaven, R.E., (1997). *A Geophysical Investigation to Determine the Thickness and Nature of Glacial Deposits in the Buried Valleys of Afon Teifi between Cardigan and Llanybydder.* British Geological Survey Technical Report, WK/97/05 (included as Appendix 2 in Waters *et al.* 1997).

Cave, R., & Hains, B.A., (1986). Geology of the country between Aberystwyth and Machynlleth. *Memoir of the British Geological Survey, Sheet 163 (England & Wales).*

Cave, R., & Hains, B.A., (2001). *Geology of the country around Montgomery and the Ordovician rocks of the Shelve area: Memoir for 1:50,000 geological sheet 165 with part of sheet 151 (Welshpool) (England and Wales).* British Geological Survey, Stationery Office, London, 173 p.

Charlesworth, J.K., (1929). The south Wales end moraine. *Quarterly Journal of the Geological Society of London,* **85,** 335-358.

Christiansen, H.H., (1995). Observations of open system pingos in a marsh environment, Mellemfjord, Disko, central west Greenland. *Danish Journal of Geography,* **95,** 42-48.

Christiansen, H.H.; French, H.M. & Humlum, O. (2005) Permafrost in the Gruve-7 mine, Adventdalen, Svalbard. *Norwegian Journal of Geography,* 59, 109-115.

Clark, C.D., Gibbard, P.L., & Rose, J., (2004). Pleistocene glacial limits in England, Scotland and Wales. *In* Ehlers, J., & Gibbard, P.L., (eds.), *Quaternary Glaciations: Extent and Chronology, Part 1; Europe.* Developments in Quaternary Science, Elsevier, Amsterdam, 47-82.

Clark, C.D., & Meehan, R.T., (2001). Subglacial bedform geomorphology of the Irish Ice Sheet reveals major configuration changes during growth and decay. *Journal of Quaternary Science,* **16,** 483-496.

Clark, P.U., (1994). Unstable behaviour of the Laurentide Ice Sheet over deforming sediment and its implications for climate change. *Quaternary Research*, **41**, 19-25.

Clayton, L., and Moran, S.R. (1974). A glacial process form model. In Coates, D.R., (ed.) *Glacial Geomorphology*. Publications in Geomorphology, State University of New York, Binghampton, 89-119.

Comas, X., Slater, L., & Reeve, A., (2004). Geophysical evidence for peat basin morphology and stratigraphic controls on vegetation observed in a Northern Peatland. *Journal of Hydrology*, **295**, 173-184.

Comas, X., Slater, L., & Reeve, A., (2005). Stratigraphic controls on pool formations in a domed bog inferred from ground penetrating radar (GPR). *Journal of Hydrology*, **315**, 40-51.

Coope, G.R., (1977). Fossil coleopteran assemblages as sensitive indicators of climatic changes during the Devensian (last) cold stage. *Philosophical Transactions of the Royal Society of London*, **B280**, 313-340.

Coope, G.R., & Brophy, J.A., (1972).Late-glacial environmental changes indicated by a coleopteran succession from North Wales. *Boreas*, **1**, 97-142.

Coultish, T.L., & Lewkowicz, A.G., (2003). Palsa dynamics in a subarctic mountainous environment, Wolf Creek, Yukon Territory, Canada. *In*, Phillips, M., Springman, S.M., & Arenson, L.U., (eds) *Proceedings of the 8th International Conference on Permafrost, 21-25th July 2003, Zurich, Switzerland*. Swets and Zeitlinger, Lisse.

Coxon, P., (1978). The first record of a fossil naled in Britain. *Quaternary Newsletter*, **24**, 9-11.

Coxon, P. (1986). A radiocarbon dated Early Post Glacial pollen diagram from a pingo remnant near Millstreet Co. Cork. *Irish Journal of Earth Sciences*, **8**, 9-20.

Coxon, P. & O'Callaghan, P., (1987). The distribution and age of pingo remnants in Ireland. In Boardman, J., (ed.), *Periglacial processes and landforms in Britain and Ireland*. Cambridge University Press, Cambridge, 195-202.

Craig, J., (1987). The structure of the Llangranog Lineament, west Wales: A Caledonian transpression zone. *Geological Journal*, **22**, 167-181.

Crampton, C.B., & Taylor, J.A., (1967). Solifluction terraces in south Wales. *Biuletyn Peryglacjalny*, **16**, 15-36.

Crimes, T.P., Chester, D.K., Hunt, N.C., Lucas, G.R., Mussett, A.E., Thomas, G.S.P., & Thompson, A., (1994). Techniques used in aggregate resource analysis of four areas in the UK. *Quarterly Journal of Engineering Geology*, **27**, 165-192.

Crimes, T.P., Lucas, G.R., Chester, D.K., Thomas, G.S.P., James, P.A., McCall, G.J., Hunt, N.C., Chapman, A., & Lancaster, K., (1992). *An appraisal of the land based sand and gravel resources of South Wales.* Open file report, Engineering Geology Unit, University of Liverpool, for the Department of the Environment (Welsh Office), Cardiff. p. 88.

Cruickshank, J.G., & Colhoun, E.A., (1965). Observations on pingos and other landforms in Schuchertdal, northeast Greenland. *Geografiska Annaler*, **47**, 224-236.

Culver, S.J., & Bull, P.A., (1979). Late Pleistocene rock basin lakes in South Wales. *Geological Journal*, **14**, 107-116.

Currant, A.P., Stringer, C.B., & Collcutt, S.N., (1984). Bacon Hole Cave. *In* Bowen, D.Q., & Henry, A., (eds.), *Wales: Gower, Preseli and Fforest Fawr.* Quaternary Research Association Field Guide, April 1984, 38-44.

D

Dahlin, T., (1996). 2D resistivity surveying for environmental and engineering applications. *First Break*, **14**, 275-283.

Dallimore, S.R., & Davis, J.L., (1987). Ground probing radar investigations of massive ground ice and near surface geology in continuous permafrost. *Geological Survey of Canada*, Paper **87-1A**, 913-918.

Dallimore, S.R., & Davis, J.L., (1992). Ground penetrating radar investigations of massive ground ice. In Pilon, J.A., (ed.). *Ground Penetrating Radar, Geological Survey of Canada Paper*, **90-4**, 41-48.

van Dam, R.L., van den Berg, E.H., Schaap, M.G., Boekma, L.H., & Schlager, W., (2003). Radar reflections from sedimentary structures in the vadose zone. In Bristow, C.S., & Jol, H.M., (eds.) *Ground Penetrating Radar in Sediments.* Geological Society, London, Special Publications, **211**, 257-273.

David, J.E., (1883). On the evidence of glacial action in south Brecknockshire and east Glamorganshire. *Quarterly Journal of the Geological Society of London*, **39**, 39-54.

Davies, D.C. (1988). *The amino-stratigraphy of British Pleistocene glacio-deposits.* Unpublished Ph.D. thesis, University of Wales, Aberystwyth.

Davies, J.R., Fletcher, C.J.N., Waters, R.A., Wilson, D., Woodhall, D.G., & Zalasiewicz, J.A., (1997). Geology of the country around Llanilar and Rhayader *Memoir of the British Geological Survey*, Sheets 178 and 179 (England and Wales). British Geological Survey, Nottingham.

Davies, J.R., Waters, R.A., Wilby, P.R., Williams, M., & Wilson, D., (2003). Geology of the Cardigan and Dinas Island district – a brief explanation of the geological map. *Sheet Explanation of the British Geological Survey*, 1:50,000 Sheet 193 (including part of Sheet 210) Cardigan and Dinas Island (England and Wales).

Davis, J.L., & Annan, A.P. (1989). Ground-penetrating radar for high-resolution mapping of soil and rock stratigraphy. *Geophysical Prospecting*, **37**, 531-551.

Davis, J.L., Scott, W.J., Morey, R.M., & Annan, A.P., (1976). Impulse radar experiments on permafrost near Tuktoyaktuk, Northwest Territories. *Canadian Journal of Earth Sciences*, **13**, 1584-1590.

De Gans, W. (1981). *The Drentsche Aa valley, system: a study in Quaternary geology*. Thesis, Vrije Universiteit te Amsterdam, pp. 132.

De Gans, W. (1988). Pingo scars and their identification. *In*, Clark, M.J., (ed). *Advances in periglacial geomorphology*. Wiley, Chichester, 299-322.

De Geer, G., (1940). *Geochronologia Suecica, Principles*. Kuglica Svenska Vetenskab Akademiens Handlingar 18, 1-90.

Delaney, A.J., & Arcone, S.A., (1984). Dielectric measurements of frozen silt using time domain reflectometry. *Cold Regions Science and Technology*, **9**, 39-46.

Delaney, A., Sellmann, P., & Arcone, S., (1988). Seasonal variations in resistivity and temperature in discontinuous permafrost. In K. Senneset (ed.): Proceedings of the 5th International Conference on Permafrost. Vol. 1. pp. 927–932. Trondheim: Tapir Publishers.

Delisle, G., Allard, M., Fortier, R., Calmels, F., & Larrivée, É., (2003). Umiujag, northern Quebéc: innovative techniques to monitor the decay of a lithalsa in response to climate change. *Permafrost and Periglacial Processes*, **14**, 375-385.

Dionne, J.-C., (1978). Formes et phénomènes périglaciaires en Jamésie, Québec subarctique. *Géographie Physique et Quaternaire*, **37**, 127-146.

Domack, E.W., & Lawson, D.E., (1985). Pebble fabric in an ice-rafted diamicton. *Journal of Geology*, **93**, 577-592.

Donnelly, R., (1988). *Glacial sediments at sites of opencast coal extraction in South Wales*. Unpublished Ph.D thesis, University of Wales, Cardiff.

Doolittle, J.A., Hardisky, M.A., & Black, S., (1992). A ground-penetrating radar study of Goodream palsas, Newfoundland, Canada. *Arctic and Alpine Research*, **24**, 173-178.

Dowdeswell, J.A., & Sharp, M.J., (1986). Characterisation of pebble fabrics in modern terrestrial glacigenic sediments. *Sedimentology*, **33**, 699-710.

Dwerryhouse, A.R., and Miller, A.A., (1930). The glaciation of Clun Forest, Radnor Forest and some adjoining districts. *Quarterly Journal of the Geological Society of London*, **86**, 96-129.

E

Etienne, J.L., Hambrey, M.J., Glasser, N.F., & Jansson, K.N., (2005). West Wales. *In* Lewis, C.A., & Richards, A.E., (eds.), *The Glaciations of Wales and Adjoining Areas*, Logaston Press, Bristol, 85-100.

Etienne, J.L., Jansson, K.N., Glasser, N.F., Hambrey, M.J., Davies, J.R., Waters, R.S., Maltman, A.J., & Wilby, P.R., (2006). Palaeoenvironmental interpretation of an ice-contact glacial lake succession: an example from the late Devensian of southwest Wales, UK., *Quaternary Science Reviews*, **25**, 739-762.

Evans, D.J.A., Owen, L.A., & Roberts, R., (1995). Stratigraphy and sedimentology of Devensian (Dimlington Stadial) glacial deposits, east Yorkshire, England. *Journal of Quaternary Science*, **10**, 241-265.

Evans, D.J.A., & Twigg, D.R., (2002). The active temperate glacial landsystem: a model based on Breidamerkurjökull and Fjallsjökull, Iceland. *Quaternary Science Reviews*, **21**, 2143-2177.

Eyles, N., Boyce, J.I., & Barendregt, R.W., (1999). Hummocky moraine: sedimentary record of stagnant Laurentide Ice Sheet lobes resting on soft beds. *Sedimentary Geology*, **123**, 163-174.

Eyles, N., & McCabe, A.M., (1989). The Late Devensian (<22, 000BP) Irish Sea Basin: the sedimentary record of a collapsed ice sheet margin. *Quaternary Science Reviews*, **8**, 307-351.

Eyles, N., McCabe, A.M., & Bowen, D.Q., (1994). The stratigraphic and sedimentological significance of late Devensian ice sheet surging in Holderness, Yorkshire, U.K. *Quaternary Science Reviews*, **13**, 727-759.

F

Ferrians, O.J., (1983). Pingos on the Arctic Coastal Plain, northeastern Alaska. *In* Permafrost, Fourth International Conference, Fairbanks, Alaska, July 18-22, 1983, Abstracts and program: University of Alaska, 105-106.

Ferrians, O.J., (1988). Pingos in Alaska: a review. *In* Senneset, K., (ed.), Permafrost 5th International Conference Proceedings. Tapir Publishers, Trondheim, 734-739.

Fitches,W.R., & Woodcock, N.H., (1987). Sedimentation and tectonics in the Welsh Basin: Introduction. *Geological Journal*, **22**, 1-5.

Flemal, R.C., (1976). Pingo scars: their characteristics, distribution and utility in reconstructing former permafrost environments. *Quaternary Research*, **6**, 37-53.

Flemal, R.C., Hinkley, K.C., & Hesler, J.L., (1973). DeKalb Mounds: a possible Pleistocene (Woodfordian) pingo field in north-central Illinois. *Geological Society of America, Memoir*, **136**, 229-250

Fletcher, C.J., & Siddle, H.J., (1998). Development of glacial Llyn Teifi, west Wales: evidence for lake-level fluctuations at the margins of the Irish Sea ice sheet. *Journal of the Geological Society, London*, **155**, 389-399.

Forman, S.L., Lubinski, D.J., Ingólfsson, Ó., Zeeberg, J.J., Snyder, J.A., Siegert, M.J., & Matishov, G.G., (2004). A review of postglacial emergence on Svalbard, Franz Josef Land and Novaya Zemlya, northern Eurasia. *Quaternary Science Reviews*, **23**, 1391-1434.

Fortier, R., Lévesque, R., Seguin, M.K., & Allard, M., (1991). Caractérisation du pergélisol de buttes cryogènes à l'aide de diagraphies électriques au Nunavik, Québec. *Permafrost and Periglacial Processes*, **2**, 79–93.

Francis, T.J.G., (1964). A seismic refraction section of the pre-glacial Teifi valley near Cenarth. *Geological Magazine*, **101**, 108-112.

French, H.M., (1975). Pingos investigations and terrain disturbance studies, Banks Island, District of Franklin. *Geological Survey of Canada, Paper 75-1A*, 459-464.

French, H.M., (1979). Periglacial geomorphology. *Progress in Physical Geography*, **3**, 264-273.

French, H.M., & Dutkiewcz, L., (1976). Pingos and pingo-like forms, Banks Island, western Canadian Arctic. *Biuletyn Peryglacjalny*, **26**, 211-222.

French, H.M., Harry, D.G., & Clark, M.J., (1982). Ground ice stratigraphy and late-Quaternary events, south-west Banks Island, Canadian Arctic. *In* French, H.M., (ed), *The Roger J.E. Brown memorial volume. Proceedings of the Fourth Canadian Permafrost Conference, Calgary, Alberta, 2-6 March 1981*. National Research Council of Canada, pp. 81-90.

Furuberg, T., & Berggren, A.-L., (1988) In K. Senneset (ed.): Proceedings of the 5th International Conference on Permafrost. Vol. 1. pp. 1078-1084. Trondheim: Tapir Publishers.

G

Gangloff, P., & Pissart, A., (1983). Évolution géomorphologique et palses minerals dans la region du Kuujjuak (Fort-Chimo, Québec). *Bulletin de la Société Géographique de Liège*, **19**, 119-132.

Gell, W.A., (1978). Fabrics of icing-mound and pingo ice in permafrost. *Journal of Glaciology*, **20**, 563-569.

George, T.N., (1942). The development of the Towy and Upper Usk drainage pattern. *Quarterly Journal of the Geological Society of London*, **98**, 89-137.

George, T.N., (1970). *British regional geology. South Wales* (third edition). H.M.S.O., London.

Gravenor, C.P., & Kupsch, W.O., (1959). Ice-disintegration features in western Canada. *Journal of Geology*, **67**, 48-64

Gray, J.M., & Coxon, P., (1991). The Loch Lomond Stadial glaciation in Britain and Ireland. In Ehlers, J., Gibbard, P.L., & Rose, J., (eds.), *Glacial Deposits in Great Britain and Ireland*, Rotterdam, Balkema, 89-105.

Greenhouse, J.P., & Morgan, A.V., (1977). Resistivity mapping of fossil permafrost patterns in southwestern Ontario. *Canadian Journal of Earth Sciences*, **14**, 496-500.

Gregersen, O., Phukan, A., & Johansen, T., (1983). Engineering properties and foundation design alternatives in marine Svea clay, Svalbard. Proceedings of the 4th International Conference on Permafrost, Fairbanks, Alaska. pp. 384-388.

Gregersen, O., & Eidsmoen, T., (1988). Permafrost conditions in the shore area at Svalbard. In K. Senneset (ed.): Proceedings of the 5th International Conference on Permafrost. Vol. 1. pp. 933-936. Trondheim: Tapir Publishers.

Gregory, K.J., & Bowen, D.Q., (1966). Fluvioglacial deposits between Newport (Pembrokeshire) and Cardigan. *In* Price, R.J., (ed.), *Deglaciation*. Occasional Publication of the British Geomorphological Research Group, **2**, 25-28.

Griffiths, D.H., & Barker, R.D., (1993). Two-dimensional resistivity imaging and modelling in areas of complex geology. *Journal of Applied Geophysics*, **29**, 211-226.

Griffiths, D.H., & Turnbull, J., (1985). A multi-electrode array for resistivity sounding. *First Break*, **3**, 16-20.

Griffiths, J.C. (1940). *The glacial deposits west of the Taff.* Unpublished PhD thesis, University of London.

Gurney, S.D., (1994). *Investigations of the Geomorphology and Sedimentology of Permafrost Related Pingos and Palsas, Ancient and Modern.* Unpublished PhD thesis, University of Reading.

Gurney, S.D. (1995). A reassessment of the relict Pleistocene "pingos" of west Wales: Hydraulic pingos or mineral palsas. *Quaternary Newsletter*, **77**, 6-16.

Gurney, S.D. (1998). Aspects of the genesis and geomorphology of pingos: perennial permafrost mounds. *Progress in Physical Geography*, **22**, 307-324.

Gurney, S.D. (2000). Relict cryogenic mounds in the UK as evidence of climate change. In, McLaren, S.J. & Kniveton, D.R., (eds), *Linking climate change to land surface change*. Kluwer Academic Publishers, Netherlands, 209-229.

Gurney, S.D., (2001). Aspects of the genesis, geomorphology and terminology of palsas: perennial cryogenic mounds. *Progress in Physical Geography*, **25**, 249-260.

Gurney, S.D. & Worsley, P. (1996). Relict cryogenic mounds at Owlbury, near Bishops Castle, Shropshire. *Mercian Geologist*, **14**, 14-21.

Gurney, S.D., & Worsley, P., (1997). Genetically complex and morphologically diverse pingos in the Fish Lake area of south west Banks Island, N.W.T., Canada. *Geografiska Annaler*, **79A**, 41-56.

H

Haeberli, W., & Vonder Mühll, D., (1996). On the characteristics and possible origins of ice in rock glacier permafrost. *Zeitschrift für Geomorphologie Supplement*, **104**, 43-57.

Hagedoorn, J.G., (1959). The plus-minus method of interpreting seismic refraction sections. *Geophysical Prospecting*, **7**, 158-192.

Hambrey, M.J., Davies, J.R., Glasser, N.F., Waters, R.A., Dowdeswell, J.A., Wilby, P.R., Wilson, D., Etienne, J.L., (2001). Devensian glacigenic sedimentation and landscape evolution in the Cardigan area of southwest Wales. *Journal of Quaternary Science*, **16**, 455-482.

Hamilton, T.D. & Obi, C.M. (1982). Pingos in the Brooks range, northern Alaska, USA. *Arctic and Alpine Research*, **14**, 13-20.

Handa, S. & Moore, P.D. (1976). Studies in the vegetational history of mid Wales No. IV: Pollen analysis of some pingo basins. *New Phytologist*, **77**, 205-225.

Harada, K., & Yoshikawa, K., (1996). Permafrost age and thickness near Adventfjorden, Spitsbergen. *Polar Record*, **20**, 267-281.

Harris, C., (1981). *Periglacial Mass Wasting: A Review of Research*. Norwich: Geo Abstracts.

Harris, C., (1991a). Glacial deposits at Wylfa Head, Anglesey, north Wales,: evidence for Late Devensian deposition in a non-marine environment. *Journal of Quaternary Science*, **6**, 67-77.

Harris, C., (1991b). Glacially deformed bedrock at Wylfa Head, Anglesey, North Wales. In Forster, A., Culshaw, M.G., Cripps, J.C., Little, J.A., & Moon, C.F., (eds). *Quaternary Engineering Geology*, Geological Society Engineering Geology Special Publication No. 7, 135-142.

Harris, C., (1998). The micromorphology of paraglacial and periglacial slope deposits: a case study from Morfa Bychan, west Wales, UK. *Journal of Quaternary Science*, **13**, 73-84.

Harris, C., (2001a). Llanon. In Walker, M.J.C., & McCarroll, D., (eds.), *The Quaternary of West Wales: Field Guide*. Quaternary Research Association, London, 65-66.

Harris, C., (2001b). Ground ice depressions, Cledlyn valley. In Walker, M.J.C., & McCarroll, D., (eds.), *The Quaternary of West Wales: Field Guide*. Quaternary Research Association, London, 67-70.

Harris, C., (2002). Middle and late Quaternary permafrost and periglacial environments in the UK: A review of geological evidence. *Report for United Kingdom NIREX Ltd.*

Harris, C., & Donnelly, R., (1991). The glacial deposits of south Wales. In: Ehlers, J. Gibbard, P.L., & Rose, J., (eds). *Glacial deposits in Great Britain and Ireland.* A.A. Balkema, 279-290.

Harris, C., Ross, N., and Sheppard, H., (2005). *Geological Mapping Solutions for Quaternary Ground-Ice Systems; Final Report March 2005.* British Geological Survey UCAC Report. p. 64.

Harris, C., Williams, G., Brabham, P.J., Eaton, G., & McCarroll, D., (1997). Glaciotectonized Quaternary sediments at Dinas Dinlle, Gwynedd, North Wales, and their bearing on the style of deglaciation in the eastern Irish Sea. *Quaternary Science Reviews,* 16, 109-127.

Harris, C., & Wright, M.D., (1980). Some last glaciation drift deposits near Pontypridd, South Wales. *Geological Journal,* 15, 7-20.

Harris, S.A. (1993). Palsa like mounds developed in a mineral substrate, Fox Lake, Yukon Territory. *Proceedings, 6th International Conference on Permafrost, Beijing,* 238-243.

Harris, S.A., (1998). A genetic classification of the palsa-like mounds in western Canada, *Biuletyn Peryglacjalny,* 37, 115-130.

Harris, S.A., French, H.M., Heginbottom, J.A., Johnston, G.H., Ladanyi, B., Sego, D.C., & van Everdingen, R.O., (1988). *Glossary of Permafrost and Related Ground-Ice Terms.* Permafrost Subcommittee, Associate Committee on Geotechnical Research, National Research Council of Canada, Ottwawa, Technical Memorandum, 142, 156 p.

Hart, J.K., (1994). Till fabric associated with deformable beds. *Earth Surface Processes and Landforms,* 19, 15-32.

Hart, J.K., (1995). Subglacial erosion, deposition and deformation associated with deformable beds. *Progress in Physical Geography,* 19, 173-191.

Hart, J.K., & Boulton, G.S., (1991). The inter-relation of glaciotectonic and glaciodepositional processes within the glacial environment. *Quaternary Science Reviews,* 10, 335-350.

Hättestrand, C., & Kleman, J., (1999). Ribbed moraine formation. *Quaternary Science Reviews,* 18, 43-61.

Hauck, C., (2002). Frozen ground monitoring using DC resistivity tomography. *Geophysical Research Letters,* 29, 2016.

Hauck, C., Guglielmin, M., Isaksen, K., & Vonder Mühll, D., (2001). Applicability of frequency-domain and time-domain electromagnetics for mountain permafrost studies. *Permafrost and Periglacial Processes*, **12**, 39-52.

Hauck, C., Isaksen, K., Vonder Mühll, D., & Sollid, J.L., (2004). Geophysical surveys designed to delineate the altitudinal limit of mountain permafrost: an example from Jotunheimen, Norway. *Permafrost and Periglacial Processes*, **15**, 191-205.

Hauck, C., & Vonder Mühll, D., (2003a). Inversion and interpretation of two-dimensional geoelectrical measurements for detecting permafrost in mountainous regions. *Permafrost and Periglacial Processes*, **14**, 305-318.

Hauck, C., & Vonder Mühll, D., (2003b). Permafrost monitoring using time-lapse resistivity tomography. In Phillips, M., Springman, S.M., & Arenson, L.U., (eds.), *Permafrost. Proceedings of the Eighth International Conference on Permafrost, 21-25th July 2003, Zurich, Switzerland*. Swets & Zeitlinger, Lisse, 361-366.

Hauck, C., & Vonder Mühll, D., (2003c). Evaluation of geophysical techniques for application in mountain permafrost studies. In Schrott, L., Hoerdt, A., Dikau, R. (eds.), *Geophysical Methods in Geomorphology, Zeitschrift für Geomorphologie Supplement*, **132**, 161-190.

Hauck, C., Vonder Mühll, D., & Maurer, H., (2003). Using DC resistivity tomography to detect and characterize mountain permafrost. *Geophysical Prospecting*, **51**, 273-284.

Heaven, R.E., Raines, M.G., & Napier, B., (1999). *A Geophysical Study to Determine the Thickness and Nature of Glacial Deposits in the Buried Valleys of Afon Teifi Between Cardigan and Lampeter*. British Geological Survey Technical Report WK/98/13. p. 31.

Helm, D.G., & Roberts, B., (1975). A re-interpretation of the origin of sands and gravels around Banc-y-Warren, near Cardigan, west Wales. *Geological Journal*, **10**, 131-146.

Hicks, H., (1885). In T.G. Bonney: On the so-called Diorite of Little Knott (Cumberland), with further remarks on the occurrence of Picrite in Wales. *Quarterly Journal of the Geological Society of London*, **41**, 511-522.

Hicock, S.R., & Dreimanis, A., (1992). Deformation till in the Great Lakes region: implications for rapid flow along the south central margim of the Laurentide Ice Sheet. *Canadian Journal of Earth Sciences*, **29**, 1565-1579.

Hiemstra, J.F., Rijsdijk, K.F., Evans, D.J.A., & van der Meer, J.M., (2005). Integrated micro- and macro-scales analyses of Last Glacial Maximum Irish Sea Diamicts from Abermawr and Traeth y Mwnt, Wales, UK. *Boreas*, **34**, 61-74.

Hiemstra, J.F., Evans, D.J.A., Scourse, J.D., McCarroll, D., Furze, M.F.A., & Rhodes, E., (2006). New evidence for a grounded Irish Sea glaciation of the Isles of Scilly, UK. *Quaternary Science Reviews*, **25**, 299-309.

Hinkel, K.M., Doolittle, J.A., Bockheim, J.G., Nelson, F.E., Paetzold, R., Kimble, J.M., & Travis, R., (2001). Detection of subsurface permafrost features with ground-penetrating radar, Barrow, Alaska. *Permafrost and Periglacial Processes,* **12**, 179-190.

Hiscock, K., & Paci, A., (2000). Groundwater resources in the Quaternary deposits and Lower Palaeozoic bedrock of the Rheidol catchment, west Wales. *In* Robins, N.S., & Misstear, B.D.R., (eds) *Groundwater in the Celtic Regions: Studies in Hard Rock and Quaternary Hydrogeology.* Geological Society, London, Special Publications, **182**, 141-155.

Hobbs, N., (1986). Mire morphology and the properties and behaviour of some British and foreign peats. *Quarterly Journal of Engineering Geology,* **19**, 7-80.

Hoekstra, P., & Delaney, A.J., (1974). Dielectric properties of soils at UHF and microwave frequencies. *Journal of Geophysical Research,* **79**, 1699-1708.

Hoekstra, P., Sellmann, P.V., & Delaney, A., (1975). Ground and airborne resistivity surveys of permafrost near Fairbanks, Alaska. *Geophysics,* **40**, 641-656.

Holmes, G.W., Hopkins, D.M., & Foster, H. L. (1968). Pingos in central Alaska. *United States Geological Survey Bulletin,* 1241-H, 40pp.

Hooyer, T.S., & Iverson, N.R., (2000). Clast-fabric development in a shearing granular material: Implications for subglacial till and fault gouge. *Geological Society of America Bulletin,* **112**, 683-692.

Hope McDonald, H.A., (1961). Some erratics from Teifi Estuary, western Cardiganshire. *Geological Magazine,* **98**, 81-84.

Hoppe, G., (1952). Hummocky moraine regions with special reference to the interior of Norrbotten. *Geografiska Annaler,* **34**, 1-72.

Hoppe, G., (1957). Problems of glacial morphology and the ice age. *Geografiska Annaler,* **39**, 1-18.

Hoppe, G., (1959). Glacial morphology and inland ice recession in northern Sweden. *Geografiska Annaler,* **41**, 193-212.

Horvath, C.L., (1998). An evaluation of ground-penetrating radar for investigation of palsa evolution, Macmillan Pass, NWT, Canada. In Lewkowicz, A.G., & Allard, M. (eds.), *Proceedings Seventh International Permafrost Conference,* Laval University Press, 473-478.

Hughes, O.L., (1969). *Distribution of open-system pingos in central Yukon territory with respect to the glacial limits.* Geological Survey of Canada Paper 69-34, pp. 8.

Humlum, O., Instanes, A., & Sollid, J.L., (2003). Permafrost in Svalbard: a review of research history, climatic background and engineering challenges. *Polar Research*, **22**, 191-215.

Hussen, S.A., (1998). *The exploration of onshore Quaternary deposits using high resolution shallow seismic techniques*. Unpublished Ph.D. Thesis. University of Wales, Cardiff.

I

Iannicelli, M., (2003). Reinterpretation of the original DeKalb Mounds in Illinois. *Physical Geography*, **24**, 170-182.

Isaksen, K., Ødegaard, R.S., Eiken, T., & Sollid, J.L., (2000). Composition, flow and development of two tongue-shaped rock glaciers in the permafrost of Svalbard. *Permafrost and Periglacial Processes*, **11**, 241-257.

Isaksen, K., Holmlund, P., Sollid, J. L. & Harris, C. (2001). Three deep alpine-permafrost boreholes in Svalbard and Scandinavia. *Permafrost Periglacial Processes*, **12**, 13–25.

Isarin R.F.B., (1997). Permafrost distribution and temperatures in Europe during the Younger Dryas. *Permafrost and Periglacial Processes*, **8**, 313–333.

J

Jehu, T.J., (1904). The glacial deposits of northern Pembrokeshire. *Transactions of the Royal Society of Edinburgh*, **41**, 53-87.

John, B.S., (1970a). Pembrokeshire. *In* Lewis, C.A. (ed.). *The glaciations of Wales and adjoining regions*. Longman, London, 229-265.

John, B.S., (1970b). The Pleistocene drift succession at Porth Clais, Pembrokeshire. *Geological Magazine*, **107**, 439-457.

John, B.S., (1973). Vistulian periglacial phenomena in south-west Wales. *Biuletyn Peryglacjalny*, **22**, 185-213.

Johnson, P.G., (1997). Spatial and temporal variability of ice-dammed lake sediments in alpine environments. *Quaternary Science Reviews*, **16**, 635-647.

Johnson, W.H., & Menzies, J., (2002). Supraglacial and ice-marginal deposits and landforms. *In* J. Menzies (ed.), *Modern and Past Glacial Environments – revised student edition*. Butterworth-Heinemann, Oxford, pp. 317-333.

Jol, H.M., (1995). Ground penetrating radar antennae frequencies and transmitter powers compared for penetration depth, resolution and reflection continuity. *Geophysical Prospecting*, **43**, 693-709.

Jol, H.M., & Bristow, C.S., (2003). GPR in sediments: advice on data collection, basic processing and interpretation, a good practice guide. In Bristow, C.S., & Jol,

H.M., (eds.) *Ground Penetrating Radar in Sediments.* Geological Society, London, Special Publications, **211**, 9-27.

Jol, H.M., & Smith, D.G., (1995). Ground penetrating radar surveys of peatlands for oilfield pipelines in Canada. *Journal of Applied Geophysics*, **34**, 109-123.

Jones, O.T., (1912). The geological structure of central Wales and the adjoining regions. *Quarterly Journal of Geological Society of London*, **68**, 328-344.

Jones, O.T., (1938). On the evolution of a geosyncline. *Quarterly Journal of the Geological Society*, **94**, lx-cx.

Jones, O.T., (1942). The buried channel of the Tawe Valley near Ynystawe, Glamorganshire. *Quarterly Journal of the Geological Society of London*, **98**, 61-88.

Jones, O.T., (1965). The glacial and post-glacial history of the lower Teifi valley. *Quarterly Journal of the Geological Society of London*, **121**, 247-281.

Juvigne, E., (1983). Two different volcanic ash-falls of Alleröd age in High Belgium. *Geologie en Mijnbouw*, **62**, 545-549.

K

Kearey, P., & Brooks, M., (1991). *An Introduction to Geophysical Exploration* (2nd edition). Blackwell, Oxford.

Keeping, W., (1882). The glacial geology of central Wales. *Geological Magazine*, **9**, 251-257.

King, M.S., Zimmerman, R.W., & Corwin, R.F., (1988). Seismic and electrical properties of unconsolidated permafrost. *Geophysical Prospecting*, **36**, 349-364.

Kjær, K.H., & Krüger, J., (1998). Does clast size influence fabric strength? *Journal of Sedimentary Research*, **68**, 746-749.

Knight, J., & McCabe, A.M., (1997). Identification and significance of ice-flow-transverse subglacial ridges (Rogen moraines) in northern central Ireland. *Journal of Quaternary Science*, **12**, 519-524.

Knudsen, C.G., Larsen, E., Sejrup, H.P., & Stalsberg, K., (2006). Hummocky moraine landscape on Jæren, SW Norway – implications for glacier dynamics during the last deglaciation. *Geomorphology*, **77**, 153-168.

Kovacs, A. & Morey, R.M. (1985). Impulse radar sounding of frozen ground. In Brown, J., Metz, M.C. & Hoekstra, P. (eds.) *Workshop in Permafrost Geophysics, Golden, Colorado, 23–24 October 1984.* U.S. Army Cold Regions Research and Engineering Laboratory, Special Report, **85-5**, 28–40.

L

Lagerbäck, R., (1988). The Veiki moraines in northern Sweden – widespread evidence of an Early Weichselian deglaciation. *Boreas*, **17**, 469-486.

Lagerbäck, R., & Rodhe, L., (1985). Pingos in northernmost Sweden. *Geografiska Annaler*. **67A**, 239-245.

Lagerbäck, R., & Rodhe, L., (1986). Pingos and palsas in northermost Sweden. preliminary notes on recent investigations. *Geografiska Annaler*, **68A**, 149-154.

Lagarec, D., (1973). Eléments de la morphologie cryogène du Golfe de Richmond, Nouveau Québec. *Cahiers Géographie Québec*, **17**, 465– 482.

Lagarec, D., (1976). Etude géomorphologique de palses dans la région de Fort Chimo, Nouveau Québec, Canada. *Cahiers Géologiques*, **92**, 153–163.

Lagerec, D., (1982). Cryogenic mounds as indicators of permafrost conditions, northern Québec. *Proceedings of the Fourth Canadian Permafrost Conference, the Roger J.E. Brown Memorial Volume*, Ottawa, National Research Council of Canada, 43-48.

Lamplugh, G.W., (1911). On the shelly moraine of the Sefstromglacier and other Spitsbergen phenomena illustrative of the British glacial conditions. *Proceedings of the Yorkshire Geological Society*, **17**, 216-241.

Landvik, J. Y., Bondevik, S., Elverhøi, A., Fjeldskaar, W., Mangerud, J., Siegert, M.J., Salvigsen, O., Svendsen, J.I., & Vorren, T.O., (1998). The last glacial maximum of Svalbard and the Barents Sea area: ice sheet extent and configuration. *Quaternary Science Reviews*, **17**, 43-76.

Landvik, J. Y., Mangerud, J. & Salvigsen, O. (1988). Glacial history and permafrost in the Svalbard area. In K. Senneset (ed.): Proceedings of the 5th International Conference on Permafrost. Vol. 1. pp. 194–198. Trondheim: Tapir Publishers.

Lankston, R.W., (1989). The seismic refraction method: A viable tool for mapping shallow targets in the 1990s. *Geophysics*, **54**, 1535-1542.

Lankston, R.W., (1990). High-resolution refraction seismic data acquisition and interpretation. In Ward, S.H. (ed.), *Geotechnical and Environmental Geophysics. Investigations in Geophysics no. 5. Vol 1 Review & Tutorial.* Society of Exploration Geophysicists, Tulsa, 45-73.

Larsen, E., Longva, O., Follestad, B.A., (1991). Formation of De Geer moraines and implications for deglaciation dynamics. *Journal of Quaternary Science*, **6**, 263-277.

Lear, D., (1986). *The Quaternary deposits of the Lower Teifi valley*. Unpublished PhD thesis. University of Wales, Aberystwyth.

Lear, D.L. (2003). Some observations on recent ideas about the Teifi Valley, West Wales. *Quaternary Newsletter*, **99**, 19-24.

Lear, D.L., & Bowen, D.Q., (1984). The lower Teifi valley. *In* Bowen, D.Q. & Henry, A. (eds.). *Wales: Gower, Preseli, Fforest Fawr.* Quaternary Research Association Field Guide, April 1984, 78-81.

Leffingwell, E. de K. (1919). The Canning River region, Northern Alaska. U.S. Geological Survey Professional Paper 109, 251 pp.

Leopold, M., & Völkel, J., (2003). GPR images of periglacial slope deposits beneath peat bogs in the Central European Highlands, Germany. In Bristow, C.S., & Jol, H.M., (eds.) *Ground Penetrating Radar in Sediments.* Geological Society, London, Special Publications, **211**,181-189.

Lewis, C.A., (1966). The Breconshire end-moraine. *Nature*, **212**, 1559-1561.

Lewis, C.A., (1970). The upper Wye and Usk regions. *In* C.A. Lewis (ed), *The Glaciations of Wales and Adjoining Regions*, Longman, London, 147-173.

Lewis, C.A., (1985). Periglacial features. In: Edwards, K.J., & Warren, W.P., *The Quaternary History of Ireland.* Academic Press, London. 95-113.

Lewis, C.A., & Thomas, G.S.P. (2005). The upper Wye and Usk regions. In Lewis, C.A., & Richards, A.E., (eds.), *The Glaciations of Wales and Adjoining Areas*, Logaston Press, Bristol, 101-128.

Liestøl, O. (1977). Pingos, springs, and permafrost in Spitsbergen. *Norsk Polarinstitutt, Årbok* 1975, 7-29.

Liestøl, O. (1996). Open-system pingos in Spitsbergen. *Norsk Geografisk Tidsskrift*, **50**, 81-84.

Likens, G.E., & Johnson, P.L., (1966). A chemically stratified lake in Alaska, *Science*, **153**, 875-877.

Lindén, M., & Möller, P., (2005). Marginal formation of De Geer moraines and their implications to the dynamics of grounding-line recession. *Journal of Quaternary Science*, **20**, 113-133.

Lindsay, R., (1995). *Bogs : the ecology, classification and conservation of ombrotrophic mires.* Scottish Natural Heritage, Edinburgh. 120 p.

Loke, M.H., (2000). Topographic modelling in resistivity imaging inversion. 62nd EAGE Conference & Technical Exhibition Extended Abstracts, D-2.

Loke, M.H., (2004a). Res2dinv ver. 3.54. Rapid 2-D resistivity and IP inversion using the least-squares method. Geoelectrical Imaging 2-D & 3-D, Geotomo Software, March 2004. www.geoelectrical.com, 124 p.

Loke, M.H., (2004b). Tutorial: 2-D and 3-D electrical imaging surveys. www.geoelectrical.com, 128 p.

Loke, M.H., & Barker, R.D., (1995). Least-squares deconvolution of apparent resistivity pseudosections. *Geophysics*, **60**, 1682-1690.

Loke, M.H., & Barker, R.D., (1996a). Rapid least-squares inversion of apparent resistivity pseudosections by a quasi-Newton method. *Geophysical Prospecting*, **44**, 131-152.

Loke, M.H., & Barker, R.D., (1996b). Practical techniques for 3D resistivity surveys and data inversion. *Geophysical Prospecting*, **44**, 499-523.

Longva, O., & Bakkejord, K.J., (1990). Iceberg deformation and erosion in soft sediments, southeast Norway. *Marine Geology*, **92**, 87-104.

Longva, O., & Thoresen, M.K., (1991). Iceberg scours, iceberg gravity craters and current erosion marks from a gigantic Preboreal flood in southeastern Norway. *Boreas*, **20**, 47-62.

Lønne, I. & Nemec, W., (2004) High-arctic fan delta recording deglaciation and environment disequilibrium. *Sedimentology*, **51**, 553-589.

Lønne, I., & Lauritsen, T., (1996). The architecture of a modern push moraine at Svalbard as inferred from ground-penetrating radar measurements. *Arctic and Alpine Research*, **28**, 488-495.

Lowe, J.J., Birks, H.H., Brooks, S.J., Coope, G.R., Harkness, D.D., Mayle, F.E., Sheldrick, C., Turney, C.S.M., & Walker, M.J.C., (1999). The chronology of palaeoenvironmental changes during the Last Glacial-Holocene transition: towards an event stratigraphy for the British Isles. *Journal of the Geological Society of London*, **156**, 397-410.

Lowe, J.J., Coope, G.R., & Sheldrick, C., (1995). Direct comparison of UK temperatures and Greenland snow accumulation rates, 15 000-12 000 yr ago. *Journal of Quaternary Science*, **10**, 175-180.

Lowe, J.J., & Lowe, S., (2001). Llyn Gwernan. *In* Walker, M.J.C., & McCarroll, D., (eds.), *The Quaternary of West Wales: Field Guide*. Quaternary Research Association, London, 132-152.

Luckman, B.H., (1970). The Hereford Basin. In: Lewis, C.A., (ed.) *The Glaciations of Wales and adjoining regions*. Longman, London, 175-196.

Lundqvist, G., (1953). Tillägg till palsfragan. *Geol. Fören. Förhandl.*, **73**, 149–154.

Lundqvist, J., (1981). Moraine morphology. *Geografiska Annaler*, **63A**, 127-138.

Lundqvist, J., (1989a). Rogen (ribbed) moraine – identification and possible origin. *Sedimentary Geology*, **62**, 281-292.

Lundqvist, J., (1989b). Late glacial ice lobes and glacial landforms in Scandinavia. In Goldthwait, R.P., & Matsch, C.L., (eds.). *Genetic Classification of Glacigenic Deposits*, A.A. Blakema, Rotterdam, 217-225.

Lundqvist, J., (2000). Palaeoseismicity and De Geer Moraines. *Quaternary International*, **68-71**, 175-186.

M

MacDonald, R.J., (1994). *The application of shallow seismic reflection to onshore Quaternary studies*. Unpublished Ph.D. Thesis, University of Wales, Cardiff.

Mackay, J.R., (1962). Pingos of the Pleistocene MacKenzie River delta area, *Geographical Bulletin*, **18**, 21-63.

Mackay, J.R., (1963). The Mackenzie Delta Area, N.W.T. Geographical Branch, Canadian Department of Mines and Technical Survey., Memoir, **8**, 202pp.

Mackay, J.R., (1966). Pingos in Canada. Proceedings of the International Conference on Permafrost, Lafayette, Indiana, 1963. Washington, NAC-NRC Publication 1287, 71-76.

Mackay, J.R., (1972). The world of underground ice. *Annals of the Association of American Geographers*, **62**, 1-22.

Mackay, J.R., (1973). The growth of pingos, Western Arctic coast, Canada. *Canadian Journal of Earth Sciences*, **14**, 979-1004.

Mackay, J.R., (1977). Pulsating pingos, Tuktoyaktuk Peninsula, N.W.T., *Canadian Journal of Earth Sciences*, **14**, 209-222.

Mackay, J.R., (1978a). Sub-pingo water lenses, Tuktoyaktuk Peninsula, Northwest Territories. *Canadian Journal of Earth Sciences*, **15**, 1219-1227.

Mackay, J.R., (1978b). Contemporary pingos: a discussion. *Biuletyn Peryglacjalny*, **27**, 133-154.

Mackay, J.R., (1979). Pingos of the Tuktoyaktuk Peninsula Area, Northwest Territories. *Géographie physique et Quaternaire*, **33**, 3-61.

Mackay, J.R., (1981). Aklisuktuk (growing fast) Pingo, Tuktoyaktuk Peninsula, Northwest Territories, Canada. *Arctic*, **34**, 270-273.

Mackay, J.R., (1983). Pingo growth and subpingo water lenses, Western Arctic Coast, Canada. *In* Permafrost: Fourth International Conference, Proceedings, Fairbanks, Alaska. National Academy Press, Washington, D.C., 762-766.

Mackay, J.R., (1985). Pingo ice of the western Arctic coast, Canada. *Canadian Journal of Earth Sciences*, **22**, 1452-1464.

Mackay, J.R., (1986). Growth of Ibyuk Pingo, Western Arctic Coast, Canada, and some implications for environmental reconstructions. *Quaternary Research*, **26**, 68-80

Mackay, J.R., (1987). Some mechanical aspects of pingo growth and failure, western Arctic coast, Canada. *Canadian Journal of Earth Sciences*, **24**, 1108-1119.

Mackay, J.R., (1988). Pingo collapse and paleoclimatic reconstruction. *Canadian Journal of Earth Sciences*, **25**, 495-511.

Mackay, J.R., (1990). Seasonal growth bands in pingo ice. *Canadian Journal of Earth Sciences*, **27**, 1115-1125.

Mackay, J.R., (1998). Pingo growth and collapse, Tuktoyaktuk Peninsula area, Western Arctic Coast, Canada: A long term field study. *Geographique physique et Quaternaire*, **52**, 271-323.

Mackay, J.R., (2000). Thermally induced movements in ice-wedge polygons, western arctic coast: a long-term study. *Geographie Physique et Quaternaire*, **54**, 41-68.

Mackay, J.R., & Stager, J.K., (1966). The structure of some pingos in the Mackenzie Delta area, N.W.T.. *Geographical Bulletin*, **4**, 360-368.

Maizels, J., (1992). Boulder ring structures produced during jökulhaup flows. *Geografiska Annaler*, **74A**, 21-33.

Major, H., Haremo, P., Dallmann, W.K., & Andresen, A., (2000). Geological map of Svalbard 1:100,000 sheet C9G Adventdalen (revised after Major 1964). *Norsk Polarinstitutt Temakart nr. 31*.

Mark, D.M., (1973). Analysis of axial orientation data, including till fabrics. *Geological Society of America Bulletin*, **84**, 1369-1374.

Mark, D.M., (1974). On the interpretation of till fabrics. *Geology*, **2**, 101-104.

Matsuoka, N., Sawguchi, S., & Yoshikawa, K., (2004). Present-day periglacial environments in Central Spitsbergen, Svalbard. *Geographical Review of Japan*, **77**, 276-300.

Matthews, J.A., Dahl, S., Berrisford, M.S., & Nesje, A., (1997). Cyclic development and thermokarstic degradation of palsas in the mid-Alpine zone at Leirpullan, Dovrefjell, southern Norway. *Permafrost and Periglacial Processes*, **8**, 107-122.

McCabe, A.M., Knight, J., & McCarron, S., (1999). Ice-flow stages and glacial bedforms in north central Ireland: a record of rapid environmental change during the last glacial termination. *Journal of the Geological Society, London*, **156**, 63-72.

McCarroll, D., (1991). Ice directions in western Lleyn and the status of the Gwynedd readvance of the last Irish sea glacier. *Geological Journal*, **26**, 137-143.

McCarroll, D., (1995). Geomorphological evidence from the Lleyn Peninsula constraining models of the magnitude and rate of isostatic rebound following deglaciation of the Irish Sea Basin. *Geological Journal*, **30**, 157-163.

McCarroll, D., (2001). Deglaciation of the Irish Sea Basin: a critique of the glaciomarine hypothesis. *Journal of Quaternary Science*, **16**, 393-404.

McCarroll, D., & Harris, C., (1992). The glacigenic deposits of western Lleyn, north Wales: terrestrial or marine? *Journal of Quaternary Science*, **7**, 19-29.

McCarroll, D., & Rijsdijk, K.F., (2003). Deformation styles as a key for interpreting glacial depositional environments. *Journal of Quaternary Science*, **18**, 473-489.

Meier, K.-D., (1987). Studien zur periglaziären Landshaftsformung in Finmark (Nordnorwegen). Jahrbuch des Geographischen Gesellschaft zu Hannover. Sonderheft, vol. 13. Hannover, 298 pp.

Menzies, J., & Shilts, W.W., (2002). Subglacial environments. *In* J. Menzies (ed.), *Modern and Past Glacial Environments – revised student edition*. Butterworth-Heinemann, Oxford, pp. 183-278.

van der Meulen, S., (1988). The spatial facies of a group of pingo remnants on the southeast Frisian till plateau (the Netherlands). *Geologie en Mijnbouw*, **67**, 61-74.

Miall, A.D., (1983). Glaciofluvial transport and deposition. *In* N. Eyles (ed), *Glacial Geology. An Introduction for Engineers and Earth Scientists*. Pergamon Press, Oxford. 168-183.

Mickelson, D.M., & Berkson, J.M., (1974). Till ridges forming above and below sea level in Wachusett Inlet, Glacier Bay, Alaska. *Geografiska Annaler*, **56A**, 111-119.

Milsom, J., (2002) *Field Geophysics*, 3rd edition. Wiley, Chichester, 232 p.

Mitchell, G.F., (1960). The Pleistocene history of the Irish Sea. *British Association for the Advancement of Science*, **17**, 313-325.

Mitchell, G.F. (1971). Fossil pingos in the south of Ireland. *Nature*, **230**, 43-44.

Mitchell, G.F., (1972). The Pleistocene history of the Irish Sea: a second approximation. *Scientific Proceedings of the Royal Dublin Society Series* **A4**, 181-199.

Mitchell, G.F. (1973). Fossil pingos at Camaross Townland, County Wexford. *Proceedings of the Royal Irish Academy*, **73**, 269-282.

Mollard, J.D., (1983). The origin of reticulate and orbicular patterns on the floor of the Lake Agassiz Basin. *In* J.T. Teller & L. Clayton (eds), *Glacial Lake Agassiz*, Geological Association of Canada, Special Paper 26, 355-374.

Mollard, J.D., (2000). Ice-shaped ring-forms in Western Canada: their airphoto expression and manifold polygenetic origins. *Quaternary International*, **68-71**, 187-198.

Moore, J. (1980). *A study of pingo scars at Bwlch-derwin, North Wales*. Unpublished B.Sc. dissertation, University of London.

Moorman, B.J., & Michel, F.A., (2000). Glacial hydrological system characterisation using ground penetrating radar. *Hydrological Processes*, **14**, 2645-2667.

Moorman, B.J., Robinson, S.D., & Burgess, M.M., (2003). Imaging periglacial conditions with ground-penetrating radar. *Permafrost and Periglacial Processes*, **14**, 319-329.

Mückenhausen, V.E., (1960). Eine besondere art von pingos am Hohen Venn/Eifel. *Eiszeitalter und Gegenwart*, **11**, 5-11.

Müller, F. (1959). Beobachtungen über Pingos. *Meddelelser om Grønland*, **153**, 127 pp. (Translated by D.A. Sinclair: Observations on Pingos, National Research Council of Canada Translation 1073, 117 pp. (1963).)

Müller, F., (1962). Analysis of some stratigraphical observations and radiocarbon dates from two pingos in the Mackenzie Delta Area, N.W.T., *Arctic*, **15**, 278-288.

Mullenders, W. & Gullentops, F. (1969). The age of pingos in Belgium. In Péwé, T.L., (ed.). *The Periglacial Environment*. Montreal: McGill-Queens University Press, 321-336.

N

Neal, A., (2004). Ground-penetrating radar and its use in sedimentology: principles, problems and progress. *Earth Science Reviews*, **66**, 261-330.

Nunn, K.R., & Boztas, M., (1977). Shallow seismic reflection profiling on land using a controlled source. *Geoexploration*, **15**, 87-97.

O

O' Brien, R., (1971), Observations on pingos and permafrost hydrology in Schuchert Dal, N.E. Greenland. *Meddelelser om Grønland*, **195**, 1-20.

Ó Cofaigh, C. and Evans, D.J.A., (2001). Deforming bed conditions associated with a major ice stream of the last British ice sheet. *Geology*, **29**, 795-798.

Orvin, A.K. (1944). Litt om kilder på Svalbard. *Norsk Geografisk Tidsskrift*, **10**, 1-26.

van Overmeeren, R.A., & Ritsema, I.L., (1988). Continuous vertical electrical sounding. *First Break*, **6**, 313-324.

Owen, G., (2001). Bedrock geology of west Wales. *In* Walker, M.J.C., & McCarroll, D., (eds.), *The Quaternary of West Wales: Field Guide*. Quaternary Research Association, London, 2-8.

P

Palmer, D., (1981). An introduction to the generalized reciprocal method of seismic refraction interpretation. *Geophysics*, **46**, 1508-1518.

Parizek, R.R., (1969). Ice contact rings and ridges. *Geological Society of America, Special Paper (United States Contribution to Quaternary Research)* **123**, 49-102.

Paul, M.A., (1983). The supraglacial landsystem. In Eyles, N. (ed.) *Glacial Geology. An Introduction for Engineers and Earth Scientists*. Pergamon, Oxford, 71-90.

Payette, S., Samson, H., & Lagarec, D., (1976). The evolution of permafrost in the taiga and in the forest-tundra, western Québec-Labrador Peninsula. *Canadian Journal of Forest Research*, **6**, 203-220.

Payette, S., & Seguin, M.K., (1979). Les buttes minérales cryogènes dans les basses terres de la rivière aux Feuilles, Nouveau-Québec. *Géographie Physique et Quaternaire*, **33**, 339-358.

Pękala, K., & Repelewska-Pękalowa, J., (2004). Pingos in the South Bellsund Region (Spitsbergen). In Styszyńska, A and Marsz, A.A. (eds). *Polish Polar Studies*, XXX International Polar Symposium, Gydnia 2004. 293-305.

Pettersson, J.K., & Nobes, D.C., (2003). Environmental geophysics at Scott Base: ground penetrating radar and electromagnetic tools for mapping contaminated ground at Antarctic research bases. *Cold Regions Science and Technology*, **37**, 187-195.

Péwé, T.L., (1975) *Quaternary geology of Alaska*, US Geological Survey Professional Paper **835**, pp. 145.

Phillips, F.M., Bowen, D.Q., & Elmore, D., (1994). Surface exposure dating of glacial features in Great Britain using cosmogenic Chlorine-36: preliminary results. *Mineralogical Magazine*, **58A**, 722-723.

Pihlainen, J.A., Brown, R.J.E., & Legget, R.F., (1956). Pingos in the Mackenzie Delta, Northwest Territories, Canada. Bulletin of the Geological Society of America, **67**, 1119-1122.

Piotrowski, J.A., Mickelson, D.M., Tulaczyk, S., Krzyszkowski, D., & Junge, F.W., (2002). Reply to the comments by G.S. Boulton, K.E. Dobbie, S. Zatsepin on: Deforming soft beds under ice sheets: how extensive were they? *Quaternary International*, **97-98**, 173-177.

Piper, D.J.W., & Porritt, C.J., (1966). Some pingos in Spitsbergen. *Norsk Polarinstitutt, Årbok* 1965. 80-84.

Pissart, A. (1956). L'origine périglaciaire des viviers des Hautes Fagnes. *Annales de la Société géologique de Belgigue*, **79**, 119-131.

Pissart, A. (1963). Les traces de pingos du Pays de Galles (Grande Bretagne) et du Plateau des Hautes Fagnes (Belgigue). *Zeitschrift für Geomorphologie, 7*, 381-392.

Pissart, A., (1965). Les pingos des Hautes Fagnes: les problèmes de leur genèse. *Annales de la Société géologique de Belgigue*, **88**, B277-B289.

Pissart, A., (1967). Les pingos de L'Ile Prince Patrick (76°N, 120°W), *Geographical Bulletin*, **9**, 189-217.

Pissart, A. (1974). Les Viviers des Hautes Fagnes sont des traces de buttes periglaciaires. Mais s'agissait-il réellement de pingos? *Annales de la Société géologique de Belgigue*, **97**, 359-381.

Pissart, A., (1976). Les dépôts et la morphologie périglaciaires de la Belgique. In: Pissart, A. (ed.), Géomorphologie de la Belgique. Hommage au professeur P. Macar. Laboratoire de Géologie et de Géographie Physique, Université de Liège, pp. 115–135.

Pissart, A., (1983). Remnants of periglacial mounds in the Hautes Fagnes (Belgium): structure and age of the ramparts. *Geologie en Mijnbouw*, **62**, 551-555.

Pissart, A., (1988). Pingos: an overview of the present state of knowledge. *In*, Clark, M.J., (ed), *Advances in periglacial geomorphology*. Wiley, Chichester, 279-297.

Pissart, A., (2000). Remnants of lithalsas of the Hautes Fagnes, Belgium: a summary of present-day knowledge. *Permafrost and Periglacial Processes*, **11**, 327-355.

Pissart, A., (2002). Palsas, lithalsas and remnants of these periglacial mounds. A progress report. *Progress in Physical Geography*, **26**, 605-621.

Pissart, A., (2003). The remnants of Younger Dryas lithalsas on the Hautes Fagnes Plateau in Belgium and elsewhere in the world. *Geomorphology*, **52**, 5-38.

Pissart, A., & French, H.M., (1976). Pingo investigations, north-central Banks Island, Canadian Arctic. *Canadian Journal of Earth Sciences*, **13**, 937-946.

Pissart, A. & Gangloff, P., (1984). Les palses minérales et organiques de la vallee de l'Aveneau, près de Kuujjuaq, Québec Subartique. *Géographie physique et Quaternaire*, **38**, 217-228.

Pissart, A. & Juvigne, E., (1980). Genése et âge d'une trace de butte périglaciaire (pingo ou palse) de la Konnerzvenn (Hautes Fagnes, Belgigue). *Annales de la Société Géologique de Belgique, 103*, 73-86.

Pissart, A., Juvigné, E., Woillard, G., Thorez, J., (1972). Les cicatrices de pingos de le Brackvenn (Hautes Fagnes). Compte rendu de l'excursion du 3 juillet 1971. Les Congrès et Colloques de l'Université de Liège 67, 281–294.

Pissart, A., Bastin, B., & Juvigné, E., (1975). L'origine des viviers des Hautes Fagnes: traces de pingos ou de palses? *Hautes Fagnes*, 1, 9 – 38.

Pissart, A., Bastin, B., & Juvigne, E., (1981). Les traces de buttes périglaciaires (pingos? Palses?) des Hautes Fagnes. *Biuletyn Peryglacjalny*, 28, 333-339.

Pissart, A., Harris, S.A., Prick, A., Van Vliet-Lanoe., B., (1998). La signification paleoclimatique des lithalses (palsas minerales), *Biuletyn Peryglacjalny*, 37, 141-154.

Plewes, L.A., & Hubbard, B., (2001). A review of the use of radio-echo sounding in glaciology. *Progress in Physical Geography*, 25, 203-236.

Pollard, W.H., & French, H.M., (1983). The occurrence of seasonal frost mounds, North Fork Pass, Ogilvie Mountains, Yukon Territory. *Proceedings, Fourth International Conference on Permafrost*, National Academy Press, Washington, DC, 1000-1004.

Pollard, W.H., & French, H.M., (1984). The groundwater hydraulics of seasonal frost mounds, Northern Yukon. *Canadian Journal of Earth Sciences*, 21, 1073-1081.

Pollard, W.H., & French, H.M., (1985). The internal structure and ice crystallography of seasonal frost mounds. *Journal of Glaciology*, 31, 157-162.

Porsild, A.E., (1938). Earth mounds in unglaciated Arctic northwestern America. *Geographical Review*, 28, 46-58.

Potts, A.S., (1971). Fossil cryonival features in central Wales. *Geografiska Annaler*, 53A, 39-51.

Price, A., (1976). *Quaternary deposits of the middle Teifi valley, Dyfed, between the Llanllwni and Allt-y-cafan gorges*. Unpublished MSc thesis, University of Wales, Aberystwyth.

Price, R.J., (1973). *Glacial and Fluvioglacial Landforms*. Oliver and Boyd, Edinburgh. p. 242

R

Rampton, V.N., & Mackay, J.R., (1971). *Massive ice and icy sediments throughout the Tuktoyaktuk Peninsula, Richards Island, and nearby areas, District of Mackenzie.* Geological Survey of Canada Paper, 71-21, 16p.

Rampton, , V.N., & Walcott, R.I., (1974). Gravity profiles across ice-cored topography. *Canadian Journal of Earth Sciences*, 11, 110-122.

Rapp, A., Rudberg, D., (1960). Recent periglacial phenomena in Sweden. *Biuletyn Peryglacjalny*, 8, 143– 154.

Reade, T.M., (1896). Notes on the drift of the mid-Wales coast. *Quarterly Journal of the Geological Society of London*, 53, 341-348.

Reynolds, J.M., (1997). *An Introduction to Applied and Environmental Geophysics.* John Wiley & Sons Ltd, Chichester.

Richards, A.E., (2005). Herefordshire. In Lewis, C.A. and Richards, A.E. (eds.), *The Glaciations of Wales and Adjoining Areas*, Logaston Press, Bristol, 129-144.

Rijsdijk, K. F., (2000). Late Devensian Glaciation of the Southern Irish Sea Basin: Testing of Competing Hypotheses. Ph.D. thesis, University of Wales, Swansea, 357 pp.

Rijsdijk, K.F., (2001). Density-driven deformation structures in glacigenic consolidated diamicts: examples from Traeth y Mwnt, Cardiganshire, Wales, U.K. *Journal of Sedimentary Research*, 71, 122-135.

Rijsdijk, K.F., & McCarroll, D., (2001). Abermawr. In Walker, M.J.C., & McCarroll, D., (eds.), *The Quaternary of West Wales: Field Guide.* Quaternary Research Association, London, 32-38.

Rijsdijk, K.F., Owen, G., Warren, W.P., McCarroll, D., & van der Meer, J.J.M., (1999). Clastic dykes in over-consolidated tills: evidence for subglacial hydrofracturing at Killiney Bay, eastern Ireland. *Sedimentary Geology*, 129, 111-126.

Roberts, M.C., Pullan, S.E., & Hunter, J.A., (1992). Applications of land-based high resolution seismic reflection analysis to Quaternary and geomorphic research. *Quaternary Science Reviews*, 11, 557-568.

Robins, N.,S., Shand, P., & Merrin, P.D., (2000). Shallow groundwater in drift *In* Robins, N.S., & Misstear, B.D.R., (eds) *Groundwater in the Celtic Regions: Studies in Hard Rock and Quaternary Hydrogeology.* Geological Society, London, Special Publications, 182, 123-131.

Rogers, V.A., (1998a). *A preliminary investigation of a number of geomorphological features and other characteristics of a site on the Lleyn Peninsula, North Wales.* Unpublished CCW Report pp. 29.

Rogers, V.A., (1998b). Pingo! Relict Ice mounds..... *Earth Heritage*, 9, 17.

Ross, N., Harris, C., Brabham, P.J., Campbell, S., & Sheppard, T.H., (2005a). *Ramparted Ground-ice Depressions and Related Cryogenic Landforms in Wales: Distribution, Character and Conservation Status.* CCW Contract Science Report No. 668. p. 133.

Ross, N., Harris, C., Christiansen, H.H., & Brabham, P.J., (2005b). Ground-penetrating radar investigations of open system pingos, Adventdalen, Svalbard. *Norwegian Journal of Geography*, 59, 129-138.

Rudeforth. C.C., Hartnup, R., Lea, J.W., Thompson, T.R.E, & Wright, P.S., (1984). *Soils and their use in Wales.* Bulletin No. 11, Soil Survey of England and Wales, Harpenden.

Ruuhijärvi, R., 1960. Uber die regionale Einteilung der nord-finnischen Moore. Ann. Botan. Soc. "Vanamo" 31 (1) (360 pp.).

S

Saunders, G.E., (1973). Vistulian periglacial environments in the Lleyn Peninsula. *Biulteyn Peryglacjalny*, **22**, 257-269.

Scholz, H., & Baumann, M., (1997). An 'open system pingo' near Kangerlussuaq (Søndre Strømfjord), West Greenland. *Geology of Greenland Survey Bulletin*, **176**, 104-108.

Schuncke, E. (1983). Zur morphodynamic der thufur und palsas in den Arktischen tundren Nordamerikas und Nordeuropas. In Schroeder-Lanz, H. (ed.), *Late- and Post-Glacial Oscillations of Glaciers: Glacial and Periglacial Forms*. Balkema, Rotterdam, pp. 371-387.

Schwamborn, G.J., Dix, J.K., Bull, J.M., & Rachold, V., (2002). High-resolution seismic and ground penetrating radar – geophysical profiling of a thermokarst lake in the western Lena Delta, northern Siberia. *Permafrost and Periglacial Processes*, **13**, 259-269.

Scott, W.J., Campbell, K.J., & Orange, A.S., (1974). EM pulse survey method in permafrost. *Natural Research Council of Canada, Technical Memoir*, **113**, 92-96.

Scott, W.J., Sellmann, P.V., & Hunter, J.A., (1990). Geophysics in the study of permafrost. In Ward, S.H. (ed.), *Geotechnical and Environmental Geophysics. Investigations in Geophysics no. 5. Vol 1 Review & Tutorial*. Society of Exploration Geophysicists, Tulsa, 355-384.

Scourse, J.D., Furze, M.F.A., (2001). A critical review of the glaciomarine model for Irish Sea deglaciation: evidence from southern Britain, the Celtic shelf and adjacent continental slope. *Journal of Quaternary Science*, **16**, 419–434.

Schofield, D.I., Davies, J.R., Waters, R.A., Wilby, P.R., Williams, M., & Wilson, D., (2004). Geology of the Builth Wells district – a brief explanation of the geological map. *Sheet Explanation of the British Geological Survey*. 1:50 000 Sheet 196 Builth Wells (England and Wales). Keyworth, Nottingham: British Geological Survey.

Seguin, M. K., (1986) Geophysics of permafrost mounds. *Eos*. **67**, 1401.

Seguin, M.K., & Allard, M., (1984). Le pergèlisol et les processus thermkarstiques de la region de la rivière Nastapoca, Nouveau-Québec. *Géographie Physique et Quaternaire*, **38**, 11-25.

Seppälä, M., (1972a). The term 'palsa'. *Zeischrift für Geomorphologie*, **16**, 463.

Seppälä, M., (1972b). Pingo-like remnants in the Peltojärvi area of Finnish Lapland. *Geografiska Annaler*, **54A**, 38-45.

Seppälä, M., (1982). An experimental study of the formation of palsas. *Proceedings of the Fourth Canadian Permafrost Conference*, National Research Council of Canada, Ottawa, 36-42.

Seppälä, M. (1988a). Rock pingos in northern Ungava Peninsula, Quebec, Canada. *Canadian Journal of Earth Sciences*, **25**, 629-634.

Seppälä, M., (1988b). Palsas and related forms. In: Clark, M.J., (ed.), *Advances in Periglacial Geomorphology*, pp. 247-278. John Wiley, Chichester.

Seppälä, M., (1995). How to make a palsa: a field experiment on permafrost formation. *Zeitschrift für Geomorphologie, Supplementbände*, **99**, 91-96.

Sharp, M., (1985). "Crevasse-fill" ridges – a landform type characteristic of surging glaciers? *Geografiska Annaler*, **67A**, 213-220.

Sheppard, T.H., (2003). *Late Pleistocene and Holocene Geology of the Upper Afon Teifi Valley*. British Geological Survey Internal Report, IR/03/097. p. 22.

Shotton, F.W. & Williams, R.E.G. (1973). Birmingham University radiocarbon dates VII. *Radiocarbon*, **15**, 451-468.

Shotton, F.W., Williams, R.E.G. & Johnson, A.S., (1974). Birmingham University radiocarbon dates VIII. *Radiocarbon*, **16**, 285-303.

Shotton, F.W., Williams, R.E.G. & Johnson, A.S., (1975). Birmingham University radiocarbon dates IX. *Radiocarbon*, **17**, 255-275.

Shumskii, P.A., (1959). *Principles of Geocryology (permafrost studies). Part 1, General Cryology*. Academy of Sciences of the U.S.S.R., V.A. Obruchec Institute of Permafrost Studies, Moscow.

Sissons, J.B., (1979). The Loch Lomond Stadial in the British Isles. *Nature*, **280**, 199-203.

Slater, L.D., & Lesmes, D., (2002). IP interpretation in environmental investigations. *Geophysics*, **67**, 77-88.

Slater, L.D., & Reeve, A., (2002). Investigating peatland stratigraphy and hydrogeology using integrated electrical geophysics. *Geophysics*, **67**, 365-378.

Smith, D.G. and Jol, H.M., (1995). Ground penetrating radar: antenna frequencies and maximum probable depths of penetration in Quaternary sediments. *Journal of Applied Geophysics*, **33**, 93-100.

Smith, M.J., Rose, J., & Booth, S., (2006). Geomorphological mapping of glacial landforms from remotely sensed data: An evaluation of the principal data sources and an assessment of their quality. *Geomorphology*, **76**, 148-165.

Solheim, A., (1986). Submarine evidence of glacier surges. *Polar Research*, **4**, 91-95.

Sollid, J.L., & Carlsson, A.B., (1984). De Geer moraines and eskers in Pasvik, north Norway. *Striae*, **20**, 55-61.

Sollid, J.L., & Sørbel, L., (1974). Palsa bogs at Haugtjørnin, Dovrefjell, South Norway, *Norsk Geografisk Tidssskrift*, **28**, 53-60.

Soloviev, P.A., (1973). Thermokarst phenomena and landforms due to frost heaving in Central Yakutia. *Biuletyn Peryglacjalny*, **23**, 135-155.

Sone, T., & Takahashi, N., (1993). Palsa formation in the Daisetsu Mountains, Japan. *Proceedings, 6th International Conference on Permafrost, Beijing*, 1231-1234.

Sparks, B.W., Williams, R.B.G., & Bell, F.G., (1972). Presumed ice depressions in East Anglia. *Proceedings of the Royal Society*, **A327**, 329-343.

Stager, J.K., (1956). Progress report on the analysis of the characteristics and distribution of pingos east of the Mackenzie Delta. *The Canadian Geographer*, **7**, 13-20.

Stalker, A., MacS., (1960). Ice pressed drift forms and associated deposits in Alberta. *Geological Survey of Canada, Memoirs*, **57**, 38pp.

St-Onge, D.A., & Pissart, A., (1990). Un pingo en système fermé dans des dolomies palèozoïques de l'Arctique canadien. *Permafrost and Periglacial Processes*, **1**, 275-282.

Strahan, A., Cantrill, T.C., Dixon, E.E.L., & Thomas, H.H., (1909). The Geology of the South Wales Coalfield. Part 10. The country around Carmarthen. Memoir of the Geological Survey of Great Britain. H.M.S.O., London.

Strömberg, B., (1965).Mappings and geochronological investigations in some moraine areas of south-central Sweden. *Geografiska Annaler*, **47A**, 73-82.

Sutcliffe, A.J., & Currant, A., (1984). Minchin Hole Cave. In: Bowen, D.Q. & Henry, A. (eds.). *Wales: Gower, Preseli, Fforest Fawr*. Quaternary Research Association Field Guide, April 1984, 33-37.

Svensson, H., (1964a). Structural observations in the minerogenic core of a palsa. *Svensk Geografisk Arsbok*, **40**, 137–142.

Svensson, H, (1964b). Traces of pingo-like frost mounds. *Svensk geografiska Årsbok*, **40**, 93-106.

Svensson, H., (1969). A type of circular lakes in northernmost Norway. *Geografiska Annaler*, **51A**, 1-12

Svensson, H., (1971). Pingos i ytre delen av Adventdalen. *Norsk Polarinstitutt Årbok 1969*, 168-174.

Svensson, H., (1976). Pingo problems in the Scandinavian countries. *Biuletyn Peryglacjanlny*, **26**, 33-40.

Svensson, H., (1986). Permafrost. Some morphoclimatic aspects of periglacial features of northern Scandinavia. *Geografiska Annaler*, **68A**, 123-130.

Synge, F.M., (1963). A correlation between the drifts of south-east Ireland with those of west Wales. *Irish Geographer*, **4**, 360-366.

Synge, F.M., (1964). The glacial succession in west Caernarvonshire. *Proceedings of the Geologists' Association*, **75**, 431-444.

T

Tarnocai, C., & Netterville, J.A., (1976). Some characteristics of a pingo in the Simpson Peninsula, N.W.T. *Canadian Journal of Earth Sciences*, **13**, 490-492.

Taylor, J.A., (1987). *Timescales of Environmental Change*. University College of Wales, Aberystwyth, 45 pp.

Theimer, B.D., Nobes, D.C., Warner, B.G., (1994). A study of the geoelectrical properties of peatlands and their influence on ground penetrating radar surveying. *Geophysical Prospecting*, **42**, 179–209.

Thomas, G.S.P., Chester, D.K., & Crimes, P., (1998). The late Devensian glaciation of the eastern Lleyn peninsula, North Wales: evidence for terrestrial depositional environments. *Journal of Quaternary Science*, **13**, 255-270.

Thompson, R., (1978). Resistivity investigation of an infilled kettle hole. *Quaternary Research*, **9**, 231-237.

Trotman, D.M., (1963a). Peat deposits within a pingo remnant near Llangurig, Wales. *Zeitschrift für Geomorphologie*, **7**, 381-392.

Trotman, D.M., (1963b). *Data for late-glacial and post-glacial history in South Wales*. Unpublished Ph.D. thesis, University of Wales, Swansea.

Turesson, A., & Lind, G., (2005). Evaluation of electrical methods, seismic refraction and ground-penetrating radar to identify clays beneath sands – two case studies in SW Sweden. *Near Surface Geophysics*, **3**, 59-70.

V

Vaughan, D.G., Corr, H.F.J., Doake, C.S.M. & Waddington, E.D., (1999). Distortion of isochronous layers in ice revealed by ground-penetrating radar. *Nature*, **398**, 323-326.

Völkel, J., Leopold, M., & Roberts, M.C., (2001). The radar signatures and age of periglacial slope deposits, Central Highlands of Germany. *Permafrost and Periglacial Processes*, **12**, 379-387.

Vonder Mühll, D., Hauck, C., & Gubler, H., (2002). Mapping of mountain permafrost using geophysical methods. *Progress in Physical Geography*, **26**, 643-660.

Vonder Mühll, D., Hauck, C., Gubler, H., McDonald, R., & Russill, N., (2001). New geophysical methods of investigating the nature and distribution of mountain permafrost with special reference to radiometry techniques. *Permafrost and Periglacial Processes*, **12**, 27-38.

Vonder Mühll, D., Hauck, C., & Lehmann, F., (2000). Verification of geophysical models in Alpine permafrost using borehole information. *Annals of Glaciology*, **31**, 300-306.

W

Walker, D.A., Walker, M.D., Everett, K.R., & Weber, P.J., (1985). Pingos of the Prudhoe bay region, Alaska. *Arctic and Alpine Research*, **17**, 321-336.

Walker, M.J.C., Buckley, S.L., & Caseldine, A.E., (2001). Landscape change and human impact in west Wales during the Lateglacial and Flandrian. *In* Walker, M.J.C., & McCarroll, D., (eds.), *The Quaternary of West Wales: Field Guide*. Quaternary Research Association, London, 17-29.

Walker, M.J.C., Coope, G. R., Sheldrick, C., Turney, C. S. M., Lowe, J. J., Blockley S. P. E. & Harkness D. D., (2003). Devensian Lateglacial environmental changes in Britain: a multi-proxy environmental record from Llanilid, South Wales, UK. *Quaternary Science Reviews*, **22**, 475-520.

Walker, M.J.C., & James, J.H., (2001). A pollen record from a ground ice depression ('Pingo U'), Cledlyn valley. In, Walker, M.J.C., & McCarroll, D., (eds), *The Quaternary of West Wales: Field Guide*. Quaternary Research Association, London.

Wang, B., & French, H.M., (1995). Permafrost on the Tibet Plateau, China. *Quaternary Science Reviews*, **14**, 255-274.

Ward, S.H., (1990). Resistivity and induced polarisation methods. In Ward, S.H. (ed.), *Geotechnical and Environmental Geophysics. Investigations in Geophysics no. 5. Vol 1 Review & Tutorial*. Society of Exploration Geophysicists, Tulsa. 147-189.

Warner, B.G., Nobes, D.C., & Theimer, B.D., (1990). An application of ground penetrating radar to peat stratigraphy of Ellice Swamp, southwestern Ontario. *Canadian Journal of Earth Sciences*, **27**, 932-938.

Warren, W.P., (1991). Fenitian (Midlandian) glacial deposits and glaciation in Ireland and the adjacent offshore regions. *In* J., Ehlers, P.L., Gibbard, & J., Rose (eds.), *Glacial Deposits in Great Britain and Ireland*, Balkema: Rotterdam, 79–88.

Washburn, A.L., (1979). *Geocryology: A Survey of Periglacial Processes and Environments*. Edward Arnold, London, 320 pp.

Washburn, A.L., (1980). Permafrost features as evidence of climatic change. *Earth Science Reviews*, **15**, 327-402.

Washburn, A.L., (1983). What is a palsa? In: Poser, H., Schunke, E. (eds.), Mathematisch–Physikalische Klasse, Dritte Folge. Mesofirmen des Reliefs im Heutingen Periglazialraum. Bericht über ein Symposium, Göttingen, Vandenhoeck and Ruprecht, vol. 35, 34–47.

Waters, R. A., Davies, J.R., Wilson, D., Prigmore, J.K., (1997). *A Geological Background for Planning and Development in the Afon Teifi Catchment.* British Geological Survey Technical Report WA/97/35; British Geological Survey: Keyworth.

Watson, E., (1965). Periglacial structures in the Aberystwyth region of central Wales. *Proceedings of the Geologists Association*, **76**, 443-462.

Watson, E., (1968). The periglacial landscape of the Aberystwyth region. In Bowen, E.G., Carter, H., & Taylor, J.A. (eds), *Geography at Aberystwyth.* University of Wales Press, Cardiff, 35-49.

Watson, E., (1970). The Cardigan Bay area. *In* Lewis, C.A., (Ed) *The Glaciations of Wales and Adjoining Regions.* Longman, London, 125-145.

Watson, E. (1971). Remains of pingos in Wales and the Isle of Man. *Geological Journal,* **7**, 381-392.

Watson, E. (1972). Pingos of Cardiganshire and the latest ice limit. *Nature*, **238**, 343-344.

Watson, E. (1975). Remains of round and linear pingos in the Cledlyn and Cletwr basins. In Watson, E., (ed) *Co-ordinating committee for periglacial research. Working group of the International Geographical Union Symposium: Guide to field excursion 1-10th July 1975.* University College of Wales, Aberystwyth.

Watson, E. (1976). Field excursions in the Aberystwyth region (1-10 July 1975). *Biuletyn Peryglacjalny,* **26**, 79-112.

Watson, E., (1977). The periglacial environment of Great Britain during the Devensian. *Philosophical Transactions of the Royal Society of London,* **B280**, 183-198.

Watson, E., (1981). Characteristics of ice-wedge casts in west central Wales. *Biuletyn Peryglacjalny,* **28**, 164-177.

Watson, E., (1982). Remains of pingos in the Cledlyn Valley near Lampeter. In Bassett, M.G., (ed) *Geological excursions in Dyfed, south-west Wales.* National Museum of Wales, Cardiff, 303-312.

Watson, E. & Watson, S. (1967). The periglacial origin of the drifts at Morfa Bychan, near Aberystwyth. *Geological Journal,* **5**, 419-440.

Watson, E. & Watson, S. (1971). Vertical stones and analogous structures. *Geografiska Annaler*, **53**, 107-114.

Watson, E. & Watson, S. (1972). Investigation of some pingo basins near Aberystwyth, Wales. *Report of the 24th International Geological Congress (Montreal)*, **12**, 212-233.

Watson, E. & Watson, S. (1974). Remains of pingos in the Cletwr basin, south-west Wales. *Geografiska Annaler*, **56A**, 213-225.

Watson, S. (1996). Relict ground-ice mounds in west Wales – pingos or palsas? *Quaternary Newsletter*, **80**, 64-65.

Williams, K.E., (1927). The glacial drifts of western Cardiganshire. *Geological Magazine*, **64**, 205-227.

Wirtz, D., (1953). Zur stratigraphie des Pleistozäns in western der Britischen Inseln. *Neues Jahrbuch für Geologie und Paläontologie*, **96**, 267-303.

Wisén, R., Auken, E., & Dahlin, T., (2005). Combination of 1D laterally constrained inversion and 2D smooth inversion of resistivity data with a priori data from boreholes. *Near Surface Geophysics*, **3**, 71-79.

Wood, A., & Smith, A.J., (1959). The sedimentation and sedimentary history of the Aberystwyth Grits (Upper Llandoverian). *Quarterly Journal of the Geological Society*, **114**, 163-195.

Woodcock, N.H., (1977). Specification of fabric shapes using an eigenvalue method. *Geological Society of America Bulletin*, **88**, 1231-1236.

Woodland, A.W., & Evans, W.B., (1964). *The geology of the South Wales Coalfield, Part 4. The country around Pontypridd and Maesteg*. Memoir of the Geological Survey of great Britain. H.M.S.O., London.

Worsley, P., (1977). Periglaciation. *In* Shotton, F.W., (ed.), *British Quaternary Studies*, Clarendon, Oxford, 205-219.

Worsley, P., (1984). Banc-y-Warren. In: Bowen, D.Q. & Henry, A. (eds). *Wales: Gower, Preseli, Fforest Fawr*. Quaternary Research Association Field Guide, Cambridge, 68-77.

Worsley, P., (1997). The preservation potential of icings. *Quaternary Newsletter*, **83**, 52-54.

Worsley, P., & Gurney, S.D., (1996). Geomorphology and hydrogeological significance of the Holocene pingos in the Karup Valley area, Traill Island, northern east Greenland. *Journal of Quaternary Science*, **11**, 249-262.

Worsley, P., Gurney, S.D., Colllins, P.E.F. (1995). Late Holocene 'mineral palsas' and associated vegetation patterns: a case study from Lac Hendry, Northern Quebec,

Canada and significance for European Pleistocene thermokarst. *Quaternary Science Reviews,* **14,** 179-192.

Worssam, B.C., & Taylor, J.H., (1969). Geology of the Country around Cambridge. Memoir of the British Geological Survey, Sheet 188 (England and Wales). The Stationery Office, London.

Wramner P., (1967). Studier av palsmyrar i Laivadalen, Lappland. Teknik och Natur, (Göteborg): 435–449.

Wramner, P., (1972). Palslika bildningar i mineraljord. Nagra iakttagelser fran Taavavuoma, Lappland (Summary: Palsa-like formation in mineral soil. Some observations from Taavavuoma, Swedish Lapland). Göteborgs Universitet Naturgeografiska Institutionen, Guni Rapport 1. 60 pp.

Wramner, P., 1973. Palsmyrar i Taavavuoma, Lappland (Summary: Palsa bogs in Taavavuoma, Swedish Lapland). Göteborg Universitets Naturgeografiska Institutionen, Guni Rapport 3. 140 pp.

Wright, W.B., (1914). *The Quaternary Ice Age.* Macmillan, London.

Y

Yoshikawa, K., (1991). Age of growth of two pingos, Sarqaq Dalen, west central Greenland. *Permafrost and Periglacial Processes,* **2,** 245-252.

Yoshikawa, K., (1993). Notes on open-system pingo ice, Adventdalen, Spitsbergen. *Permafrost and Periglacial Processes,* **4,** 327-334.

Yoshikawa, K., & Harada, K., (1995). Observations on nearshore pingo growth, Adventdalen, Spitsbergen. *Permafrost and Periglacial Processes,* **6,** 361-372.

Yoshikawa, K., Leuschen, C., Ikeda, A., Harada, K., Gogineni, P., Hoekstra, P., Hinzman, L., Sawada, Y., & Matsuoka, N., (2006). Comparison of geophysical investigations for detection of massive ground ice (pingo ice). *Journal of Geophysical Research,* **111,** E06S19.

Yoshikawa, K., & Nakamura, T., (1996). Pingo growth ages in the delta area, Adventdalen, Spitsbergen. *Polar Record,* **32,** 347-352.

Yoshikawa, K., Nakamura, T., & Igarashi, Y., (1996). Growth and collapse history of pingos, Kuganquaq, Disko Island, Greenland. *Polarforshung,* **64,** 109-113.

Z

Zilliacus, H., (1989). Genesis of De Geer moraines in Finland. *Sedimentary Geology,* **62,** 309-317.

Zoltai, S.C., (1972). Palsas and peat plateaus in central Manitoba and Saskatchewan. *Canadian Journal of Forest Research,* **2,** 291-302.

Zoltai, S.C., (1983). Pingos on Bylot Island, NWT, Canada. *Polarforschung*, **53**, 43-48.

Zoltai, S.C., & Tarnocai, C. (1975). Perennial frozen peatlands in the western Arctic and subarctic of Canada. *Canadian Journal of Earth Sciences*, **12**, 28-43.